

Recharge and discharge mechanism and dynamics in the mountainous northern Upper Jordan River Catchment, Israel

By Heike Briemann, Rostock

A thesis submitted to the Faculty of Geosciences
at Ludwig-Maximilians-University, Munich
in partial fulfilment of the
requirements for the
Ph.D. degree

January 2008

Day of examination: 29.04.2008
Dean: Prof. Dr. Wolfram Mauser
1st Reviewer: Prof. Dr. Klaus-Peter Seiler
2nd Reviewer: Prof. Dr. Christian Wolkersdorfer

To Marie & Josef Ciupa and Margret Crusius.

„Like the Eskimos' reputedly rich vocabulary for snow, the Hebrew language has separate words for the first and last rainfall, dew, different levels of floods, and half a dozen types of drought. The word „water“ itself appears 580 times in the Old Testament. The Hebrew patriarchs concerned themselves with digging and protecting wells. Water is a prerequisite for a variety of ritual purifications. There is no more common metaphor in the religious liturgy.“

Alon Tal (2002), Pollution in a Promised Land – An Environmental History of Israel.

Table of contents

Table of contents	i
Table of figures.....	iii
Table of tables	vii
Acknowledgements	xiii
Zusammenfassung.....	I
1. Introduction	1
1.1 Background data and tasks in the Upper Jordan River Catchment.....	2
1.2 Special research goals and approaches.....	9
2. Review of existing knowledge, concepts and techniques.....	10
2.1 Concepts on groundwater flow systems.....	10
2.1.1 Karst.....	10
2.1.2 Basalt.....	12
2.2 Techniques for residence time estimation	13
2.2.1 Lumped-parameter models and water isotopes	14
2.2.2 Radiocarbon dating in groundwater	15
2.3 Concepts on runoff generation processes	17
2.3.1 Runoff generation in Mediterranean semi-arid environments	22
2.4 Hydrograph separation techniques	23
2.4.1 Baseflow analysis	24
2.4.2 Recession analysis	25
2.4.3 Tracer-based hydrograph separation techniques.....	27
2.4.4 Natural tracers	31
3. Study area	40
3.1 Location and physiography	40
3.2 Climate	41
3.3 Soils.....	43
3.4 Vegetation and land use	45
3.5 Geology	46
3.5.1 Hula Valley.....	47
3.5.2 Mount Hermon	50
3.5.3 Golan Heights.....	55
3.5.4 Naftali Mountains.....	58
3.6 Hydrology	59
3.7 Hydrochemistry.....	63
3.8 Knowledge gaps and research needs	65
4. Sampling network and sampling program	66
5. Hydrochemical and stable isotopic characterization of precipitation in the mountainous northern Upper Jordan River Catchment	71
5.1 Orographic precipitation	72
5.2 Chemical composition of precipitation	75
5.3 Stable isotope composition of precipitation	76
5.3.1 Mean isotope composition and the local meteoric water line.....	76
5.3.2 Seasonal variations	80
5.3.3 Temperature and amount effect.....	81
5.3.4 Influence of wind direction	82
5.3.5 The influence of the synoptic system	83
5.3.6 Inter- and intra-storm variability	85
5.3.7 Altitude effect.....	87
5.3.8 Snowpack chemistry and stable isotope composition.....	88

6. Hydrochemical and stable isotopic characterization of groundwater in the mountainous northern Upper Jordan River Catchment	92
6.1 Chemical composition of groundwater	94
6.1.1 General hydrochemical characteristics	94
6.1.2 Hydrochemical facies and ionic ratios	98
6.1.3 Equilibrium conditions of groundwater	101
6.2 Stable isotope composition of groundwater	104
6.3 Mixing of groundwater sources in the UJRC	107
6.3.1 Hermon springs	108
6.3.2 Golan springs	111
6.4 Estimation of recharge altitudes and groundwater recharge rates	113
6.4.1 Recharge altitude	113
6.4.2 Groundwater recharge rates	115
6.5 Temporal variations in groundwater chemistry and isotopic content	118
6.5.1 Hermon springs	119
6.5.2 Golan 'Side springs'	125
6.6 Banias spring – long-term hydrograph separation	127
6.6.1 Two-component mixing model using $\delta^{18}\text{O}$ as tracer	127
6.6.2 Three-component mixing model using $\delta^{18}\text{O}$ and sulfate as tracers	130
6.7 Dan spring - hydrograph separation	132
6.7.1 Two-component mixing model comparing $\delta^{18}\text{O}$, chloride and sulfate as natural tracers	132
6.8 Groundwater residence times	136
6.8.1 Tritium content and mean residence time of groundwater	136
6.9 Radiocarbon dating	142
6.9.1 Carbon (^{13}C , ^{14}C) isotopes	144
6.9.2 Initial ^{14}C activity and radiocarbon ages	147
7. Runoff generation in the main tributaries of the Upper Jordan River	154
7.1 Long-term streamflow hydrograph separation	155
7.2 Baseflow recession analyses	159
7.3 Tracer-based investigation of runoff generation processes	164
7.3.1 General pattern of streamflow response	166
7.3.2 Hydrometric observations	169
7.3.3 Event chronology	173
7.3.4 Chemographs	177
7.3.5 End-member differentiation	186
7.3.6 Two-component hydrograph separation	189
Extended summary	197
References	203
Appendix	233
List of common abbreviations	233
Stratigraphy of Mount Hermon and geology of the study area	234
Analytical methods	237
Sample collection	237
Electrical conductivity, temperature and pH	237
Anions and cations	238
Dissolved silicic acid (Silica)	238
^{18}O and ^2H	239
Dissolved organic carbon (DOC)	240
Carbonate alkalinity	240
Tritium	241
Carbon-13 and carbon-14	241
TSS	241
Supplementary data	242
Supplementary data - Chapter 5	242
Supplementary data – Chapter 6	258
Supplementary data – Chapter 7	278
Curriculum Vitae	305

TABLE OF FIGURES

Figure 1:	The Upper Jordan River Catchment (UJRC), Israel (from EXACT, U.S. Geological Survey, 1998).	2
Figure 2:	Mean annual water fluxes into Lake Kinneret and out of the lake. Dashed lines indicate inflows, solid black lines losses and numbers represent water volumes in million cubic meter ($=10^6\text{m}^3$). Adapted from Gvirtzman (2002).	5
Figure 3:	Conceptual discharge model of the Upper Jordan River catchment.	6
Figure 4:	Conceptual model of water flow and storage in a karst aquifer. Modified according to MALOSZEWSKI et al. (2002), PERRIN et al. (2003) and EINSIEDL (2005). Flow is indicated by arrows. Q_D = diffusive flow, Q_C = conduit flow, Q_{SO} = saturation overland flow, Q_T = total flow, P = precipitation, ET = evapotranspiration.	11
Figure 5:	Conceptual model of groundwater flow in a basalt aquifer according to DAFNY et al. (2006). The regional, deep aquifer is overlain by several smaller perched aquifers in the unsaturated zone.....	13
Figure 6:	Mechanism of runoff generation (adapted from BEVEN, 1986).	19
Figure 7:	The groundwater ridging mechanism of pre-event water discharge. Hypothetical water table profiles (a) prior to the event and (b) at peak runoff (adapted from CLOKE et al., 2006).	22
Figure 8:	The Upper Jordan River Catchment and its location in the State of Israel (EXACT, 1998). Numbers represent gauging stations of the Hydrological Service of Israel (HSI).	40
Figure 9:	Map of the main faults in the northern Jordan Rift Valley (HEIMANN, 1990; ZILBERMAN, 2000).	47
Figure 10:	Schematic block model of the Hula trough, showing the groundwater circulation below the Hula plain (adapted from KAFRI and LANG, 1979). (Brick signature = carbonates, circles = gravel/sands, waves = clay/silt, black bars = peat, arrows = direction of water movement.)	49
Figure 11:	The topography of the Mount Hermon region and its hydrological network (GUR et al., 2003 adapted from GILAD and SCHWARTZ, 1978). The size of circles is proportional to the respective spring discharge (see legend on the bottom right).	52
Figure 12:	Geological cross sections of springs emerging on the southern foot slopes of Mount Hermon. The flow direction of water is indicated by arrows (GUR et al., 2003 adapted from GILAD and SCHWARTZ, 1978).	53
Figure 13:	North-south hydrogeological cross section along the Golan Heights (DAFNY et al., 2003). Groundwater flows both from east to west into the Kinneret-Hula basin and from west to east towards the upper Yarmouk River.	56
Figure 14:	(a) Location map and (b) hydrological background map (DAFNY et al., 2006) showing major springs, major streams and rivers, major wells, yearly rain isohyets (1961–1990 average), sedimentary outcrops and the computerized model boundaries defined by DAFNY et al. (2003). MCM/year equals 10^6 m^3 per year.	57
Figure 15:	Scheme of the Upper Jordan River and its main tributaries (Dan, Hermon, Senir). Additionally given are rivulets and springs investigated within this study. Springs that are underlined and given in italic letters were not accessible for sampling.	59
Figure 16:	Hydrological regime and annual distribution of mean monthly flow (open symbols) versus mean monthly high flow (filled symbols) of the main waters in the Upper Jordan River Catchment. The fluctuation coefficient FC represents the mean monthly discharges compared to the long-term annual mean. The latter one is corresponding to the zero line (\cong mean). Based on data and periods of time summarized in Table 5.	62
Figure 17:	Precipitation sampling network in the Upper Jordan River catchment. Modified from EXACT (1998).	72
Figure 18:	Stable isotope composition of precipitation in the northern UJRC. Relationship between $\delta^{18}\text{O}$ and $\delta^2\text{H}$ of daily rainfall in 2002-2004.	79

Figure 19:	Stable isotope composition of precipitation in the northern UJRC. Relationship between $\delta^{18}\text{O}$ and $\delta^2\text{H}$ of weekly rainfall and snow in 2002-2004.....	79
Figure 20:	Monthly means of ^{18}O in rainfall in the northern UJRC for the years 2002-2004.....	80
Figure 21:	Relationship between the arithmetic mean monthly $\delta^{18}\text{O}$ values of all investigated stations and the number of rain days in the adequate month, rain season 2003/04.	80
Figure 22:	Relationship between $\delta^{18}\text{O}$ in rain water and maximum daily air temperature (left) and the daily rain depths (right) in the northern UJRC, in the years 2002-2004. “**” denotes that results are significant at $p<0.01$ (two-sided).....	81
Figure 23:	The distribution of the stable ^{18}O isotope composition of precipitation in relation to the prevailing wind direction and mean rain depths in the UJRC determined in this thesis.....	82
Figure 24:	Mean stable isotope composition ($\delta^{18}\text{O}$) of rain water (squares) and the relative number of days with rain (bars) for each synoptic system class determined for daily rain samples taken at Tel Dan during 2002/03 and 2003/04. Descriptions of the synoptic system classes are given in Figure 66.83	
Figure 25:	Inter- and intra-storm variability of $\delta^{18}\text{O}$ in daily rainfall samples of the Banias Nature Reserve, 2002-2004. The V-shaped pattern in the temporal evolution of stable isotopes during the rain events is emphasized by the respective symbol (V).	86
Figure 26:	Snowpack chemistry and stable isotopic composition of two snow profiles investigated during January and February 2004.....	90
Figure 27:	Groundwater sampling network in the Upper Jordan River Catchment. Modified from EXACT (1998).	93
Figure 28:	Relationship between concentrations of Na^+ and Cl^- in the investigated springs (left figure). Lines illustrate common ratios of Na^+ versus Cl^- in the analyzed groundwaters. The 1:1 ratio equals the seawater dilution line. Relationship between alkali and earth-alkali metals (right figure). Gray circles comprise all Golan springs which plot very close to each other.	98
Figure 29:	Piper plot of the mean chemical composition of groundwater sampled in the northern UJRC during the study period 2002-2004. Open circles represent the Hermon springs, open squares the Golan springs. Symbol diameter reflects the electrical conductivity of each spring.....	99
Figure 30:	Relationship between concentrations of SO_4^{2-} and Cl^- (left figure). Relationship between concentrations of HCO_3^- and $\text{Cl}^-+\text{SO}_4^{2-}$ in the investigated groundwater (right figure). Lines illustrate common ion ratios in the analyzed springs. Gray circles comprise all Golan springs which plot very close to each other.	101
Figure 31:	Relationship between mean $\delta^{18}\text{O}$ and $\delta^2\text{H}$ values for springs sampled in the northern UJRC. Figure a) distinctive grouping of groundwaters emerging in the Hermon Mountains and in the Golan Heights, Figure b) mean stable isotope composition of the Golan “Side Springs”, Figure c) seasonal stable isotope composition of the Hermon springs.....	106
Figure 32:	Relationship between mean oxygen isotopic composition and mean chloride concentration in the sampled Hermon spring waters and in Mt. Hermon snow. For the Banias and Kezinim spring, mean seasonal compositions are given. The error bars represent 1σ uncertainty.....	108
Figure 33:	Relationship between mean sulfate and mean chloride composition in the sampled Hermon spring waters and Mt. Hermon snow. For the Banias and Kezinim spring, mean seasonal compositions are given. Grey frames indicate the suggested end-members. The error bars represent 1σ uncertainty.....	109
Figure 34:	Relationship between mean oxygen isotopic composition and mean SiO_2 concentrations in the investigated Golan “Side springs”. Groundwaters (with the exception of the Elmin Jedida spring) plot along a perfect mixing line as indicated by the given correlation coefficient. The error bars represent 1σ uncertainty.....	111
Figure 35:	Relationship between tritium and mean dissolved SiO_2 concentrations in the investigated Golan “Side springs”. Groundwaters (with the exception of the Elmin Jedida spring) plot along a mixing line further indicated by the given correlation coefficient. The error bars represent 1σ uncertainty..	112

Figure 36:	Local “Enrichment” Lines (LELs) of the investigated Hermon springs plotted against the Local Meteoric Water line (LMWL) . Frames indicate the initial stable isotopic composition ($\delta^{18}\text{O}$, $\delta^2\text{H}$) of the recharged groundwaters.....	114
Figure 37:	Altitude versus $\delta^{18}\text{O}$ in precipitation in the southern Hermon Mountains. The line is a best-fit to daily rainfall samples taken during 2002-2004. Isotopic composition of the springs was corrected for enrichment effects (see Figure 36). Their main recharge elevation is inferred by determining the altitude at which precipitation has approximately the same isotopic composition.	115
Figure 38:	Seasonal development of monthly discharge, temperature, electrical conductivity, major ions and stable isotopes ($\delta^{18}\text{O}$, $\delta^2\text{H}$) in the Banias spring during the study period 2002-2004. Also shown are the annual accumulated rain amounts measured at the Banias Nature Reserve. The parameter that is mentioned first in the legends above the graphs refers to the left axis, the second one to the right axis.....	121
Figure 39:	Seasonal development of monthly discharge, temperature, electrical conductivity, major ions and stable isotopes ($\delta^{18}\text{O}$, $\delta^2\text{H}$) in the Dan spring during the study period 2002-2004. Also shown are the annual accumulated rain amounts measured at the Dan Nature Reserve. The parameter that is mentioned first in the legends above the graphs refers to the left axis, the second one to the right axis	122
Figure 40:	Temporal variations of temperature, electrical conductivity, sulfate, chloride and the stable water isotopes during three subsequent rain events in December 2002. Also shown are daily rain values and monthly discharges measured at the Banias Nature Reserve. The parameter that is mentioned first in the legends above the graphs refers to the left axis, the second one to the right axis.....	124
Figure 41:	Input function of ${}^3\text{H}$ for precipitation over the Upper Jordan River catchment, (GNIP, 2005) ...	138
Figure 42:	Calculated ${}^3\text{H}$ output concentrations obtained as best fit of the dispersion model (DM) and the exponential model (EM) to the data measured in the Senir (upper left), Dan (lower left) and Hermon (lower right) streams during baseflow conditions. The respective parameters are given in Table 31.....	139
Figure 43:	${}^{14}\text{C}$ activity (left chart) and pH (right chart) versus $\delta^{13}\text{C}$ content in the Hermon springs, the Golan springs and the Senir stream.....	146
Figure 44:	EC (left chart) and $\log P_{\text{CO}_2}$ (right chart) versus ${}^{14}\text{C}$ activity in the Hermon springs (H), the Golan springs (G) and the Senir stream. The Dupheila spring belonging to the Golan springs is displayed separately.....	146
Figure 45:	Relationship between calculated mean residence times (MRT) of baseflow in the Dan stream and annual precipitation prior to the respective recession period.....	163
Figure 46:	Investigated stream network in the northern UJRC. Underlined and italic fonts denote springs that were not sampled due to their location on the borderline between Israel and Syria or Israel and Lebanon.....	165
Figure 47:	Rain (bars) and mean air temperature (dots) at Pichmann farm from November 2002 to May 2004. Also presented are continuous discharge (black line), electrical conductivity (light grey line) and stream temperature (dark grey line) in the Dan, Hermon, Senir and Orevim stream for the study period. Data gaps are due to technical and logistical problems.....	167
Figure 48:	Rain (bars) and mean air temperature (dots) at Pichmann farm from November 2002 to May 2004. Also presented is the continuous Sion discharge during the study period.....	168
Figure 49:	Hourly and accumulated rain at Pichmann farm and discharge, electrical conductivity and stream temperature for the Hermon stream (storm runoff event 1/13/2004-1/22/2004).	174
Figure 50:	Hourly and accumulated rain at Pichmann farm. Also given are discharge and electrical conductivity for the Sion stream (storm runoff event 1/14/2004-1/16/2004).	175
Figure 51:	Hourly and accumulated rain at Pichmann farm. Also given are discharge, electrical conductivity and stream temperature for the Orevim stream (storm runoff event 1/13/2004-1/18/2004).....	176
Figure 52:	Daily and accumulated rain at Mayan Barukh. Also given are discharge and electrical conductivity for the Senir stream (storm runoff event 2/13/2003-2/18/2003).	177

Figure 53:	Time-series of discharge, electrical conductivity, temperature, $\delta^{18}\text{O}$, deuterium excess and major anions during 1/13/2004-1/22/2004 in the Hermon stream.....	178
Figure 54:	Time-series of discharge, electrical conductivity, temperature, major cations, SiO_2 and DOC during 1/13/2004-1/22/2004 in the Hermon stream.....	179
Figure 55:	Time-series of discharge, electrical conductivity, temperature, $\delta_{18}\text{O}$, deuterium excess and major anions during 1/13/2004-1/18/2004 in the Orevim stream.....	181
Figure 56:	Time-series of discharge, electrical conductivity, temperature, major cations, SiO_2 and DOC during 1/13/2004-1/18/2004 in the Orevim stream.....	182
Figure 57:	Relative natural tracer concentration in the Hermon stream during 1/13/2004-1/22/2004.....	184
Figure 58:	Relative tracer concentration in the Orevim stream during 1/13/2004-1/18/2004.....	185
Figure 59:	Mixing diagrams of $\delta^{18}\text{O}$ and Cl^- for the investigated events in the Hermon, Orevim and Senir stream. R indicates the correlation coefficient.....	186
Figure 60:	Mixing diagrams of HCO_3^- and Ca^{2+} for the investigated events in the Hermon, Orevim and Senir stream. R indicates the correlation coefficient.....	187
Figure 61:	Results of the two-component hydrograph separation for the Hermon stream (left) and Orevim stream (right) using $\delta^{18}\text{O}$ and Cl^- as tracer. Given are the $\delta^{18}\text{O}$ scenarios each that best reproduced the results of the chloride-based mixing model. Q_T denotes total discharge while Q_{PE} refers to pre-event water.	193
Figure 62:	Results of the two-component hydrograph separation for the Senir stream using $\delta^{18}\text{O}$ and Cl^- as tracer. Presented are the $\delta^{18}\text{O}$ scenarios that best reproduced the results of the chloride-based mixing model.....	195
Figure 63:	Stratigraphy and hydrological characteristics of the Hermon area adapted from GUR et al. (2003).....	234
Figure 64:	Geological map of the study area according to SNEH et al., 1998. The legend is given in Figure 65.	235
Figure 65:	Legend explaining the geological map of the study area (Figure 64).....	236
Figure 66:	Explanation of the synoptic systems classified for the Eastern Mediterranean region.....	255
Figure 67:	Time-series of discharge, electrical conductivity, temperature, $\delta^{18}\text{O}$, deuterium excess and major anions during 2/14/2003-2/18/2003 in the Senir stream.....	291
Figure 68:	Time-series of discharge, electrical conductivity, temperature, major cations, SiO_2 and DOC during 2/14/2003-2/18/2003 in the Senir stream.....	292
Figure 69:	Time-series of discharge, electrical conductivity, temperature, $\delta^{18}\text{O}$, deuterium excess and major anions during 1/14/2004-1/18/2004 in the Sion stream.	293
Figure 70:	Time-series of discharge, electrical conductivity, temperature, major cations, SiO_2 and DOC during 1/14/2004-1/18/2004 in the Sion stream.	294

TABLE OF TABLES

Table 1:	Annual water resources and water withdrawal in Israel and its neighboring countries. Numbers were retrieved from the FAO AQUASTAT database and are representative for the period 1998-2002. Quantities of withdrawal and resources in the Palestinian Authority area (PA) are cited from BOU-ZEID and EL-FADEL (2002) [*] and ALATOUT (2000) [**].....	3
Table 2:	Springs fed (at least in part) by recharge on Mount Hermon and their corresponding average annual yields.....	51
Table 3:	Major “Side springs” fed by recharge on the Golan Heights and their corresponding average annual yields (MICHELSON, 1996)	58
Table 4:	Springs fed by recharge on the Naftali Mountains and their corresponding average annual yields (MICHELSON, 1996)	59
Table 5:	Hydrological classification numbers of the main Jordan tributaries in the Upper Jordan River Catchment. Data provided by the HSI.....	60
Table 6:	Streamflow sampling network in the UJRC and sampling frequency. Coordinates are given according to the New Israeli Grid. Station numbers are according to the Hydrological Service of Israel (HSI).	67
Table 7:	Rainfall sampler locations in the UJRC and sampling intervals, (W: weekly, D: daily). Coordinates are given according to the New Israeli Grid.....	68
Table 8:	Locations of groundwater sampling and sampling program. Coordinates are given according to the New Israeli Grid. N is the number of samples taken.....	69
Table 9:	Quantiles of accumulated rain amounts at Kefar Giladi for the period 1969-1999.....	72
Table 10:	Location of stations in the UJRC and accumulated quantities of rain measured during the period 2002-2004. Correlation of the station-characteristic rain amount with data recorded at Kefar Giladi. Coordinates are given in the New Israeli Grid.....	73
Table 11:	Rain depths at Mount Hermon during 2002-04. Results were estimated by multiple regression analysis. Coordinates are given according to the New Israeli Grid. Easting not shown.....	74
Table 12:	Median and mean ion concentrations of daily rain samples and snow in the UJRC. Sampled rain amounts were too small to analyze for HCO_3^-	75
Table 13:	Arithmetic mean (δ) and amount-weighted (δ_w) mean stable isotope composition of daily rainfall in the northern UJRC. Also, the deuterium excess (d) is given each. Stations are arranged according to increasing altitudes (see Table 7). Samples were taken during 2002-2004.	77
Table 14:	Arithmetic mean (δ) and amount-weighted (δ_w) mean stable isotope composition of weekly rainfall and snow in the northern UJRC. Also, the deuterium excess (d) is given each. Stations are arranged according to increasing altitudes (see Table 7). Samples were taken during 2002-2004. 78	78
Table 15:	Mean stable isotope composition, the relative number of rain days (n) and mean rain amounts for each synoptic system determined for daily rain samples taken at five stations in the northern UJRC during 2002/03 and 2003/04. Synoptic systems are explained in Figure 66.	84
Table 16:	Altitude gradients of stable water isotopic composition in the northern UJRC and neighboring regions in the Eastern Mediterranean. The global isotopic lapse rate is given as a reference.	87
Table 17:	Physico-chemical characteristics and concentrations of DOC and SiO_2 of groundwater in the northern UJRC.....	94
Table 18:	Mean major ion concentrations of groundwaters emerging in the northern UJRC. For numbers of samples refer to Table 17. TDI is total dissolved ions, R.E. is the reaction error based on mean values.....	95
Table 19:	Mean partial pressure of carbon dioxide and saturation indices of selected minerals of groundwaters sampled in the UJRC during the study period 2002-04. Saturation indices for magnesite, dolomite, calcite, anhydrite, gypsum, aragonite, sepiolite and silica (gel) are SI_{mag} , SI_{dol} , SI_{cal} , SI_{an} , SI_{gyp} , SI_{ara} , SI_{sep} and SI_{sil} , respectively.....	102

Table 20:	Mean stable isotope composition of spring waters in the northern UJRC during 2002-2004.	105
Table 21:	Estimated groundwater recharge rates for the investigated springs in the UJRC. Cl_{GW} represents the mean concentration of chloride during baseflow (winter), P the mean annual precipitation for the Hermon region1) and Cl_p the median concentration of chloride in snow (Hermon springs) and rain (Golan springs). R is the calculated recharge rate given in mm/year and % of mean annual precipitation.....	117
Table 22:	Seasonal distribution of mean natural tracer concentrations in the major Hermon springs (autumn: October-November, winter: December-March, spring: April-May, summer: June-September).....	120
Table 23:	Seasonal distribution of mean tracer concentrations in the Golan “Side springs” (autumn: October-November, winter: December-March, spring: April-May, summer: June-September).	126
Table 24:	Monthly portions of event (P_E) and pre-event water (P_{PE}) of total discharge at the Banias spring as determined by two-component hydrograph separation using ^{18}O as a natural tracer.	128
Table 25:	Input tracer concentrations of rain/snow (C_{RS}) = event water (C_E), vadose (C_{VAD}) and diffusive flow (C_{DF}) used in the three-component mixing model for the Banias spring.....	131
Table 26:	Monthly portions of rain/snow (P_{RS}), vadose (P_{VAD}) and diffusive flow (P_{DF}) of total discharge at the Banias spring as determined by three-component hydrograph separation using ^{18}O and sulfate as a tracer.....	131
Table 27:	Input tracer concentrations for $\delta^{18}O$, sulfate and chloride of the event (C_E) and pre-event (C_{PE}) components used in the two-component mixing models for the Dan spring.....	134
Table 28:	Monthly portions of event and pre-event water in the Dan spring as determined by two-component hydrograph separation using ^{18}O , sulfate and chloride as tracer, respectively.....	134
Table 29:	Tritium content in precipitation accumulating in the Upper Jordan River Catchment.	137
Table 30:	Tritium content in groundwaters emerging in the UJRC.....	137
Table 31:	Results of the conducted lumped parameter modeling using tritium contents in precipitation and baseflow (representing the outflow of the fissured-porous aquifer) of the main Jordan tributaries. DM is the Dispersion model with tp as the mean transit time of tracer in the fissured-porous aquifer, while EM is the exponential model with t as the mean transit time of tracer.....	141
Table 32:	Literature review on ranges of $\delta^{13}C$ contents in CO_2 , rocks and vegetation.....	144
Table 33:	Carbon isotopes (^{13}C , ^{14}C) in sampled Hermon and Golan groundwater. Electrical conductivity, pH, $\log P_{CO_2}$ and isotopic characterization of DIC.	145
Table 34:	Corrected initial ^{14}C activities and subsequently calculated groundwater mean residence times of the sampled Hermon springs. The measured in situ activities are given as ‘Original data’.	151
Table 35:	Corrected initial ^{14}C activities and subsequently calculated groundwater mean residence times of the sampled Golan springs (I). The measured in situ activities are given as ‘Original data’.....	152
Table 36:	Corrected initial ^{14}C activities and subsequently calculated groundwater mean residence times of the sampled Golan springs (II). The measured in situ activities are given as ‘Original data’.....	153
Table 37:	Mean flow and mean baseflow of the five investigated streams in the UJRC determined by different hydrograph separation techniques.....	156
Table 38:	Separated discharge components of the five investigated streams in the UJRC.....	157
Table 39:	Baseflow index (BFI) of the five investigated streams in the UJRC. The BFI value equals the monthly mean low flow according to Kille (MoMLF _K) as presented in Table 37.	158
Table 40:	Characteristics of baseflow recession in the Upper Jordan River Catchment including the recession constant α , the mean residence time of baseflow T_B , the initial baseflow discharge Q_0 , the estimated volume of water in the baseflow reservoir V_B , the recession length Δt_B and the reservoir change $V_{\Delta t_B}$. Estimations for the Dan, Hermon and Senir stream are based on a 32-year record (1969-2000); for the Jordan River a 10-year record (1991-2000) was available. The complete dataset of the extracted recessions is given in the appendix in Table 76, Table 77, Table 78 and Table 79.	161

Table 41:	Correlation and cross correlation (CC) of monthly rain depth at Kefar Giladi with mean monthly stream discharge in the UJRC	162
Table 42:	Estimated aquifer thickness for the Dan and Hermon catchments.	164
Table 43:	Hydrological characteristics of runoff events in 2002/03 and 2003/04 in four streams of the UJRC. All discharges (Q) are reported as median values except for the maximum discharge (Q_{\max}). Q_{initial} , Q_{final} and Q_{peak} are the discharges at the beginning, and at the end of the event, and during peak flow, respectively. N is the number of major events differentiated from the hydrograph. N_s is the number of sampled events. Single event characteristics are given in the appendix in Table 80, Table 81, Table 82 and Table 83.	171
Table 44:	Temporal features of runoff events in 2002/03 and 2003/04 for four streams of the UJRC and antecedent precipitation indices based on records of the meteorological station at Banias Nature Reserve. N is the number of major events differentiated from the hydrograph. The antecedent precipitation index (API) is calculated as the 2- or 5-day sum of precipitation preceding the storm event.	172
Table 45:	Relative natural tracer concentrations in the investigated streams at peak discharge during the investigated events.....	185
Table 46:	Results of the conducted principal component analyses for the investigated events in the Hermon, Orevim and Senir stream. Principal components (PC) are given with their component matrix. Italic letters indicate principal components with eigenvalues smaller than 1. Var(PC) indicates the variance explained by the respective principal component.	188
Table 47:	Results of the conducted two-component hydrograph separations using $\delta^{18}\text{O}$ and Cl^- as tracer. Maximum (max) and mean event water contributions are presented as well as the event water input at peak discharge (peak). Event water contributions are given as percentage of total discharge (% Q_T).	192
Table 48:	Details on pretreatment and storage of the collected water samples.	237
Table 49:	Specifications of the IC-analyzer at the Institute of Groundwater ecology, GSF.....	238
Table 50:	Specifications of the TOC/DOC analyzer at the Institute of Groundwater ecology, GSF.....	240
Table 51:	Ion concentrations in daily rain samples at the Banias Nature Reserve. N.d.: not determined....	242
Table 52:	Ion concentrations in daily rain samples at the Dan Nature Reserve. N.d.: not determined.....	243
Table 53:	Natural tracer concentrations from snow samples of different snow courses taken on Mount Hermon (Israel). N.d.: not determined.....	244
Table 54:	Natural tracer concentrations from snow samples of different snow profiles taken on Mount Hermon (Israel). N.d.: not determined.....	246
Table 55:	Stable isotope composition ($\delta^{18}\text{O}$, $\delta^2\text{H}$) and amounts of daily rain in the Banias and Dan Nature Reserves.....	247
Table 56:	Stable isotope composition ($\delta^{18}\text{O}$, $\delta^2\text{H}$) and amounts of daily rain in Kibutz Mayan Barukh, the Nimrod Nature Reserve and Moshav Shear Yeshuv. N.d.: not determined.....	250
Table 57:	Stable isotope composition ($\delta^{18}\text{O}$, $\delta^2\text{H}$) and amounts of weekly rain in the Banias and Dan Nature Reserves and Kibutz Mayan Barukh.	252
Table 58:	Stable isotope composition ($\delta^{18}\text{O}$, $\delta^2\text{H}$) and amounts of weekly rain in Moshav Neve Ativ, the Nimrod Nature Reserve and Moshav Shear Yeshuv. N.d.: not determined.....	253
Table 59:	Stable isotope composition ($\delta^{18}\text{O}$, $\delta^2\text{H}$) and amounts of weekly rain in the Orevim catchment and Kibutz Shamir. N.d.: not determined.....	254
Table 60:	Single altitude gradients determined on weekly bulk samples of up to five stations based on $\delta^{18}\text{O}$. NA = Neve Ativ, NNR = Nimrod Nature Reserve, BNR = Banias Nature Reserve, TDNR = Tel Dan Nature Reserve, MSY = Moshav Shear Yeshuv. N.d.: not determined.	256
Table 61:	Single altitude gradients determined on weekly bulk samples of up to five stations based on $\delta^2\text{H}$. NA = Neve Ativ, NNR = Nimrod Nature Reserve, BNR = Banias Nature Reserve, TDNR = Tel Dan Nature Reserve, MSY = Moshav Shear Yeshuv. N.d.: not determined.	257

Table 62:	Physico-chemical parameters and natural tracer concentrations of the Bet HaMekhes spring from 2002 to 2004. N.d.: not determined.	258
Table 63:	Physico-chemical parameters and natural tracer concentrations of the Divsha spring from 2002 to 2004. N.d.: not determined.	259
Table 64:	Physico-chemical parameters and natural tracer concentrations of the Dupheila spring from 2002 to 2004. N.d.: not determined.	260
Table 65:	Physico-chemical parameters and natural tracer concentrations of the Elmin Jedida spring from 2002 to 2004. N.d.: not determined.	261
Table 66:	Physico-chemical parameters and natural tracer concentrations of the Gonon spring from 2002 to 2004. N.d.: not determined.	262
Table 67:	Physico-chemical parameters and natural tracer concentrations of the Hamroniya spring from 2002 to 2004. N.d.: not determined.	263
Table 68:	Physico-chemical parameters and natural tracer concentrations of the Jalabina spring from 2002 to 2004. N.d.: not determined.	264
Table 69:	Physico-chemical parameters and natural tracer concentrations of the Notera spring from 2002 to 2004. N.d.: not determined.	265
Table 70:	Physico-chemical parameters and natural tracer concentrations of the Sion spring / stream from 2002 to 2004. N.d.: not determined.	266
Table 71:	Physico-chemical parameters and natural tracer concentrations of the Barid spring from 2002 to 2004. N.d.: not determined.	266
Table 72:	Physico-chemical parameters and natural tracer concentrations of the Leshem spring from 2002 to 2004. N.d.: not determined.	267
Table 73:	Physico-chemical parameters and natural tracer concentrations of the Dan spring from 2002 to 2004. N.d.: not determined.	270
Table 74:	Physico-chemical parameters and natural tracer concentrations of the Banias spring from 2002 to 2004. N.d.: not determined.	273
Table 75:	Physico-chemical parameters and natural tracer concentrations of the Kezinim spring from 2002 to 2004. N.d.: not determined.	276
Table 76:	Characteristics of baseflow recessions in the Dan stream from 1969 to 2000. X_1 and X_2 both denote the interpolation points of the recession curve, X_0 is the time of the initial baseflow discharge (reconstructed from the recession curve), X_{end} is the end of the recession. Given are the recession constant α , the respective intercept β , the mean residence time of baseflow T_B , the initial baseflow discharge Q_0 , the estimated volume of water in the baseflow reservoir V_B , the recession length Δt_B and the baseflow reservoir change $V_{\Delta t B}$	278
Table 77:	Characteristics of baseflow recessions in the Hermon stream from 1969 to 2000. X_1 and X_2 both denote the interpolation points of the recession curve, X_0 is the time of the initial baseflow discharge (reconstructed from the recession curve), X_{end} is the end of the recession. Given are the recession constant α , the respective intercept β , the mean residence time of baseflow T_B , the initial baseflow discharge Q_0 , the estimated volume of water in the baseflow reservoir V_B , the recession length Δt_B and the baseflow reservoir change $V_{\Delta t B}$	280
Table 78:	Characteristics of baseflow recessions in the Senir stream from 1969 to 2000. X_1 and X_2 both denote the interpolation points of the recession curve, X_0 is the time of the initial baseflow discharge (reconstructed from the recession curve), X_{end} is the end of the recession. Given are the recession constant α , the respective intercept β , the mean residence time of baseflow T_B , the initial baseflow discharge Q_0 , the estimated volume of water in the baseflow reservoir V_B , the recession length Δt_B and the baseflow reservoir change $V_{\Delta t B}$	282
Table 79:	Characteristics of baseflow recessions in the Jordan River from 1991 to 2000. X_1 and X_2 both denote the interpolation points of the recession curve, X_0 is the time of the initial baseflow discharge (reconstructed from the recession curve), X_{end} is the end of the recession. Given are the recession constant α , the respective intercept β , the mean residence time of baseflow T_B , the initial baseflow discharge Q_0 , the estimated volume of water in the baseflow reservoir V_B , the recession length Δt_B and the baseflow reservoir change $V_{\Delta t B}$	284

Table 80:	Hydrological characteristics of runoff events in the Hermon stream in 2002/03 and 2003/04. Q denotes discharges where Q_{initial} , Q_{final} and Q_{peak} are the discharges at the beginning, and at the end of the event and during peak flow, respectively. Temporal features are given as T: times, where T_{start} , T_{end} , T_{peak} are the start, end or peak time of the runoff event. T_{duration} , T_{BF} , T_{interval} and T_{response} denote the duration of the runoff event, the duration of baseflow preceding the event, the interval between events and the time between the start and the peak of the runoff event, respectively. The antecedent precipitation index (API) is calculated as the 2-day or 5-day sum of precipitation preceding the storm event.....	285
Table 81:	Hydrological characteristics of runoff events in the Senir stream in 2002/03 and 2003/04. Q denotes discharges where Q_{initial} , Q_{final} and Q_{peak} are the discharges at the beginning, and at the end of the event and during peak flow, respectively. Temporal features are given as T: times, where T_{start} , T_{end} , T_{peak} are the start, end or peak time of the runoff event. T_{duration} , T_{BF} , T_{interval} and T_{response} denote the duration of the runoff event, the duration of baseflow preceding the event, the interval between events and the time between the start and the peak of the runoff event, respectively. The antecedent precipitation index (API) is calculated as the 2-day or 5-day sum of precipitation preceding the storm event.....	286
Table 82:	Hydrological characteristics of runoff events in the Orevim stream in 2002/03 and 2003/04. Q denotes discharges where Q_{initial} , Q_{final} and Q_{peak} are the discharges at the beginning, and at the end of the event and during peak flow, respectively. Temporal features are given as T: times, where T_{start} , T_{end} , T_{peak} are the start, end or peak time of the runoff event. T_{duration} , T_{BF} , T_{interval} and T_{response} denote the duration of the runoff event, the duration of baseflow preceding the event, the interval between events and the time between the start and the peak of the runoff event, respectively. The antecedent precipitation index (API) is calculated as the 2-day or 5-day sum of precipitation preceding the storm event.....	288
Table 83:	Hydrological characteristics of runoff events in the Sion stream in 2002/03 and 2003/04. Q denotes discharges where Q_{initial} , Q_{final} and Q_{peak} are the discharges at the beginning, and at the end of the event and during peak flow, respectively. Temporal features are given as T: times, where T_{start} , T_{end} , T_{peak} are the start, end or peak time of the runoff event. T_{duration} , T_{BF} , T_{interval} and T_{response} denote the duration of the runoff event, the duration of baseflow preceding the event, the interval between events and the time between the start and the peak of the runoff event, respectively. The antecedent precipitation index (API) is calculated as the 2-day or 5-day sum of precipitation preceding the storm event.....	290
Table 84:	Discharge and natural tracer concentrations of the investigated Hermon runoff event (1/13-1/22/2004). N.d.: not determined.....	295
Table 85:	Discharge and natural tracer concentrations of the investigated Orevim runoff event (1/13-1/18/2004). N.d.: not determined.....	298
Table 86:	Discharge and natural tracer concentrations of the investigated Senir runoff event (2/14-2/18/2003). N.d.: not determined.....	301
Table 87:	Discharge and natural tracer concentrations of the investigated Sion runoff event (1/14-1/16/2004). (At times, Sion discharge was just a trickle and was recorded as "zero" by the gauges of the Hydrological Service.) N.d.: not determined.....	303

Acknowledgements

I am extremely grateful for the guidance and support of the following people in preparation of this dissertation:

Prof. Dr. Klaus-Peter Seiler, Professor at the Ludwig-Maximilians-University, Munich and former head of the Institute of Hydrology at the GSF – National Research Center, provided support and guidance in understanding the concepts presented in this thesis. I am especially grateful for his confidence allowing me to work independently, for his fruitful suggestions and constructive criticism during the final processing of this work.

Prof. Dr. Iggy M. Litaor, Tel-Hai College, Israel, provided support at the best possible rate, allowing me to realize the extensive sampling campaigns and helped with constructive criticism during the writing of this thesis.

Prof. Dr. Christian Wolkersdorfer read this thesis critically and thoroughly and provided constructive criticism. For that I am very grateful.

Willibald Stichler, Peter Trimborn, Harald Lowag, Nadia Kadlec, Petra Seibel, Environmental Isotope Group at the Institute of Groundwater Ecology (former Institute of Hydrology), GSF-National Research Center, Neuherberg, conducted countless numbers of isotope analyses thus providing a big part of the data used in this study. I am especially grateful to Willibald Stichler who shared his extensive expertise to the subject matter.

Rony Silberberg, Jacob Braslav and Jacob Arzi, Migal Galilee Technology Center, Kiryat Shmona, Israel, practically enabled my stay in Israel, provided extensive support concerning any administrative problem and always had an encouraging smile.

Benny Rophe, Rita Chudinov, Tzadik Amran, Hydrological Service of Israel (HSI), granted access to many of the sampling sites. They also reliably supported me with much needed hydrological data.

Benny Teltsch, Mekorot, Israel, provided access to sampling sites and data.

The staff of the Meteorological Service of Israel (IMS), provided me with data.

Members of the GLOWA Jordan River project, particularly Alon Rimmer, Yigal Salingar, Harald Kunstmann and Pinhas Alpert offered fruitful suggestions and data.

The staff of the Society of Protection of Nature, Israel (SPNI) provided access to sampling sites and supported me with precipitation sampling. I am especially grateful to Eytan and Jacques (Tel Dan), Rina (Banias), Hagai (Senir) and Assad (Nimrod).

The staff of the Mount Hermon Skiing site, provided access and equipment for snow sampling.

Members of Kibutz Mayan Barukh, helped with rain sampling.

Dr. Igal Bar-Ilan, Edna Hadar, Gershon Melman, Migal Galilee Technology Center, Kiryat Shmona, Israel, provided extensive technical support enabling me to conduct the major part of my hydrochemical analyses on spot.

Dr. Moshe Meron and Dr. Joseph Tsipris, Migal Galilee Technology Center, Kiryat Shmona, Israel, provided meteorological data and useful suggestions concerning precipitation sampling.

Michael Stoeckl, Dietmar Jurat, Hilge Halder, Institute of Groundwater Ecology (former Institute of Hydrology), GSF-National Research Center, Neuherberg, introduced me to IC and DOC/TOC analyses providing technical support.

Dipl.-Ing. Volker Mueller, Institute of Groundwater Ecology (former Institute of Hydrology), GSF – National Research Center, Neuherberg, simply made everything that seemed impossible possible.

The staff of the Hazbani Kajak Site/Mayan Barukh provided access and support during sampling.

The staff of Migal Galilee Technology Center, Israel, especially Bella, Rachamim, Shosh, Yulia and Alona created a friendly and comfortable working atmosphere.

The staff of the former Institute of Hydrology, GSF - National Research Center, Neuherberg, in particular Iris Vomberg, Dr. Petr Marusak, Dr. Reinhard Zapata-Blosa created a friendly and comfortable working atmosphere.

The staff of the Institute of Groundwater Ecology, GSF - National Research Center, was continuously supportive and created a great working atmosphere. I am particularly grateful to Christine Stumpp who critically reviewed part of this thesis and helped with constructive criticism. My thanks and appreciation goes to Dr. Tillmann Lueders for patience and ongoing support. Thanks to Eva Fritz for always seeing the bright side of life. Thanks to Bettina Anneser for never giving up on asking me out.

Shuka Ravek enabled me to sample the Sion spring, showed me a beautiful part of the Hermon Mountain and taught me a lot on its geology and botany on a single afternoon.

The members of Kibutz Kfar Blum helped to make me feel at home.

Oren Reichman, Gonen Eshel, Maria Belzer, Idan Barnea, Yotam Gonen and their families created a home to me, taught me everything good I could learn about Israel and provided neverending support (and I simply miss them). I am extremely grateful to Dror Wald for his support during sampling, for humus at Kfar Yasif and time “al nahar”. Thanks to Igor Yagmour for patience and affection. Thanks to Alex, Ayelet and Idan.

Thomas Ruelke, Stefan Rieger, Cornelia Haase, Antje Mueller, Susanne Roeber, Stefan Mueller & Kathi Schrader, Ute Weidmann and their families offered ongoing support, patience and confidence in my ability “to finish”. Thank you.

My parents and my brother.

Christian.

Zusammenfassung

Das Ziel der vorliegenden Arbeit bestand zum einen darin, die Frischwasserressourcen im Einzugsgebiet des Oberen Jordan (UJCR = Upper Jordan River Catchment) im Hinblick auf ihre Anfälligkeit gegenüber Klimaveränderungen zu bewerten und das Prozessverständnis der Abfluss- und Grundwasserneubildung im Einzugsgebiet zu verbessern. Zum anderen galt es, die Erkenntnisse aus den durchgeführten Untersuchungen in vorhandene konzeptionelle Modelle zur Grundwasserneubildung und Abflussbildung zu integrieren und diese weiterzuentwickeln.

Trink- bzw. Frischwasser ist von begrenzter Verfügbarkeit in semi-ariden und ariden Gebieten, eine Lage, die sich mit den erwarteten Klimaveränderungen noch zu verschärfen droht. Das grenzüberschreitende Einzugsgebiet des Oberen Jordan umfasst Gebiete in Israel, Libanon und Syrien und liefert etwa 27 % von Israels aktuellem Wasserbedarf. Das UJRC ist Israels nördlichstes Wassereinzugsgebiet und umfasst eine Fläche von circa 1700 km². Die Hauptneubildungsgebiete des Grundwassers liegen im Karst des Hermongebirges (2814 m NN) und des Antilibanon Gebirges und in den basaltischen Golanhöhen (1000 m NN). Das Einzugsgebiet wird vom Jordanfluss dräniert, der das Hula-Tal durchquert und den See Genezareth mit Frischwasser speist.

Die schwierigen politischen Gegebenheiten im Bereich des UJCR haben zu einem Mangel an grenzüberschreitenden Untersuchungen der hydrogeologischen Eigenschaften der Quellen des Oberen Jordan geführt. Das Einzugsgebiet ist nur in Teilen untersucht worden und veröffentlichte Daten sind rar. Für eine nachhaltige Bewirtschaftung der Wasserressourcen im Einzugsgebiet werden aber dringend Informationen über die Art und den Anteil von Abflusskomponenten, Wasservolumina, mittlere Verweilzeiten, die Ausdehnung der unterirdischen Einzugsgebiete und Grundwasserneubildungsraten benötigt.

Aus diesem Grund wurden in den Jahren 2002 bis 2004 im Rahmen der vorliegenden Arbeit Grundwasserneubildungs- und Abflussbildungsprozesse mit Hilfe einer Kombination verschiedener Methoden im Einzugsgebiet des Oberen Jordan untersucht. Der räumliche Schwerpunkt lag dabei auf den gebirgigen Hermon- und Golangebieten, wo ein wesentlicher

Teil der Grundwasserneubildung erfolgt. Die Methodenkombination umfasste Hydrographenuntersuchungen, Zeitreihenanalysen und die Untersuchungen von Isotopen und geochemischen Tracern. Zu den Freilanduntersuchungen gehörte das durchgehende Monitoring von fünf Hauptzuflüssen im Einzugsgebiet. Regensammler und 14 Quellen wurden regelmäßig beprobt, während die Untersuchung von Schnee, Schneeschmelze und Überlandabfluss stichprobenartig erfolgte. Die gewonnenen Proben wurden auf bis zu 14 Wasserqualitätsparameter hin untersucht. Diese umfassten die Hauptionen, DOC, TSS, gelöstes Silikat, Kohlenstoff-14 und Kohlenstoff-13, Tritium und die stabilen Wasserisotope. Die Ergebnisse dieser Untersuchungen werden in der vorliegenden Arbeit in drei thematisch unterteilten Kapiteln dargestellt und sind untergliedert in (1) die hydrochemische und isotopische Charakterisierung des Niederschlags, (2) die hydrochemische und isotopische Beschreibung des Grundwassers und (3) die Abflussbildung in den Hauptzuflüssen des Oberen Jordan.

Die Umwandlung von **Niederschlag** in Grundwasserneubildung und Abfluss wird im wesentlichen von der Eingangsgröße – dem Niederschlag – selbst kontrolliert. Im Rahmen dieser Studie wurde, das erste Mal für dieses Einzugsgebiet, die isotopische und chemische Zusammensetzung des Niederschlages und seine zeitliche und räumliche Variabilität umfassend untersucht. Die chemische Zusammensetzung des Niederschlages variierte in Abhängigkeit der Herkunft der wetterbestimmenden Luftmassen und in Abhängigkeit von der Mineralogie der Gesteine, mit denen diese Luftmassen auf ihrem Weg ins Einzugsgebiet in Berührung kamen. Der gesammelte Niederschlag zeigte im allgemeinen eine geringe Mineralisierung ($\sim 20 \mu\text{S}/\text{cm}$).

Auf der Basis der Analyse der stabilen Wasserisotope im Niederschlag wurde für das Einzugsgebiet des Oberen Jordan eine Lokale Meteorische Wasserlinie (LMWL) konstruiert ($\delta^2\text{H} = 7,23 \delta^{18}\text{O} + 16,21$). Der Höheneffekt verursacht im Hermongebiet eine Abreicherung von ca. $-0,26 \text{‰}$ und $-1,10 \text{‰}$ pro 100 m für $\delta^{18}\text{O}$ bzw. $\delta^2\text{H}$ und wurde anschließend verwendet, um die mittleren Einzugsgebietshöhen für die bedeutendsten Quellen im Hermon zu bestimmen. Zusätzlich konnte gezeigt werden, dass die Menge und isotopische Zusammensetzung des Niederschlages im wesentlichen von der Jahreszeit und dem

vorherrschenden synoptischen System beeinflusst werden. So waren Kaltfronten wie das *Zyperntief* in der Regel mit starken Niederschlägen und leichten Isotopenwerten verbunden, während das *Rote-Meer-Tief* durch geringe Regenmengen und schwere Isotopenwerte gekennzeichnet war. Die gefundenen Zusammenhänge zwischen der Zusammensetzung der stabilen Wasserisotope und der Temperatur, der Niederschlagsmenge und der Windrichtung sind durch die oben beschriebenen Zusammenhänge bedingt. Die isotopische Zusammensetzung eines untersuchten Schneeprofils zeigte eine signifikante Anreicherung von bis zu 4,3 ‰ für $\delta^{18}\text{O}$ über die Zeit.

Das **Grundwasser** der ergiebigsten Quellen im Hermongebirge und den Golanhöhen, das in das Einzugsgebiet des Oberen Jordan abfließt, wurde auf seine Umwelttracersignaturen hin untersucht, um detaillierte Informationen über Grundwasserneubildungsgebiete und -raten, Wasseraufenthaltszeiten, Wasseralter und Aquiferabmessungen zu erhalten. Ihre unterschiedliche chemische und isotopische Zusammensetzung erlaubte die klare Unterscheidung von Grundwässern aus dem Golan oder dem Hermon.

Die untersuchten Golanquellen („Side springs“) waren durch einen Ca-Na-HCO₃- oder einen Na-Ca-HCO₃-Wassertyp gekennzeichnet und besaßen erhöhte Silikatkonzentrationen. Die Quellwässer gruppieren sich um eine Mischungsgerade ($\delta^2\text{H} = 6,41 \delta^{18}\text{O} + 10,73$), die durch eine geringere Steigung als die dargestellte LMWL gekennzeichnet ist, was darauf hinweist, dass diese Wässer Evaporation in der ungesättigten Zone unterliegen. Die Golanquellen können zum einen vom regionalen Basaltaquifer gespeist sein (mit Wasseraufenthaltszeiten > 50 Jahre), zum anderen kann ihr Wasser aus einer Mischung aus regionalem Grundwasser sowie Wässern aus lokalen gespannten Grundwasserleitern (mit Wasseraufenthaltszeiten < 50 Jahre) zusammengesetzt sein. Die Wasseralter wurden mit Hilfe von Tritium und radioaktivem Kohlenstoff bestimmt.

Im allgemeinen scheint die chemische und isotopische Zusammensetzung der Golanquellen einen Nord-Süd-Gradienten aufzuweisen und bildet damit die klimatischen und geologischen Gegebenheiten in den Golanhöhen ab. Der nördliche Golan ist durch einen vergleichsweise mächtigen Grundwasserleiter, eine ausgeprägte ungesättigte Zone und hohe Niederschlagsmengen gekennzeichnet. Die dort entspringenden Quellen, wie z.B. die Hamroniya-, Gonen-

und Notera-Quelle, zeigen einen hohen Anteil an Wasser aus der ungesättigten Zone an, das in Grundwasser mit hohen Tritiumwerten, geringen Chlorid- und hohen Silikatkonzentrationen resultiert. Im Süden, wo Verdunstungseinflüsse zunehmen und Neubildungsraten abnehmen, sind die Bet HaMekhes- und Jalabina-Quelle durch geringe Tritiumkonzentrationen und hohe Chloridgehalte charakterisiert. Grundwasserneubildungsraten für die untersuchten Golanquellen, die aufgrund von Chloridmassenbilanzen ermittelt wurden, liegen zwischen 12 und 16 % des Jahresniederschlages; die Größe ihrer unterirdischen Einzugsgebiete variiert zwischen 0,6 und 3 km².

Die untersuchten Quellen im Hermon sind (a) von zwei Einzugsgebieten - die durch die Sion-Rachaya-Störung getrennt werden – gespeist und stammen (b) aus lokalen oder regionalen Grundwassersystemen, wie durch ihre chemische und isotopische Zusammensetzung deutlich wurde. Außerdem (c) erhalten sie unterschiedliche Anteile ihres Wassers aus dem Drainageraum (Kluft) bzw. dem Speicherraum (Gesteinsmatrix). Alle Quellen sind durch geringe Leitfähigkeiten und einen Ca-Mg-HCO₃-Wassertyp gekennzeichnet. Allerdings weisen die Quellen aus dem östlichen Einzugsgebiet (Banias und Kezanim) gewisse Mengen an gelöstem Dolomit, Gips und Anhydrit auf. Diese Lösungsvorgänge konnten für das westliche Einzugsgebiet in dem die Dan-, Barid- und Leshem-Quellen liegen, nicht beobachtet werden. Die Hermonquellen zeigen eine deutliche saisonale Verteilung der Grundwasserneubildung, wobei die höchsten Raten im Frühjahr erreicht werden. Das wurde insbesondere durch abgereicherte Werte im $\delta^{18}\text{O}$ und $\delta^2\text{H}$, durch die Abnahme der Grundwassertemperatur und Verdünnungseffekte in den Ionenkonzentrationen des Quellausflusses durch Schneeschmelzwässer deutlich. Die Bedeutung der Schneeschmelze für die Grundwasserneubildung in den Hermonquellen wird vor allen Dingen durch den in den Quellwässern nachgewiesenen erhöhten Deuteriumexzess im Frühjahr erkennbar. Diese Beobachtung war auch die Grundlage für die Bestimmung der mittleren Einzugsgebietshöhen der Quellen. Methodisch wurde dafür die mittlere $\delta^{18}\text{O}$ -Zusammensetzung um ihre Anreicherung durch Fraktionierungsprozesse während der Schneeschmelze korrigiert. Anschließend konnten mit Hilfe des ermittelten Höheneffekts in der Isotopenzusammensetzung des Niederschlages die mittleren Einzugsgebietshöhen für die

Banias- und Kezanim-Quelle (~1260 m NN), für die Dan-, Barid- und Leshem-Quelle (~ 1560 m NN) und für die Sion-Quelle (~ 1320 m NN) bestimmt werden.

Die Kezanim-Quelle und der Basisabfluss in der Banias-Quelle verweisen in ihren Eigenschaften auf den Einfluss eines thermischen Regimes und die höchste Mineralisierung unter den Hermonquellen. Insbesondere zeichnen sie sich durch hohe Konzentrationen an Sulfat, Silikat und Chlorid aus. Zusätzlich zeigen diese Quellen angereicherte $\delta^{18}\text{O}$ und $\delta^2\text{H}$ - Werte und insbesondere die Kezanim-Quelle unterliegt geringen saisonalen Schwankungen in ihrer isotopischen und chemischen Zusammensetzung. Daraus ließ sich schlussfolgern, dass die Kezanim-Quelle und der Basisabfluss in der Banias-Quelle durch Grundwasser aus einem regionalen, diffusiven System gespeist werden, und dass sie außerdem im Kontakt mit der triassischen Muheila-Formation stehen. Diese Annahme wurde zudem durch die mittlere Aufenthaltszeit (> 1000 Jahre) für die Wässer der Kezanim-Quelle bestätigt, welches auf der Grundlage von radioaktivem Kohlenstoff berechnete wurde. Im Unterschied dazu, stammen die Grundwasser der Dan-, Barid- und Leshem-Quelle aus einem flachen lokalen System, das von aktuellem Wasser dominiert wird und in dem der Wassertransport zu wechselnden Anteilen sowohl durch Klüfte als auch durch die Gesteinsmatrix erfolgt.

Die Bedeutung von schnellen und langsamen Abflusskomponenten für verschiedene Grundwässer im Hermongebiet wurde am Beispiel der Banias- und Dan-Quelle im Detail untersucht. Die Banias-Quelle reagierte von allen Hermon-Quellen am schnellsten und intensivsten auf Niederschläge. Ihr Quellabfluss wird von folgenden drei Komponenten kontrolliert: dem Direktabfluss, dem Abfluss aus der ungesättigten Zone (Epikarst) und dem Abfluss aus der gesättigten Zone. Die verschiedenen Abflüsse konnten mit Hilfe eines Dreikomponenten-Mischungsmodels auf der Basis von $\delta^{18}\text{O}$ - und Sulfatmessungen quantifiziert werden. Danach waren die schnellen und mittelschnellen Abflusskomponenten im Februar 2003 zu 88 % am Gesamtabfluss beteiligt und im Juni 2003 betrug ihr Anteil immer noch 70 %. Das ist ein deutlicher Hinweis auf das klimakontrollierte Abflussregime dieser Quelle. Im Gegensatz dazu reagierte die Dan-Quelle ausgewogen und nur mit geringen Schwankungen der gemessenen physikalischen, chemischen und isotopischen Parameter auf Niederschläge. Trotzdem konnte auf Grundlage von Zwei-Komponenten-Massenbilanzen auf

der Basis von $\delta^{18}\text{O}$, Chlorid oder Sulfat nachgewiesen werden, dass ca. 40 % des Gesamtabflusses in der Dan-Quelle aus der aktuellen Grundwasserneubildung stammen, dabei sind die höchsten Anteil von Ereigniswasser im Früh- und Spätsommer gemessen worden. Zusammenfassend konnte geschlussfolgert werden, dass die Banias-Quelle über einen limitierten Speicherraum und einen ausgeprägten Drainageraum verfügt und deshalb unmittelbar auf Niederschläge reagiert während die Dan-Quelle ein enormes, gut durchmisches Reservoir umfasst, in dem neuankommendes Wasser stark verdünnt wird. Grundwasserneubildungsraten, die auf der Grundlage von Chloridmassenbilanzen ermittelt wurden, liegen zwischen 12 und 20 % des mittleren Jahresniederschlages. Im Vergleich dazu wurden Grundwasserneubildungsraten, welche anhand mittlerer Verweilzeiten festzustellen waren, mit Werten von 19 bis 30 % des mittleren Jahresniederschlages bestimmt. Auf der Grundlage der vorliegenden Ergebnisse konnte erstmalig im Rahmen dieser Arbeit eine Abschätzung der unterirdischen Einzugsgebiete für die Danquelle und für die Baniasquelle erfolgen. Diese Gebiete überschreiten mit 1.324 km² (Dan) und 523 km² (Banias) bei weitem die Abmessungen des Oberflächeneinzugsgebietes und reichen weit über Israels politische Grenzen hinaus. Die Qualität dieser Abschätzungen hängt erheblich von der Treffsicherheit der Bestimmung der mittleren jährlichen Gebietsniederschlagsmengen im Hermongebirge ab, deren weitere Verbesserung Bestandteil zukünftiger Untersuchungen sein sollte.

In einem dritten Schritt wurden die **Abflussbildungsprozesse** für die Hauptzuflüsse des Oberen Jordan, das heißt für den Hermon-, Senir- und den Dan-Bach untersucht. Methodisch erfolgte das zum einem auf der Basis von Hydrographenanalysen an langen Datenreihen und zum anderen auf der Tracer-basierten Untersuchung von Abflussereignissen. Zusätzlich zu den drei Jordanzauflüssen wurde vergleichsweise ein Bach aus den basaltischen Golanhöhen beprobt. Für beide geologischen Gegebenheiten, Karst und Basalt, konnten drei Abflusskomponenten identifiziert werden. Während der Dan-Bach ausschließlich durch Basisabfluss gespeist wird, machen die Überland- und die Zwischenabflusskomponente (ermittelt auf der Grundlage einer 30-jährigen Datenreihe) bis zu 46 % beziehungsweise 58 % des Gesamtabflusses im Hermon- und Senir-Bach aus. Im Basalt (Orevim-Bach) trugen die schnelle und mittelschnelle Abflusskomponente sogar bis zu 75 % zum Gesamtabfluss bei.

Während die Zwischenabflusskomponente im Karstgebiet auf das Schneereservoir des Hermongebirges zurückgeführt wird, das mit der Schneeschmelze zum Abflussgeschehen beiträgt, ist der Zwischenabfluss im Basaltgebiet eher auf die Struktur des Untergrundes und dabei insbesondere auf die Existenz von hydraulischen Grenzflächen zurückzuführen.

Die große Bedeutung der schnellen Abflusskomponenten konnte durch die Untersuchung von Abflussereignissen bestätigt werden. Im Ergebnis dieser Analysen betrug der Anteil von Ereigniswasser am Gesamtabfluss zum Zeitpunkt der Abflussspitze für den Hermon-, den Senir- und den Orevim-Bach circa 52 %, 69 % beziehungsweise 77 %. Die Beteiligung einer flachen unterirdischen Abflusskomponente konnte zudem aufgrund von sogenannten *End-member*-Mischungsrechnungen nachgewiesen werden.

Die mittleren Verweilzeiten des Basisabflusses im Hermon-, Senir- und Dan-Bach rangierten zwischen einigen Monaten bis zu 4 Jahren und wurden mit Hilfe von Rückgangsanalysen am Hydrographen bestimmt. Das Vorherrschen von jungen Wässern im Einzugsgebiet konnte zusätzlich durch Tritiummessungen bestätigt werden, mit denen mittlere Verweilzeiten von 24 Jahren für den Hermon-, 28 Jahren für den Dan- und 33 Jahren für den Senir-Bach bestimmt wurden. Auf Grundlage der berechneten mittleren Verweilzeiten ist die Mächtigkeit des aktiven Grundwasserumsatzraumes im Einzugsgebiet des Dan zu zwischen 11 und 103 m bestimmt worden, wobei die mittlere Mächtigkeit in etwa 32 m beträgt. Im Einzugsgebiet des Hermon-Baches besitzt diese Zone nur eine mittlere Mächtigkeit von ca. 13 m.

Im Ergebnis der vorgestellten Untersuchungen kann geschlussfolgert werden, dass die für das Untersuchungsgebiet zu erwartenden Klimaänderungen, die durch einen geringereren Gesamtniederschlag, eine Temperaturerhöhung und die Häufung extremer Regenereignisse gekennzeichnet sein werden, eine große Herausforderung für die Bewirtschaftung der Wasserressourcen im Einzugsgebiet des Oberen Jordan bedeuten.

Insgesamt dominiert junges Wasser die aktuell sichtbaren Fließsysteme im Karst und im Basalt. Eine Temperaturerhöhung könnte demnach zu einer Verringerung des Schnee/Regen-Verhältnisses und einem beschleunigtem Abschmelzen von Schnee führen. Das wird einerseits voraussichtlich sogar zu einer erhöhten Grundwasserneubildung im Karst des Hermongebirges mit seinen hohen Infiltrationskapazitäten führen. Andererseits wird sich

dadurch auch das Risiko des Auftretens von Hochwasserereignissen erhöhen. Wenn in Zukunft häufiger extreme Regenereignisse, wie für das Gebiet vorhergesagt, auftreten werden, nimmt die Eintrittswahrscheinlichkeit von Hochwasserereignissen aus dem Hermongebirge und den Golanhöhen zu. Das wiederum könnte zusätzlich zu einer Verschlechterung der Wasserqualität im Oberen Jordan und dem See Genezareth führen, weil das Auftreten von Hochwässern mit dem vermehrten Austrag von Nährstoffen und suspendierten Stoffen verbunden ist.

In einem Szenario mit steigenden Temperaturen und geringerem Gesamtniederschlag wird die Reduzierung des Schneeniederschlages und damit der Schneeschmelze zu einer signifikanten Abnahme des Basisabflusses im Oberen Jordan führen und die Bewirtschaftung des See Genezareths nachhaltig beeinflussen.

Vor dem Hintergrund aktueller Klimaprognosen sollten die Ergebnisse dieser Arbeit als ein Beitrag zum besseren Verständnis der hydrogeologischen Prozesse im bezeichneten Wassereinzugsgebiet des Oberen Jordan verstanden werden und dazu beitragen, dass nachfolgende Forschungen bezüglich der betrachteten Wasserressourcen noch zielgerichteter auf die Bewältigung von möglichen Konsequenzen der prognostizierten Klimaänderungen ausgerichtet werden können.

1. Introduction

Freshwater is a limited resource on Earth. While the Earth's total water content is about 1.39 billion cubic kilometer, all freshwater accounts for only 2.5 % of the global water budget. Approximately 70 % of freshwater is stored in polar icecaps, glaciers, and permanent snow, while only 30 % represents mobile freshwater that is easily accessible for men and ecosystems (GLEICK, 1996).

Freshwater originates through the water cycle and is renewable both in the short and long run. Accordingly, mean residence times range from present to millions of years and are unevenly distributed along climate zones (horizontally) and within strata of rock and sediments (vertically).

On the global scale, mobile freshwater resources are subject to numerous pressures. Worldwide population growth and increasing living standards lead to a growing demand for good quality water. Increasing demand for water in combination with insufficient protection and management strategies of freshwater resources (accompanied by an often poor wastewater management) results in their overexploitation and contamination. Additional stress on water resources is expected from the growing threat of men induced climate and land use changes (HOUGHTON et al., 2001). While the former processes are certain and observed on a global scale, a big uncertainty is how climate will change and what will be the influence of global and regional climate changes on water resources.

It is difficult to assess the meteorological boundary conditions and intrinsic parameters that influence short term freshwater recharge and discharge. Thus, flexibility is the best policy for water resource management to be able to control floods and droughts, surpluses and shortages (BOUWER, 2003). This required flexibility in water management is among others based on a thorough knowledge of recharge/discharge mechanisms and dynamics in a respective watershed.

The present study intends to outline mechanisms of discharge, discharge quantities and qualities under present boundary and intrinsic conditions in the Upper Jordan River Catchment (UJRC, Figure 1) and to develop a conceptual hydrogeologic model for the study

area. This will serve as a base for future mathematical models to develop water protection and management strategies under future boundary conditions.

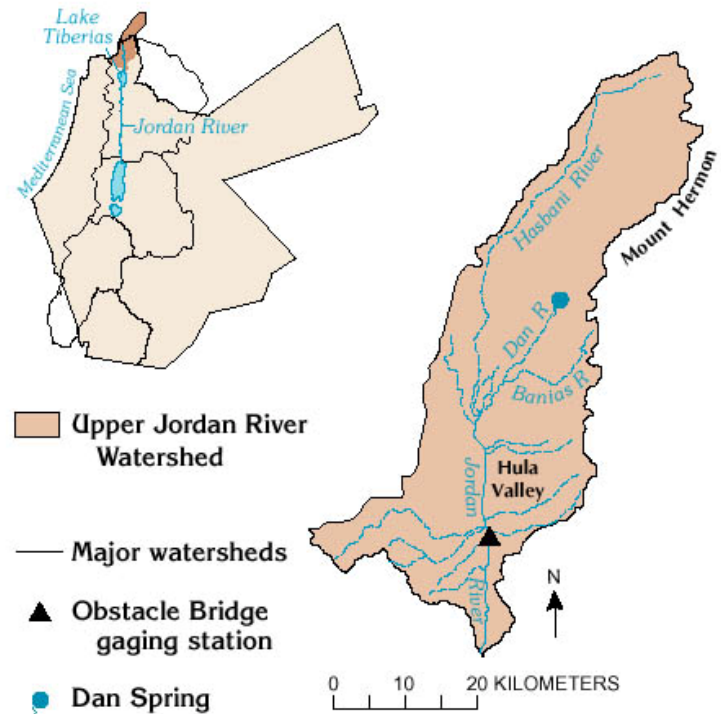


Figure 1: The Upper Jordan River Catchment (UJRC), Israel (from EXACT, U.S. Geological Survey, 1998).

1.1 BACKGROUND DATA AND TASKS IN THE UPPER JORDAN RIVER CATCHMENT

Groundwater is formed by the surplus of precipitation over direct runoff and evapotranspiration. While for humid climates, about 40 % of the precipitation ends up in groundwater; in semi-arid and arid Mediterranean type climates less than 25 % respectively 5 % contributes to groundwater recharge causing water to be a scarce resource in these regions. In fact, the Middle East and North Africa is considered one part of the world where water scarcity is severe and precarious (BERKOFF, 1994). Nine out of the 14 countries in this area dispose of less than 1000 m³ water per capita and year and thus – based on the classification developed by FALKENMARK et al. (1989) – suffer under water stress. Moreover, these countries are subject to rapid population growth and increasing urbanization resulting in additional pressures on the often already overused water resources.

In fact, important water resources of the Middle East region such as the Jordan, Euphrates, Tigris and Nile Rivers are shared by two or more countries, in other words belong to transboundary basins, thus adding a political dimension to the issue of water management (BEAUMONT, 2000; AMERY and WOLF, 2000; MEDZINI and WOLF, 2004). It also emphasizes a special need for a detailed understanding of hydrogeological processes in the considered watershed as an essential basis for any water resources assessment or political negotiations on water.

Table 1: **Annual water resources and water withdrawal in Israel and its neighboring countries. Numbers were retrieved from the FAO AQUASTAT database and are representative for the period 1998-2002. Quantities of withdrawal and resources in the Palestinian Authority area (PA) are cited from BOU-ZEID and EL-FADEL (2002) [*] and ALATOUT (2000) [**].**

Country	P mm/year	TRWR $10^9 \text{ m}^3/\text{year}$	TRWR $\text{m}^3/\text{capita*year}$	TW-WD $\text{m}^3/\text{capita*year}$	%WD-TRWR %
Israel	435	1.7	265	325	123
Lebanon	661	4.4	1226	384	31
Syria	252	26.3	1511	1148	76
Jordan	111	0.9	165	190	115
Egypt	51	58.3	827	969	117
PA	350*	0.2*	92*	165**	179

P = Precipitation, TRWR = Total Renewable Water Resources, TW-WD = Total Water Withdrawal, %WD-TRWR = Percent Withdrawal of Total Renewable Water Resources.

Quantitative numbers on water resources in the Eastern Mediterranean are difficult to access. Estimated amounts differ according to the source and period of consideration. Statistics on water resources and water withdrawal in Israel and its neighboring countries presented in Table 1 have thus to be assessed cautiously, especially since they represent a period of time coinciding with extreme droughts in the region. According to the numbers published by the Food and Agriculture Organization of the United Nations (FAO, 2005) Israel holds about 265 m^3 freshwater per capita and year and uses about 123 % of its renewable water resources; agricultural, industrial and domestic usage account for about 62 %, 7 % and 31 % of total water withdrawal, respectively (FAO, 2005).

Among the Eastern Mediterranean countries, the water demand of Israel, Jordan and the Palestinian Authority exceeds the renewable water resources by far ($< 500 \text{ m}^3/\text{capita/year}$),

hence, these areas were classified as regions under extreme water stress (FALKENMARK et al., 1989). According to the same classification Egypt faces high water stress (500 – 1000 m³/capita/year) while Lebanon, and Syria encounter moderate water stress (1000 – 1700 m³/capita/year).

Israel's main freshwater reservoirs are 1) Lake Kinneret¹, 2) the coastal aquifer and 3) the mountain (Yarkon-Taninim) aquifer, providing about 27, 22, and 17 % of the countries water demand. The focus of this thesis will be on the quantitative state of the actual water resources in the Upper Jordan River Catchment (UJRC) feeding Lake Kinneret.

Lake Kinneret is the lowest freshwater lake of the world, covering a surface area of about 167 km² and reaching an average depth of about 26 m. The average annual water inflow into Lake Kinneret is 800 10⁶m³ (GVIRTZMAN, 2002). The lake provides annually about 380 10⁶m³ to Israel's water demand via the National water carrier connecting the UJRC with the country's dry central and southern areas. On average, 280 10⁶m³ of water per year leave the lake through evaporation and about 80 10⁶m³ through overflow into the southern Jordan River.

Accordingly, the national awareness for the importance of this reservoir is high; in winter for example lake levels are reported on the front page of newspapers. During the period of investigation (2002-2004) the lake level rose due to above-average rainfalls from a low of 214.42 m below sea level by about 4.7 m.

¹ Also Lake Tiberias, Sea of Galilee, Sea of Gennesareth

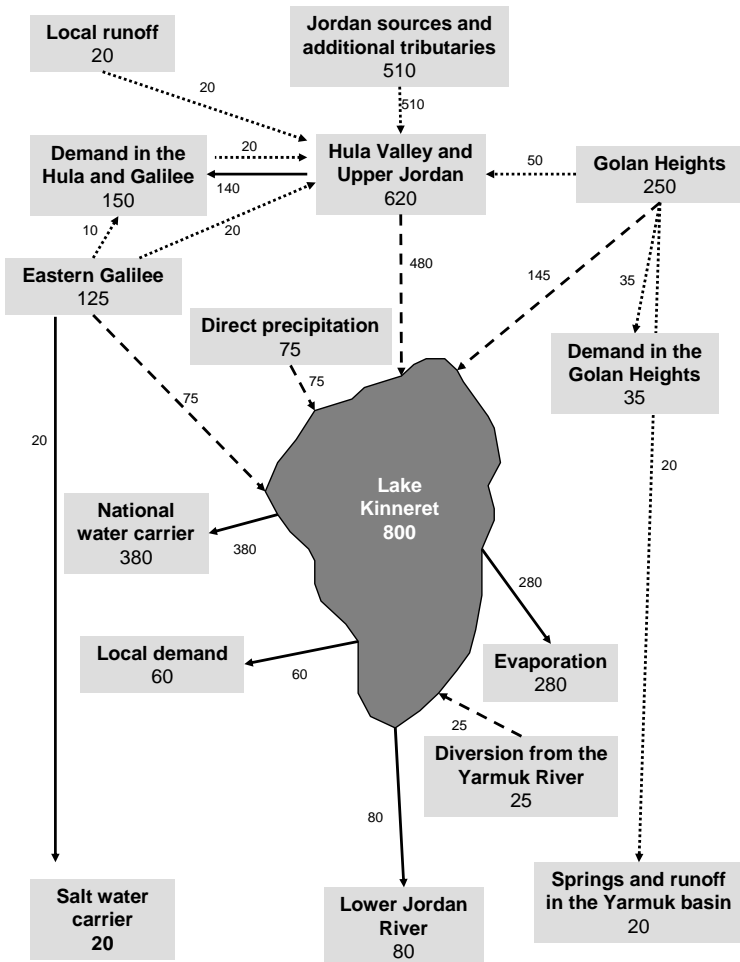


Figure 2: Mean annual water fluxes into Lake Kinneret and out of the lake. Dashed lines indicate inflows, solid black lines losses and numbers represent water volumes in million cubic meter ($=10^6\text{m}^3$). Adapted from Gvirtzman (2002).

About $480 \text{ } 10^6 \text{m}^3$ out of $800 \text{ } 10^6 \text{m}^3$ of the inflow into Lake Kinneret originate from the **Upper Jordan River** north of Lake Kinneret (Figure 2). The Upper Jordan River receives its major contributions from runoff that is generated in the mountainous Hermon, Antilibanon and Golan and the southern Beka'a Valley. Referring to the scheme given in Figure 3, the Upper Jordan River is fed by three types of runoff:

- overland runoff and
- interflow, both with short mean residence times, and
- baseflow with medium to high mean residence times.

These discharge components are either produced by rain or snowmelt. Any dominance of one of the runoff components depends on topographical and geological features of the catchment as well as on the type, amount, and distribution of infiltration.

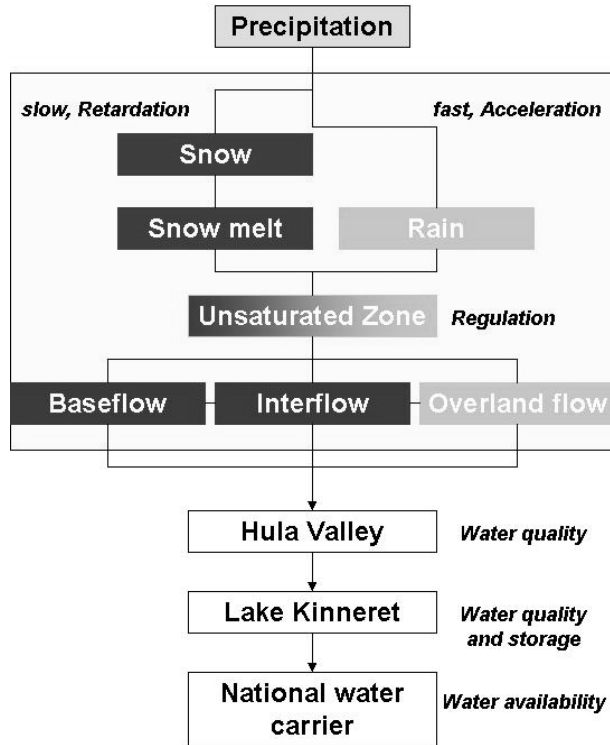


Figure 3: Conceptual discharge model of the Upper Jordan River catchment.

Rain and snow are the dominating types of precipitation in the Upper Jordan River region. Dependent on the hydrological properties of the interface atmosphere-litosphere-biosphere, precipitation is either intercepted by plants, stored at the land surface as snow or produces runoff. Runoff generates overland flow or infiltrates into the unsaturated zone. This unsaturated zone has a regulating function on discharge generation: according to local, hydrogeological characteristics it generates interflow or baseflow from infiltrating precipitation. Given a sufficient replenishment of the unsaturated zone or the existence of preferential flow paths, rain is rather rapidly transformed into discharge. In contrast, the snow cover residing on Mount Hermon and the southern Lebanon mountains during winter acts as an external reservoir and causes significant runoff retardation. Accordingly, snowmelt

contributes to the discharge of the Upper Jordan River tributaries until late spring and early summer, months after the rainy season ended.

Beside human impacts, the physico-chemical conditions of through-flow reservoirs in the Upper Jordan River Catchment and the specific contribution of each discharge component strongly influence the water quality in the Hula Valley and consequently, that of Lake Kinneret. For example, runoff of the Jordan River is usually accompanied by high loads of nutrients and suspended matter from the surrounding mountains and the Hula wetland, raising the potential for eutrophication in Lake Kinneret. Thus, the amount of water flowing into Lake Kinneret during a certain period of time and subsequently the water availability for the national water carrier depends not only on the precipitation input function but also on the recharge and discharge mechanisms in the Upper Jordan River Catchment and the interaction of discharge components with the geologic boundary conditions and the land use.

This actual situation will change with global climate changes. The determination and assessment of climate changes is a challenging task and has to be done with caution. The output of such studies varies not only according to the methods applied but also according to the length of records available for the considered parameters. For Israel, BEN-GAI et al. (1999) determined a significant decreasing trend of temperatures during the cold season, and an increasing trend during the warm season. They also state that the frequency of occurrence of extreme temperature events, with low winter and high summer temperatures, has increased. KUTIEL (2000) analyzed the yearly distributions of rains in Israel during the period 1976-2000 and found that the duration of the winter season shortened over this period, particularly in the last decade. An overall trend of decreasing rainfall and increasing frequencies of high-intensity rains was shown by ALPERT et al. (2002).

Predictions on future climate changes in Israel are summarized by PE'ER and SAFRIEL (2000). Accordingly, possible trends from the beginning of the industrial age until 2100 include:

- a mean temperature increase of 1.6 to 1.8 °C,
- a reduction in precipitation by 8 to 4 % and,
- an increase in evapotranspiration by 10 %.

Additionally, rain intensities will increase while the rainy season will shorten and the arrival of winter rains will delay. Seasonal temperature variability will increase as well as the frequency and severity of extreme climate events. In general, a greater spatial and temporal climate uncertainty is expected.

Considering these predictions and referring to the conceptual discharge model (Figure 3), different scenarios should be taken into account to develop appropriate future water management strategies for an already water scarce region. An increase in temperature will almost certainly lead to a decreasing snow/rain-ratio, an accelerated melting of snow and subsequently, an increased potential of floods. This will enhance erosion in fine to medium grained sediments; increase the overland runoff/interflow ratio and enhance unproductive evaporation losses from artificial reservoirs (SEILER and GAT, 2007).

On the contrary, in karstic regions with bare rocks and quasi unlimited infiltration capacities a reduction of rain may even increase groundwater recharge when antecedent moisture conditions and groundwater levels do not allow generating direct runoff (overland plus interflow). However, since the general reduction in precipitation is predicted to coincide with increasing rain intensities, the reduction of groundwater recharge and an increasing flood potential might be a more likely scenario. Nevertheless, the impact of climate change – on groundwater resources in particular – is difficult to assess (SEILER and GAT, 2007).

Known mean residence times in the study area range from months to tens of thousands of years. Consequently, especially old, transient groundwater is independent from recent recharge or at least delays the response on climate change. Therefore, the age of groundwater is important in terms of water management. Only groundwater that is part of the recent hydrological cycle can be used for sustainable exploitation, the use of groundwater that is not actively recharged leads to groundwater overexploitation; in other words, old groundwater is a limited resource.

Consequently, two tasks derived: Which parameters must be determined to assess the sensitivity of the Upper Jordan River catchment against climate change? Which suitable watershed management strategies should be developed as a consequence?

1.2 SPECIAL RESEARCH GOALS AND APPROACHES

In 2000, the German Federal Ministry of Education and Research (BMBF) launched the GLOWA² program as an interdisciplinary and integrative research project that aims to develop strategies for the sustainable management of water resources on a regional scale. Five large cluster projects (Danube, Elbe, IMPETUS, Jordan River, and Volta) have been selected to investigate issues like

- climate and precipitation variability
- interactions between the hydrological cycle, the biosphere and landuse,
- water availability and conflicting water utilization.

The subproject of GLOWA Jordan River is a case study of Eastern Mediterranean environments and is directed to evaluate the actual vulnerability of water resources and ecosystems in the Jordan River watershed. For these purposes, hydrogeology contributes with a combined method approach comprising hydrograph time-series analysis, and isotopic (¹⁸O, ²H, ³H, ¹⁴C) and geochemical tracer analysis of discharge. The aim in this study was to achieve:

- the separation of snowmelt runoff, direct runoff and groundwater runoff
- the estimation of mean residence times of the three discharge components
- the assessment of water volumes and
- the determination of groundwater recharge rates.

These data are considered to define a clear conceptual model on discharge mechanisms, forming the base of a mathematical model on future discharge scenarios.

2. Review of existing knowledge, concepts and techniques

The first part of the review summarizes concepts on groundwater flow systems and presents techniques used for the estimation of groundwater quantities and ages (respectively mean residence times). The focus is thereby on karst aquifers since this type of flow system represents the major freshwater source in the study area. The tools presented include lumped parameter models and radioactive isotope dating.

Subsequently, different techniques to study discharge and recharge mechanism in a mesoscale catchment were evaluated and summarized. The review includes a synopsis of the current knowledge on runoff generation processes with special emphasis on their occurrence and characteristics in semi-arid Mediterranean catchments. Furthermore, tools to study runoff generation and to assess the different discharge components are introduced. These tools comprise classical hydrograph evaluations such as baseflow and recession analysis as well as tracer-based hydrograph separation techniques such as the mass-balance concept and end-member mixing analysis (EMMA). Additionally, difficulties and uncertainties immanent in these approaches are discussed.

2.1 CONCEPTS ON GROUNDWATER FLOW SYSTEMS

The study area is characterized by two types of groundwater bearing rocks: carbonates and basalts. The Hula valley itself which is characterized by unconsolidated sediments was not in the scope of this study. The karst and basalt aquifers are fissured consolidated rocks but differ significantly from one another considering mineralogy, porosities, hydraulic conductivities and groundwater quality.

2.1.1 Karst

Karst environments are heterogeneous, multiple-porosity systems. Karst develops in fractured soluble rocks such as limestone, dolostone and gypsum, which contain a variety of primary fractures like bedding planes and master fissures that are permeable to water.

Groundwater flow in karst areas is dominated by three types of porosities: intergranular matrix porosity, fracture/fissure porosity and conduit porosity (WHITE, 1988). While the majority of transport occurs in conduits (if existent), the majority of storage takes place in the rock matrix and fissures. The two latter are generally considered a combined diffusive flow component. Assuming the existence of an underlying regional groundwater table, the exchange of water between the different porosities can be described as follows: During normal and low flow conditions water enters the conduits from matrix porosity and narrow fractures, while under flood conditions and sufficient hydraulic gradients, water enters from conduits to the matrix (MARTIN and SCREATON, 2001). Consequently, diffusive matrix flow (Q_D) controls spring discharge during baseflow conditions, while conduit flow (Q_C) dominates spring discharge after storm events.

Conduit flow is usually fast and shows large variations in temperature, flow rate and water chemistry depending on the frequency, intensity and duration of storm events. The same parameter varies little throughout the year in diffusive flow (LEE and KROTHE, 2003).

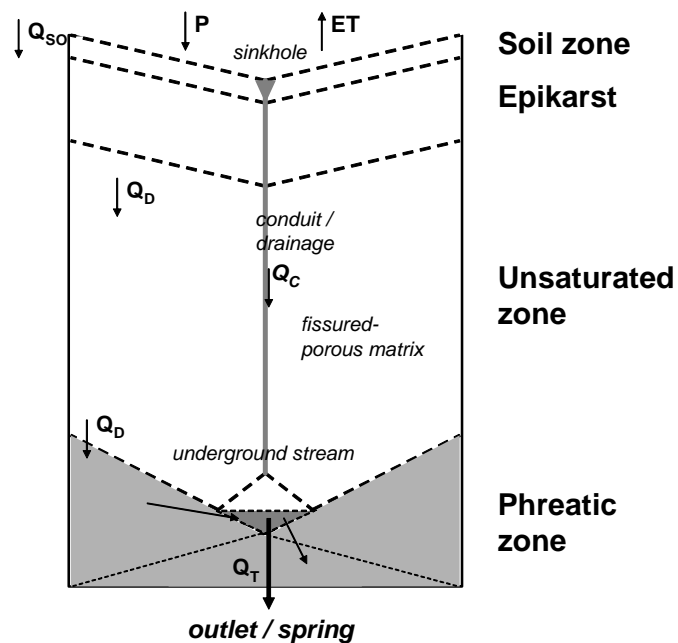


Figure 4: Conceptual model of water flow and storage in a karst aquifer. Modified according to MALOSZEWSKI et al. (2002), PERRIN et al. (2003) and EINSIEDL (2005). Flow is indicated by arrows. Q_D = diffusive flow, Q_C = conduit flow, Q_{SO} = saturation overland flow, Q_T = total flow, P = precipitation, ET = evapotranspiration.

Tracer-based hydrograph separation in karst areas ranges from the application of simple two-component mixing models separating event (quickflow) from pre-event water (baseflow) (SHUSTER and WHITE, 1971; HALLBERG, 1983; DREISS, 1989; LAKEY and KROTHE, 1996; MASSEI et al. 2003; PERRIN et al., 2003) to more sophisticated attempts such as the four-component mixing model of LEE and KROTHE (2001). In this paper, Lee and Krothe separate the karst spring hydrograph into rain, soil, epikarstic and phreatic water by analyzing sulfate, dissolved inorganic carbon (DIC), $\delta^2\text{H}$, $\delta^{18}\text{O}$ and $\delta^{13}\text{C}_{\text{DIC}}$ as tracers.

NATIV et al. (1999) used stable and radioactive isotopes, CFC's and He to separate groundwater flow components from different recharge altitudes in a karst environment.

MALOSZEWSKI et al. (2002) determined mean transit times and volumes in both, the matrix and the conduit flow system. In order to do so they applied a lumped parameter approach in combining $\delta^{18}\text{O}$ and tritium data in high and low discharges separately. A similar approach and artificial tracer tests were used by EINSIEDL (2005) to determine flow velocities, storage volumes and mean residence times in a karst aquifer. For detailed information on numerical modeling of the natural response of karst aquifers, refer to EISENLOHR et al. (1997a,b), SCANLON et al. (2003) and KOVACS et al. (2005) as this is not subject of this study.

2.1.2 Basalt

Groundwater flow in basalt lava tubes is most likely governed by two types of porosity, the rock matrix and fracture porosity. In contrast to karst formations, fractures are of planar-type, either with displacement (faults) or without displacement (fissures). In certain rock formations fractures may provide the primary pathway for flow and transport but as fractures drain, flow and transport through the rock matrix will become dominant (EVANS et al., 2001; OXTOBEE and NOVAKOWSKI, 2002). In such volcanic aquifers, basalt flows are often interbedded with fossil soils or sediments controlling the vertical flow. These sediment layers are generally highly compacted and of low permeability acting as hydraulic barriers to infiltrating waters (OKI et al., 1998; DAFNY et al., 2006). Depending on the extension of these soil/sediment lenses perched aquifers control the local or regional hydrogeology.

DAFNY et al. (2006) used geochemical and isotopic tracer to investigate groundwater flow in the basaltic Golan Heights aquifer, Israel, and to differentiate between waters from the perched and regional aquifer. Results of their study are further evaluated in chapter 3.5.3.

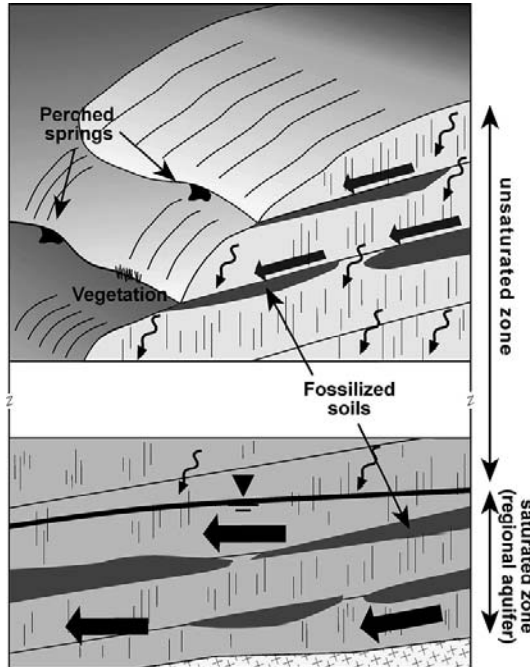


Figure 5: Conceptual model of groundwater flow in a basalt aquifer according to DAFNY et al. (2006). The regional, deep aquifer is overlain by several smaller perched aquifers in the unsaturated zone.

2.2 TECHNIQUES FOR RESIDENCE TIME ESTIMATION

The **mean residence time** (MRT) of water is the average time that water spends in the subsurface system before it reaches the watershed outlet or a designated point on its either vertical or horizontal flow path (MALOSZEWSKI and ZUBER, 1982). Knowledge about the mean residence time of water allows conclusions on the immediate or delayed system response to climate changes or land-use changes. Additionally, the MRT is a valuable measure to evaluate the fate of contaminants in the aquifer. Thus, the mean water residence time is an important parameter to assess the water quality in a hydrogeological system.

2.2.1 Lumped-parameter models and water isotopes

Generally, estimations of mean residence times are generated by tracer studies and the application of **lumped parameter models**. In such black-box models, spatial variations of parameters are not evaluated in detail and the system is described by adjustable (fitted) parameters. In other words, MRTs are directly derived from the transfer of the input to the output tracer concentrations by a fitting procedure. Accordingly, the detailed transport mechanisms within a system are simplified and are represented by the choice of a specific system response (transfer) function (SIMIC and DESTOUNI, 1999).

Commonly, the determination of MRTs is based on the key papers of MALOSZEWSKI and ZUBER (1982, 1996) who developed several transfer functions to describe the MRT in a flow system. A short summary of other available techniques is given by MCGUIRE et al. (2002) including the determination of groundwater mean residence times by *sine-wave analysis of stable isotope data* (MALOSZEWSKI et al., 1983; BURNS and McDONNELL, 1998; SOULSBY et al., 2000), *multi-parameter response function models* (AMIN and CAMPANA, 1996; HAITJEMA, 1995), *direct simulation* (ETCHEVERRY and PERROCHET, 2000; GOODE, 1996), *fractal analysis* (KIRCHNER et al., 2000, 2001) and *stochastic-mechanistic models* (SIMIC and DESTOUNI, 1999). In the course of this thesis, the response function models as described by MALOSZEWSKI and ZUBER (1982, 1996) were applied.

The fundamental model theory is reviewed in the following paragraphs.

2.2.1.1 *Model theory*

For a system with steady flow and an ideal tracer such as $\delta^{18}\text{O}$, $\delta^2\text{H}$ or tritium the tracer concentration in the output is related to the input concentration by the convolution integral:

$$C(t) = \int_{-\infty}^0 C_{in}(t-t')g(t') \exp(-\lambda t')dt'$$

where $C(t)$ is the output, C_{in} the input signature of the tracer, t' is the time of entry, t the calendar time, $(t-t')$ the transit time, λ the radioactive decay constant and $g(t')$ is the system response function representing the travel time probability distribution.

Theoretical models developed to describe the distribution of MRTs in an aquifer system (MALOSZEWSKI and ZUBER, 1996) comprise:

- the **piston-flow model (PFM)**: where a single mean residence time represents the modeled system; hydrodynamic dispersion and molecular diffusion are supposed negligible,
- the **exponential model (EM)**: with the underlying assumption that the exponential distribution of residence times corresponds to a probable situation of decreasing permeability with the aquifer depth,
- the combined **exponential-piston-flow model (EPM)**: where the system is presumed to constitute of two consecutive systems. One is approximated by the piston flow model and the other exhibits an exponential distribution of residence times,
- the **linear model (LM)**: describes an aquifer with linearly increasing thickness and a constant hydraulic gradient, a situation rarely met under natural conditions. Also the combined **linear-piston flow model (LPM)** describes conditions hardly met in nature,
- the **dispersion model (DM)**: accounts, at least to a certain extent, for the heterogeneity of a system. In the model, the one-dimensional solution to the dispersion equation for a semi-infinite medium is used as the response function (KREFT and ZUBER, 1978).

The introduced models on residence time distribution and their transfer functions have been formalized in the software package FLOWPC (MALOSZEWSKI and ZUBER, 1996) and are thus easily available.

2.2.2 Radiocarbon dating in groundwater

Carbon-14 (^{14}C) has been widely used to determine groundwater mean residence times in the range of 1000 to 25000 years and to draw conclusions on groundwater flow directions and fluxes, recharge rates, hydraulic conductivities, and effective porosity (ZHU and MURPHY, 2000). Reviews on radiocarbon dating and its inherent challenges are given by FONTES and

GARNIER (1979), PLUMMER et al. (1991), FONTES (1992), KALIN (1999), GEYH (2000), ZHU and MURPHY (2000).

In nature, ^{14}C is produced in the outer atmosphere by the interaction of nitrogen and cosmic radiation. The evolving free ^{14}C nuclides are rapidly oxidized to $^{14}\text{CO}_2$, washed out by precipitation and photosynthetically fixed into the biomass; after the decay of biomass it is incorporated into the soil carbon pool. Infiltrating water charges with soil CO_2 , which can react with the calcium of the rocks, together contributing to dissolved inorganic carbon (DIC). Infiltrating water also charges with dissolved organic carbon (DOC). DIC and DOC contain ^{14}C and can both be used for groundwater dating. In this study, the focus is on ^{14}C -dating with DIC alone. For information on radiocarbon dating of DOC, the reader is referred to AIKEN (1985), LEENHEER (1981) and GEYER (1994).

Radiocarbon dating of groundwater is based on the knowledge of both the ^{14}C half-life time (5730 ± 40 years) and the initial ^{14}C activity at the time of infiltration. Assuming the ^{14}C activity decreases by radioactive decay alone and no dilution occurs, groundwater mean residence time is determined according to the decay equation:

$$T = \frac{T_{1/2}}{\ln 2} \ln \frac{A_0}{A_m}$$

where T is the groundwater mean residence time, $T_{1/2}$ is the half-life time of ^{14}C , A_0 is the initial ^{14}C activity at the time of groundwater recharge and A_m is the measured ^{14}C activity of the sample.

Generally, the ^{14}C activity of subsurface water is reported as percent modern carbon (pmc). However, the determination of the initial ^{14}C activity of dissolved inorganic carbon (DIC) is a challenging task since it is affected by a variety of geochemical reactions. Among these are:

- the dissolution of either carbonate minerals in an open or closed subsurface system,
- or the weathering of silicates,
- the oxidation of sulfides, followed by carbonate dissolution,
- the oxidation of “old” organic matter present in the aquifer or
- the diffusion of ^{14}C into the aquifer matrix ,

- the influence of volcanic CO₂

all of which lead to an addition of dissolved inorganic ¹²C diluting the ¹⁴C/¹²C-ratio activity in groundwater. Thus, the initial ¹⁴C content needs to be corrected for isotope exchange processes within the groundwater-soil-rock system. The most common correction models applied to account for this dilution are introduced in chapter 6.9.

2.3 CONCEPTS ON RUNOFF GENERATION PROCESSES

In the scope of global change, both climate and land-use changes can severely influence runoff generation. Climate change effects control the input parameter ‘precipitation’. Modifications in land-use affect runoff processes by altering storage capacities or saturation states. An overview of potential impacts of land-use changes on surface and near-surface hydrological processes is given by BRONSTERT et al. (2002).

The assessment of the vulnerability of particular catchments towards anticipated global change effects requires a thorough understanding of runoff generation dynamics. Based on multiple catchment studies in primarily northern temperate climates hydrologists so far agree that:

- Catchments store water for considerable times but release it promptly during storm events, *i.e.*, **pre-event water dominates storm runoff** (KIRCHNER, 2003; McDONNELL, 2003).
- **The chemistry of old water is highly variable during runoff** (BISHOP et al., 2004).
- **Hydrological processes are highly irregular in space and time** (SEIBERT and McDONNELL, 2002; WEILER and McDONNELL, 2004). UHLENBROOK (2006) states that so-called ‘hot spots’ and ‘hot moments’ control stormflow. These terms refer to hydrologically very active areas and short periods of time that exhibit disproportionately high and intense runoff generation.

Conceptual models to explain the ‘old water paradigm’ and techniques to investigate runoff generation processes on the catchment scale are introduced in the following paragraphs.

Particularly, studies investigating runoff generation in Mediterranean semi-arid environments were reviewed.

Simplifying, runoff generation can be described as follows: The part of total precipitation that is not lost through e.g. evapotranspiration contributes directly to surface runoff, this is the so-called *effective rainfall*. This *direct runoff* component is further separated into *surface runoff* = *overland flow* (precipitation flowing on the ground surface) and *interflow* (= prompt subsurface flow). Total discharge measured at a gauge comprises of direct flow and *baseflow* (e.g. groundwater). Conceptual models to explain runoff generation include:

Hortonian overland flow (HORTON, 1933) that occurs when rainfall intensity exceeds the infiltration capacity at the interface atmosphere-litosphere. This flow type is considered the dominant runoff generation process at the local scale in semi-arid environments where high rainfall intensities and sparse vegetation covers prevail (YAIR and LAVEE, 1985; PUIGDEFABREGAS et al., 1998; GUENTNER and BRONSTERT, 2004). The occurrence of Hortonian overland flow is additionally promoted by conditions that lead to a reduction of the near-surface saturated hydraulic conductivity (BUTTLE, 1998). These conditions can be caused by urbanization and the associated sealing of surfaces (ZIEGLER et al., 2004b), by the elimination of natural vegetation, which reduces evapotranspiration and lowers the soil's ability to absorb precipitation (HEWLETT, 1982), by the crusting of soil surfaces (PATRICK, 2002) or by agricultural techniques.

Saturation overland flow is caused by precipitation falling on water saturated areas (ESHLEMAN et al., 1993; BUTTLE, 1994) for example near stream channels or in depressions. In semi-arid catchments, saturation overland flow is of importance only under specific conditions such as during rainy periods in valley bottoms (CEBALLOS and SCHNABEL, 1998) or on shallow soils/weathering zones above bedrocks of low hydraulic conductivity (PUIGDEFABREGAS et al., 1998) where high infiltration capacity opposes low storage capacity.

Direct channel precipitation, in the strict sense, is a form of saturation overland flow and is the part of runoff that is generated by precipitation which falls directly on to the stream channel. Its importance is highest at the beginning of large, intense rainstorms when only a limited surface area contributes to river runoff (WILLIAMS et al., 2002).

Pressure wave translatory flow was proposed as part of the variable source area concept, independently derived by CAPPUS (1960), HEWLETT and HIBBERT (1961, 1967) and TSUKAMOTO (1961). The concept opposes Horton's theory and implies that subsurface flow dominates storm runoff via translatory flow. Precipitation on the upper hillslope displaces the existing water at depth and at the base of the hillslope. When the upslope additions of water exceed the drainage capacity of the downslope areas water will come to the surface as return flow causing areas near the stream to saturate. These areas can vary in size between storms and during the course of a single storm (CHORLEY, 1978). They are thus termed 'variable source areas'. Their extent depends on the initial soil moisture content, storage capacity, and rainfall duration and intensity (CHORLEY, 1978).

55

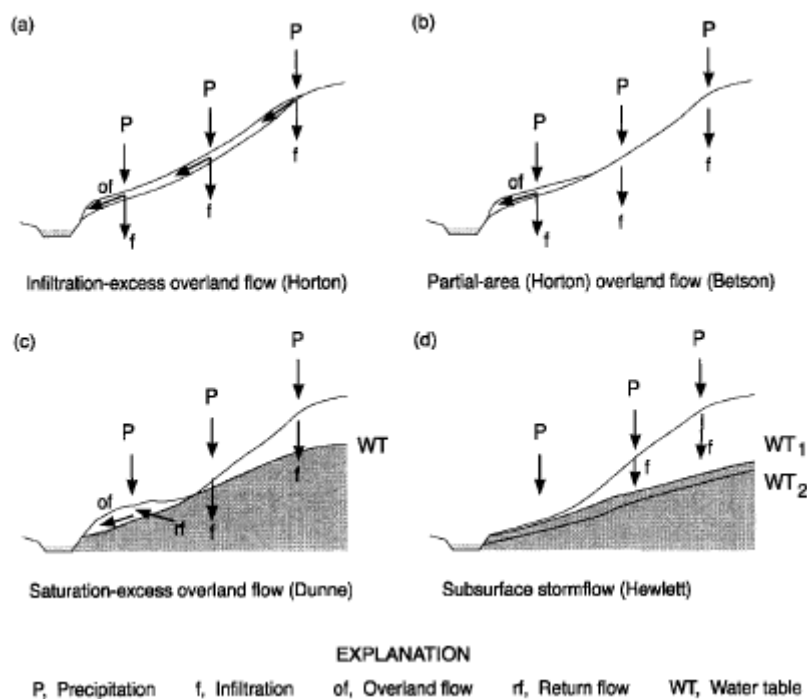


Figure 6: Mechanism of runoff generation (adapted from BEVEN, 1986).

The term **preferential flow** comprises all rapid, nonuniform subsurface flow processes where water and solutes move along certain pathways, while bypassing a fraction of the porous media (BEVEN and GERMANN, 1982; HENDRICKX and FLURY, 2001). An additional characteristic of preferential flow is the non-equilibrium situation with respect to the pressure head or the solute concentrations (WANG, 1991). Consequently, preferential flow mechanism play a significant role concerning the increase of infiltration and an accompanying reduction of overland flow or the rapid transfer of agrochemicals (CHRISTIANSEN et al., 2004) through the soil towards groundwater. The modeling of preferential flow in the vadose zone is reviewed by SIMUNEK et al. (2003), CHRISTIANSEN et al. (2004) and others.

Different categories of preferential flow have been distinguished:

Macropore flow (or alternatively pipeflow) refers to the rapid movement of water in a well-connected pore system that originates e.g. due to the activity of soil fauna and plant roots, the existence of cracks and fissures; or natural soil pipes that developed as a result of erosional subsurface flow (BEVEN and GERMANN, 1982). The importance of macropore flow in hillslope runoff, threshold values and antecedent soil moistures were investigated by PILGRIM et al. (1979), MOSLEY (1982), GERMANN (1986), JONES (1987), LUXMORE et al. (1990), UCHIDA et al. (1999) among others.

Interflow or funneled flow (KUNG, 1990), first observed by GARDNER (1960), is a form of lateral flow that occurs at sloping interfaces between sediments of different permeability where, *e.g.* a fine grained sediment is overlaying a coarse grained. Especially during low flow situations, when the matrix potential at the textural interface is so low that it prevents water from entering into the coarse, underlying soil a capillary barrier is developing which restricts vertical water flux and forces the water to move laterally along the bedding interface (WALTER et al., 2000). Water entry values and flow mechanism have been studied by HILLEL and GARDNER (1970), SEILER and BAKER (1985), HILLEL and BAKER (1988), KUNG (1993), HEILIG et al. (2003) among others.

An additional flow mechanism generating rapid subsurface stormflow is that of lateral flow along the sediment-bedrock interface. Flow velocities of preferential flow can reach rates comparable with and even exceeding that of overland flow (BEFANI, 1966, 1967 in SMAKHTIN, 2002; BEVEN and GERMANN, 1982; JONES, 1987; SEILER et al., 2002).

Preferential flow mechanisms are generally of minor importance in semi-arid environments apart from karstic environments. Nevertheless, BERGKAMP et al. (1996) and CALVO-CASES et al. (2003) for example report macropore flow in soils on semi-arid limestones slopes.

One concept to explain the dominance of pre-event water during runoff generation is **groundwater ridging**, a process first observed and suggested by RAGAN (1968), GILLHAM (1984) and ABDUL and GILLHAM (1989).

According to this model, the pre-storm groundwater table is overlain by a tension-saturated capillary fringe with the extension of the fringe primarily depending on the grain size distribution and antecedent moisture of the soil. During storm conditions additional water percolates down to this zone, the tension saturation is obliterated and the pressure state of water changes from negative to positive consequently inducing an immediate rise in the water table and thus increasing the net hydraulic gradient towards the seepage face. Given the thin unsaturated zone, the accumulation of fine-grained material and the – compared to upslope segments – moist conditions in broad near-stream environments, this is where groundwater ridging is most likely to occur. The same mechanism might as well lead to return or saturation overland flow where the rising water table coincides with the soil surface (ABDUL and GILLHAM, 1989). Indirect evidence of this effect by tracer-hydrograph studies was offered by SKLASH and FARVOLDEN (1979), SKLASH et al. (1986), LADOCHE et al. (2001) and during snowmelt events by BUTTLE and SAMI (1992) and BUTTLE (1994). SANDSTROM (1996) reports rainfall-dependent importance of groundwater ridging for a semi-arid catchment in East Africa.

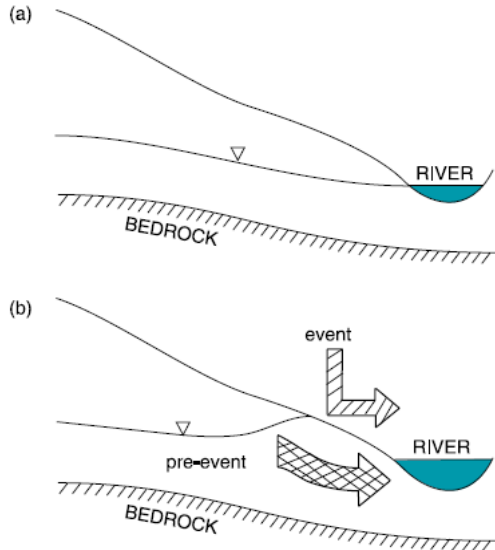


Figure 7: The groundwater ridging mechanism of pre-event water discharge. Hypothetical water table profiles (a) prior to the event and (b) at peak runoff (adapted from CLOKE et al., 2006).

2.3.1 Runoff generation in Mediterranean semi-arid environments

Runoff generation in Mediterranean semi-arid environments differs significantly from that under humid conditions insofar as it is nonuniform in space and time (CALVO-CASES et al., 2003). Additionally, runoff patches in semi-arid climates show poor hydrological connectivity (PUIGDEFABREGAS et al., 1998). These peculiarities of runoff generation in Mediterranean regions are primarily due to the prevailing climate conditions and secondarily caused by the geomorphologic heterogeneity within these catchments.

Precipitation in the Mediterranean region is restricted to a few months, rain events are infrequent and of short duration. Consequently, the rate of evaporation equals or even exceeds the rate of precipitation thus leaving only little amounts of water to runoff. On the other hand, rain events are often of high intensity resulting in overland flow being the dominant runoff process at the local scale (YAIR and LAVEE, 1985).

Mediterranean slopes have often been described as a mosaic of runoff (source) and runoff (sink) areas (NICOLAU et al., 1996; PUIGDEFABREGAS and SANCHEZ, 1996; BERGKAMP, 1998; LAVEE et al., 1998). High spatial variability of lithology, slope morphology, soil development as well as past and present land uses cause local differences in infiltration capacities and mosaic-like soil moisture distributions (WESTERN et al., 1998a,b).

The neighborhood of vegetation patches and bare soil surfaces introduces additional heterogeneity. Thus, vegetation patches have been shown to lead to increased infiltration and reduced overland flow (BERGKAMP, 1998), a result of plant-modified soil properties such as the greater density of macropores (BERGKAMP et al., 1996). Generally, bare soils will tend to act as overland runoff sources while vegetation patches will receive the runoff for re-infiltration (BROMLEY et al., 1997). At the hillslope scale, footslope areas or river cone deposits in the valley bottoms will usually act as sink areas for runoff (CEBALLOS and SCHNABEL, 1998) while runoff is generated on upslope segments (PUIGDEFABREGAS et al., 1998).

2.4 HYDROGRAPH SEPARATION TECHNIQUES

The transformation of precipitation into discharge involves complex hydrological processes (see above). To study complex recharge and discharge processes in a selected catchment, scientists refer to abstract input-output model systems where precipitation is the input and discharge the output parameter. The transformation process itself is on the one hand determined by relatively steady catchment properties such as geology, topography, soil, and vegetation cover. On the other hand, the dynamic control on the evolution of discharge is the input parameter itself i.e., precipitation falling within a certain catchment and the resulting antecedent moisture conditions.

Different perceptions on recharge and discharge processes and consequently different methods to separate discharge components have been developed. Generally, one distinguishes between source areas (surface/subsurface water, shallow/deep groundwater) or response times of discharge components (fast and slow discharge components). However, the complexity of discharge processes is reflected by the lack of unambiguous denomination of discharge components, for example terms such as interflow, lateral flow, prompt subsurface flow and hypodermic flow are often used interchangeably.

UHLENBROOK and LEIBUNDGUT (1997) distinguish three different techniques to investigate discharge processes:

Process-based methods. Of main interest are runoff-generating processes and the associated flow paths. Tracerhydrological and hydraulic methods are applied.

Residence-time-based methods. Discharge components are separated based on tracer-hydrologically determined residence times within the catchment.

Dynamic-based methods. Discharge components are separated according to their temporal occurrence in the hydrograph which is achieved with a variety of empirical and graphical techniques.

The appropriate method is chosen according to the question at issue. Hydrograph methods e.g., separate slow and fast discharge components, tracer methods consider pre-event and event components. A comparison of discharge components that have been received by the different methods is often limited or dependent on certain boundary conditions.

2.4.1 **Baseflow analysis**

Baseflow is the portion of streamflow that is contributed by groundwater and is referred to as dry weather flow. To separate baseflow from streamflow and to receive a characteristic baseflow hydrograph, several techniques have been developed that are reported by HALL (1968), MATTHESS and UBELL (1983), NATHAN and MACMAHON (1990), HOELTING and COLDEWEY (2005) and SMAKHTIN (2001a).

Event-based separation methods such as *straight line*, *slope line* and *concave separation* (LINSLEY et al., 1982) are used to calculate the portion of baseflow during a single runoff event. Major challenge is thereby to determine the shape of the hydrograph which is done by choosing the appropriate peak, beginning point and inflection point of the hydrograph, the latter describing the end of the recession limb.

Continuous separation techniques such as base wave line (NATERMANN, 1951) are applied to generate baseflow hydrographs on a long-term basis and to quantify groundwater recharge in the observed period. These approaches make often use of some kind of digital filtering realized for example in the *smoothed minima method* (INSTITUTE OF HYDROLOGY, 1980) or the *recursive digital filtering* technique (NATHAN and MACMAHON, 1990).

PETTYJOHN and HENNING (1979) developed three algorithms for systematical separation of baseflow from the hydrograph, which were later automated by SLOTO and CROUSE (1996) within the HYSEP software provided by the USGS (chapter 7.1).

Another option to gain information about the baseflow portion and thus groundwater recharge is the application of modified frequency and duration analysis of low flow discharge; see for example WUNDT (1958), KILLE (1970) and DEMUTH (1993). WUNDT (1958) assumed that *monthly mean low flow* ($MoMLF_W$) is exclusively fed by groundwater. Accordingly, *mean monthly low flow during summer* ($SuMoMLF_W$) corresponds to minimum groundwater flow. However, especially in catchments affected by delayed discharge such as snowmelt, low flows are influenced by interflow and overland flow components. Hence, KILLE (1970) developed an algorithm to exclude direct runoff components from monthly mean low flows ($MoMLF_K$), which was later automated (and thus objectified) by DEMUTH (1993). Monthly low flows of a long-term record are organized in ascending order and graphically displayed. The lower 5 % of values are excluded from the analysis due to anthropogenic interference. Values between 5 and 50 % correspond approximately to a straight line. Hence, a best fit line is constructed and values plotting above are reduced to this line to eliminate the portion of direct runoff components. The mean value of the best fit line equals the mean, long-term baseflow which – in the German-speaking literature – is equated with the mean, long-term groundwater recharge.

However, no standardization concerning baseflow analysis exists and the prevalent graphical approaches have a limited physical basis. Additionally, the location of the spring/gauge relative to the local groundwater flow field determines the significance of the calculated baseflow values (PFAFF, 1987). In other words, how significant is the contribution of groundwater originating in the aquifer below the spring/gauge level? A question that is particularly important in semi-arid to arid areas where long dry periods prevail.

2.4.2 **Recession analysis**

The recession limb of the hydrograph, which represents the dry weather discharge, depicts the storage-discharge relationship of a catchment area. This relationship mainly depends on

catchment geology (e.g. transmissivity, storativity of the aquifers) and distance from stream channels to basin boundaries (SMAKHTIN, 2001b).

Recession of the different discharge components varies in its magnitude. The steep part of the recession curve represents overland flow, which – after a storm event – ceases quickly within hours or days. With ongoing dry weather, the recession curve flattens until it represents outflow from groundwater storage that can endure for decades. For the hydrologist it is still difficult to interpret recession curves as the recession rates of the different discharge components overlap and there is no clear distinction between the single components.

Assuming the storage-discharge relationship to be linear and underlying the mass balance approach, the recession curve is described by an exponential function:

$$Q(t) = Q_0 e^{-t/K}$$

where $Q(t)$ is the discharge at any time t during recession, Q_0 the discharge at the beginning point of the considered recession curve (often coinciding with the peak) and K is the recession constant that gives an indication about the mean residence time in the system.

Usually more than a single storage influences the depletion of a water source thus often composite exponential functions are used to describe the recession behavior. WITTENBERG (1990) claims that a non-linear storage algorithm explains baseflow recession in an unconfined aquifer physically more accurately.

Most recession analyses aim to determine a master recession curve and the appending recession constant, which then represent the mean recession behavior of the investigated water source. Common techniques such as the *correlation method* (HALL, 1968) or the *matching strip method* (NATHAN and MACMAHON, 1990) are described in MATTHESS and UBELL (1983), NATHAN and MACMAHON (1990), HOELTING and COLDEWEY (2005), TALLAKSEN (1995) and SMAKHTIN (2001a).

2.4.3 Tracer-based hydrograph separation techniques

2.4.3.1 *Hydrograph separation based on the mass balance concept*

The classical hydrograph separation technique is extensively described in KENDALL and McDONNELL (1998) and HOEG et al. (2000).

Hydrograph separation analyses are based on simple steady state mass balance equations of water and tracer fluxes in a catchment. Commonly a two-component mixing model (PINDER and JONES, 1969) is used to quantify two different discharge components based on their tracer concentrations and discharge volumes.

Theoretically, this concept allows the determination of **n** runoff components based on the observation of **n-1** tracers and solving the following **n** linear mixing equations (HOEG et al., 2000):

$$Q_T = Q_1 + Q_2 + \dots + Q_n$$
$$c_T^{t_i} Q_T = c_1^{t_i} Q_1 + c_2^{t_i} Q_2 + \dots + c_n^{t_i} Q_n$$

whereas Q_T is the total runoff, Q_1, Q_2, \dots, Q_n are the different runoff components and $c_1^{t_i}, c_2^{t_i}, \dots, c_n^{t_i}$ are the concentrations of one observed tracer t_i . Because $c_1^{t_i}, c_2^{t_i}, \dots, c_n^{t_i}$ represent the extreme possible concentrations for c_T they are known as end-members (HOOPER et al., 1990). The application of this separation technique is restricted by several boundary conditions (SKLASH and FARVOLDEN, 1979):

- The tracer concentrations of the different runoff components are significantly different.
- Each input tracer concentration is constant in space and time or its variation is known.
- The tracer behaves conservatively.
- Contributions of an additional component are negligible, or their composition is identical to that of another component.

Especially the demand for the tracer concentrations being constant in space and time or their variations being known is often insufficiently met in reality. In that way, introduced uncertainties have to be taken into account and quantified.

Hydrograph separation based on two-component mixing models was first applied in the 1970's and used to determine the proportion of event and pre-event water contributing to storm runoff (SKLASH and FARVOLDEN, 1979; RODHE, 1981; OBRADOVIC and SKLASH et al., 1986; STICHLER, 1987; WELS et al., 1991a). Thereby event water refers to the water that is added to a catchment's surface as rainfall or snowmelt during a storm event while pre-event water was held in the catchment prior to, and has been discharged into the stream channel during a storm event (BUTTLE, 1998).

Pre-event water was found to dominate largely the streamflow generation regardless of catchment scale, physical properties and climatic conditions (GENEREUX and HOOPER, 1998; MARC et al., 2001). This implies that catchments store water for considerable periods of time but then release it promptly during storm events (KIRCHNER, 2003).

It was soon understood that two components could not satisfactorily account for the variation of isotopic and chemical composition in the stream during stormflow. In more sophisticated studies three-component models were used to divide pre-event water further into soil water and groundwater (HOOPER et al., 1990; McDONNELL et al., 1991; OGUNKOYA and JENKINS, 1993; HOEG et al., 2000) addressing rather the geographic than the time source of storm runoff components. The concept was further extended by MEROT et al. (1995), LEE and KROTHER (2001), UHLENBROOK and HOEG (2003) by refining the division of discharge components applying four- and five-component hydrograph separation.

2.4.3.2 *End-member mixing analysis (EMMA)*

End-member mixing analysis (EMMA) is an analytical approach developed by CHRISTOPHERSEN et al. (1990) and HOOPER et al. (1990) that is closely connected to and often combined with the classical hydrograph separation technique. It allows to model stream water chemistry as a mixture of representative end-members and to separate the hydrograph using multiple tracers simultaneously.

CHRISTOPHERSEN et al. (1990) observed that the chemical species in stream water that are closely correlated with flow, are the same ones that exhibit marked differences in concentrations across soil horizons. They concluded that the extremes among the solutions, the so-called end-members, must mix in proportions such that their combined chemistry equates the observed stream water chemistry.

The restrictive assumptions for tracers mentioned before in the scope of hydrograph separation (2.4.3.1) are also valid within the framework of end-member mixing analysis. The end-member contributions are estimated by solving a constrained, overdetermined set of linear equations applying a least-square procedure.

End-member mixing analysis have been enhanced by introducing multivariate data analysis techniques – in particular *principal component analysis (PCA)* – to indicate the approximate rank of the mixture in question and thus to estimate the minimum number of end-members needed to describe the observed data (CHRISTOPHERSEN and HOOPER, 1992). The application of principal component analysis enables to study the structure of variance within the data and results in a more efficient coordinate system describing the observed stream water chemistry. The detailed EMMA procedure is outlined by CHRISTOPHERSEN and HOOPER (1992) and summarized in BROWN et al. (1999).

Though the EMMA approach itself has been less applied compared to the vast literature covering the use of classical hydrograph separation, clearly its advantages consist in:

- its compatibility with classical hydrograph separation,
- the generation of testable hypotheses that focus future field efforts,
- the identification of geographical source areas,
- the simultaneous application of multiple tracers and
- the overdetermination of the algebraic solution

(CHRISTOPHERSEN et al., 1990; HOOPER et al., 1990; CHRISTOPHERSEN and Hooper, 1992; MULHOLLAND, 1993; OGUNKOYA and JENKINS, 1993; BAZEMORE et al., 1994, ELSENBEEER et al., 1995, BROWN et al., 1999; BURNS et al., 2001).

Common end-members identified have been soil water, groundwater, organic horizon water, hillslope subsurface water, riparian zone water or event (rain) water to name just a few.

Temporal variations of end-member chemistry have been taken into account by OGUNKOYA and JENKINS (1993) who tested “fixed”, “time-invariant” and “temporally varying” end-member concentrations. Depending on the size of variation, BURNS et al. (2001) allowed end-member chemistry to vary over time (large variations) or to be represented by their median value (small variations).

2.4.3.3 *Uncertainty analysis*

The validity of conclusions drawn from EMMA-based hydrograph separation is largely dependent on the conducted uncertainty analysis.

The success of EMMA-based hydrograph separation and the determination of end-member proportions are based on the adequate chemical differentiation of these source waters (JOERIN et al., 2002). Given that, at the catchment scale, spatial and temporal variability in end-member composition is usually unknown or difficult to characterize (HOEG et al., 2000) and that the determination of tracer concentrations can be subject to sampling and analytical errors, it is evident that the hydrograph separation approach inherits large uncertainties. In addition to parametric and natural uncertainties the strong simplistic model hypotheses that mixing models refer to (JOERIN et al., 2002) introduce significant uncertainties into the obtained results. While the former sources of error can be summarized as statistical uncertainty, the latter is referred to as model uncertainty.

Among other, UHLENBROOK and HOEG (2003) conclude that results of hydrograph separations should not be taken as exact numbers and are of mostly qualitative nature unless combined with additional field data. The following paragraphs offer a brief introduction to uncertainty analysis in conjunction with EMMA-based hydrograph separation.

Focusing on parametric variability only, early research (RODHE, 1981; NEAL et al., 1990; McDONNELL et al., 1991) addresses uncertainty in terms of *sensitivity analysis* where tracer concentrations change within the range of observed data and requantification of the models results in an array of end-member proportions. HOOPER et al. (1990) introduced *first-order Taylor series expansion* into sensitivity analysis and where thus the first to invoke a formalized statistical approach.

Concentrating on both, the tracer concentrations used to perform the hydrograph separation and the uncertainties in the tracer concentrations itself, GENEREUX (1998) uses *Gaussian error propagation* to determine uncertainties in the computed mixing fractions of two- and three-component hydrograph separation. This technique was frequently applied (BROWN et al., 1999; HOEG et al., 2000; BURNS et al., 2001), extended to an even higher number of end-members and refined concerning the addressed uncertainty sources (UHLENBROOK and HOEG, 2003).

BAZEMORE et al. (1994) incorporated both the effects of spatial variability of the end-member concentrations as well as the laboratory analytical error into uncertainty analysis and were the first to apply the, to some extent advanced, *Monte Carlo approach*. This computer-based method simulates probability distributions of possible end-member contributions for each collected stream sample, a technique applied and adapted by DURAND and TORRES (1996), RICE and HORNBERGER (1998) among others.

JOERIN et al. (2002) investigated for the first time both the **statistical uncertainty** of mixing models due to chemical variability inside components applying a less restricted Monte Carlo method, and the **model uncertainty** by comparison of alternative hypotheses.

Recently SOULSBY et al. (2003) used a *Bayesian model* (BREWER et al., 2002) to estimate uncertainty. Therein, end-members are assumed to arise from bivariate normal distributions whose mean vectors and co-variance matrices can be estimated. Markov Chain-Monte Carlo methods are used to model the average and 95 percentile upper and lower bounds of end-members during storm events. This method, its implicit assumptions and shortcomings are discussed in detailed by BEVEN (2004) who concludes that subjectivity, for example in the choice of model structures or input and boundary condition errors, will remain a significant part of uncertainty estimation for the foreseeable future.

2.4.4 Natural tracers

2.4.4.1 Temperature

Temperature can certainly not be considered a conservative tracer since the temperature observed in a stream is controlled by a variety of factors such as direct solar radiation, stream

shape and volume, shading, substrate type and others (JOHNSON, 2004). Nevertheless, stream temperature has been used as a tracer to separate stream flow during snowmelt into shallow and deep flow (KOBAYASHI, 1985; PANGBURN et al., 1992). This hydrograph separation technique is based on the assumption that precipitation or snow shows significantly different temperature fingerprints than soil water or groundwater. SHANLEY and PETERS (1988) investigated runoff processes in a small, forested catchment availing the temperature contrast in rainfall and groundwater. KOBAYASHI et al. (1999) used stream temperature to evaluate contributions of shallow and deep flow during rainstorms in summer, compared them to results received during snowmelt runoff and succeeded to determine the depth of a major subsurface flowpath by additionally investigating soil temperature profiles.

2.4.4.2 *Electrical conductivity*

Electrical conductivity (EC), sometimes referred to as specific conductance, is a measure of the ability of water to conduct an electrical current and is usually expressed in microsiemens per centimeter [$\mu\text{S}/\text{cm}$] at 25°C. The electrical conductivity is strongly correlated to the type and concentrations of ions in solution and can thus be used to infer the total dissolved solid (TSS) content in natural waters. Although TSS is commonly about 65 % of the electrical conductivity, this relationship should be evaluated individually *in situ*.

The advantages of using electrical conductivity in mixing and hydrograph separation studies consist in its low costs, its easy monitoring and the immediate assessment of the water composition (MCNAMARA et al., 1997; LAMBS, 2000). Based on the assumption that precipitation which becomes surface runoff is not subject to significant chemical enrichment on its way to the stream, NAKAMURA (1971) or KOBAYASHI et al. (1999) used electrical conductivities to separate the hydrograph into an overland and a subsurface component.

PILGRIM et al. (1979), DEBOER and CAMPBELL (1990) as well as LAUDON and SLAYMAKER (1997) pointed out the inherent instabilities of this tracer approach. While the former claim the change of variations in specific ion concentrations throughout different stages of the event, the latter refer to the different dissolution kinetics and different valences of the substances included in the electrical conductivity. To account for the variations in the new

(surface) water component PILGRIM et al. (1979) developed laboratory relationships between soil contact time and specific electric conductivity. For the same purpose, McNAMARA et al. (1997) additionally monitored the specific conductivity in a small hillslope water track during the length of the events. They also suggested the combined use with other tracers and apply both electrical conductivity and ^{18}O to divide stormflow in an Arctic region into an old and new water component finding similar water proportions for both tracers. LAMBS (2000) successfully used the same tracer combination to discriminate between snowmelt and glacier melt in a Himalayan valley and between river water and phreatic water in the Garonne catchment (France).

In a karst spring, DESMARAIS and ROJSTACZER (2002) observed increased values of EC during storm events and attributed these to the flushing of pre-storm water.

2.4.4.3 *Stable isotopes of water (^{18}O and ^2H)*

The stable isotopes ^{18}O and ^2H are components of the water molecule and therefore ideal tracers for a variety of hydrological questions. The input of water isotopes into the hydrological system occurs spatially distributed and in variable concentrations via precipitation. This variability in the isotopic composition is caused by isotope fractionation during phase transition processes such as evaporation and condensation and by mixing. Isotope fractionation is temperature-dependent, thus, isotope effects observed on the catchment scale are often closely correlated to temperature. The most important effects are:

- **Seasonal effect:** In the warm seasons precipitation is isotopically heavier than in the cold seasons.
- **Altitude effect:** With increasing altitude, precipitation gets isotopically light.
- **Amount effect:** The isotopic composition of precipitation varies with its intensity. Precipitation becomes isotopically light with increasing rain amounts because of the kinetics of isotope fractionation.
- **Continental effect:** With increasing distance from the ocean coast, (source of evaporation) precipitation becomes isotopically light due to repeated condensation.

- **Atmospheric moisture effect:** With decreasing atmospheric moisture, isotope concentrations in the vapor phase become more enriched.

Additionally, high temporal variability was observed between storms and during the course of single storms (HEATHCOTE and LLOYD, 1986; NATIV and MAZOR, 1987; RINDSBERGER et al., 1990, ADAR et al., 1998; KUBOTA and TSUBOYAMA, 2003; CELLE-JEANTON et al., 2004). The main factors determining the extent of this variability are the temperature of condensation, the origin of air mass vapor and evaporation and the isotopic exchange between the atmospheric moisture and the falling raindrops (DANSGAARD, 1964; GAT and DANSGAARD, 1972; EHHALT et al., 1963; STEWART, 1975).

If the mentioned effects result in a distinctive isotopic signature of precipitation (event water), compared to the ground and pre-event water stored in the catchment isotopic hydrograph separation can be applied (compare 2.4.3.1). Among the first to use this approach were DINCER et al. (1970), MARTINEC et al. (1974), FRITZ et al. (1976), SKLASH and FARVOLDEN (1979), RODHE (1981), STICHLER and HERMANN (1982), PEARCE et al. (1986) and others. While a vast amount of studies were conducted in a variety of catchments most of the studies showed that pre-event water supplies at least 50 % of streamflow at peak discharge. However, most investigations were performed in mid- and high-latitude regions and event-based hydrograph separations in Mediterranean environments (LOYE-PILOT and JUSSERAND, 1990; MARC et al., 2001; TEKELI and SORMANN, 2003) are scarce.

2.4.4.3.1 Rain

Catchments in humid and semi-arid climate zones receive their major input of water from rainfall. The isotopic composition of rain varies spatially and temporally (see 2.4.4.3) which has to be considered applying isotope based hydrograph separation. This is especially true for mesoscale studies and catchments where convective rainfall events dominate.

Generally, several bulk rainfall samples are collected for an event, analyzed for isotopes, and combined in a weighted mean value that is used for hydrograph separation. McDONNELL et al. (1990) developed two additional weighting techniques, the *incremental mean* and the *incremental intensity*. The incremental mean allows only for the isotopic content of rain that

has fallen until the time of separation. The temporal variability of rain events is taken into account by applying the incremental intensity technique, which accounts for rain intensity data and is based on sequential rain sampling techniques (KENNEDY et al., 1979; KRUPA, 2002). Spatial variability is usually taken into account by installing a network of rainfall samplers at different altitudes and topographic transects.

Especially in forested and densely vegetated catchments, rainfall is subject to canopy interception, which can lead to a certain amount of re-evaporation and hence isotopic enrichment of throughfall (e.g. GAT and TZUR, 1967; DEWALLE and SWISTOCK, 1994; BRODERSEN et al., 2000). In Mediterranean environments isotopic enrichment of 0.3-0.5 ‰ was observed (PICHON et al., 1996).

2.4.4.3.2 Snow

Snow can account for a significant amount of precipitation in catchments situated in the appropriate climate zones or altitudes. This is also true for several Mediterranean catchments that receive recharge from high altitude mountains. The importance of snowmelt in those catchments became only recently a focus of research (SMITH et al., 2003). Astonishingly, more water is immobilized in the snow cover in the Mediterranean coastal zone than in the snow cover on the mountains of continental Europe (AOUAD-RIZK, 2005).

This has been attributed on the one hand to the long way that clouds travel along the Mediterranean during which they collect moisture. Additionally, for Mount Lebanon it was observed that snow produced there had twice the water content as the same volume of snow falling at the same altitude on the Alps (AOUAD-RIZK et al., 2005). This fact was attributed to the steep slopes of the Lebanon Mountains and its vicinity to the coast allowing a very rapid cooling of the clouds.

To quantify the influence of snow on runoff and groundwater recharge via isotopic hydrograph separation, it is necessary to determine the actual isotope input from snow cover outflows (STICHLER, 1981) which are the amount-weighted isotope input values (UNNIKRISHNA et al., 2002). In early studies, depth-integrated snow cores were used to describe the event component (RODHE, 1981; BOTTOMLEY et al., 1986; INGRAHAM and

TAYLOR, 1989). However, it was shown that large variations of isotopic composition occur within individual melt episodes – in particular the enrichment of melt water in heavy stable isotopes (STICHLER et al., 1981; UNNIKRISHNA et al., 2002).

Consequently, snowmelt lysimeters were widely used to account for the temporal variability of the isotopic composition during melt periods (HOOPER and SHOEMAKER, 1986; STICHLER et al., 1986; MAULÉ and STEIN, 1990; KENDALL et al., 1999; SHANLEY et al., 2002; UNNIKRISHNA et al., 2002). Additionally, the latter approach allows accounting for rain falling on the snow pack and infiltrating through it (SINGH et al., 1997).

2.4.4.4 *Major anions*

Of the major anions, particularly chloride and sulfate have been used in hydrograph separation studies. Generally, chloride and (up to a certain extent) sulfate can be regarded as natural conservative tracers (RIBOLZI et al., 1993) as they derive mainly from atmospheric input and, on the event scale, geogenic contributions are of minor importance.

During dry periods, evaporation concentrates soil water and groundwater with respect to these tracers and thus allows for the separation of pre-event and event water contributing to the stormflow hydrograph (OGUNKOYA and JENKINS, 1993; PETERS and RATCLIFFE, 1998).

RIBOLZI et al. (1996) compared hydrograph deconvolutions applying hydrochemical and isotopic tracer and found good correlations between residual alkalinity, chloride and ^{18}O . KENDALL et al. (2001) derived higher pre-event portions using chloride and silicate as tracers than for isotopic hydrograph separation which was attributed to the fact that event quickflow picked up sizeable amounts of chloride and silicate during its rapid, very surficial contact with the soil.

Nitrate has been frequently used as a tracer to study transfer and export mechanisms of nutrients (and other agrochemicals) in watersheds (BURT and ARKELL, 1987; DURAND and JUAN-TORRES, 1996; CREED and BAND, 1998; HYER et al., 2001; MOLÉNAT et al., 2002, JARVIE et al., 2005). Though nitrate is generally considered reactive, it was shown that denitrification processes are negligible on the event scale (RIBOLZI et al., 2000). INAMDAR et al. (2004) used nitrate and DOC to separate till groundwater and near-surface soil waters

during summer storm events in a glaciated forested catchment. RIBOLZI et al. (2000) applied chloride and nitrate in a mixing model, and derived three locally distinct storm flow components: pre-event water deriving from the depression groundwater, event water and pre-event water of plateau groundwater.

2.4.4.5 *Major cations*

WHITE (1998) states that over the normal range of pH in natural waters, assuming no precipitation and dissolution and excluding biotic processes, the principle conservative ions are sodium, potassium, calcium, magnesium, chloride, sulfate and nitrate since these ions are usually fully dissociated from their conjugated acid and bases. During transport, however, cations are subject to a variety of processes such as cation exchange with the clay–humus complex, dissolution of calcite and dolomite or precipitation of calcite with CO₂ degassing (RIBOLZI et al., 2000) constricting their conservative nature. Thus, cations have been rarely applied as tracers in hydrograph separation.

Generally, cation concentrations and stream discharge are negatively correlated in temperate latitudes. In these environments, cations derive from weathering of primary minerals and are at their highest concentrations during baseflow conditions. The addition of new surface or subsurface water with low ionic strengths leads to the dilution of stream cations concentrations during high flow conditions (DREVER, 1997; MARKEWITZ et al., 2004).

Accordingly, MCGLYNN et al. (1999) used calcium as a tracer to distinguish deep riparian water in a snowmelt-influenced small headwater catchment while TARDY et al. (2004) referred to sodium for the identification of deep groundwater reservoir contributions to the hydrograph in a semi-arid catchment on granitic rocks.

2.4.4.6 *Dissolved silica*

In natural waters dissolved silica derives primarily from the weathering and subsequent dissolution of silicates and aluminosilicates in bedrocks and soils (DREVER, 1997). The dominant species of silicon in natural waters is Si(OH)₄, above pH 9.8 silicic acid dissociates into dihydrogen and trihydrogen silicate ions (H₃SiO₄⁻, H₂SiO₄²⁻). Weathering rates of silicate

minerals depend not only on pH but also on temperature (WHITE and BLUM, 1995), lithology (MEYBECK, 1987, TAYLOR et al., 1999), vegetation (MOULTON and BERNER, 1998) and concentration of metal species (HAINES and LLOYD, 1985) or alkaline and alkaline-earth ions (TANAKA et al., 2004) in the waters.

In tracer-based hydrograph separation, dissolved silica is considered a geogenic tracer, its specific concentration in a flow component resulting from the weathering of the rock or the soil matrix in its respective area of origin. The use of dissolved silica as a conservative tracer in hydrograph separation is based on the finding that the dissolution of silica occurs very quickly (KENNEDY, 1971) as well as that dissolved silica reaches an approximately steady-state concentration within a short period of time and maintains these concentration during the event (HENDERSHOT et al., 1992). Considering these properties and assuming the dissolved silica content in precipitation to be virtually zero, dissolved silica was used to quantify the fast runoff components by means of hydrograph separation (HOOPER and SHOEMAKER, 1986; KENNEDY et al., 1986; WELS, 1991; MAULÉ and STEIN, 1990; HINTON et al., 1994; UHLENBROOK et al., 2002). The use of dissolved silica as a conservative tracer was doubted by BUTTLE and PETERS (1997) who demonstrated, that some dilution occurs even during the event.

Because silicate minerals are subject to enduring, relatively slow weathering reactions make dissolved silica concentrations in groundwater are a suitable tool for residence time determinations (HAINES and LLOYD, 1985; LINDENLAUB, 1998). The concentration of dissolved silica in water is determined by its contact time with the silicate minerals. Thus, if the water has a sufficiently high residence time in the reservoir former influences of flow pathways are eliminated.

2.4.4.7 *DOC*

The carbon fraction of organic matter (TOC – total organic carbon) is subdivided into particulate organic carbon (POC), and dissolved organic carbon (DOC) where, by definition, dissolved substances are those that pass through a 0.45 µm filter. In natural waters, DOC concentrations generally range from <1 mg/L in precipitation and groundwater (WHITE,

1998; BROWN et al., 1999; LADOUCHE et al. 2001; NEAL et al., 2005) up to 20-40 mg/L (and more) in the interstitial waters of the upper soil layer (WHITE, 1998; CAREY and QUINTON, 2005). River waters have intermediate concentrations of about 5-7 mg/L (WHITE, 1998). The given values are mean concentrations and can vary on a broad scale.

SACHSE et al. (2005) presented a short review of factors governing DOC concentration in natural waters. Thus, 'dissolved organic carbon in surface waters is influenced by natural and anthropogenic allochthonous sources in the catchment and by autochthonous production and degradation processes'. Stream water concentrations of DOC are controlled by the rates of DOC production in soils, the rates of its absorption in mineral soils (MCDOWELL and WOOD, 1984), the flowpath of water (MOORE and JACKSON, 1989) and landscape types within the catchment (DILLON and MOLOT, 1997). Seasonal variations of DOC concentrations are caused for example by changes in rainfall, biological productivity and microbial activity (WHITE, 1998).

In the scope of hydrograph separation studies DOC concentrations have often been observed to increase with rising stream discharge (BROWN et al., 1999; MACLEAN et al., 1999; LADOUCHE et al., 2001; SHANLEY et al., 2002). This has been attributed to the rising water table during high flow conditions and the subsequent flushing of DOC-enriched in the upper soil horizons where DOC accumulates during low flow conditions (HORNBERGER et al., 1994; BOYER et al., 1997). Especially in snowmelt-influenced or permafrost catchments, DOC proved to be a suitable tracer to separate an upper (organic) soil horizon flow component - caused by rapid lateral subsurface flow - from the streamflow hydrograph (KENDALL et al., 1999; MACLEAN et al., 1999; CAREY and QUINTON, 2005). BISHOP et al. (1994) and LISCHIED (2002) evaluated the importance of the riparian zone as control on DOC stream chemistry. TARDY et al. (2004) monitored DOC in a semi-arid tropical catchment and attributed the DOC response to an organic superficial soil horizon. Though DOC cannot generally be considered a conservative tracer (see above), biological activity is usually assumed negligible at the event scale. Additionally, the major fraction of DOC is often refractory (LADOUCHE et al., 2001).

3. Study area

3.1 LOCATION AND PHYSIOGRAPHY

The study area is part of the Upper Jordan River Catchment (UJRC), Israel's northernmost watershed (Figure 8). The $\approx 1700 \text{ km}^2$ Upper Jordan River orographic catchment, of which $\approx 900 \text{ km}^2$ are situated within the State of Israel, comprises the northern Jordan Rift valley, which is the northward extension of the Dead Sea Rift Transform (DSRT). The latter evolved, as the African and Arabian tectonic plates started to drift and separate about 30 Ma ago. The DSRT, a tectonic graben, runs from the spreading Red Sea through the whole length of the State of Israel and continues through Lebanon and Syria, approaching the Taurus zone of convergence in Turkey. Its formation is still a matter of dispute, which is further discussed in SNEH (1996). Several small faults and left-stepping displacements of the Dead Sea fault are additionally shaping the UJRC (Figure 9).

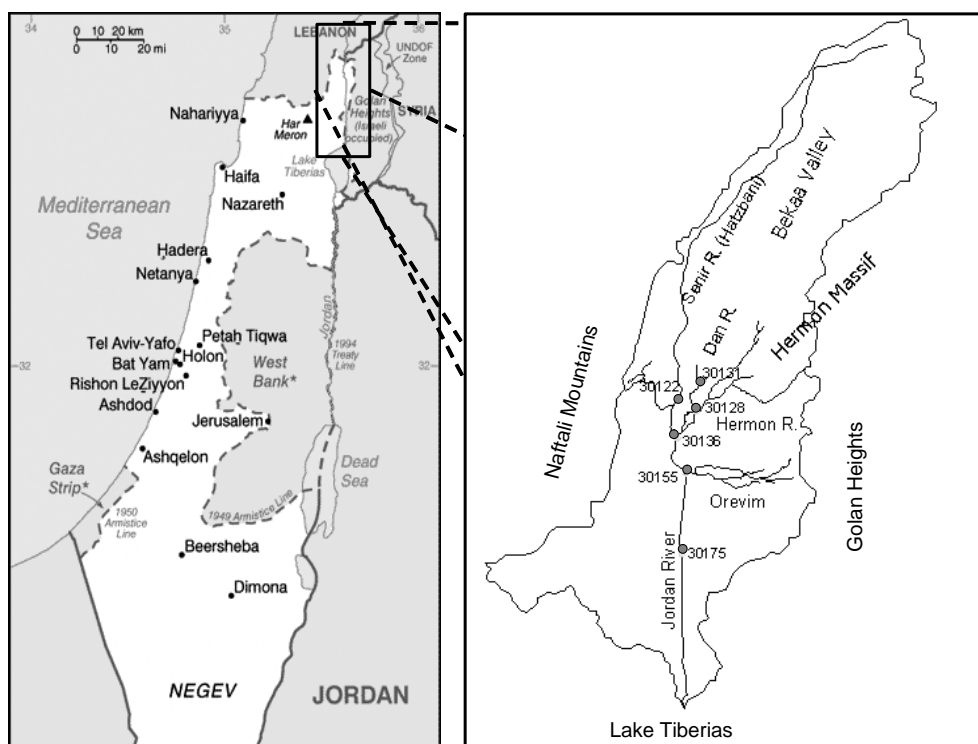


Figure 8: The Upper Jordan River Catchment and its location in the State of Israel (EXACT, 1998). Numbers represent gauging stations of the Hydrological Service of Israel (HSI).

The Upper Jordan River drains part of the southern Beka'a Valley, the Hermon Mountains, the Golan Heights, the eastern Naftali Mountains, and the Hula Valley north of Lake Tiberias. It is fed by three main perennial streams, emerging on the southern flanks of the Hermon Mountains and by additional small, predominantly intermittent rivulets draining the eastern and western plateau and escarpments that enclose the Hula Valley (Figure 8).

The topography of the study area - with altitudes ranging from about 210 m b.s.l. (Lake Kinneret) to 70 m a.s.l. in the Hula Valley to about 1000 m a.s.l. on the Golan plateau and more than 2.800 m a.s.l. on top of Mount Hermon - causes high relief energy and a potential for fast hillslope runoff processes.

3.2 CLIMATE

The study area is located in the Eastern Mediterranean, a transition zone between the temperate European and the arid Sahara-Arabian climate. The Eastern Mediterranean climate is characterized by hot, dry summers, cool, wet winters and short transitional terms that are often overlapped by the two prevailing seasons.

ALPERT et al. (2004) defined the seasons in the Eastern Mediterranean based on synoptic systems that dominate the region. According to him:

- **Summer** lasts from the end of May until the mid of September and is influenced by the persistent *Persian trough* weather condition which is marked by high temperatures and high humidity and by north/north-easterly winds.
- **Autumn**, which lasts from the mid of September until the beginning of December, is dominated by the *Red Sea trough* associated with south/south-easterly winds, low humidity, and medium to high temperatures.
- **Winter**, which persists from December until the end of March, is influenced by the *Cyprus low* that brings low temperature, strong winds, and high-intensity precipitation.
- The short, 2-month **spring** season is dominated by the *Sharav low* accompanied by hot and dusty winds, low humidity and medium to high temperatures.

All climate parameters show high spatial variability. Mean annual precipitation ranges from more than 1600 mm/year in the upper Mount Hermon range (GILAD and SCHWARTZ, 1978; SIMPSON and CARMI, 1983) to 900 mm/year in the upper Golan and to 500 mm/year at the southern tip of the UJRC. In a recent study, RIMMER and SALINGAR (2006) applied an empirical “precipitation-elevation-seasonal equation” to model a representative annual precipitation of the Hermon region of about 958 mm. However, their model is restricted to a limited data basis (until now, there are no precipitation gauges in the upper Hermon region) and the topographic catchment area of the three major tributaries which is most likely much smaller than the actual recharge area of these streams. Additionally, no systematic estimation of snow water equivalents on Mount Hermon were conducted so far.

On the Hermon Massif most of the precipitation is falling as snow, which accumulates from December to April but can last until early summer (GILAD and BONNE, 1990). Snow on the Golan Heights and Naftali Mountains is rare and usually melts within a day. The wet season lasts from October to April but about 90% of the annual total rain falls during November until March. Spatial and temporal variability of precipitation is highest during the transitional seasons (BEN-GAI, 1998).

Mean potential evaporation based on long-term (1970-2000) daily measurements of pan evaporation in the UJRC is about 1900 mm/year (RIMMER and SALINGAR, 2006); it varies with altitude, soil and vegetation covers. Limited data availability, in particular information on sublimation, evaporation from snowmelt, or evapotranspiration and the scarce spatial distribution of meteorological stations within the UJRC do not allow for reliable estimations of actual evapotranspiration so far.

Temperatures strongly fluctuate with season and altitudes. KESSLER (1980) reported a temperature gradient of about -0.5 to - 0.6 K per 100 m on Mt. Hermon. Mean daily temperature in August for an altitude of about 2100 m a.s.l. is 16.9 °C, for an altitude of about 1130 m a.s.l. (Majdal Shams) 20.7 °C. In January, the mean daily temperature at 2100 m a.s.l. is -1.6 °C, at 1130 m a.s.l. 5.1 °C. In the Golan Heights (Qneitra, 900 m a.s.l.) mean daily temperature in August is about 23.4 °C and in January, the coldest month, about 6.4 °C (DAN and SINGER, 1973).

The climate in the research area was shown to depend on several global weather phenomena such as the Atlantic Oscillation (AO), the North Atlantic Oscillation (NAO), the Mediterranean Oscillation (MO) and the El Niño Southern Oscillation (ENSO). The MO has been first described by CONTE et al. (1989) and was later confirmed by KUTIEL et al. (1996) and MAHERAS et al. (1999) to be the most important regional circulation-rainfall relationship. DUENKELOH and JACOBET (2003) state that the MO is not an independent large-scale circulation mode, it rather comprises those parts of the AO/NAO that are linked with Mediterranean precipitation variability. Generally, it was shown that during a positive NAO, conditions are colder and drier than average in the Mediterranean (KRICHAK and ALPERT, 2005; VISBECK et al., 2001). Both the MO and its connection to the AO/NAO are best developed during winter. PRICE et al. (1998) found a significant correlation between El Niño events and above average precipitation since the 1970's. In addition, extreme summer temperatures were shown to be linked to the Indian Monsoon (ALPERT et al., 2005).

3.3 SOILS

Soil formation is controlled by the prevailing climate, bedrock, topography and by men's activities. The Eastern Mediterranean climate with its wet and cool winters and hot and dry summers promotes xeric (\approx dry) soil moisture regimes in most of the region. The excess of rainfall over evapotranspiration during winter enhances the dissolution of carbonate rocks as well as the slow hydrolytic weathering of silicate minerals. A common feature of many Mediterranean soils – the reddish color – derives from the release of iron compounds during mineral weathering. These compounds, such as iron oxyhydroxides precipitate as ferrihydrites and ferridehydrates and recrystallize into hematite when the soil dries. They coat the fine (clays) and coarse grained particles and cause the reddish color (YAALON, 1997; SINGER et al., 1998).

An influence of aeolian (Saharan) dust on soil formation within the Eastern Mediterranean was recognized by YAALON and GANOR, 1973; MACLEOD, 1980; NIHLEN and OLSSON, 1995. YAALON (1997) claims that in soils derived from hard limestone up to 50 % of the material could be of aeolian origin. GANOR and MAMANE (1982) estimated the annual dust

deposition in Israel as 20 to 40 tons km^{-2} . The effects of airborne additions of dust to soils are manifold and of varying importance. It may affect horizon differentiation, physical and hydraulic properties of soils, or levels of fertility (SIMONSON, 1995).

Another important factor is the anthropogenic impact. Man has cultivated Mediterranean lands for more than 5000 years, thus significantly influencing soil formation processes. Deforestation on naturally occurring steep slopes for example, accelerated erosion, which exceeded the slow weathering, processes leaving bare mountain slopes and creating local valley fills.

On the calcareous bedrocks of the southern Hermon Mountains, weathering led to the formation of soil types such as *terra rossa*, *brown rendzina*, and *pale rendzina* (DAN et al., 1976, 1983). Carbonates and sulfides are dissolved and leached by infiltrating water while the remaining silicates and oxides accumulate and undergo further soil formation processes. Which soil type develops, depends on the pedoclimate, biotic activity, organic matter content, pH, redox and soil water conditions. The formation of hematite, causing the characteristic color of *terra rossa* soils, is promoted in dry and warm pedoenvironments, for example on the upper parts of a toposequence, in sub soils and on hard limestones. Goethite, imparting a yellow-brown color onto the typical *rendzina* soil profile, forms under wet soil conditions on gentil slopes, in top soils or on soft limestones with low iron contents (CORNELL and SCHWERTMANN, 1996; SINGER et al. 1998). Generally, soil covers on Mount Hermon are thin and soil depth decreases with increasing altitudes and slopes.

The Golan plateau is a syncline covered with Plio-Pleistocene basalts. It decreases gradually in altitude from about 1000 m a.s.l. in the north to 300 m a.s.l. on the southern edge. While the southern Golan is dominated by late Pliocene cover basalt and a semi-arid climate, the northern part is characterized by younger overlying Pleistocene basalts and a humid Mediterranean climate. These gradients in geology, topography, and climate caused the formation of a variety of soil types on the Golan Heights. Shallow and gravelly basaltic Brown Mediterranean soils prevail on the young Pleistocene basalts in the north. These soils are slightly acidic, contain a considerable amount of silt, and predominately form kaolinite minerals. Smectite brown grumusols, basaltic protogrumusols, or pale rendzinas in contrast

cover most basaltic plateaus of the dry, southern Golan (SINGER, 1971). Additionally, they are also found in undrained depressions of the northern part (DAN and SINGER, 1973). Soil depths range from a few decimeters down to 2 m, with the deep soils found on the lower parts of a toposequence or in hydromorphic depressions.

3.4 VEGETATION AND LAND USE

Mediterranean wood- and shrublands dominate the Golan Heights, the Naftali Mountains and the low slopes of Mt. Hermon, while the upper regions (>1300 m) are characterized by an oro-Mediterranean mountainous vegetation. Plant communities of the Golan Heights include:

- *Quercus ithaburensis* park forests at altitudes of 0-500 m accompanied by *Pistacia atlantica*, *Ziziphus spina-christi* and *Ziziphus lotus*. The open areas in between support rich annual herbaceous vegetation dominated by *Triticum dicoccoides*, *Hordeum spontaneum* and *Avena sterilis*.
- *Quercus calliprinos* woodlands at altitudes above 500 m accompanied by *Quercus boissieri*, *Crataegus monogyna*, *Crataegus aronia*, *Pistacia palaestina*, *Prunus ursine* and a species rich ephemeral vegetation (DANIN and ARBEL, 1998; DANIN, 2004).

On Mt. Hermon, more than 900 different plant species have been found so far. A multifaceted topography and resulting microclimates offer habitats for a variety of species. West facing, wind exposed, often desiccated slopes are covered by spiny, rounded, dense and small shrubs known as “cushion-plants” including species such as *Astragalus cruentiflorus*, *Onobrychis cornuta*, *Acantholimon libanoticum*, *Acantholimon echinus* and *Astragalus echinus*. These in turn offer environments for geophytes, annuals and other plants with soft stems. Temporally wet areas following snowmelt are covered with *Romulea nivalis* and *Ranunculus demissus* while *Polygonum cedrorum* grows on the waterlogged soils of dolinas (DANIN, 2004).

The primary land use on the shallow soils of the Golan Heights is cattle grazing. Livestock is kept for dairy and beef farming. The more permeable red soils of the upper northern Golan are used for orchards; locally deep soils are utilized for dry farming of small grains. The

application of chemical fertilizers and pesticides is common in those areas and poses a potential risk for water quality in the area. The lower Hermon region is characterized by orchards and olive groves managed by the resident Druze population. Both the Hermon and the Golan area comprise a number of nature reserves and hiking areas but are also in use for military purposes. The Hula Valley is managed primarily with intensive irrigated agriculture, the major crops being: corn, wheat, peanuts, and alfalfa. Fish farming is common in the northern parts of the valley, near the Jordan River sources. About 8 km² of the valley center comprise a new-created lake and are developed as a resting area for migratory birds and in parts for eco-tourism.

3.5 GEOLOGY

The study area (Figure 17, Figure 27) is characterized by four main geological units (Figure 64 – Appendix), which are subsequently described considering their genesis, tectonics, petrography, and the resulting hydrogeological characteristics:

- the **Hula Valley** (Figure 9, Figure 10), a pull-apart basin evolved during the Pliocene-Pleistocene tectonic activity of the Dead Sea Transform; its sedimentary fill consists mainly of organic and inorganic lake deposits interbedded with Quaternary basalt and interfingering with gravel and sands from river cones that developed from the bordering mountains.
- the **Mount Hermon** (Figure 9, Figure 11), an isolated, uplifted anticline is dominated by Mid-Jurassic Bathonian to Callovian limestones,
- the **Golan Heights** (Figure 9, Figure 13), a syncline, is covered with Plio-Pleistocene basalts of the Bashan Group and,
- The **Naftali Mountains (= Galilee Mountains)** (Figure 9), an anticline, with limestones of the Cretaceous Judean Group.

3.5.1 Hula Valley

The central geological feature of the Upper Jordan River Catchment is the rhomb-shaped Hula Valley, about 20 km in length and about 6 km wide. The pull-apart basin developed between left-stepping segments of the Dead Sea Transform during the Plio-Pleistocene (GARFUNKEL et al., 1981).

The Qiryat Shemona master fault (Figure 9) borders the valley to the west and splits further north into the Roum and Yammuneh faults. The eastern Jordan River fault turns northeast at Mount Hermon branching into the Rachaya and Serjaya faults (HEIMANN, 1990; GOMEZ et al., 2003). While several echelon faults limit the Hula graben towards the south, the northern margin comprises a series of gradual step faults (HEIMANN, 1990).

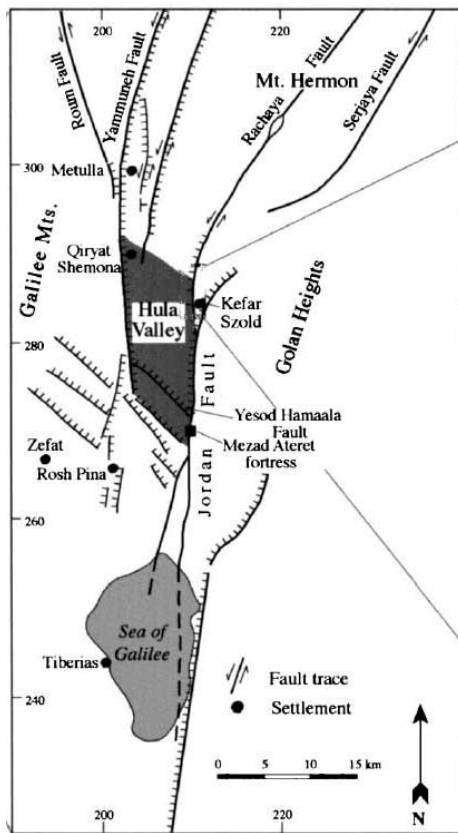


Figure 9: Map of the main faults in the northern Jordan Rift Valley (HEIMANN, 1990; ZILBERMAN, 2000).

The basin fill was investigated during several oil, gas, and lignite exploration campaigns (KAFRI and LANG, 1979, 1987 among others). It reaches a thickness of more than 4-5 km (BEN-GAI, 2002; RYBAKOV et al., 2003). The bedrock of the subsided Hula block was never

reached by drillings so far but is assumed to consist of Eocene, Senonian or Cenomanian limestones and dolostones. Sedimentation of the valley fill is assumed to have started in Middle-Late Miocene leading to the accumulation of predominantly fluvio-lacustrine fresh water deposits comprising marls, lacustrine limestones, sands, gravels, and peat. These fluvio-lacustrine sediments alternate with layers of Early and Late Pleistocene basalt flows and tuffs as well as with sediments of river cones originating from the surrounding areas (PICARD, 1965; HOROWITZ, 1973). The sequence ends with peat in most of the area, only the elevated northern part of the valley is extensively covered by travertines (PICARD, 1965; HOROWITZ, 1973; HEIMANN and SASS, 1989).

The rivers that discharge from the surroundings into the Hula basin caused the formation of debris cones that interfinger with the basin fill and consist of coarse-grained, relatively unsorted material. Thus, significant flow paths along the valley edges are generated (KAFRI et al., 1979, Figure 10), being a typical characteristic of extremely deep valley fills (SEILER, 1977). Additionally, gravitational forces produced valley-parallel fissures and fractures with high opening widths in the valley bordering rocks, causing high hydraulic conductivities. Consequently it is assumed, that

- an essential part of the groundwater recharge entering the Hula valley subsurface from the bordering mountains or by river infiltration along the valley borders leaves the valley subterraneously along the valley borders, and
- that only a minor part of groundwater recharge passes the valley center (KAFRI et al., 1979).

NEUMAN and DASBERG (1977) investigated the shallow groundwater system within the Hula Valley and stated the existence of a low hydraulic gradient from north to south and a pronounced vertical gradient that is probably caused by upraising groundwater recharged in the surrounding mountains. At shallow depths, the bordering faults are considered to act as hydraulic barriers but according to the conducted environmental stable isotope investigations, this must not be true for the entire length of the faults or at great depths. Since the research of NEUMAN and DASBERG (1977) the Hula Valley has undergone significant changes such as

ongoing soil erosion and an extension of the canal network as well as the re-flooding of the Agmon Lake; all these activities raised the formerly lowered groundwater table. Originally, the Hula Valley was drained to rule out malaria diseases. Later it was restored to a certain extent because drainage enhanced e.g., the eutrophication of Lake Kinneret and the occurrence of peat fires.

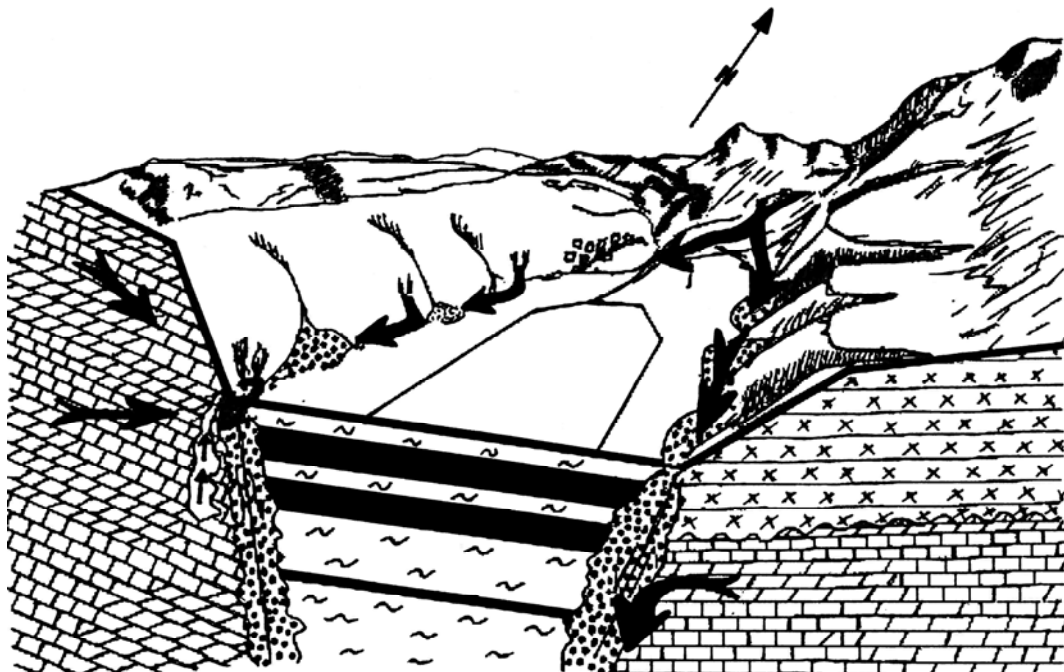


Figure 10: Schematic block model of the Hula trough, showing the groundwater circulation below the Hula plain (adapted from KAFRI and LANG, 1979). (Brick signature = carbonates, circles = gravel/sands, waves = clay/silt, black bars = peat, arrows = direction of water movement.)

In a recent work about the shallow groundwater system of the Hula Valley (ESHEL, 2004) two horizontal hydrological units have been identified: A shallow part with a maximum depth of 5 m, characterized by a network of macropores and cracks which serve subsurface water as preferential flow conduits and thus resulting in high horizontal hydraulic conductivities (≈ 100 m/day). A deep part from the bottom of the cracks down to more than 15 m consists of silty sediments with low hydraulic conductivities (≈ 0.1 m/day).

3.5.2 Mount Hermon

The Hermon block, with a maximum length of about 55 km and 35 km in its maximum width, comprises an area of about 1.250 km² and includes the eastern part of the Damascus basin in Syria. About 750 km² of the area belong to the Jordan River orographic watershed (GILAD and BONNE, 1990). The area is hydrologically shared between Israel, Lebanon, and the Syrian Arab Republic. The Hermon massif is characterized by steep slopes; its summit reaches an altitude of 2,814 m.

Early work on the Jurassic stratigraphy of Mount Hermon rocks was conducted by FRAAS (1877), DIENER (1885), NOETLING (1886), BLANCKENHORN (1912), PICARD and SOYER (1927), VAUTRIN (1934), BURDON and SAFADI (1964) and was summarized by DUBERTRET (1955) and WOLFART (1966). Recent studies on the geology of Mount Hermon have been accomplished by SALZMAN (1968), GOLDBERG (1969), MICHELSON (1975), HOROWITZ (1979), HIRSCH (1996), EDGELL (1997), MOUTI (2000) and were in part compiled by GUR et al. (2003) (Figure 63).

Mount Hermon and its northern extension, the Anti-Lebanon Mountains, are both part of the Syrian Arc fold system, a semi-continuous belt extending from western Egypt through the North Sinai, the Negev Desert and adjacent offshore waters of the SE Mediterranean to Syria in the east. The Hermon massif is a NNE-SSW trending anticline that was rapidly uplifted in response to Neogene activity along the DST fault system (WILSON et al., 2000).

The Sion-Rachaya fault (Figure 9), which parallels the axis of the Hermon anticline, divides the Hermon Massif into two main blocks: the western Sion shoulder³ and the central and eastern Hermon Range, the latter comprising the Sirion and Hermon ridges (Figure 11).

The eastern block is mainly composed of Mid-Jurassic Bathonian to Callovian limestones overlain by Oxfordian marls and shales near the top of the Jurassic section and is known for its abundant basaltic rocks, dolomitization, and mineralization (SHIMRON, 1989). None of this is found in the Sion (Har Dov) Range whose low western slopes are characterized by exposures of Lower Cretaceous and Cenomanian-Turonian carbonates and sandstones. The thickness of exposed Jurassic at Mt. Hermon was estimated to be about 2700 m (GOLDBERG

³ Arkub, Har Dov

et al., 1981). Further to the west, the Har Dov Range merges with the Hazbani Valley, which is characterized by Pliocene basalts, Cenomanian limestone, and dolomites of the Sannine formation and Cretaceous sandstone and shales. Marls, as well as Senonian and Eocene chalks, are common (GUR et al., 2003). Chronostratigraphies of the Hermon region were compiled by WOLFART (1966) and GOLDBERG et al. (1981).

Table 2: Springs fed (at least in part) by recharge on Mount Hermon and their corresponding average annual yields.

Spring	Annual yield 10^6m^3	Altitude m a.s.l.	Reference
Tanur (I)	0.6	300	HSI (2002)
Barid (I)	5.0	243	HSI (2002)
Sa'ar (I)	5.0	1030	GUR et al. (2003)
Sion (I)	20 – 25	1000	GUR et al. (2003)
Kezinim (I)	24	340	GUR et al. (2003)
El-Hazbani (L)	25 – 30	575	GILAD and SCHWARTZ (1978)
Wazani (L)	40 – 50	280	GILAD and SCHWARTZ (1978)
Shreid, Aicha & Cheba'a springs, Hazbani Valley (L/S)	50		GILAD and SCHWARTZ (1978)
Banias (I)	70	390	HSI (2002)
Beit Jean & Sabarani (S)	100	1280	GILAD and SCHWARTZ (1978)
Barada (S)	101	1100	BURDON and SAFADI (1964)
Figeh (S)	235	860	BURDON and SAFADI (1964)
Dan (I)	254	180	GUR et al. (2003)

Israel (I), Lebanon (L), and Syrian Arab Republic (S)

The hydrogeology of this region was first studied by MICHELSON (1975) and GILAD and SCHWARTZ (1978). The formation of cracks and fissures led to a deep karstification providing high permeability anisotropies. The Arad Group Aquifer is the source of a few big and several small springs that drain towards the south and southwest, thus forming the source area of the Upper Jordan River. However, considerable yields were also monitored for a variety of springs replenishing the Barada and Aawaj rivers towards the east and northeast of the Hermon Massif. While the Aawaj River is fed by recharge generated on the Mount Hermon ridges, the Barada River receives recharge both from the Anti-Lebanon and Hermon mountains (KATTAN, 1997b). In Table 2 the biggest springs of the region and

their corresponding yields are summarized. Within this study, the focus is on springs that are contributing to the Upper Jordan River tributaries only.

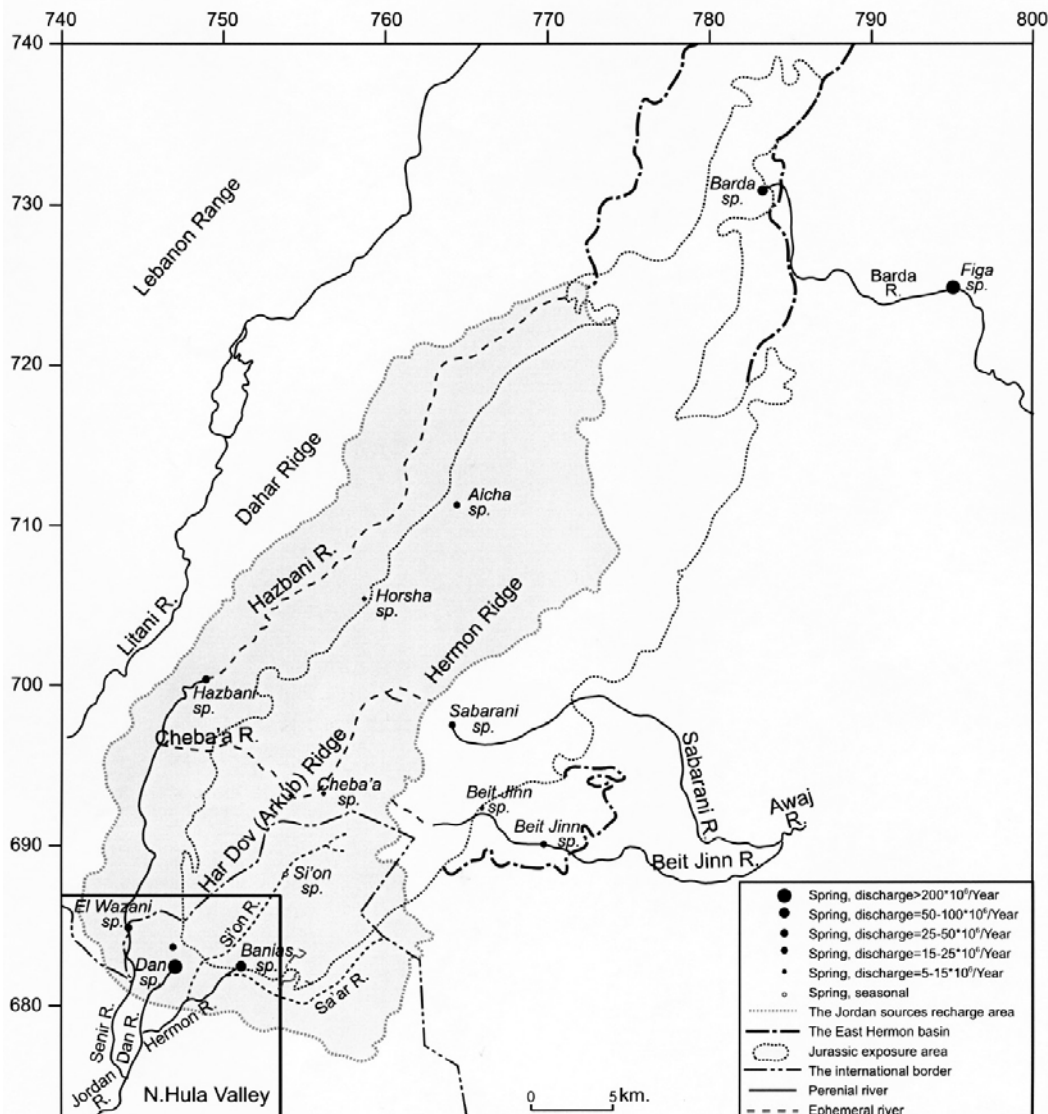


Figure 11: The topography of the Mount Hermon region and its hydrological network (GUR et al., 2003 adapted from GILAD and SCHWARTZ, 1978). The size of circles is proportional to the respective spring discharge (see legend on the bottom right).

The most yielding spring of the region – the Dan spring – crowns a horst structure at an elevation of 180 m a.s.l. that developed along an underground fault line forming a hydraulic short cut between Jurassic carbonates and Lower Cretaceous sandstones and marls (Figure 12-b). This is also where the Leshem side spring emerges. The springs feed the Dan tributary.

A variety of springs contribute to the Hermon river at the south-eastern foot of the Hermon; the biggest of them – Banias – at 390 m a.s.l. It surges along a vertical interface between the

carbonates of the Hermon formation and low-permeable quaternary sediments (Figure 12-a). An additional water source within this group is the Kezinim spring; whose unique characteristics and significant input to the flow of the Hermon stream was only recently emphasized (GUR et al., 2003).

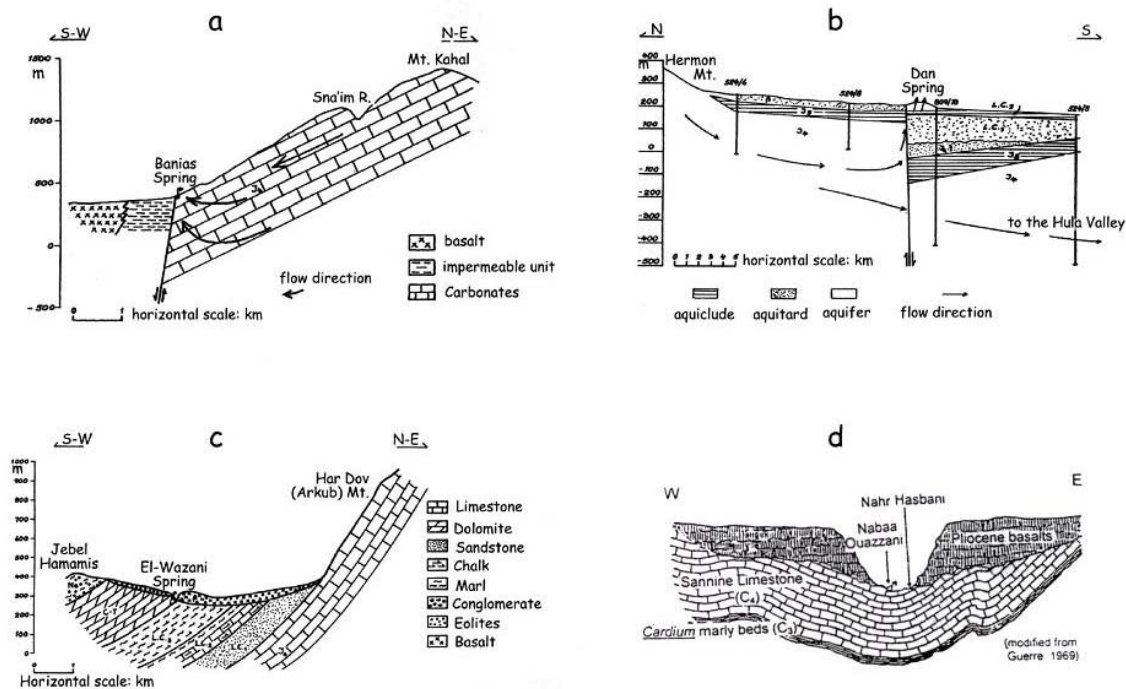


Figure 12: Geological cross sections of springs emerging on the southern foot slopes of Mount Hermon. The flow direction of water is indicated by arrows (GUR et al., 2003 adapted from GILAD and SCHWARTZ, 1978).

The Senir stream is fed by two perennial springs both emerging in the Hazbani Valley at the southwestern border of the Hermon Massif: Wazani and El-Hazbani (Figure 12-c,d). The Wazani spring is situated in Lebanon close to the border with Israel at an elevation of 280 m a.s.l. It contacts between overlaying Pliocene basalts and Cenomanian limestone of the Sannine formation (EDGELL, 1997). The El-Hazbani spring is located approximately 15 km upstream at an elevation of 575 m a.s.l. According to MEINZER (1923), the Banias, Dan, and Wazani springs can be classified as first-magnitude springs indicating a large area of supply and easy subsurface-groundwater communication.

Several researchers tried to determine the dominating discharge components in the mountainous areas of the Upper Jordan River Catchment. Early work was done by

MICHELSON (1975) who – based on hydrograph analyses – already stated the existence of an interflow component for the main tributaries emerging from the karstic Hermon region.

SIMPSON and CARMI (1983) used hydrographical and isotopic methods to characterize reservoirs feeding the main tributaries of the Jordan River. They claim the existence of a dual reservoir system consisting of a baseflow component with mean residence times of 11-20 months and an additional interflow component for the Senir and Hermon streams with a mean residence time of about 1 month. Their hydrograph analyses were based on mean daily discharge values, which do not allow for conclusions concerning a fast discharge component such as overland flow. According to their assumptions, baseflow of the three streams is fed by the same regional groundwater aquifer. The interflow reservoir is explained to be located in the near-surface karst and to be additionally supplied by snowmelt. Isotopic analysis showed further on that the springs are dominated by water with short residence times, 90 % being less than 3 years old. Deep groundwater residence times based on ^{14}C analysis have been investigated by CARMI et al. (1985) who found that the residence time for Hermon and Dan is < 20 yr.

GILAD and BONNE (1990) investigated the contribution of snowmelt to the main sources of the Jordan River. According to their analysis, the Mt. Hermon snowmelt represents about 10 % of the annual yield of the upper Jordan River sources and 30 % of the dry weather discharge during late spring and early summer.

EDGELL (1997) studied the hydrogeology of karst areas in Lebanon and stated for the Wazani spring, which partly feeds the Senir stream, a steep decline of discharge from winter (up to 6 m^3/s) to summer (just above 1 m^3/s) which indicates an extended subsurface catchment with low storage capacities because of significant karstification.

GUR et al. (2003) applied hydrochemical and isotopic methods to emphasize the importance of an additional spring in the Hermon Massif, the Kezinim spring. They also showed that the Banias spring is governed by two different discharge components: conduit and diffusive flow. They state that these two components are best represented by the Dan and Kezinim spring. According to GUR et al. (2003), the Dan spring represents the outlet of a relatively shallow and well-washed karstic system being recharged over the flanks of Mt. Hermon, whereas the

Kezinim spring water is recharged at the summit of the geological structure and flows through deep parts of the anticline structure.

3.5.3 Golan Heights

The Golan Heights cover an area of 1044 km² within the western part of the Hula Valley. The northern limit of the plateau is shaped by Wadi Sa'ar, which separates it from the Hermon Mountains. The Golan decreases in altitude gradually from about 1000 m a.s.l. in the north to about 300 m a.s.l. in the south where the Yarmuk River divides it from the Gilad Mountains. Towards the west, the Golan Heights slope down to the Hula Valley and Lake Kinneret. The transition zone is marked by several cliffs reflecting the morphology of the main border and a series of step faults of the Jordan Rift. The Syrian Hauran plateau is the eastern continuation of the Golan Heights.

The Golan syncline extends between the Hermon anticline in the north and the Ajlun anticline (Jordan) in the south (MICHELSON, 1979). Volcanic activities during the Plio-Pleistocene issued in an elevated basaltic cover, which is attributed to the Bashan Group (MOR, 1986). The basalt flows reach a thickness of > 600 m in the center of the plateau and overlay sedimentary rocks. While volcanic cones characterize the eastern part of the Golan, the southern and southwestern parts are carved by deep gorges. These gorges developed during the Pleistocene as a concomitant phenomenon to the formation of the Jordan Rift Valley and the accompanying lowering of the erosion base. The general discharge direction within these valleys is from east to west with the exception of the Meshushim stream that flows southwards. Early studies on the hydrogeology of the Golan Heights have been conducted by BURDON (1954) and WOLFART (1966). A variety of studies published in Hebrew such as those from MERO and BONNE (1967), KIDRON (1972), MICHELSON (1972, 1996) focused on water balances and exploration of water production capacities. Resent research by DAFNY et al. (2003) led to the development of a conceptual and numerical hydrogeological model describing the groundwater flow field in the Golan basalt aquifer.

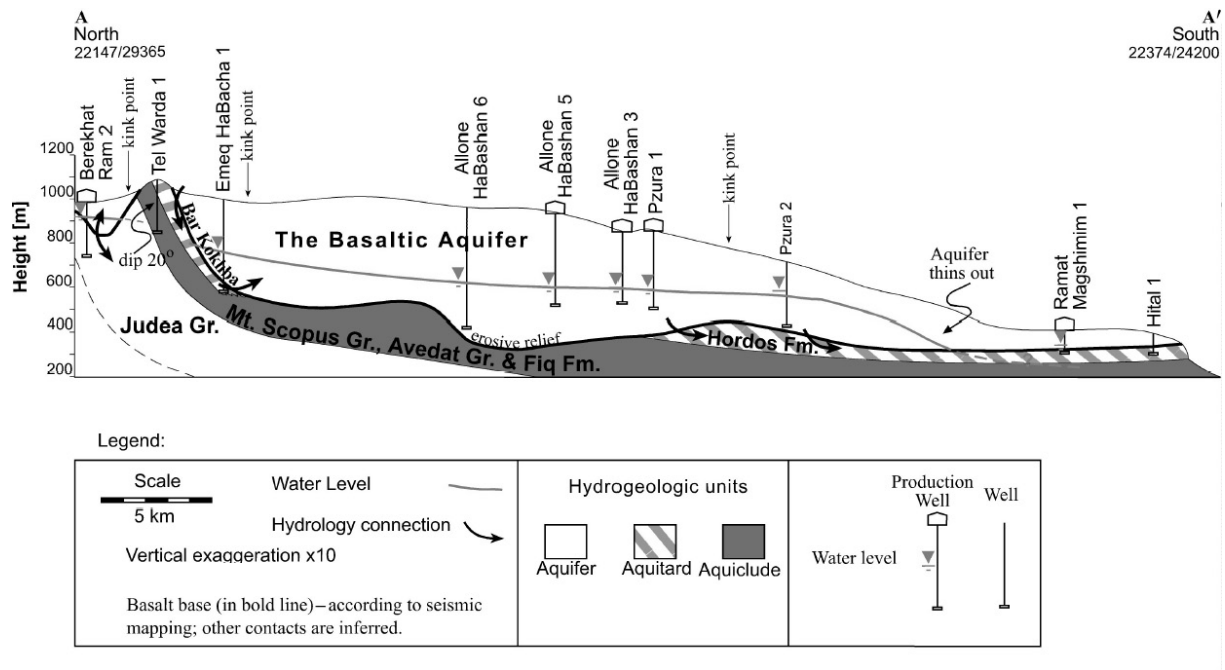


Figure 13: North-south hydrogeological cross section along the Golan Heights (DAFNY et al., 2003). Groundwater flows both from east to west into the Kinneret-Hula basin and from west to east towards the upper Yarmouk River.

According to DAFNY et al. (2003), a phreatic basalt aquifer extends over the north and central parts of the Golan. An aquiclude complex comprising the low permeable Mount Scopus, Avedat Groups, and Fiq Formation forms the base of the basaltic aquifer (Figure 13). Though, hydraulic connections have been shown to exist between the Berekhat Ram region and Judea Group aquifer (MICHELSON, 1979; GILAD, 1988b), the Tel Warda area and the Bar Kokhba Formation aquitard as well as the southern part of the basalt aquifer and the Hordos Formation aquitard (MICHELSON, 1979); (Figure 13).

The basalt aquifer is subdivided into two main basins with the subsurface water divide located east of the volcanic cones in the northern Golan. The western basin drains to Lake Kinneret and the Hula Valley; it yields about $85 \text{ } 10^6 \text{ m}^3$ of freshwater per year. This basin is further separated by a pre-basaltic topographic ridge that acts as a hydraulic barrier. The resulting subbasins are the source of the northern and central ‘Side springs’ yielding approximately $50 \text{ } 10^6 \text{ m}^3$ annually (Figure 14). Mean annual yields of the major ‘Side springs’ are given in Table 3. The basin east of the subsurface water divide extends mainly into Syria and drains towards the Yarmouk River.

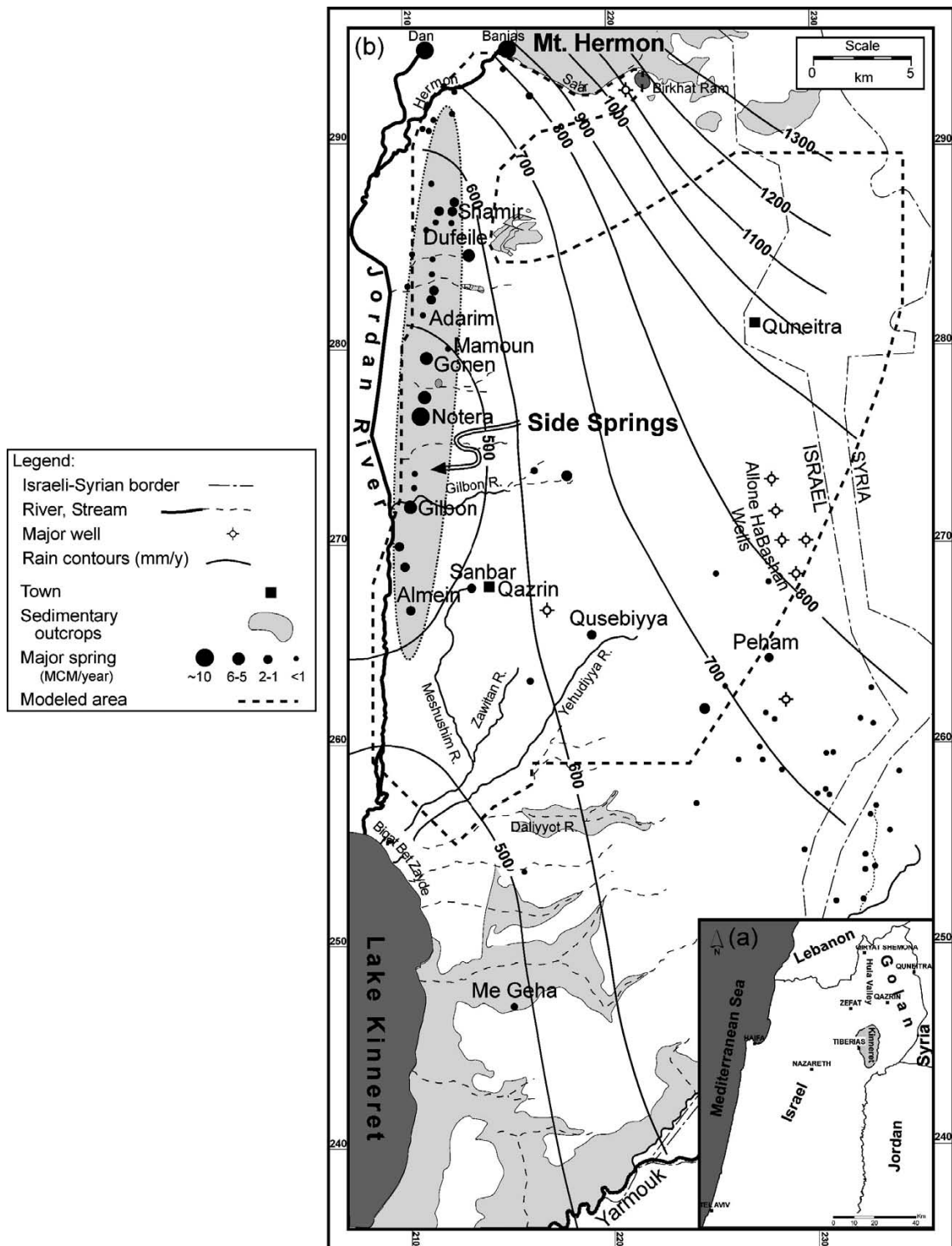


Figure 14: (a) Location map and (b) hydrological background map (DAFNY et al., 2006) showing major springs, major streams and rivers, major wells, yearly rain isohyets (1961–1990 average), sedimentary outcrops and the computerized model boundaries defined by DAFNY et al. (2003). MCM/year equals 10^6 m^3 per year.

The flow regime of the Golan “Side springs” is controlled by two types of aquifer: a regional basalt aquifer and several local perched aquifers that developed on interbedded paleosols.

Table 3: Major “Side springs” fed by recharge on the Golan Heights and their corresponding average annual yields (MICHELSON, 1996).

Spring	Annual yield 10^6m^3	Altitude m a.s.l.
Dupheila	6.1	300
Ela	0.5	75
Shamir & Hamroniya	4.2	200
HaRofe	0.5	120
Lehavot	1.6	130
Gonen	5.8	155
Divsha	5.7	168
Notera	10.5	95
Gilabun	6.0	110
Elmin Jedida	1.8	170
Durijat	1.1	110

3.5.4 Naftali Mountains

The Naftali Mountains border the Upper Jordan River catchment towards the east. The densely faulted rock outcrops belong to the Judean Limestone Group and consist mainly of limestone, dolostones and some chalks and marls. These rocks overlay the Albian Tzalmon Formation and underlie the Senonian Mount Scopus Group. The sequence reaches a thickness of about 700 m (GERSON, 1974).

The hydrogeology of the area was described by GERSON (1974) and GILAD (1988a). The limestone aquifer is drained by several springs that emerge along the Rift Valley fault line. The major ones are the Enan springs and the Te'o spring which emerge from different aquifers. Additional springs in the area have become partly dry due to the drainage of the Hula Valley and intensive pumping. Available mean annual yields of springs in the Naftali Mountains are given in Table 4.

As compared to the karst systems of Mount Hermon, the Upper Galilean karst is less evolved, which results from rapid saturation of water in the uppermost portion of the karst system, high evaporation and tectonic instability in the past leading to the rapid uplifting of rocks and insufficient time for karst evolution (GERSON, 1974). Karst depressions have developed mostly on fault lines restricted to areas with moderate initial slopes.

Table 4: Springs fed by recharge on the Naftali Mountains and their corresponding average annual yields (MICHELSON, 1996).

Spring	Annual yield 10^6m^3	Altitude m a.s.l.
Zahav	4.30	138
Te'o	4.75	70
Enan	no data	no data
Qadesh	no data	440

3.6 HYDROLOGY

The **Upper Jordan River Catchment (UJRC)** is part of the Jordan River network, which additionally comprises the watersheds of Lake Kinneret, the Yarmouk River, the Zarqua River and the Lower Jordan River. Three major tributaries (and a few minor) contribute to the Upper Jordan River: the Dan, Hermon and Senir streams (Figure 8, Figure 15).

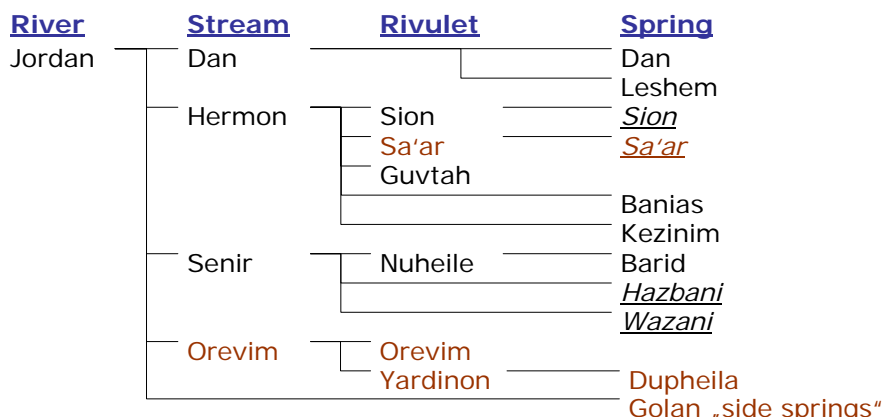


Figure 15: Scheme of the Upper Jordan River and its main tributaries (Dan, Hermon, Senir). Additionally given are rivulets and springs investigated within this study. Springs that are underlined and given in italic letters were not accessible for sampling.

The orographic catchment area of the **Dan stream** is virtually zero since it is mainly fed by the Dan spring, which turns into a broad, gushing rivulet in the immediate vicinity of the source. This spring has a mean discharge volume of $254 \text{ } 10^6 \text{m}^3$ per year and is one of the largest karst springs in the region. One of the smaller springs emerging from the same horst structure and contributing to the flow of the Dan stream is the Leshem spring (Figure 15). The

hydrographs recorded at the Dan gauging station (HSI 30131) are influenced by upstream water withdrawals.

The **Hermon** tributary has a surface drainage area of 158 km² at its gauging station. The steep gradient that characterizes the Hermon stream, led to the development of deep canyons with a number of rapids and waterfalls. The river is fed by its two main springs, Banias and Kezinim as well as by its three intermittent tributaries Guvtah, Sa'ar and Sion (Figure 15).

The **Senir** stream has a surface drainage area of 563 km², which lays mainly in Lebanon. The major gauging station is situated approximately 20 km downstream from the main contributing springs and also records minor contributions of the Nuheile surface drainage area (7.6 km²) and the outlet of a number of fishponds receiving its water originally from the Dan River. The mean discharge volume is 108 10⁶m³ per year.

Table 5: Hydrological classification numbers of the main Jordan tributaries in the Upper Jordan River Catchment. Data provided by the HSI.

	Dan*	Hermon	Senir	Orevim	Dishon	Hazor	Jordan
period	1969- 2000	1969- 2000	1969- 2000	1985- 2000	1984- 2000	1986- 2000	1991- 2000
station no. (HSI)	30131	30128	30122	30155	30165	30170	30175
AMaF [m ³ /s]	12.4 8/2/1993	38.6 2/6/1992	107.0 12/2/1994	12.9 2/6/1992	9.2 2/4/1992	2.6 2/8/1995	126.1 2/6/1992
MHF [m ³ /s]	8.5	5.5	8.0	0.7	0.37	0.10	22.0
MF [m ³ /s]	8.0	3.3	3.4	0.2	0.08	0.01	13.6
MLF [m ³ /s]	7.7	2.5	2.1	0.1	0.01	0.00	10.3
AMiF [m ³ /s]	3.2 12/19/1990	0.7 9/6/1999	0.5 12/13/1999	0.0	0.00	0.00	2.8 6/16/1999
volume [10 ⁶ m ³]	254	105	108	6	2.63	0.34	430
surface drainage [km ²]	0	158	563	40	91	32	1380
yield [L/s km ²]		21.1	6.1	4.6	0.92	0.33	9.9
runoff [mm/d]		1.8	0.5	0.4	0.08	0.03	0.9

*Discharge values are corrected for amounts pumped upstream of the gauging station (data supplied by Alon Rimmer, Kinneret Limnological Laboratory).

AMaF = Absolute Maximum Flow, MHF = Mean annual High Flow, MF = Mean annual Flow, MLF = Mean annual Low Flow, AMiF = Absolute Minimum Flow.

Within the focus of this study is also the **Orevim** stream that emerges in the basaltic Golan Heights and represents the combined discharges of the Yardenit stream and Wadi Orevim (Figure 15). While the perennial Yardenit stream is fed by the Dupheila spring, Wadi Orevim

is intermittent and responds to strong and intense precipitation. The mean annual yield of the Orevim stream is about $6 \cdot 10^6 \text{ m}^3$. Pumping from the Dupheila spring provides water to Kibbutz Shamir and upstream of the Orevim stream locates a small reservoir collecting water during precipitation events.

Classification numbers of the upper Jordan River, its major headwaters and two intermittent streams emerging in the Naftali Mountains are given in Table 5. Referring only to the known surface drainage areas, specific discharges of the subcatchments vary according to their respective geological and meteorological conditions. Precipitation amounts are highest over the northern part of the UJRC leading to significantly bigger yields for the headwaters Dan, Hermon and Senir. While the orographic catchment area of the Dan spring is zero, its actual groundwater basin is unknown thus making it difficult to determine its specific yield. Estimates of the catchment area of the Dan spring based on hydrographic and tracer investigations are given within this thesis (see chapter 6.4.2). Comparing the Hermon and Senir streams shows that despite the small catchment area of the Hermon stream, its yield is considerably higher than that of the Senir stream. While the Hermon stream drains a mountainous catchment area, the Senir stream receives its major contributions from the Beka'a Valley. Hence, recharge derived from the melting of the snow cover on Mt. Hermon might be the reason for a higher specific yield in the Hermon stream. Furthermore, the groundwater basin of the Hermon stream might significantly exceed the surface drainage basin in size.

The annual hydrological regime of the different tributaries varies considerably (Figure 16). The streams Dan, Hermon and Senir can be classified as Mediterranean *pluvio-nival* systems that are governed by rain and additionally influenced by snowmelt. Snowmelt recharge that continues during spring and early summer leads to an attenuated summer low flow. The steadiest hydrological regime has been observed for the Dan stream (spring) where the proportion of summer discharge (34 %) equals approximately the proportion of winter discharge (33 %). Flow declines below the long-term annual mean only by September. In addition, the comparison between the mean monthly discharges (MF) and the mean monthly

high discharges (MHF) (Table 5) indicate a balanced system that is ascribed to an extended groundwater basin area with favorable storage properties in a karst environment.

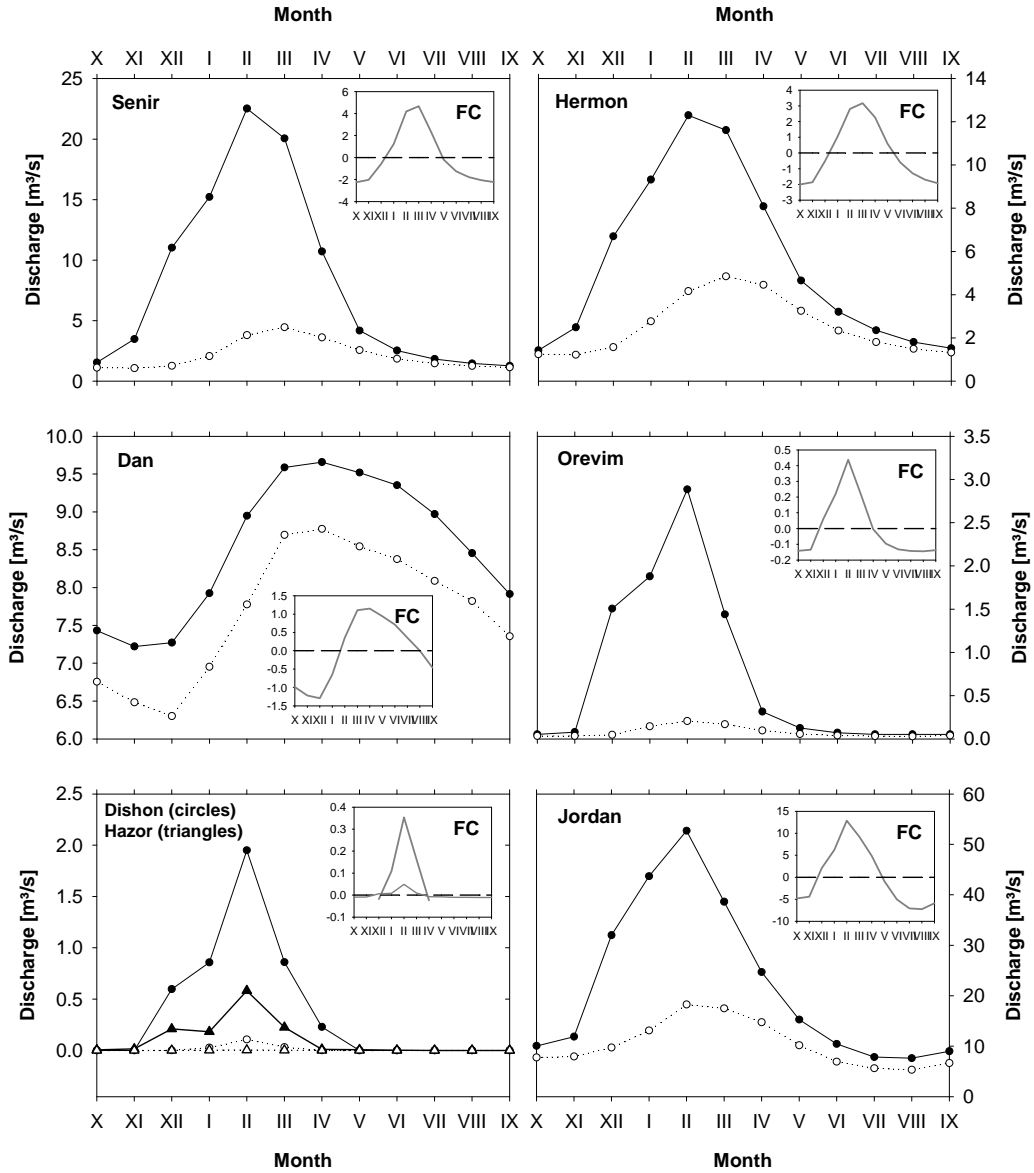


Figure 16: Hydrological regime and annual distribution of mean monthly flow (open symbols) versus mean monthly high flow (filled symbols) of the main waters in the Upper Jordan River Catchment. The fluctuation coefficient FC represents the mean monthly discharges compared to the long-term annual mean. The latter one is corresponding to the zero line (\cong mean). Based on data and periods of time summarized in Table 5.

The hydrological regimes of the Hermon and Senir stream reflect the precipitation patterns in the corresponding subbasins. About 56 % of the annual discharge in the Senir stream is generated during winter, 22 % during spring and 16 % during summer. In the Hermon stream, the seasonal discharge proportions are 49 %, 24 % and 20 %, respectively. The bigger amount

of discharge during winter and the higher variations in discharge throughout the years in the Senir stream point toward a more rain-fed system while the comparatively bigger proportions of spring and summer discharge in the Hermon stream show a bigger influence of snow melt contributions.

The Orevim stream fed by the basaltic aquifer as well as the Dishon and Hatzor streams rising in the Naftali Mountains are all characterized by an instantaneously responding *pluvial* system. Discharge culminates in February lagging the precipitation peak by about one month. Between March and April, discharge declines below the long-term annual mean. About 76 % of the annual discharge in the Orevim stream and 94 and 90 % respectively in the Dishon and Hazor stream are released during the 4-month winter period demonstrating the importance of direct runoff in these areas. While the Dishon falls dry during summer, the Hazor and Orevim recede to rivulets.

The Jordan River discharges a combination of these different regimes and is as well characterized by a Mediterranean pluvio-nival system with an attenuated summer low flow and the peak discharge lagging the rainfall maximum by one month. This lag month is most likely caused by the replenishing of subsurface reservoirs and by the time needed to reach antecedent soil moisture conditions within the catchments that allow for runoff generation.

3.7 HYDROCHEMISTRY

Several aspects of hydrochemistry were investigated in the Upper Jordan River Catchment. Generally, the groundwater of the springs emerging from the Arad Group aquifer – such as the Dan, Banias and Kezinim – are fresh waters of the Ca-Mg-HCO₃-type with low salinities. The NO₃ content in these fresh water sources was found to be below 10 mg/L and anthropogenic pollution seems to be negligible (KAFRI et al., 2002). Differences in the hydrochemistry of these springs are caused by changes in lithology, residence time of water and distance from the sea. The Banias spring for example differs significantly from the Dan spring in its hydrochemical characteristics which is caused by the different bedrocks of the respective intake areas. Thus, Banias water is characterized by higher contents of Cl, Li, Rb, Sr and V as well as higher equivalent SO₄/Cl and Na/Cl ratios. As mentioned earlier the

Banias intake area is known for its abundant basaltic volcanism, dolomitization, and mineralization within the aquifer, all of which are absent in the intake area of the Dan spring (SHIMRON, 1989, KAFRI et al., 2002).

GUR et al. (2003) studied the hydrochemistry of the main Jordan River sources with special emphasis on the Kezanim spring. Kezanim spring water is typified by higher TDS, SO₄, Sr, and Mg than Dan and Banias waters. Its hydrochemistry is characterized by dissolution proportions of 29 % dolomite, 48 % gypsum, and 23 % calcite based on mixing calculations. The Cover Basalt aquifer water sources are also of the bicarbonate type with higher amounts of Na than in the carbonate aquifers, derived from the basaltic host rocks. Salinities are low while the waters are characterized by high contents of SiO₂, Rb and V and a low equivalent ratio of rU/rCl (KAFRI et al., 2002).

Few researchers investigated the stable and radioactive isotope composition of the Upper Jordan River tributaries. GAT and DANSGAARD (1972) used the stable isotopes of water to develop a flow model for the Upper Jordan system. SIMPSON and CARMI (1983) distinguished, based on the evaluation of ¹⁸O measurements, different catchments for the main Jordan springs and reach the conclusion that interflow occurs in the near-surface part of the regional groundwater reservoir. Their tritium analyses suggest that 90 % of the groundwater is less than 3 years old. CARMI et al. (1985) investigated also the effect of atmospheric ¹⁴C variations on the ¹⁴C levels in the Jordan River system and determined the initial ¹⁴C activity of groundwater in this region to be about 44 % of the atmospheric isotopic composition.

NISSENBAUM (1978) conducted a study on the sulfur isotope distribution in sulfates of surface water in the Upper Jordan River Catchment. He concluded that the fresh water emerging north of Lake Kinneret represents almost exclusively sulfates derived from recharging rainwater. An exception is the Hermon river whose ³⁴S-enriched sulfates, especially in the summer, largely appear to originate from marine sulfate. This finding is confirmed by BURG et al. (2003), who found even more enriched sulfate in the Kezanim spring.

3.8 KNOWLEDGE GAPS AND RESEARCH NEEDS

Considering the importance of the Upper Jordan River Catchment in terms of water supply for the State of Israel, only few hydrogeological studies were conducted to investigate the dominating recharge and discharge mechanism and dynamics in this area. RIMMER and SALINGAR (2006) recently summarized existing gaps of knowledge concerning the Hermon region including:

- the amount of snow and rainfall on Mt. Hermon (due to the lack of meteorological stations in the upper part of the mountain) as well as the local rainfall distribution,
- a complete water balance for the region (due to the lack of data for springs, streams and meteorological parameters for Syria and Lebanon),
- aquifer characteristics such as: the thickness and boundaries of aquifers (*i.e.*, the actual subsurface area of the recharge areas), water level fluctuations, hydraulic characteristics (*i.e.*, conductivity and porosity), annual recharge as well as the location and subsurface recharge area,
- the quantitative evaluation of the discharge components.

Hence, this study addresses part of the open questions, in particular, I tried to qualitatively and quantitatively describe the different components involved in discharge generation in the UJRC. Additionally, the estimation of parameters that allow to evaluate the vulnerability of the UJRC water resources towards anticipated climate effects was aimed at. In particular, recharge rates, mean residence times, recharge areas and reservoir volumes were investigated.

4. Sampling network and sampling program

The sampling network and program was designed to understand the dominating runoff generation mechanisms, the contributing groundwater reservoirs, and their temporal and spatial variability by combining hydrological, hydrochemical and environmental isotopic methods. According to LEIBUNDGUT (1984) the discharge dynamics as well as physical, hydrochemical and isotopic properties of a system are determined by its physiographic and geologic settings. Thus, any information about the system is enclosed in its discharge and is observed at the observation gauge. To decode this information tracerhydrological and traditional methods have to be applied. The resulting information will then represent area- and time-integrated properties of the particular catchment.

Main objective of this work is to determine the influence of global climate change on water resources in the Upper Jordan River catchment. Consequently, the four major sampling stations were predefined to be located at the major headwaters of the Jordan River, near existing gauges. An additional station was installed at the Sion stream, since this is an intermittent rivulet predominantly fed by rain and snowmelt in a karstic catchment located in the upper regions of the Israeli Hermon Mountains. Moreover, a gauging station of the HSI at this location enabled for recording of a continuous stream hydrograph, a precondition for the intended analysis. The sampling network is detailed in Table 6 and shown in Figure 8. Most stations were equipped with programmable liquid samplers (ISCO Inc., Lincoln, NE), the sampling interval was adjusted according to the discharge behavior. Sampling was intensified during rising discharge and peak flow and reduced during recession flow. Additionally, electrical conductivity and temperature were monitored continuously in intervals from 1 hour to 10 minutes. For storm events, samples were analyzed for a variety of parameters including ^{18}O , ^2H , major anions, major cations, SiO_2 , DOC and TSS. The monitoring of stable isotopes and major anions/cations was pursued also during low flow conditions, however only weekly to monthly timesteps were retained.

Table 6: Streamflow sampling network in the UJRC and sampling frequency. Coordinates are given according to the New Israeli Grid. Station numbers are according to the Hydrological Service of Israel (HSI).

Sub catchment	Easting	Northing	Station (HSI)	Sampling	Period	Interval
	km	km				
Dan	260.80	794.55	30131	ISCO sampler, EC, T	11/02-05/04	up to 1 hour
Hermon	260.25	791.31	30128	ISCO sampler, EC, T	11/02-05/04	up to 1 hour
Senir	257.70	792.20	30122	ISCO sampler, EC, T	11/02-05/04	up to 1 hour
Orevim	260.12	783.75	30155	ISCO sampler, EC, T	11/03-04/04	up to 1 hour
Sion ^E	263.16	795.12	30118	manually ISCO sampler	12/02-06/03 12/03-04/04	up to 1 day up to 1 hour
Sa'ar ^E	266.00	793.83	30124	manually	12/02-04/04	weekly
Guvtah ^E	264.89	795.00	-	manually	11/02-03/04	weekly
Nuheile ^E	259.50	797.73	-	manually	11/02-06/04	weekly

E = runoff event based

EC: continuous registration of electrical conductivity, T: continuous registration of temperature.

The necessary hydrometric measurements were provided by the Hydrological Service of Israel (HSI) that is operating stage recorders at the major tributaries in the area (see Figure 8).

Rain amounts and rain composition are one of the predefined end-members for the intended tracer-based hydrograph separation; they are known to be subject to a high spatial and temporal variability in mesoscale ($= 10^{-1}$ to 10^3 km^2) catchments. Thus, the rain-sampling network required to be designed in a way that a representative input function was received for the particular period under consideration. Still the sampling network needed to be a compromise between the call for representative sampling (exhaustive) and the call for feasibility (point sampling).

To receive an input function that sufficiently describes spatial heterogeneity of precipitation within the UJRC, at least one sampler at a time representative for each of the investigated subcatchments was installed. Additional rain samplers were set up along altitude gradients to account for isotopic and chemical properties of rains. The precipitation sampling network is

detailed in Table 7 and shown in Figure 17. Rain samplers were constructed in a way that evaporative effects on rain samples were minimized, yet the intrusion of dust especially into the bulk samplers could not be prevented. However, these effects were much smaller for daily samples.

Table 7: Rainfall sampler locations in the UJRC and sampling intervals, (W: weekly, D: daily). Coordinates are given according to the New Israeli Grid.

Location	Altitude m a.s.l.	Easting km	Northing km	Sub catchment	Sampling	Period
Moshav Shear Yeshuv	100	261.00	793.10	Dan/Hermon	W/D	2002-04
Kibutz Mayan Barukh	200	256.99	793.97	Senir	W/D	2002-04
Tel Dan Nature Reserve	227	260.94	794.57	Dan	W/D	2002-04
Banias Nature Reserve	360	265.09	794.74	Hermon	W/D	2002-04
Nimrod Nature Reserve	700	267.50	796.30	Hermon	W/D	2002-04
Moshav Neve Ativ	1000	270.50	796.50	Hermon	W	2002-04
Kibutz Shamir	200	262.20	786.20	Orevim	W	2002-04
Orevim – tap road	810	264.70	785.00	Orevim	W	2003-04

The temporal variability during single rain events plays an important role in tracer-based hydrograph separation, especially if stream response is fast. Both, temporal variability during single rain events and quick stream response were observed in the considered sub catchments. Therefore, it was originally planned to install two additional sequential rain samplers, yet that turned out to be logically impossible during the course of this project.

The spatial variability of snow's chemical and isotopic composition was accounted for by frequent sampling of fresh fallen snow along several snow transects. Transects were chosen such, that altitude gradients in chemical and isotopic composition of snow could be determined. For other effects, such as due to the location of sample in drift or non-drift areas could not be accounted for. Isotopic homogenization of snow packs and progressive enrichment of ^{18}O in snowmelt are known phenomena (STICHLER, 1987, TAYLOR et al., 2001). To study the former, a snow pit was dug and different snow layers were sampled twice during the season 2003/04. The temporal development of snowmelt, especially information such as the beginning of snowmelt, snowmelt amounts over time or the isotopic enrichment of snowmelt are generally important input functions for the separation of snowmelt from the

stream hydrograph. Yet, this exceeded the scope of this project and has to be addressed in succeeding projects for example by the installation of snowmelt lysimeters in representative areas.

The design of the **groundwater** sampling program was based upon earlier works by GILAD and BONNE (1990), DAFNY et al. (2003) and GUR et al. (2003) and was intended to shed further light on the hydrogeological characteristics of the predominant groundwater source areas. Springs were selected according to their discharge behavior, as well as their bulk hydro- and physico-chemical characteristics. Thus sampling focused on the major headsprings of the Upper Jordan River as well as the 'Side springs' emerging in the Golan Heights which are also significantly contributing to the Upper Jordan River. While springs were sampled at least on a seasonal basis (see Table 8), four of the springs were sampled on a monthly basis. During high flow conditions, sampling was intensified to weekly or even daily sampling. Due to logistic reasons, sampling was interrupted for three months during summer 2003.

Table 8: Locations of groundwater sampling and sampling program. Coordinates are given according to the New Israeli Grid. N is the number of samples taken.

Spring	Altitude m a.s.l.	Easting km	Northing km	Station (HSI)	Sampling	Period	n
<i>Hermon springs</i>							
Dan	180	260.95	794.92	-	monthly**	10/02-07/04	66
Leshem	180	261.10	794.90	-	monthly**	10/02-07/04	67
Banias	390	265.20	794.90	30250	monthly**	10/02-08/04	60
Kezinim (Ain Hilu)	340	264.50	794.70	-	monthly**	11/02-07/04	46
Sion	800	268.00	800.10	-	snowmelt	13/03/04	3
Barid	243	260.95	796.25	30308	seasonal	02/03-07/04	5
<i>Golan springs</i>							
Hamroniya	210	262.40	787.00	30439	seasonal*	10/02-07/04	17
Dufaila	300	263.20	784.50	30474	seasonal*	10/02-07/04	18
Gonen	155	261.02	779.52	30515	seasonal*	10/02-07/04	14
Divsha	170	260.90	777.32	30535	seasonal*	10/02-07/04	14
Notera	90	260.60	772.20	30538	seasonal*	10/02-05/04	18
Jalabina	90	260.50	772.10	30568	seasonal*	10/02-07/04	14
Bet HaMekhes	110	259.40	768.60	30575	seasonal*	10/02-07/04	14
Elmin Jedida	170	260.20	766.70	30580	seasonal*	10/02-07/04	14

*up to monthly

** up to weekly

Since most of the springs are part of nature reserves or protected areas, permission for sampling was granted by the Society for the Protection of Nature in Israel (SPNI). Springs were monitored in situ for temperature and electrical conductivity; pH and alkalinity were determined in the lab on the day of sampling. All samples were analyzed for ^{18}O , ^2H , major anions and cations. Additional parameters determined were SiO_2 and DOC. To receive further information about the distribution of mean residence times in the groundwater source areas, the majority of springs was sampled on reference dates in autumn 2003 and 2004 for tritium analysis. During this season, baseflow dominates the hydrograph. Another reference date sampling for ^{13}C - and ^{14}C -analysis was conducted in July 2004. In addition, a selection of samples was analyzed for major elements by inductively coupled plasma mass spectrometry (ICP-MS).

All the necessary hydrometric measurements were provided by the Hydrological Service of Israel (HSI) which is operating stage recorders at the major tributaries in the area (see Figure 8) and which is regularly conducting flow measurements at the majority of springs in the region.

Meteorological parameters such as radiation, temperature, relative humidity, and precipitation were downloaded from the Mop Zafon website (<http://www.mop-zafon.org.il/> csv/index.html, in Hebrew), an organization which operates a meteorological network in the Upper Galilee region for agricultural purposes. Sequential rainfall data were provided by the Crop Ecology research group (Moshe Meron, Joseph Tsipris) of the MIGAL Galilee Technology Center, Israel, which is also part of the Mop Zafon network. Data on wind speed and direction in northern Israel were extracted from the database on air quality of the Israeli ministry of environment (see <http://avir.sviva.gov.il/DocGenerator.asp>, in Hebrew). Weather and snow forecasts were retrieved from <http://www.israelweather.co.il> website (in Hebrew and English).

Unfortunately, there is currently no fully equipped weather station on Mt. Hermon itself, leading to uncertainties considering the climatic conditions on high altitudes.

5. Hydrochemical and stable isotopic characterization of precipitation in the mountainous northern Upper Jordan River Catchment

A preliminary condition for applying tracer-based hydrograph separation techniques and end-member mixing analyses to investigate the transformation of precipitation into runoff is the comprehensive description of the spatial and temporal variation of the input tracer concentration, i.e. the chemical and isotopic composition of precipitation. Hence, from October 2002 to September 2004, the isotopic and chemical composition of precipitation and its temporal and spatial distributions was investigated for the semi-arid mountainous northern Upper Jordan River Catchment (UJRC), Israel.

The amount of precipitation and its isotopic and chemical composition determined at a certain measuring station depends on parameters such as the prevailing synoptic system, topographic features, or the altitude. Synoptic patterns in particular determine the stable isotopic signature of precipitation samples by isotope fractionation occurring during the evaporation of seawater and condensation of water vapor (DANSGAARD, 1964). On a global scale, the stable isotope (^{18}O , ^2H) composition of precipitation is described by the so-called global meteoric water line (GMWL) equation:

$$\delta^2\text{H} = 8 \cdot \delta^{18}\text{O} + 10 \text{ (CRAIG, 1961).}$$

Local meteoric water lines (LMWL) have to be established to account for regional variabilities in precipitation and isotopic fractionation processes during evaporation and condensation of air humidity along weather trajectories. Particularly when runoff events are investigated, it is necessary to know the short-term temporal heterogeneity of the stable isotope composition in rain or snow (see chapter 2.4.4.3). Thus, the objectives of this part of the study were to a) characterize the isotopic composition of precipitation by establishing a local meteoric water line for the northern UJRC, b) to compare it to other LMWLs found in the region, and c) to investigate specific factors determining the spatial and temporal variability of precipitation and its isotopic as well as chemical pattern.

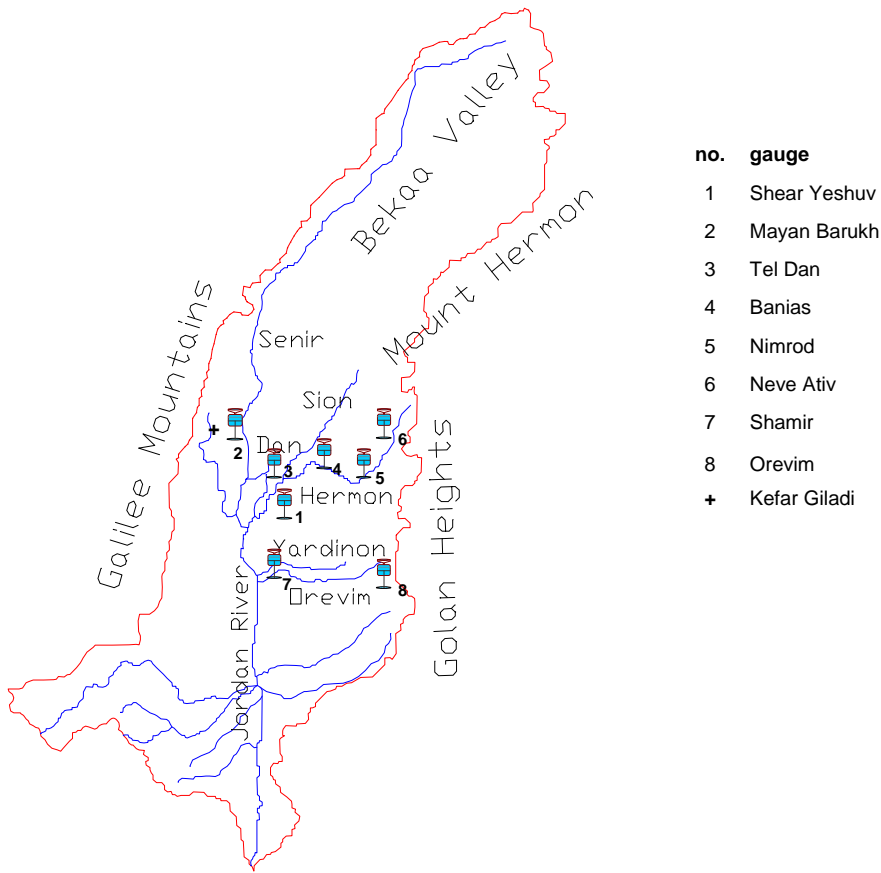


Figure 17: Precipitation sampling network in the Upper Jordan River catchment. Modified from EXACT (1998).

5.1 OROGRAPHIC PRECIPITATION

Records on the amounts of rain during the study period 2002-2004 were available for 16 stations in the UJRC provided by the Israeli Meteorological Service and the Mop Zafon network (chapter 4). The distribution of sampling stations setup in the scope of this study within the UJRC is shown in Figure 17. Additionally, a long-term record of monthly rain data was accessible for the station at Kefar Giladi. Based on this record the 5th-, 25th-, 50th-, 75th- and 95th-quantiles of the accumulated rain during the period 1969-99 were calculated to investigate the distribution of precipitation over time.

Table 9: Quantiles of accumulated rain amounts at Kefar Giladi for the period 1969-1999.

quantile	[%]	5	25	50	75	95
rain	[mm]	480	619	772	937	1117

The data summarized in Table 9 suggest that only 5 % of the considered rain years had less than 480 mm of accumulated rain. Comparing the rain data of the study period to the quantile values shows that the hydrological year 2002/03 was an extreme rain year with an amount of 1117 mm (Kefar Giladi), which is exceeded in only 5 % of the cases. On the other hand, the hydrological year 2003/04 was characterized by rain amounts just below the average.

Table 10: Location of stations in the UJRC and accumulated quantities of rain measured during the period 2002-2004. Correlation of the station-characteristic rain amount with data recorded at Kefar Giladi. Coordinates are given in the New Israeli Grid.

Location	Altitude m a.s.l.	Easting km	Northing km	Rain 2002/03 mm	Rain 2003/04 mm	r
Kefar Giladi	340	254	794	1117	699	
Mayan Barukh	240	257	794	989	702	0.980**
Dafna	150	260	793	964	725	0.955**
Tel Dan	160	260	793	1037	737	0.951**
Kefar Blum	75	257	786	689	429	0.944**
Banias	375	265	794	1031	673	0.943**
El Rom	1046	272	787	1506	932	0.905**
Merom Golan	940	276	781	1360	no data	0.890**
Neot Mordekhay	75	255	785	972	579	0.889**
Ayyelet HaShahar	175	254	769	669	463	0.878**
Har Kenaan	934	247	764	969	707	0.866**
Ged Sade	180	253	791	929	640	0.793**
Bet Seida	180	259	757	636	403	0.790**
Gadot	100	258	769	575	437	0.773**
Pichmann	1100	276	792	1333	932	0.746**
Matityau	700	243	774	1107	676	0.541**

**result is significant at a level of $p < 0.01$ (two-sided)

Rain depths of all available stations correlate significantly with rain at Kefar Giladi (Table 10), though this correlation seems to diminish with increasing distance from this station.

A clear disadvantage of this study is the lack of continuous rain measurements on Mt. Hermon at altitudes higher than 1000 m a.s.l. To overcome this gap of information, rain depths are generally estimated by geostatistical methods. However, the lack of area-wide topographical data in particular forced a more simple approach. Hence rain depths were estimated based on multiple regression analysis, which accounted for the topographic location of rain stations. As a result, rain amounts in the UJRC were found to be a function of altitude

and latitude. Although latitudes are seldom used to explain the distribution of precipitation, latitude dependent variability in precipitation was shown among others by LEGATES and WILLMOTT (1990). The State of Israel is characterized by a distinct north-to-south climate gradient, hence, it seemed reasonable to introduce latitude into the regression analyses to explain the observed variabilities in precipitation.

Simple regression analysis for the dependent variable *rain* and the independent variable *altitude* resulted in correlation coefficients of 0.78 and 0.74 for the hydrological years 2002/03 and 2003/04 respectively. Including *latitude* (northing) into the regression analysis led to an even stronger correlation with $r = 0.939$ and $r = 0.946$ correspondingly. Adding longitude to the model did not improve the correlation. Thus, the following empirical relationships were established:

$$\text{Rain (2002/03) [mm]} = 0.56 \text{ Altitude [m a.s.l.]} + 11.3 \text{ Latitude [km]} - 8109$$

$$\text{Rain (2003/04) [mm]} = 0.34 \text{ Altitude [m a.s.l.]} + 7.6 \text{ Latitude [km]} - 5447$$

According to these equations, the amounts of rain were estimated for three stations on Mt. Hermon and are given in Table 11. Recently, a meteorological station collecting data on quantities of rain and snow, air temperature, wind direction and speed has been installed at Mount Hermon at an altitude of about 2000 m and will provide new insight into the distribution of precipitation in the recharge area of the Upper Jordan River.

Table 11: Rain depths at Mount Hermon during 2002-04. Results were estimated by multiple regression analysis. Coordinates are given according to the New Israeli Grid. Easting not shown.

Location	Northing	Altitude	Rain 2002/03	Rain 2003/04
	km	m a.s.l.	mm	mm
Majdal Shams	797	1170	1552	1008
Mizpe Shlagim	803	2224	2210	1412
Mount Hermon	815	2814	2676	1704

SIMPSON and CARMI (1983) used a linear extrapolation between rainfall depth and altitude to estimate precipitation on the summit of Mt. Hermon to exceed rain depths at Majdal Shams

by 50 %. Based on multiple regression analyses conducted in this study, precipitation at Mount Hermon exceeds rain depths at Majdal Shams even by about 70 %. At watershed scale, more complex methods that include data on terrain slope, wind speed or advection models were used to predict orographic precipitation. For further information, see DALY et al., 1994; MARQUINEZ et al., 2003; SMITH, 2003; SMITH et al., 2003; ALPERT and SHAFIR, 1989a.

5.2 CHEMICAL COMPOSITION OF PRECIPITATION

The chemical composition of rain water, in particular the concentrations of major anions and cations, is an important input variable for the intended mass-balance approaches and mixing models. Yet, continuously monitoring of precipitation chemistry was not in the scope of this study. In this study, 92 samples were collected and analyzed to describe the mean chemical composition of precipitation in the study area. Table 12 provides both, the mean and median ion concentrations and electrical conductivities, for two rain stations (Banias, Tel Dan) and snow on Mount Hermon. For comparison, the chemical composition of precipitation in the Golan region as reported by HERUT et al. (2000) is included. Besides the mean values assumed to be normally distributed, median values are also given because they account much better for the low number of samples and the asymmetric distribution of ion concentrations.

Table 12: Median and mean ion concentrations of daily rain samples and snow in the UJRC. Sampled rain amounts were too small to analyze for HCO_3^- .

Location	n	Na^+	K^+	Ca^{2+}	Mg^{2+}	SO_4^{2-}	Cl^-	NO_3^-	HCO_3^-	EC
		$\mu\text{eq/L}$	$\mu\text{eq/L}$	$\mu\text{eq/L}$	$\mu\text{eq/L}$	$\mu\text{eq/L}$	$\mu\text{eq/L}$	$\mu\text{eq/L}$	$\mu\text{eq/L}$	$\mu\text{S/cm}$
Banias	Median	27	80	6.6	312	38	54	101	19	n.d.
	Mean		144	16	430	60	70	128	35	n.d.
Tel Dan	Median	23	83	5.1	157	38	48	79	19	n.d.
	Mean		163	9.0	225	49	62	120	26	n.d.
Snow (Mt. Hermon)	Median	42	30	2.8	33	35	19	37	23	350
	Mean		58	4.7	70	58	19	73	21	420
Golan (HERUT et al., 2000)	Median	36	56	4.7	42	24	73	68	17	n.g.
	Mean	-	111	6.7	116	50	85	128	30	47

n.d.: not determined, n.g.: not given.

Analyses of snow (and rain) revealed the following ion sequences at the southeastern footslopes and on higher altitudes of Mount Hermon: $[\text{Ca}^{2+}] > [\text{Na}^+] > [\text{Mg}^{2+}] > [\text{K}^+]$ and

$[\text{HCO}_3^-] > [\text{Cl}^-] > [\text{SO}_4^{2-}]$ (while HCO_3^- was not analyzed in the rain samples). This sequence is identical to results obtained by NATIV and MAZOR (1987) for the Maktesh Ramon basin (Negev). In snow samples, ion sequences were similar but ion concentrations tend to be much lower than those measured at Dan and Banias Nature Reserve. In the Golan Heights, HERUT et al. (2000) observed a different pattern with: $[\text{Na}^+] > [\text{Ca}^{2+}] > [\text{Mg}^{2+}] > [\text{K}^+]$ and $[\text{Cl}^-] > [\text{SO}_4^{2-}] > [\text{HCO}_3^-]$. For precipitation in Israel, two distinct sources for dissolved ions are inferred. First, Ca^{2+} and HCO_3^- are attributed to dust derived from chalk and limestones as shown by GANOR and MAMANE (1982) and NATIV and MAZOR (1987), second, Na^+ , Mg^{2+} , Cl^- and SO_4^{2-} are assumed to derive from cloud-borne sea spray. Hence, the absence of carbonate rock sources in the Golan Height explains its sea-salt dominated rain chemistry. Considering the rain sampling technique used, the influence of local over regional dust patterns on rain water composition cannot be entirely excluded.

5.3 STABLE ISOTOPE COMPOSITION OF PRECIPITATION

5.3.1 Mean isotope composition and the local meteoric water line

Both, the arithmetic and the amount-weighted means of stable isotope composition were determined for 268 daily rain samples from five stations and 118 weekly bulk samples from eight stations (Figure 17) given in Table 13 and Table 14. The amount-weighted means for each of the sampled stations were calculated according to YURTSEVER and GAT (1981) with:

$$\delta_w = \sum_i^n [p_i \cdot \delta_i] \Big/ \sum_i^n [p_i]$$

where δ_w = amount-weighted mean, p_i = amount of weekly or daily precipitation, respectively and δ_i = isotopic composition of rainfall for the week or the day i . The standard deviation $\sigma(\delta_w)$ of the amount-weighted mean values δ_w , were calculated as follows:

$$\sigma(\delta_w) = \left\{ \sum_i p_i \cdot (\delta_i - \overline{\delta_w})^2 \Big/ \left[\sum_i p_i \cdot \left(\sum_i p_i - 1 \right) \right] \right\}^{1/2}$$

The arithmetic mean isotopic composition of $\delta^{18}\text{O}$ and $\delta^2\text{H}$ in daily rainfall samples was determined with -5.71 ‰ and -25.1 ‰ , respectively. Values range between -13.02 ‰ and

2.31 ‰ for $\delta^{18}\text{O}$ and -82.6 ‰ and 24.3 ‰ for $\delta^2\text{H}$. Similar isotopic compositions are found in weekly rainfall samples where the mean concentration was -6.33 ‰ and -28.8 ‰ for $\delta^{18}\text{O}$ and $\delta^2\text{H}$. More depleted concentrations were found for stations at higher altitudes such as Nimrod and Neve Ativ (Table 13, Table 14) while extreme enriched values can be attributed to evaporative effects. The mean deuterium excess in the northern UJRC rains, *i.e.* 20.59 ‰ and 21.86 ‰ for daily and weekly samples respectively, equals the one determined for the eastern Mediterranean meteoric waters ($d = 22$ ‰).

Table 13: Arithmetic mean (δ) and amount-weighted (δ_w) mean stable isotope composition of daily rainfall in the northern UJRC. Also, the deuterium excess (d) is given each. Stations are arranged according to increasing altitudes (see Table 7). Samples were taken during 2002-2004.

Location	n	$\delta^{18}\text{O}$ ‰	$\pm\sigma$ ‰	$\delta^2\text{H}$ ‰	$\pm\sigma$ ‰	d ‰	$\pm\sigma$ ‰	$\delta^{18}\text{O}_w$ ‰	$\pm\sigma_w$ ‰	$\delta^2\text{H}_w$ ‰	$\pm\sigma_w$ ‰	d_w ‰	$\pm\sigma_w$ ‰
Mayan													
Barukh	43	-4.73	2.56	-19.9	18.3	18.0	6.3	-6.23	0.09	-29.2	0.8	20.7	0.22
Tel Dan	87	-5.76	2.55	-25.7	19.4	20.4	6.6	-6.63	0.06	-32.2	0.5	20.9	0.19
Shear Yeshuv	23	-5.81	2.23	-26.2	18.7	20.3	5.5	-6.57	0.11	-31.0	0.9	21.5	0.22
Banias	78	-5.66	2.69	-24.7	20.2	20.5	6.2	-6.64	0.07	-31.2	0.6	21.9	0.16
Nimrod	37	-6.75	2.57	-29.6	22.1	24.4	5.4	-7.31	0.09	-33.1	0.8	25.4	0.21

The amount-weighted stable isotope composition showed generally more depleted values (Table 13, Table 14) than the non-weighted indicating the importance and abundance of convective rain spells when strong convective motions result in the mixing of surface air with air from higher altitudes that is partially depleted in heavy isotopes (RINDSBERGER et al., 1990). Normally, there should be no differences between the mean values of daily or weekly amount-weighted isotope compositions given the same period of observation is covered. However, for several reasons full coverage both for daily as well as weekly samples was not achieved during this study, hence the differentiation.

Plotting $\delta^{18}\text{O}$ and $\delta^2\text{H}$ -values in a respective diagram showed that UJRC values generally plotted above the GMWL and the MMWL (Figure 18, Figure 19). The observed high deuterium excess of the samples is a common feature of Mediterranean precipitation and is attributed to isotopic exchange with the moisture originating from the Mediterranean Sea,

which is characterized by lower relative humidity conditions (DINCER and PAYNE, 1971, YURTSEVER and GAT, 1981). Generally, deuterium excess is highest at high altitudes and at the Golan stations.

Table 14: Arithmetic mean (δ) and amount-weighted (δ_w) mean stable isotope composition of weekly rainfall and snow in the northern UJRC. Also, the deuterium excess (d) is given each. Stations are arranged according to increasing altitudes (see Table 7). Samples were taken during 2002-2004.

Location	n	$\delta^{18}\text{O}$ ‰	$\pm\sigma$ ‰	$\delta^2\text{H}$ ‰	$\pm\sigma$ ‰	d ‰	$\pm\sigma$ ‰	$\delta^{18}\text{O}_w$ ‰	$\pm\sigma_w$ ‰	$\delta^2\text{H}_w$ ‰	$\pm\sigma_w$ ‰	d_w ‰	$\pm\sigma_w$ ‰
Mayan Barukh	8	-6.32	2.36	-31.3	17.8	19.2	3.5	-6.93	0.07	-35.1	0.6	20.3	0.1
Tel Dan	19	-6.12	2.15	-27.6	18.1	21.3	4.0	-6.43	0.04	-29.1	0.4	22.3	0.1
Shear Yeshuv	12	-5.62	1.92	-25.5	15.1	19.5	4.2	-6.32	0.05	-30.1	0.4	20.5	0.1
Banias	19	-5.84	2.65	-26.9	19.8	19.8	5.3	-6.71	0.04	-31.7	0.3	22.0	0.1
Nimrod	21	-6.63	2.45	-29.9	18.6	23.1	5.4	-7.43	0.04	-34.5	0.3	24.9	0.1
Neve Ativ	21	-7.37	2.47	-34.9	19.0	24.1	4.7	-8.13	0.04	-39.9	0.3	25.2	0.1
Shamir	10	-5.78	1.16	-24.1	11.1	22.2	5.3	-6.12	0.05	-27.0	0.5	21.9	0.2
Orevim	8	-6.24	1.66	-25.5	13.6	24.4	3.7	-6.53	0.06	-27.3	0.5	24.9	0.1
Snow	50	-7.59	1.63	-34.2	12.3	26.5	3.8						

The Local Meteoric Water Line (LMWL) was estimated by determining a least square regression line fitting all daily or weekly rain data collected during the study period. Accordingly, the LMWL of the northern UJRC is given by:

$$\delta^2\text{H} = (7.23 \pm 0.14) \delta^{18}\text{O} + (16.21 \pm 0.89) \text{ (daily rain)}$$

$$\delta^2\text{H} = (7.15 \pm 0.17) \delta^{18}\text{O} + (17.57 \pm 1.18) \text{ (weekly rain)}$$

Regression parameters are given with standard errors. The established LMWLs (which are not significantly different when comparing the regression parameters by t-tests) are characterized by slopes that are slightly lower than the MMWL and with lower intercepts. This is due to evaporation of precipitation on its way to the ground. Samples that plot below the GMWL have most likely undergone evaporation.

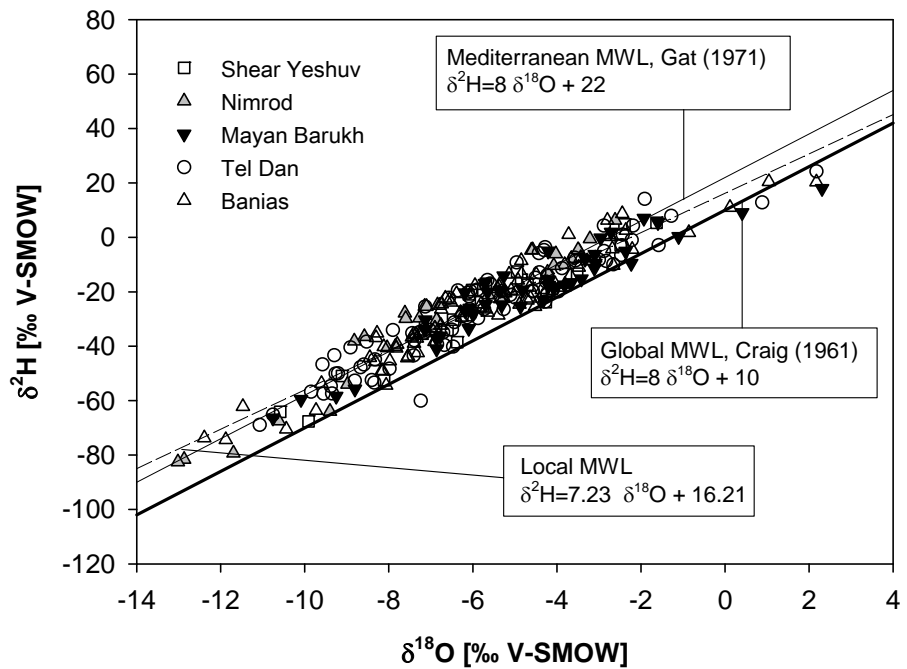


Figure 18: Stable isotope composition of precipitation in the northern UJRC. Relationship between $\delta^{18}\text{O}$ and $\delta^2\text{H}$ of daily rainfall in 2002-2004.

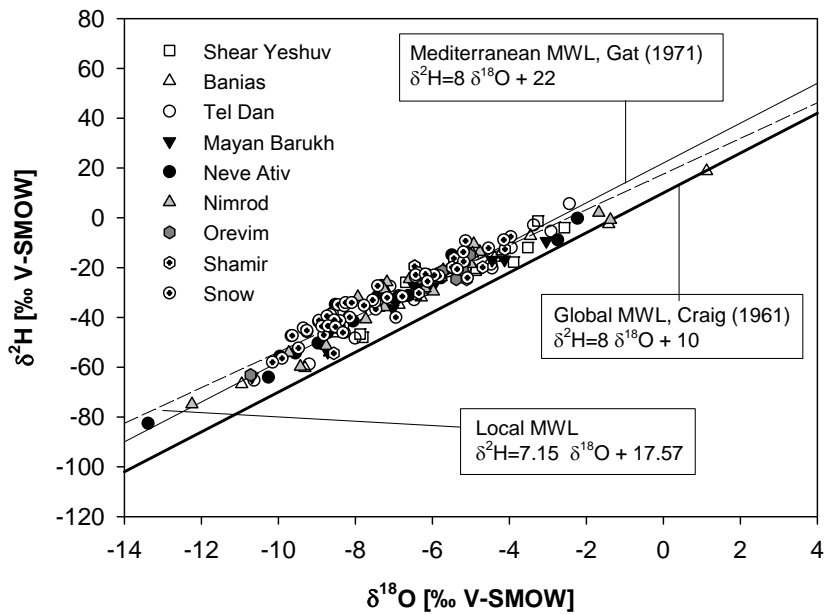


Figure 19: Stable isotope composition of precipitation in the northern UJRC. Relationship between $\delta^{18}\text{O}$ and $\delta^2\text{H}$ of weekly rainfall and snow in 2002-2004.

5.3.2 Seasonal variations

For the two-year period of observation, the collected isotope data demonstrated a pronounced monthly variation. In November, at the beginning of the rainy season when relative humidity is low, precipitation tended to be more enriched in heavy stable water isotopes. December rain showed the biggest variation considering its stable isotope composition. This variation is explained by the different origin of air masses since two types of synoptic systems, the *Red Sea Trough* and the *Winter Lows* (ALPERT et al., 2004a), dominate during that period (chapter 3.2.).

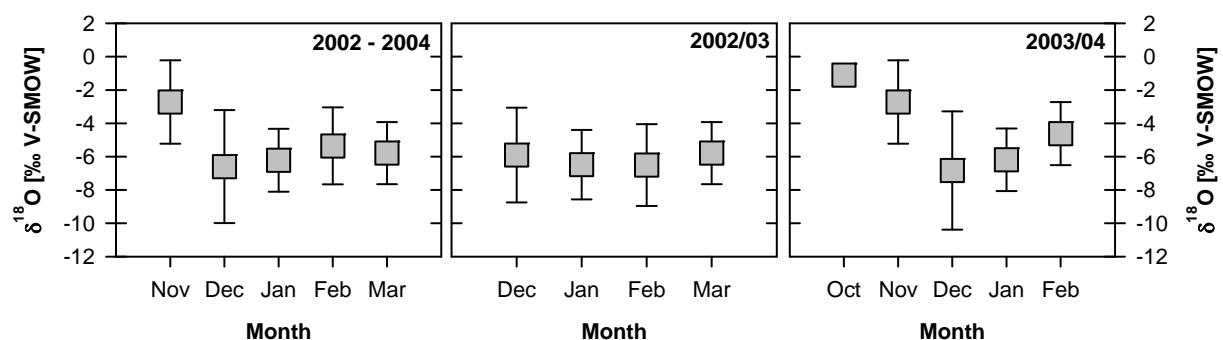


Figure 20: Monthly means of $\delta^{18}\text{O}$ in rainfall in the northern UJRC for the years 2002-2004.

The observed seasonal effects in the isotopic composition of precipitation varied throughout the years. While in 2002/03 the monthly variations were less distinct and ranged about a mean value of -6.19 ‰ $\delta^{18}\text{O}$, the 2003/04 rain season exhibited a distinct monthly pattern (Figure 20).

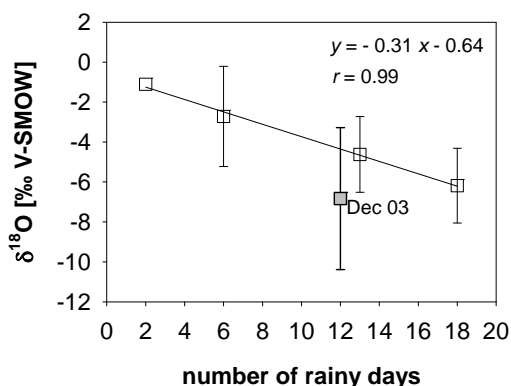


Figure 21: Relationship between the arithmetic mean monthly $\delta^{18}\text{O}$ values of all investigated stations and the number of rain days in the adequate month, rain season 2003/04.

In 2003/04, the isotopic composition of precipitation showed enriched values during autumn followed by gradual depletion later in the rainy season, and enriched again as the rain ceased. In fact, the mean monthly $\delta^{18}\text{O}$ composition significantly correlated with the number of rainy days in a month, emphasizing increasing evaporative effects as the number of rain days decreased. However, the $\delta^{18}\text{O}$ values in December clearly deviated from this relationship and thus were excluded from the regression (Figure 21).

5.3.3 Temperature and amount effect

Plotting $\delta^{18}\text{O}$ values of daily rainfall samples against the daily maximum air temperature revealed a positive correlation (Figure 22), in which increasing temperature resulted in high stable isotope ratios in rain water. A complete record of maximum and mean daily air temperature was only available for the Mop Zafon station at Qiryat Shemona (chapter 4). Expectedly, the correlation was most significant for rainfall samples taken at Mayan Barukh ($r = 0.53$) which is in short distance of the Mop Zafon station.

The effect is well known (DANSGAARD, 1964) and was widely used to trace seasonal recharge and to estimate mean residence times (SIEGENTHALER and OESCHGER, 1980; MALOSZEWSKI et al., 1983; UHLENBROOK et al., 2002; RODGERS et al., 2005).

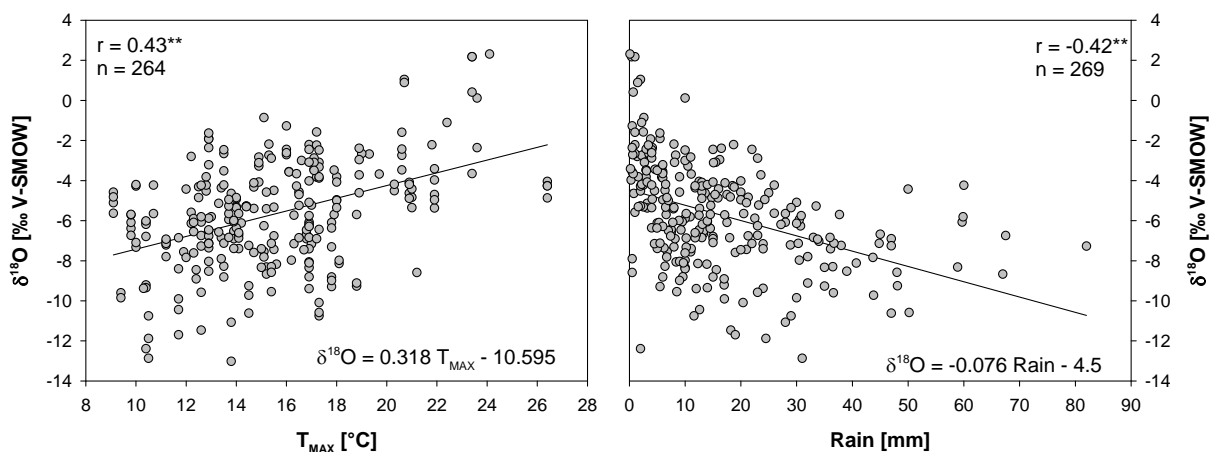


Figure 22: Relationship between $\delta^{18}\text{O}$ in rain water and maximum daily air temperature (left) and the daily rain depths (right) in the northern UJRC, in the years 2002-2004. “**” denotes that results are significant at $p < 0.01$ (two-sided).

The amount effect, representing the isotopic enrichment of precipitation with decreasing size of rainstorms, was clearly observed for the daily rainfall samples of the northern UJRC (Figure 22). The effect is especially observed during light rains or at the beginning of rainstorms, when precipitation passes an atmosphere of low relative humidity on its way to the ground.

Although the relationship between increasing rain amount and the depletion in $\delta^{18}\text{O}$ was significant ($p < 0.05$) for all the stations, it was most pronounced in Mayan Barukh, Tel Dan, and Banias, which might be due to number of samples.

5.3.4 Influence of wind direction

HERUT et al. (2000) investigated the effect of wind direction on the chemical composition of rain in Israel. They found that southern winds display higher continental contribution as depicted by higher pH and higher concentrations of non-sea-salt derived Ca^{2+} . This analysis was conferred to the isotopic composition of precipitation revealing a relationship between the origin and genesis of precipitation and the ^{18}O composition. Generally, northern winds were characterized by higher mean rain depths and more depleted $\delta^{18}\text{O}$ values (Figure 23). Highest mean rain depths and most depleted $\delta^{18}\text{O}$ coincided with north northeasterly and northwesterly winds.

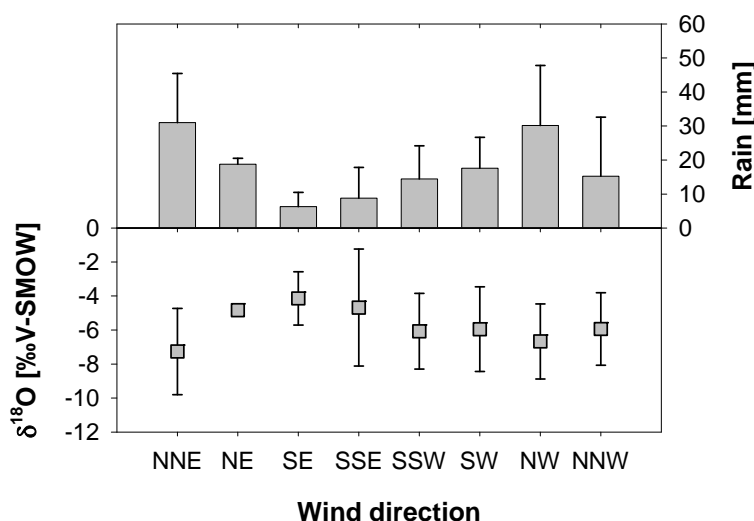


Figure 23: The distribution of the stable ^{18}O isotope composition of precipitation in relation to the prevailing wind direction and mean rain depths in the UJRC determined in this thesis.

Wind directions generally change according to the prevailing weather system. Thus, a subsequent step was to investigate the influence of synoptic systems on the isotopic pattern in precipitation provided by Alpert, 2006, personal communication.

5.3.5 The influence of the synoptic system

Most of the precipitation reaching the Eastern Mediterranean and thus the Upper Jordan River catchment during winter is caused by cold fronts and the air masses following these fronts (SHARON and KUTIEL, 1986; ALPERT et al., 1990; GOLDREICH and MOZES, 2004; ZIV et al., 2006). In particular, the passage of extratropical cyclones called *Cyprus Lows* brings significant rain amounts to the region. The rest of the annual rainfall events are associated with *Red Sea troughs* which are generally confined to the transitional seasons (GOLDREICH and MOZES, 2004, ZIV et al. 2006).

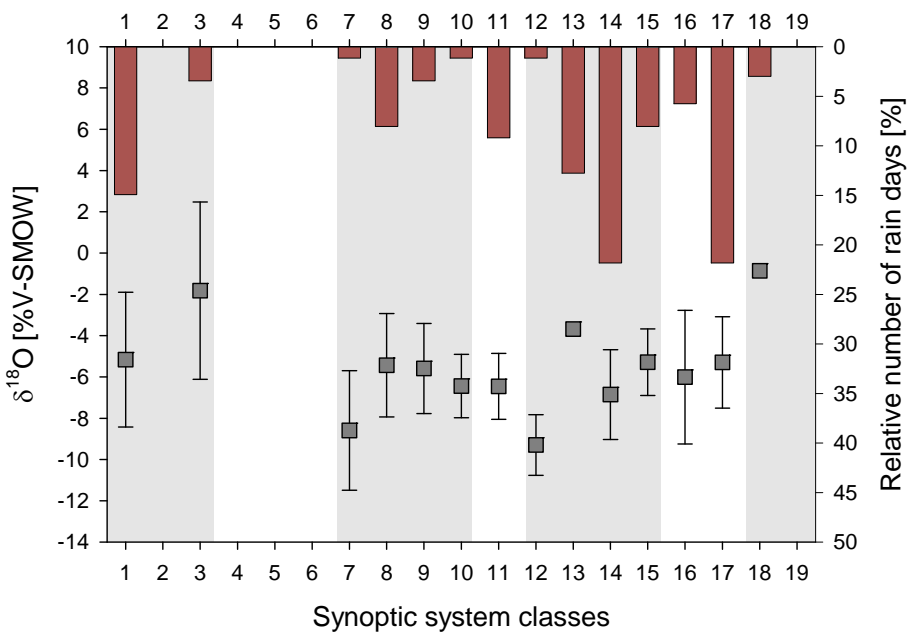


Figure 24: Mean stable isotope composition ($\delta^{18}\text{O}$) of rain water (squares) and the relative number of days with rain (bars) for each synoptic system class determined for daily rain samples taken at Tel Dan during 2002/03 and 2003/04. Descriptions of the synoptic system classes are given in Figure 66.

To investigate the influence of the synoptic systems on the isotopic composition of precipitation and rain amounts, daily precipitation samples were assigned to the respective synoptic class at that day. Subsequently, mean isotopic compositions and the relative number

of days with rain were calculated for each synoptic class and the results are given in Figure 24 and Table 15.

Table 15: Mean stable isotope composition, the relative number of rain days (n) and mean rain amounts for each synoptic system determined for daily rain samples taken at five stations in the northern UJRC during 2002/03 and 2003/04. Synoptic systems are explained in Figure 66.

Class	Synoptic system	n	Amount mm	$\delta^{18}\text{O}$ ‰	$\pm\sigma$ ‰	$\delta^2\text{H}$ ‰	$\pm\sigma$ ‰	d ‰	$\pm\sigma$ ‰
1	RST _E	29	231	-4.95	3.03	-22.14	22.17	17.47	5.43
3	RST _C	8	17	-1.14	3.47	4.57	16.85	13.72	11.47
7	H _E	6	38	-3.10	2.89	-3.99	21.71	20.82	7.34
8	H _W	16	155	-5.01	2.18	-21.19	15.09	18.86	4.75
9	H _N	5	20	-5.40	1.58	-19.48	9.35	23.70	3.32
10	H _C	5	40	-3.83	1.53	-11.91	11.09	18.74	1.67
11	L _E -D	19	263	-7.03	1.93	-29.60	15.73	26.64	4.65
12	CL _S -D	5	33	-7.61	1.47	-42.36	7.57	18.54	7.24
13	CL _S -S	1	11	-3.68		-14.00		15.44	
14	CL _N -D	58	1895	-7.07	2.09	-35.39	18.19	21.21	6.49
15	CL _N -S	26	428	-5.85	2.63	-24.11	21.78	22.71	4.88
16	L _W	33	478	-5.37	2.44	-20.53	20.34	22.41	5.54
17	L _E -S	55	621	-5.65	2.10	-25.90	16.34	19.31	6.11
18	SL _W	1	3	-0.86		1.80		8.68	

As expected, the highest abundance of rain days and the biggest amount of precipitation in the investigated seasons was monitored for cold fronts (Figure 24, Table 15). Particularly, the *Cyprus Lows* (Deep; class 14) with a northward orientation and *Lows (Shallow) to the East* (class 17) were associated with high amounts of rain and high abundance of rain days (Figure 24, Table 15). Especially for the *deep Cyprus Lows* (class 14), depleted values of $\delta^{18}\text{O}$ and $\delta^2\text{H}$ were monitored. Rain originating from these synoptic patterns forms within cold air masses of European origin that enter the Mediterranean region from the northwest. While moving over warmer Mediterranean waters, the air masses then gain moisture and become conditionally unstable (ZIV et al., 2006). No rain at all was monitored for the *Persian trough*, a barometric trough originating from the Persian Gulf with its trajectory mainly over land terrain which is characterized by limited humidity and dominates Israeli weather during summer (HASHMONAY et al., 1991; chapter 3.2).

Enriched values of $\delta^{18}\text{O}$ and $\delta^2\text{H}$ but also significant amounts of rain were monitored for *Red Sea troughs* that extend from East Africa through the Red Sea towards the East Mediterranean and dominate rainfall during the transitional seasons as well as for the *Sharav Low*, a spring cyclone that moves along the North African coast before turning north near the southeastern Mediterranean (ALPERT and ZIV, 1989b). Clearly, origin and trajectory of these synoptic patterns are responsible for the observed evaporative effects on their stable isotopic composition.

5.3.6 Inter- and intra-storm variability

Inter- and intra-storm variability of stable isotope composition in precipitation in the northern UJRC is high (Figure 25). A common feature already stated by RINDSBERGER et al. (1990) was the V-shaped pattern in the temporal evolution of stable isotopes which was also observed for several rain events in the UJRC during the study period. At the beginning of a rain storm when humidity and rain intensity were comparatively low, enriched values dominate while at the peak of the storm rain intensities were high and strong convective motions resulted in the mixing of surface air with air from higher altitudes that is partially depleted in heavy isotopes (RINDSBERGER et al., 1990; CELLE-JEANTON et al., 2004). Looking at major runoff events like those occurring on 20th December 2002, 21st January 2003 and 24th January 2004 (see 7.3) each time cold fronts, either *deep Cyprus Lows to the North*, *Cold Lows to the West*, or *Lows to the East* dominated the weather pattern.

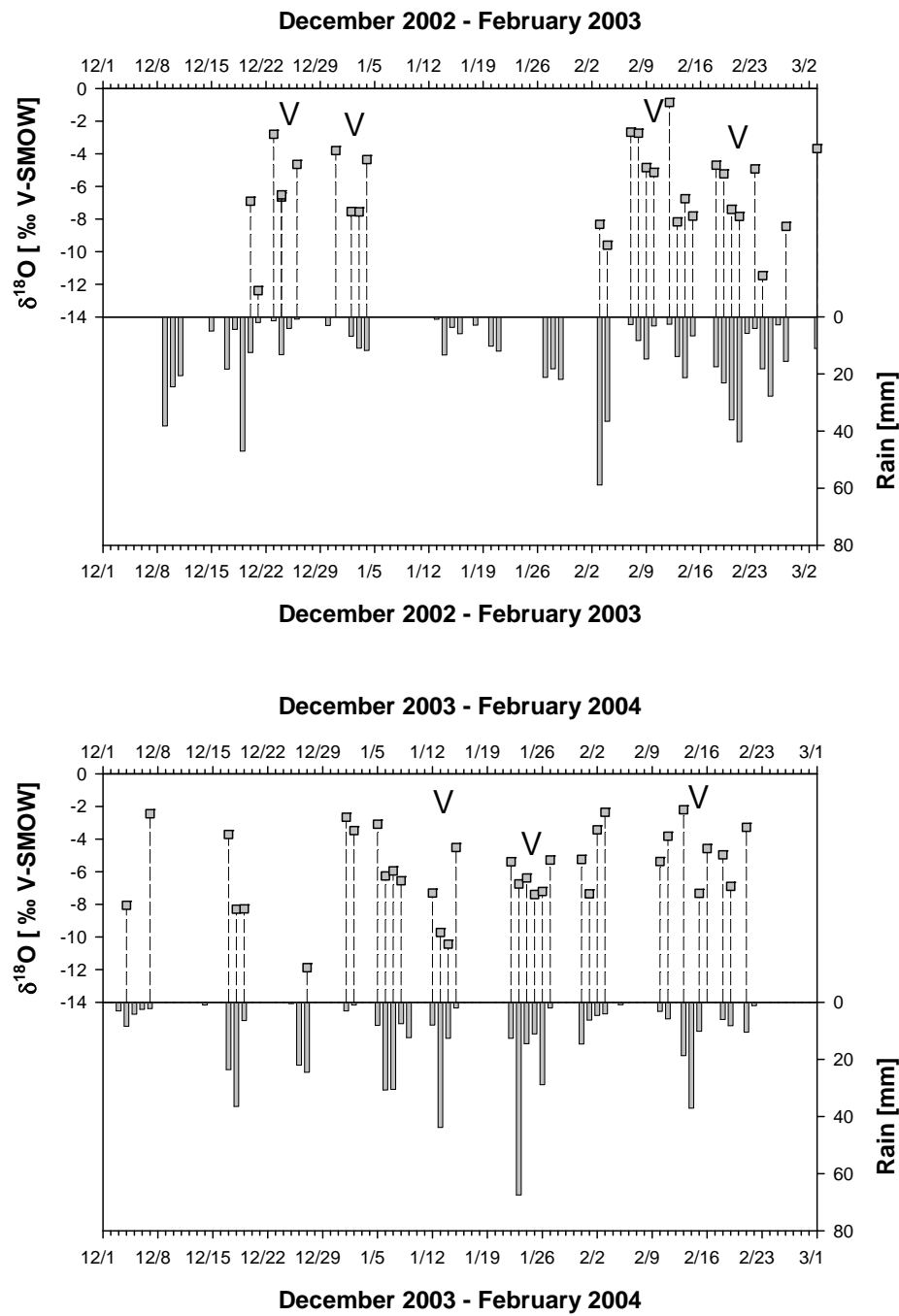


Figure 25: Inter- and intra-storm variability of $\delta^{18}\text{O}$ in daily rainfall samples of the Banias Nature Reserve, 2002-2004. The V-shaped pattern in the temporal evolution of stable isotopes during the rain events is emphasized by the respective symbol (V).

5.3.7 Altitude effect

With increasing altitude, the stable isotopic composition of precipitation decreases towards more depleted values. Thus, the resulting altitude gradient is strongly dependent on the local climate which in turn depends on factors such as topography and microclimate, e.g., orientation towards the wind (weather side/lee-side) and distance from the coast. The establishment of this effect within a specific research area is a useful tool in tracing groundwater recharge and potential recharge areas (PAYNE and YURTSEVER, 1974; CHRISTODOULOU et al., 1993; LEONTIADIS et al., 1996 among others) or for quantifying paleo-elevational changes of mountain belts (POAGE and CHAMBERLAIN, 2001).

Table 16: Altitude gradients of stable water isotopic composition in the northern UJRC and neighboring regions in the Eastern Mediterranean. The global isotopic lapse rate is given as a reference.

Location	$\delta^{18}\text{O}$ gradient ‰ per 100 m	$\delta^2\text{H}$ gradient ‰ per 100 m	Reference
northern UJRC	-0.26	-1.10	this study (daily rainfall)
northern UJRC	-0.25	-1.42	this study (weekly rainfall)
southern Mount Hermon	-0.30	-2.41	this study (snow) 23.02.2003
northern Jordan Rift valley	-0.13		GAT and DANSGAARD, 1972
Damascus region	-0.19		PRIZGONOV et al., 1988
western Syria	-0.23	-1.65	KATTAN, 1997a
Jezireh (Syria/Turkey)	-0.29	-2.23	KATTAN, 2001
global (except for extreme latitudes and high altitudes)	-0.28		POAGE and CHAMBERLAIN, 2001

For the determination of the altitude effect on the stable isotope composition of daily and weekly rainfall samples only datasets comprising at least three different elevations with a linearity of $r \geq 0.975$ ($r^2 \geq 0.95$) were included into the analysis (Table 60). In the northern UJRC, the altitude effect of daily rainfall samples was represented by a gradual depletion of the stable isotopes of about -0.26 ‰ and -1.10 ‰ per 100 m for $\delta^{18}\text{O}$ and $\delta^2\text{H}$, respectively. However, altitude effects determined for single events during November 2003 until February 2004 ranged between -1.06 to 0.26 ‰ per 100 m for $\delta^{18}\text{O}$. For the weekly rain samples, the progressive reduction of the isotopic concentrations with altitude was slightly lower for $\delta^{18}\text{O}$

and slightly higher for $\delta^2\text{H}$ (Table 16). Gradients ranged in between -0.35 to -0.17 ‰ per 100 m for $\delta^{18}\text{O}$ (Table 60, Table 61).

Four snow transects with an altitude range of 1390 to 2060 m a.s.l. were sampled on the southern Hermon Mountain during the winters 2002/03 and 2003/04 (Table 53). Only one transect showed a significant linear relationship ($r = 0.79$) between altitude and the stable water isotopic composition. According to this single gradient (-0.30 ‰ per 100 m for $\delta^{18}\text{O}$), the depletion of heavy stable isotopes in precipitation of higher altitudes in the southern Mount Hermon is more pronounced compared with those further downslope. The three other transects did not show any significant linear relationship between altitude and ^{18}O composition which might be due to superimposed snowdrift effects, especially since not all of the transects could be sampled on the actual snow day. Often, access to Mt. Hermon was restricted on snowy days. MARGARITZ (in SIMPSON and CARMI, 1983) suggested a gradient of about -0.6 ‰ per 100 m for $\delta^{18}\text{O}$ in snow, much higher than the one determined here. However, generally, the estimated altitude gradients agree well with those established by other researchers for adjacent regions and they are close to the global gradient of -0.28 ‰ per 100 m for $\delta^{18}\text{O}$ found by POAGE and CHAMBERLAIN (2001). The observed variability in altitude gradients is most likely caused by dominating weather pattern during the rainfall event and by drift phenomena in the case of snow.

5.3.8 Snowpack chemistry and stable isotope composition

A significant fraction of recharge in the UJRC originates from snowmelt on the upper slopes of Mount Hermon. GILAD and BONNE (1990) estimated the snowmelt contribution to the main Jordan River springs to be about 30 % of dry weather discharge. One objective of this study is to verify this assumption by applying chemical and isotope based mass balance approaches, which are based on the chemical and isotopic characterization of the pre-event (snowmelt) component.

Samples of fresh fallen snow were taken on four occasions during the study period. Their chemical and isotopic composition is presented in Table 12 and Table 54. Snow samples exhibited significantly lower ion concentrations and more depleted stable isotope

compositions than rain samples from the foot slopes of the Hermon Mountain. Additionally, snow samples were characterized by high values of deuterium excess with a mean of $d = 26.5\text{\textperthousand}$. However, snowpack chemistry and stable isotopic composition was shown to vary considerably with the ongoing season and the accompanying melting of the snow cover (STICHLER et al., 1981; TAYLOR et al., 2001; UNNIKRISHNA et al., 2002; STOTTELYER, 2001). Hence, snowmelt discharging from the bottom of the snowpack and infiltrating into the ground cannot be represented by samples of fresh snow.

During the study period, access to Mount Hermon was temporarily restricted. Additionally, logistic reasons did not allow for the installation of snowmelt lysimeters and the continuous monitoring of snowmelt. It is questionable at all, if single snowmelt lysimeters can deliver representative values that reflect the variability of snowpack and snowmelt chemistry over an area as multifaceted and large as Mount Hermon. Of course, the catchment size might have a homogenizing effect on local variations but particularly in areas with pronounced preferential flow paths, such as the karstic Hermon region, local variations might in fact affect the resulting chemical and isotopic composition of recharged waters.

Within this study, a snow profile was sampled on two reference dates to monitor the evolution of snowpack chemistry and stable isotope chemistry with the ongoing winter season (Figure 26). Since snowpack sampling could not proceed past February although the snow cover prevailed until late spring/early summer on Mount Hermon, it was impossible to account for the total seasonal variability of snowpack chemistry within this study.

The maximum range of the $\delta^{18}\text{O}$ variation for the January-profile was about $1.8\text{\textperthousand}$. Isotopic composition was most depleted on top of the profile and increases towards more enriched values at a depth of about 80 cm below the snow surface. The isotopic composition of snow at the bottom of the profile in turn, showed more depleted $\delta^{18}\text{O}$ -values again. At the beginning of the snow season, this variability in snowpack isotopic composition originated from isotopic variability of precipitation that contributed to the different snow layers rather than by isotopic fractionation processes accompanying the melting and refreezing of snow.

In the February-profile, a considerable enrichment of $\delta^{18}\text{O}$ in the lower snow layers of the profile was observed. This supports findings by STICHLER et al. (1981) and TAYLOR et al.

(2001). STICHLER et al. (1981) assumed that, due to isotopic fractionation, the light isotopes will prevail in the initial runoff followed by a steady increase of heavy isotope contents in the course of ablation. The maximum range of the $\delta^{18}\text{O}$ variation in the February-profile is about 4.3 ‰, the profile having a depth of about 160 cm. However, snow depths in the study area, varied considerably according to altitude, topography, and wind exposure of the sampling location.

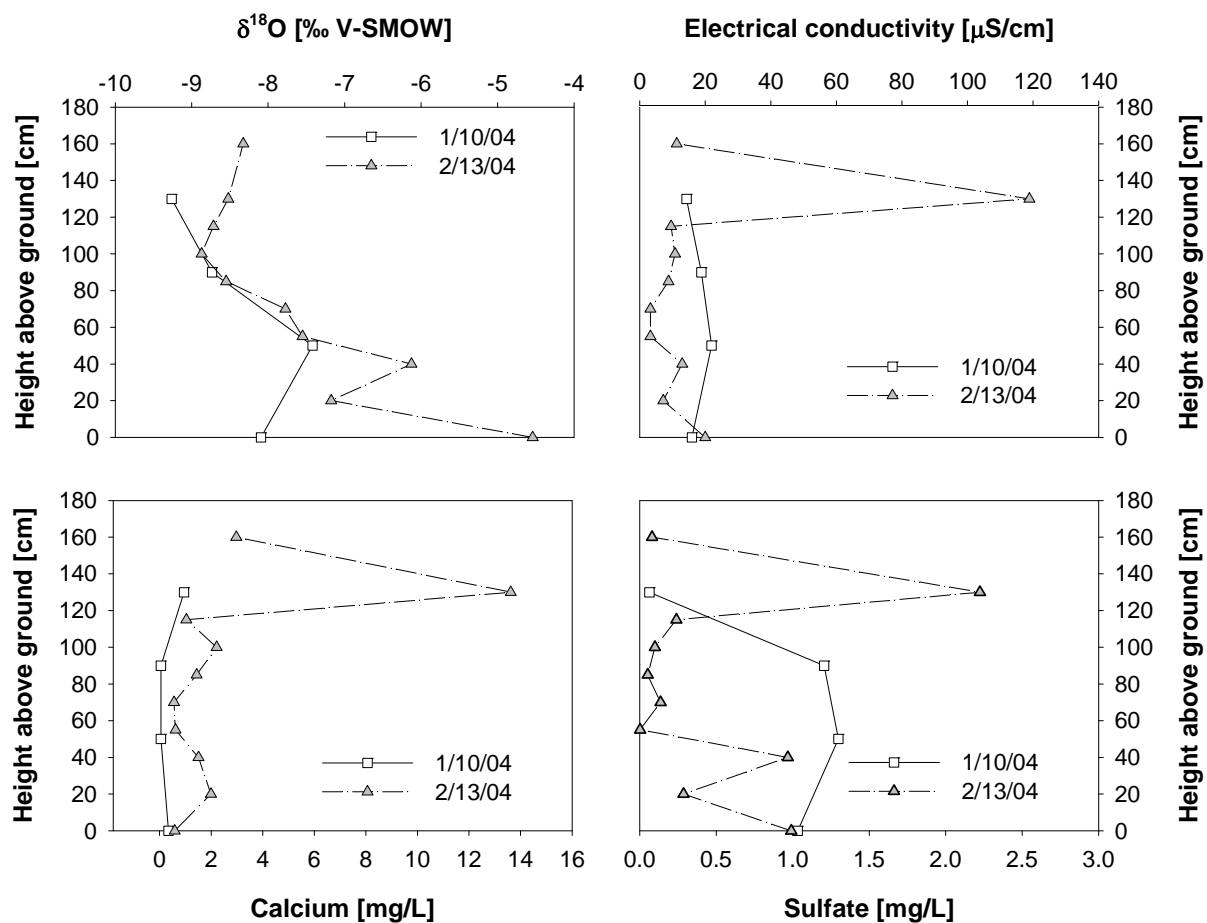


Figure 26: Snowpack chemistry and stable isotopic composition of two snow profiles investigated during January and February 2004.

Electrical conductivity gives information on ion concentrations in the considered solutions. Comparing the two profiles investigated in winter 2004 clearly showed that ion concentrations decreased with the ongoing winter season indicating the elution of certain ions (Figure 26). Focusing on the individual ions revealed that the concentration of ions originating from cloud-borne sea spray such as Cl^- , SO_4^{2-} , K^+ , Na^+ and Mg^{2+} (chapter 5.2)

decreased towards February while concentrations of dust derived ions such as Ca^{2+} and HCO_3^- increased.

The high ion concentrations of the February snow sample at a depth of about 30 cm below snow surface are attributed to the fact that a considerably amount of dust accumulated on this layer before snowfall continued. In the field, this layer appeared grayish. Though the sampling location was situated apart from the skiing area on Mount Hermon, anthropogenic influences caused by military vehicles could not be fully excluded.

6. Hydrochemical and stable isotopic characterization of groundwater in the mountainous northern Upper Jordan River Catchment

The chemical and isotopic composition of groundwater is determined by a number of factors such as the initial composition of the infiltrating precipitation and aquifer lithology. Host rock lithology (through mineral dissolution and water-rock interactions) in particular, controls groundwater flowpaths and ages and hence, the resulting groundwater chemistry and isotopic composition. Additional controls on groundwater characteristics are anthropogenic activities such as the pumping and pollution of groundwater.

Groundwater that emerges at a spring or well is often a mixture of waters from different flowpaths and of different ages. This is particularly true in heterogeneous systems such as well-developed karst and fractured rocks. Dependent on the dominance of certain flowpaths and groundwater bearing rocks, groundwater chemistry and isotopic composition varies with time. Decoding the hydrographic, chemical and isotopic information measured at the groundwater outlet, allows to draw conclusions on groundwater sources, evolution and mixing.

Preceding studies on the hydrogeology and hydrochemistry of groundwater in northern Israel and in particular, of the main Jordan River sources, were conducted by GAT and DANSGAARD (1972), GILAD and SCHWARTZ (1978), GILAD and BONNE (1990), SIMPSON and CARMI (1983), KAFRI et al. (2002) and GUR et al. (2003). In more recent publications, RIMMER and SALINGAR (2006) describe the karstic nature of the Hermon region by modeling precipitation-streamflow processes, while DAFNY et al. (2006) identified two types of aquifers (a regional one and several smaller perched aquifers) dominating the groundwater flow regime in the basaltic Golan Heights aquifer (chapter 3.5). The objectives of this study were to identify and characterize water types both in the Hermon karst and Golan basalt aquifer and to infer information on the origin and flowpaths of recharge waters. Another goal was to estimate mean residence times and water volumes of the assumed reservoirs and to determine mean recharge rates with the help of chemical and isotope tracer information. Temporal variations in groundwater composition were investigated to characterize the response of the recharge systems and to estimate the influence of snowmelt on the Upper Jordan River sources. This

information allows to deduce the sensitivity of the UJRC groundwater systems towards climate change. One hypothesis is that, if seasonal variations in the springs discharge, chemical and isotopic composition are high and spring responses are flashy, groundwater is mainly controlled by climate. Consequently, groundwater would be highly vulnerable towards anticipated changes in temperature and precipitation pattern.

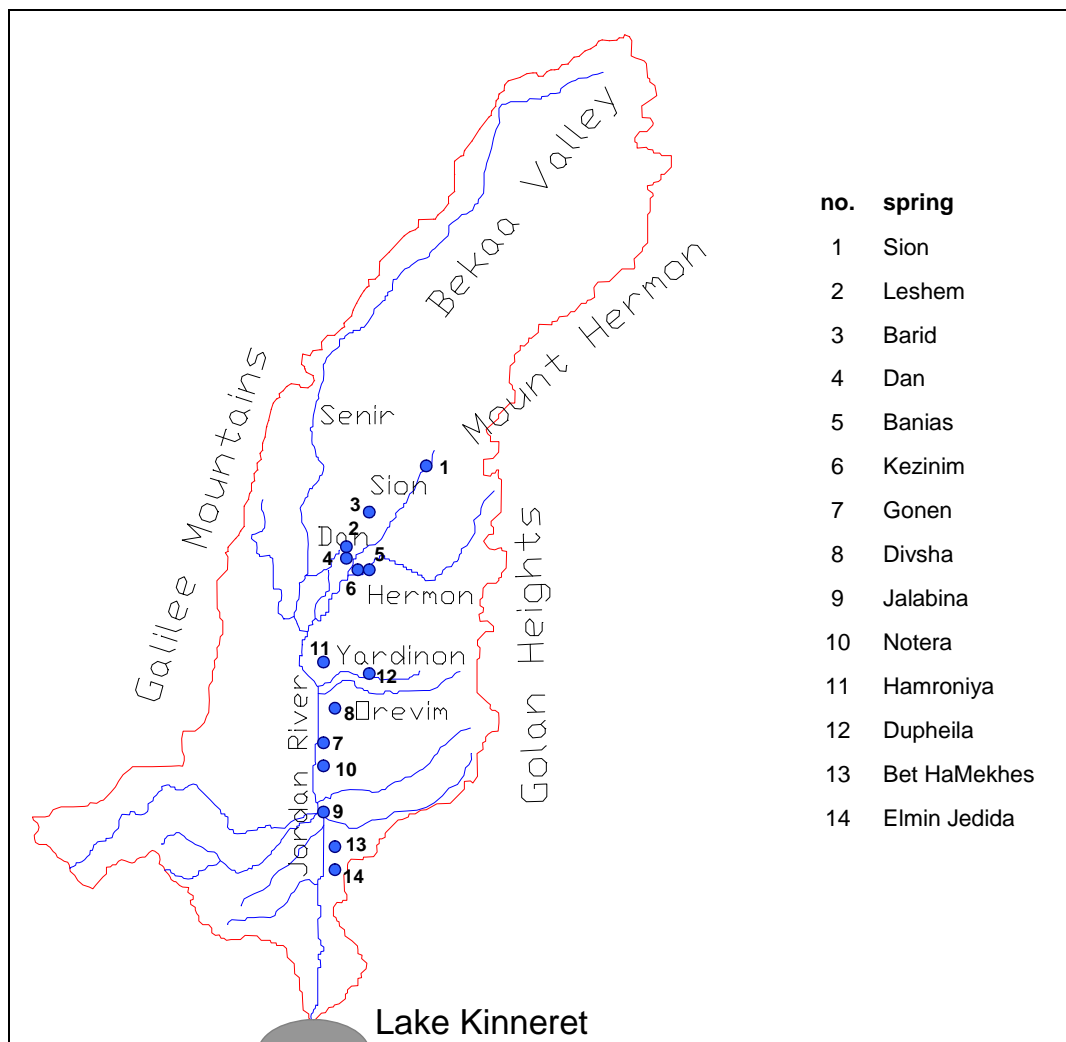


Figure 27: Groundwater sampling network in the Upper Jordan River Catchment. Modified from EXACT (1998).

6.1 CHEMICAL COMPOSITION OF GROUNDWATER

6.1.1 General hydrochemical characteristics

Major physico-chemical bulk parameters and the concentration of DOC and SiO₂ of the investigated groundwater are given in Table 17. The investigated groundwaters in the study area are cold springs. Mean temperatures during the study period ranged from 11.7-19.8 °C in the Hermon springs and 18.9-20.4 °C in the Golan springs. With the exception of the Kezinim spring, mean temperature was comparatively low in the Hermon springs, which was attributed to the fact that a major portion of their waters is recharged at high altitudes, is generated during the snowmelt season and travels along preferential, shallow flowpaths such as karstic conduits and fissures. The Sion spring for example, that is known to be the outlet of a karstic conduit, had a mean temperature of about 11.7 °C. Within this work, there was no opportunity to directly monitor snowmelt at the Sion dolina but temperatures in the range of 7-13 °C were observed in other intermittent streams of the Hermon area fed by snowmelt.

Table 17: Physico-chemical characteristics and concentrations of DOC and SiO₂ of groundwater in the northern UJRC.

Location	n	T	± σ	pH	± σ	EC	± σ	DOC*	± σ	SiO ₂ *	± σ
		°C	°C			μS/cm	μS/cm	mg/L	mg/L	mg/L	mg/L
<i>Hermon springs</i>											
Sion	3	11.7	1.3	8.1	0.1	258	17	1.1	0.3	3.2	1.0
Leshem	67	15.2	0.3	7.6	0.2	319	17	2.2	3.9	4.3	0.6
Barid	5	15.6	0.6	7.9	0.1	327	24	0.8	0.5	4.8	-
Dan	66	15.9	0.3	7.5	0.1	342	16	2.5	6.5	5.3	0.5
Banias	60	15.2	0.5	7.5	0.1	395	66	1.1	0.6	7.4	2.2
Kezinim	46	19.8	0.5	7.4	0.1	561	39	1.2	0.5	10.5	1.4
<i>Golan springs</i>											
Gonen	14	18.9	1.0	8.4	0.2	313	9	1.1	0.2	33.6	2.8
Divsha	14	19.9	1.0	8.4	0.4	328	10	1.2	0.4	35.4	2.6
Jalabina	14	19.2	1.9	8.1	0.2	329	9	1.6	1.0	29.8	2.6
Notera	18	19.2	0.9	8.3	0.2	339	19	1.2	0.5	34.2	2.5
Hamroniya	17	19.0	0.6	8.1	0.3	343	17	1.0	0.3	37.0	2.0
Dupheila	14	19.9	1.8	8.1	0.2	352	18	1.1	0.3	32.5	1.8
Bet HaMekhes	14	19.9	1.1	8.3	0.3	358	7	1.3	2.1	26.7	1.4
Elmin Jedida	14	20.4	0.3	7.7	0.1	399	8	1.1	0.4	34.9	1.6

n is the number of samples taken, “*” for DOC and SiO₂ less samples than n were available, see chapter 6.

Table 18: Mean major ion concentrations of groundwaters emerging in the northern UJRC. For numbers of samples refer to Table 17. TDI is total dissolved ions, R.E. is the reaction error based on mean values.

	Ca^{2+} mg/L	$\pm \sigma$	Mg^{2+} mg/L	$\pm \sigma$	Na^+ mg/L	$\pm \sigma$	K^+ mg/L	$\pm \sigma$	HCO_3^- mg/L	$\pm \sigma$	SO_4^{2-} mg/L	$\pm \sigma$	Cl^- mg/L	$\pm \sigma$	NO_3^- mg/L	$\pm \sigma$	TDI mg/L	$\pm \sigma$	R.E. %
<i>Hermon springs</i>																			
Sion	50.0	6.8	2.6	0.7	4.1	1.3	0.4	0.2	160	8	4.6	0.6	7.0	2.2	1.6	0.9	207	36	-1.0
Barid	54.5	9.9	3.0	0.7	3.5	0.4	0.6	0.1	194	17	5.3	0.7	6.0	0.8	3.8	1.0	271	28	6.3
Leshem	55.3	5.2	3.1	0.9	3.5	0.4	0.6	0.1	209	15	5.5	1.0	5.9	0.6	3.9	1.1	287	17	8.2
Dan	57.6	5.7	4.2	0.8	4.2	0.4	0.7	0.1	211	17	7.0	1.0	6.6	0.7	4.2	1.4	295	20	6.0
Banias	61.5	7.8	8.3	3.2	7.9	2.5	1.1	0.4	208	20	32.5	21.5	9.9	2.1	4.6	1.4	334	54	3.7
Kezanim	84.1	6.2	15.2	2.2	10.0	1.3	1.6	0.3	231	17	101.1	1.0	10.9	18.7	4.4	0.6	457	33	2.8
<i>Golan springs</i>																			
Gonen	24.0	1.9	12.8	1.0	20.8	1.3	3.8	0.4	169	9	6.0	0.8	14.9	0.9	11.8	2.3	263	11	3.8
Divsha	26.0	1.7	12.2	4.5	20.6	1.5	3.4	0.3	178	5	7.1	1.4	15.1	1.0	11.1	2.3	275	6	4.4
Jalabina	17.3	1.7	13.4	1.2	31.0	2.9	3.4	0.4	181	13	4.5	0.8	17.2	0.6	10.0	1.8	278	13	4.3
Notera	21.2	2.0	14.9	2.1	24.7	1.3	4.7	0.6	177	15	6.0	1.0	17.4	1.3	13.8	2.2	279	16	3.6
Hamroniya	22.5	1.8	13.7	1.0	24.7	2.5	4.8	0.5	180	13	5.8	0.8	17.1	1.3	15.2	1.2	282	14	4.6
Dupheila	28.6	4.0	13.8	1.6	22.2	2.8	3.8	0.8	186	20	6.7	1.6	16.1	1.7	13.4	3.1	291	22	3.3
Bet HaMekhes	16.6	1.0	14.3	1.1	35.0	3.0	4.3	0.4	193	11	3.9	0.9	20.7	0.9	11.2	0.9	301	12	5.2
Elmin Jedida	27.7	1.8	17.2	1.2	27.2	2.1	3.8	0.3	213	8	5.0	0.6	19.7	0.6	16.1	0.8	330	8	3.9

Mean water temperatures measured in springs and wells reflect groundwater temperatures attained at depth and hence provide information on the depth of circulation (given that groundwater velocities are low). In shallow, fast flowing systems the influence of the mean annual temperature at the surface superimposes the conductive geothermal heat flux resulting in groundwater temperatures that are close to the mean annual surface temperatures. Based on a 10-year temperature record of Majdal Shams (DEGANI and INBAR, 1993), a village located at an altitude of 1170 m a.s.l. on Mount Hermon, the mean annual air temperature at this altitude was determined to be about 14.7 °C. The Kezinim spring is assumed to be recharged at similar or even higher altitudes. Accordingly, the higher mean temperature in the Kezinim spring must be caused by contributions of groundwater from deep parts of the anticline structure as already proposed by BURG et al. (2003) and as suggested for other thermal, sulfate-rich springs emerging from carbonate rocks (WORTHINGTON and FORD, 1995; GUNN et al., 2006).

Mean annual surface temperatures in the Golan Heights ranged in between 15 °C to 17 °C (DEGANI and INBAR, 1993), hence, Golan springs as well might receive deep flow contributions. Mean groundwater temperatures within the Golan springs differ by about 1.5 °C, suggesting minor differences in the circulation depths of the contributing groundwater.

The Hermon springs have pH values in the range 7.5-8.1. Within these spring systems, the low initial pH of infiltrating groundwater is buffered by the weathering of minerals such as calcite, dolomite and gypsum. At the observed pH, the dominating dissolved inorganic carbon species is bicarbonate. Average pH values in the Golan springs are in the range 7.7-8.4. pH-values such as these are common in basalt-sourced groundwaters where water chemistry is dominated by minerals such as silicates and aluminosilicates, which tend to raise the pH to values of 9-10 or even higher (LANGMUIR, 1997).

Sampled groundwater in the northern UJRC are fresh and of low salinities. Throughout the sampling period mean electrical conductivities were in the range of between 258-561 µS/cm and 313-399 µS/cm in the Hermon and Golan springs, respectively. Low salinities in the carbonatic groundwater suggest that CO₂ dissolution with infiltration is low which is

attributed to the thin or absent soil covers on Mount Hermon. Golan soil covers are comparatively thick, however, silicate weathering is a slow process once it reached a threshold concentration thus limiting the mineralization of the Golan groundwater. Within the Hermon springs, highest EC values and highest variation of EC were recorded for the Banias and Kezinim spring indicating both abundant mineralizations within the aquifer (SHIMRON, 1989) and – considering the Banias spring - a highly responsive system. Variation of electrical conductivity was comparatively low in the Dan, Leshem and Barid springs indicating large intake areas and distinctive mixing processes. Lowest and highly variable electrical conductivities were recorded for the Sion spring where short residence times of groundwater in the karstic conduits limit the mineralization of water. Tracer tests resulted in residence times as short as 17 hours for water entering the Sion dolina and emerging at its spring (YOSSI LEVANON, personal communication).

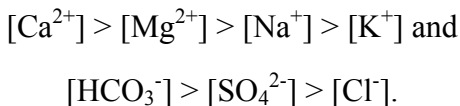
Within the Golan springs, the variation of EC throughout the sampling period was generally low. Differences in solute concentrations for the investigated springs could be explained with groundwater residence times where high water ages result in stronger mineralization of waters. Additionally, the contribution of shallow groundwater components with low residence time in the aquifer will lead to lower values of electrical conductivity.

Mean concentrations of dissolved silica ranged between 3.4-10.5 mg/L in the Hermon springs. The abundance of silicate minerals in the hosting aquifer (SHIMRON, 1989; KAFRI et al., 2002) of the Banias and Kezinim spring leads to high SiO₂ concentrations in these springs. Dissolved silica in the Hermon springs originates as a byproduct of carbonate weathering. However, carbonate bedrocks have generally low contents of silicate minerals when compared to basaltic bedrocks for example. Hence, in the Golan springs, mean concentrations of dissolved silica ranged between 26.7-37.0 mg/L. These comparatively high concentrations are caused by silicate mineral weathering processes within the Golan basalt aquifer.

Mean DOC concentrations in the investigated springs were all about 1 mg/L reflecting the natural DOC concentrations commonly found in groundwater (chapter 2.4.4.7).

6.1.2 Hydrochemical facies and ionic ratios

Groundwater in the Hermon springs emerging from the Jurassic Arad Group aquifer was characterized by a calcium-magnesium and bicarbonate water type with the following ionic sequences:



Calcium and bicarbonate dominate ion concentrations in these springs (Figure 29). Mean concentrations ranged between 50-84 mg/L and 160-231 mg/L, respectively (Table 18). Low Mg/Ca ratios ranging between 0.09-0.30 emphasize the dominance of calcite over dolomite dissolution. The highest Mg/Ca ratios and high levels of SO₄ (33 and 101 mg/L, respectively) were observed in the Banias and Kezinim spring suggesting the dissolution of dolomite, gypsum and anhydrite within these source areas. BURG et al. (2003) investigated the stable sulfate isotope composition of groundwater in these springs and found values similar to marine sources. Consequently, BURG et al. (2003) concluded that these springs receive contributions from groundwater flowing through the upper Triassic Mohila Formation (Figure 63). Sulfate levels in the other Hermon springs are close to that of natural precipitation implying that rain and snow are the only sources of sulfate within these springs.

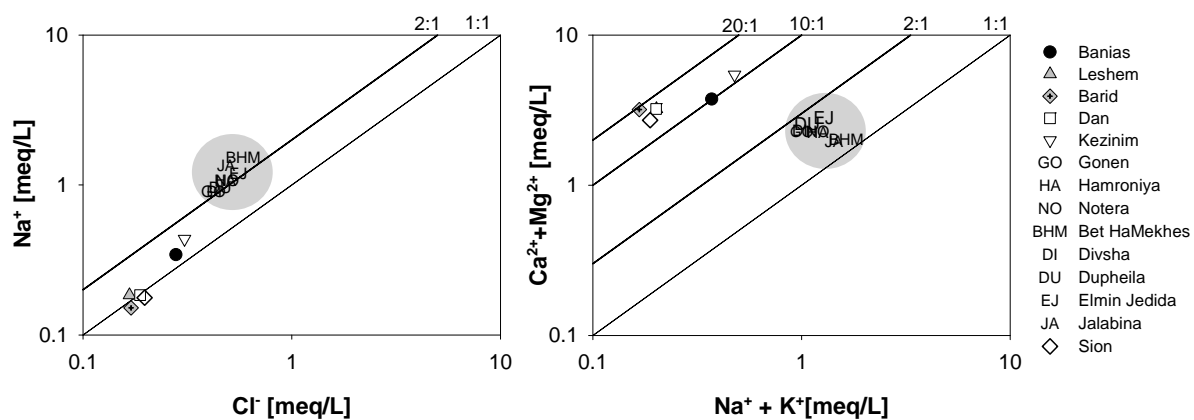


Figure 28: Relationship between concentrations of Na^+ and Cl^- in the investigated springs (left figure). Lines illustrate common ratios of Na^+ versus Cl^- in the analyzed groundwaters. The 1:1 ratio equals the seawater dilution line. Relationship between alkali and earth-alkali metals (right figure). Gray circles comprise all Golan springs which plot very close to each other.

Mean concentrations of Na and Cl were in the range of 3.5-10.0 mg/L and 5.9-10.9 mg/L, respectively. Slightly higher values of Na and Cl in the Banias and Kezinim spring are attributed to halite beds known to occur in the evaporite series (BURDON and SAFADI, 1964) (chapter 3.5.2.) In the other Hermon springs, no lithological source of chloride is known and human activity in the catchment is negligible. Hence, chloride concentrations are solely attributed to atmospheric inputs. This is supported by the fact that the Sion, Dan, Barid and Leshem spring all plot on the seawater-dilution line (Figure 28), while the Banias and Kezinim spring plot above. Hence, chloride concentrations can be used to estimate groundwater recharge rates via chemical mass-balance approach.

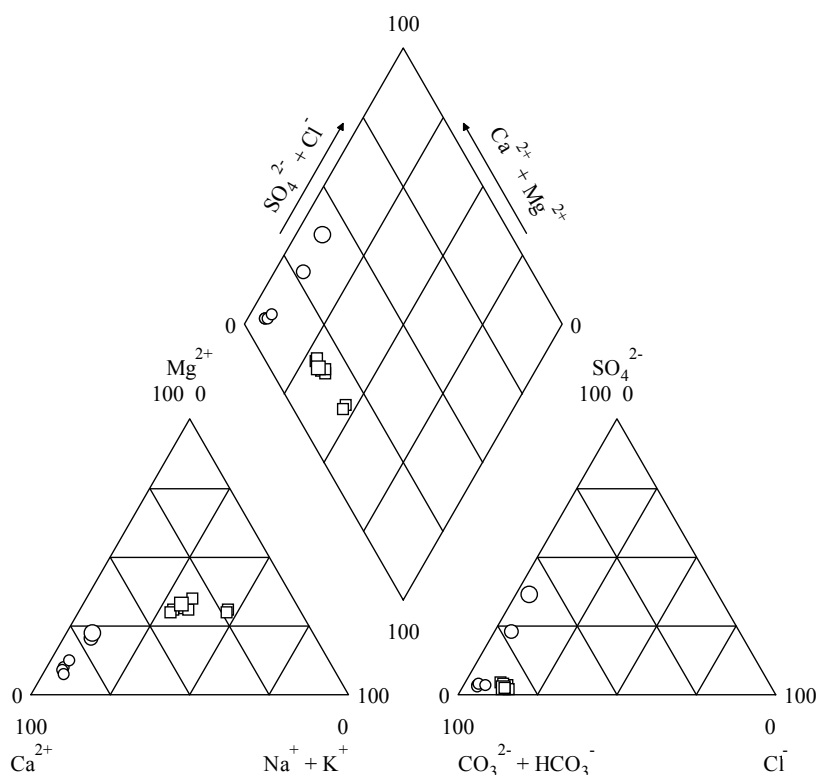
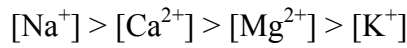
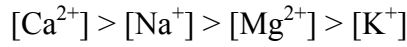


Figure 29: Piper plot of the mean chemical composition of groundwater sampled in the northern UJRC during the study period 2002-2004. Open circles represent the Hermon springs, open squares the Golan springs. Symbol diameter reflects the electrical conductivity of each spring.

Mean concentrations of potassium were low, in the range of 0.5-1.6 mg/L since there is no substantial mineral source of K^+ in these aquifers. Nitrate levels were below 5 mg/L in all of the Hermon springs emphasizing their good water quality (Table 18).

The investigated “Side springs” that emerge from the Golan basalt aquifer are represented by a calcium-sodium or sodium-calcium and bicarbonate water type with the following ionic sequences:



In the Golan springs, bicarbonate is by far the most dominant anion. The mean HCO_3^- concentrations were in the range of 169-213 mg/L. As rainwater moves through the soil zone, it rapidly dissolves CO_2 leading to increased carbonate concentrations in the infiltrating water. Under pH conditions such as found in the observed groundwaters (pH 7-9), bicarbonate is the most abundant carbonate species. Dominant cations of the basaltic groundwaters were Ca^{2+} , Na^+ and Mg^{2+} , with mean concentration ranges of 16.6-28.6 mg/L, 20.6-35.0 mg/L and 12.2-17.2 mg/L, respectively. Silicate and alumino-silicate minerals such as Ca-rich plagioclase, pyroxene and olivine are the major rock-forming minerals in basalt groundwaters (CRUZ and AMARAL, 2004). Accordingly, the prevailing weathering reaction in basalt aquifers is silicate hydrolysis. In general, silicate weathering leads to decreasing concentrations of alkali metals, alkali-earth metals and silicic acid in the host rocks, which preferably dissolve in groundwater (VOIGT, 1990).

In addition, ion exchange reactions determine groundwater chemistry in the basaltic host rocks. These reactions are dependent on the amount of exchangeable ions present in both the solid and the liquid phases, on the contact time between water and rock, and on the flow velocity of the water through the contact layers. With increasing contact time between water and rock, Na^+ will be replaced by Ca^{2+} at the exchange site of the clay mineral leading to higher concentrations of sodium in the groundwater. Hence, ion exchange reactions might explain the different cation sequences and the high Na:Cl-ratio (Figure 28) in the basaltic groundwater. On the other hand, these differences can also be attributed to the different evolution of the rocks (EVANS et al., 2001; CRUZ and AMARAL, 2004) and rock composition as suggested by SENDLER (1981) for basaltic groundwater of the central and southern Golan.

In comparison to the Hermon springs, the Golan springs exhibited significantly higher mean concentration of K^+ in the range of 3.4-4.8 mg/L, which is reasonable due to the abundance of K^+ -bearing silicate minerals in the aquifer. Mean nitrate concentrations were considerably higher than in the Hermon springs ranging between 10.0-16.1 mg/L. This is still by far lower than the drinking water standard (50 mg/L, WHO) and might correspond to natural concentrations of nitrate caused by biogenic activities in the uppermost soil layers.

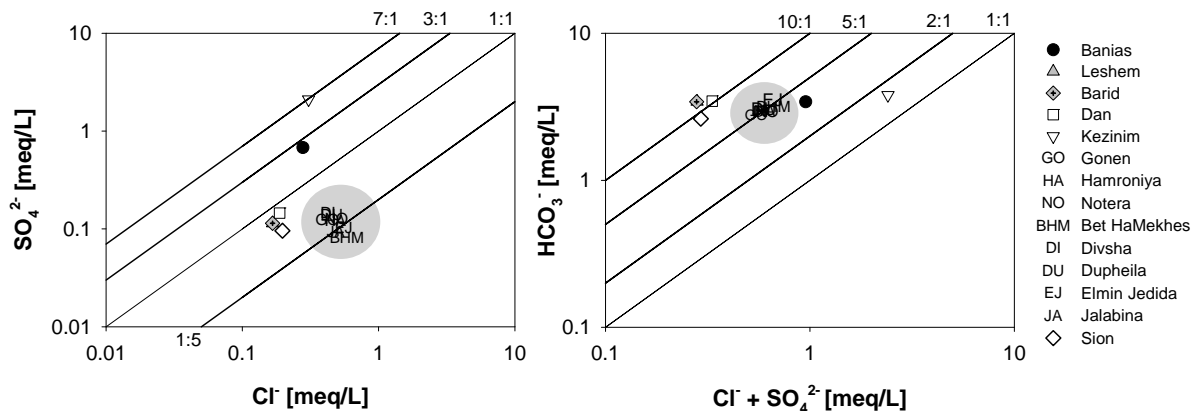


Figure 30: Relationship between concentrations of SO_4^{2-} and Cl^- (left figure). Relationship between concentrations of HCO_3^- and $Cl^- + SO_4^{2-}$ in the investigated groundwater (right figure). Lines illustrate common ion ratios in the analyzed springs. Gray circles comprise all Golan springs which plot very close to each other.

In contrast to the ‘Side springs’ emerging in the Golan Heights, Hermon springs exhibit a wide range of sulfate concentrations with the highest values in the Kezinim and Banias spring. While groundwater of the Dan, Barid, Leshem and Sion spring display a $SO_4:Cl$ ratio of 1 suggesting that both salts are solely derived from precipitation, these ratios are three to seven times higher in the Banias and Kezinim spring indicating an additional geogenic source of sulfate (Figure 30). Marine evaporites and gypsum as the sulfate source were proposed by BURG et al. (2003).

6.1.3 Equilibrium conditions of groundwater

The hydrochemical equilibrium conditions of groundwater and mineral phases of the aquifer rocks can be evaluated using saturation indices. The saturation index ($SI_{mineral}$) of a certain mineral is defined as the (logarithmic) ratio of the ion activity product to the equilibrium

constant ($\log(IAP/K)$). When a mineral is in equilibrium with respect to a solution, the SI is zero. Undersaturation is indicated by a negative SI and supersaturation by a positive SI. The concept is described in detail by DOMENICO and SCHWARTZ (1990), STUMM and MORGAN (1996), LANGMUIR (1997) among others.

Table 19: Mean partial pressure of carbon dioxide and saturation indices of selected minerals of groundwaters sampled in the UJRC during the study period 2002-04. Saturation indices for magnesite, dolomite, calcite, anhydrite, gypsum, aragonite, sepiolite and silica (gel) are SI_{mag} , SI_{dol} , SI_{cal} , SI_{an} , SI_{gyp} , SI_{ara} , SI_{sep} and SI_{sil} , respectively.

Sample	$\log P_{CO_2}$	SI_{mag}	SI_{dol}	SI_{cal}	SI_{an}	SI_{gyp}	SI_{ara}	SI_{sep}	SI_{sil}
<i>Hermon springs</i>									
Sion	-2.96	-1.29	-1.00	0.37	-3.19	-2.94	0.22	-4.86	-1.11
Barid	-2.68	-1.25	-0.96	0.34	-3.13	-2.88	0.19	-4.90	-0.99
Leshem	-2.34	-1.52	-1.49	0.07	-3.11	-2.86	-0.08	-6.22	-1.03
Dan	-2.28	-1.43	-1.43	0.04	-3.00	-2.75	-0.11	-5.92	-0.95
Banias	-2.29	-1.18	-1.19	0.03	-2.34	-2.09	-0.12	-4.94	-0.79
Kezanim	-2.05	-0.98	-0.94	0.05	-1.79	-1.55	-0.10	-4.64	-0.69
<i>Golan springs</i>									
Divsha	-3.25	-0.03	0.53	0.57	-3.31	-3.08	0.42	1.20	-0.18
Gonen	-3.19	-0.15	0.26	0.42	-3.42	-3.18	0.27	0.80	-0.19
Notera	-3.06	-0.15	0.13	0.29	-3.47	-3.23	0.14	0.57	-0.18
Bet HaMekhes	-3.06	-0.08	0.19	0.27	-3.77	-3.53	0.12	0.38	-0.30
Jalabina	-2.89	-0.34	-0.28	0.06	-3.67	-3.43	-0.08	-0.33	-0.24
Hamroniya	-2.86	-0.37	-0.24	0.14	-3.46	-3.22	-0.01	-0.15	-0.14
Dupheila	-2.86	-0.31	-0.03	0.28	-3.30	-3.07	0.14	-0.22	-0.21
Elmin Jedida	-2.41	-0.54	-0.59	-0.05	-3.46	-3.22	-0.20	-1.48	-0.18

The dissolution and redistribution of gaseous CO_2 with the infiltrating water significantly affects the chemical signature of groundwater. Atmospheric inputs into the hydrogeological system such as rain or snow generally have a partial CO_2 pressure of $10^{-3.5}$ atm, within the soil zone, due to root and microbial respiration, values can be up to 500 times higher. The calculated P_{CO_2} for sampled groundwater can offer insight into the nature of the correspondent aquifers. In an *open system* P_{CO_2} is constant, i.e. there is a constant supply of CO_2 , while in a *closed system* no CO_2 is added, and P_{CO_2} decreases as CO_2 is depleted by the dissolution of carbonates (DREVER, 1997).

The thermodynamic equilibrium condition controlling the groundwater in the investigated Hermon and Golan springs given in Table 19 were computed using the PHREEQC software (WATEQ database) (PARKHURST and APPELO, 1999). Variations in the saturation state of the investigated groundwaters towards certain minerals occur mainly due to the chemical composition of infiltrating water (e.g. pH, log P_{CO_2}) or due to temperature fluctuations.

Calculated partial pressures of CO_2 (log P_{CO_2}) ranged from $10^{-2.96}$ up to $10^{-2.05}$ atm in the investigated Hermon springs, while the sampled Golan springs exhibit P_{CO_2} -values of $10^{-3.25}$ to $10^{-2.41}$ atm. Hence, in both spring systems partial pressures were close to values of atmospheric log P_{CO_2} . As mentioned before, soil cover in the Hermon region is scarce or thin, hence soil zone generated CO_2 is of minor influence in this area. Within the Hermon springs, the Sion spring showed a calculated P_{CO_2} value close to that of precipitation which is due to its ephemeral nature and the dominance of conduit flow in this spring. The highest partial pressure within these springs was calculated for the Kezinim spring supporting the assumption that Kezinim spring water is in longer contact time with the rock matrix allowing a stronger depletion of CO_2 by the dissolution of carbonates than in the other Hermon springs. In the Golan springs, the Elmin Jedida spring water displayed highest partial pressure of CO_2 suggesting it has a comparatively high contact time with the rock matrix.

All Hermon springs were in saturation ($-1.5 < SI < 1$) with respect to calcite and dolomite (Table 19) indicating predominantly limestone and dolostone source rocks. As expected from the literature review, the Banias and Kezinim spring were slightly less undersaturated with respect to gypsum than the other Hermon springs suggesting a different intake area and the occurrence of these kind of minerals in that intake area. The Sion spring is ephemeral which was reflected in its highest undersaturation towards all investigated minerals except for calcite and aragonite. Kezinim spring was less undersaturated towards most minerals than all the other Hermon springs indicating a longer contact time of infiltrating water with the rock matrix and hence longer residence times.

6.2 STABLE ISOTOPE COMPOSITION OF GROUNDWATER

Similar to the hydrochemical signature, the stable isotope composition of the sampled groundwater allowed to distinguish between the two groups of groundwaters:

- groundwater recharged in the Golan basalt aquifer and
- groundwater emerging from the Arad Group aquifer of Mount Hermon.

The mean stable isotope composition of the Hermon springs during the sampling period ranged from -7.55 to -7.27 ‰ and -39.1 to -36.9 ‰ for $\delta^{18}\text{O}$ and $\delta^2\text{H}$, respectively (Table 20). The deuterium excess values varied between 20.6 ‰ and 21.7 ‰. Hermon spring groundwaters were slightly depleted compared to the isotopic composition of the Golan springs suggesting they are recharged at higher altitudes and/or lower temperatures. Additionally, springs sampled in the Hermon Mountains plot close to the local and Mediterranean MWL (Figure 31a) implying that recharge occurs by rapid infiltration with little evaporation prior to recharge as common in karstic regions that promote infiltration through sinkholes and conduits.

The $\delta^{18}\text{O}$ and $\delta^2\text{H}$ values in the Golan springs ranged between -6.86 to -6.37 ‰ and -32.1 to -25.1 ‰, respectively. The deuterium excess values show a comparatively broader range of 21.6 to 27.4 ‰. The slightly enriched stable isotope composition compared to the Hermon springs reflects recharge at low altitudes and/or high temperatures. Differences in the stable isotopic composition of groundwater in the Golan and Hermon springs ranged between -1.18 to -0.41 ‰. Referring to an altitude effect of -0.23 ‰ per 100 m for $\delta^{18}\text{O}$ in precipitation as determined within this study, mean recharge altitudes for the investigated Golan and Hermon springs would differ by just 180 to 450 m. Even if the Golan ‘Side springs’ are recharged at altitudes between 900 to 1000 m as suggested by DAFNY et al. (2006), this difference seems low when considering the total height of Mount Hermon (2814 m a.s.l.).

Table 20: Mean stable isotope composition of spring waters in the northern UJRC during 2002-2004.

Spring	$\delta^{18}\text{O}$ ‰	$\pm \sigma$ ‰	$\delta^2\text{H}$ ‰	$\pm \sigma$ ‰	d ‰	$\pm \sigma$ ‰
<i>Hermon springs</i>						
Kezinim	-7.27	0.06	-36.9	0.9	21.2	0.9
Banias	-7.49	0.11	-38.3	1.0	21.7	1.0
Dan	-7.41	0.13	-38.4	1.1	20.8	1.0
Leshem	-7.44	0.17	-39.0	1.2	20.6	1.0
Barid	-7.45	0.07	-37.9	2.3	21.7	2.4
Sion	-7.55	0.25	-39.1	0.8	21.3	2.2
<i>Golan springs</i>						
Dupheila	-6.67	0.12	-30.4	1.1	23.4	1.3
Divsha	-6.78	0.08	-32.1	0.4	22.1	0.6
Bet HaMekhes	-6.37	0.06	-28.1	0.8	22.7	0.8
Elmin Jedida	-6.38	0.05	-29.6	0.5	21.6	0.6
Gonen	-6.76	0.08	-31.3	0.8	23.0	1.0
Hamroniya	-6.86	0.09	-31.9	0.9	23.5	0.8
Jalabina	-6.50	0.13	-29.1	0.79	21.6	0.7
Notera	-6.63	0.21	-25.1	1.75	27.4	2.2

Groundwater samples of the Golan “Side springs” plot below the Mediterranean MWL indicating that infiltrating water has been subject to evaporation during its passage through the unsaturated zone. Golan groundwater plot along an evaporation line with a slope of 6.41. The most enriched values were observed for the Bet HaMekhes and Elmin Jedida springs (Figure 31), hence evaporative effects on these groundwaters were highest compared to the other ‘Side springs’. Reverting to the hydrogeological model introduced by DAFNY et al. (2006), springs with the more depleted stable isotopic compositions are fed by old (> 50 years) groundwater recharging at high altitudes and covering long flow distances. On the other hand, more enriched values of $\delta^{18}\text{O}$ specify springs fed by shallow groundwater or receiving contributions from perched aquifers recharged at low altitudes. Thus, the Bet HaMekhes and Elmin Jedida springs were assumed to collect more local recharge from surroundings of the springs which is subject to evaporation, while the Hamroniya spring receives more water from the regional aquifer.

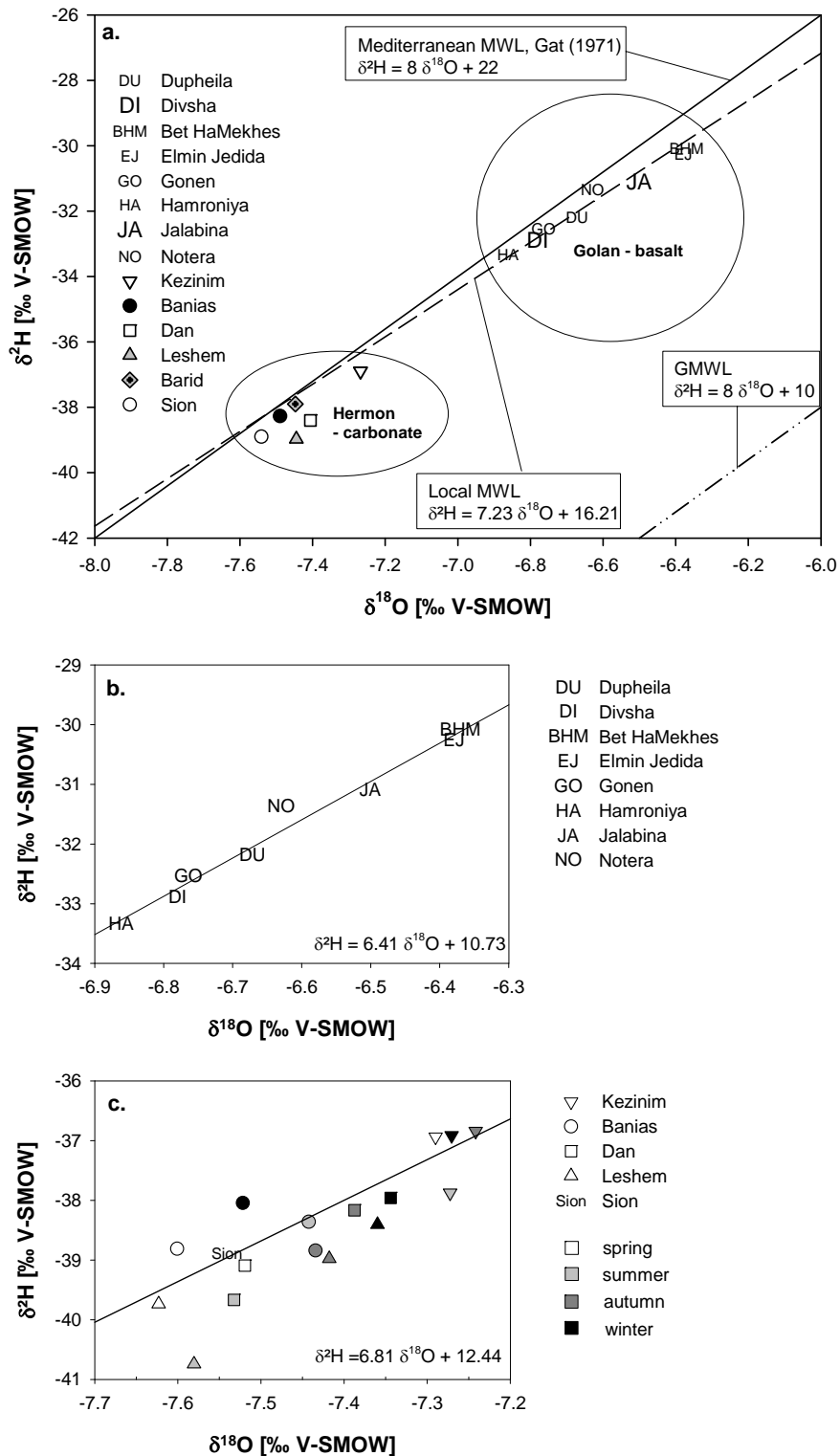


Figure 31: Relationship between mean $\delta^{18}\text{O}$ and $\delta^2\text{H}$ values for springs sampled in the northern UJRC. Figure a) distinctive grouping of groundwaters emerging in the Hermon Mountains and in the Golan Heights, Figure b) mean stable isotope composition of the Golan “Side Springs”, Figure c) seasonal stable isotope composition of the Hermon springs.

Strikingly, the $\delta^{18}\text{O}$ and $\delta^2\text{H}$ composition were quite similar for all of the Hermon springs. If the mean recharge altitudes of the springs would lay somewhere in between the altitude of the springs outlet and the top of Mount Hermon, $\delta^{18}\text{O}$ gradients between 4 to 6 ‰ could be expected based on the estimated $\delta^{18}\text{O}$ -altitude gradient. Since this is not the case, springs were assumed to be recharged at similar altitudes receiving different portions of conduit flow. Within the Hermon springs, a characteristic stable isotope pattern was recognizable. The Kezanim spring, assumed to be fed mainly by diffusive matrix flow (GUR et al., 2003) and shown to be of distinct hydrogeochemical composition (Table 17, Table 18) displays the most enriched stable isotope composition with only minor seasonal variations. Slightly more depleted in its stable isotope composition are the waters of the Dan and Leshem spring during autumn (October/November) and winter (December-March), and the Banias spring water during summer (June-September) and autumn representing baseflow conditions in the respective springs. Most depleted values of $\delta^{18}\text{O}$ and $\delta^2\text{H}$ were determined for the Sion spring, the Dan and Leshem spring during springtime (April/May) and summer and, the Banias spring in winter and spring. This depletion of $\delta^{18}\text{O}$ and $\delta^2\text{H}$ in the spring waters was attributed to significant contributions of freshly infiltrated water, in particular to the contribution of melt waters originating on the high slopes of Mount Hermon.

6.3 MIXING OF GROUNDWATER SOURCES IN THE UJRC

One objective of this study was to define the different end-members contributing to the discharge of the Hermon and Golan springs. The determination of end-members is a precondition for the intended application of mass-balance approaches and mixing models (see chapter 2.4.3.1), techniques that allow to quantify the contribution of single flow components to spring discharge. Generally, conservative natural tracers such as chloride, $\delta^2\text{H}$ and $\delta^{18}\text{O}$ that don't interact with the rock matrix and are assumed to originate exclusively from precipitation are combined in mixing models to identify different discharge components. However, sometimes one natural tracer alone will fail to recognize all end-members involved in discharge generation. Instead, the use of different tracers representative either for

anthropogenic pollution or for the contribution of waters from certain lithogenic layers might lead to more meaningful results (LEE and KROTHE, 2001; TARDY et al., 2004 among others).

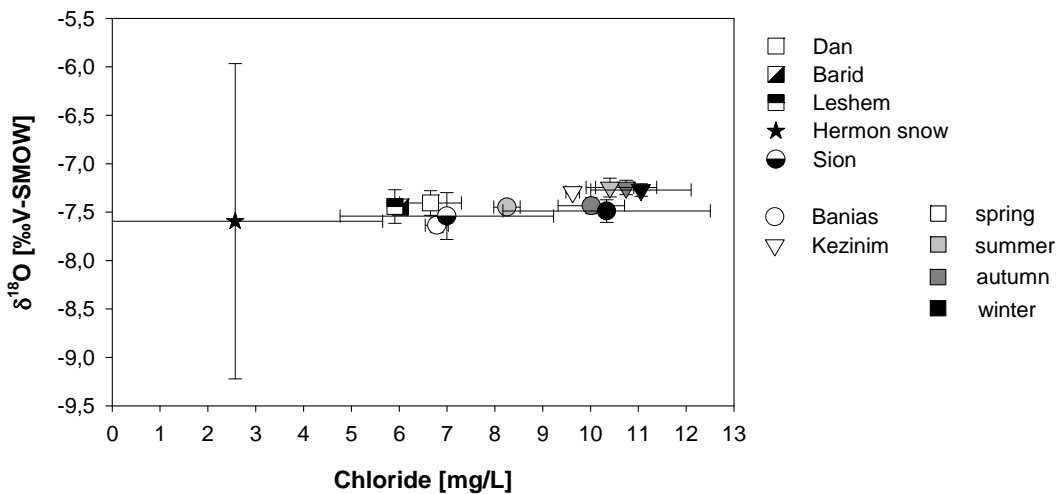


Figure 32: Relationship between mean oxygen isotopic composition and mean chloride concentration in the sampled Hermon spring waters and in Mt. Hermon snow. For the Banias and Kezanim spring, mean seasonal compositions are given. The error bars represent 1σ uncertainty.

6.3.1 Hermon springs

For the Hermon springs, chloride and sulfate were used as tracer in addition to the stable water isotopes (see chapter 6.2). Plotting $\delta^{18}\text{O}$ versus chloride for the investigated springs (Figure 32) revealed a linear relationship suggesting the mixing of two end-members: 1) precipitation represented by Hermon snow and 2) diffusive flow characterized by the chemical and isotopic composition of Kezanim groundwater (in particular during autumn). The Dan, Leshem, Barid, Sion and Banias groundwater fall on a mixing line between both components. Seasonal variations are highest for Banias water. During spring, the groundwater source tended to the precipitation end-member while it was close to the diffusive flow end-member during autumn and winter. KAFRI et al. (2002) suggested that the Sion-Rachaya fault divides the southern Hermon into an eastern and western recharge area. Hence, the Kezanim and Banias springs emerging in the southeastern part of Mt. Hermon receive geogenic contributions that cause the observed high chloride concentrations. These geogenic contributions are absent in the western recharge area.

Since sulfur is known to originate from marine sources within the recharge area of the Kezinim and Banias spring, sulfate was plotted versus chloride to further investigate the springs hydrogeology. While the Dan, Barid and Leshem spring water corresponded to the second end-member of a perfect mixing line between Mt. Hermon snow and these groundwater (Figure 33) suggesting no additional source of sulfate, a different pattern is observed for the Banias and Kezinim spring. Accordingly, the chemical composition of the Kezinim spring during summer and autumn represents the diffusive flow end-member. This end-member originates from parts of the aquifer containing evaporites (a possible gypsum source). Springs with high sulfate concentrations are frequently found in carbonate aquifers as a result of evaporite dissolution (GUNN et al., 2006). Banias spring water plot along a mixing line between the diffusive end-member and waters that are - in their chemical composition - similar to waters emerging at the Dan or Barid spring.

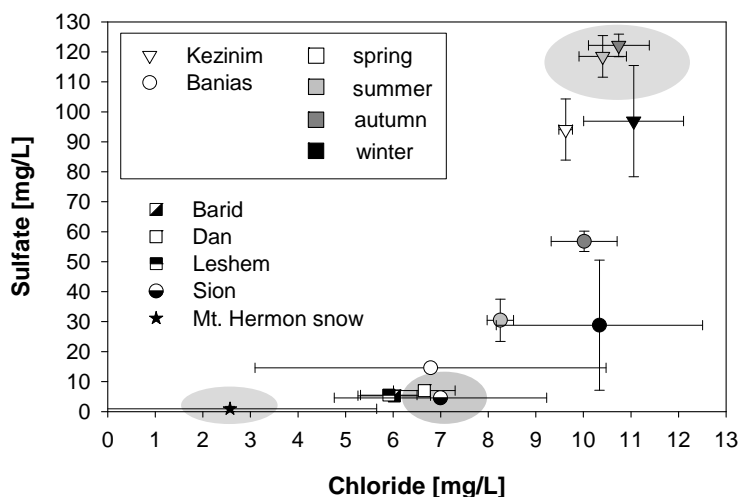


Figure 33: Relationship between mean sulfate and mean chloride composition in the sampled Hermon spring waters and Mt. Hermon snow. For the Banias and Kezinim spring, mean seasonal compositions are given. Grey frames indicate the suggested end-members. The error bars represent 1σ uncertainty.

Groundwater systems can receive local, intermediate and regional recharge depending on topography, basin depth and geological heterogeneity in the catchment (TÓTH, 1963). Theoretically, the hydrogeologic boundary conditions met in the UJRC (chapter 3.5) promote both, local flow and deep circulation of groundwater. Based on the conducted physico-

chemical and stable isotope analyses, it is assumed that the Kezinim spring is characterized by:

- a thermal regime (spring temperature is more than 5 K higher than the local mean annual temperature),
- highest mineralization within the Hermon springs,
- in particular, high concentrations of sulfate, chloride and silicate
- comparatively enriched values of $\delta^{18}\text{O}$ and $\delta^2\text{H}$,
- and low seasonal variations in its isotopic and chemical composition,

indeed represents a diffusive (matrix flow) component migrating to deep parts of the aquifer that are in contact with evaporites beds before rising back to the surface, the flow possibly directed by fault zones. The Banias spring also receives contribution of this diffusive flow component during baseflow as shown by its high sulfate concentration during autumn and summer (Figure 33). In contrast, water of the Dan, Barid, Leshem and Sion spring represent a shallow (local) calcium-bicarbonate type of groundwater where transport occurs in changing portions through both conduit/fissure and matrix flow. This is supported by the fact that the Sion spring, an ephemeral outlet known to be recharged through dolinas and conduits reveals similar hydrochemical characteristics as the Dan, Barid and Leshem springs. These assumptions were further supported through the conducted estimations of mean water residence times (chapter 6.8.1).

Consequently, three end-members are suggested to contribute to the Banias spring discharge:

- a direct (local) component with short residence times representing snow and rain recharge quickly transferred to the spring via conduits,
- an indirect (interflow) component with medium residence times representing infiltrated snow and rain stored in the epikarst zone and that, after this zone is saturated, travels to the spring through conduits and fissures,
- an indirect component with long residence times representing the diffusive flow component from the phreatic aquifer and dominating the Banias spring discharge during summer and autumn.

While the epikarst component is represented by the chemistry of the Sion spring, Kezinim water corresponds to the diffusive flow end-member as shown before. These results agree well with a study of GUR et al. (2003) who investigated the different end-members contributing to the flow of the Hermon springs.

6.3.2 Golan springs

DAFNY et al. (2006) developed a conceptual hydrogeological model for the Golan basalt aquifer suggesting the contribution of a regional aquifer and local perched aquifers to the Golan springs outflow. In the present study the focus was on the Golan “Side springs”. These emerge on the western flanks of the plateau and contribute with about $50 \text{ } 10^6 \text{ m}^3$ per year significantly to the discharge of Upper Jordan River. In addition to tritium, ^{18}O and deuterium, dissolved silica (SiO_2) was chosen to be a meaningful natural tracer in the groundwaters of this basaltic environment.

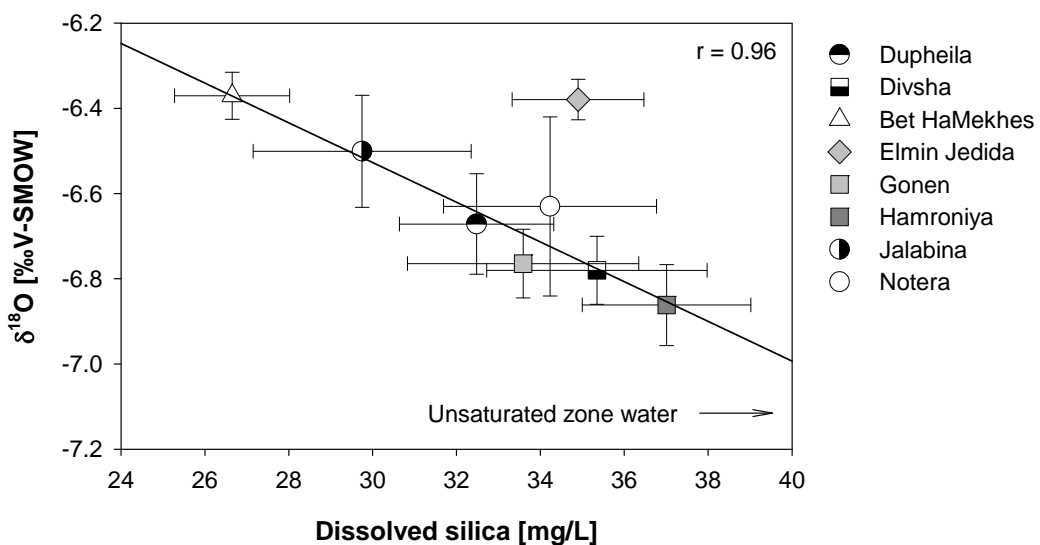


Figure 34: Relationship between mean oxygen isotopic composition and mean SiO_2 concentrations in the investigated Golan “Side springs”. Groundwaters (with the exception of the Elmin Jedida spring) plot along a perfect mixing line as indicated by the given correlation coefficient. The error bars represent 1σ uncertainty.

Golan groundwaters plot on a mixing line between two end-members. One end-member is characterized by comparatively enriched values of $\delta^{18}\text{O}$, as well as generally high chloride

concentrations but low concentrations of silica (Figure 34, Figure 35). This end-member represents groundwater from the regional aquifer that is recharged in the eastern part of the Golan Heights (partly in Syria) traveling east to west through deep parts of the aquifer. Low tritium concentrations of about 0-0.9 TU indicating groundwater mean residence times > 50 years in these springs support this assumption (Figure 35). Springs with significant contributions of this end-member are the Elmin Jedida, Bet HaMekhes and Jalabina spring. These springs are geographically the southernmost of the investigated ‘Side springs’. Springs that receive different portions of the second end-member are distinguished by more depleted $\delta^{18}\text{O}$, low concentrations of chloride and high concentrations of silicate (Figure 34, Figure 35). Since these characteristics coincide with tritium concentrations close to recent atmospheric tritium, it is assumed that the second end-member represents local recharge that derives its chemical pattern mainly in the unsaturated zone. Hence, springs that receive significant portions of recharge through the unsaturated zone will be characterized by depleted $\delta^{18}\text{O}$, low chloride and high silicate concentrations such as the Hamroniya, Gonen, Notera, Divsha and Dupheila springs.

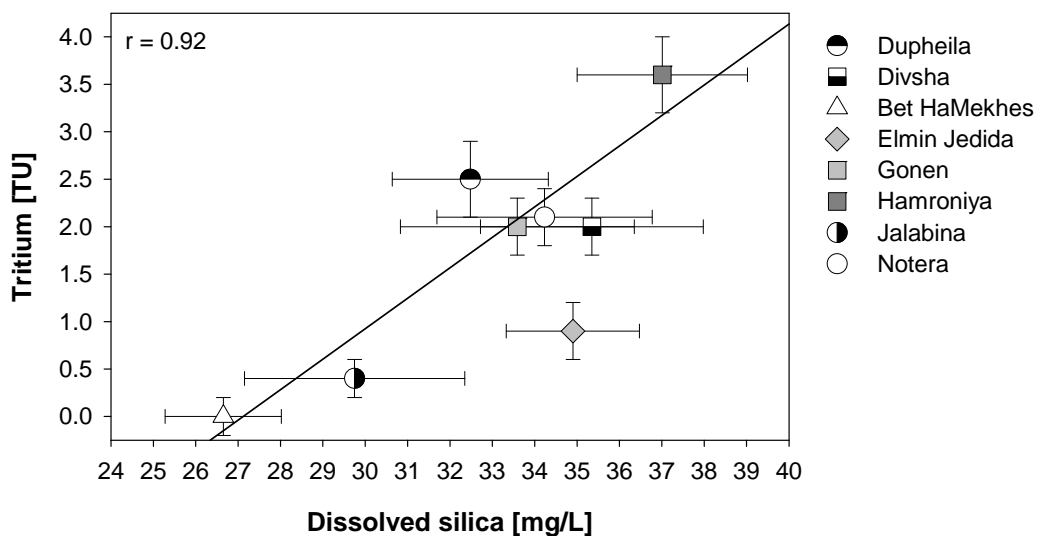


Figure 35: Relationship between tritium and mean dissolved SiO_2 concentrations in the investigated Golan ‘Side springs’. Groundwaters (with the exception of the Elmin Jedida spring) plot along a mixing line further indicated by the given correlation coefficient. The error bars represent 1σ uncertainty.

In contrast to dissolved chloride, silicate originates through weathering of the basaltic rocks. Generally, the dissolution of silica occurs very quickly (KENNEDY, 1971) and rainwater infiltrating into the basaltic rocks of the Golan Heights reached chemical equilibrium within one month as shown by SENDLER (1981) in lab experiments. However, ongoing infiltration of (in respect to silicate) undersaturated rainwaters into the unsaturated zone of the Golan Heights enables for high dissolution rates of silicate and subsequently, higher silicate concentrations in the shallow groundwaters compared to groundwater from the regional aquifer. The observed silicate concentrations in the “Side springs” correspond well to the concentration range (28-36 mg/L) monitored by KAFRI et al. (2002) for basaltic groundwaters in northern Israel.

Generally, the chemical and isotopic composition of the Golan ‘Side springs’ seem to follow a north-to-south gradient in that way reproducing the climatic and geological gradient observed for the Golan Heights (see chapter 3.2 and 3.5.3). The northern Golan is characterized by a comparatively thick aquifer, a thick unsaturated zone and high amounts of precipitation and recharge. Here, ‘Side springs’ such as the Hamroniya, Gonen and Notera springs display high contributions of unsaturated zone water resulting in tritium-rich groundwater with low chloride and high silicate concentration. In the south, where evaporative effects increase and comparatively less recharge through the unsaturated zone occurs, low-tritium water with high amounts of chloride are found in the Bet HaMekhes and Jalabina spring.

6.4 ESTIMATION OF RECHARGE ALTITUDES AND GROUNDWATER RECHARGE RATES

6.4.1 Recharge altitude

The established relationship between the stable isotope ($\delta^{18}\text{O}$, $\delta^2\text{H}$) composition of precipitation and altitude as given in chapter 5.3.7 allows to identify the mean replenishment areas for the investigated springs. For the southern Hermon Mountains, the observed gradient is about -0.26 ‰ per 100 m altitude for $\delta^{18}\text{O}$ (Figure 37). The major springs in this area all emerge at low slopes of the Hermon Mountain at altitudes between 180 m to 390 m. Since their mean isotopic composition is very alike ranging between -7.27 ‰ and -7.55 ‰ for $\delta^{18}\text{O}$,

one would assume that they are recharged at similar altitudes. However, Hermon springs are mainly fed by snowmelt recharge. The melting of snow is usually accompanied by fractionation processes resulting in the enrichment of infiltrating waters (STICHLER et al., 1981; UNNIKRISHNA et al., 2002). TAYLOR et al. (2002) showed that the isotopic enrichment in a snowpack during a melting event was about 3 to 5 ‰ with high local variations. That means infiltrating snowmelt does not possess the isotopic altitude information anymore.

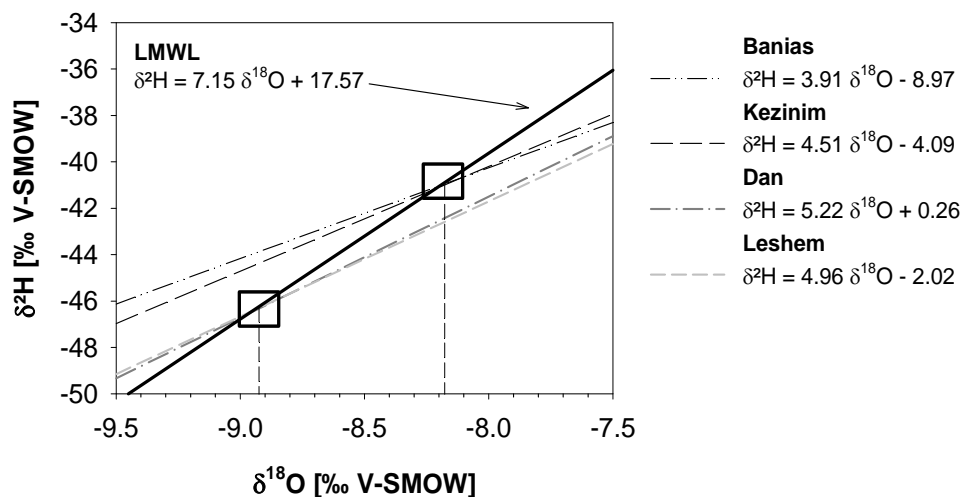


Figure 36: Local “Enrichment” Lines (LELs) of the investigated Hermon springs plotted against the Local Meteoric Water line (LMWL) based on weekly bulk samples of precipitation. Frames indicate the initial stable isotopic composition ($\delta^{18}\text{O}$, $\delta^2\text{H}$) of the recharged groundwaters.

In this study, the mean isotopic ($\delta^{18}\text{O}$) composition of precipitation infiltrating into the recharge area of the respective spring was suggested to be retraceable. For each spring, so-called local enrichment lines (LEL)⁴ were plotted against the local meteoric water line (LMWL) determined for weekly precipitation samples in the northern UJRC. Intersects of LELs with the LMWL were assumed to represent the spatially integrated, amount-weighted stable isotope composition of precipitation (Figure 36).

Based on the corrected mean isotopic composition of infiltrating waters mean recharge altitudes were estimated (Figure 37). As a result, the mean recharge altitudes of the Banias

⁴ Generally, local **evaporation** lines are plotted against the LMWL to define the initial stable isotope composition of lake waters or brines before evaporation (GAMMONS et al., 2006). In our case however, the deviation of the groundwaters from the meteoric water line can be due to enrichment during snowmelt also. Hence, the regression lines are called local **enrichment** lines comprising both evaporation and snowmelt effects.

and Kezanim springs were calculated to be about 1260 m. The Dan, Leshem and Barid are replenished from a mean recharge altitude of about 1560 m, while the Sion springs mean recharge altitude is at about 1320 m. However, since the extent and location of the springs subsurface catchment areas are still unknown it is difficult to verify these estimations. Based on an altitude gradient of -0.25 ‰ per 100 m for $\delta^{18}\text{O}$ in shallow groundwater of the Golan Heights, DAFNY et al. (2006) estimated the recharge altitudes for the Golan “Side springs” to be about 750-900 m.

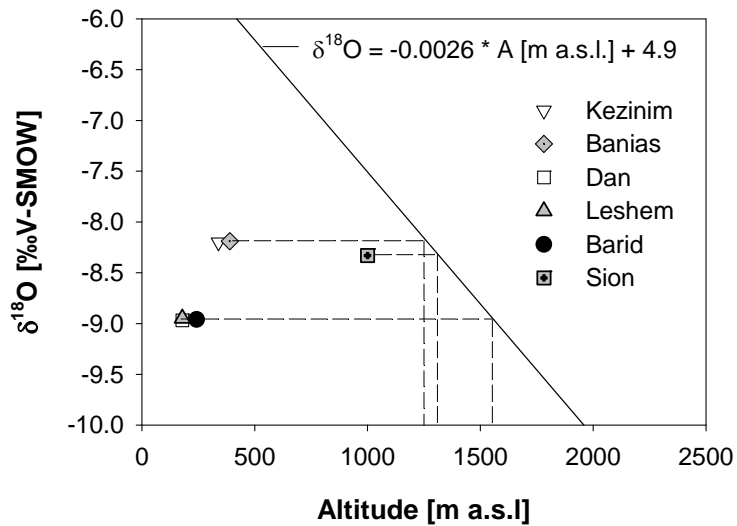


Figure 37: Altitude versus $\delta^{18}\text{O}$ in precipitation in the southern Hermon Mountains. The line is a best-fit to daily rainfall samples taken during 2002-2004. Isotopic composition of the springs was corrected for enrichment effects (see Figure 36). Their main recharge elevation is inferred by determining the altitude at which precipitation has approximately the same isotopic composition.

6.4.2 Groundwater recharge rates

The term *groundwater recharge* describes the infiltration of water (precipitation) through the unsaturated zone and its addition to the aquifer. Given that infiltration is spatially distributed over large areas, the term *diffusive (direct) recharge* is being used. In semi-arid areas, *(indirect) localized recharge* at wadis (dry stream beds), ephemeral streams, lakes or through preferential flow in fractured rocks are common phenomena (SCANLON et al., 2006).

A review on techniques to quantify groundwater recharge in the unsaturated or saturated zones by physical, chemical, isotopic or modelling approaches is given by LERNER (1990),

HENDRICKX and WALKER (1997), ZHANG (1998), KINZELBACH et al. (2002), SANFORD (2002), VRIES and SIMMERS (2002), and SCANLON et al. (2002). However, the method most widely used to estimate groundwater recharge rates in unsaturated as well as saturated zones is the chloride mass balance (CMB) which is also applied in this study. This technique is based on the assumption that chloride behaves conservatively and that Cl^- concentrations in groundwater solely increase because of evaporation in the upper part of the unsaturated zone and remain constant below this depth. Chloride concentrations can be reliably determined for atmospheric deposition and groundwaters, thus a mass balance approach allows to quantify groundwater recharge locally or on a regional scale. Accordingly,

$$R = \frac{P \times \text{Cl}_P}{\text{Cl}_{GW}}$$

where R [mm/year] is the annual recharge rate, P [mm/year] the mean annual precipitation, Cl_P [mg/L] the average chloride concentration in precipitation, and Cl_{GW} the average chloride concentration in groundwater.

In this study, recharge rates were estimated separately for the Hermon and Golan springs, the results are presented in Table 21. Since mean annual chloride concentrations determined in the Hermon springs are significantly influenced by fast flow components resulting in the dilution of Cl^- concentrations, mean chloride concentrations during winter (baseflow conditions) were chosen to represent diffusive groundwater flow.

Based on the mean annual precipitation for the Hermon region determined by RIMMER et al. (2006), recharge in the Hermon springs ranged between 12 to 13 % of P for the Banias and Kezinim spring to about 20 % of P for the Barid, Leshem and Dan springs. Since the Banias and Kezinim spring both receive chloride contributions from the aquifer as shown earlier (chapter 6.1.2), recharge rates for these springs are underestimated. For the Golan “Side springs”, recharge estimates differed between 12 % to 16 % of mean annual precipitation and agreed well with the suggested 10 to 30 % of the total precipitation as received by other authors for this region (DAFNY et al. 2006; BURDON, 1954; MERO and KAHANOVITZ, 1969; MICHELSON and MICHALI, 1971; MICHELSON, 1979).

Table 21: Estimated groundwater recharge rates for the investigated springs in the UJRC. Cl_{GW} represents the mean concentration of chloride during baseflow (winter), P the mean annual precipitation for the Hermon region¹⁾ and Cl_P the median concentration of chloride in snow (Hermon springs) and rain (Golan springs). R is the calculated recharge rate given in mm/year and % of mean annual precipitation.

Spring	Cl_{GW} mg/L	P mm/year	Cl_P mg/L	R mm/year	R % P
<i>Hermon springs</i>					
Barid	6.4	958 ¹⁾	1.31	196	20
Leshem	6.3	958 ¹⁾	1.31	199	21
Dan	6.9	958 ¹⁾	1.31	182	19
Banias	10.3	958 ¹⁾	1.31	122	13 (+ geogenic chloride)
Kezanim	11.1	958 ¹⁾	1.31	113	12 (+ geogenic chloride)
<i>Golan springs</i>					
Gonen	14.9	800 ²⁾	2.41 ³⁾	129	16
Divsha	15.1	800 ²⁾	2.41 ³⁾	128	16
Jalabina	17.2	800 ²⁾	2.41 ³⁾	112	14
Notera	17.4	800 ²⁾	2.41 ³⁾	111	14
Hamroniya	17.1	800 ²⁾	2.41 ³⁾	113	14
Dupheila	16.1	800 ²⁾	2.41 ³⁾	120	15
Bet HaMekhes	20.7	800 ²⁾	2.41 ³⁾	93	12
Elmin Jedida	19.7	800 ²⁾	2.41 ³⁾	98	12

1) RIMMER et al. (2006)

2) HARRIS (1978), NAOR and COHEN (2003)

3) HERUT et al. (2000)

Another hydrogeological problem so far unsolved for the Upper Jordan River Catchment was the determination of the subsurface recharge areas (RIMMER et al., 2006). Orographic catchment areas as given in Table 5 cannot account for the observed recharge rates. Thus, based on the estimated recharge rates (Table 21), subsurface catchment areas were approximated by applying:

$$A_R = \frac{MF}{R}$$

where A_R [km²] is the recharge area of the respective spring (or stream), MF [L/s] is the mean annual discharge measured for the spring (or stream), and R [L/s km⁻²] is the estimated recharge rate as presented in Table 21. Assuming that the Dan and Leshem spring are the major contributors to mean annual discharge in the Dan stream, the combined subsurface recharge area for these two springs was calculated to be about 1324 km². Hence, recharge to

the Dan stream generates from a big part of the Anti-Lebanon/Hermon mountain range (actually laying in Lebanon and Syria). The combined subsurface catchment area for the Banias and Kezinim spring was estimated to be about $\approx 523 \text{ km}^2$ based on mean flow of the Hermon stream and a recharge rate of 20 % P , thus exceeding the surface catchment area of the Hermon stream (105 km^2) by far. The same might be true for the Senir stream, however, within the scope of this study there were no means to study the hydrochemistry of the contributing Wazani and El-Hazbani springs. However, the quality of these estimations is limited by uncertainty in the determination of the mean annual precipitation on Mount Hermon, a problem to be addressed in future investigations. Subsurface recharge areas for the Golan springs ranged between 0.6 to 3 km^3 based on the yields given by MICHELSON (1996; Table 3).

6.5 TEMPORAL VARIATIONS IN GROUNDWATER CHEMISTRY AND ISOTOPIC CONTENT

Temporal variations observed or absent at groundwater outlets such as springs and wells comprise a variety of information about the nature of the underlying groundwater system. Continuous recharge to an aquifer of homogeneous porosity results in uniform discharge patterns. In contrast, heterogeneous (seasonal) recharge to a double-porosity system such as karst can lead to high variations of discharge and a broad range of tracer concentrations monitored at the systems outlet.

A variety of chemical or isotopic tracer techniques are available to decode the nature of a specific aquifer (chapter 2.4.4). The dilution of non-reactive natural tracers indicates the addition of new water, *i.e.* recharge to the hydrogeological system. The stable isotopes of water in particular, were shown to be functional tracers to detect the arrival of new (event) water such as snowmelt or rain recharge. Snowmelt recharge for instance, is generally detected by depleted $\delta^{18}\text{O}$ or $\delta^2\text{H}$ concentrations in discharge compared to groundwater since the rapid melting of snow is characterized by a loss of light isotopes in respect to the remaining snow cover (RODHE, 1981; STICHLER et al., 1981; TAYLOR et al., 2001). However, although still lighter than groundwater, subsequent meltwaters generally show a progressive

enrichment of stable water isotopes (TAYLOR et al., 2002), a fact to be considered when applying hydrograph separation techniques. In this study, the main goal was to detect and quantify the contribution of different reservoirs to discharge measured at the springs and thus to deduce the vulnerability of the groundwater system towards climate change. Although a broad range of natural tracers were monitored for the Hermon and Golan springs, the understanding of the underlying hydrogeology was based particularly on the selection of natural tracers given in Table 22 and Table 23.

6.5.1 Hermon springs

Temperature and electrical conductivity are both easy-to-monitor tracers. Temperature measurements might indicate the arrival of new water when observing cold spring temperatures during the recharge season. These originate through the dilution of heat originally added by geothermal warming (MANGA and KIRCHNER, 2004).

Changes in electrical conductivity on the other hand, point to dilution or enrichment of baseflow chemistry. Chloride was chosen because at least for the Hermon springs Sion, Dan, Barid and Leshem it acts as a conservative tracer as does sulfate. For the Banias and Kezinim spring, sulfate represents contributions from the phreatic part of the aquifer (compare chapter 6.3.1) while chloride, though plotting close to the seawater-dilution-line, does not behave conservative due to the occurrence of halite beds in the aquifer feeding these two springs. The stable water isotopes, as mentioned above, help to distinguish new (event) water from pre-event waters while the deuterium excess value reveals information either on the origin of recharge-generating precipitation or on fractionation effects during recharge. Two different intake areas have been suggested for the Hermon springs (KAFRI et al., 2002). An eastern intake area for the Banias and Kezinim spring on the one hand and a western one for the Dan, Leshem and Barid spring on the other hand. A hypothesis that is further supported by the findings of the conducted temporal analyses in this study.

Table 22: Seasonal distribution of mean natural tracer concentrations in the major Hermon springs (autumn: October-November, winter: December-March, spring: April-May, summer: June-September).

Spring	Season	T °C	EC μS/cm	Cl ⁻ mg/L	SO ₄ ²⁻ mg/L	δ ¹⁸ O ‰	δ ² H ‰	d ‰
Barid	autumn	16.0	321	6.0	5.2	-7.42	-39.4	20.0
	winter	15.7	335	6.4	5.7	-7.42	-36.3	23.0
	spring	-	-	-	-	-	-	-
	summer	15.0	312	4.8	4.2	-7.54	-39.6	20.7
Leshem	autumn	15.2	320	5.8	6.2	-7.41	-39.0	20.3
	winter	15.3	328	6.3	5.9	-7.36	-38.4	20.5
	spring	14.9	303	5.6	4.7	-7.62	-39.5	21.3
	summer	14.8	302	5.1	4.7	-7.63	-40.9	20.2
Dan	autumn	16.0	349	6.8	7.7	-7.39	-38.2	20.6
	winter	16.0	345	6.9	7.2	-7.35	-38.0	20.8
	spring	16.0	336	6.4	6.5	-7.52	-37.8	21.9
	summer	15.7	328	5.9	6.2	-7.56	-40.0	20.5
Banias	autumn	15.6	462	10.0	56.8	-7.43	-37.9	21.5
	winter	15.2	387	10.3	28.8	-7.49	-38.3	21.6
	spring	14.5	331	6.8	14.6	-7.64	-38.0	23.1
	summer	15.1	385	8.3	30.5	-7.44	-39.1	20.5
Kezanim	autumn	20.4	607	10.7	122.2	-7.25	-36.9	21.1
	winter	19.6	553	11.1	96.9	-7.27	-36.9	21.3
	spring	19.8	546	9.6	94.1	-7.29	-36.7	21.9
	summer	20.6	591	10.4	118.5	-7.25	-37.4	20.5

The Dan spring was - compared to the two other springs of the western intake area - Barid and Leshem, the most stable when looking at the temporal development of its water chemistry. All three springs exhibited more or less the same seasonal pattern. The highest temperatures, electrical conductivities, ion concentrations and most enriched values of δ¹⁸O and δ²H were observed during autumn and winter indicating baseflow conditions. On the other hand, the lowest temperatures, electrical conductivities, ion concentrations and most depleted stable water isotopes were monitored during spring and summer demonstrating the influence of recent (winter) recharge. The most significant contribution of recharge to these sources occurred in springtime accompanied by high discharge and strong dilution effects on the groundwater chemistry (Table 22, Figure 38).

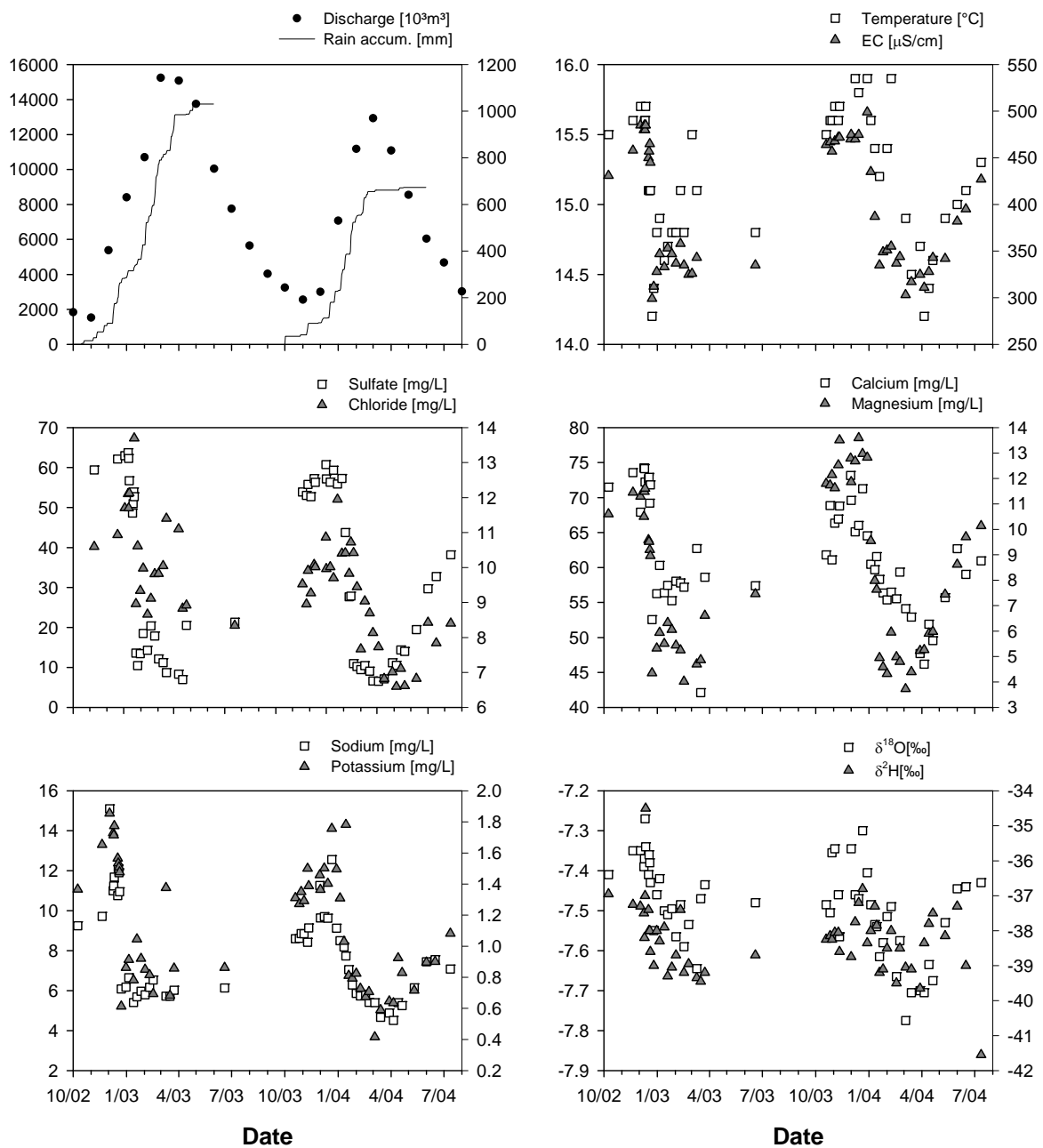


Figure 38: Seasonal development of monthly discharge, temperature, electrical conductivity, major ions and stable isotopes ($\delta^{18}\text{O}$, $\delta^2\text{H}$) in the Banias spring during the study period 2002-2004. Also shown are the annual accumulated rain amounts measured at the Banias Nature Reserve. The parameter that is mentioned first in the legends above the graphs refers to the left axis, the second one to the right axis.

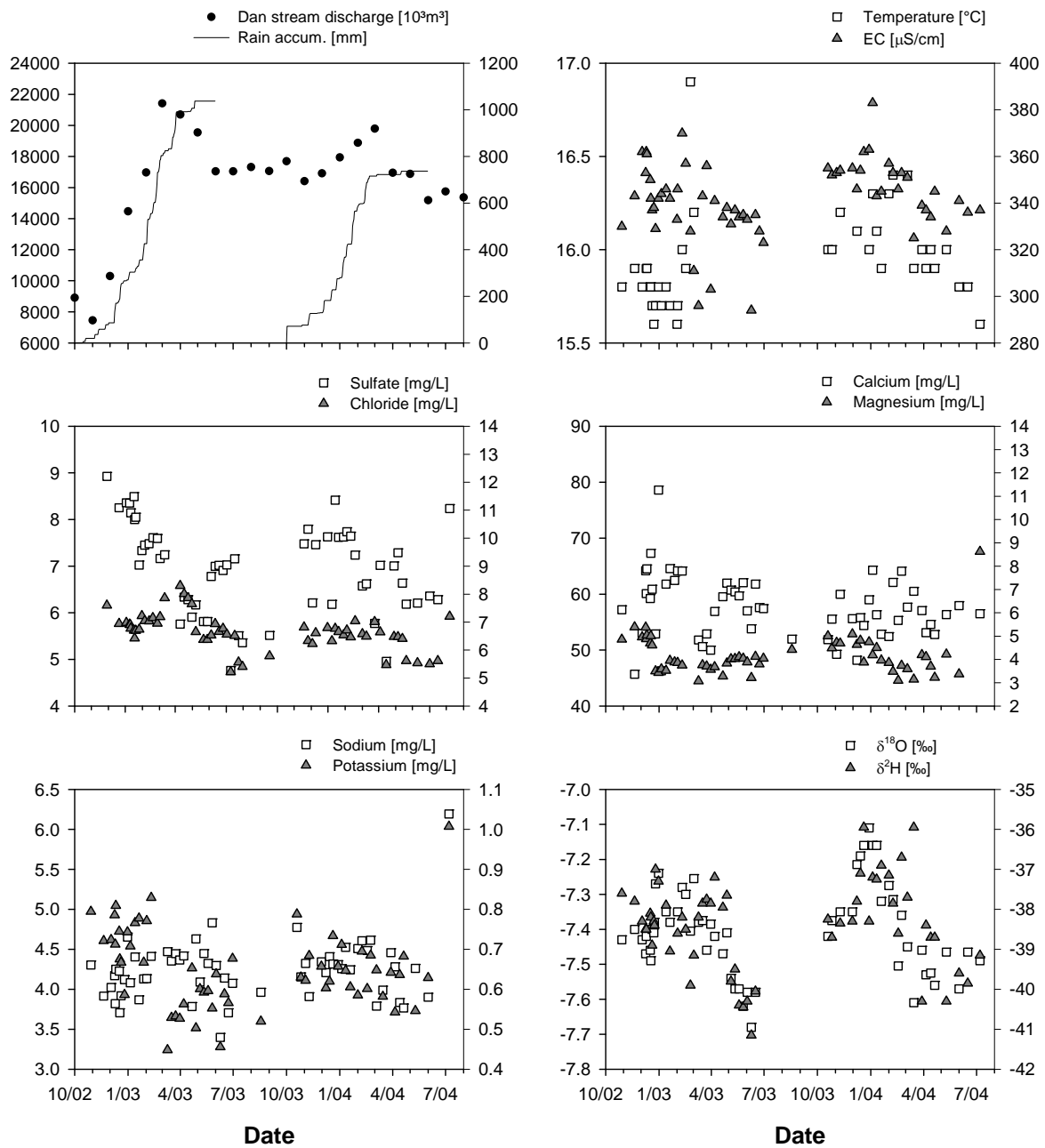


Figure 39: Seasonal development of monthly discharge, temperature, electrical conductivity, major ions and stable isotopes ($\delta^{18}\text{O}$, $\delta^2\text{H}$) in the Dan spring during the study period 2002-2004. Also shown are the annual accumulated rain amounts measured at the Dan Nature Reserve. The parameter that is mentioned first in the legends above the graphs refers to the left axis, the second one to the right axis.

No direct response to winter precipitation was detected for these springs because of three-month delay suggesting a vast intake area where incoming water is significantly diluted. Another reasonable explanation could be, that the Dan, Leshem and Barid spring are recharged at higher altitudes where winter precipitation is stored as snow. Hence, recharge is

only activated when rising temperatures in spring cause the snow to melt. Consequently, the discharge delay is not caused by the nature of the hydrogeological flow system but by the snow cover on Mount Hermon that acts as an external reservoir distributing recharge over time. The importance of snowmelt recharge during spring was additionally confirmed by high values of deuterium excess monitored during that time (Table 22). At first, this appears contradictorily to conclusions drawn before on the enriched stable isotope composition ($\delta^{18}\text{O}$, $\delta^2\text{H}$) of snowmelt in comparison to precipitation (fresh fallen snow) (see chapter 6.4.1). However, this is not the case. The overall composition of snowmelt that recharges the Hermon springs is enriched in comparison to precipitation on Mt. Hermon because of fractionation processes during the melting of the snowpack. Yet, the initial melting of a snowcover is accompanied by the release of melt water with light water isotopes (STICHLER et al., 1981; UNNIKRISHNA et al., 2002; HUTH et al., 2004). Since the early melting events are also those with the highest release of meltwater into the Hermon aquifer as shown by the Sion stream hydrograph (Figure 50), meltwater that quickly reaches the spring will display comparatively light stable isotopic composition and high deuterium excess values.

The same occurrence of elevated deuterium excess values was observed for the springs of the eastern intake area, Banias and Kezanim, indicating the importance of snowmelt for these two springs as well. However, while the Kezanim spring exhibits a relatively stable groundwater chemistry and isotopic composition over time representing its diffusive flow nature, the karstic character of the Banias springs is clearly shown by its variable spring chemistry. In contrast to the springs of the western intake area, the Banias spring showed an immediate response to winter precipitation accompanied by the dilution of geochemical tracers and depleted values of stable water isotopes (Table 22, Figure 40). Highest temperatures, electrical conductivities, ion concentrations and most enriched values of $\delta^{18}\text{O}$ and $\delta^2\text{H}$ are observed during summer and autumn indicating baseflow conditions.

The importance of conduit flow to the Banias spring becomes even more evident when looking at Banias spring runoff in December 2002 (Figure 40). From December 9th to 12th, 83.3 mm of accumulated rain were measured at the Banias Nature Reserve resulting in a slight but immediate contribution of new water to the springs discharge leading to lower

temperatures, electrical conductivities, ion concentrations and slightly more depleted concentrations of $\delta^{18}\text{O}$ and $\delta^2\text{H}$. Additional 95.2 mm of precipitation from December 17th to 21st led to increased concentrations of chloride and sulfate and enriched values of the stable water isotopes pointing to the activation of more mineralized water. Another rain spell on December 24th produced major dilution effects on groundwater chemistry, low water temperatures and a peak of light $\delta^{18}\text{O}$ and $\delta^2\text{H}$. This type of temporal isotopic and chemical signature is explained by an epikarst storage-displacement mechanism.

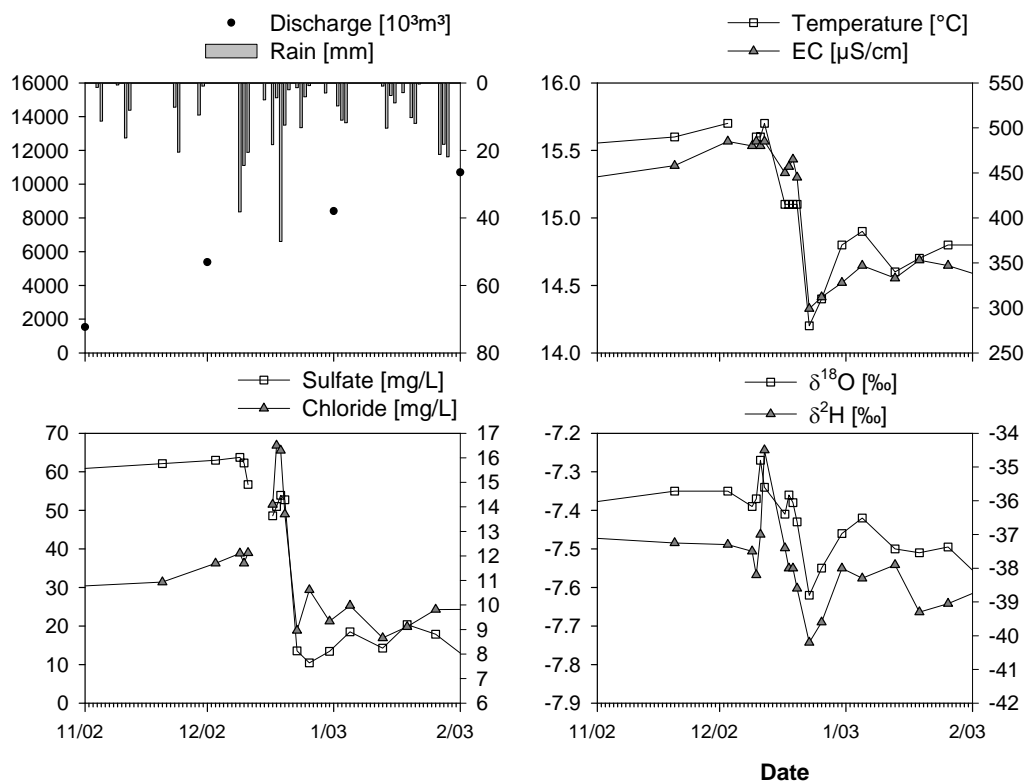


Figure 40: Temporal variations of temperature, electrical conductivity, sulfate, chloride and the stable water isotopes during three subsequent rain events in December 2002. Also shown are daily rain values and monthly discharges measured at the Banias Nature Reserve. The parameter that is mentioned first in the legends above the graphs refers to the left axis, the second one to the right axis.

The first rain event led to the saturation of the epikarst zone which was thus connected to the main drainage system via conduit flow and resulted in the arrival of some of the low-mineralized precipitation waters at the springs outlet. However, part of the water was stored within the epikarst and reacted with salts and minerals that were concentrated in the soil and epikarst zone by evaporation throughout the preceding dry season. During the second rain

event, precipitation from the previous event stored in the epikarst zone was displaced by the newly incoming waters and resulted in the observed flushing effects. Since the epikarst zone was already saturated during the third event, the additional precipitation led to the immediate displacement of now diluted epikarst water via the major drainage network leading to the monitored occurrence of depleted stable water isotopes and low-mineralized waters in the Banias spring (Figure 40).

Since the delay of water is only within the range of a few days, the epikarst zone feeding the Banias spring is assumed to be a limited reservoir. For subsequent hydrograph separation studies it has to be taken into account that water monitored during a high discharge event (***n***) at the spring originates most likely from the previous precipitation event (***n-1***) as observed for other karst systems (AQUILINA et al., 2006). Within the scope of this study however, there were no means to continuously monitor discharge at the Banias spring in order to enable for event hydrograph separation.

One of the objectives of this study was to estimate the contribution of snowmelt recharge to the sources of the Upper Jordan River. However, event-based analyses of single springs were not in the scope of this work. Additionally, discharge data, provided by the Hydrological Service of Israel, were only available for some of the springs. For the Kezanim spring for example, a measuring weir was installed only after the end of our field investigations. Nonetheless, contributions of different reservoirs to spring outflow were roughly estimated based on monthly discharge and mean monthly chemical and isotopic data for the Banias and Dan spring.

6.5.2 Golan ‘Side springs’

Snowmelt is negligible on the Golan Heights and therefore rain is the principal recharge input. As described before, two types of aquifers control the discharge behaviour of most of the Golan “Side springs”, a deep regional and smaller perched aquifers (DAFNY et al., 2006). Since water from the deep aquifer has tritium ages > 50 years, only local recharge from the perched aquifers can lead to a seasonal bias in spring chemistry.

Table 23: Seasonal distribution of mean tracer concentrations in the Golan “Side springs” (autumn: October-November, winter: December-March, spring: April-May, summer: June-September).

Spring	Season	T °C	EC μS/cm	Cl mg/L	SO ₄ mg/L	δ ¹⁸ O ‰	δ ² H ‰	d ‰
Gonen	autumn	19.4	306	15.7	5.5	-6.78	-31.8	22.4
	winter	18.0	316	14.8	5.8	-6.81	-32.8	21.6
	spring	19.1	312	13.9	5.7	-6.72	-33.2	20.6
	summer	19.9	317	15.0	6.4	-6.70	-32.3	21.3
Divsha	autumn	21.3	315	14.8	7.3	-6.85	-32.8	22.0
	winter	19.4	325	14.7	6.6	-6.82	-33.1	21.4
	spring	19.5	336	15.8	7.8	-6.71	-33.1	20.6
	summer	20.5	336	16.0	6.9	-6.72	-32.5	21.3
Jalabina	autumn	20.3	326	18.0	4.2	-6.54	-31.5	20.8
	winter	18.2	332	17.1	4.6	-6.47	-30.7	21.1
	spring	18.4	328	16.5	5.0	-6.44	-30.6	21.0
	summer	20.3	328	17.4	4.4	-6.53	-31.4	20.8
Notera	autumn	19.7	327	17.4	6.4	-6.70	-31.6	22.0
	winter	19.4	333	16.7	6.6	-6.71	-30.6	23.1
	spring	19.3	328	16.3	6.5	-6.50	-32.1	19.9
	summer	19.7	337	17.8	5.9	-6.62	-31.7	21.2
Hamroniya	autumn	19.4	365	17.9	6.5	-6.80	-32.3	22.1
	winter	19.2	341	16.9	5.8	-6.87	-33.4	21.5
	spring	18.6	344	16.3	5.6	-6.90	-33.7	21.5
	summer	19.0	340	17.7	5.7	-6.86	-33.5	21.3
Dupheila	autumn	19.4	367	17.6	7.6	-6.71	-31.8	21.9
	winter	19.4	347	16.0	5.1	-6.73	-31.9	21.9
	spring	19.4	349	15.6	5.5	-6.51	-32.2	19.9
	summer	19.7	362	15.6	7.3	-6.61	-34.0	18.9
Bet HaMekhes	autumn	20.6	350	21.0	4.1	-6.42	-30.5	20.8
	winter	19.1	361	21.0	4.3	-6.37	-29.9	21.1
	spring	20.4	358	19.7	2.6	-6.33	-29.3	21.3
	summer	21.1	356	20.4	3.8	-6.36	-30.7	20.2
Elmin Jedida	autumn	20.4	392	19.7	5.3	-6.39	-30.5	20.6
	winter	20.3	398	19.5	5.1	-6.39	-30.2	21.0
	spring	20.5	404	19.2	5.1	-6.34	-30.0	20.8
	summer	20.8	403	20.1	4.6	-6.37	-30.4	20.5

However, temporal variations in the investigated Side springs are small with a minor trend towards lower temperatures, electrical conductivities and more depleted δ¹⁸O values during

winter and spring (Table 23). The thickness of the unsaturated zone and extensive mixing of incoming waters with baseflow cause the observed balanced chemical and isotopic composition of the groundwater outlets.

6.6 BANIAS SPRING – LONG-TERM HYDROGRAPH SEPARATION

The Banias spring is a perennial spring that responds quickly to precipitation (see above). This responsiveness is accompanied by large variations of the spring's chemical and isotopic composition indicating the rapid mixing of event with pre-event water. However, during baseflow conditions, discharge and the isotopic and chemical composition of the Banias spring are constant. It thus seems evident that the diffusive flow system controls the spring discharge during baseflow and the conduit flow system dominates the spring after rain or snowmelt events, *i.e.* during recharge conditions (see also 2.1.1). Hence, in a first step, a two-component mixing model using $\delta^{18}\text{O}$ as tracers was applied to divide the observed spring discharge into an event (conduit flow) and a pre-event (diffusive flow) component.

6.6.1 Two-component mixing model using $\delta^{18}\text{O}$ as tracer

The theoretical basis of this kind of analysis was given in chapter 2.4.3. Thus, the two-component mass balance for pre-event water (diffusive flow) mixing with event water (conduit flow) in the Banias spring is given as:

$$Q_T = Q_E + Q_{PE}$$

$$Q_T \delta_T = Q_E \delta_E + Q_{PE} \delta_{PE}$$

where Q_T is the total discharge measured at the Banias spring, Q_E is the amount of event flow (rain or snow that is rapidly transferred through conduits or fissures) and Q_{PE} is the amount of pre-event flow which is assumed to approximate baseflow. Delta notation represents $\delta^{18}\text{O}$ for total discharge δ_T , event flow δ_E , or pre-event flow δ_{PE} . Combining the two equations results in:

$$Q_E = Q_T \frac{\delta_T - \delta_{PE}}{\delta_E - \delta_{PE}}$$

Although the available discharge, chemical and isotopic data allowed for a rough estimation of discharge components only, a necessary precondition was to define the isotopic composition of the event component (δ_E) as accurately as possible. Given the altitude-dependent distribution of precipitation and its isotopic composition are known, a spatially integrated, amount-weighted value for the stable isotopic composition of the event component can be calculated with the help of GIS tools. Here, a different approach was applied. For each spring, so-called local enrichment lines (LEL) were plotted against the local meteoric water line (LMWL) determined for weekly precipitation samples in the northern UJRC. Intersects of LELs with the LMWL were assumed to represent the spatially integrated, amount-weighted stable isotope composition of precipitation (see chapter 6.4.1, Figure 36). Precipitation is believed to have more or less the same chemical and isotopic ($\delta^{18}\text{O}$, $\delta^2\text{H}$) composition as the event component.

The isotopic composition of the pre-event component was determined as the $\delta^{18}\text{O}$ concentration of the month were baseflow conditions prevail which is indicated by the most enriched values for $\delta^{18}\text{O}$ and $\delta^2\text{H}$. In the investigated case, the stable water isotope composition of the Banias spring during November 2002 and December 2003 was chosen to represent baseflow conditions. Input data for the conducted two-component hydrograph separations are given in Table 25.

Monthly portions of the two flow components (event, pre-event water) determined for the hydrological years 2002/03 and 2003/04 in the Banias spring are given in Table 24.

Table 24: Monthly portions of event (P_E) and pre-event water (P_{PE}) of total discharge at the Banias spring as determined by two-component hydrograph separation using ^{18}O as a natural tracer.

	Oct	Nov	Dec	Jan	Feb	Mar	Apr	May	Jun	Jul	Aug	Sep
2002/03												
P_E	%	0	5	16	23	20	n.d.	n.d.	15	n.d.	n.d.	n.d.
P_{PE}	%	100	95	84	77	80	n.d.	n.d.	85	n.d.	n.d.	n.d.
2003/04												
P_E	%	0	20	21	42	35	17	6	4	n.d.	n.d.	n.d.
P_{PE}	%	100	80	80	58	65	83	94	96	n.d.	n.d.	n.d.

n.d.: not determined.

Spring discharge at the Banias spring and the contribution of the different discharge components depend on the prevailing recharge pattern. The hydrological year 2002/03 was in terms of precipitation an extraordinary year following an average rain year in 2001/02. In 2002/03 patches of snow persisted until midsummer on Mt. Hermon enabling ongoing recharge to the springs located in the area. The year 2003/04 in turn, was again an average precipitation year with the last major rain falling in February.

Although pre-event water dominated the discharge of the Banias spring throughout the two investigated years (Table 24), event water which was assumed to represent the conduit flow system could account for up to 42 % of the springs total discharge. Unfortunately, sampling did not cover each month, however, for 2003/04 it could be shown, that the highest event water contributions occurred in March and April 2004 during the major melting of snow on Mt. Hermon. However, it seems unreasonable that the pre-event component represents diffusive (phreatic) flow alone since this water was shown to travel to great depths before rising to the surface again (chapter 6.3.1). Additionally, the strong dilution of sulfate concentrations that are representative for the diffusive (phreatic) flow component (Figure 38) suggests that pre-event water does not equal phreatic zone water but comprises an additional component.

Epikarst storage was shown to play an important role in the flow system of the Banias spring (chapter 6.5.1) and other karst systems (PERRIN et al., 2003; EINSIEDL, 2005; LEE and KROTH, 2003). The term *epikarst* generally describes the uppermost portions of the limestone where major carbonate dissolution takes place and conduits develop. Conduit development decreases with depth as the percolating water becomes less aggressive. Epikarst is situated beneath the soil zone, but above the permanently saturated (phreatic) zone. Hence, water passing through the epikarst must be understood as vadose (unsaturated) zone water although perched water tables might form during recharge events. This vadose zone water has a chemical and isotopic composition deriving from both the soil and the epikarst zone. In the case of the Banias spring, the Sion spring was chosen to represent the epikarst outlet conditions (see Figure 33).

6.6.2 Three-component mixing model using $\delta^{18}\text{O}$ and sulfate as tracers

The pre-event component was further delineated into a vadose (unsaturated) zone component deriving its chemical and isotopic signature from the epikarst and soil zone, and a phreatic diffusive flow component using $\delta^{18}\text{O}$ and sulfate as tracers. This tracer combination was proven to display distinctly significant concentrations in all of the three flow components (Table 25) and has been used by Lee and Krothe (2001) for another karst terrain. High sulfate concentrations in particular, are representative for the diffusive (phreatic) flow component. Three-component mass balance equations describing the flow pattern at the Banias karst spring are written as follows:

$$Q_T = Q_{RS} + Q_{VAD} + Q_{DF}$$

$$Q_T C_T = Q_{RS} C_{RS} + Q_{VAD} C_{VAD} + Q_{DF} C_{DF}$$

where Q and C represent discharge (in 10^3m^3) and concentration of dissolved sulfate (in mg/L) in rain/snow flow (RS) (= event water), vadose (VAD) and phreatic diffusive flow (DF) components, respectively. Eliminating Q_T from the equations above results in the following terms:

$$1 = Q'_{RS} + Q'_{VAD} + Q'_{DF}$$

$$C_T = Q'_{RS} C_{RS} + Q'_{VAD} C_{VAD} + Q'_{DF} C_{DF}$$

where $Q'_{RS} = Q_{RS}/Q_T$, $Q'_{VAD} = Q_{VAD}/Q_T$ and $Q'_{DF} = Q_{DF}/Q_T$ are the proportions of rain/snow flow, vadose and diffusive flow contributing to the total discharge at the Banias spring respectively. Rearranging these equations leads to the following relationships:

$$Q'_{VAD} = \frac{C_{DF}(Q'_{RS} - 1) + C_T - Q'_{RS} C_{RS}}{C_{VAD} - C_{DF}}$$

$$Q'_{DF} = 1 - (Q'_{RS} + Q'_{VAD})$$

To solve these equations the rain/snow component (event water) is identified by the two-component mixing model introduced above using $\delta^{18}\text{O}$ as a natural tracer. Subsequently, the portions of vadose and phreatic flow can be calculated. Again, it is a necessary requirement to determine the input tracer concentrations for the single discharge components. Direct flow

was assumed to be represented by the mean sulfate concentration of 50 snow samples taken on Mount Hermon. Mean sulfate concentrations of the ephemeral Sion spring were chosen to correspond to vadose flow sulfate signals. Diffusive flow was represented by sulfate concentrations measured at the spring during baseflow conditions (Table 25).

Table 25: **Input tracer concentrations of rain/snow (C_{RS}) = event water (C_E), vadose (C_{VAD}) and diffusive flow (C_{DF}) used in the three-component mixing model for the Banias spring.**

Hydr. year	$\delta^{18}\text{O}$		Sulfate		
	C_E ‰	C_{PE} ‰	C_{RS} mg/L	C_{VAD} mg/L	C_{DF} mg/L
2002/03	-8.19	-7.35	0.9	4.6	62.2
2003/04	-8.19	-7.40	0.9	4.6	57.2

Monthly portions of the two assumed discharge components (pre-event, event) determined for the hydrological years 2002/03 and 2003/04 in the Dan spring are given in Table 28.

Table 26: **Monthly portions of rain/snow (P_{RS}), vadose (P_{VAD}) and diffusive flow (P_{DF}) of total discharge at the Banias spring as determined by three-component hydrograph separation using ^{18}O and sulfate as a tracer.**

	Oct	Nov	Dec	Jan	Feb	Mar	Apr	May	Jun	Jul	Aug	Sep
2002/03												
P_{RS}	%	0	5	16	23	20	n.d.	n.d.	15	n.d.	n.d.	n.d.
P_{VAD}	%	0	25	60	65	66	n.d.	n.d.	55	n.d.	n.d.	n.d.
P_{DF}	%	100	70	24	12	14	n.d.	n.d.	30	n.d.	n.d.	n.d.
2003/04												
P_{RS}	%		0	20	21	42	35	17	6	4	n.d.	n.d.
P_{VAD}	%		0	42	70	48	47	54	43	32	n.d.	n.d.
P_{DIF}	%		100	38	10	10	18	29	51	64	n.d.	n.d.

n.d.: not determined.

Evidently, the rain/snow and vadose zone component play a significant role in the discharge behavior of the Banias spring and almost completely mask baseflow from January to May. In 2002/03, direct flow (rain/snow) varied between 16 to 20 % during the precipitation rich-months (January-March). In 2003/04 however, the water level in the epikarst zone was still

high and this reservoir quickly saturated resulting in rain/snow contributions of up to 42 %. Direct flow ceases in early summer and the importance of snow recharge is clearly seen by the magnitude of vadose zone flow during the investigated summer months. In June and July, epikarst contributions were between 32 to 54 %. Unfortunately, the data did not allow to detect the end of the recharge season. Since the storage capacity of the epikarst zone is limited, the importance of the vadose zone consists mainly in the delay of direct flow in that way distributing recharge over time.

Obviously, discharge at the Banias spring is directly connected to current weather patterns. A long-residing snow cover on Mount Hermon will continuously supply recharge to the spring resulting in balanced flow and slow discharge recessions. On the other hand, average years with short precipitation seasons will lead to steep recessions and a quick depletion of the epikarst reservoir. Hence, the Banias spring is highly vulnerable towards potential climate effects suggested for the region (chapters 1.1, 3.2).

6.7 DAN SPRING - HYDROGRAPH SEPARATION

6.7.1 Two-component mixing model comparing $\delta^{18}\text{O}$, chloride and sulfate as natural tracers

Dan spring waters plot along a perfect two-component mixing line when looking at conservative tracers such as $\delta^{18}\text{O}$, chloride and sulfate that were shown to have no additional source than precipitation in this aquifer (Figure 32, Figure 33). Thus, Dan spring chemistry and its isotopic composition represent a mixture of groundwater that is present in the aquifer and newly arriving recharge with an isotopic and chemical signal close or equal to that of precipitation. The discharge behaviour of the Dan spring is characterized by minor variations and a slow response indicating a vast diffusive reservoir and the absence of direct discharge (Figure 39). However, the conducted cross-correlation analyses showed that the spring responds with a lag of three months to precipitation (Table 41) proposing the existence of a fast to medium flow component in addition to baseflow. Also, the minimum rain depth needed to increase discharge in the spring is 150 mm (GUR et al., 2003), a rain amount often reached by December at the beginning of the rainy season. GILAD and SCHWARTZ (1978)

stated that the hydraulic head in the Dan spring groundwater reservoir is much higher than its topographic level when compared to the other Hermon springs, an assumption further evaluated by RIMMER et al. (2006). Also in the Dan spring, the first increase in discharge is accompanied by rising levels of electrical conductivity and chloride indicating the activation of older waters. SIMPSON and CARMI (1983) showed the appearance of older “pocket storage” water by means of tritium observations in the Dan spring discharge.

The two-component mass balance for pre-event water (baseflow) mixing with event water (precipitation) in the Dan spring corresponds to the one applied for the Banias spring and is given as:

$$Q_T = Q_E + Q_{PE}$$

$$Q_T C_T = Q_E C_E + Q_{PE} C_{PE}$$

where Q_T is the total discharge measured at the Dan spring, Q_E is the amount of event flow (rain or snow that is rapidly transferred through conduits or fissures) and Q_{PE} is the amount of pre-event flow which is assumed to approximate baseflow. “C” notation represents $\delta^{18}\text{O}$, chloride or sulfate concentrations for total discharge C_T , event flow C_E , or pre-event flow C_{PE} . Combining the two equations results in:

$$Q_E = Q_T \frac{C_T - C_{PE}}{C_E - C_{PE}}$$

The isotopic composition of the event component (C_E) was assumed to equal the one of the event component in the Banias spring hydrograph separation. Accordingly, the reconstructed spatially integrated, amount-weighted stable isotope composition of precipitation (Figure 36) was used for C_E . The isotopic composition of the pre-event discharge component was determined as the ^{18}O , chloride or sulfate concentration of the month with baseflow conditions which is indicated by the most enriched values for $\delta^{18}\text{O}$ and highest concentrations of chloride and sulfate. In the investigated case, the isotopic and chemical composition of the Dan spring during October was chosen to represent baseflow in both hydrological years. Input data for the conducted two-component hydrograph separations are given in Table 27.

Table 27: Input tracer concentrations for $\delta^{18}\text{O}$, sulfate and chloride of the event (C_E) and pre-event (C_{PE}) components used in the two-component mixing models for the Dan spring.

Hydr. Year	$\delta^{18}\text{O}$		Sulfate		Chloride	
	C _E	C _{PE}	C _E	C _{PE}	C _E	C _{PE}
	‰	‰	mg/L	mg/L	mg/L	mg/L
2002/03	-8.19	-7.43	0.9	8.9	1.3	7.6
2003/04	-8.19	-7.40	0.9	7.6	1.3	6.6

Monthly portions of the two assumed discharge components (pre-event, event) determined for the hydrological years 2002/03 and 2003/04 in the Dan spring are given in Table 28.

Table 28: Monthly portions of event and pre-event water in the Dan spring as determined by two-component hydrograph separation using ^{18}O , sulfate and chloride as tracer, respectively.

	Oct	Nov	Dec	Jan	Feb	Mar	Apr	May	Jun	Jul	Aug	Sep
2002/03												
P _E - $\delta^{18}\text{O}$	%	0	(-4)	(-4)	(-9)	(-13)	(-8)	0	19	24	n.d.	n.d.
P _{PE} - $\delta^{18}\text{O}$	%	100	(104)	(104)	(109)	(113)	(108)	100	81	76	n.d.	n.d.
P _E -SO ₄	%	0	10	12	9	1	(-6)	18	14	28	n.d.	29
P _{PE} -SO ₄	%	100	90	88	91	99	(106)	82	86	72	n.d.	71
P _E -Cl	%	0	8	12	17	21	36	37	25	37	n.d.	43
P _{PE} -Cl	%	100	92	88	83	79	64	63	75	63	n.d.	57
2003/04												
P _E - $\delta^{18}\text{O}$	%	0	(-6)	(-29)	(-23)	(-4)	14	18	9	15	12	n.d.
P _{PE} - $\delta^{18}\text{O}$	%	100	(106)	(129)	(123)	(104)	86	82	91	85	88	n.d.
P _E -SO ₄	%	0	7	2	1	16	16	12	18	16	(-7)	n.d.
P _{PE} -SO ₄	%	100	93	98	99	84	84	88	82	84	(107)	n.d.
P _E -Cl	%	0	1	0	(-3)	(-2)	7	8	20	19	(-12)	n.d.
P _{PE} -Cl	%	100	99	100	103	102	93	92	80	81	(112)	n.d.

n.d.: not determined.

Discharge portions of event and pre-event water determined with the three different tracers ($\delta^{18}\text{O}$, SO₄²⁻ and Cl⁻) are only to some extent reproducible. Low overall variation in the springs $\delta^{18}\text{O}$ composition close to the analytical error of $\pm 0.15\text{ ‰}$ introduces a high uncertainty to the mixing model calculations. This is particularly evident when looking at the calculated negative portions of event water (and the subsequently overestimated portions of

pre-event water) in the Dan spring during November 2002 to March 2003 as well as from November 2003 to February 2004 (Table 28).

Though variations in chloride and sulfate concentrations in the Dan springs discharge are more distinct allowing for a more accurate discrimination of discharge components, also components calculated with these tracers are only in part reproducible. Hence, the mixing model is interpreted in a qualitative rather than a quantitative way. Generally, addition of new water to the Dan system doesn't show in the springs outlet until March confirming the cross-correlation results. Portions of new water in early and mid summer can contribute up 40 % as shown for the year 2002/03. In the following year, event water accounted for only up to 20 % of the streams flow, a result of less precipitation over the recharge area. Although the Dan spring is a comparatively well-balanced system mainly due to its vast intake area, the results show that event water amounts for a high portion of total discharge in the spring indicating the vulnerability of the system towards changes in recharge patterns and amounts. Infiltration of water into the karst system is fast and evaporative effects in the unsaturated zone are minor as shown by the springs stable isotopic composition, however, water is rapidly transferred through the system and the diffusive matrix storage can delay effects of drought only for a few years.

A comprehensive discussion of validity of end-member mixing model based hydrograph separations is given in chapter 2.4.3.3. Besides the parametric and natural uncertainties due to sampling and analytical errors summarized as statistic uncertainties, the strong simplistic model hypotheses that mixing models refer to introduce significant uncertainties into the obtained results (JOERIN et al., 2002). So, understanding of the hydrograph separation results are rather qualitative in nature and should be combined with additional field data. In this study, additional uncertainties originated from the difficulties to adequately chemically and isotopically differentiate the source waters.

6.8 GROUNDWATER RESIDENCE TIMES

6.8.1 Tritium content and mean residence time of groundwater

Tritium (${}^3\text{H}$) is the short-lived isotope of hydrogen, has a half-life of 12.43 years (IAEA) and decays to ${}^3\text{He}$. Nuclear testing starting in the early 1950's led to elevated concentrations of tritium in the atmosphere and hence, in precipitation. Atmospheric tritium levels culminated in 1963 and declined back to natural levels in the early 1990s. Since hydrogen is directly incorporated into the water molecule, tritium concentrations can serve as indicators of groundwater mean residence time given bomb tritium is still detectable in precipitation. This semi-quantitative technique to estimate groundwater mean residence times is based on the comparison of groundwater tritium values with historic records of nuclear-testing tritium in precipitation. Accordingly, water with tritium levels below detection limit (0.7 TU) has a pre-1952 age (>50 years), water with tritium is of a post-1952 age (MAZOR, 2004).

A more sophisticated approach is the use of lumped-parameter (MALOSZEWSKI et al., 2002) or numerical models (BORONINA et al., 2005) where – based on the known tritium input in precipitation - residence times are estimated by simulating the transport of tritium through an aquifer, so that the simulated concentrations match the observed values (see also chapter 2.2.1).

In the scope of this study precipitation was sampled for tritium analysis along an altitudinal gradient on two reference dates in January 2004 (Table 29). The conducted analyses revealed that the tritium content of precipitation accumulating in the UJRC has reached natural background levels ranging between 2.7 - 3.2 TU. Therefore, tritium concentrations in groundwater alone are no longer a reliable tool for estimating groundwater mean residence times so that other tracers or more sophisticated models have to be applied.

Table 29: Tritium content in precipitation accumulating in the Upper Jordan River Catchment.

Location	Altitude m a.s.l.	Date	^3H TU	$\pm 2\sigma$ TU
Kibutz Mayan Barukh	205	1/10/2004	3.2	0.4
Tel Dan Nature Reserve	227	1/10/2004	2.8	0.4
Banias Nature Reserve	360	1/10/2004	2.8	0.4
Nimrod Nature Reserve	750	1/10/2004	2.9	0.4
Moshav Neve Ativ	1000	1/10/2004	2.7	0.4
Mount Hermon	1403	1/11/2004	2.9	0.4
Mount Hermon	1500	1/11/2004	2.9	0.4
Mount Hermon	1629	1/11/2004	3.2	0.4
Mount Hermon	1725	1/11/2004	2.6	0.4
Mount Hermon	1830	1/11/2004	2.7	0.4
Mount Hermon	1927	1/11/2004	2.7	0.4
Mount Hermon	2027	1/11/2004	3.2	0.4

During this study, 14 springs in the Hermon Mountains and Golan Heights were sampled for tritium analysis in order to obtain an estimate of groundwater residence times in these areas. Sampling was conducted during October 2003 with the aim to exclude possible interflow contributions and to study baseflow conditions. Tritium concentrations in the Hermon springs range between 4.1 and 6 TU (Table 30) indicating that these groundwaters are dominated by recent recharge or a mixture of pre- and post-nuclear testing waters.

Table 30: Tritium content in groundwaters emerging in the UJRC.

Hermon springs	^3H	$\pm 2\sigma$	Golan springs	^3H	$\pm 2\sigma$
	TU	TU		TU	TU
Kezinim	4.1	0.5	Dupheila	2.5	0.4
Banias	5.0	0.5	Divsha	2.0	0.3
Dan	5.6	0.5	Bet HaMekhes	n.d.	n.d.
Leshem	6.0	0.6	Elmin Jedida	0.9	0.3
Barid	4.9	0.5	Gonen	2.0	0.3
Sion	4.3	0.4	Hamroniya	3.6	0.4
			Jalabina	0.4	0.2
			Notera	2.1	0.3

n.d.: non-detectable.

In the Golan springs, tritium levels are lower than in the Hermon springs and range between non-detectable to 3.6 TU. Three springs, that is the Bet HaMekhes, Jalabina and Elmin Jedida springs show tritium levels below or close to detection limit thus suggesting that they are mainly recharged by water of pre-1952 age. All the other springs seem to be fed by a mixture of pre- and post-bomb waters. As mentioned above singular measurements of tritium in groundwater allow only for semi-quantitative estimations of groundwater residence times. Unfortunately, no long-term records of tritium are available for any of these springs in the Upper Jordan River Catchment. SIMPSON and CARMI (1983) conducted during the early 1980s a continuous monitoring of tritium content in the discharge of the three major headwaters of the Upper Jordan River. These data, together with the present analyses allowed for lumped parameter modeling of mean residence times in the three major Jordan headwaters.

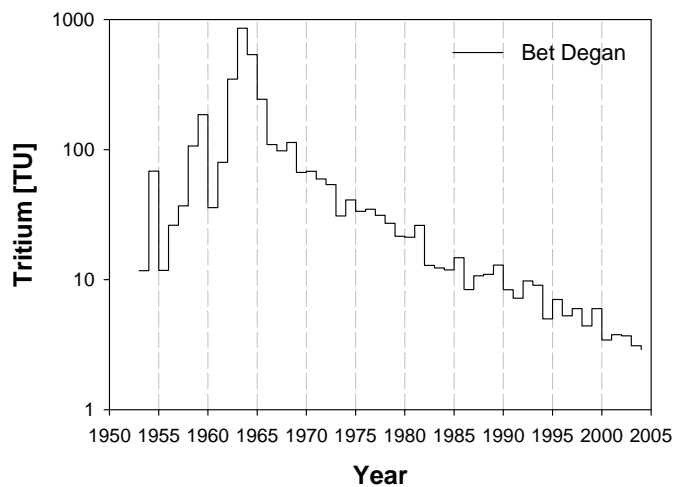


Figure 41: Input function of ${}^3\text{H}$ for precipitation over the Upper Jordan River catchment, (GNIP, 2005).

The required tritium input function for the intended lumped parameter modeling of the mean residence time was reconstructed based on tritium records of Bet Degan and Har Kenaan, which are the closest IAEA network stations in the vicinity of the study area. The available data sets for Bet Degan and Har Kenaan covered the periods 1961-2001 and 1961-1991, respectively. The annual input function (Figure 41) was reconstructed back to 1953 based on the high logarithmic correlation ($r = 0.91$) between Bet Degan and Ottawa, the latter station

representing the longest globally existing tritium record. Data gaps in the Bet Degan record were closed by referring to the high logarithmic correlation with Har Kenaan ($r = 0.94$). In 1953, mean annual tritium concentrations in precipitation were about 11.7 TU at Bet Degan. By 1963, tritium concentrations had increased to about 857 TU. Highest monthly tritium concentrations of 1940 and 4230 TU (Har Kenaan) were measured in April and May 1963. The tritium data obtained through the monitoring network in the UJRC were used to extend the dataset until recent. In terms of mean residence time estimations by lumped parameter modeling, karst environments are often considered a double-porosity system (BENISCHKE et al., 1988; SEILER et al., 1989; MALOSZEWSKI et al., 2002). While karstic channels are mainly supplied from sinkholes and provide fast response to rain events, the fissured-porous aquifer contains mobile water in the fissures and quasi-stagnant water in the microporous matrix which exchange by slow diffusion processes. Generally, transit times and storage capacities of karstic channels are approximately one order of magnitude lower than in the fissured-porous aquifer.

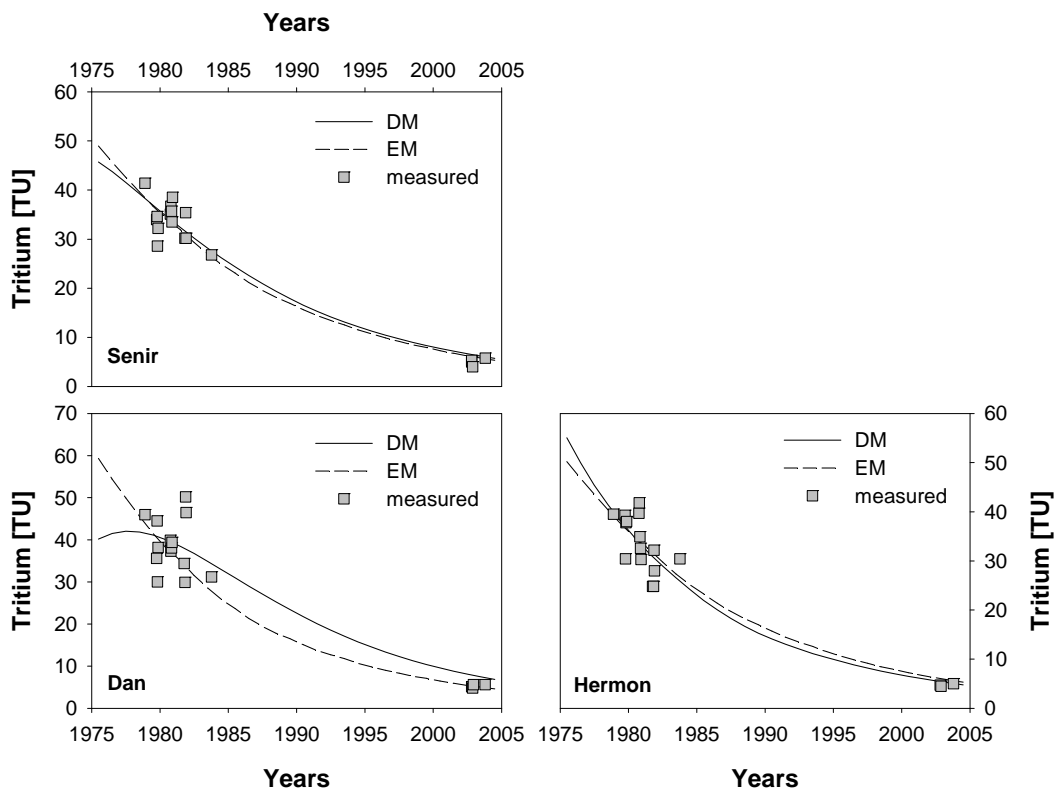


Figure 42: Calculated ${}^3\text{H}$ output concentrations obtained as best fit of the dispersion model (DM) and the exponential model (EM) to the data measured in the Senir (upper left), Dan (lower left) and Hermon (lower right) streams during baseflow conditions. The respective parameters are given in Table 31.

For estimates of groundwater mean residence time in the fissured-porous aquifers of the Dan, Hermon and Senir streams, tritium contents during baseflow conditions were extracted from the already available dataset and combined with our own measurements. According to MALOSZEWSKI and ZUBER (1982, 1985, 1996), MALOSZEWSKI et al. (1992), MALOSZEWSKI et al. (2002) and EINSIEDL (2005), the transit time distribution function of a tracer in a fissured-porous aquifer system can be adequately described by the dispersion model (DM) where P_D is a bulk dispersion parameter and t_p is the mean transit time of tracer. Within this study, both the exponential model (EM) and the dispersion model have been applied to simulate the observed tritium values in streamflow.

An apparent drawback of the conducted modeling was the lack of tritium data during the period 1985-2002 for the investigated streams which somehow lessens the reliability of the retrieved mean residence times of groundwater. However, both the dispersion and exponential model applied well to the measured data whereas the dispersion model performed slightly better (Figure 42) yielding mean transit times of tracer (t_p) of about 28, 24 and 33 years for the baseflow component of the Dan, Hermon and Senir stream under dry weather conditions. The bulk dispersion parameter P_D relates to the distribution of travel times within the investigated system and usually ranges between values of 0.05 and 0.5. The higher this dispersion parameter, the wider the distribution of travel times (ZUBER and MALOSZEWSKI, 2000). Accordingly, travel times seem to be widely distributed in the groundwater sources feeding the Hermon stream, of intermediate distribution in the Senir stream and most consistent in the Dan springs (Table 31). Yet, as mentioned above, the non-continuous character of the tritium data set for the investigated streams significantly restricts the quality of the modeled transit times of the tracer and calculated mean transit times have to be assessed cautiously.

According to MALOSZEWSKI and ZUBER (1992) and EINSIEDL (2005) the mean transit time t_p can be used to calculate the water volume in the fissured-porous aquifer applying:

$$V_p = t_p \times Q_p$$

where V_p is the water volume at baseflow conditions, t_p is the mean transit time of tracer and Q_p the discharge in the fissured-porous aquifer. Using the transit times determined by

applying the dispersion model to the observed tritium contents in groundwater and precipitation and referring to the calculated annual minimum flow, water volumes in the fissured-porous aquifer were determined (Table 31). Based on these estimates, the fissured-porous aquifer supplying the Dan stream contains a water volume which is about five times higher than that stored in the aquifers contributing to the Hermon and Senir stream. However, it is assumed that this is due to the significantly larger intake area of the Dan and Leshem springs in comparison to the recharge areas of the sources feeding the Hermon and Senir stream (see chapter 6.4.2).

Table 31: Results of the conducted lumped parameter modeling using tritium contents in precipitation and baseflow (representing the outflow of the fissured-porous aquifer) of the main Jordan tributaries. DM is the Dispersion model with t_p as the mean transit time of tracer in the fissured-porous aquifer, while EM is the exponential model with t as the mean transit time of tracer.

Stream	DM			EM			
	t_p year	P_D	σ year	t year	σ year	V_p km ³	R mm/year
Dan	28	0.18	1.28	13	1.40	2.83	250
Hermon	24	0.91	0.91	20	0.93	0.53	291
Senir	33	0.46	0.69	21	0.69	0.52	181

Another parameter that can be deduced with the help of tritium-based mean transit times is the recharge rate of an aquifer given the mean thickness and effective porosity of the system are known or can be reasonably estimated. Assuming a mean aquifer thickness of 700 m for the Jurassic (J4) Bathonian-Callovian formation (Dan and Hermon stream) and of 600 m for the Cretaceous Cenomanian aquifer (Senir stream) (GUR et al., 2003) as well as an effective karst porosity of 1 % (DOMENICO and SCHWARTZ, 1990), recharge rates for the Dan, Hermon and Senir catchments have been calculated. Recharge rates were estimated according to:

$$R = \frac{H \times n_e}{t_p}$$

where t_p [year] is the mean transit time of tracer, H [m] is the mean aquifer thickness, n_e is the effective porosity and R is the recharge rate in mm/year. Estimated recharge rates range

between 181 to 291 mm/year and are thus by about 7 to 17 % higher than those determined for the springs themselves by chloride mass balances. However, the real extent and thickness of the contributing aquifers as well as the effective porosity are not precisely known, hence aquifer thicknesses might be overestimated.

6.9 RADIOCARBON DATING

Groundwater mean residence time dating based on the measurement of ^{14}C in groundwaters is a challenging task. As soon as water infiltrates through the unsaturated zone under open system conditions, a variety of geochemical processes start to alter its carbon isotope composition, interactions that will continue and control carbon isotope geochemistry even under closed system conditions in the saturated zone. A variety of correction models have been developed to retrace initial ^{14}C activities of infiltrating waters and hence to eliminate uncertainties in groundwater mean residence time evaluation that derive from the dilution of ^{14}C activities in dissolved inorganic carbon (DIC) due to geochemical processes (in particular carbonate dissolution) in the aquifer zone.

Generally, the correction procedure includes two steps: (1) determination of the initial ^{14}C activity (A_0) in the recharge zone; and (2) adjustment of the initial ^{14}C activity for geochemical reactions along the flowpath. The most common correction models applied to account for this dilution are:

- the **chemical mixing model** (TAMERS, 1967, 1975; TAMERS and SCHARPENSEEL, 1970) that corrects for the dissolution of solid carbonates assumed to occur in the recharge zone,
- the **Vogel model** (VOGEL, 1967; VOGEL et al., 1970; VOGEL and EHHALT, 1963), where the initial ^{14}C content of DIC in a open system is assumed to be 85 % modern,
- the **isotope mixing model** (INGERSON and PEARSON, 1964; FONTES and GARNIER, 1979) that accounts for the dissolution of carbonates based on ^{13}C data for the inorganic carbon system,

- the chemical mixing and **isotope exchange model** (MOOK, 1972, 1976, 1980; FONTES and GARNIER, 1979), that corrects for isotope exchange reactions during infiltration to the aquifer,
- and the model according to EICHINGER (1983), an extension of the Pearson model additionally accounting for **equilibrium isotope exchange** for introduction of soil CO₂ into the water.

For a detailed description of the correction models the reader is referred to the textbook of CLARK and FRITZ (1997) or the NETPATH user guide of PLUMMER et al. (1991). While these correction models allow for the determination and adjustment of A_0 in a single step, PLUMMER et al. (1991) developed an advanced, widely used inverse-mass balance model (NETPATH) that accounts for the determination of A_0 and the correction for reaction effects in two distinct steps. Provided that water chemistry has been measured in an “initial” upgradient well and a “final” downgradient well, NETPATH first estimates A_0 of the “initial water” by accounting for reaction effects in the recharge zone or upgradient of the final well. Then, in a second step, reaction effects between the upgradient and downgradient well are calculated, resulting in the determination of A_{nd} which represents the ¹⁴C activity the final water would have in the absence of radioactive decay. Subsequently, the groundwater mean residence time of the final water is calculated as (PLUMMER et al., 1991):

$$T = \frac{T_{1/2}}{\ln 2} \ln \frac{A_{nd}}{A_m}$$

where A_m is the measured ¹⁴C activity in the sample.

NETPATH considers 9 possible means of defining the initial ¹⁴C which include: (1) original data, (2) mass balance, (3) Vogel, (4) Tamers, (5) Ingerson and Pearson, (6) Mook, (7) Fontes and Garnier, (8) Eichinger, and (9) user-defined. Applying NETPATH and the correction models included within, requires a thorough understanding of geochemical processes in the study area and comprehensive water chemical investigations. In particular, it is necessary to directly determine the $\delta^{13}\text{C}$ of soil zone CO₂, the ¹⁴C content of atmospheric CO₂ and the ¹⁴C activity of carbonate rocks in the study area or to rely on reasonable assumptions. While

extensive water chemical analyses of spring waters in the Hermon and Golan area were conducted within the scope of this study, we did not have the means to investigate all of the compartments involved in groundwater radiocarbon evolution. Table 32 therefore provides an overview about previously determined ^{13}C contents in the relevant phases.

Table 32: Literature review on ranges of $\delta^{13}\text{C}$ contents in CO_2 , rocks and vegetation.

Reservoir	^{13}C ‰V-PDB	Lower limit ‰V-PDB	Upper limit ‰V-PDB	Reference
atmospheric CO_2	-7	-8	-6	CERLING et al., 1991
rain (pH 4 – 6.5)	-7			CLARK and FRITZ, 1997
marine carbonates (limestones)	0	-3.5	1	HOEFS, 1987
basalt (silicic crust)	-6	-6	-5	SVEINBJORNSDOTTIR, 1995
soil CO_2 (C3)	-23			CLARK and FRITZ, 1997
soil CO_2 (C4)	-9			CLARK and FRITZ, 1997
C_3 -vegetation	-27	-30	-24	VOGEL, 1993
C_4 -vegetation	-12.5	-16	-10	VOGEL, 1993
CAM-plants	-15.5	-17	-14	CLARK and FRITZ, 1997

6.9.1 Carbon (^{13}C , ^{14}C) isotopes

In July 2004, springs emerging on Mount Hermon and feeding the main Upper Jordan tributaries as well as the majority of the Golan “Side springs” were sampled for analyses of ^{13}C content and ^{14}C activity. Since the Wazani and El-Hazbani springs that are feeding the Senir stream are located in Lebanon and were not accessible for sampling, water for carbon isotope analyses was taken approximately 34 km downstream of the Senir sources. Sampling time was assumed to represent baseflow conditions and hence, the admixture of fast flow components with an altering effect on the carbon isotope composition of groundwater was supposed to be minor.

Previously conducted tritium analyses revealed that except for the Bet HaMekhes, Elmin Jedida, and Jalabina springs, tritium was detectable at a level > 1 TU in all of the investigated groundwaters indicating the contribution of young waters to spring discharges (Table 30). For

the Hermon springs, lumped parameter modeling resulted in tritium mean residence times of 24 to 33 years for baseflow in the main Jordan River tributaries.

The ^{14}C activity of dissolved inorganic carbon (DIC) ranges between 46.6 pmc and 62.0 pmc in the Hermon springs (Table 33). Highest ^{14}C activity was detected for the Senir stream pointing to the exchange of river water with atmospheric CO_2 that leads to elevated ^{14}C levels (CARMI et al., 1985). The ^{13}C content of DIC in the Hermon springs varies between -10.6 ‰ and -7.2 ‰, while the Senir stream shows the most depleted $\delta^{13}\text{C}$ value (Table 33). The measured ^{13}C contents for the Hermon springs and the Senir stream lay within the range of $\delta^{13}\text{C}$ values determined by CARMI et al. (1985) who found $\delta^{13}\text{C}$ concentrations of -8.3 ‰ to -10.3 ‰ V-PDB in the Hermon, Dan and Senir stream while the Jordan River showed $\delta^{13}\text{C}$ values up to -6.0 ‰ V-PDB. ^{14}C activities in 1983 however, were significantly higher indicating the importance of recently recharged (post-1950) waters on the sources of the Jordan River. In fact, based on their investigations, CARMI et al. (1985) constrained mean residence times in the Hermon aquifer to be < 20 years.

Table 33: Carbon isotopes (^{13}C , ^{14}C) in sampled Hermon and Golan groundwater. Electrical conductivity, pH, $\log \text{P}_{\text{CO}_2}$ and isotopic characterization of DIC.

Spring	^{13}C ‰ V-PDB	$A_m^{14}\text{C}$ pmc	EC μS/cm	pH	$\log \text{P}_{\text{CO}_2}$
<i>Hermon springs</i>					
Kezinim	-7.2	46.6	607	7.40	-2.07
Banias	-10.6	55.9	427	7.51	-2.26
Dan	-10.0	56.7	337	7.56	-2.29
Leshem	-8.2	60.6	312	7.69	-2.45
Barid	-9.3	62.0	312	7.70	-2.46
Senir stream	-15.4	75.1	382	7.60	-2.34
<i>Golan springs</i>					
Dupheila	-11.5	54.6	364	7.85	-2.61
Divsha	-14.7	64.3	342	8.14	-2.94
Bet HaMekhes	-17.1	73.7	361	8.23	-2.98
Elmin Jedida	-17.0	81.6	408	7.68	-2.38
Gonen	-13.6	67.1	332	8.30	-3.11
Hamroniya	-9.4	67.6	358	7.75	-2.51
Jalabina	-17.7	66.5	332	8.42	-3.20
Notera	-16.8	67.2	331	8.45	-3.25

In the Golan springs, ^{14}C activity ranges from 54.6 pmc to 81.6 pmc and $\delta^{13}\text{C}$ is in the range of -17.1 ‰ to -9.4 ‰ V-PDB. Highest ^{14}C activities and most depleted $\delta^{13}\text{C}$ values have been monitored for the Elmin Jedida and Bet HaMekhes springs (Table 33). Generally, carbon isotope analyses reveal a trend of decreasing ^{14}C activity with enriched $\delta^{13}\text{C}$ contents (Figure 43) suggesting that isotope mass transfer occurs throughout the geochemical and hydrogeologic evolution of the groundwater.

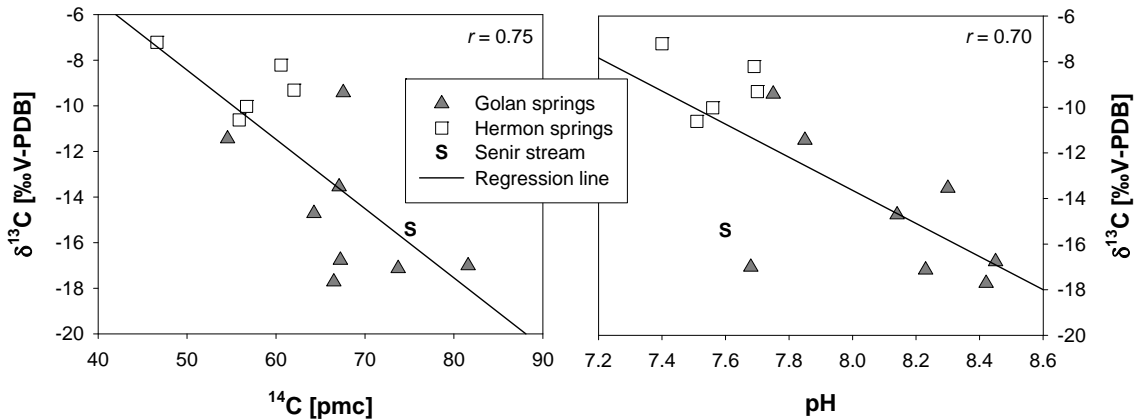


Figure 43: ^{14}C activity (left chart) and pH (right chart) versus $\delta^{13}\text{C}$ content in the Hermon springs, the Golan springs and the Senir stream.

This is particularly evident for the Hermon springs, plotting at low activities and enriched $\delta^{13}\text{C}$ values. Here, carbonate reactions take place within the aquifer matrix. The Golan springs plot at higher ^{14}C activities and lighter $\delta^{13}\text{C}$ contents indicating groundwater is recharged under shallow, unconfined conditions retaining $\delta^{13}\text{C}$ values and ^{14}C activities of the soil zone.

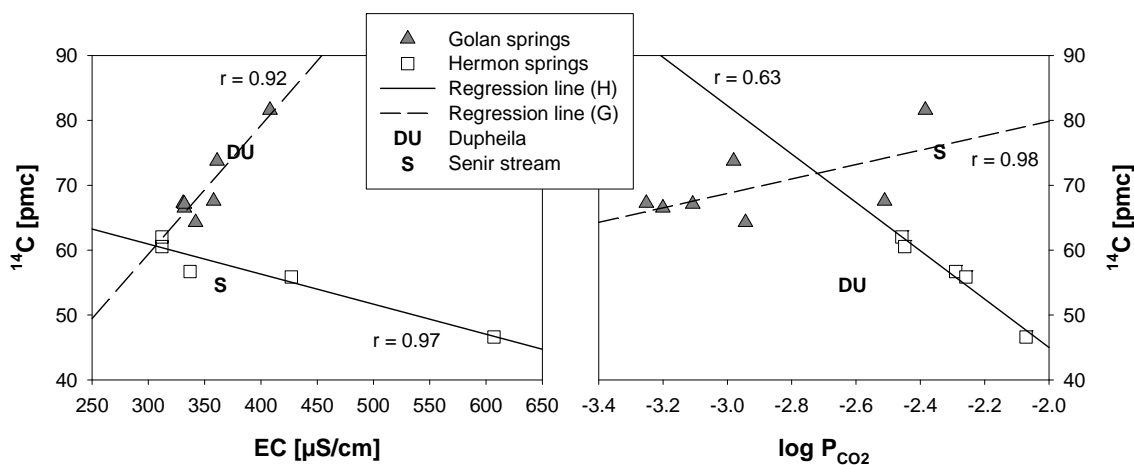


Figure 44: EC (left chart) and $\log \text{P}_{\text{CO}_2}$ (right chart) versus ^{14}C activity in the Hermon springs (H), the Golan springs (G) and the Senir stream. The Dupheila spring belonging to the Golan springs is displayed separately.

The main reaction affecting the ^{14}C activity in the Hermon springs feeding the Upper Jordan River tributaries seems to be the dissolution of carbonates evidenced by the increase of electrical conductivity and $\log \text{P}_{\text{CO}_2}$ with decreasing ^{14}C activity as shown in Table 33. Additionally, karstic aquifers are generally assumed closed systems since infiltrating water quickly reaches the water table. Under closed system conditions CO_2 is limited in amount and rapidly consumed, leading to P_{CO_2} levels below equilibrium with the atmosphere (Figure 44). Based on the high correlation ($r = 0.98$) between $\log \text{P}_{\text{CO}_2}$ and ^{14}C activity for the Hermon springs and assuming that carbonate dissolution is indeed the main reaction that governs groundwater radiocarbon, an initial ^{14}C activity of **103 pmc** can be calculated for the atmospheric CO_2 in the Hermon region. For the Golan springs, where ^{14}C contents and stable carbon concentrations are controlled by different parameters such a relationship was not observed.

Waters discharging through the Golan springs are assumed to be dominated by silicate weathering which fixes soil CO_2 but does not yield any additional carbon from a solid phase. Hence, P_{CO_2} values will decrease but ^{14}C activities and $\delta^{13}\text{C}$ values of the resulting groundwater will be close to carbon isotopes measured in soil zone CO_2 . However, ^{14}C activities decrease with decreasing partial CO_2 pressure suggesting dilution by “dead” carbon.

6.9.2 Initial ^{14}C activity and radiocarbon ages

Within this work, several approaches to estimate the initial ^{14}C activities of the spring waters were applied. Results are given in Table 34, Table 35 and Table 36. CARMI et al. (1985) in their study accounted for the exchange of CO_2 between river water and the atmosphere and concluded that the ^{14}C level in the Mount Hermon aquifer baseflow and the ^{14}C level in the atmospheric CO_2 is at a constant ratio of approximately 0.44.

Assuming that carbonate dissolution alone causes the dilution of the initial ^{14}C activity, BAJJALI et al. (1994, 1997, 2006) suggested that the dilution factor q can be calculated by:

$$q_{\text{recharge}} = {^{14}\text{C}_{\text{recharge}}} / {^{14}\text{C}_{\text{atmosphere}}}$$

where $^{14}\text{C}_{\text{recharge}}$ and $^{14}\text{C}_{\text{atmosphere}}$ are average values of ^{14}C measured in the recharge area and the atmosphere respectively. In this study, the ^{14}C content of atmospheric CO_2 is considered to be about 103 pmc (see above). Hence, the dilution factor for the Hermon springs is about 0.56, while for the Golan springs it averages to about 0.68. CLARK and FRITZ (1997) quote dilution factors of 0.65-0.75 for karst systems. Within this study, we did not correct for geochemical reactions along the flowpath (A_{nd}), which is left to future studies and more extensive investigations of carbon chemistry in the study area.

An additional precondition for the determination of corrected radiocarbon ages was the assignment of $\delta^{13}\text{C}$ values in soil CO_2 as input parameter for some of the correction models. Literature values of ^{13}C content in soil CO_2 dependent on the type of vegetation are given in Table 32. At present, C_3 -plants dominate vegetation in the Eastern Mediterranean region, hence soil CO_2 generally ranges between -27 to -24 ‰ V-PDB (CERLING et al., 1991; CERLING and QUADE, 1993). Accounting for diffusive fractionation of soil CO_2 by microbial activity of about 4 ‰ (CERLING et al., 1991), $\delta^{13}\text{C}$ of soil CO_2 in most C_3 landscapes is generally about -23 ‰ V-PDB (CLARK and Fritz, 1997). This value was thus assigned to soil CO_2 in the Golan region and for the intake area of the Senir stream.

In the Hermon region however, soil covers are thin or absent and soil waters in other karst regions have been shown to have higher $\delta^{13}\text{C}$ values of about -14.7 ‰ V-PDB (LEE and KROTH, 2001). BAR-MATTHEWS et al. (1996) investigated carbon isotopes in a close-by Mediterranean karst area. Assuming that fast infiltrating seepage waters have dissolved both soil CO_2 derived from the C_3 -type vegetation and marine carbonate host rock and given that the $^{12}\text{C}/^{13}\text{C}$ fractionation between bicarbonate ion and C_3 -type organic matter is -7.5 ‰ at $T \approx 20^\circ\text{C}$ (HENDY, 1971), the isotopic composition of DIC in equilibrium with C_3 organic matter is around -19.5 to -16.5 ‰ V-PDB (BAR-MATTHEWS et al., 1996). Therefore, a value of -19.5 ‰ V-PDB was assumed for soil CO_2 in the Hermon area.

The results of the isotopic and geochemical calculations of the initial activities A_0 and the corrected water ages according to the different models and assumptions are summarized in Table 34, Table 35 and Table 36. Groundwater mean residence times derived from the original data, the Mass Balance model, the Vogel model and the dilution factor of CLARK and

FRITZ (1997) for karst systems vary widely and are unrealistic. The Mook model did not apply to the data. However, there is some consistency for the remaining models (Tamers, Ingerson and Pearson, Fontes and Garnier, Eichinger) and assumptions (CARMI et al., 1985; BAJJALI et al., 1994, 1997) indicating the **dominance of recent water in the Hermon springs** which agrees with groundwater residence times derived on tritium analyses and earlier investigations in the study area (CARMI et al., 1985). However, **Kezanim water** seems to have significantly **larger mean residence times** than the other spring waters which is reasonable considering that this spring is dominated by matrix flow and shows little variations in discharge over time (GUR et al., 2003). Starting with the highest groundwater mean residence time, Hermon springs can be ranked in the following order:

Kezanim > Banias > Dan > Leshem > Barid.

In the Golan area, the situation seems to be more complex. The calculated A_0 values and the derived groundwater mean residence times vary broadly and a consistency between the models such as for the Hermon springs was not observed, except for the Dupheila spring which seems to be dominated by recent water. Referring to the Bajjali model most of the spring waters seem to have mean residence times below 1000 years.

A significant drawback of the conducted radiocarbon based age estimations is that *in situ* ^{13}C concentrations of soil CO_2 and the initial atmospheric ^{14}C activity could not be determined. Parameter uncertainty was shown to lead to age uncertainties of up to several thousand years, especially where $\delta^{13}\text{C}$ values of groundwater are less negative than -12 ‰ (PEARSON, 1992). Subsequent studies should thus include the measurement of soil CO_2 for carbon isotopes in the respective recharge zones. Additionally, the determination of the carbon isotope composition at epikarstic outlets in the Hermon area could provide NETPATH input data (“initial well”) that allow to account for geochemical reactions along the flow path as well. In the Golan area, an extensive network of boreholes exist that should be included in future studies.

Additional uncertainties in mass-balance based radiocarbon dating may derive from:

- the overestimation of the ^{14}C -age due to transport delays of ^{14}C without significant $\delta^{13}\text{C}$ changes (MALOSZEWSKI & ZUBER, 1991)
- the influence of isotope exchange (AESCHBACH-HERTIG, et al., 2002)
- the diffusive exchange of ^{14}C into the matrix (between aquifer and aquitards) resulting in the overestimation of ^{14}C -age (SUDICKY and FRIND, 1981)
- sulphate reduction (BAJJALI et al., 1997; KATTAN, 2002)
- the incorporation of geogenic CO_2 (BARNES et al., 1978; GASPARINI et al., 1990; KATTAN, 2002) or
- methanogenesis.

However, the existent data did not support additional modelling.

Table 34: Corrected initial ^{14}C activities and subsequently calculated groundwater mean residence times of the sampled Hermon springs. The measured *in situ* activities are given as 'Original data'.

	Kezanim		Banias		Dan		Leshem		Barid		Senir	
	A_0 pmc	Age year										
<i>NETPATH model</i>												
<i>Original Data</i>	46.6	6130	55.9	4675	56.7	4560	60.6	4030	62.0	3835	75.1	2300
<i>Mass Balance</i>	62.2	2388	60.6	675	63.1	879	62.6	269	63.5	199	57.2	Recent
<i>Vogel</i>	85.0	4967	85.0	3469	85.0	3348	85.0	2803	85.0	2604	85.0	1025
<i>Tamers</i>	55.5	1443	55.0	Recent	54.7	Recent	53.9	Recent	53.9	Recent	54.3	Recent
<i>Ingerson and Pearson</i>	38.1	Recent	56.1	34	53.0	Recent	43.4	Recent	49.2	Recent	69.0	Recent
<i>Mook</i>											110.2	3174
<i>Fontes and Garnier</i>	37.5	Recent	57.1	174	52.9	Recent	43.2	Recent	49.1	Recent	78.2	337
<i>Eichinger</i>	33.3	Recent	52.9	Recent	49.7	Recent	39.9	Recent	45.9	Recent	67.0	Recent
<i>Other</i>												
<i>Clark and Fritz (1997)</i>	67.0	2994	67.0	1496	67.0	1375	67.0	829	67.0	631	67.0	Recent
<i>Carmi et al. (1985)</i>	45.3	Recent										
<i>Bajjali et al. (1997)</i>	57.7	1762	57.7	264	57.7	143	57.7	Recent	57.7	Recent	57.7	Recent

Table 35: Corrected initial ^{14}C activities and subsequently calculated groundwater mean residence times of the sampled Golan springs (I). The measured *in situ* activities are given as ‘Original data’.

	Dupheila		Divsha		Bet HaMekhes		Elmin Jedida		Gonen	
	A_0 pmc	Age yr								
<i>NETPATH model</i>										
<i>Original Data</i>	54.6	4865	64.3	3550	73.7	2445	81.6	1635	67.1	3205
<i>Mass Balance</i>	61.8	1031	62.4	Recent	71.1	Recent	64.7	Recent	62.7	Recent
<i>Vogel</i>	85.0	3665	85.0	2310	85.0	1175	85.0	337	85.0	1955
Tamers	53.1	Recent	52.3	Recent	52.2	Recent	53.7	Recent	52.1	Recent
Ingerson and Pearson	51.3	Recent	65.9	208	76.7	326	76.2	Recent	60.7	Recent
<i>Mook</i>	33.9	Recent	101.7	3793	145.9	5643	139.2	4413	80.1	1467
Fontes and Garnier	51.2	Recent	74.1	1180	91.2	1760	89.6	777	65.9	Recent
Eichinger	48.6	Recent	63.7	Recent	74.9	125	74.6	Recent	58.4	Recent
<i>Other</i>										
Bajjali et al. (1997)	70.0	2065	70.0	709	70.0	Recent	70.0	Recent	70.0	354

Table 36: Corrected initial ^{14}C activities and subsequently calculated groundwater mean residence times of the sampled Golan springs (II). The measured *in situ* activities are given as ‘Original data’.

	Hamroniya	Jalabina		Notera		
	A_0 pmc	Age yr	A_0 pmc	Age yr	A_0 pmc	Age yr
<i>NETPATH model</i>						
Original Data	67.6	3150	66.5	3275	67.2	3190
Mass Balance	67.0	Recent	71.9	645	66.1	Recent
Vogel	85.0	1898	85.0	2029	85.0	1938
Tamers	53.5	Recent	51.9	Recent	51.9	Recent
Ingerson and Pearson	42.2	Recent	79.4	1460	75.1	914
Mook			162.3	7378	146.7	6450
Fontes and Garnier	41.9	Recent	95.9	3025	89.3	2344
Eichinger	39.1	Recent	77.4	1254	73.0	677
<i>Other</i>						
Bajjali et al. (1997)	70.0	298	70.0	429	70.0	337

7. Runoff generation in the main tributaries of the Upper Jordan River

One major goal of the work at hand was to identify and quantify the contribution of single discharge components to overall and to storm runoff which, as a result, allows for the vulnerability assessment of the investigated catchments towards possible climate changes.

Initially, existent long-term discharge data of the relevant streams were evaluated by well-known hydrograph separation techniques. These techniques allow to deduce dynamic-based discharge components, i.e. those defined by their temporal occurrence on the hydrograph. Additionally, tracer-based hydrograph separation techniques allowed to differentiate runoff processes and flowpaths.

Based on the analyses of the geomorphologic, hydrogeological, and pedological conditions in the study area, the following hypotheses were proposed for the headwaters of the Upper Jordan River:

In the long-term, overland flow plays a minor role considering runoff generation in the Hermon Mountains which is both due to rapid infiltration of precipitation into the porous karst aquifers and due to high evapotranspiration rates. In the Golan area however, soil covers are thicker and more developed hence, the occurrence of overland flow will mainly depend on the saturation status of the soil which in turn depends on the intensity, duration, and temporal succession of rain events. Generally, overland flow is a known phenomenon in semi-arid and arid regions. However, it is usually restricted to the occurrence of certain topographical features such as valley bottoms or to soil processes such as rain-induced soil surface sealing (ASSOULINE, 2004).

Interflow is a significant portion of discharge in both geological settings: basalt and karst. In karst, interflow that is fed by rain and snowmelt, is temporarily stored in the vadose (epikarst) zone and discharges mainly through conduit flow paths. In basalt, a hydraulic interface between bedrock and soil, between bedrock and paleosoils or between soil layers of different hydraulic conductivity is likely to cause lateral flow.

The ratio of long-term, medium-term and quick components and thus the importance of baseflow contributions to the stream discharge of interest can be induced by calculating

discharge coefficients. The ratio of MLF/MHF as given in chapter 3.6 is a measure of the responsiveness of a system. The baseflow component size is dependent on storage properties such as porosity, hydraulic conductivity and aquifer thickness as well as on the size of the respective catchment area. **Assuming that a major part of the Hermon/Anti-Lebanon-Mountains is actually part of the Upper Jordan River hydrogeological system, baseflow contributes significantly to the headwaters discharge.** However, compared to humid areas, baseflow contributions will be small since baseflow generation is restricted to the 4-month rainy season. The existence of an older (ancient) underlying groundwater resource that contributes to the baseflow of the Upper Jordan River could be excluded for most of the springs indicating that the Jordan Rift might act as a drain towards deeper aquifers (see chapter 6.8.1 and 6.9). However, in the Kezinim spring, old groundwater that might be upwelling along a fault zone was detectable.

7.1 LONG-TERM STREAMFLOW HYDROGRAPH SEPARATION

To quantitatively estimate the anticipated discharge components a selection of baseflow separation methods was combined. Considering the inherent assumptions and restrictions of the techniques introduced before (see 2.4.1), the *sliding interval method* (SIM) developed by PETTYJOHN and HENNING (1979) which corresponds approximately to the *base wave line method* by NATERMANN (1951) was presumed to enable the **separation of overland flow** from the long-term mean discharge (MF). Referring to KILLE (1970) and DEMUTH (1993), the *monthly mean low flow* (MoMLF_K) according to KILLE (1970) was assumed to represent solely **baseflow**. Subsequently, the **interflow** portion is calculated as the difference between baseflow determined by the sliding interval method (Q_B(SIM)) (containing interflow portions) (PETTYJOHN and HENNING, 1979) and the MoMLF_K method (excluding interflow portions) (KILLE, 1970; DEMUTH, 1993).

In short:

$$\text{Overland flow} = \text{MF} - Q_B(\text{SIM}),$$

$$\text{Interflow} = Q_B(\text{SIM}) - \text{MoMLF}_K,$$

$$\text{Baseflow} = \text{MoMLF}_K.$$

Baseflow estimates derived by the different methods are given in Table 37; the resulting portions of the single discharge components for the five investigated streams are presented in Table 38.

Table 37: Mean flow and mean baseflow of the five investigated streams in the UJRC determined by different hydrograph separation techniques.

HSI no.	Dan		Hermon		Senir		Orevim		Jordan	
	1969-1999 30131	1969-1999 30128	1969-2001 30120	1985-2001 30155	1991-2004 30175					
unit	m ³ /s	%MF	m ³ /s	%MF	m ³ /s	%MF	m ³ /s	%MF	m ³ /s	%MF
MF	8.0	100	3.3	100	3.4	100	0.18	100	14.2	100
MoMLF _W	7.7	95	2.5	76	2.1	63	0.08	43	10.0	71
SuMoMLF _W	7.5	93	1.6	47	1.3	38	0.03	19	6.7	47
MoMLF _K	7.9	99	1.8	54	1.4	42	0.05	25	8.2	58
LMM _{P&H}	7.9	99	2.9	88	2.7	78	0.12	66	11.2	79
SIM _{P&H}	8.0	99	3.0	90	2.8	83	0.14	75	11.7	83
FIM _{P&H}	8.0	99	3.0	91	2.8	83	0.14	74	11.1	78

W = according to WUNDT (1958)

K = according to KILLE (1970)

P&H = according to PETTYJOHN and HENNING (1979)

MF: mean flow, MoMLF: monthly mean low flow, SuMoMLF: monthly low flow in summer, LMM: local minimum method, SIM: sliding interval method, FIM: fixed interval method.

Generally, one can distinguish three different discharge behaviors: (1) The Dan stream is – out of a dynamic-based perception - exclusively fed by baseflow (Table 37), (2) for the Hermon and Senir streams the ratio of short- and medium-term flow components to baseflow is rather balanced (Table 38), while (3) the Orevim stream is dominated by fast flow components. The Upper Jordan River receives its major contributions from the Dan stream and is subsequently also dominated by baseflow, however, the fast flow components contribute to about 40 % of the mean annual discharge.

The applied techniques delivered baseflow portions of 93 to 99 % of mean discharge (Table 37) for the Dan stream indicating a highly permeable and well-balanced system. Due to this high permeability, it is assumed that an increase in the frequency or intensity of rain events as suggested in climate predictions (see chapter 1.1) might even enhance groundwater recharge in the Dan catchment, while the absence of rain will lead to a gradually decreasing discharge.

The impact of snowmelt recharge on Dan discharge as shown before (see 6.5.1, 6.7.1) suggests that an increase of winter temperatures and a shortened residence time of the snow cover on Mt. Hermon might considerably decrease total discharge in the Dan stream.

Both the Hermon and Senir stream receive significant portions of baseflow and discharge through interflow (Table 38). Hydrograph separation also allowed to deduce overland flow components for both catchments accounting for about 9 and 17 % of the mean annual discharge, respectively. For the Hermon catchment, overland and interflow were mainly observed as return flow and discharge of contributing ephemeral streams when rain intensity was high and rain events occurred with high frequency. The surface catchment area of the Senir stream comprises a big, elevated plane with thick soil covers that collects water from a wide area. Subsequently, higher portions of surface runoff are generated given that antecedent moisture conditions allow for overland flow.

In terms of water resource management a reduction of rain intensities and frequencies might not necessarily cause the decrease of total discharge but favor medium- and long-term discharge components. An increase of winter temperatures however, will lead to increased overland and interflow since precipitation is discharged directly as rain and not longer stored and gradually released with the snow cover on Mount Hermon.

Table 38: Separated discharge components of the five investigated streams in the UJRC.

	Dan m ³ /s	Hermon m ³ /s	Senir m ³ /s	Orevim m ³ /s	Jordan m ³ /s
overland flow	0.1	0.3	0.6	0.045	2.5
interflow	0.0	1.2	1.4	0.090	3.5
baseflow	7.9	1.8	1.4	0.045	8.2

The Orevim stream emerging in the basaltic Golan area is dominated by overland and interflow accounting for about 25 and 50 % MF, respectively. This catchment is characterized by relatively steep slopes, deep soils and perched aquifers favoring the occurrence of lateral flow (interflow) which prevents that a major portion of infiltrating water reaches the groundwater reservoir for recharge. The responsive nature of this watershed was already

indicated by the MLF/MHF-ratio calculated in chapter 3.6 and is reflected again in its baseflow index (Table 39).

The baseflow index (BFI) represents the ratio of baseflow to streamflow and indicates the proportion of discharge that is contributed mainly by groundwater storage. It hence gives a measure of catchment geology and geomorphology and is often used in comparative catchment analyses (NATHAN and MCMAHON, 1992; LACEY and GRAYSON, 1998; SMAKHTIN, 2001a). A low BFI value points to an impermeable, responsive catchment while catchments with most of the flow coming from groundwater, being permeable and non-responsive, show high BFI-indices. The established BFI values can be used in future investigations of baseflow, e.g. by digital filtering techniques (ECKHARDT, 2005) where these estimations are a necessary precondition to separate streamflow components.

Table 39: **Baseflow index (BFI) of the five investigated streams in the UJRC. The BFI value equals the monthly mean low flow according to KILLE (MoMLF_K) as presented in Table 37.**

	Dan	Hermon	Senir	Orevim	Jordan
BFI	0.99	0.54	0.42	0.25	0.58

The conducted separation of discharge components is based on their temporal occurrence on the hydrograph. On the one hand, factors such as the temporal distribution of the precipitation input cause the different retardation times of single discharge components. For example, as long as a snow cover resides in the catchment, it will constantly contribute to discharge via snowmelt. On the other hand, topographical features such as the steepness of slopes or the widths of valley floors as well as hydrogeological characteristics such as varying vertical and horizontal conductivities can accelerate or delay flow. Although there is no statistical evidence due to the low number of investigated streams and the lack of parameters describing topography or hydraulic conductivities, the established proportions of discharge components evidently reflect characteristics of the UJR subcatchments.

However, how reliable are the obtained proportions of the discharge components?

All of the investigated streams are subject to pumping and diverting of water upstream of the hydrological gauge introducing instationarity and uncertainties to hydrograph separation analyses. The Dan hydrograph in particular was reconstructed by adding averaged amounts of withdrawals to the measured hydrograph (data Alon Rimmer, KLL). Moreover, the applied techniques allowed for the separation of at most three flow components, however, a smooth transition between the different reservoirs is more likely than a sharp distinction.

Nonetheless, the determined discharge components seem to be of reasonable size since the combined portions of the estimated overland and interflow components closely relate to mean flow generated during the 4-month winter season. For the Hermon stream, 49 % of the mean annual discharge is generated during winter, as a comparison, the combined overland/interflow discharge is 47 % MF. Considering the other streams these values are 56 (58 % MF), 76 (75 % MF) and 51 (42 % MF) for the Senir, Orevim and Jordan River, respectively (compare chapter 3.6).

7.2 BASEFLOW RECESSION ANALYSES

In the previous paragraphs, mean portions of discharge components dominating streamflow in the subcatchments of the Upper Jordan River have been described. In terms of water management under changing climate conditions it is however important, to gain information on residence times and storage sizes of the particular discharge components as well. Hydrograph recession analyses allow for the estimation of these parameters by referring to the linear-storage concept. The linear-storage concept was first introduced by MAILLET (1905) and is based on the assumption that storage relates linearly proportional to outflow, a correlation that is described by:

$$V(t) = T \times Q(t)$$

with $V(t)$ representing the storage volume at time t , $Q(t)$ is the discharge at time t and T represents the mean residence time of water in storage. Including the mass-balance (continuity condition):

$$Q(t) = \frac{-dV(t)}{dt}$$

the equation given above is derived as:

$$Q(t) = -T \times \frac{dQ}{dt} = Q_0 \times e^{-t/T}$$

where Q_0 equals discharge at $t = 0$.

In the literature, the exponential coefficient $1/T$ is often given as α , the recession constant. In semi-arid climates such as prevalent in northern Israel, precipitation is restricted to the 4 month winter season with the last heavy events occurring in March or early April. Hence, during the subsequent dry season streamflow is dominated by baseflow contributions until precipitation recommences in November/December. In contrast, in humid regions it is often difficult for the hydrologist to derive baseflow characteristics since recession periods are frequently masked by successive rain events.

To determine mean residence times and reservoir sizes of baseflow for the major Jordan River tributaries and the Upper Jordan River itself, long-lasting recession segments were extracted from the hydrograph and mean residence times of baseflow were estimated by the equations given before. Results of the baseflow recession analysis are presented in Table 40. Unfortunately, out of the five investigated streams, only four stream hydrographs were suitable for the intended recession analysis. During low-flow conditions discharge data recorded at the Orevim gauge fluctuated intensely rendering the identification of a definite recession curve impossible. Since the water level in the Orevim stream bed during summer and autumn is very low already, being solely fed by the contributions of the Dupheila spring, the observed fluctuations are readily caused by water withdrawal from the adjacent settlements, due to changing evapotranspiration rates as the vegetation cover matures or to water loss in sediment and fractures.

The recession constants, mean residence times, and water volumes presented below are representative for the baseflow component in the four investigated streams. However, one has to keep in mind that this baseflow component – since it is observed on the hydrograph – actively participates in the water cycling of the considered subcatchments but does not necessarily represent the oldest contributing groundwater component (compare chapter 6.8.1).

Table 40: Characteristics of baseflow recession in the Upper Jordan River Catchment including the recession constant α , the mean residence time of baseflow T_B , the initial baseflow discharge Q_0 , the estimated volume of water in the baseflow reservoir V_B , the recession length Δt_B and the reservoir change $V_{\Delta t B}$. Estimations for the Dan, Hermon and Senir stream are based on a 32-year record (1969-2000); for the Jordan River a 10-year record (1991-2000) was available. The complete dataset of the extracted recessions is given in the appendix in Table 76, Table 77, Table 78 and Table 79.

		n		α	T_B	Q_0	V_B	Δt_B	$V_{\Delta t B}$
				-1/d	d	m ³ /s	km ³	d	km ³
Dan	26	median	-0.0018	542	9.19	0.43	214	0.140	
		minimum	-0.0007	1527	10.33	1.36	328	0.239	
		maximum	-0.0035	284	5.61	0.14	140	0.079	
Hermon	16	median	-0.0047	213	3.78	0.07	238	0.047	
		minimum	-0.0020	496	5.91	0.13	283	0.083	
		maximum	-0.0068	148	1.21	0.04	128	0.012	
Senir	10	median	-0.0027	370	1.87	0.06	265	0.031	
		minimum	-0.0019	525	11.14	0.13	301	0.114	
		maximum	-0.0107	94	1.27	0.03	207	0.020	
Jordan	7	median	-0.0135	74	23.97	0.15	74	0.148	
		minimum	-0.0065	155	48.13	0.64	329	0.545	
		maximum	-0.0171	58	9.29	0.05	242	0.046	

Referring to Table 40 above, the median of the recession constant α and the initial baseflow discharge Q_0 were calculated for the analyzed recession hydrographs describing the most frequent recession behavior in the investigated catchments. The median was chosen over the mean since recession constants showed to be asymmetrically distributed in the conducted analyses. Minimum T_B and maximum T_B refer to the lowest and highest observed recession constants (α) and initial discharges (Q_0), respectively.

Generally, mean baseflow residence times are comparatively short ranging from a few months up to about 4 years indicating the fast cycling of actual rechargeable water in these catchments and the high vulnerability towards man-induced or climate changes. The Dan stream shows the highest baseflow residence times lasting between 9 to 50 months, whereas the most frequently observed mean residence time for this stream is about 18 months (Table 40). Although there is no immediate response towards rain in the Dan stream due to its domination by baseflow, cross-correlation analysis of rain and discharge show, that Dan flow

responds with a lag time of about 3 months towards precipitation measured at Kefar Giladi (Table 41).

Table 41: Correlation and cross correlation (CC) of monthly rain depth at Kefar Giladi with mean monthly stream discharge in the UJRC.

	Dan	Hermon	Senir	Orevim	Jordan
rain	-0.07	0.52**	0.57**	0.65**	0.62**
rain (CC)	0.50**	0.75**	0.69**	0.69**	0.75**
lag [months]	3	2	1	1	1
n	372	372	372	180	108

“**” indicate significance at $p < 0.01$.

Baseflow in the Dan stream strongly depends on winter precipitation that precedes the observed recession (Figure 45). For example, the highest mean residence time in the Dan stream was observed in autumn/summer of 1992. This recession period was headed by an extraordinary rainy season when 1402 mm (>95 %-quantile) were measured at Kefar Giladi. The shortest mean residence time was measured in 1990 (referring to the 32-year streamflow record) which was preceded by two rather unproductive winter seasons (556 mm and 624 mm measured in 1988 and 1989 at Kefar Giladi, respectively).

Mean residence times of baseflow in the Hermon and Senir stream range between 5 to 16 and 3 to 17 months, respectively. Hence, the minimum recession constants in these streams are equivalent to the most frequent observed recession constant in the Dan stream. Additionally, the estimated maximum dischargeable baseflow reservoirs in the Hermon and Senir stream are by about a factor 10 lower than that of the Dan stream. The shortest mean residence times of baseflow in the Hermon and Senir stream were 5 and 3 months, most likely representing the transition to mean residence times of interflow. Most frequently observed values of T_B were 7 and 12 months for the Hermon and Senir stream, respectively. Although both streams are significantly correlated to rain measured at Kefar Giladi showing a lag phase of 2 months for the Hermon stream and of 1 month for the Senir stream (Table 41), no such significant correlation could be determined for mean residence times of baseflow and the accumulated rain which might be due to the influence of interflow on baseflow recession.

The derived recession characteristics for the Upper Jordan River have to be assessed cautiously since they might not satisfactorily reflect baseflow conditions in the Upper Jordan River. Discharge of the Upper Jordan River is monitored at the Obstacle Bridge (about 30 km upstream of Lake Kinneret) and combines the inflow of its major contributaries as well as water withdrawals and additions from the Hula Valley. The staggered arrival of discharge from the different contributaries as well as anthropogenic influences such as pumping might mask the baseflow characteristics of the Upper Jordan River.

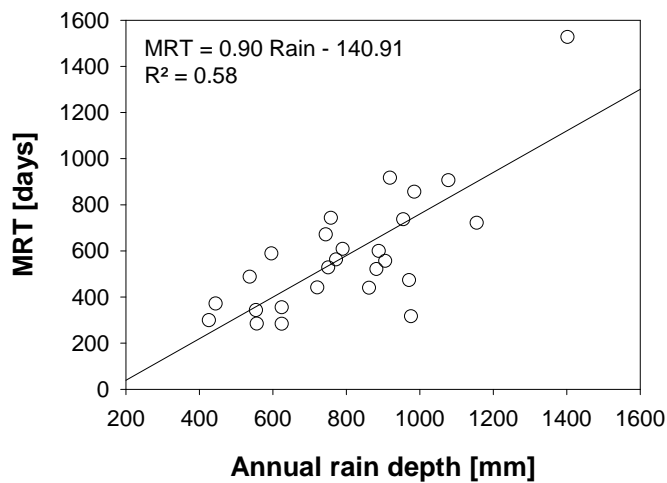


Figure 45: Relationship between calculated mean residence times (MRT) of baseflow in the Dan stream and annual precipitation prior to the respective recession period.

The conducted baseflow recession analysis additionally allowed for the estimation of aquifer thickness in the study area. Based on:

$$V_T = \frac{V_B}{n_p}$$

where V_T [km^3] represents the rock volume of the catchment area, V_B [km^3] is the water volume of the baseflow reservoir given in Table 40 and n_p is the effective porosity (fissures and rock matrix) the rock volume of the catchment area was calculated. DOMENICO and SCHWARTZ (1990) cite effective porosities of about 0.1 to 5 % for limestone and dolostone, here an effective porosity of 1 % was assumed for the estimation of aquifer thickness. For calculation of the rock volume, different water volumes of the baseflow reservoir calculated from the observed minimum, maximum and median recession constants (Table 40) were used.

Table 42: Estimated aquifer thickness for the Dan and Hermon catchments.

Catchment	Recession constant	Water volume	V_B km ³	n_p	V_T km ³	A km ³	M m
Dan	minimum	maximum	1.36	0.01	136	1324	103
	maximum	minimum	0.14	0.01	14	1324	11
	median	median	0.43	0.01	43	1324	32
Hermon	minimum	maximum	0.13	0.01	13	523	25
	maximum	minimum	0.04	0.01	4	523	8
	median	median	0.07	0.01	7	523	13

V_B : water volume of the baseflow reservoir, V_T : rock volume of the catchment area, n_p : effective porosity, A: catchment area and M: aquifer thickness.

Referring to the subsurface catchment sizes determined in chapter 6.4.2, mean aquifer thickness (= zone of active groundwater cycling) for the Dan catchment ranges between 11 to 103 m, while for the Hermon catchment aquifer thickness was calculated to be inbetween 8 to 25 m. Based on the recession characteristics that prevail the most often in the Dan and Hermon catchment, aquifer thicknesses can be assumed to be 32 and 13 m, respectively.

If the effective porosity was overestimated, mean aquifer thickness will be even lower. If catchment areas were overvalued, mean aquifer thickness will be higher. The results show that aquifer thickness will vary throughout the catchment depending, e.g. on the geomorphology of the area.

7.3 TRACER-BASED INVESTIGATION OF RUNOFF GENERATION PROCESSES

As described in chapter 4, discharge of five streams (Dan, Hermon, Senir, Orevim and Sion) was continuously recorded by the Hydrological Service of Israel (Figure 47, Figure 48). Out of these five streams, four (Dan, Hermon, Senir, Orevim) were continuously monitored for electrical conductivity and stream temperature. Except for the Dan stream (that does not show direct storm response), all streams were sampled on an event basis during winter 2002/03 and winter 2003/04 to trace the dominating runoff. Automatic samplers installed at these stations allowed for continuous sampling during flood events. Sampling intervals decreased up to 30 minutes during peak flow. In addition, three smaller contributing streams (Sa'ar, Guvtah

and Nuheile) were sporadically sampled during events to trace contributing catchment areas (Figure 46).

Main objective of this analysis was to determine the portions of pre-event and event water contributing to storm runoff generation in the investigated subcatchments. Quantified discharge components and the received ratio of pre-event and event water facilitate to assess the vulnerability of the Upper Jordan River tributaries towards predicted climate changes such as increasing precipitation intensities or a shortening of the wet season. Stable water isotopes allow for the determination of *temporal* hydrograph components (pre-event/ event water) as described in chapter 2.4.3 and 2.4.4.3. In addition, geochemical tracers enable for the delineation of *spatial* runoff sources, i.e. by identification of certain contributing areas such as hillslopes, soil or riparian zones (see chapter 2.4.4).

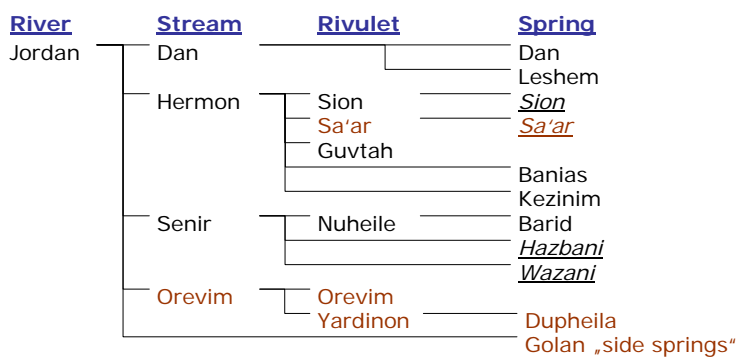


Figure 46: Investigated stream network in the northern UJRC. Underlined and italic fonts denote streams and springs that were not sampled due to their location on the borderline between Israel and Syria or Israel and Lebanon.

Mixing models and hydrograph separations based on isotopic and geochemical tracer information were widely applied to separate two, three and even four discharge components (OGUNKOYA and JENKINS, 1993; LEE and KROTHE, 2001; UHLENBROOK and HOEG, 2003, TARDY et al., 2004). However, these kind of investigations were generally restricted to hillslope studies and experimental watersheds (microscale) (BAZEMORE et al., 1994; RICE and HORNBERGER, 1998; KENDALL and McDONNELL, 2001), while hydrograph separation analyses in mesoscale large catchments are rare (TARDY et al., 2004) and often accompanied by a variety of assumptions when defining end-member concentrations. In addition, the

application of mass balances and mixing models requires either time-invariant tracer concentrations (SKLASH and FARVOLDEN, 1979) or the characterization of temporally variable end-member concentrations (GENEREUX and HOOPER, 1998), a precondition hard to meet in mesoscale catchments. Surface catchment areas of the major tributaries of the Upper Jordan River range between 40 and 563 km² (excluding the Dan stream whose surface catchment area is zero) rendering the acquisition of the temporal and spatial variability of potential discharge components almost impossible. In addition, investigating runoff processes in semi-arid catchments is of particular challenge since runoff events can be extremely rare.

7.3.1 General pattern of streamflow response

The study period (November 2002 – May 2004) was characterized by a particularly precipitation rich year in 2002/03 followed by a year with average precipitation amounts in 2003/04. However, the observed climatic pattern represented only part of the natural climate conditions in the Mediterranean region since droughts are natural occurring phenomena in the Mediterranean and a normal part of climatic variability.

For the investigated period, discharge in all of the monitored streams mimiced precipitation pattern to variable extents. The Dan stream has virtually no surface catchment area, accordingly no signals of fast flow components occured on the Dan hydrograph (Figure 47). Dan discharge steadily increased in winter 2002/03 and remained at a comparatively high level in summer and autumn 2003. With the winter season 2003/04, discharge rose again reaching peak values by March 2003. Stream temperature varied little over time (15.2 - 16.1°C). However, increases of discharge at the beginning of the winter seasons were always accompanied by slight increases in temperature while during summer and autumn, decreasing stream temperatures were registered. A similar pattern is evident for electrical conductivities monitored in the Dan stream.

Generally, a rising Dan hydrograph is accompanied by slightly decreasing EC (down to 314 µS/cm) indicating the arrival of new water with low solute concentrations. However, during the initial rising of the hydrograph at the beginning of the winter seasons, electrical

conductivities increased (up to 364 $\mu\text{S}/\text{cm}$) pointing to the activation or displacement of old, more mineralized water from the system (Figure 47).

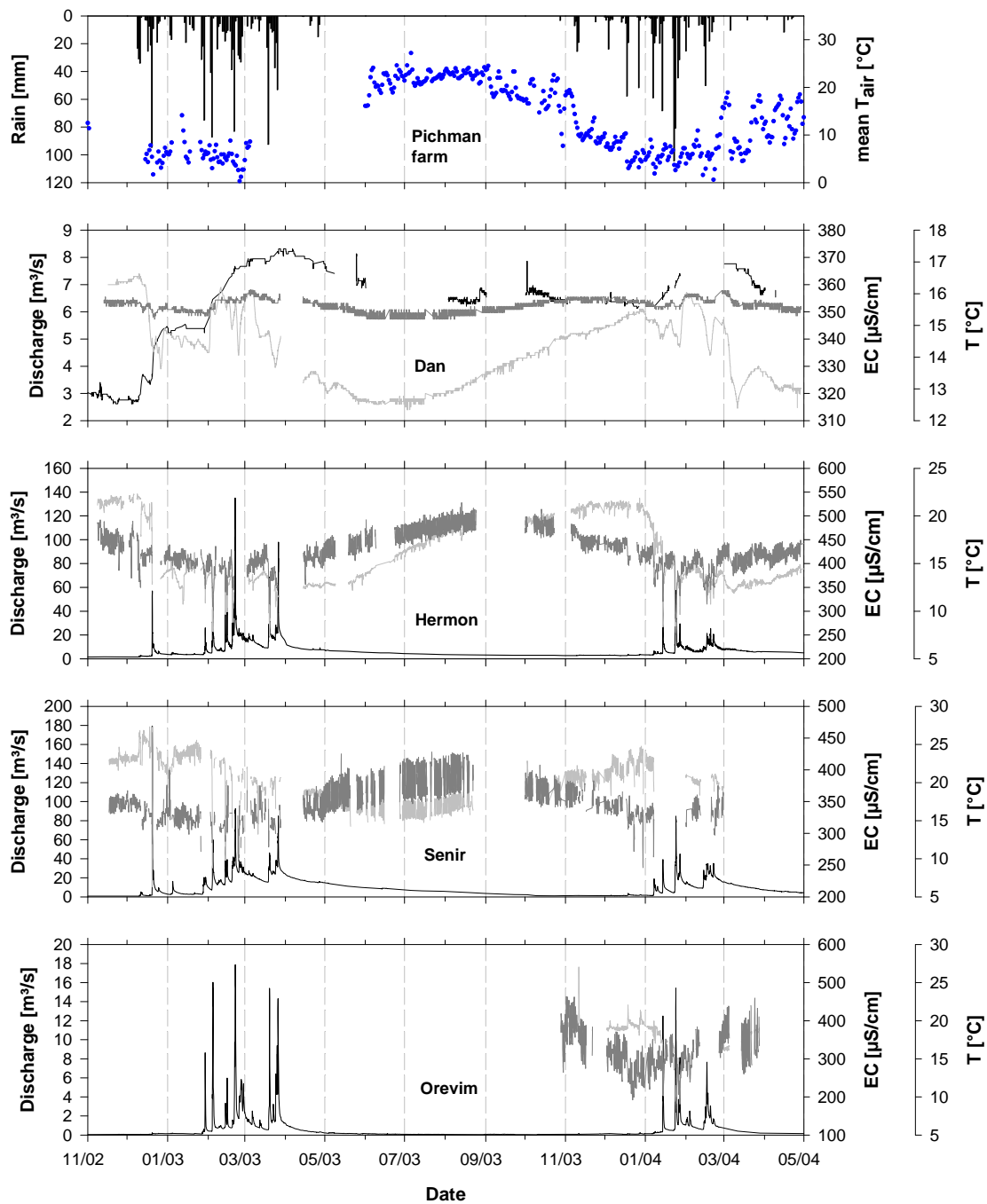


Figure 47: Rain (bars) and mean air temperature (dots) at Pichmann farm from November 2002 to May 2004. Also presented are continuous discharge (black line), electrical conductivity (light grey line) and stream temperature (dark grey line) in the Dan, Hermon, Senir and Orevim stream for the study period. Data gaps are due to technical and logistical problems.

Precipitation and subsequently stormflow in the UJRC is restricted to winter (December-April). Hence, the Hermon, Senir, Orevim and Sion stream were characterized by the rapid succession of runoff events during winter and early spring. During summer and autumn the hydrographs receded to baseflow conditions (Hermon, Senir, Orevim) or to zero flow (Sion). In the Hermon stream, both on the long-run and during short events, increases in discharge were accompanied by decreasing electrical conductivities (Figure 47, Figure 56). The ongoing dilution effect concerning electrical conductivity during spring and summer was caused by snowmelt as shown for the Banias spring (see chapter 6.6.1), the main source of the Hermon stream. Snowmelt recharge through karstic flowpaths also explains the drop in stream temperatures (down to 8.8 °C) that accompanied the dilution effects. During events, a small but steep increase of electrical conductivities indicating flushing effects during initial runoff is followed by significant decreases of electrical conductivities coinciding with peak discharges. Thus, fast flow components such as overland flow influence Hermon stream discharge.

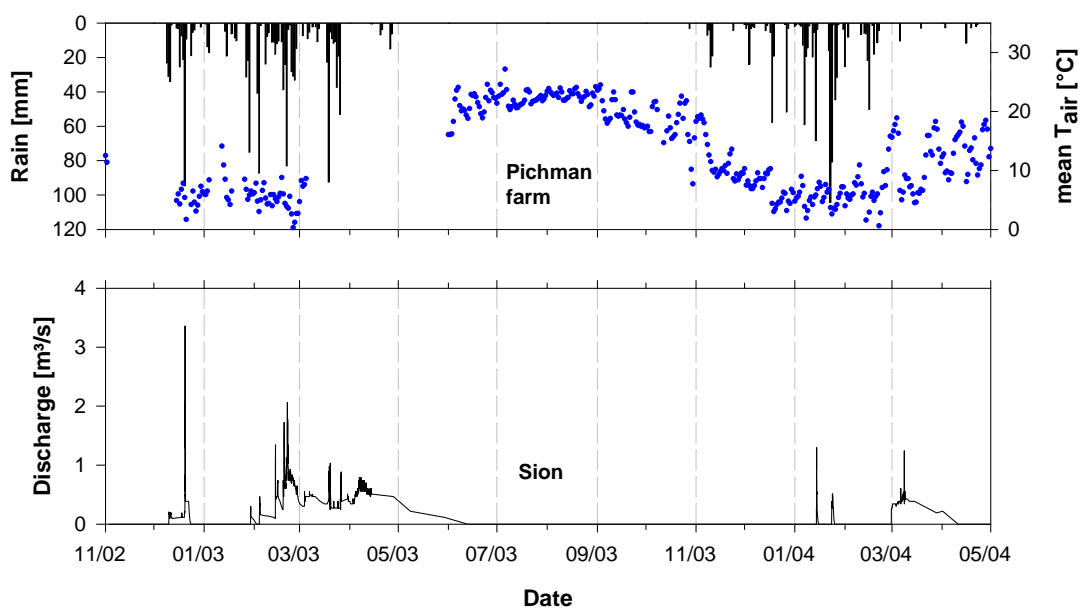


Figure 48: Rain (bars) and mean air temperature (dots) at Pichmann farm from November 2002 to May 2004. Also presented is the continuous Sion discharge during the study period.

Similar but less distinct patterns in discharge, stream electrical conductivities and temperatures were observed for the Senir stream. However, longterm dilution effects were

comparatively smaller and less abrupt at the beginning of the rainy season than in the Hermon stream (Figure 47). Also the Orevim stream rapidly responded to precipitation and Orevim storm runoff events were accompanied by significant dilution effects on stream electrical conductivities and low stream temperatures (Figure 47). Due to financial limitations no continuous measurements of temperature and electrical conductivities were available for the Sion stream.

7.3.2 Hydrometric observations

Runoff generation events in the investigated streams differed in terms of frequency, size and duration (Table 43 and Table 44). During winter, events occurred in rapid succession as indicated by the short periods in which discharge returned to baseflow conditions (T_{baseflow}), if at all. Median return periods in between peak discharges (T_{interval}) ranged between 2 to 10 days. The median response time (T_{response}), *i.e.* the lag time between the initial rising of discharge and the occurrence of peakflow was 42 hours in 2002/03 and 85 hours in 2003/04 for the Senir stream. In comparison, the Sion stream displayed the lowest median response times of 6 to 13 hours, for 2002/03 and 2003/04, respectively. Discharge reaction of the Hermon and Orevim stream occurred within 16 to 30 hours. Response times did not relate to the calculated antecedent precipitation indices (APIs), however, continuative studies should investigate the influence of catchment characteristics such as size, slope, land-use and stream length on the temporal and hydrological features of runoff events. Maximum seasonal discharges varied significantly in size, ranging from 1.3 m³/s in the Sion stream up to 135 m³/s (2/21/2003) and 179 m³/s (12/20/2002) in the Hermon and Senir stream, respectively.

Based on the timing, duration and size of the runoff events alone, the Sion and Orevim stream were the most responsive towards precipitation. This responsiveness is probably caused by comparatively small catchment areas and shorter travel distances of water to the stream channels. Catchment size appeared also to be reflected in the duration of the events which was shortest for the Orevim and Sion stream and varied most widely for the Senir stream. The Sion and Orevim as well as the Senir stream also exhibited high variability in the ratio of

peak-to-initial discharge while Hermon stream response seemed rather balanced. This pattern is attributed to the fact that the Hermon stream receives higher portions of baseflow than the three other streams, a conclusion derived from the conducted baseflow analyses (see chapter 7.2). The high variability in the duration and size of Senir events was ascribed to the respective catchment area. The large catchment area of the Senir stream might cause patchy and time-variant responses depending on the spatial and temporal distribution of precipitation during the ongoing and preceding event.

Table 43: Hydrological characteristics of runoff events in 2002/03 and 2003/04 in four streams of the UJRC. All discharges (Q) are reported as median values except for the maximum discharge (Q_{max}). $Q_{initial}$, Q_{final} and Q_{peak} are the discharges at the beginning, and at the end of the event, and during peak flow, respectively. N is the number of major events differentiated from the hydrograph. N_s is the number of sampled events. Single event characteristics are given in the appendix in Table 80, Table 81, Table 82 and Table 83.

Stream	Hydr. Year	n	n_s	Q_{max} m ³ /s	$Q_{initial}$ m ³ /s	$\pm\sigma$ m ³ /s	Q_{final} m ³ /s	$\pm\sigma$ m ³ /s	Q_{peak} m ³ /s	$\pm\sigma$ m ³ /s	$Q_{peak}/Q_{initial}$ m ³ /s	$\pm\sigma$ m ³ /s	$Q_{final}/Q_{initial}$ m ³ /s	$\pm\sigma$ m ³ /s
Hermon	2002/03	9	8	135	8.6	5.8	14.0	5.9	41.8	36.1	6.8	3.1	1.3	0.5
	2003/04	6	5	57	8.5	3.0	10.0	2.5	35.1	13.8	3.0	4.7	1.1	0.5
Senir	2002/03	12	1	179	9.9	8.8	12.7	8.4	29.7	35.6	5.1	40.3	1.4	0.6
	2003/04	4	3	85	4.0	3.2	6.6	3.0	30.3	18.6	12.3	6.7	1.6	0.8
Orevim	2002/03	14	-	18	0.8	0.7	1.1	0.7	5.6	6.2	3.8	20.9	1.3	0.9
	2003/04	6	4	15	0.9	0.3	1.0	0.2	7.7	5.1	8.9	12.8	1.1	0.4
Sion	2002/03	13	-	3.4	0.3	0.2	0.3	0.3	0.9	0.9	3.3	573.1	1.3	320.1
	2003/04	3	3	1.3	0.02	0.01	0.0	0.0	1.2	0.4	41.3	19.7	0.0	0.0

Table 44: Temporal features of runoff events in 2002/03 and 2003/04 for four streams of the UJRC and antecedent precipitation indices based on records of the meteorological station at Banias Nature Reserve. N is the number of major events differentiated from the hydrograph. The antecedent precipitation index (API) is calculated as the 2- or 5-day sum of precipitation preceding the storm event.

Stream	Hydr. Year	n	T _{duration}	±σ	T _{baseflow}	±σ	T _{interval}	±σ	T _{response}	±σ	2-day API	±σ	5-day API	±σ
			d	d	d	d	d	d	h	h	mm	mm	mm	mm
Hermon	2002/03	9	4.5	2.0	2.5	13.1	4.1	12.7	24.3	14.9	45	22	61	27
	2003/04	6	2.7	2.6	0.9	10.2	2.8	7.3	16.9	7.5	45	27	80	37
Senir	2002/03	12	6.9	7.2	0.0	1.7	2.6	4.0	42.4	64.9	38	26	59	37
	2003/04	4	15.3	13.9	0.0	0.0	1.9	8.3	84.8	66.2	60	27	66	28
Orevim	2002/03	14	2.5	1.6	3.4	6.2	5.9	6.5	16.0	20.3	55	36	105	41
	2003/04	6	4.1	2.7	0.6	3.8	4.4	4.6	29.8	21.0	54	44	87	87
Sion	2002/03	13	1.3	19.3	3.4	11.5	6.3	12.1	6.0	30.8	69	30	98	28
	2003/04	3	2.2	22.8	8.0		9.9		12.5	106.8	107	55	131	70

7.3.3 Event chronology

A variety of runoff events were monitored for the investigated streams during the two extensive sampling campaigns in winter 2002/03 and winter 2003/04. Though automated samplers were installed for high-frequency sampling during runoff events, the successful sampling of single runoff events depended on a number of parameters. Since samplers could not be started automatically with rising discharge levels or by rain sensors (which were both tried), sampling campaigns were initiated according to weather forecasts and anticipated precipitation events. The duration and intensity of the precipitation event was not predictable either, thus sampling lengths and frequencies were adjusted during the ongoing event depending on experience and – luck. Hence, only a small number of the actually occurring events (Table 44) were successfully sampled and out of these only a part was suitable for the application of mass balances and mixing models. The following problems were encountered:

- Increases in discharge and variations in tracer concentrations were too small to conduct meaningful hydrograph separations.
- When conducting ^{18}O -based two-component hydrograph separations, isotopic compositions of the pre-event and event component were too similar, thus violating one of the boundary conditions restricting hydrograph separation (see chapter 2.4.3.1).
- The rapid succession of events did not allow to reliably determine the composition of the pre-event component.

Consequently, one storm runoff event for each of the streams was chosen for the quantification of discharge components and indepth analysis of the governing flowpaths and runoff generation processes. The comparative evaluation of additional runoff events was reserved to future publications and would exceed the scope of this work.

Fortunately, three of the investigated streams were successfully sampled for one and the same runoff event providing the possibility to compare runoff generation mechanisms and dynamics for different settings.

On January 11, 2003, precipitation amounts of 320 mm and 356 mm had accumulated at the meteorological stations of Banias and Pichmann, respectively. Four succeeding rain days starting on January 12, 2003 caused first major storm runoffs in all of the investigated streams (Figure 47, Figure 48). During this rain period, 66.4 mm and 91.8 mm of precipitation were measured at Banias and Pichmann, respectively. Highest overall rain intensities were monitored for January 14, 2004 between 8 to 9 a.m. at Pichmann station where hourly recordings were conducted. In the Hermon stream, this first major flood was preceded by only smaller increases in discharge of up to 6.5 m³/s (mean discharge is 3.3 m³/s). The antecedent precipitation 5-day API (defined as the rainfall during the 5 days prior to the storm event) was 64 mm. At the beginning of the event on January 13, 2004 at 10 p.m. discharge was about 4.4 m³/s. Peak discharge (47 m³/s) occurred on January 14, 2004 at around 11.30 a.m. with a response time of 13 hours after the first initial increase in discharge. Peak discharge lagged about 2-3 hours behind highest rain intensity. Discharge receded until January 22, 2004 at 10.30 a.m. back to a level of 4.7 m³/s. Thus, the whole event lasted for about 8.5 days (Figure 49).

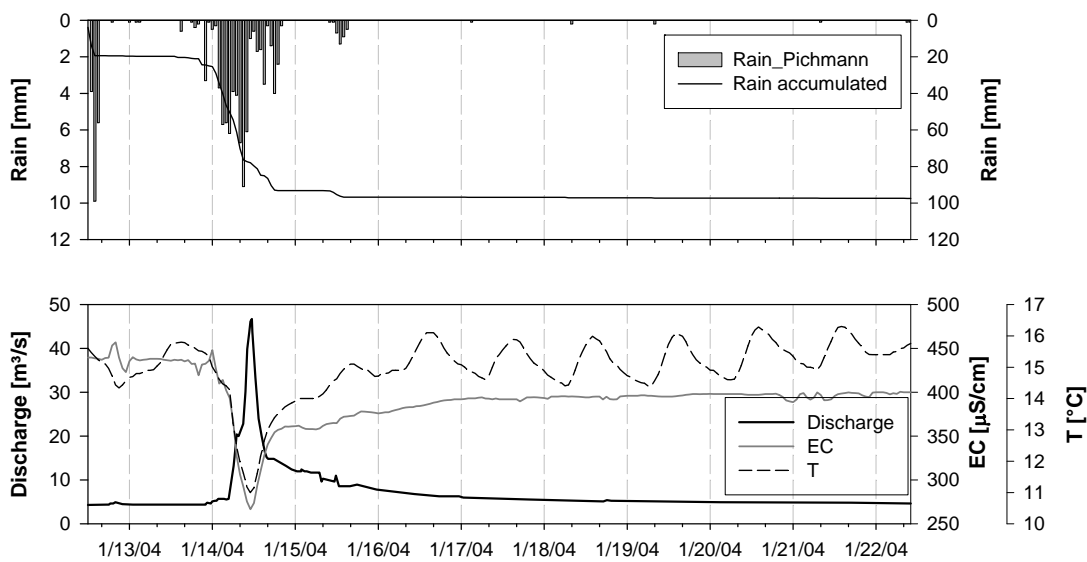


Figure 49: Hourly and accumulated rain at Pichmann farm and discharge, electrical conductivity and stream temperature for the Hermon stream (storm runoff event 1/13/2004-1/22/2004).

Sion stream flow (Figure 50) (which contributes to Hermon stream discharge) started to increase on January 14, 2002 at around 8 a.m. thus immediately responding to highest rain intensities. Peak discharge ($1.03 \text{ m}^3/\text{s}$) occurred on the same day at around 10:40 a.m. preceding peak discharge in the Hermon stream by about 50 minutes. Storm runoff ended when discharge faded to zero on January 15, 2003 at about 7 p.m. In the Sion stream, the whole event lasted for 1.5 days suggesting the absence of any medium or long-term flow component at this time of the year. Generally, this discharge behaviour was assumed to be representative for other contributing rivulets originating on Mount Hermon, such as the Guvtah and Hazuri. The Sa'ar stream receiving major recharge by the basaltic Golan Heights stopped flowing only in spring 2004 matching the end of the rain and snowmelt season.

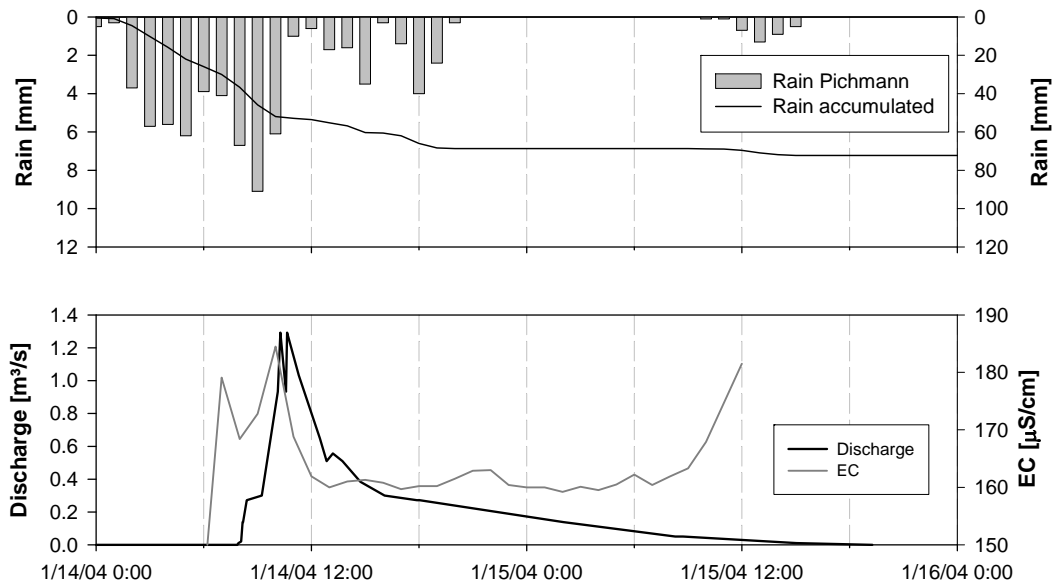


Figure 50: Hourly and accumulated rain at Pichmann farm. Also given are discharge and electrical conductivity for the Sion stream (storm runoff event 1/14/2004-1/16/2004).

In the Orevim stream (Golan) (Figure 51), the event lasted 4.7 days and started on January 14, 2004 at 3 a.m. with an initial discharge of $0.4 \text{ m}^3/\text{s}$. Peak discharge ($12.5 \text{ m}^3/\text{s}$) was reached on the same day at around 9:30 a.m. coinciding with highest rain intensities recorded at Pichmann which is located in the basaltic Golan Heights as well. Discharge returned to baseflow conditions on January 18, 2004 to a level of about $0.5 \text{ m}^3/\text{s}$. Duration of the runoff

events, that were 4.7 and 8.5 days in the Orevim and Hermon streams respectively, indicates the contribution of a medium-term component to storm runoff.

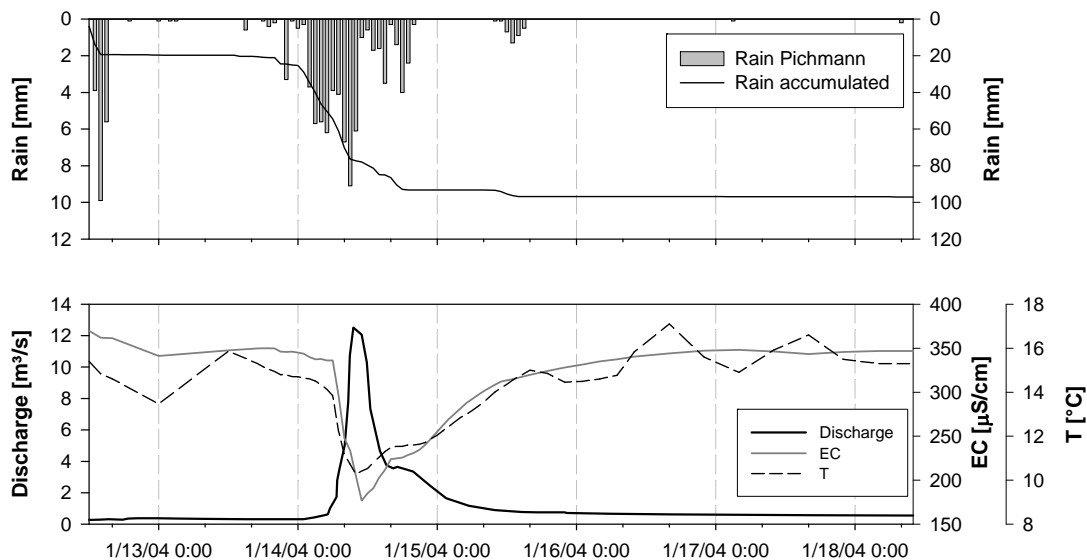


Figure 51: **Hourly and accumulated rain at Pichmann farm. Also given are discharge, electrical conductivity and stream temperature for the Orevim stream (storm runoff event 1/13/2004-1/18/2004).**

For the Senir stream (Figure 52), two consecutive storm events (2/13/2003-2/18/2003) were analyzed in detail. In contrast to the event investigated for the Hermon, Sion and Orevim stream, this storm runoff event occurred in the middle of the rainy season when 530.5 mm had accumulated at Mayan Barukh, a meteorological station about 30 km downstream of the main springs feeding the Senir River. Baseflow conditions had controlled streamflow for only a day when rain started again on February 13, 2003 lasting for four days altogether. The antecedent precipitation 5-day API was 39 mm. In total, 43.4 mm of precipitation accumulated during the flood event with the highest amount falling on February 14. Discharge started to increase on February 13 at about 7 p.m. from an already high level of 12.9 m^3/s (mean discharge is 3.4 m^3/s) to a peak discharge of about 52.5 m^3/s on February 14 at about 3 a.m. A second peak of 39 m^3/s occurred on February 15, 2003 at 11 a.m.; discharge returned to a pre-storm level (15.3 m^3/s) on February 18, 2003. Runoff conditions lasted for 5.1 days, however, recession characteristics were overwritten by a successive rain event.

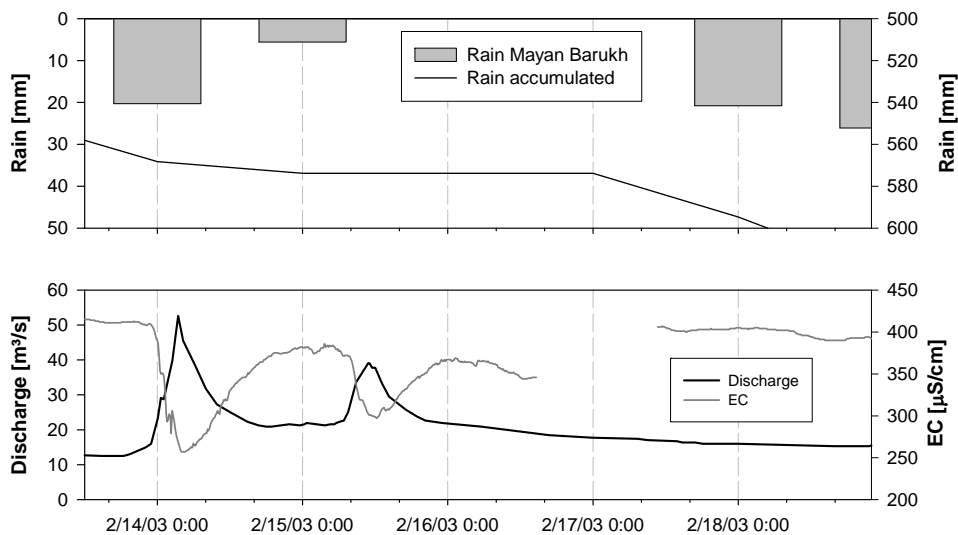


Figure 52: Daily and accumulated rain at Mayan Barukh. Also given are discharge and electrical conductivity for the Senir stream (storm runoff event 2/13/2003-2/18/2003).

7.3.4 Chemographs

Up to 15 parameters were monitored during storm runoff events in the four investigated streams. Hydrographs, chemographs and temporal variations of $\delta^{18}\text{O}$ during the course of the investigated flood event are given in Figure 53 and Figure 54 for Hermon stream, in Figure 55 and Figure 56 for Orevim stream, in Figure 67 and Figure 68 for the Senir stream and in Figure 69 and Figure 70 for the Sion stream.

7.3.4.1 Hermon stream

The chemical and isotopic tracer species monitored in Hermon stream discharge showed a broad response pattern during the investigated storm runoff event. The first initial increase in discharge was accompanied by a rapid increase in electrical conductivity, which in turn reflected the behaviour of Cl^- , SO_4^{2-} and to a lesser extent that of HCO_3^- , Mg^{2+} and SiO_2 (Figure 53, Figure 54). This initial increase represented most likely flushing effects within the catchment when ions that accumulated during preceding dry periods were washed from the upper soil horizons. The rapid increase was immediately followed by declining ion concentrations.

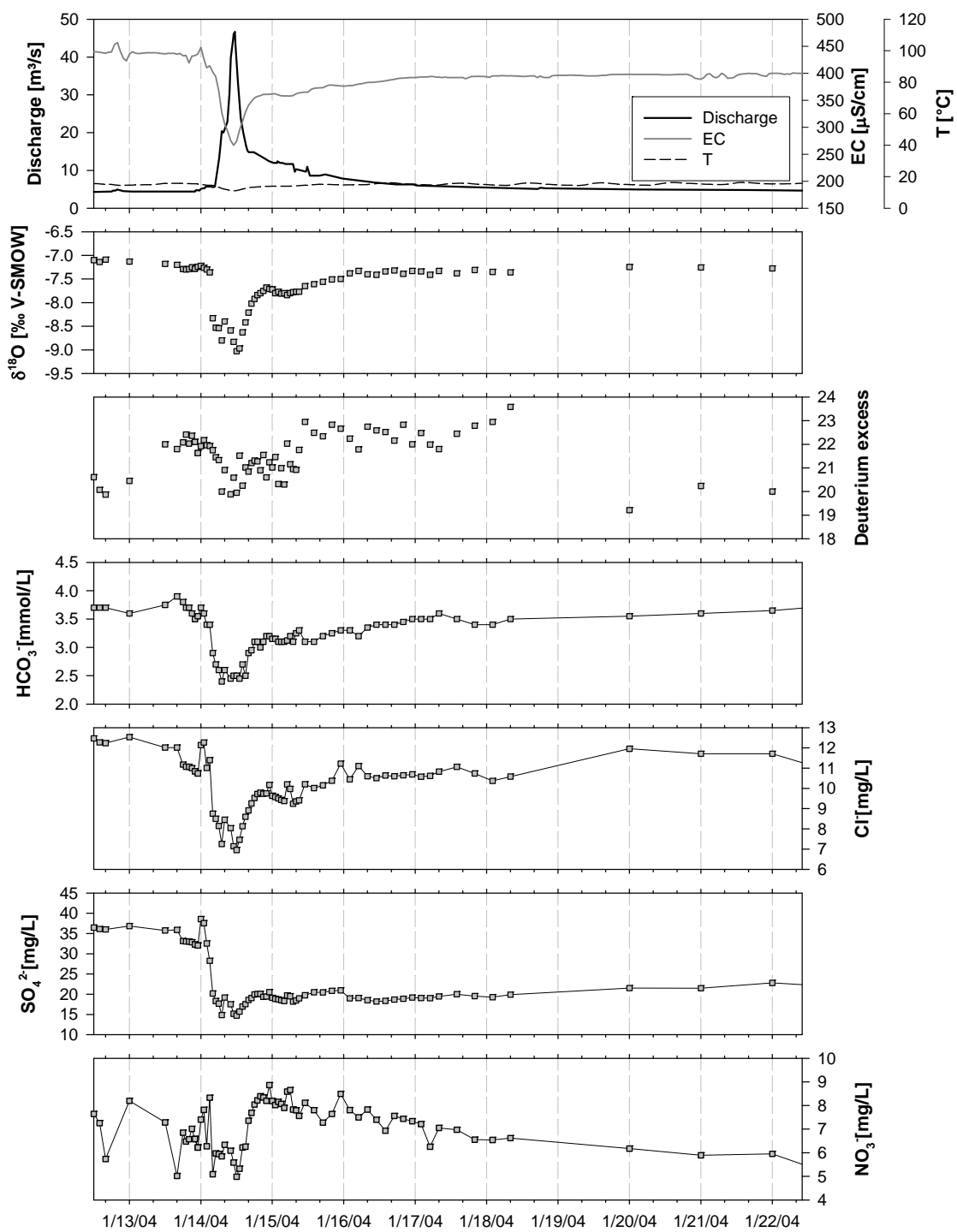


Figure 53: Time-series of discharge, electrical conductivity, temperature, $\delta^{18}\text{O}$, deuterium excess and major anions during 1/13/2004-1/22/2004 in the Hermon stream.

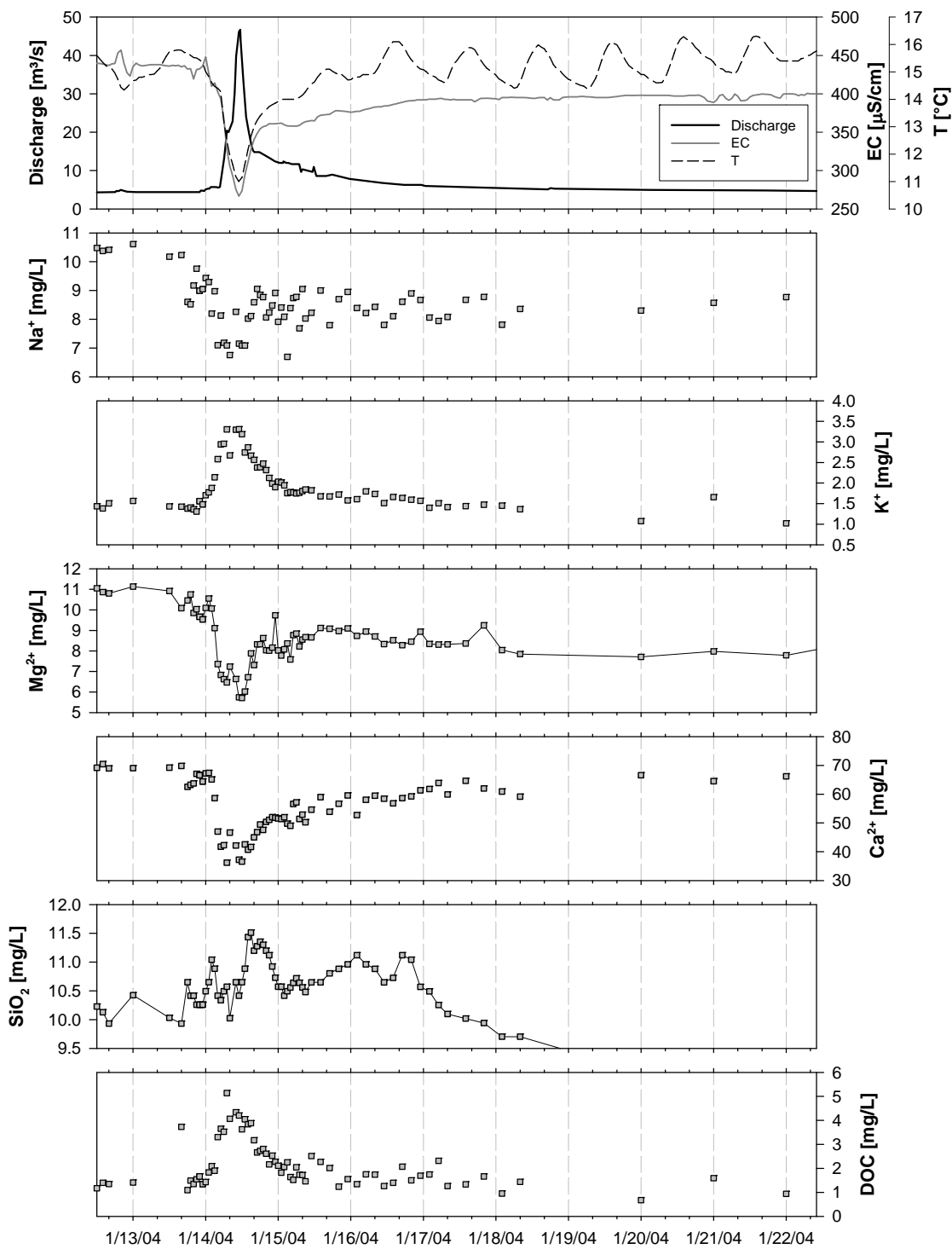


Figure 54: Time-series of discharge, electrical conductivity, temperature, major cations, SiO_2 and DOC during 1/13/2004-1/22/2004 in the Hermon stream.

Peak discharge went along with a strong shift towards more negative (more depleted) $\delta^{18}\text{O}$ values and a significant decrease of ion concentrations in the order:

$$[\text{SO}_4^{2-}] (0.45) > [\text{Ca}^{2+}] (0.54) > [\text{Mg}^{2+}] (0.67) > [\text{Cl}^-] (0.67) > [\text{HCO}_3^-] (0.69) > [\text{Na}^+] (0.79),$$

where numbers in brackets indicate the respective dilution factor. The strongest dilution at peak discharge relative to initial concentrations in baseflow was observed for sulfate. Increasing concentrations were measured for DOC (by a factor 2.5 at peak discharge), K^+ (2.1) and SiO_2 (1.03).

During the recession phase, the stable isotope composition ($\delta^{18}O$) and concentrations of Cl^- , HCO_3^- , Ca^{2+} and Na^+ returned to pre-storm conditions representing baseflow. However, K^+ , Mg^{2+} , SO_4^{2-} , DOC and SiO_2 had not regained their initial concentration at the end of the recession period (Figure 54). This effect was most evident for sulfate and might indicate the contribution of an additional water component with residence times bigger than overland flow. One possible explanation could be the participation of vadose zone water contributing to Banias spring discharge (see chapter 6.6.2). However, none of these tracers are considered conservative in the Hermon catchment and chemical processes on the flowpath might alter their concentrations.

7.3.4.2 *Orevim stream*

Storm runoff in the Orevim stream that emerges in the basaltic Golan Heights showed a slightly different pattern of chemical and isotopic tracer response. The initial increase in Orevim discharge was accompanied by a distinct increase of SO_4^{2-} concentrations and to a lesser extent by an increase of HCO_3^- . However, these pattern were not reflected in the streams electrical conductivity (Figure 55). Peak discharge went along with a strong shift towards more negative (more depleted) $\delta^{18}O$ values and a significant decrease of ion concentrations in the order:

$$[Mg^{2+}] (0.50) > [Na^+] (0.54) > [NO_3^-] > [Cl^-] (0.59) > [HCO_3^-] (0.63) > [Ca^{2+}] (0.71).$$

In the Orevim stream, the strongest dilution effect was observed for magnesium. Increases in concentrations occurred for DOC (by a factor 3.1 at peak discharge), K^+ (1.3) and SO_4^{2-} (1.1). During the recession phase, the stable isotope composition ($\delta^{18}O$) and the concentrations of all investigated tracers returned to pre-storm conditions representing baseflow (Figure 55, Figure 56). The only exception to this pattern was the DOC concentration that did not regain

its initial concentration at the end of the recession period but was slightly higher suggesting the ongoing contribution of water from the upper soil zones.

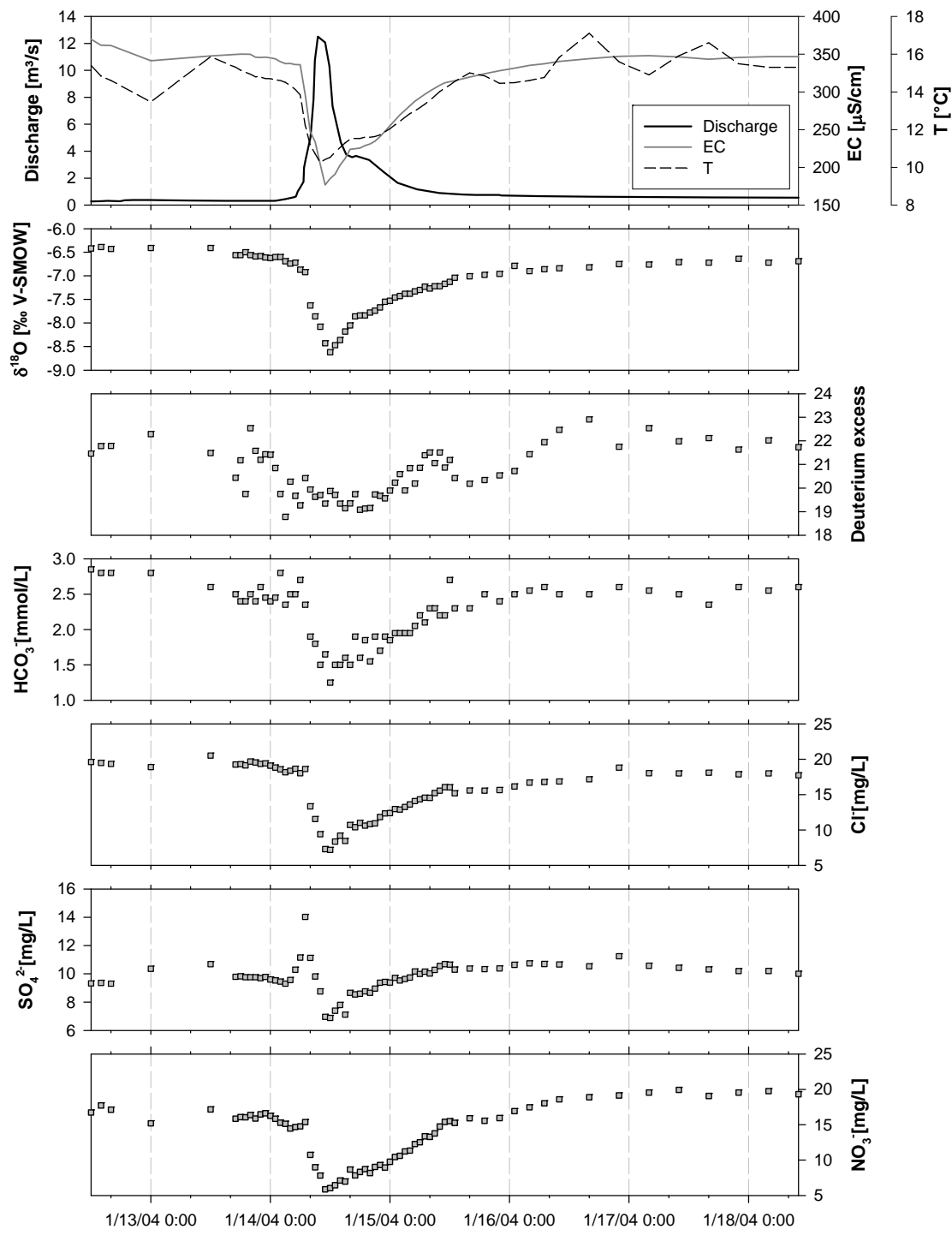


Figure 55: Time-series of discharge, electrical conductivity, temperature, $\delta^{18}\text{O}$, deuterium excess and major anions during 1/13/2004-1/18/2004 in the Orevim stream.

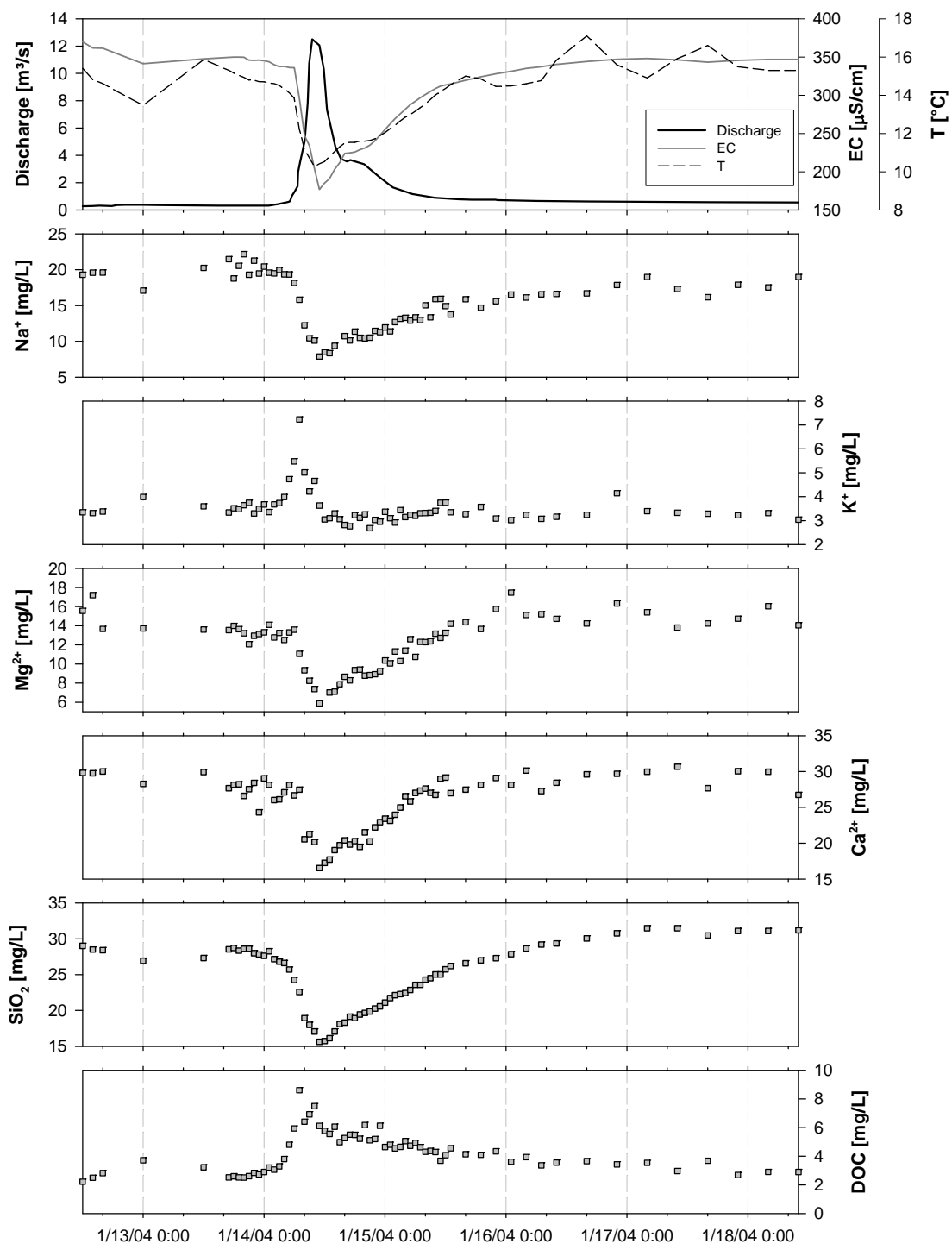


Figure 56: Time-series of discharge, electrical conductivity, temperature, major cations, SiO_2 and DOC during 1/13/2004-1/18/2004 in the Orevim stream.

7.3.4.3 *Sion stream*

As suggested before (see 7.3.3), Sion storm runoff seemed to be fed by overland flow alone during the investigated event, an assumption confirmed by the observed tracer responses. With the onset of discharge, $\delta^{18}\text{O}$ concentrations in stream discharge decreased from -8.47 ‰ to -11.41 ‰ V-SMOW which could be a result of the amount effect, *i.e.* precipitation becoming isotopically lighter with increasing rain amounts. However, this isotopic signature might also reflect the delayed arrival of runoff from high altitudes knowing that with increasing altitude precipitation gets isotopically depleted (see chapter 2.4.4.3).

A steep initial increase followed by an ongoing gradual rise in concentrations was observed for Na^+ and Cl^- to about 5 mg/L and 4.5 mg/L, respectively (Figure 69, Figure 70). A steep concentration increase followed by a rather stable behaviour was monitored for SO_4^{2-} , HCO_3^- and Ca^{2+} while the reverse effect (initial decline followed by stable concentrations) was observed for Mg^{2+} . Nitrate concentrations showed a heterogeneous signature because of its dependence on nitrate concentrations in precipitation itself. Additional nitrate sources could be excluded for the Sion catchment. DOC , K^+ and SiO_2 concentrations peaked at the beginning of the event and showed decreasing or stable (low) concentrations during recession suggesting the initial flushing of upper soil zones within the catchment.

7.3.4.4 *Senir stream*

Peak discharge in the Senir stream was accompanied by a strong shift towards negative (more depleted) $\delta^{18}\text{O}$ values from -6.67 ‰ down to -8.10 ‰ V-SMOW and a significant dilution effect on most of the ion concentrations (Figure 67, Figure 68). The most distinct dilution at peak discharge relative to initial concentrations in baseflow was observed for nitrate. Increasing concentrations were measured for DOC (by a factor 1.4 at peak discharge) and K^+ (2.1).

During the recession phase, the stable isotope composition ($\delta^{18}\text{O}$, $\delta^2\text{H}$) and the concentrations of all investigated tracers returned to pre-storm conditions with the exception of DOC that did not regain its initial concentration at the end of the recession period but was slightly lower.

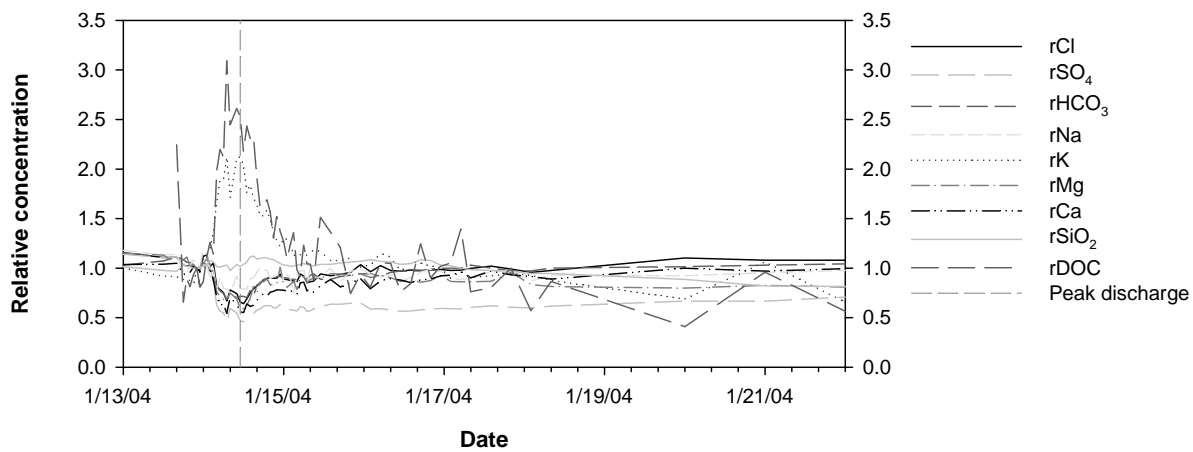


Figure 57: Relative natural tracer concentration in the Hermon stream during 1/13/2004-1/22/2004.

Generally, an inverse relationship between weathering-related determinants (Ca^{2+} , Mg^{2+} , HCO_3^- and Na^+) and discharge was observed in the Hermon, Orevim and Senir stream suggesting the dilution of base-rich, mineralized groundwater with less mineralized inputs from overland flow or flow through shallow soil horizons. This did not apply to the Sion stream that was solely fed by overland flow at this point of time and whose storm runoff was characterized by the chemical signature of precipitation (Na^+ , Cl^- , NO_3^-), the activation of dust-derived constituents (Ca^{2+} , Mg^{2+} , SiO_2) as well as that of biologically cycled materials (DOC, K^+).

Determinants associated with the upper soil layer (DOC and K^+) were positively related with discharge in all of the streams, the extent of this relationship however, was different for each of them (Table 45). Also, maximum concentrations of DOC and K^+ were always measured before the arrival of peak discharge (Figure 57, Figure 59). The investigation of various soil and sediment profiles showed that DOC and K^+ concentrations increase towards the soil surface (BROWN et al., 1999; HANGEN et al., 2001; LADOUCHE et al., 2001; BISHOP et al., 2004). Thus it is suggested that lateral flow through superficial flowpaths (especially in the riparian zone) lead to the observed initial increase of DOC and K^+ in stream flow (see also 2.4.4.7). With ongoing precipitation additional runoff areas will be connected to the stream through rainfall-excess or infiltration-excess overland flow (see 2.3.1) causing the positive correlation between discharge and these tracers.

Table 45: Relative natural tracer concentrations in the investigated streams at peak discharge during the investigated events.

Tracer	Sion	Hermon	Orevim	Senir
EC	1.83	0.61	0.63	0.71
T	-	0.71	0.70	-
Cl ⁻	1.87	0.67	0.59	0.79
SO ₄ ²⁻	1.91	0.45	1.05	0.90
HCO ₃ ⁻	1.76	0.69	0.63	0.76
NO ₃ ⁻	0.90	0.73	0.54	0.66
Na ⁺	2.11	0.79	0.54	0.87
K ⁺	1.08	2.12	1.26	1.44
Mg ²⁺	1.21	0.67	0.52	0.74
Ca ²⁺	1.73	0.54	0.71	0.99
SiO ₂	1.61	1.02	0.62	0.85
DOC	1.41	2.50	3.12	1.43
TSS	50	181	22	-

Dissolved silica (SiO₂) responded differently in the investigated streams. While in the Sion and Hermon stream, SiO₂ positively correlated with discharge, its relation with flow was negative in the Orevim and Senir stream. It is suggested that in the Hermon catchment, (including the Sion), SiO₂ accumulates in the upper soil or epikarst layers as a product of carbonate weathering thus causing the positive correlation to discharge during storm runoff. In the Orevim and Senir catchment on the other hand, SiO₂ concentrations are highest in deep parts of the unsaturated and in the saturated zone (chapter 6.3.2) causing its dilution through water arriving on superficial flowpaths with less SiO₂ dissolution taking place.

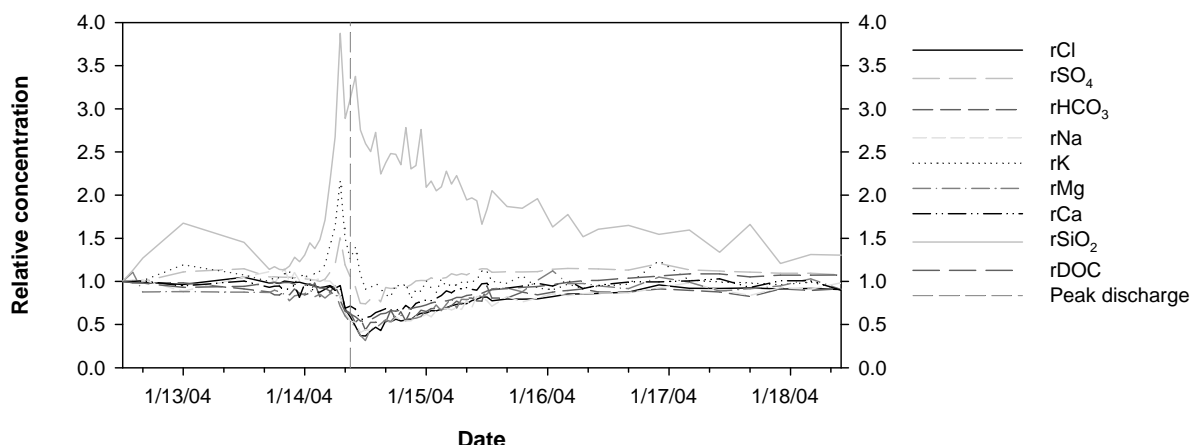


Figure 58: Relative tracer concentration in the Orevim stream during 1/13/2004-1/18/2004.

7.3.5 End-member differentiation

A precondition for the application of mass balances and mixing models to quantitatively determine the contribution of different water bodies to streamflow generation is the reliable identification of the involved end-member. If runoff generation is explained by two components, the relationship between tracer and discharge must be linear (SKLASH and FARVOLDEN, 1979). A two-component mixing model will then allow to differentiate pre-event from event water whereas pre-event water is considered to represent groundwater contributions while event water equals to precipitation traveling at the surfaces of the catchment. In order to test the two-component hypothesis, correlation matrices using the non-reactive tracer $\delta^{18}\text{O}$ and Cl^- assumed to identify pre-event and event water contributions as well as the reactive tracer Ca^{2+} and HCO_3^- were plotted for the Orevim, Hermon and Senir streams (Figure 59, Figure 60). Based on groundwater and precipitation analyses (see 5.2 and 6.1), the latter tracer combination was suggested to enable the separation of groundwater contributions (high Ca^{2+} and HCO_3^-) from overland flow (low Ca^{2+} and HCO_3^-). Although Ca^{2+} and HCO_3^- are reactive tracers, they are often assumed to behave conservative at the event scale enabling their application in mass-balances and mixing models (SOULSBY, 1995; MCGLYNN et al., 1999; SHANLEY et al., 2002).

The Sion stream was excluded from this type of analysis since for the respective event it was shown to be fed by overland flow alone (see chapter 7.3.4.3 and Table 45).

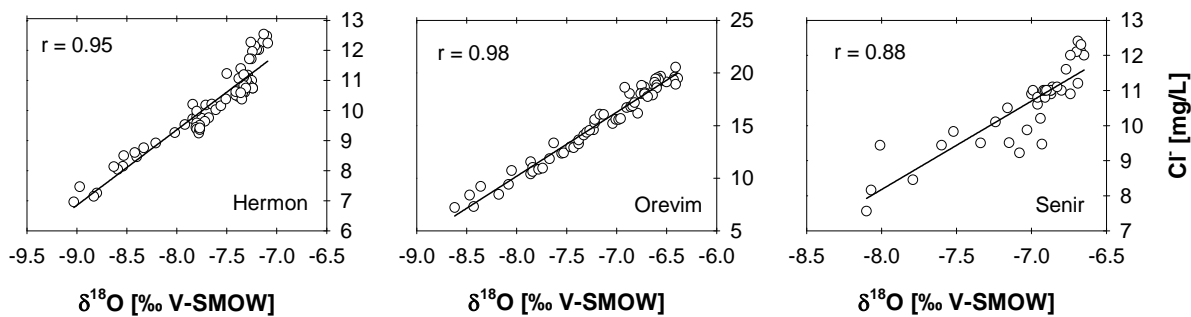


Figure 59: Mixing diagrams of $\delta^{18}\text{O}$ and Cl^- for the investigated events in the Hermon, Orevim and Senir stream. R indicates the correlation coefficient.

Analysis of the mixing charts for the assumed conservative tracers showed that discharge in the Hermon, Orevim and Senir stream can be mainly explained by the mixing of two obvious end-members (Figure 59, Figure 60). One end-member is characterized by depleted $\delta^{18}\text{O}$ and low concentrations of Cl^- , Ca^{2+} and HCO_3^- and is assumed to represent event water that travels on overland flowpaths. The second end-member shows enriched $\delta^{18}\text{O}$, and high concentrations of Cl^- , Ca^{2+} and HCO_3^- and thus displays the signature of pre-event water that is assumed to equal groundwater contributions. However, a somewhat exceptional pattern was observed for the Senir stream; when plotting HCO_3^- versus Ca^{2+} values scattered widely and a third component with high concentrations of HCO_3^- but comparatively low values of Ca^{2+} seemed to be involved in runoff generation.

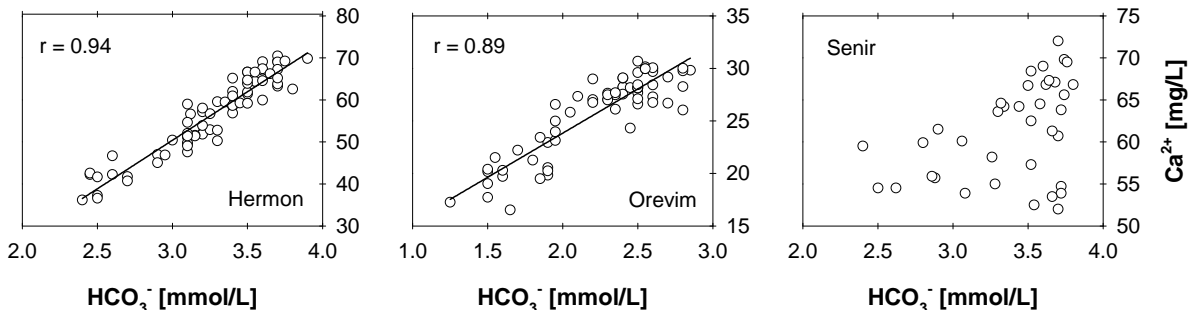


Figure 60: Mixing diagrams of HCO_3^- and Ca^{2+} for the investigated events in the Hermon, Orevim and Senir stream. R indicates the correlation coefficient.

A potential weakness of two-component mixing models is the underlying assumption of no contribution of pre-event soil water to stream discharge. However, soil water was frequently shown to contribute to storm runoff generation (BAZEMORE et al., 1994). Hence, in a second step principal component analysis (PCA) were performed to test for the assumption of two-component mixing and to identify the most important end-members describing the observed variance in stream chemistry for the investigated storm events. The technique of PCA and end-member mixing analysis was outlined by CHRISTOPHERSEN and HOOPER (1992) and BURNS et al. (2001) and described in detail in chapter 2.4.3.2.

For the Hermon, Orevim and Senir storm runoff events, a dataset of the concentrations of eight natural tracers ($\delta^{18}\text{O}$, Cl^- , Ca^{2+} , Mg^{2+} , SO_4^{2-} , DOC, K^+ and SiO_2) was obtained to

represent the observed variability in stream tracer response. These data were standardized such that constituents with great variation would not exert more influence on the model than those with less variation. Standardization was conducted according to:

$$x_{std} = \frac{x - \bar{x}}{s}$$

where x is the raw value of a chemical or isotopic parameter in the sample, \bar{x} is the mean value of the respective parameter for all of the samples, and s is the standard deviation of the respective parameter for all of the samples. Subsequently, a PCA was performed on the correlation matrix using all eight parameters; the results are given in Table 46.

Table 46: **Results of the conducted principal component analyses for the investigated events in the Hermon, Orevim and Senir stream. Principal components (PC) are given with their component matrix. Italic letters indicate principal components with eigenvalues smaller than 1. Var(PC) indicates the variance explained by the respective principal component.**

Event	PC	$\delta^{18}\text{O}$	Cl^-	Ca^{2+}	Mg^{2+}	SO_4^{2-}	DOC	K^+	SiO_2	Var(PC) %
Hermon	PC 1	0.969	0.968	0.973	0.857	0.810	-0.856	-0.925	-0.417	74.70
	PC 2	0.013	0.036	-0.046	0.452	0.315	0.157	0.178	0.830	87.86
Orevim	PC 1	0.976	0.963	0.957	0.950	0.683	-0.772	0.119	0.968	71.39
	PC 2	0.007	0.088	0.036	-0.068	0.619	0.583	0.934	-0.151	91.79
Senir	PC 1	0.900	0.949	0.371	0.954	0.908	-0.806	-0.883	0.862	71.91
	PC 2	<i>0.005</i>	<i>-0.049</i>	<i>0.909</i>	<i>-0.115</i>	<i>-0.005</i>	<i>0.343</i>	<i>-0.047</i>	<i>0.061</i>	83.97

Generally, an arbitrary number of principal components will describe overall variance in a dataset. However, since each derived component **n** requires **n+1** end-members in terms of mixing models, the number of components used in further analysis is usually restricted to those having an eigenvalue greater than 1 (DOCTOR et al., 2006). In the case of the investigated events for the Hermon, Orevim and Senir stream, two components (suggesting three end-members) accounted for 87 %, 92 % and 84 % of variance in the datasets, respectively. For all of the three streams, the first principal component (PC 1) is characterized by high-loadings of groundwater related constituents such as Ca^{2+} , Mg^{2+} , SO_4^{2-} , Cl^- and a high loading of $\delta^{18}\text{O}$ confirming the assumption of mixing between two end-members

(groundwater/overland flow) as introduced before. However, the contribution of a soil water component to storm runoff is suggested by comparatively high values of DOC, K⁺ and SiO₂ for the Hermon stream (Table 46) and by high values of DOC and K⁺ for the Orevim stream. For the Senir stream event the results are less clear, the third end-member being characterized by high loadings of DOC and Ca²⁺. Since Ca²⁺ generally increase with increasing soil depth, it seems unlikely that the third end-member represents soil water contributions. Further investigations have to be conducted to evaluate the origin of this discharge end-member. The application of EMMA for quantitative hydrograph separation requires the definition of the chemical and isotopic composition of the suggested end-members. Within the scope of this study, there were no means to establish representative end-member concentrations for soil zone contributions in the Hermon and Orevim catchment. In the Orevim catchment suction cups were temporarily installed to collect soil water from depths of 10 to 30 cm. However, the installation was followed by a dry period rendering the collection of soil water impossible. Thus, the characterization of any such component has to be reserved to future studies. Here, two-component mixing models were applied to separate event (overland flow) from pre-event water (baseflow).

7.3.6 Two-component hydrograph separation

The theoretical basis and the underlying assumptions of two-component hydrograph separations were described in chapter 2.4.3.1. Hydrograph separations were already applied in the context of discriminating Banias and Dan spring discharge components (see chapter 6.6.1 and 6.7.1). Here, $\delta^{18}\text{O}$ was used to separate event from pre-event water and Cl⁻ was applied to differentiate between overland flow and baseflow in storm runoff of the Hermon, Orevim and Senir stream. Hence, the two-component mixing model is given as:

$$Q_T C_T = Q_E C_E + Q_{PE} C_{PE}$$

where Q_T is the total discharge measured at the respective stream, Q_E is the amount of event flow (overland flow) and Q_{PE} is the amount of pre-event flow which is assumed to approximate baseflow. “C” notation represents $\delta^{18}\text{O}$ or chloride concentrations for total

discharge C_T , event flow C_E , or pre-event flow C_{PE} . Thus, the portion of the event component is calculated as:

$$Q_E = Q_T \frac{C_T - C_{PE}}{C_E - C_{PE}}$$

The relative contributions of event and pre-event water were calculated for each streamflow sample taken during the investigated storm runoff event. The isotopic and chemical composition of stream discharge prior to the event represented the pre-event component and baseflow, respectively.

A major challenge to chemical and isotopic hydrograph separations is the definition of the event component, especially in mesoscale catchments where the chemical and isotopic signature is known to vary spatially and over time (MCDONNELL et al., 1990; KENDALL and MCDONNELL, 1998; WISSMEIER and UHLENBROOK, 2007). Despite the intensive precipitation sampling campaign (chapter 5) it rendered impossible to account for the total chemical and isotopic variability of the precipitation input during storm runoff, especially since there was no possibility to sequentially sample the precipitation input as suggested by MCDONNELL et al. (1990), WISSMEIER and UHLENBROOK (2007) and others. Consequently, different scenarios for the definition of the event component were applied and compared for the investigated events in the Hermon, Orevim and Senir stream, simultaneously providing an uncertainty estimation of the conducted two-component hydrograph separation.

For chloride based hydrograph separations, the median chloride concentration of 50 snow samples taken on Mt. Hermon was assumed to represent the event component for the investigated Hermon (1/13-1/22/2004) and Senir (2/13-2/18/2003) runoff events. For the Orevim stream that emerges in the Golan area, median chloride concentrations of precipitation in the Golan determined by Herut et al. (2000) (Table 12) were believed to sufficiently characterize the event component during January 13th to 18th, 2004.

For stable isotope based ($\delta^{18}\text{O}$) hydrograph separation, the event concentrations were defined as follows: Daily precipitation sampled at Nimrod station (700 m a.s.l.) was assumed to represent the event component for the Hermon event (**Scenario A**). In a second step, these data were corrected for the known isotope-altitude gradient in precipitation (-0.26‰ per

100 m; chapter 5.3.7) assuming that major event runoff contributing to the Hermon stream is generated at an altitude similar to the mean recharge altitudes of the Banias and Kezinim springs (1260 m a.s.l.; chapter see 6.4.1). (**Scenario B**). The Sion stream collects its discharge from the upper slopes of the southeastern Hermon Mountain, contributes to Hermon stream discharge and was shown to be fed by overland flow alone during the investigated event (1/14-1/16/2004). Hence, in a third step, the measured isotopic composition of Sion discharge was assumed to characterize the temporal variation in the precipitation input contributing to Hermon storm runoff (**Scenario C**).

For the investigated storm runoff event in the Orevim stream, first, the isotopic composition of a weekly bulk precipitation sample from the Orevim catchment (station at 810 m a.s.l., see Figure 17) for that period was assumed to represent the event component (**Scenario D**). Second, the isotopic signature of the event component was recalculated from the high correlation between stream $\delta^{18}\text{O}$ and stream Cl^- during storm runoff as shown in Figure 59. Using the median chloride concentration of Golan precipitation (HERUT et al., 2000) as input variable to the regression equation, the bulk isotope composition of the precipitation end-member was reconstructed for the event (**Scenario E**).

Definition of the event component for the investigated Senir storm runoff was somewhat arbitrary because of the lack of representative precipitation input data. As described earlier (see chapter 3.6), the catchment area of the Senir stream lays for the most part in Lebanon. Hence, the isotope composition of a weekly bulk sample taken at Neve Ativ (1000 m a.s.l.) was expected to represent the event component (**Scenario F**). Enrichment effects on precipitation due to canopy interception was assumed to be negligible in the investigated subcatchments due to the sparse vegetation cover.

Estimated maximum event water contributions to storm runoff ranged from 33 % to 52 % Q_T for $\delta^{18}\text{O}$ -based separations in the Hermon stream (Table 47). For the chloride-based hydrograph separation, maximum event contribution was 49 % Q_T of total Hermon stream discharge during 1/13-1/22/2004. Maximum event water input generally occurred just after peak discharge. Mean event water contributions ranged between 10 % to 20 % Q_T for the Hermon event depending on the chosen model. Scenario E, where the stable isotopic

composition of the Sion discharge was defined to represent the event water input agreed best to the chloride-based two-component mixing model. Although sequential sampling of the precipitation input was not conducted in the scope of this study, the usage of continuously measured Sion stream $\delta^{18}\text{O}$ to define the event end-member seemed to be a good substitution. Hence, Sion stream $\delta^{18}\text{O}$ did not only include the temporal variation of $\delta^{18}\text{O}$ in precipitation but also indicated the arrival of water from different recharge altitudes (see chapter 5.3.7)

Table 47: Results of the conducted two-component hydrograph separations using $\delta^{18}\text{O}$ and Cl^- as tracer. Maximum (max) and mean event water contributions are presented as well as the event water input at peak discharge (peak). Event water contributions are given as percentage of total discharge (% Q_T).

Scenario	Event	$Q_E - \delta^{18}\text{O}$			$Q_E - \text{Cl}^-$		
		max % Q_T	mean % Q_T	peak % Q_T	max % Q_T	mean % Q_T	peak % Q_T
A	Hermon	42	12	38	49	20	48
B		33	10	29	49	20	48
C		52	16	45	49	20	48
D	Orevim	103	34	67	72	24	47
E		77	25	50	72	24	47
F	Senir	69	19	33	42	14	24

For the Orevim stream, estimated maximum event water contributions to storm runoff ranged from 77 % to 103 % Q_T for $\delta^{18}\text{O}$ -based separations (Table 47). The overestimation of the event water contribution ($> 100\% Q_T$) in scenario D results from the uncertainty of the input parameter. However, scenario E was in good agreement with results received for the chloride-based hydrograph separation which yielded a maximum event water contribution of 72 % Q_T . Mean event water contributions ranged between 24 % to 34 % Q_T .

Maximum event water contribution to the Senir stream was 69 % Q_T for the $\delta^{18}\text{O}$ -based hydrograph separation and 42 % Q_T for the chloride-based mixing model (Table 47). Mean contributions ranged between 14 % Q_T and 19 % Q_T . Both in the Orevim and Senir stream, maximum event contributions occurred right after peak discharge.

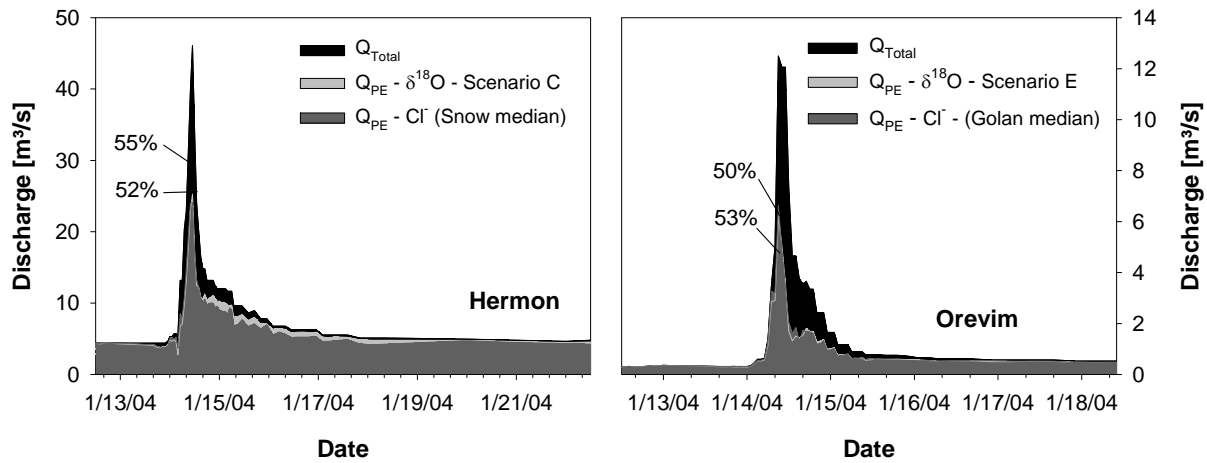


Figure 61: Results of the two-component hydrograph separation for the Hermon stream (left) and Orevim stream (right) using $\delta^{18}\text{O}$ and Cl^- as tracer. Given are the $\delta^{18}\text{O}$ scenarios each that best reproduced the results of the chloride-based mixing model. Q_T denotes total discharge while Q_{PE} refers to pre-event water.

During the investigated storm events in the Hermon, Orevim and Senir stream, total discharge (Q_T) was dominated by pre-event water (*i.e.* baseflow) accounting in average for 66 % to 88 % Q_T (Table 47). The predominance of pre-event water during storm runoff was already shown for a variety of catchment scales and climatic conditions (KENDALL and McDONNELL, 1998; MARC et al., 2001) and implies that catchments store water for a considerable amount of time but then release it promptly during storm events (KIRCHNER, 2003). Mechanisms suggested to explain this phenomena were groundwater ridging (RAGAN, 1968; GILLHAM, 1984) or pressure wave translatory flow (CAPPUS, 1960; HEWLETT and HIBBERT, 1967; TSUKAMOTO, 1961) (see chapter 2.3).

However, although pre-event water dominates total stream discharge during storm runoff in the investigated catchments, event water was shown to account for a significant portion of total flow at the time of peak discharge demonstrating the importance of overland or interflow pathways. For the Hermon stream, event contribution to peak discharge was 45 % and 48 % Q_T for the $\delta^{18}\text{O}$ - and Cl^- -based mixing models (scenario C), respectively (Figure 61). Though overland flow as such was seldom monitored in the Hermon catchment, return flow, where water rapidly infiltrates into the upper parts of the soil or epikarst and returns to surface due to hydraulic interfaces downslope of the infiltration area was frequently observed. Return flow represents a type of interflow that is difficult to separate from overland flow or baseflow

in terms of $\delta^{18}\text{O}$ -based two-component mixing models. However, results of the conducted EMMA (chapter 7.3.5) already indicated the contribution of a third component.

In general, infiltration capacities in the Hermon catchment were limited during the storm runoff event thus favoring fast flow components. However as described earlier, runoff generation in semi-arid Mediterranean catchments exhibits a patchy pattern, depending on hillslope structure, bedrocks and vegetation covers (CALVO-CASES et al., 2003; PUIDGEFABREGAS et al., 1998; BERGKAMP, 1998) suggesting that infiltration capacities show a high spatial heterogeneity in all of the investigated catchments.

For the Orevim stream, event water contribution to peak discharge was 50 % or 47 % Q_T for $\delta^{18}\text{O}$ - and Cl^- -based hydrograph separation, respectively (Figure 61, Table 47). Maximum event water contributions even ranged between 72 and 77 % Q_T indicating that the fast flow components (overland and interflow) are even more important in the basaltic setting as was already shown by long-term hydrograph separation analyses (chapter 7.1.) Both, overland flow mechanism and re-emerging shallow subsurface flow were observed at first hand during runoff event sampling in the Orevim catchment. These observations agree with results received by the conducted principal component analyses (see chapter 7.3.5) that indicated the contribution of an interflow component traveling through the upper soil layers.

In comparison, calculated event contributions to peak discharge during the investigated storm event in the Senir stream were low ranging between 33 and 24 % Q_T for $\delta^{18}\text{O}$ and Cl^- -based hydrograph separation, respectively (Table 47, Figure 62). However, also for this stream, the contribution of a fast interflow component could not be excluded. The Sion stream contributing to Hermon stream discharge, was - as already mentioned – fed by overland flow (and potentially by rapid return flow) alone.

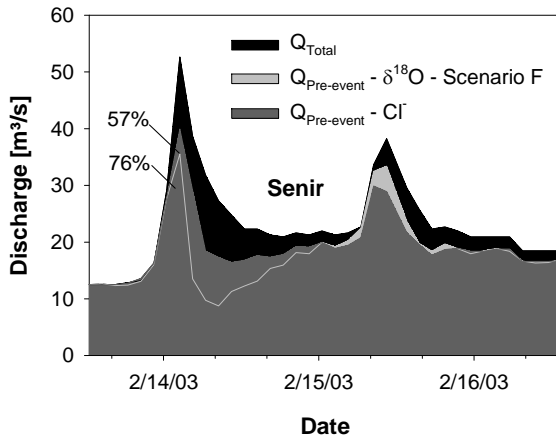


Figure 62: Results of the two-component hydrograph separation for the Senir stream using $\delta^{18}\text{O}$ and Cl^- as tracer. Presented are the $\delta^{18}\text{O}$ scenarios that best reproduced the results of the chloride-based mixing model.

Hydrograph separation and end-member mixing analyses are subject to numerous uncertainties as described in 2.4.3.3. Generally, one distinguishes between statistical uncertainties (due to sampling and analytical errors) and model uncertainty (due to the strong simplistic model hypotheses that mixing models refer to) (JOERIN et al., 2002). In this study, uncertainties were not calculated by any of the introduced techniques (see 2.4.3.3) because of insufficient data. However, an indication of uncertainty was derived by comparison of the different scenarios (Table 47). The definition and input regionalization of precipitation and $\delta^{18}\text{O}$ is of particular importance in mesoscale catchments and might result in large uncertainties (WISSMEIER and UHLENBROOK, 2007). In this study, the choice of the $\delta^{18}\text{O}$ input concentration for the event component resulted in differences of 6 % and 9 % Q_T for mean event contributions in the Hermon and Orevim stream, respectively (Table 47).

Additional uncertainty for the two-component mixing model derives from the assumption that no pre-event soil water contributes to stream discharge during storm runoff. However, both end-member mixing analyses (see chapter 7.3.5) and the visual evaluation of the retrieved chemographs (Figure 54, Figure 56) suggests the contribution of a fast interflow component that travels through the upper layers of the soil or the epikarst. Since it is unlikely that precipitation infiltrating to the soil or epikarst reaches the stream channel without altering its chemical or isotopic composition (BAZEMORE et al., 1994), the event water component might be overestimated in case soil water is mobilized. On the other hand, if event water is a

mixture of event and soil water flowing through or directly below the shallow organic soil horizon, the event water component might be underestimated. Thus, in future studies, soil and return flow should be tried to be sampled at the hillslope scale for spatial and temporal characterization of this discharge component.

Also, mixing models are based on the assumption of wave (or pressure) celerity and water (or solute) velocity, a theory that was questioned for large scale catchments in particular (WISSMEIER and UHLENBROOK, 2007). Additional uncertainties might thus derive from the delay of solutes behind the wave.

The importance of fast flow components was shown for storm runoff generation in the investigated subcatchments of the Upper Jordan River. In terms of the anticipated climate change effects such as less overall precipitation, a shortent rainy season accompanied by increasing precipitation intensities (see chapter 1.1), the runoff regime in the Upper Jordan River catchment will change. First, the overall frequency of runoff events might decrease while the occurrence of floods might increase provided that precipitation amounts allow for runoff generating moisture conditions.

Since overland and interflow significantly influence runoff generation in the investigated catchments, the occurrence of floods will be accompanied by high loadings of particulate and dissolved matter resulting in a deterioration of the quality of surface water that are feeding Lake Kinneret. Additionally, if the occurrence of dry intervals between runoff events increases or lengthens, the occurrence of first flush effects will be more frequent since soil and vegetation particles can accumulate more frequently in the dry river beds. Thereby, the term “first flush effect” refers to a hydrological process where different kinds of solutes are washed from the catchment into the stream during a runoff event. This process might result in a peak in solute concentrations that either precedes the hydrograph peak if flushing is supply-limited or occurs only after the hydrograph when flushing is transport-limited such as often observed for DOC (BURNS, 2005). Although water quality might deteriorate, the amount of water reaching Lake Kinneret and thus the short-term availability of water resources might even increase due to the already observed limited infiltration capacities and - with increasing peak discharges - the increasing significance of fast flow components.

Extended summary

One objective of this study was to assess the vulnerability of the main water resources in the Upper Jordan River Catchment (UJRC), Israel, towards climate change and to increase the knowledge about recharge and discharge mechanism and dynamics in this basin. Another objective was to refine the existing conceptual models of recharge and runoff generation in the UJRC based on the results of the conducted experimental investigations.

High quality freshwater is a limited resource in semi-arid and arid zones, the anticipated effects of global and climate change may even worsen the actual situation. The Upper Jordan River catchment, a transboundary basin shared by Israel, Lebanon and Syria, which was subject of this study provides about 27 % of the State of Israel's water demand. The UJRC, Israel's northernmost watershed comprises a surface area of about 1700 km² and receives its major recharge from the karstic Hermon/Anti-Lebanon mountains (2814 m a.s.l.) and the basaltic Golan Heights (1000 m a.s.l.). The catchment is drained by the Jordan River that passes the Hula basin and feeds Lake Kinneret.

The difficult political circumstances resulted in a general lack of studies concerning the hydrogeological features of the main Upper Jordan River sources. Only parts of the basin were studied and published data are scarce. For a sustainable management of the basins water resources, detailed information regarding the type and portion of discharge components, water volumes, mean residence times, the extent of subsurface recharge areas and recharge rates are urgently required.

For this purpose, characteristics of recharge and discharge in the UJRC with focus on the mountainous Hermon and Golan recharge areas were investigated from 2002 to 2004, applying a combined-method approach. This approach comprised hydrographic techniques, time-series analyses, isotopic and natural geochemical tracers. Field sampling included the continuous monitoring of five major streams. Rain collectors and 14 groundwater outlets were sampled on a regular basis, while snow, snowmelt and overland flow were tested occasionally. Samples were analyzed for up to 14 water quality parameters including major ions, DOC, TSS, dissolved silica, ¹⁴C and ¹³C, tritium and the stable isotopes of water.

The results of these investigations are presented in three thematically divided chapters within this thesis and deal with (1) the hydrochemical and isotopic characterization of precipitation, (2) the hydrochemical and isotopic characterization of groundwater and finally with (3) runoff generation in the main tributaries of the Upper Jordan River.

The dynamic control on the transformation process of **precipitation** into recharge and discharge is the input variable itself, *i.e.* precipitation. Within the scope of this study, the isotopic and chemical composition of precipitation and its temporal and spatial distribution was – for the first time – extensively investigated for the mountainous northern UJRC. The chemical composition of precipitation varied depending on the origin of air-masses and the mineralogy of dusts of bedrocks passed on their way. Precipitation showed generally low electrical conductivities (20 $\mu\text{S}/\text{cm}$).

Stable isotope data in precipitation were used to construct a local meteoric water line (LMWL) for the UJRC ($\delta^2\text{H} = 7.23 \delta^{18}\text{O} + 16.21$). The altitude effect causes a depletion of -0.26 ‰ and -1.10 ‰ per 100 m for $\delta^{18}\text{O}$ and $\delta^2\text{H}$ in the Hermon area, respectively and was used to determine mean recharge altitudes for the major Hermon springs. Additionally, precipitation amounts and stable isotope patterns were influenced by seasons and the prevailing synoptic system, e.g. high amounts of rain and depleted isotope compositions were associated with cold fronts such as the *Cyprus Low*, while low rain amounts and enriched $\delta^{18}\text{O}$ in precipitation were connected to the *Red Sea trough*. The observed isotopic trends subject to temperature, precipitation amount and wind direction were closely connected to these phenomena. The isotopic composition of an investigated snowpack showed significant enrichment over time (up to 4.3 ‰ for $\delta^{18}\text{O}$).

Groundwaters from the major springs in the Hermon Mountains and Golan Heights recharging into the UJRC were investigated for their environmental tracer signatures to derive detailed information on recharge areas and rates, mean residence times of the water and aquifer dimensions. Based on their distinct chemical and isotopic pattern, Golan and Hermon springs were differentiated.

Golan “Side springs” were represented by a calcium-sodium or sodium-calcium and bicarbonate water type and showed elevated concentrations of silicate compared to the Hermon springs. The springs plot along a mixing line ($\delta^2\text{H} = 6.41 \delta^{18}\text{O} + 10.73$) with a slope lower than the LMWL indicating that infiltrating water has been subject to evaporation in the unsaturated zone. Golan “Side springs” are either fed by the regional basalt aquifer (with groundwater residence times > 50 years) or by a mixture of regional groundwater with water from local perched aquifers (with groundwater residence times < 50 years). Water mean residence times were determined with the help of tritium and radiocarbon measurements.

Generally, the chemical and isotopic composition of the springs seems to follow a north-to-south gradient in that way reproducing the climatic and geological gradient observed for the Golan Heights. The northern Golan is characterized by a comparatively thick aquifer, a thick unsaturated zone and high amounts of precipitation and recharge. Here, “Side springs” such as the Hamroniya, Gonen and Notera display high contributions of unsaturated zone water resulting in tritium-rich groundwater with low chloride and high silicate concentration. In the south, where evaporative effects increase and comparatively less recharge through the unsaturated zone occurs, low tritium water with high amounts of chloride are found in the Bet HaMekhes and Jalabina spring. Recharge rates for the Golan “Side springs” range between 12 to 16 % of mean annual precipitation based on chloride mass balances. Their subsurface recharge areas size between 0.6 to 3 km².

The investigated Hermon springs are (a) fed by two recharge areas (divided by the Sion-Rachaya fault) and (b) exhibit patterns of local and regional recharge systems indicated by the isotopic and chemical signatures of their groundwater. In addition, (c) they receive different contributions of conduit and diffusive matrix flow. All springs are characterized by low salinities and a Ca-Mg-HCO₃-water type. However, springs of the eastern intake area such as the Banias and Kezinim spring show dilution of dolomite, gypsum and anhydrite all of which are absent in the western recharge area feeding the Dan, Barid and Leshem spring.

Generally, Hermon springs exhibit a seasonal recharge bias with most inflow occurring in the spring season as indicated by depleted values in $\delta^{18}\text{O}$ and $\delta^2\text{H}$, a drop of groundwater temperatures and diluted ion concentrations in spring discharge. The dominance of snowmelt

recharge in the Hermon springs is particularly indicated by elevated deuterium excess values in groundwater during spring. This observation also allowed to retrace the mean recharge altitudes of the springs. Mean $\delta^{18}\text{O}$ composition of groundwater were corrected for enrichment due to fractionation processes during snowmelt, combined with the altitude effect on precipitation $\delta^{18}\text{O}$ and resulted in mean recharge elevations of about 1260 m a.s.l. for the Banias and Kezinim spring, about 1560 m a.s.l. for the Dan, Barid and Leshem springs and about 1320 m a.s.l for the Sion spring.

The Kezinim spring as well as the baseflow discharge of the Banias spring display a thermal regime and highest mineralization within the Hermon springs, in particular, high concentrations of sulfate, chloride and silicate were measured. Additionally, these two water exhibit comparatively enriched values of $\delta^{18}\text{O}$ and $\delta^2\text{H}$ and, the Kezinim spring in particular, low seasonal variations in its isotopic and chemical composition. Thus, it was concluded that the Kezinim spring and Banias baseflow are fed by diffusive matrix flow that originates from a regional groundwater system that is in contact with the Triassic Muheila Formation. This assumption was additionally supported by the derived comparatively high (> 1000 years) radiocarbon residence time for the waters of the Kezinim spring. In contrast, water of the Dan, Barid and Leshem springs represent a relatively shallow (local) groundwater flow system dominated by young water where transport occurs in changing portions through both conduit/fissure and matrix flow.

The importance of fast and slow flow components for Hermon groundwater was investigated in detail for the Banias and Dan spring. The Banias spring showed the most rapid and flashy response towards precipitation within the Hermon springs. The springs discharge is controlled by direct, vadose zone and phreatic flow that were quantified based on a three-component mixing model using $\delta^{18}\text{O}$ and sulfate as natural tracer. Fast and medium flow components accounted for up to 88 % of total discharge in February 2003 and still for up to 70 % in June 2003, emphasizing the climate-controlled recharge dynamics of this spring. In contrast, Dan spring response was well-balanced and minor variations of physical, chemical and isotopic parameters were monitored in response to precipitation. However, two-component mass balances using $\delta^{18}\text{O}$, chloride or sulfate revealed that up to 40 % of the total discharge

originated from newly arriving water with the highest contributions in early and mid summer. Summarizing, it was concluded that the Banias spring comprises a system with limited storage and well developed drainage and responds fast to rain and snowmelt while the Dan spring is characterized by a vast, well-mixed reservoir where newly arriving waters are subject to strong dilution.

Recharge rates for the Hermon springs range between 12 to 20 % of mean annual precipitation based on chloride mass balances, in comparison to 19 to 30 % based on mean residence time estimations. For the first time, estimations of subsurface recharge areas for the Dan and Banias spring could be calculated sizing between 1324 km² and 523 km², respectively. Hence, the subsurface catchment area of the major springs contributing to the Upper Jordan River outnumbers considerably the orographic catchment area and reaches far beyond Israel's political borders. The quality of these estimations is limited by uncertainty in the determination of the mean annual precipitation on Mount Hermon, an input parameter of the recharge estimations. This problem needs to be addressed in future field investigations.

In a third step, **runoff generation processes** based on (a) existing hydrographic long-term data and (b) natural tracer-based during storm runoff events were investigated for the major tributaries of the Upper Jordan River, i.e. the Hermon, Senir and Dan stream. Additionally, the Orevim stream emerging in the basaltic Golan Heights was studied for comparison. Three main runoff components were identified for both geological settings: basalt and karst. While the Dan stream is solely fed by baseflow of the Dan and Leshem springs; the overland and interflow component together amounted – based on a 30-year record - to 46 % and 58 % of total stream discharge in the Hermon and Senir stream, respectively. In the basalt area (Orevim stream), the fast and medium flow component contributed with about 75 % to total discharge. While in the karst area the interflow component is attributed to the snow reservoir on Mount Hermon feeding snowmelt to streamflow, in the basalt area the interflow reservoir is rather due to the structure of the subsurface system, *i.e.* the existence of hydraulic interfaces.

The importance of the fast flow components was again emphasized by the conducted storm runoff hydrograph separations. During the investigated floods, event water contributed with

about 52 %, 69 % and 77 % to peak discharge in the Hermon, Senir and Orevim stream, respectively. End-member mixing analyses supported the assumption of shallow subsurface flow in both settings. Mean baseflow residence times ranged from a few months to about 4 years for the Hermon, Senir and Dan stream based on recession analyses. The dominance of young waters was additionally supported by ${}^3\text{H}$ -measurements resulting in mean residence times of 24, 28 and 33 years for the Hermon, Dan and Senir stream, respectively. Based on the retrieved mean residence times, the thickness of the aquifer (*i.e.* the zone where groundwater is actively cycled) was determined to size in between 11 to 103 m in the Dan subcatchment, whereas the mean aquifer thickness is about 32 m. In the Hermon catchment this zone sizes to about 13 m.

Based on the conducted investigations it has to be concluded that the anticipated climate changes such as less overall precipitation, increasing temperatures and increasing frequency of rain extremes will significantly challenge the water resource management in the Upper Jordan River Catchment.

Altogether recent water dominates the flow system of the Hermon karst area as well as that of the Golan basalt area. Hence, an increase in temperature will lead to a decreasing snow/rain-ratio and an accelerated melting of snow. On the one hand, this might even lead to enhanced groundwater recharge given the high infiltration capacities in the karstic Mount Hermon, on the other hand it will also cause an increased potential of floods. If rain extremes will occur more often as suggested for the region, the frequency of extreme flood events both in the Hermon area and the Golan Heights will increase. Additionally, this might lead to a deterioration of water quality in the Upper Jordan River and Lake Kinneret since floods were observed to cause the flushing of nutrients and suspended materials from the different catchments.

Under a predicted scenario of increasing temperatures and less overall precipitation, the reduction of snow precipitation and snowmelt will significantly reduce baseflow in the Upper Jordan River tributaries thus strongly impacting the water supply management of Lake Kinneret.

References

Abdul, A.S., Gillham, R.W., 1989. Field studies of the effects of the capillary fringe on streamflow generation. *Journal of Hydrology* 112: 1-18.

Adar, E.M., Dody, A., Geyh, M.A., Yair, A., Yakirevich, A., Issar, A.S., 1998. Distribution of stable isotopes in arid storms. I. Relation between the distribution of isotopic composition in rainfall and in the consequent runoff. *Hydrogeology Journal* 6: 50-65.

Aeschbach-Hertig, W., Stute, M., Clark, J.F., Reuter, R.F., Schlosser, P., 2002. A paleotemperature record derived from dissolved noble gases in groundwater of the Aquia Aquifer (Maryland, USA). *Geochemica et Cosmochimica Acta* 66(5): 797-817.

Aiken, G.R., 1985. Isolation and concentration techniques for aquatic humic substances. In: G.R. Aiken, G.R., MacCarthy, P. (Eds.), *Humic substances in soil, sediment and water*. Wiley, New York, pp. 363-386.

Alatout, S., 2000. Water Balances in Palestine: Numbers and Political Culture in the Middle East. In: David B. Brooks and Ozay Mehmet (eds.), *Water Balances in the Eastern Mediterranean*. Ottawa, Canada: International Development Research Center.

Alpert, P., Shafir, H., 1989a. Scale distribution of orographic precipitation: numerical study and comparison with precipitation derived from radar measurements. *Journal of Applied Meteorology* 28: 1105-1117.

Alpert, P., Ziv, B., 1989b. The Sharav Cyclone: Observations and some theoretical considerations. *Journal of Geophysical Research*, 94: 18495-18514.

Alpert, P., Abramsky, R., Neeman, B.U., 1990. The prevailing summer synoptic system in Israel - Subtropical high, not Persian trough. *Israel Journal of the Earth Sciences* 39: 93-102.

Alpert P, Ben-Gai T, Baharad A, Benjamini Y, Yekutieli D, Colacino M, Diodato L, Ramis C, Homar V, Romero R, Michaelides S, Manes A., 2002. The paradoxical increase of Mediterranean extreme daily rainfall in spite of decrease in total values. *Geophysical Research Letters* 29: 31-1-31-4.

Alpert, P., Silverman, D., 2003. Vulnerability of water resources in Eastern Mediterranean ecosystems due to climate change - an integrated approach to sustainable management. Report.

Alpert, P., Osetinsky, I., Ziv, B., Shafir, H., 2004a. A new seasons definition based on classified daily synoptic systems: an example for the Eastern Mediterranean. *International Journal of Climatology* 24: 1013-1021.

Alpert, P., Osetinsky, I., Ziv, B., Shafir, H., 2004b. Semi-objective classification for daily synoptic systems: application to the Eastern Mediterranean climate change. *International Journal of Climatology* 24: 1001-1011.

Alpert, P., Price, C., Krichak, S.O., Ziv, B., Saaroni, H., Osetinsky, I., Barkan, J., Kishcha, P., 2005. Tropical tele-connections to the Mediterranean climate and weather. *Advances in Geosciences* 2: 157-160.

Amery, H.A., Wolf, A.T., 2000. Water Resources and the Geography of Peace in the Middle East: An Introduction. In Amery, H. A. and A. T. Wolf (eds.) *Water in the Middle East: A Geography of Peace.*.. Austin: University of Texas Press. Pp. 1-18.

Amin, I.E., Campana, M.E., 1996. A general lumped parameter model for the interpretation of tracer data and transit time calculation in hydrologic systems. *Journal of Hydrology* 179: 1-21.

Aouad-Rizk, A., Job, J.-O., Khalil, S., Touma, T., Bitar, C., Boquillon, C., Najem, W., 2005. Snow in Lebanon: A preliminary study of snow cover over Mount Lebanon and simple snowmelt model. *Hydrological Sciences Journal* 50(3): 555-569.

Aquilina, L., Ladouce, B., Dorfliger, N., 2006. Water storage and transfer in the epikarst of karstic systems during high flow periods. *Journal of Hydrology* 327(3-4): 472-485.

Asaf, L., Nativ, R., Shain, D., Hassan, M., Geyer, S., 2004. Controls on the chemical and isotopic compositions of urban stormwater in a semiarid zone. *Journal of Hydrology* 294(4): 270-293.

Assouline, S., 2004. Rainfall-induced soil surface sealing: a critical review of observations, conceptual models, and solutions. *Vadose Zone Journal* 3: 570-591.

Bajjali, W., 1994. Recharge and regional circulation of thermal groundwater in northern Jordan using isotope geochemistry. PhD Thesis, University of Ottawa, Canada, 257 pp.

Bajjali, W., 2006. Recharge mechanism and hydrochemistry evaluation of groundwater in the Nuaimeh area, Jordan, using environmental isotope techniques. *Hydrogeology Journal* 14(1-2): 180-191.

Bajjali, W., Clark, I.D., Fritz, P., 1997. The artesian groundwaters of northern Jordan: insights into their recharge history and age. *Journal of Hydrology* 192: 355-382.

Bar-Matthews, M., Ayalon, A., Matthews, A., Sass, E., Halicz, L., 1996. Carbon and oxygen isotope study of the active water-carbonate system in a karstic Mediterranean cave: Implications for paleoclimate research in semiarid regions. *Geochimica et Cosmochimica Acta* 60(2): 337-347.

Barnes, I., Irwin, W.P., White, D.E., 1978. Global distribution of carbon dioxide discharges and major zones of seismicity; United States Geological Survey, Water Resource Investigations Open File Report 78-39.

Bazemore, D.E., Eshleman, K.N., Hollenbeck, K.J., 1994. The role of soil water in storm flow generation in a forested headwater catchment: synthesis of natural tracer and hydrometric evidence. *Journal of Hydrology* 162: 47-75.

Beaumont, P., 2000. The Quest for Water Efficiency - Restructuring of Water Use in the Middle East. *Water, Air, & Soil Pollution* 123(1-4): 551-564.

Ben-Gai, T., Bitan, A., Manes, A., Alpert, P., Rubin, S., 1998. Spatial and temporal changes in rainfall frequency distribution patterns in Israel. *Theoretical and Applied Climatology* 61: 177-190.

Ben-Gai, T., Bitan, A., Manes, A., Alpert, P., Rubin, S., 1999. Spatial and temporal trends of temperature patterns in Israel. *Theoretical and Applied Climatology* 64: 163-177.

Ben-Gai, Y., 2002. Near-surface geophysical studies in a drained wetland - the Hula Basin, Upper Jordan River Valley. *Geophysical Institute of Israel, Report*. No. 836/216/02.

Benischke, R., Zojer, H., Fritz, P., Malosszewski, P., Stichler, W., 1988. Environmental and Artificial Tracer Studies in an Alpine Karst Massif (Austria). *Karst Hydrogeology and Karst Environment Protection. Volume 2. Proceedings of the 21st Congress of the International Association of Hydrogeologists, Guilin, China October 10-15, 1988. IAHS Publication No. 176*: 938-947.

Bergkamp, G., 1998. A hierarchical view of the interactions of runoff and infiltration with vegetation and microtopography in semi-arid shrublands. *Catena*, 33: 201-220.

Bergkamp, G., Cammeraa, L.H., Martinez Fernandez, J., 1996. Water movement and vegetation patterns on shrubland and an abandoned field in two desertification threatened areas in Spain. *Earth Surface Processes and Landforms* 21: 1073-1090.

Berkoff, J., 1994. A strategy for managing water in the Middle East and North Africa. *WORLD BANK, WASHINGTON, D.C. (USA)*. 96 pp.

Beven, K.J., 1986. Hillslope runoff processes and flood frequency characteristics. *Hillslope Processes*, A. D. Abrahams, Ed., Allen and Unwin, 187-202.

Beven, K.J., 2004. Does an interagency meeting in Washington imply uncertainty? *Hydrological Processes* 18: 1747-1750.

Beven, K.J., Feyen, J., 2002. The future of distributed hydrological modeling. *Hydrological Processes* 16: 169-172.

Beven, K.J., Germann, P., 1982. Macropores and water flow in soils. *Water Resources Research* 18: 1311-1325.

Bishop, K., Pettersson, C., Allard, B. Lee, Y.-H., 1994. Identification of the riparian sources of aquatic dissolved organic carbon. *Environment International* 20(1): 11-19.

Bishop, K., Seibert, J., Köhler, S., Laudon, H., 2004. Resolving the Double Paradox of rapidly mobilized old water with highly variable responses in runoff chemistry. *Hydrological Processes* 18: 185-189.

Blanckenhorn, M., 1912. Kurzer Abriß der Geologie Palästinas. *Zeitschrift des deutschen-palästinesischen Vereins* 35: 113-139.

Boronina, A., Balderer, W., Renard, P., Stichler, W., 2005. Study of stable isotopes in the Kouris catchment (Cyprus) for the description of the regional groundwater flow. *Journal of Hydrology* 308(1-4): 214-226.

Bottomley, D.J., Craig, D., Johnston, L.M., 1986. Oxygen-18 studies of snowmelt runoff in a small Precambrian shield watershed: implications for streamwater acidification in acid-sensitive terrain. *Journal of Hydrology* 88: 213-234.

Bouwer, H., 2003. Integrated water management for the 21st century: problems and solutions. *Food, Agriculture & Environment*, 1: 118-127.

Bou-Zeid, E., El-Fadel, M., 2002. Climate Change and Water Resources in Lebanon and the Middle East. *Journal of Water Resource Planning and Management* 128(5): 343-355.

Boyer, E.W., Hornberger, G.M., Bencala, K.E., McKnight, D.M., 1997. Response characteristics of DOC flushing in an alpine catchment. *Hydrological Processes* 11: 1635-1647.

Bredenkamp, D.B., Vogel, J.C., 1970. Study of a dolomitic aquifer with carbon-14 and tritium. In: *Isotope Hydrology*, 1970, Proceedings Symposium of International Atomic Energy Agency and UNESCO, Vienna, March 9-13, 1970. Vienna, International Atomic Energy Agency STI/PUB/255, Paper No SM-129/21, P 349-372.

Brewer, M.J., Dunn, S.M., Soulsby, C., 2002. A Bayesian model for compositional data analysis. *Proceedings of Compstat 2002*, Berlin, Germany, pp. 105-110.

Brodersen, C., Pohl, S., Lindenlaub, M., Leibundgut, C., vWilpert, K., 2000. Influence of vegetation structure on isotope content of throughfall and soil water. *Hydrological Processes* 14(8): 1439-1448.

Bromley, J., Brouwer, J., Barker, A.P., Gaze, S.R., Valentin, C., 1997. The role of surface water redistribution in an area of patterned vegetation in a semi-arid environment, south-west Niger. *Journal of Hydrology* 198: 1-29.

Bronstert, A., Niehoff, D., Bürger, G., 2002. Effects of climate and land-use change on storm runoff generation: present knowledge and modelling capabilities. *Hydrological Processes* 16: 509-529.

Brown, V.A., McDonnell, J.J., Burns, D.A., Kendall, C., 1999. The role of event water, a rapid shallow flow component, and catchment size in summer stormflow. *Journal of Hydrology* 217: 171-190.

Burdon, D.J., 1954. Infiltration rates in the Yarmouk basin of Syria-Jordan. *International Association Science Hydrology* 37: 343-355.

Burdon, D.J., Safadi, C., 1964. The karst groundwaters of Syria. *Journal of Hydrology* 2: 324-347.

Burg, A., Gavrieli, I., Bein, A., 2003. Identification of recharge areas and flow paths by natural tracers; the Upper Jordan spring system. *Geophysical Research Abstracts* 5: 10074.

Burns, D.A., McDonnell, J.J., 1998. Effects of a beaver pond on runoff processes: comparison of two headwater catchments. *Journal of Hydrology* 205: 248-264.

Burns, D.A., McDonnell, J.J., Hooper, R.P., Peters, N.E., Freer, J.E., Kendall, C., Beven, K., 2001. Quantifying contributions to storm runoff through end-member mixing analysis and hydrologic measurements at the Panola Mountain Research Watershed (Georgia, USA). *Hydrological Processes* 15: 1903-1924.

Burns, D.A., 2005. What do hydrologists mean when they use the term flushing? *Hydrological Processes* 19(6): 1325-1327.

Burt, T.P., Arkell, B.P., 1987. Temporal and spatial patterns of nitrate losses from an agricultural catchment. *Soil Use and Management* 3(4): 138-142.

Buttle, J. M. and Peters, D. L. 1997. Inferring hydrological processes in a temperate basin using isotopic and geochemical hydrograph separation: A re-evaluation. *Hydrological Processes* 11: 557-573.

Buttle, J.M., 1994. Isotope hydrograph separations and rapid delivery of pre-event water from drainage basins. *Progress in Physical Geography* 18: 16-41.

Buttle, J.M., 1998. Fundamentals of small catchment hydrology. In: Kendall, C, McDonnell, J.J. (Eds.), *Isotope Tracers in Catchment Hydrology*, Elsevier, pp. 1-43.

Buttle, J.M., Sami, K., 1992. Testing the groundwater ridging hypothesis of streamflow generation during snowmelt in a forested catchment. *Journal of Hydrology* 135(1-4): 53-72.

Calvo-Cases, A., Boix-Fayos, C., Imeson, A.C., 2003. Runoff generation, sediment movement and soil water behaviour on calcareous (limestone) slopes of some Mediterranean environments in southeast Spain. *Geomorphology* 50: 269-291.

Cappus, P., 1960. Bassin expérimental d'Alrance - Étude des lois de l'écoulement - Application au calcul et à la prévision des débits. *La Houille Blanche* A: 493-520.

Carey, S.K., Quinton, W.L., 2005. Evaluating runoff generation during summer using hydrometric, stable isotope and hydrochemical methods in a discontinuous permafrost alpine catchment. *Hydrological Processes* 19: 95-114.

Carmi, I., Stiller, M., Kaufman, A., 1985. The effect of atmospheric ^{14}C variations on the ^{14}C levels in the Jordan River system. *Radiocarbon* 27: 305-313.

Ceballos, A., Schnabel, S., 1998. Hydrological behaviour of a small catchment in the dehesa land use system (Extremadura, SW Spain). *Journal of Hydrology* 210: 146-160.

Celle-Jeanton, H., Gonfiantini, R., Travi, Y., Sol, B., 2004. Oxygen-18 variations of rainwater during precipitation: application of the Rayleigh model to selected rainfalls in Southern France. *Journal of Hydrology* 289: 165-177.

Cerling, T.E., Quade, J., 1993. Stable carbon and oxygen isotopes in soil carbonates. In: Swart, P.K., Lohmann, K.C., McKenzie, J., Savin, S. (eds) *Climate Change in Continental Isotope Records*, Geophys. Monogr. 78. Washington, DC: Am. Geophys. Union. 374 pp.

Cerling, T.E., Quade, J., Ambrose, S.H., Sikes, N.E., 1991. Fossil soils, grasses, and carbon isotopes from Fort Ternan, Kenya: grassland or woodland? *Journal of Human Evolution* 21: 295– 306.

Chorley, R.J., 1978. The hillslope hydrological cycle. In: Kirkby, M.J. (Ed.), *Hillslope Hydrology*, John Wiley, New York, pp. 1-42.

Christiansen, J.S., Thorsen, M., Clausen, T., Hansen, S., Refsgaard, J.C., 2004. Modelling of macropore flow and transport processes at catchment scale. *Journal of Hydrology* 299: 136-158.

Christodoulou, T., Leontiadis, I.L., Morfis, A., Payne, B.R., Tzimourtas, S., 1993. Isotope hydrology study of the Axios River plain in northern Greece. *Journal of Hydrology* 146: 391-404.

Christophersen, N., Hooper, R.P., 1992. Multivariate analysis of stream water chemical data: The use of principal components analysis for the end-member mixing problem. *Water Resources Research* 28: 99-107.

Christophersen, N., Neal, C., Richard, H., Vogt, R. D., Andersen, S., 1990. Modelling streamwater chemistry as a mixture of soil-water end-members – a step towards second generation acidification models. *Journal of Hydrology* 116: 307-320.

Clark, I.D., Fritz, P., 1997. Environmental isotopes in hydrogeology; Lewis Publishers, New York, 328 p.

Cloke, H.L., Anderson, M.G., Renaud, J.-P., 2006. Development of a modelling methodology for the investigation of riparian hydrological processes. *Hydrological Processes* 20(1): 85-107.

Cornell, R.M., Schwertmann, U., 1996. The iron oxides. Structure, properties, reactions, occurrence and uses. VCH Weinheim, pp. 395-432.

Craig, H., 1961. Isotopic variations in meteoric waters. *Science* 133:1702.

Creed, I.F., Band, L.E., 1998. Export of nitrogen from catchments within a temperate forest: Evidence for a unifying mechanism regulated by variable source area dynamics. *Water Resources Research* 34(11): 3105.

Cruz, J.V., Amaral., C.S., 2004. Major ion chemistry of groundwater from perched-water bodies of the Azores (Portugal) volcanic archipelago. *Applied Geochemistry* 19: 445–459.

Dafny, E., Burg, A., Gvirtzman, H., 2006. Deduction of groundwater flow regime in a basaltic aquifer using geochemical and isotopic data: The Golan Heights, Israel case study. *Journal of Hydrology* 330: 506-524.

Dafny, E., Gvirtzman, H., Burg, A., Fleischer, A., 2003. The hydrogeology of the Golan basalt aquifer, Israel. *Israeli Journal of Earth Sciences* 52: 139-153.

Daly, C., Neilson, R.P., Phillips, D.L., 1994. A statistical-topographic model for mapping climatological precipitation over mountainous terrain. *Journal of Applied Meteorology* 33: 140-158.

Dan, J., 1983. Soil chronosequences of Israel. *Catena* 10: 287-319.

Dan, J., Singer, A., 1973. Soil evolution on basalt and basic pyroclastic materials in the Golan Heights. *Geoderma* 9: 165-192.

Dan, J., Yaalon, D.H., Koyumdjiski, H., Raz, Z., 1972: The soil association map of Israel. *Israeli Journal of Earth Sciences* 21: 29–49.

Danin, A. and Arbel, A., 1998. The fauna and flora of the Holyland. Carta, Jerusalem, 144 pp. (in Hebrew).

Danin, A., 2004. Distribution atlas of plants in the flora Palaestina area. Israel Academy for Science and Humanities, Jerusalem.

Dansgaard, W., 1964. Stable isotopes in precipitation. *Tellus* 16: 436-438.

DeBoer, D.H. and Campbell, I.A., 1990. Runoff chemistry as an indicator of runoff sources and routing in semi-arid, badland drainage basins. *Journal of Hydrology* 121: 379-394.

Degani, A., Inbar, M., 1993. The lands of the Golan and Hermon. Ministry of Defense Publishing House, Tel Aviv (in Hebrew).

Demuth, S., 1993. Untersuchungen zum Niedrigwasser in Westeuropa. Freiburger Schriften zur Hydrogeologie. Band 1, Freiburg, Germany.

Denic-Jukic, V., Jukic, D., 2003. Composite transfer functions for karst aquifers. *Journal of Hydrology* 274: 80-94.

Desmarais, K. and Rojstaczer, S. 2002. Inferring groundwater flow paths from measurements of carbonate spring response to storms. *Journal of Hydrology* 260: 118-134.

DeWalle, D.R., Swistock, B.R., 1994. Causes of episodic acidification in five Pennsylvania streams on the northern Appalachian Plateau. *Water Resources Research* 30(7): 1955-1964.

Diener, C., 1885. Die Struktur des Jordanquellgebietes. *Sitzungs-Bericht der kaiserlichen Akademie der Wissenschaften. Wien*, 92: 633-642.

Dillon, P.J., Molot, L., 1997. Dissolved organic and inorganic carbon mass balances in central Ontario lakes. *Biogeochemistry* 36: 29-42.

Dinçer, T., Payne, B.R., 1971. An environmental isotope study of the south-western part karst region of Turkey. *Journal of Hydrology* 14: 233-258.

Dinçer, T., Payne, B.R., Florkowski, T., Martinec, J., Tongiorgi, E., 1970. Snowmelt runoff from measurements of tritium and oxygen-18. *Water Resources Research* 6: 110-124.

Doctor, D.H., Alexander, E.C., Petric, M., Kogovsek, J., Urbanc, J., Loyen, S., Stichler, W., 2006. Quantification of karst aquifer discharge components during storm events through end-member mixing analysis using natural chemistry and stable isotopes as tracers. *Hydrogeology Journal* 14(7): 1171-1191.

Domenico, P.A., Schwartz, F.W., 1990. Physical and chemical hydrogeology. John Wiley and Sons, New York.

Dreiss, S.J., 1989. Regional scale transport in a karst aquifer: 1. Component separation of spring flow hydrographs. *Water Resources Research* 25(1): 117-125.

Drever, J.I., 1997. The Geochemistry of Natural Waters: Surface and Groundwater Environments. 3rd ed., Prentice-Hall, Upper Saddle River, NJ (436pp.).

Dubertret, L., 1955. Carte géologique du Liban au 1/200000 avec notice explicative. République Libanaise, Ministère des Travaux Publics, Beirut, p. 74.

Duenkeloh, A., Jacobbeit, J., 2003. Circulation dynamics of Mediterranean precipitation variability 1948-98. *International Journal of Climatology* 23: 1843-1866.

Durand, P., Torres, J.L.J., 1996. Solute transfer in agricultural catchments: the interest and limits of mixing models. *Journal of Hydrology*, 181, 1-22.

Edgell, H.S., 1997. Karst and hydrogeology. *Carbonates and Evaporites* 12: 220-235.

Ehhalt, D., Knott, K., Nagel, J.F., Vogel, J.C., 1963. Deuterium and oxygen 18 in rain water. *Journal of Geophysical Research* 68: 3775.

Eichinger, L., 1983. A contribution to the interpretation of ^{14}C groundwater ages considering the example of a partially confined sandstone aquifer. *Radiocarbon* 25: 347–356.

Einsiedl, F., 2005. Flow system dynamics and water storage of a fissured-porous karst aquifer characterized by artificial and environmental tracers. *Journal of Hydrology*, 312: 312-321.

Eisenlohr, L., Bouzelboudjen, M., Kiraly, L., Rossier, Y., 1997a. Numerical versus statistical modelling of natural response of a karst hydrogeological system. *Journal of Hydrology* 2: 244-262.

Eisenlohr, L., Kiraly, L., Bouzelboudjen, M., Rossier, I., 1997b. A numerical simulation as a tool for checking the interpretation of karst springs hydrographs. *Journal of Hydrology* 193: 306-315.

Elsenbeer, H., Lorieri, D., Bonnell, M., 1995. Mixing model approaches to estimate storm flow sources in an overland flow-dominated tropical rain forest catchment. *Water Resources Research* 31(9): 2267-2278.

Eshel, G., 2004. Geohydrological and geochemical characterization of the groundwater in the Hula Valley, Israel. M.Sc. Thesis, Hebrew University of Jerusalem.

Eshleman, K.N., Pollard, J.S., Kuebler O'Brien, A., 1993. Determination of contributing areas for saturation overland flow from chemical hydrograph separations. *Water Resources Research*, 29: 3577-3587.

Etcheverry, D., Perrochet, P., 2000. Direct simulation of groundwater transit-time distributions using the reservoir theory. *Hydrogeology Journal* 8: 200-208.

Evans, D.D., Nicholson, T.J. and Rasmussen, T.C., 2001. Flow and transport through unsaturated fractured rock. American Geophysical Union, Washington, 196p.

EXACT, 1998. Executive Action Team. Multilateral Working Group on Water Resources. United States, Geological Survey; Jordan, Ministry of Water and Irrigation; Palestinian Water Authority, Nablus and Israeli Hydrological Service, Jerusalem. *Overview of Middle East water resources : water resources of Palestinian, Jordanian, and Israeli interest*. Washington, DC, USA, US Geological Survey. <http://exact-me.org/overview/index.htm>

Falkenmark, M., Lundqvist, J., Widstrand, C., 1989. Macro-scale water scarcity requires micro-scale approaches. Aspects of vulnerability in semi-arid development. *Natural Resources Forum* 13(4):258-67.

FAO, 2005. http://www.fao.org/ag/agl/aglw/aquastat/water_res/index.stm. AQUASTAT database.

Fontes, J.-C., 1992. Chemical and isotopical constraints on ^{14}C dating of groundwater. In: Taylor, R.E., Long, A., Kra, R.S. (Eds.), *Radiocarbon after four decades*, Springer, Berlin – New York, pp. 243-261.

Fontes, J.-C., Garnier, J.M., 1979. Determination of the initial ^{14}C -activity of the total dissolved carbon: a review of the existing methods and a new approach. *Water Resources Research* 15: 399-413.

Fraas, O., 1877. *Juraschichten am Hermon*. N. Jb. Miner. etc., Stuttgart, Germany, pp.17-30.

Fritz, P., Cherrry, J.A., Weyer, K.U., Sklash, M.G., 1976. Storm runoff analyses using environmental isotopes and major ions, in interpretation of environmental isotope and hydrochemical data in groundwater hydrology. International Atomic Energy Agency, Vienna. pp. 111-131.

Ganor, E., Mamane, Y., 1982. Transport of Saharan dust across the eastern Mediterranean. *Atmospheric Environment* 16: 581-587.

Garfunkel, Z., Zak, I., Freund, R., 1981. Active faulting in the Dead Sea Rift. *Tectonophysics* 80: 1-26.

Gasparini, A., Custudio, E., Fontes, J.C., Jimenez, J., Nunez, J.A., 1990. Exemple d'étude géochimique et isotopique de circulations aquifères en terrain volcanique sous climat semi-aride (Amurga, Gran Canaria, Iles Canaries). *Journal of Hydrology* 114: 61-91.

Gat, J. and Gonfianti, R. (Eds.), 1981. *Stable Isotope Hydrology: Deuterium and Oxygen-18 in the Water Cycle*. IAEA Technical Report Series No. 210, Vienna, 337p.

Gat, J.R., 1971. Comments on the stable isotope method in regional groundwater investigations. *Water Resources Research* 7: 980-993.

Gat, J.R., Dansgaard, W., 1972. Stable isotope survey of the fresh water occurrences in Israel and the northern Jordan Rift valley. *Journal of Hydrology* 16: 177-212.

Gat, J.R., Tzur, Y., 1967. Modification of the isotopic composition of rain water by processes which occur before groundwater recharge. In: *Proceedings of a symposium on isotope hydrology, nos 49-60*. International Atomic Energy Agency, Vienna, 740 pp.

Gat, J.R., 1980. The isotopes of hydrogen and oxygen in precipitation. In *Handbook of Environmental Isotope Geochemistry*, Fritz P, Fontes JC (eds). Elsevier: New York; 21-47.

Genereux, D. P., 1998. Quantifying uncertainty in tracer-based hydrograph separations. *Water Resources Research* 34: 914-918.

Genereux, D.P., Hooper, R.P., 1998. Oxygen and Hydrogen Isotopes in Rainfall-Runoff Studies. In: Kendall, C., McDonnell, J.J. (Eds.) *Isotope Tracers in Catchment Hydrology*, Elsevier, pp. 319-343.

Germann, P.F., 1986. Rapid drainage response to precipitation. *Journal of Hydrological Processes*, 1, 3-13.

Gerson, R., 1974. Karst processes of the eastern Upper Galilee, northern Israel. *Journal of Hydrology* 21: 131-152.

Geyer, S., 1994. Isotopengeochemische Untersuchungen an Fraktionen von gelöstem organischen Kohlenstoff (DOC) zur Bestimmung der Herkunft und Evolution des

DOC im Hinblick auf die Datierung von Grundwässern. GSF-Bericht, Institut für Hydrologie, 4/94, Neuherberg, Germany, 184 pp.

Geyh, M.A., 2000. An overview of ^{14}C analysis in the study of groundwater. *Radiocarbon* 42(1): 1-180.

Gilad, D., 1988a. Hydrogeology of the Naftali Moutain springs. Israeli Hydrological Service Report (in Hebrew).

Gilad, D., 1988b. Mt. Hermon, the major water source of Israel, In: Klein, M., ed. *Ofakim Be-Geographia*. University of Haifa, pp. 39-50. (in Hebrew).

Gilad, D., Bonne, J., 1990. Snowmelt of Mt. Hermon and its contribution to the sources of the Jordan River. *Journal of Hydrology* 114: 1-15.

Gilad, D., Schwartz, S., 1978. Hydrogeology of the Jordan sources aquifers. Israeli Hydrological Service Report Hydro/5/78, 58pp. (in Hebrew).

Gillham, R.W., 1984. The effect of the capillary fringe on water-table response. *Journal of Hydrology* 67: 307-324.

Gleick, P.H., 1996. Basic water requirements for human activities: Meeting basic needs. *Water International* 21: 83-92.

Goldberg, M., 1969. The Jurassic of Majdal Shams area, Mt. Hermon. Israeli Geological Society. Proceedings of the Annual Meeting., p.25 (Abstract).

Goldberg, M., Hirsch, F., Mimran, Y., 1981. The Jurassic sequence of Mount Hermon. Israeli Geological Society, Proceedings of the Annual Meeting, (Abstract).

Goldreich, Y., Mozes, H., D., 2004. Radar analysis of cloud systems and their rainfall yield in Israel. *Israel Journal of Earth Sciences* 53: 63-76.

Gomez, F., Meghraoui, M., Darkal, A.N., Hijazi, F., Mouty, M., Suleiman, Y., Sbeinati, R., Darawcheh, R., Al-Ghazzi, R., Barazangi, M., 2003. Holocene faulting and earthquake recurrence along the Serghaya branch of the Dead Sea fault system in Syria and Lebanon – erratum. *Geophysical Journal International* 155: 749-750.

Goode, D.J., 1996. Direct simulation of groundwater age. *Water Resources Research* 32(2): 289-296.

Guentner, A., Bronstert, A., 2004. Representation of landscape variability and lateral redistribution processes for large-scale hydrological modelling in semi-arid areas. *Journal of Hydrology* 297: 136-161.

Gunn, J., Bottrell, S.H., Lowe, D.J., Worthington, S.R.H., 2006. Deep groundwater flow and geochemical processes in limestone aquifers: evidence from thermal waters in Derbyshire, England, UK. *Hydrogeology Journal* 14(6): 868-881.

Gur, D., Bar-Matthews, M., Sass, E., 2003. Hydrochemistry of the main Jordan River sources: Dan, Banias, and Kezinim springs, north Hula Valley, Israel. *Israel Journal of Earth Sciences* 52: 155-178.

Gvirtzman, H., 2002. Israel Water Resources, Chapters in Hydrology and Environmental Sciences, Yad Ben-Zvi Press, Jerusalem, 301 p (in Hebrew).

Haines, T.S., Lloyd, J.W., 1985. Controls on silica in groundwater environments in the United Kingdom. *Journal of Hydrology* 81: 277-295.

Haitjema, H.M., 1995. Analytic Element Modeling of Groundwater Flow. Academic Press: San Diego; 393 pp.

Hall, F.R., 1968. Base-flow recessions – A review. *Water Resources Research* 4: 973-983.

Hallberg, G.R., Hoyer, B.E., Bettis, E.A., Libra, R.D., 1983. Hydrogeology, water quality, and land management in the Big Spring basin, Clayton County, Iowa, Iowa Geological Survey Open File Report 83-3, Iowa Geological Survey, Iowa City, Iowa.

Hangen, E., Lindenlaub, M., Leibundgut, C., vWilpert, K., 2001. Investigating mechanisms of stormflow generation by natural tracers and hydrometric data: a small catchment study in the Black Forest, Germany. *Hydrological Processes* 15: 183-199.

Harris, W.W., 1978. War and Settlement Change: The Golan Heights and the Jordan Rift, 1967-77. *Transactions of the Institute of British Geographers, New Series*, Vol. 3, No. 3, Settlement and Conflict in the Mediterranean World (1978), pp. 309-330.

Hashmonay, R., Cohen, A., Dayan, U., 1991. Lidar observation of the atmospheric boundary layer in Jerusalem. *Journal of Applied Meteorology* 30: 1228-1236.

Heathcote, J.A., Lloyd, J.W., 1986. Factors affecting the isotopic composition of daily rainfall at Driby, Lincolnshire. *Journal of Climatology* 6(1): 97-106.

Heilig, A., Steenhuis, T.S., Walter, M.T., Herbert, S.J., 2003. Funneled flow mechanisms in layered soil: field investigations. *Journal of Hydrology* 279: 210-223.

Heimann, A., 1990. The development of the Dead Sea Rift and its margins in Northern Israel during the Pliocene and the Pleistocene. Ph.D. thesis, Hebrew University Jerusalem and GSI Rep.28/90, 76 pp. (in Hebrew, English abstract).

Heimann, A., Sass, E., 1989. Travertines in the northern Hula Valley. *Sedimentology* 36: 95-108.

Hendershot, W.H., Savoie, S. and Courchesne, F., 1992. Simulation of streamwater chemistry. *Journal of Hydrology* 136(1/4): 237-252.

Hendrickx, J.M.H., Flury, M., 2001. Uniform and preferential flow, mechanisms in the vadose zone, *Conceptual Models of Flow and Transport in the Fractured Vadose Zone*, National Research Council, National Academy Press, Washington, DC, pp. 149–187.

Hendrickx, J., Walker, G., 1997. Recharge from precipitation. In: Simmers, I. (ed), *Recharge of phreatic aquifers in (semi-)arid areas*. AA Balkema, Rotterdam, pp 19–98.

Herut, B., Starinsky, A., Katz, A., Rosenfeld, D., 2000. Relationship between the acidity and chemical composition of rainwater and climatological conditions along a transition zone between large deserts and Mediterranean climate, Israel. *Atmospheric Environment* 34: 1281-1292.

Hewlett, J.D., Hibbert, A.R., 1961. Increases in water yield after several types of forest cutting. *Int. Assoc. Sci. Hydrol. Bull.* 6: 5-17.

Hewlett, J.D. and Hibbert, A.R., 1967. Factors affecting the response of small watersheds to precipitation in humid areas. In: Sopper, W. E., Lull, H. W. (Eds), *Forest Hydrology*, Pergamon Press, New York, pp. 275-290.

Hewlett, J.D., 1982. *Principles of forest hydrology*. University of Georgia Press, Athens, 183 pp.

Hillel, D., Gardner, W.R. Transient infiltration into crust-topped profiles. *Soil Science* 199(2): 69-76.

Hinton, M.J., Schiff, S.L., English, M.C., 1994. Examining the contributions of glacial till water to storm runoff using two- and three-component hydrograph separations. *Water Resources Research* 30: 983-993.

Hirsch, F., 1996. Geology of the southeastern slopes of Mount Hermon. *Geological Survey of Israel Current Research* 10: 22-27.

Hoeg, S., Uhlenbrook, S. and Leibundgut, Ch., 2000. Hydrograph separation in a mountainous catchment – combining hydrochemical and isotopic tracers. *Hydrological Processes* 14: 1199-1216.

Hoelting, B., Coldewey, W.G., 2005. *Hydrogeologie: Einführung in die Allgemeine und Angewandte Hydrogeologie*. 6th Edition, Elsevier GmbH, München.

Hooper, R.P., 2001. Applying the scientific method to small catchment studies: a review of the Panola Mountain experience. *Hydrological Processes* 15: 2039-2050.

Hooper, R.P., Christoffersen, N., Peters, N.E., 1990. Modelling stream water chemistry as a mixture of soil water end-members – An application to the Panola Mountain catchment, Georgia, USA. *Journal of Hydrology* 116: 321-343.

Hooper, R.P., Shoemaker, C.A., 1986. A comparison of chemical and isotopic hydrograph separation. *Water Resources Research* 22: 1444-1454.

Hornberger, G.M., Bencala, K.E., McKnight, D.M., 1994. Hydrological controls on dissolved organic carbon during snowmelt in the Snake River near Montezuma, Colorado. *Biogeochemistry* 25: 147-165.

Horowitz, A., 1979. *The Quaternary of Israel*. Academic Press, New York.

Horowitz, A., 1973. Development of the Hula basin, Israel. *Israeli Journal of Earth Sciences* 22: 107.

Horton, R.E., 1933. The role of infiltration in the hydrologic cycle. *Transactions of the American Geophysical Union* 14: 446-460.

Houghton, J.T., Ding, Y., Griggs, D.J., Noguer, M., van der Linden, P.J., Dai, X., Maskell, K., Johnson, C.A. (eds.), 2001. *Climate Change 2001: The Scientific Basis. Contribution of Working Group I to the Third Assessment Report of the Intergovernmental Panel on Climate Change*. Cambridge University Press, Cambridge, United Kingdom and New York, NY, USA, 881pp.

HSI, 2002. Hydrological Yearbook of Israel 1999. Ministry of National Infrastructures. Water Commission. Hydrological Service. Jerusalem.

Huth, A.K., Leydecker, A., Sickman, J.O., Bales, R.C., 2004. A two-component hydrograph separation for three high-elevation catchments in the Sierra Nevada, California. *Hydrological Processes* 18: 1721-1733.

Hyer, K.E., Hornberger, G.M., Herman, J.S., 2001. Processes controlling the episodic streamwater transport of atrazine and other agrichemicals in an agricultural watershed. *Journal of Hydrology* 254: 47-66.

Inamdar, S.P., Christopher, S.F., Mitchell, M.J., 2004. Export mechanisms for dissolved organic carbon and nitrate during summer storm events in a glaciated forested catchment in New York, USA. *Hydrological Processes* 18: 2651-2661.

Ingerson, I., Pearson, F.J., 1964. Estimation of age and rate of motion of groundwater by the ^{14}C -method. In: *Recent Researches in the Fields of Hydrosphere, Atmosphere and Nuclear Geochemistry*, Mazuren, Tokio, pp. 263-283.

Ingraham, N.L., Taylor, B.E., 1989. The effect of snowmelt on the hydrogen isotope ratios of creek discharge in Surprise Valley, California. *Journal of Hydrology* 106: 233-244.

Institute of Hydrology, 1980. Low flow studies. Research Report 1, Wallingford, U.K.

Jarvie, H.P., Juergens, M.D., Williams, R.J., Neal, C., Davies, J.J.L., Barrett, C., White, J., 2005. Role of river bed sediments as sources and sinks of phosphorus across two major eutrophic UK river basins: the Hampshire Avon and Herefordshire Wye. *Journal of Hydrology* 304(1/4).

Joerin, C., Beven, K.J., Iorgulescu, I., Musy, A., 2002. Uncertainty in hydrograph separations based on geochemical mixing models. *Journal of Hydrology* 255: 90-106.

Johnson, S.L., 2004. Factors influencing stream temperatures in small streams: substrate effects and a shading experiment. *Canadian Journal of Fisheries and Aquatic Sciences* 61(6): 913-923.

Jones, J.A.A., 1987. The effects of soil piping on contributing areas and erosion patterns. *Earth Surface Processes and Landforms* 12: 229-248.

Kafri, U., Lang, B., 1979. Gas shows in the lignite project exploration boreholes, Hula Basin, Geological Survey of Israel Report No. 1/79 (in Hebrew).

Kafri, U., Lang, B., Halicz, L., Yoffe, O., 2002. Geochemical characterization and pollution phenomena of aquifer waters in northern Israel. *Environmental Geology* 42: 370-386.

Kafri, U., Lang, B., 1987. New data on the Late Quaternary fill of the Hula Basin. *Israel Journal of Earth Sciences* 36: 73-81.

Kalin, R.M., 1999. Radiocarbon dating of groundwater systems. Environmental tracers in subsurface hydrology. In: P.G. Cook and A.L. Herczeg (ed.) *Environmental Tracers in Subsurface Hydrology*. Kluwer, Boston, pp. 111-144.

Kattan, Z., 1997a. Chemical and environmental isotope study of precipitation in Syria. *Journal of Arid Environments* 35: 601-615.

Kattan, Z., 1997b. Environmental isotope study of the major karst springs in Damascus limestone aquifer systems: case of the Figeh and Barada springs. *Journal of Hydrology* 193: 161-182.

Kattan, Z., 2001. Use of hydrochemistry and environmental isotopes for evaluation of groundwater in the Paleogene limestone aquifer of the Ras Al-Ain area (Syrian Jezireh). *Environmental Geology* 41: 128-144.

Kattan, Z., 2002. Effects of sulphate reduction and geogenic CO₂ incorporation on the determination of ¹⁴C groundwater ages – a case study of the Paleogene groundwater system in north-eastern Syria. *Hydrogeology Journal* 10(4): 495-508.

Kendall, C., McDonnell, J.J. 1998. Isotope tracers in catchment hydrology. Elsevier, New York, 839 pp.

Kendall, C., McDonnell, J.J., Gu, W., 2001. A look inside "black box" hydrograph separation models: a study at the Hydrohill catchment. *Hydrological Processes* 15: 1877-1902.

Kendall, K.A., Shanley, J.B., McDonnell, J.J., 1999. A hydrometric and geochemical approach to test the transmissivity feedback hypothesis during snowmelt. *Journal of Hydrology* 219: 188-205.

Kennedy, V.C., 1971. Silica variations in stream water with time and discharge. In: Hem, J. D. (Ed.). Nonequilibrium systems in natural water chemistry. Advances in Chemistry Series American Chemical Society, Washington, DC, pp. 106-130.

Kennedy, V.C., Kendall, C., Zellweger, G.W., Wyerman, T.A., Avanzino, R.J., 1986. Determination of the components of stormflow using water chemistry and environmental isotopes, Mattole River basin, California. *Journal of Hydrology* 84: 107-140.

Kennedy, V.C., Zellweger, G.W., Avanzino, R.J., 1979. Variation of rain chemistry during storms at two sites in Northern California. *Water Resources Research* 15: 687.

Kidron, Y., 1972. Central Golan Heights – Waset-Dalawe area, feasibility of the basaltic aquifers exploiting through wells. TAHAL report, Tel Aviv, 9 pp. (in Hebrew).

Kille, K. 1970. Das Verfahren MoMNQ, ein Beitrag zur Berechnung der mittleren jährlichen Grundwasserneubildung mit Hilfe der monatlichen Niedrigwasserabflüsse. – *Zeitschrift der deutschen geologischen Gesellschaft, Sonderheft Hydrogeologie und Hydrochemie*, Hannover, pp. 89-95.

Kinzelbach W., Aeschbach W., Alberich C., Goni I.B., Beyerle U., Brunner P., Chiang W.-H., Rueedi J., and Zoellmann K. (2002) A Survey of Methods for Groundwater Recharge in Arid and Semi-arid regions. Early Warning and Assessment Report Series, UNEP/DEWA/RS.02-2. United Nations Environment Programme, Nairobi, Kenya.

Kirchner, J.W., 2003. A double paradox in catchment hydrology and geochemistry. *Hydrological Processes* 17: 871-874.

Kirchner, J.W., Feng, X., Neal, C., 2000. Fractal stream chemistry and its implications for contaminant transport in catchments. *Nature* 403: 524-527.

Kirchner, J.W., Feng, X., Neal, C., 2001. Catchment-scale advection and dispersion as a mechanism for fractal scaling in stream tracer concentrations. *Journal of Hydrology* 254: 82-101.

Kobayashi, D. 1985. Separation of the snowmelt hydrograph by stream temperatures. *Journal of Hydrology* 76: 155-165.

Kobayashi, D., Ishii, Y., Kodama, Y., 1999. Stream temperature, specific conductance and runoff processes in mountain watersheds. *Hydrological Processes* 13(6): 865-876.

Kovacs, A., Perrochet, P., Kiraly, L., Jeannin, P.-Y., 2005. A quantitative method for the characterisation of karst aquifers based on spring hydrograph analysis. *Journal of Hydrology* 303: 152-164.

Kreft, A., Zuber, A., 1978. On the physical meaning of the dispersion equation and its solutions for different initial and boundary conditions. *Chemical Engineering Science* 33: 1471-1480.

Krichak, S.O., Alpert, P., 2005. Signatures of the NAO in the atmospheric circulation during wet winter months over the Mediterranean region. *Theoretical and Applied Climatology* 82(1-2): 27-39.

Krupa, S.V., 2002. Sampling and physico-chemical analysis of precipitation: a review. *Environmental Pollution* 120: 565-594.

Kubota, T., Tsuboyama, Y., 2003. Estimation of evaporation rate from the forest floor using oxygen-18 and deuterium composition of throughfall and stream water during a non-storm runoff period. *Journal of Forest Research* 9(1): 51-59.

Kung, K.-J. S., 1990. Preferential flow in a sandy vadose zone, 2, Mechanisms and implications, *Geoderma* 46: 59-71.

Kung, K.-J.S., 1993. Laboratory observation of the funnel flow mechanism and its influence on solute transport. *Journal of Environmental Quality* 22: 91-102.

Kutiel, H., Maher, P., Guika, S., 1996. Circulation indices over the Mediterranean and Europe and their relationship with rainfall conditions across the Mediterranean. *Theoretical and Applied Climatology* 54: 125-138.

Kutiel, H., 2000. Climatic uncertainty in the Mediterranean basin. In: *Natural Resources and Environment Studies*, Vol 1 (1) (In preparation)(in Hebrew).

Lacey, G.C., Grayson, R.B., 1998. Relating baseflow to catchment properties in south-eastern Australia. *Journal of Hydrology* 204: 231-250.

Ladouce, B., Probst, A., Viville, D., Idir, S., Baque, D., Loubet, M., Probst, J.-L. and Bariac, T., 2001. Hydrograph separation using isotopic, chemical and hydrological approaches (Strengbach catchment, France). *Journal of Hydrology* 242: 255-274.

Lakey, B.L. and Krothe, N.C., 1996. Stable isotopic variation of storm discharge from a Perennial Karst spring, Indiana. *Water Resources Research* 32: 721-731.

Lambs, L., 2000. Correlation of conductivity and stable isotope ^{18}O for the assessment of water origin in river system. *Chemical Geology* 164: 161-170.

Langmuir, D., 1997. *Aqueous Environmental Geochemistry*: Prentice Hall, New Jersey, 600 p.

Laudon, H. and Slaymaker, O., 1997. Hydrograph separation using stable isotopes, silica and electrical conductivity, an alpine example. *Journal of Hydrology* 201: 82-101.

Lavee, H., Imeson, A.C., Sarah, P., 1998. The impact of climate change on geomorphology and desertification along a Mediterranean arid transect. *Land Degradation and Development* 9: 407-422.

Lee, E. S. and Krothe, N.C., 2003. Delineating the karstic flow system in the upper Lost River drainage basin, south central Indiana: using sulphate and $\delta^{34}\text{S}$ - SO_4 as tracers. *Applied Geochemistry* 18(1): 145-153.

Lee, E.S., Krothe, N.C., 2001. A four-component mixing model for water in a karst terrain in south-central Indiana, USA. Using solute concentration and stable isotopes as tracers. *Chemical Geology* 179:129-143.

Leenheer, J.L., 1981. Comprehensive approach to preperative isolation and fractionation of dissolved organic carbon from natural waters and wastewaters. *Environmental Science and Technology* 15: 578-587.

Legates, D.R., Willmott, C.J., 1990. Mean seasonal and spatial variability in gauge-corrected, global precipitation. *International Journal of Climatology* 10(2): 111-127.

Leibundgut, C., 1984. Zur Erfassung hydrologischer Messwerte und deren Übertragung auf Einzugsgebiete verschiedener Dimensionen. *Geomethodica* 9: 141-170.

Leontiadis, I.L., Vergis, S., Christodoulou, T., 1996. Isotope hydrology study of areas in eastern Macedonia and Thrace, northern Greece. *Journal of Hydrology* 182: 1-17.

Lerner, D.N., 1990. Groundwater recharge in urban areas. *Atmosperic Environment* 24B: 29–33.

Lindenlaub, M. 1998. Abflusskomponenten und Herkunftsräume im Einzugsgebiet der Brugga (Runoff components and source areas in the Brugga basin) (in German). Ph.D.Thesis, Institute of Hydrology, University of Freiburg, Germany.

Linsley, R.K., Kohler, M.A. and Paulhus, J.I.H., 1982. *Hydrology for engineers*, 3rd ed., McGraw-Hill, New York, 508 pp.

Lischeid, G., Kolb, A., Alewell, C., 2002. Apparent translatory flow in groundwater recharge and runoff generation. *Journal of Hydrology* 265: 195-211.

Loye-Pilot, M.-D., Jusserand, C., 1990. Chemical and isotopic hydrograph separation for a mediterranean torrent flood. A critical view. *Revue des Sciences de l'Eau* 3(2): 211-231. (in French).

Luxmore, R.J., Jardine, P.M., Wilson, G.V., Jones, J.R., Zelazny, L.W., 1990. Physical and chemical controls of preferred path flow through a forested hillslope, *Geoderma* 46: 139–154.

MacLean, R., Oswood, M.W., Irons III, J.G., McDowell, W.H., 1999. The effect of permafrost on stream biogeochemistry: A case study of two streams in the Alaskan (U.S.A.) taiga. *Biogeochemistry* 47(3): 239-267.

MacLeod, D.A., 1980. The origin of the Red Mediterranean soils in Epirus, Greece. *Journal of Soil Science* 31: 126-136.

Maheras, P., Kuti, H., 1999. Spatial and temporal variations in the temperature regime in the Mediterranean and their relationship with circulation during the last century. *International Journal of Climatology* 19: 745-764.

Maheras, P., Kuti, H., 1999. Spatial and temporal variations in the temperature regime in the Mediterranean and their relationship with circulation during the last century. *International Journal of Climatology* 19: 745-764.

Maheras, P., Xoplaki, E., Kuti, H., 1999. Wet and dry monthly anomalies across the Mediterranean basin and their relationship with circulation, 1860-1990. *Theoretical and Applied Climatology* 64: 189-199.

Maloszewski, P., Harum, T., Benischke, R., 1992. Mathematical modelling of tracer experiments in the karst of Lurbach system. *Steirische Beiträge zur Hydrogeologie*, 43; 116-136.

Maloszewski, P., Rauert, W., Stichler, W., Herrmann, A., 1983. Application of flow models in an alpine catchment area using tritium and deuterium data. *Journal of Hydrology* 66: 319-330.

Maloszewski, P., Stichler, W., Zuber, A., Rank, D., 2002. Identifying the flow systems in a karstic-fissured-porous aquifer, the Schnealpe, Austria, by modelling of environmental ^{18}O and ^{3}H isotopes. *Journal of Hydrology* 256: 48-59.

Maloszewski, P., Zuber, A., 1982. Determining the turnover time of groundwater systems with the aid of environmental tracers: I. Models and their applicability. *Journal of Hydrology* 57: 207-231.

Maloszewski, P., Zuber, A., 1985. On the theory of tracer experiments in fissured rocks with a porous matrix. *Journal of Hydrology*, 79; 333-358.

Maloszewski, P., Zuber, A., 1991. Influence of matrix diffusion and exchange reactions on radiocarbon ages in fissured carbonate aquifers. *Water Resources Research* 27: 1937-1945.

Maloszewski, P., Zuber, A., 1996. Lumped parameter models for the interpretation of environmental tracer data. In: *Manual on mathematical models in isotope hydrogeology*. IAEA (International Atomic Energy Agency), Vienna, pp. 9-58.

Manga, M., Kirchner, J.W., 2004. Interpreting the temperature of water at cold springs and the importance of gravitational potential energy. *Water Resources Research* 40: W05110.

Marc, V., Didon-Lescot, J.-F., Michael, C., 2001. Investigation of the hydrological processes using chemical and isotopic tracers in a small Mediterranean forested catchment during autumn recharge. *Journal of Hydrology* 247(3): 215-229.

Markewitz, D., Davidson, E.A., Figueiredo, R.D.O., Victoria, R.L., Krusche, A.V., 2004. Control of cation concentrations in stream waters by surface soil processes in an Amazonian watershed. *Nature* 410: 802.

Marquinez, J., Lastra, J., Garcia, P., 2003. Estimation models for precipitation in mountainous regions: the use of GIS and multivariate analysis. *Journal of Hydrology* 270: 1-11.

Martin, J.B., Screatton, E.J., 2001. Exchange of matrix and conduit water with examples from the Floridan Aquifer. In: Kuniansky, E.L. (Ed), U.S. Geological Survey Karst Interest Group Proceedings, Water-Resources Investigations Report 01-4011.

Martinec, J., Siegenthaler, U., Oeschger, H., Tongiorgi, E., 1974. New insights into the runoff mechanism by environmental isotopes, Isotope Techniques in Groundwater Hydrology. In: Environmental isotopes as a hydrogeological tool in Nicaragua, IAEA, Proceedings of the Symposium on Isotope Techniques in Groundwater Hydrology, Vol. 1., Vienna 193 pp.

Massei, N., Wang, H.Q., Dupont, J.P., Rodet, J. and Laignel, B., 2003. Assessment of direct transfer and resuspension of particles during turbid floods at a karstic spring. *Journal of Hydrology* 275: 109-121.

Matthess, G. and Ubell, K., 1983. Allgemeine Hydrogeologie – Grundwasserhaushalt. Lehrbuch der Hydrogeologie, Verlag Gebrüder Borntraeger, Berlin/Stuttgart.

Mazor, E., 2004. Chemical and isotopic groundwater hydrology. Marcel Dekker New York, Basel.

McDonnell, J.J., 2003. Where does water go when it rains? Moving beyond the variable source area concept of rainfall-runoff response. *Hydrological Processes* 17: 1869-1875.

McDonnell, J.J., Bonell, M.K., Stewart, M.K., Pearce, A.J., 1990. Deuterium variations in storm rainfall: Implications for stream hydrograph separation. *Water Resources Research* 26: 455-458.

McDonnell, J.J., Stewart, M.K., Owens, I.F., 1991. Effect of catchment-scale subsurface mixing on stream isotopic response. *Water Resources Research* 27: 3065-3073.

McDowell, W.H., Wood, 1984. Podzolization: Soil Processes Control Dissolved Organic Carbon Concentrations in Stream Water. *Soil Science* 137(1): 23-32.

McGlynn, B.L., McDonnell, J.J., Shanley, J.B., Kendall, C., 1999. Riparian zone flowpath dynamics in a small headwater catchment. *Journal of Hydrology* 222: 75-92.

McGuire, K.J., DeWalle, D.R., Gburek, W.J., 2002. Evaluation of mean residence time in subsurface waters using oxygen-18 fluctuations during drought conditions in the mid-Appalachians. *Journal of Hydrology* 261: 132-149.

McNamara, J.P., Kane, D.L., Hinzman, L.D., 1997. Hydrograph separations in an Arctic watershed using mixing model and graphical techniques. *Water Resources Research*, 33: 1707-1719.

Medzini, A., Wolf, A., 2004. Towards a Middle East at peace: hidden issues in Arab-Israeli hydropolitics. *Water Resources Development* 20: 193-204.

Meinzer, O.E., 1923. Outline of ground-water hydrology, with definitions: U.S. Geological Survey Water-Supply Paper 494, 74pp.

Mero, F., Bonne, J., 1967. Springs, streams and wells survey in the Golan Heights. TAHAL Report No. 102872, Tel Aviv, 9 pp. (in Hebrew).

Mero, F., Kahanovitz, A., 1969. Hydrological evaluation of Berekhat Ram. TAHAL Report, Tel Aviv, 6 pp.

Merot, P., Durand, P., Morisson, C., 1995. Four-component hydrograph separation using isotopic and chemical determinations in an agricultural catchment in western France. *Physics and Chemistry of the Earth* 20: 415-425.

Meybeck, M., 1987. Global chemical weathering of surficial rocks estimated from river dissolved loads. *American Journal of Science* 287: 401–428.

Michelson, H., 1972. Hydrogeology of the southern Golan Heights. TAHAL Report HR/72/037, Tel Aviv, 89 pp. (in Hebrew).

Michelson, H., 1975. Geohydrology of the enclave and the southeastern flanks of Mount Hermon. TAHAL Report 01/75/05 (in Hebrew).

Michelson, H., 1979. The geology and paleogeography of the Golan Heights. Ph.D. thesis, Tel Aviv University, 163 pp. (in Hebrew, English abstract).

Michelson, H., 1996. Review on the Golan Heights water source. Mekorot report, unpublished (in Hebrew).

Michelson, H., Michaeli, A., 1971. Peham Springs exploitation possibilities by wells. TAHAL Report, Tel Aviv, pp. 25.

Molénat, J., Durand, P., Gascuel-Odoux, C., Davy, P. and Gruau, G., 2002. Mechanisms of nitrate transfer from soils to stream in an agricultural watershed of French Brittany. *Water Air Soil Pollution* 133: 161–183.

Mook, W.G., 1972. On the reconstruction of the initial ^{14}C content of groundwater from the chemical and isotopic composition. In: Proc 8th Int Conf on Radiocarbon Dating, vol 1, Royal Society of New Zealand, Wellington, pp 342–352.

Mook, W.G., 1976. The dissolution-exchange model for dating ground water with ^{14}C . In: Interpretation of Environmental Isotope and Hydrochemical Data in Ground-Water Hydrology. IAEA, Vienna: 213-225.

Mook, W.G., 1980. The dissolution-exchange model for dating of groundwater with ^{14}C . In: Fritz, P., Fontes, J.-C., *Handbook of Environmental Isotope Geochemistry*, Elsevier, Amsterdam, pp. 50-74.

Moore, T.R., Jackson, R.J., 1989. Dynamics of dissolved organic carbon in forested and disturbed catchments, Westlands, New Zealand II Larry River. *Water Resources Research* 25(6): 1331-1339.

Mor, D., 1986. The volcanism of the Golan Heights. Ph.D. thesis, Hebrew University Jerusalem, 159 pp., and GSI report, GSI/5/86. (in Hebrew, English abstract).

Mosley, M.P., 1982. Streamflow generation in a forested watershed, New Zealand, *Water Resources Research* 15: 795-806.

Moulton, K., Berner, R.A., 1998. Quantification of the effects of plants on weathering: studies in Iceland. *Geology* 26: 895-898.

Mouti, M., 2000. The Jurassic in Syria: an overview. Lithostratigraphic and biostratigraphic correlations with adjacent areas. In: Crasquin-Soleau, S., Barrier, E. (Eds.), *PeriTethys memoir 5: new data on Pery Tethyan sedimentary basins. Memoires de Museum National de Historie Naturé* 182: 159-168. Paris.

Mulholland, P.J., 1993. Hydrometric and stream chemistry evidence of three storm flowpaths in Walker Branch Watershed. *Journal of Hydrology* 151: 291-316.

Nakamura, R., 1971. Runoff analysis by electrical conductance of water. *Journal of Hydrology* 14: 197-212.

Naor, A., Cohen, S., 2003. Response of apple tree stem diameter, midday stem water potential and transpiration rate to a drying and recovery cycle. *Hortscience* 38(4):547-551.

Natermann, E., 1951. Die Linie des langfristigen Grundwassers (AuL) und die Trockenwetterabflusslinie (TWL). *Wasserwirtschaft* 41: Sonderheft: 12-14.

Nathan, R.J., McMahon, T.A., 1990. Evaluation of automated techniques for base flow and recession analysis. *Water Resources Research* 26: 1465-1473.

Nativ, R., Guenay, G., Hoetzl, H., Reichert, B., Solomon, D.K., Tezcan, L., 1999. Separation of groundwater-flow components in a karstified aquifer using environmental tracers. *Applied Geochemistry* 14: 1001-1014.

Nativ, R., Mazor, E., 1987. Rain events in an arid environment – their distribution and ionic and isotopic composition patterns: Makhtesh Ramon Basin. *Israel Journal of Hydrology* 89: 205-237.

Neal, C., Robson, A., Smith, C.J., 1990. Acid neutralization capacity variations for the Hafren forest stream, Mid-Wales: inferences for hydrological processes. *Journal of Hydrology*, 121, 85-101.

Neal, C., Robson, A.J., Neal, M., Reynolds, B., 2005. Dissolved organic carbon for upland acidic and acid sensitive catchments in mid-Wales. *Journal of Hydrology* 304: 203-220.

Neuman, S.P., Dasberg, S., 1977. Peat hydrology in the Hula Basin, Israel: II. Subsurface flow regime. *Journal of Hydrology* 32: 241-256.

Nicolau, J.M., Solé-Benet, A., Puigdefábregas, J., Gutiérrez, L., 1996. Effects of soil and vegetation on runoff along a catena in semi-arid Spain. *Geomorphology* 14: 297-309.

Nihlen, T., Olsson, S., 1995. Influence of eolian dust on soil formation in the Aegean area. *Zeitschrift für Geomorphologie* 39: 341-361.

Nissenbaum, A., 1978. Sulfur isotope distribution in sulfates from surface waters from the northern Jordan Valley, Israel. *Environmental Science and Technology* 12: 962-964.

Noetling, F., 1886. Entwurf einer Gliederung der Kreideformation in Syrien und Palästina. *Zeitschrift der deutschen geologischen Gesellschaft* 38: 824-875.

Obradovic, M.M., Sklash, M.G. 1986. An isotopic and geochemical study of snowmelt runoff in a small Artic watershed. *Hydrological Processes* 1: 15-30.

Ogunkoya, O.O., Jenkins, A., 1993. Analysis of storm hydrograph and flow pathways using a 3-component hydrograph separation model. *Journal of Hydrology* 142: 71-88.

Oki, D.S., Souza, W.R., Bolke, E.L., Bauer, G.R., 1998. Numerical analysis of the hydrogeologic controls in a layered coastal aquifer system, Oahu, Hawaii, USA. *Hydrogeology Journal* 6(2): 243-263.

Oxtobee, J.P.A., Novakowski, K., 2002. A field investigation of groundwater/surface water interaction in a fractured bedrock environment. *Journal of Hydrology* 269: 169-193.

Pangburn, T., Albert, M.R., Hardy, J.P., McGilvary, W.R., and Shanley, J.B., 1992. Characterization of hillslope thermal and hydrologic processes at the Sleepers River Research Watershed. 49th Eastern Snow Conference, 161-167.

Parkhurst, D.L., Appelo, C.A.J., 1999. User's guide to PHREEQC (Version 2)—A computer program for speciation, batch-reaction, one-dimensional transport, and inverse geochemical calculations: U.S. Geological Survey Water-Resources Investigations Report 99-4259, 310 p.

Patrick, E., 2002. Researching crusting soils: themes, trends, recent developments and implications for managing soil and water resources in dry areas. *Progress in Physical Geography* 26(3): 442-461.

Payne, B.R., Yurtsever, Y., 1974. Environmental isotopes as a hydrogeological tool in Nicaragua, IAEA, Proceedings of the Symposium on Isotope Techniques in Groundwater Hydrology, Vol. 1., Vienna 193 pp.

Pe'er, G., Safriel, U.N., 2000.. Climate change: Israel national report under the United Nations Framework Convention on Climate Change: Impact, vulnerability and adaptation. <http://www.bgu.ac.il/BIDR/rio/Global91-editedfinal.html>

Pearce, A.J., Stewart, M.K., Sklash, M.G., 1986. Storm runoff generation in humid headwater catchments. 1. Where does the water com from? *Water Resources Research* 22: 1263-1272.

Pearson, F.J. Jr., 1992. Effects of parameter uncertainty in modelling 14C. In: Taylor R. E., Long A. & Kra R. S., eds.: *Radiocarbon After Four Decades. An Interdisciplinary Perspective*. Springer-Verlag, New York: 262–275.

Perrin, J., Jeannin, P.-Y., Zwahlen, F., 2003. Epikarst storage in a karst aquifer: conceptual model based on isotopic data, Milandre test site, Switzerland. *Journal of Hydrology* 279: 106-124.

Peters, N.E., Ratcliffe, E.B., 1998. Tracing hydrologic pathways using chloride at the Panola Mountain Research Watershed, Georgia, USA. *Water, Air & Soil Pollution* 105(1-2): 263-275.

Pettyjohn, W.A., Henning, R., 1979. Preliminary estimate of groundwater recharge rates, related streamflow and water quality in Ohio: Ohio State University Water Resources Center Completion Report Number 552, 323 p.: cited in: Sloto, R. A. and Crouse, M.Y. 1996.

Pfaff, T., 1987. Grundwasserumsatzräume im Karst der Südlichen Frankenalb. GSF-Bericht 3/87 (in German).

Picard, L., 1965. The geological evolution of the Quaternary in the central-northern Jordan Graben, Israel. The Geological Society of America Special Paper 84: 337-366.

Picard, L., Soyer, R., 1927. Sur la présence du Jurassique, du Crétacé inférieur et moyen sur le versant ouest de l'Anti-Liban. C. R. Acad. Sci. 185: 656-658.

Pichon, A., Travi, Y., Vincent, M., 1996. Chemical and isotopic variations in throughfall in a mediterranean context. Geophysical Research Letters 32(5): 531-534.

Pilgrim, D.H., Huff, D.D. and Steele, T.D., 1979. Use of specific conductance and contact time relations for separating flow components in storm runoff. Water Resources Research 15: 329-339.

Pinder, G.F., Jones, J.F. 1969. Determination of the groundwater component of peak discharge from the chemistry of total runoff. Water Resources Research 5: 438-445.

Plummer, L.N., Prestemon, E.C., Parkhurst, D.L., 1991. An interactive code (NETPATH) for modeling net geochemical reactions along a flow path. U.S. Geological Survey, Water Resources Investigations Report 91-4078.

Poage, M.A., Chamberlain, C.P., 2001. Empirical relationships between elevation and the stable isotope composition of precipitation and surface waters: considerations for studies of paleoelevation change. American Journal of Science 301: 1-15.

Price, C., Stone, L., Huppert, A., Rajagopalan, B., Alpert, P., 1998. A possible link between El Nino and precipitation in Israel. Geophysical Research Letters 25: 3963-3966.

Prizgonov, V., Nitashov, V., Steriocovitch, P.V., 1988. Determination of recharge zone of Damascus Basin by the use of oxygen-18 in groundwater. Edition Nawca, Moscow, USSR Academy of Science (In Russian).

Puddefabregas, J., Del Barrio, G., Boer, M.M., Gutierrez, L., Sole, A., 1998. Differential responses of hillslope and channel elements to rainfall events in a semi-arid area. Geomorphology 23: 337-351.

Ragan, R.M., 1968. An experimental investigation of partial area contributions. In: hydrological aspects of the utilization of water, reports and discussions, Proceedings of the IAHS Assembly at Bern, IAHS Publ. 76: 241-251.

Ribolzi, O., Andrieux, P., Valles, V., Bouzigues, R., Bariac, T. and Voltz, M., 2000. Contribution of groundwater and overland flows to storm flow generation in a cultivated Mediterranean catchment. Quantification by natural chemical tracing. Journal of Hydrology 233: 241-257.

Ribolzi, O., Valles, V., Barbiero, L., 1993. Controle geochimique des eaux par la formation de calcite en milieu mediterraneen et en milieu tropical. Arguments d'équilibre et argument de bilan. *Science Sol* 31: 77-95.

Ribolzi, O., Valles, V., Bariac, T., 1996. Comparison of hydrograph deconvolutions using residual alkalinity, chloride, and oxygen-18 as hydrochemical tracers. *Water Resources Research* 32(4): 1051-1060.

Rice, K.C., Hornberger, G.M., 1998. Comparison of hydrochemical tracers to estimate source contributions to peak flow in a small, forested headwater catchment. *Water Resources Research* 34: 1755-1766.

Rimmer, A., Salingar, Y., 2006. Modelling precipitation-streamflow processes in karst basin: the case of the Jordan River sources, Israel. *Journal of Hydrology* 331: 524-542.

Rindsberger, M., Jaffe, S., Rahamim, S., Gat, J.R., 1990. Patterns of the isotopic composition of precipitation in time and space: data from the Israeli storm water collection program. *Tellus* 42B: 263-271.

Rodgers, P., Soulsby, C., Waldron, S., Tetzlaff, D., 2005. Using stable isotope tracers to assess hydrological flow paths, residence times and landscape influences in a nested mesoscale catchment. *Hydrology and Earth System Sciences* 9: 139-155.

Rodhe, A., 1981. Spring flood meltwater or groundwater? *Nordic Hydrology* 12: 21-30.

Rybakov, M., Fleischer, L., ten Brink, U., 2003. The Hula Valley subsurface structure inferred from gravity data. *Israel Journal of Earth Sciences* 52: 113-122.

Sachse, A., Henrion, R., Gelbrecht, J., Steinberg, C.E.W., 2005. Classification of dissolved organic carbon (DOC) in river-systems: influence of catchment and internal processes. *Organic Geochemistry* 36: 923-935.

Salzman, U., 1968. The geology of the southeastern Hermon slopes. TAHAL Report, 46pp. (in Hebrew).

Sandstrom, K., 1996. Hydrochemical deciphering of streamflow generation in semi-arid East Africa. *Hydrological Processes* 10(5): 703-720.

Sanford, W., 2002. Recharge and groundwater models: an overview. *Hydrogeology Journal* 10: 110-120.

Scanlon, B.R., Healy, R.W., Cook, P.G., 2002. Choosing appropriate techniques for quantifying groundwater recharge. *Hydrogeology Journal* 10: 18-39.

Scanlon, B.R., Keese, K.E., Flint, A.L., Flint, L.E., Gaye, C.B., Edmunds, W.M., Simmers, I., 2006. Global synthesis of groundwater recharge in semiarid and arid regions. *Hydrological Processes* 20: 3335-3370.

Scanlon, B.R., Mace, R.E., Barrett, M.E., Smith, B., 2003. Can we simulate regional groundwater flow in a karst system using equivalent porous media models? Case study, Barton Springs Edwards aquifer, USA. *Journal of Hydrology* 276: 137-158.

Seibert, J., McDonnell, J.J., 2002. On the dialog between experimentalist and modeler in catchment hydrology: Use of soft data for multicriteria model calibration. *Water Resources Research* 38: 23-1 – 23-14.

Seiler, K.-P., 1977. Hydrogeologie glazial übertiefter Täler der Bayrischen Alpen zwischen Lech und Woesner Tal. *Steirische Beiträge zur Hydrogeologie* 29: 5-118.

Seiler, K.-P., Baker, D., 1985. Der Einfluss der Schichtung auf die Sickerwasserbewegung bei punkt- bzw. linienförmiger Infiltration. *Zeitschrift der deutschen geologischen Gesellschaft* 136: 659-672.

Seiler, K.-P., Gat, J.R., 2007. Groundwater recharge from run-off and infiltration. – 241pp., Springer Verlag, Dordrecht.

Seiler, K.-P., Maloszewski, P., Behrens, H., 1989. Hydrodynamic dispersion in karstified limestone and dolomites in Upper Jura of Franconian Alb, FRG. *Journal of Hydrology*, 108; 235-247.

Seiler, K.-P., von Loewenstein, S., Schneider, S., 2002. Matrix and bypass-flow in quaternary and tertiary sediments of agricultural areas in south Germany. *Geoderma* 105: 299-306.

Sendler, A., 1981. Geochemistry of groundwater from basaltic aquifers at the Lower Galilee and the Golan. M.Sc. diss., The Hebrew University of Jerusalem, GSI Report 81/2, pp. 91 (in Hebrew, English Abstract).

Shanley, J.B., Kendall, C., Smith, T.E., Wolock, D.M., McDonnell, J.J., 2002. Controls on old and new water contributions to stream flow at some nested catchments in Vermont, USA. *Hydrological Processes* 16: 598-609.

Shanley, J.B., Peters, N.E., 1988. Preliminary observations of streamflow generation during storms in a forested Piedmont watershed using temperature as a tracer. *Journal of Contaminant Hydrology* 6(3): 349-365.

Sharon, D., Kutiel, H., 1986. The distribution of rainfall intensity in Israel, its regional and seasonal variations and its climatological evaluation. *International Journal of Climatology* 6: 277-291.

Shimron, A.E., 1989. Geochemical exploration and new geological data along the SE flanks of the Hermon range. *Geological Survey of Israel, Jerusalem, Report GSI/32/89*.

Shuster, E.T., White, W.B., 1971. Seasonal fluctuations in the chemistry of limestone springs: a possible means for characterizing carbonate aquifers. *Journal of Hydrology* 14(2): 93-128.

Siegenthaler, U., Oeschger, H., 1980. Correlation of ^{18}O in precipitation with temperature and altitude. *Nature* 285: 314-317.

Simic, E., Destouni, G., 1999. Water and solute residence times in a catchment: Stochastic-mechanistic model interpretation of ^{18}O transport. *Water Resources Research* 35: 2109-2119.

Simonson, R.W., 1995. Airborne dust and its significance to soils. *Geoderma* 65: 1-43.

Simpson, B., Carmi, I., 1983. The hydrology of the Jordan River tributaries (Israel): Hydrographic and isotopic investigation. *Journal of Hydrology* 62: 225-242.

Simunek, J., Jarvis, N.J., van Genuchten, M.Th., Gärdenäs, A., 2003. Review and comparison of models for describing non-equilibrium and preferential flow and transport in the vadose zone. *Journal of Hydrology* 272: 14-35.

Singer, A., 1971. Clay minerals in the soils of the southern Golan Heights. *Israel Journal of Earth Sciences* 20: 105-112.

Singer, A., Schwertmann, U., Friedl, J., 1998. Iron oxide mineralogy of Terre Rosse and Rendzinas in relation to their moisture and temperature regimes. *European Journal of Soil Science* 49: 385-395.

Singh, P., Spitzbart, G., Hübl, H., Weinmeister, H.W., 1997. Hydrological response of snowpack under rain-on-snow events: a field study. *Journal of Hydrology* 202: 1-20.

Sklash, M.G. and Farvolden, R.N., 1979. The role of groundwater in storm runoff. *Journal of Hydrology* 43: 45-65.

Sklash, M.G., Stewart, M.K., Pearce, A.J., 1986. Storm runoff generation in humid headwater catchments 2. A case study of hillslope and low-order stream response. *Water Resources Research* 22: 1273-1282.

Sloto, R.A., Crouse, M.Y., 1996. HYSEP – A computer program for streamflow hydrograph separation and analysis. U.S. Geological Survey. Water Resources Investigation Report 96-4040.

Smakhtin, V.U., 2001a. Low flow hydrology: a review. *Journal of Hydrology* 240: 147-186.

Smakhtin, V.U., 2001b. Estimating continuous monthly baseflow time series and their possible applications in the context of the ecological reserve. *Water SA* 27: 213.

Smakhtin, V.U., 2002. Some early Russian studies of subsurface storm-flow processes. *Hydrological Processes* 16: 2613-2620.

Smith, R.B., 2003. A linear upslope-time-delay model for orographic precipitation. *Journal of Hydrology* 282: 2-9.

Smith, R.B., Jiang, Q.F., Fearon, M.G., Tabary, P., Dorninger, M., Doyle, J.D., Benoit, R., 2003. Orographic precipitation and air mass transformation: An Alpine example. *Quarterly Journal of the Royal Meteorological Society* 129: 433-454.

Sneh, A., 1996. The Dead Sea Rift: lateral displacement and downfaulting phases. *Tectonophysics* 263: 277-292.

Sneh, A., Bartov, Y., Weissbrod, T. and Rosensaft, M., 1998. Geological Map of Israel, 1:200,000. Isr. Geol. Surv. (4 sheets).

Soulsby, C., Malcolm, R., Ferrier, R.C., Helliwell, R.C., Jenkins, A., 2000. Isotope hydrology of the Allt a'Mharcaidh catchment, Cairngorms, Scotland: implications for hydrological pathways and residence times. *Hydrological Processes* 14: 747-762.

Soulsby, C., Petry, J., Brewer, M.J., Dunn, S.M, Ott, B., Malcolm, I.A., 2003. Identifying and assessing uncertainty in hydrological pathways: a novel approach to end-member mixing in a Scottish agricultural catchment. *Journal of Hydrology* 274: 109-128.

Soulsby, C., Turnbull, D., Langan, S.J., Owen, R., Hirst, D., 1995. Long-term trends in stream chemistry and biology in North-East Scotland: Evidence for recovery. *Water, Air & Soil Pollution* 85(2): 689-694.

Stewart, M.K., 1975. Stable isotope fractionation due to evaporation and isotope exchange of falling water drops: application to atmospheric processes and evaporation of lakes. *Journal of Geophysical Research* 80: 1133-1146.

Stichler, W., 1981. Identifizierung von Grundwässern anhand ihres Gehaltes an stabilen Isotopen. Sonderdruck aus *Festschrift G. Zöttl.*, pp.147-157, Graz, Austria.

Stichler, W., 1987. Snowcover and snowmelt processes studied by means of environmental isotopes. In: Jones, H.G., Orville Thomas, W. J. (Eds.), *Biogeochemistry of seasonally snow-covered catchments. Proceedings of a Boulder Symposium, July 1-14. IAHS Publication No. 228*, Boulder, Colorado, pp. 141-155.

Stichler, W., Hermann, A., 1982. Surface and subsurface runoff modelling using environmental isotopes. *Proceedings of the International Symposium on Rainfall-Runoff Relationships*, pp. 245-260; Mississippi, USA.

Stichler, W., Maloszewski, P., Moser, H., 1986. Modelling of river water infiltration using oxygen-18 data. *Journal of Hydrology* 83 (3/4): 355-365.

Stichler, W., Rauert, W., Martinec, J., 1981. Environmental isotope studies of an alpine snowpack. *Nordic Hydrology* 12: 297-308.

Stottlemeyer, R., 2001. Processes regulating watershed chemical export during snowmelt, Fraser Experimental Forest, Colorado. *Journal of Hydrology* 245: 177-195.

Stumm, W., Morgan, J.J., 1996. *Aquatic Chemistry, Chemical Equilibria and Rates in Natural Waters*, 3rd ed. John Wiley & Sons, Inc., New York, 1022p.

Sudicky, E.A., Frind, E.O., 1981. Carbon 14 dating of groundwater in confined aquifers: implications of aquitard diffusion. *Water Resources Research* 17(4): 1060-1064.

Tallaksen, A., 1995. A review of baseflow recession analysis. *Journal of Hydrology* 165: 349-370.

Tamers, M.A., 1967. Radiocarbon ages of groundwater in an arid zone unconfined aquifer. In: *Isotope Techniques in the Hydrological Cycle*, AGU Monograph 11, pp. 143-152.

Tamers, M.A., 1975. The validity of radiocarbon dates on groundwater; *Geophysical Survey*, v. 2, p. 217-239.

Tamers, M.A., Scharpenseel, H.W., 1970. Sequential sampling of radiocarbon in groundwater. In: *Isotope Hydrology, 1970, Proceedings of symposium of international Atomic Energy Agency and UNESCO, Vienna, March 9-13, IAEA STI/PUB/255/16*, pp. 241-257.

Tanaka, M., Takahashi, K., Sahoo, Y.V., 2004. Speciation of dissolved silicates in natural waters containing alkaline and alkaline-earth ions. *Analytical and Bioanalytical Chemistry* 378: 789-797.

Tardy, Y., Bustillo, V., Boeglin, J.-L., 2004. Geochemistry applied to the watershed survey: hydrograph separation, erosion and soil dynamics. A case study: the basin of the Niger River, Africa. *Applied Geochemistry* 19: 469-518.

Taylor A.S., Lasaga A.C., and Blum, J.D., 1999. Effect of lithology on silicate weathering rates, In: Armansson H. (ed) *Geochemistry of the Earth's Surface*: Rotterdam, Balkema, p. 127-128.

Taylor, S., Feng, X., Williams, M., McNamara, J., 2002. How isotopic fractionation of snowmelt affects hydrograph separation. *Hydrological Processes* 16: 3683-3690.

Taylor, S., Feng, X.H., Kirchner, J.W., Osterhuber, R., Klaue, B. and Renshaw, C.E., 2001. Isotopic evolution of a seasonal snowpack and its melt. *Water Resources Research* 37: 759-769.

Tóth, J., 1963. A theoretical analysis of groundwater flow in small drainage basins. *Journal of Geophysical Research* 68: 4795-4812.

Tsukamoto Y., 1961. An experiment on sub-surface flow. *Journal of the Japanese Forestry Society* 43: 62-67.

Uchida, T., Kosugi, K., Mizuyama, T., 1999. Runoff characteristics of pipeflow and effects of pipeflow on rainfall-runoff phenomena in a mountainous watershed. *Journal of Hydrology* 222: 18-36.

Uhlenbrook, S., 2006. Catchment hydrology – a science in which all processes are preferential. *Hydrological Processes* 20(16): 3581-3585.

Uhlenbrook, S., Frey, M., Leibundgut, Ch., Maloszewski, P., 2002. Residence time based hydrograph separations in a meso-scale mountainous basin at event and seasonal time scales. *Water Resources Research* 38: 1-14.

Uhlenbrook, S., Hoeg, S., 2003. Quantifying uncertainties in tracer-based hydrograph separations: a case study for two, three and five component hydrograph separation in a mountainous catchment. *Hydrological Processes* 17: 431-453.

Uhlenbrook, S., Leibundgut, Ch., 1997. Abflussbildung bei Hochwasser in verschiedenen Raumskalen (Runoff processes, spatial scales and flood generation). *Wasser und Boden*, 49: 13-22.

Uhlenbrook, S., Leibundgut, Ch., 2002. Process-oriented catchment modelling and multiple-response validation. *Hydrological Processes* 16: 423-440.

Unnikrishna, P.V., McDonnell, J.J. and Kendall, C. 2002. Isotope variations in a Sierra Nevada snowpack and their relation to meltwater. *Journal of Hydrology* 260: 38-57.

USGS, 1999. Tracing and dating young ground water. USGS Fact Sheet 134-99.

Vautrin, H., 1934. Sur l'orogenèse du massif de l'Hermon (Syrie). *C. Royal Academy of Science* 199: 82.

Visbeck, M.H., Hurrell, J.W., Polvani, L., Cullen, H.M., 2001. The North Atlantic Oscillation: Past, present and future. *PNAS* 98(23): 12876-12877.

Vogel, J.C., 1967. Investigation of groundwater flow with radiocarbon. In: *Proceedings of a symposium on isotopes in hydrology*. International Atomic Energy Agency, Vienna, pp 255–368.

Vogel, J.C., 1993. Variability of carbon isotope fractionation during photosynthesis. In: Ehleringer JR, Hall AE, Farquhar GD, eds. *Stable isotope and plant carbon/water relations*, New York, USA: Academic Press, 29-46.

Vogel, J.C., Ehhalt, D., 1963. The use of carbon isotopes in groundwater studies. In: *Proceedings of a symposium on radioisotope in hydrology*. International Atomic Energy Agency, Vienna, 383 pp.

Vogel, J.C., Grootes, P.M., Mook, W.G., 1970. Isotope fractionation between gaseous and dissolved carbon dioxide. *Zeitschrift für Physik* 230: 225-238.

Voigt, H.-J., 1990. *Hydrogeochemie – Eine Einführung in die Beschaffenheitsentwicklung des Grundwassers*. Springer Verlag Berlin, Heidelberg, New York, Tokyo, 310p.

Vries de, J.J., Simmers, I., 2002. Groundwater recharge: an overview of processes and challenges. *Hydrogeology Journal* 10: 5-17.

Walter, M.T., Kim, J.-S., Steenhuis, T.S., Parlange, J.-Y., Heilig, A., Braddock, R.D., Selker, J.S., Boll, J., 2000. Funneled flow mechanisms in a sloping layered soil: Laboratory investigation. *Water Resources Research* 36(4): 841-849.

Weiler, M., McDonnell, J., 2004. Virtual experiments: a new approach for improving process conceptualization in hillslope hydrology. *Journal of Hydrology* 285: 3-18.

Wels, C., Cornett, R.J. and Lazarete, B.D. 1991a. Hydrograph separation: a comparison of geochemical and isotopic tracers. *Journal of Hydrology* 122: 253-274.

Western, A.W., Blöschl, G., Grayson, R.B., 1998a. Geostatistical characterisation of soil moisture patterns in the Tarrawarra catchment. *Journal of Hydrology* 205: 20-37.

Western, A.W., Grayson, R.B., 1998b. The Tarrawarra data set: soil moisture patterns, soil characteristics, and hydrological flux measurements. *Water Resources Research* 34: 2765-2768.

White, A.F., Blum, A.E., 1995. Effects of climate on chemical weathering in watersheds. *Geochimica et Cosmochimica Acta* 59: 1729-1747.

White, W., 1988. *Geomorphology and Hydrology of Karst Terrains*. Oxford Univ. Press, New York, 464 pp.

White, W.B., 2002. Karst hydrology: recent developments and open questions. *Engineering Geology* 65: 85-105.

White, W.M., 1998. *Geochemistry*. Online text book. Dept. Geo. Sci., Cornell University, Ithaka, New York.

Williams, A.G., Dowd, J.F., Meyles, E.W., 2002. A new interpretation of kinematic stormflow generation. *Hydrological Processes* 16: 2791-2803.

Wilson, M., Shimron, A.E., Rosenbaum, J.M., Preston, J., 2000. Early Cretaceous magmatism of Mount Hermon, Northern Israel. *Contributions to Mineralogy and Petrology* 139: 54-67.

Wissmeier, L., Uhlenbrook, S., 2007. Distributed, high-resolution modelling of ^{18}O signals in a meso-scale catchment. *Journal of Hydrology* 332: 497-510.

Wittenberg, H., 1990. Baseflow recession and recharge as nonlinear storage processes. *Hydrological Processes* 13: 715-726.

Wolfart, R., 1966. Geologie von Syrien und dem Libanon. [The geology of Syria and Lebanon]. Beiträge zur regionalen Geologie der Erde, Band 6. Verlag Gebrüder Borntraeger-Berlin.

Worthington, S.R.H., Ford, D.C., 1995. High sulfate concentrations in limestone springs: An important factor in conduit initiation? *Environmental Geology* 25(1): 9-15.

Wundt, W., 1958. Die Kleinstwasserfuehrung der Fluesse als Mass fuer die verfuegbaren Grundwassermengen. In: Grahmann, R.(Ed.), Die Grundwaesser der Bundesrepublik Deutschland und ihre Nutzung. – Forschung deutsche Landeskunde 104: 47-54, Remagen.

Yaalon, D.H., 1997. Soils in the Mediterranean region: what makes them different? *Catena* 28: 157-169.

Yaalon, D.H., Ganor, E., 1973. The influence of dust on soils during the Quaternary. *Soil Science* 116: 146-155.

Yair, A., Lavee, H., 1985. Runoff generation in arid and semi-arid zones. In: Anderson, M.G., Burt, T.P. (Eds.), *Hydrological Forecasting*. Wiley, Chichester, pp. 183-220.

Yurtsever, Y., Gat, J.R., 1981. Atmospheric waters, stable isotope hydrology: deuterium and oxygen-18 in the water cycle. Technical Report Series no 210. Vienna: IAEA. 339 pp.

Zhang, L., 1998. The basics of recharge and discharge. CSIRO, Collingwood, Australia.

Zhu, C., Murphy, W.M., 2000. On radiocarbon dating of ground water. *Ground Water* 38: 802-804.

Ziegler, A.D., Giambelluca, T.W., Sutherland, R.A., Nullet, M.A., Yarnasarn, S., Pinthong, J., Preechapanya, P., Jaiaree, S., 2004. Toward understanding the cumulative impacts of roads in upland agricultural watersheds of northern Thailand. *Agriculture, Ecosystems & Environment* 104, 145–158.

Zilberman, E., Amit, R., Heimann, A., Porat, N., 2000. Changes in Holocene Paleoseismic activity in the Hula pull-apart basin, Dead Sea Rift, northern Israel. *Tectonophysics* 321: 237-252.

Ziv, B., Dayan, U., Kushnir, Y., Roth, C., Enzel, Y., 2006. Regional and global atmospheric patterns governing rainfall in the southern Levant. *International Journal of Climatology* 26: 55-73.

Zuber, A., Maloszewski, P., 2000. Lumped parameter models. In: Mook, W.G. (Ed.), Environmental Isotopes in the Hydrological Cycle Principles and Applications. IAEA and UNESCO, Vienna, pp. 5–35.

Appendix

LIST OF COMMON ABBREVIATIONS

a.s.l.	above sea level
b.s.l.	below sea level
BFI	baseflow index
C	tracer concentration
d	deuterium excess
DIC	dissolved inorganic carbon
DOC	dissolved organic carbon
EC	electrical conductivity
HSI	Hydrological Service of Israel
MRT	mean residence time
n	number of samples
n_e	effective porosity
P	precipitation
Q	discharge
R	recharge rate
r	correlation coefficient
T	temperature
t	time
TDI	total dissolved ions
TSS	total suspend solids
TU	tritium unit
UJRC	Upper Jordan River catchment
V	water volume
V-SMOW	Vienna Standard Mean Ocean Water
V-PDB	Vienna Pee Dee Belemnite

STRATIGRAPHY OF MOUNT HERMON AND GEOLOGY OF THE STUDY AREA

Stratigraphy and hydrological characteristics of the Hermon area*				
Age	Formation	Lithology	Thickness m.	Hydrological characteristics
Late Triassic**	J ₁ —Rime (Mohila)	Black marls and black, thinly bedded limestone	?–200	aquitard
Jurassic				
Liassic	J ₁	Green Marl and dark dolomite	100–150	aquifer
Bajocian	J ₂	Dark Massive dolomite	600	aquifer
Bajocian	J ₃	Oolitic, massive limestone	150–170	aquitard
Bathonian–Callovian	J ₄ —Hermon (Zohar Fm)	Massive, grey limestone and brown dolomite, marl at the top	700–900	aquifer
Oxfordian	J ₅ —Kidod	Marl and shales, thin limestone or dolomite with pyritized fauna	100–220	aquiclude
Oxfordian–Kimmeridgian	J ₆ —Be'er Sheva J ₇ —Haluza	Grey, massive, reef limestone Biomicritic limestone	40 140	aquifer aquifer
Cretaceous				
Berriassian	Tayasir Volcanics	Basalts and tuffs, intercalated with lacustrine sediments	130	?
Barremian	Hatira	Red quartz sandstone	70–80	aquitard
Aptian	Nabi Said	Sand, marl and oolitic limestone	10–20	aquitard
Aptian	Ein El Assad	“Blanche” limestone	60	aquifer
Aptian	Hidra	Shale, sandstone, iron oolites, and limestone	70–80	aquiclude
Albian	Mas'ade (Rama)	Limestone, chalky limestone, and marl	210–230	aquitard
Cenomanian	Yagur, Deir-Hanna, Sakhnin	Grey, dolomitic limestone	590	aquifer
Turonian	Bina	Limestone and chalk, marls at the base	200	aquiclude
Senonian	Mt. Scopus Gr.	Chalk and marly white limestone	570	aquiclude
Lower Eocene	E ₁	Marl and chalk	400	aquiclude
Middle Eocene	E ₂	Nummulitic limestone	900	aquifer
Miocene	M ₁	Lacustrine marly limestone	?	aquiclude
Neogene	M _{cg}	Conglomerate	?	aquitard

* Compiled from Dubertret (1951), Salzman (1968), Goldberg (1969), Michelson (1975), and Hirsch (1996).

** J₁ is of late Triassic age, based on paleontological criteria (Mouti, 2000).

Figure 63: Stratigraphy and hydrological characteristics of the Hermon area adapted from GUR et al. (2003).

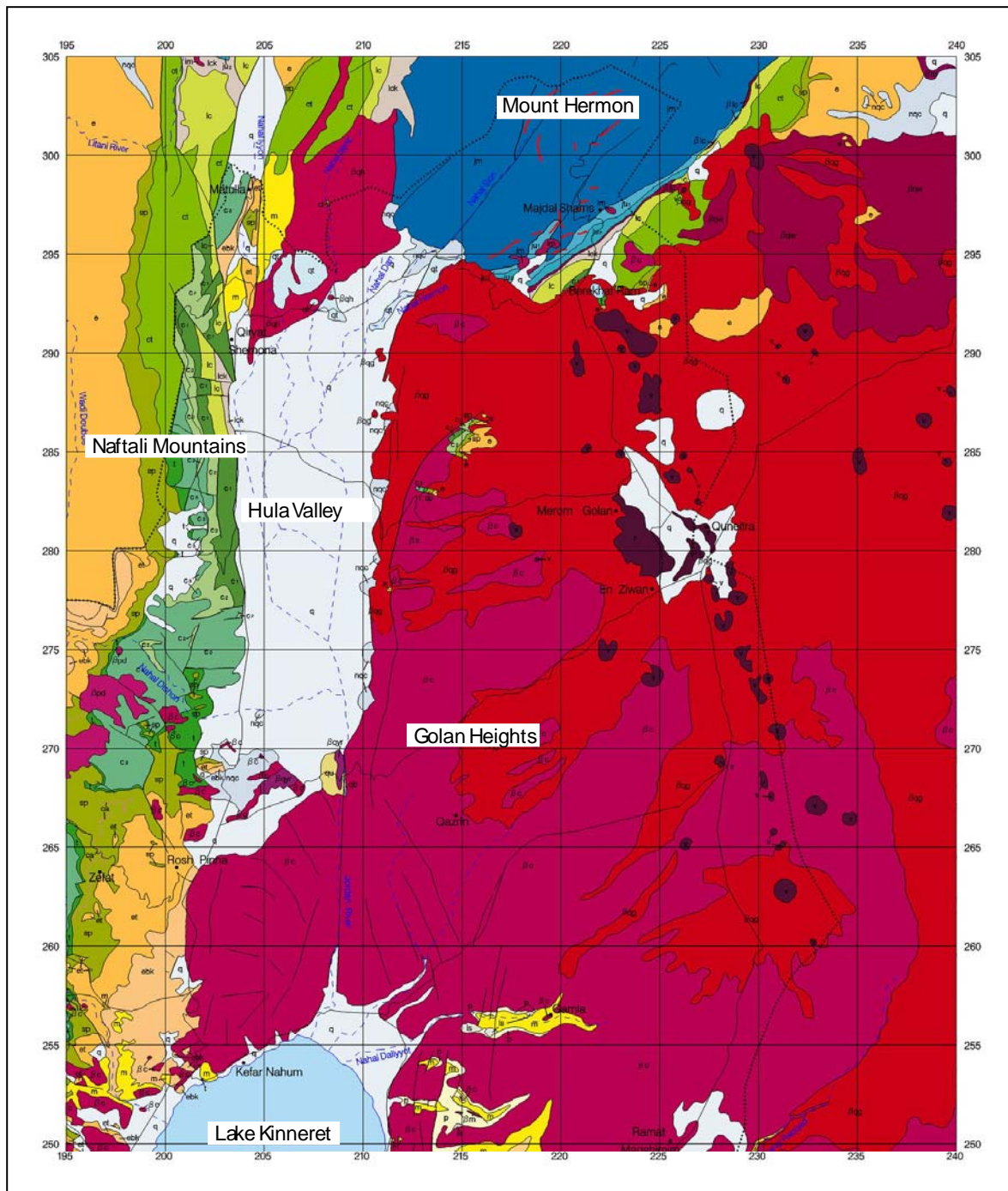


Figure 64: Geological map of the study area according to SNEH et al., 1998. The legend is given in Figure 65.

q	Alluvium (Gravel, sand, clay) <i>Quaternary</i>
qt	Travertine (Gravel, sand, silt) <i>Quaternary</i>
qu	Gadot and Mishamar Ha'Yarden fms. (Conglom., sandstone, mudst., chalk + 283m) <i>Pliocene – Pleistocene</i>
v	Volcanic cone (Basalt, basanite / flows and volcaniclastics) <i>Quaternary</i>
qw	Wa'ara Basalt (Basalt, basanite / flows and volcaniclastics) <i>Quaternary</i>
qq	Golan Basalt Raqqad Basalt (Basalt, basanite / flows) <i>Quaternary</i>
qy	Yarmouk Basalt Naharayim Basalt (Basalt, basanite / flows) <i>Quaternary</i>
qyr	Yarda Basalt (Basalt, basanite / flows) <i>Quaternary</i>
qh	Hasbani Basalt (Basalt, basanite / flows) <i>Quaternary</i>
nqc	Conglomerate units, undifferentiated (Basalt, basanite / flows) <i>Neogene – Quaternary</i>
bc	Cover basalt / Dalwe Basalt (Basalt, basanite / flows, intrusions and volcaniclastics) <i>Pliocene – Pleistocene</i>
m	Hordos Fm. / Umm Sabune Conglom. Kefar Giladi Fm. (sandst., mudst., conglom., limest. 880m) <i>Miocene</i>
e	Eocene (Chalk, limestone) <i>Oligocene</i>
ebk	Bar Kokhba Fm. (Limestone 250m) <i>Middle Eocene</i>
et	Timrat Fm. Meroz / Yizre'el fms. (Limestone, chalk, chert 380m) <i>Lower – Middle Eocene</i>
sp	Mount Scopus Group (Chalk, marl 380m) <i>Senonian – Paleocene</i>
ca	Campanian (Jordan) (Chalk, posporite, chert) <i>Maastrichtian</i>
ct	Cenomanian-Turonian in Lebanon (Limestone, dolostone) <i>Coniacian</i>
t	Bina Fm. (Limestone, marl, dolostone) <i>Turonian</i>
C3	Sakhnin and Yanuh fms. (Dolostone, limestone, chert 205m) <i>Cenomanian</i>
C2	Deir Hanna Fm. Isfiya Chalk, Beit Oren Limest. (Limest., dolostone, marl, chalk, chert 330m) <i>Cenomanian</i>
C1	Yagur Fm. Kammon Fm. (Dolostone 197m) <i>Albian-Cenomanian</i>
lc	Nabi Said, Ein el Assad, Hidra, Rama / Kefira fms. (Limest., chalk, marl, sandst. 430m) <i>Lower Cretaceous</i>
lck	Kurnub Group (Sandstone 85m) <i>Lower Cretaceous</i>
im	Intrusions and volcaniclastic rocks (Diabase, microgabro) <i>Mesozoic</i>
lc	Basalt flows (Basalt, basanite) <i>Lower Cretaceous</i>
ju	Upper Jurassic (Limestone 193m) <i>Lower Cretaceous</i>
ju2	Be'er Sheva and Haluza fms. (Limestone, marl 85m) <i>Upper Jurassic</i>
ju1	Kidot Fm. (Clay, limestone, dolostone 155m) <i>Upper Jurassic</i>
jm	Hermon Fm. (Limestone, dolostone 623m) <i>Middle Jurassic</i>

Figure 65: Legend explaining the geological map of the study area (Figure 64).

ANALYTICAL METHODS

Sample collection

Surface water and groundwater samples were collected as grab samples in the middle of the stream, rivulet, or spring unless otherwise mentioned. Samples were collected in 50 to 1000 ml high-density polyethylene bottles (Table 48).

Table 48: Details on pretreatment and storage of the collected water samples.

Parameter	Container	Amount	Pretreatment	Storage	Laboratory
^{18}O , ^2H	HDPE, narrow neck	50	none	dark, cool	GSF
^3H	HDPE, narrow neck	500	none	dark, cool	GSF
^{13}C , ^{14}C	glass, crimp seal	100	none	dark, 4°C	Leibniz
major anions	HDPE	20	filtered, 0.45 μm	4°C	GSF, MIGAL
major cations	HDPE	20	filtered, 0.45 μm	4°C	GSF
SiO_2	HDPE	50	filtered, 0.45 μm	4°C	MIGAL
DOC	HDPE	20	filtered, 0.45 μm	4°C	GSF
Major elements	HDPE	50	filtered, 0.45 μm	4°C	GSF
TSS	HDPE	up to 1000	none	4°C	MIGAL

Before filling, the sample bottles were rinsed three times with the water being collected. Bottles were filled to capacity to minimize headspace, capped tightly, and stored in a cooler for transport to the laboratory. If possible, samples were analyzed immediately, otherwise kept under refrigeration at 4°C until analysis.

Electrical conductivity, temperature and pH

Electrical conductivity and temperature were measured with a WTW Cond340i handheld conductivity meter connected to a WTW Tetracon®325 standard conductivity cell. Measurement accuracy is $\pm 0.5\%$ for electrical conductivity and $\pm 0.1\text{ K}$ for temperature. pH was measured immediately after sampling in the laboratory using a WTW glass electrode SenTix 81.

Anions and cations

Ion concentrations were determined by ion-exchange chromatography at the Institute of Groundwater ecology, GSF National Research Center, Germany. Specifications of the measurement devices are given in the table below. Samples were provided by a Dionex AS40 autosampler.

Table 49: Specifications of the IC-analyzer at the Institute of Groundwater ecology, GSF

	Anions	Cations
ion chromatograph	Dionex DX-100	Dionex DX-100
pre-column	AG4A-SC 4 mm (10-32)	CG12A 4x50 mm
column	AS4A-SC 4 mm (10-32)	CS12A 4x250 mm
eluent	3.5 mN Na ₂ CO ₃ + 1 mN NaHCO ₃	200 mN H ₂ SO ₄
flow rate	1.2 ml/min	1.0 ml/min
suppressor	ASRS-Ultra 4 mm	CSRS-Ultra 4 mm
detection	electrical conductivity	electrical conductivity

Samples were measured against a base electrical conductivity of 12 µS/cm for anions and 2 µS/cm for cations. The concentration of the sample was obtained by integration of the measured peak area using the multi-point calibration curves established in advance according to the expected concentrations. The detection limit with the applied method is about 0.1 mg/L for chloride, 0.02 mg/L for nitrite and bromide, 0.2 mg/L for sulfate and 0.01 mg/L for phosphate. For cations, the limit of determination is as follows: 0.025 mg/L for lithium, 0.1 mg/L for ammonium, 0.5 mg/L for potassium, 1 mg/L for sodium and magnesium and 2.5 mg/L for calcium. The accuracy of measurement is about 5 %.

Dissolved silicic acid (Silica)

Molybdate-reactive silica concentrations were determined on a Spectronic®20Genesys spectrometer according to Standard Methods (American Public Health Association, 1997). Analyses were conducted at the MIGAL Galilee Technology Center, Israel. Samples were acidified with 1:1 HCl to approximately pH 1.2 at which ammonium molybdate reacts with silica to form molybdisilicic acid. Any simultaneously developing molybdophosphoric acid

complexes are destroyed by the addition of oxalic acid. The intensity of the resulting yellow color is proportional to the concentration of molybdate-reactive silica. A standard calibration curve covering the expected range of concentrations was established to determine quantitatively sample silica concentrations. During analysis the usage of glassware was minimized, samples were read on the spectrometer at 410 nm with a 1 cm plastic cuvette. The detection limit is about 1 mg/L SiO₂ and the accuracy of measurement is about 5 %.

¹⁸O and ²H

Samples for the analysis of stable water isotopes were collected and stored according to standard procedures (MOSER and RAUERT, 1980, CLARK and FRITZ, 1997). The stable isotope ratios of ¹⁸O and ²H in the water samples were measured at the Institute of Groundwater ecology, GSF National Research Center Neuherberg, Germany using isotope ratio mass spectrometers (IRMS).

¹⁸O analyses were carried out by equilibrating each sample with CO₂ at 18 °C during 4 to 6 hours and subsequent measurement of CO₂ with an MAT GD 150 isotope ratio mass spectrometer. ²H analyses were conducted by converting water to hydrogen by passage over 800 °C hot uranium (BIGELEISEN et al., 1952; FRIEDMAN, 1953; GODFREY, 1962) and subsequent mass-spectrometric measurement of hydrogen at a MAT M 86 IRMS. The results are expressed as δ values [‰] relative to the Vienna Standard Mean Ocean Water (V-SMOW):

$$\delta^2H \dots \delta^{18}O = \frac{R_{Sample} - R_{Standard}}{R_{Standard}} * 1000$$

where R denotes respectively the ratio of the heavy and light isotope (²H/¹H and ¹⁸O/¹⁶O). The quantitative determination of the isotope concentrations is obtained by comparative measurements against internal laboratory standards, which in turn are calibrated against the international standard. Measurement accuracy is ± 0.15 ‰ for δ¹⁸O and ± 1.5 ‰ for δ²H.

Dissolved organic carbon (DOC)

Dissolved organic carbon (DOC) concentrations in the water samples were determined based on the NPOC-method, which is the determination of non-purgeable organic carbon via combustion catalytic oxidation. Analyses were conducted at the Institute of Groundwater ecology, GSF National Research Center, Germany. Samples were processed with the help of a total organic carbon analyzer coupled to an autosampler. Specification of the measurement devices are given in the table below.

Table 50: Specifications of the TOC/DOC analyzer at the Institute of Groundwater ecology, GSF.

Technical details	
TOC/DOC analyzer	Shimadzu TOC 5000A
autosampler	Shimadzu ASI 5000
flow rate	150 ml/min
carrier gas	oxygen 4.5
catalyst	platinum
detection	infrared spectrometry

At the beginning of the analyses, samples were automatically acidified with a 2 M HCl solution according to their buffer capacity. The non-purgeable organic carbon of the water sample was oxidized to CO₂ by addition of the carrier gas. The measured concentration of the sample was obtained by integration of the measured peak area using the three-point calibration curve developed in advance according to the expected concentrations. Each sample was measured four times, the measurement with the highest deviation was discarded and the remaining values used to calculate the mean concentration. The detection limit is about 0.3 mg/L DOC and the accuracy of measurement is about 10 %.

Carbonate alkalinity

Carbonate alkalinity in water samples was measured by acidimetric titration against a mixed indicator; color change at pH 4.3. Analyses were conducted based on the Aquamerck Alkalinity Test reagent kit. Analytical precision is ± 0.1 mmol/L.

Tritium

Tritium measurements were conducted by liquid scintillation counting of water after electrolytic enrichment of ^3H (EICHINGER et al., 1980). The detection limit of this method is ± 0.7 T.U.

Carbon-13 and carbon-14

$^{13}\text{C}/^{12}\text{C}$ and $^{14}\text{C}/^{12}\text{C}$ ratios were determined at the Leibniz Laboratory for Radiometric dating and Isotope research, Christian-Albrecht-University Kiel, Germany. For the samples taken in summer 2003, carbonate was precipitated as SrCO_3 in the field by adding SrCl_2 to 100 to 125 liter samples (depending on the bicarbonate content). The necessary alkaline environment was generated by the addition of NaOH . In July 2004, additional samples were collected in 100 ml glass bottles with a rubber stopper/crimp sealing according to standard procedures (CLARK and FRITZ, 1997).

The SrCO_3 samples were acidified with 37 % HCl to approximately pH 6, transferred into reaction phials and subsequently hydrolyzed to CO_2 at 90 °C by addition of 100 % phosphoric acid. The 100 ml samples without pretreatment were passed under cover gas through a 0.2 μm membrane filter and acidified with 30 % phosphoric acid. Afterwards CO_2 was removed by addition of nitrogen and cryotechnically absorbed. Sample CO_2 was reduced to an iron-graphite mixture under addition of H_2 on a iron catalyst at 600 °C with the mixture then being utilized for analysis at the atomic mass spectrometer (AMS).

TSS

Total suspended solids (TSS) give a measure of the turbidity of the water. TSS measurements were conducted at selected samples taken during high flow conditions. Total suspended solids were analyzed by filtering an aliquot of sampled water through 0.45 μm preweighed filters.

SUPPLEMENTARY DATA

Supplementary data - Chapter 5

Table 51: Ion concentrations in daily rain samples at the Banias Nature Reserve. N.d.: not determined.

Date	Amount mm	HCO_3^- mg/L	Cl^- mg/L	NO_3^- mg/L	SO_4^{2-} mg/L	Na^+ mg/L	K^+ mg/L	Mg^{2+} mg/L	Ca^{2+} mg/L
12/20/2002	47.0	n.d.	4.4	1.3	2.9	2.4	0.1	0.3	6.5
12/21/2002	2.0	n.d.	6.6	0.0	1.9	4.0	1.4	1.3	11.0
12/23/2002	1.4	n.d.	8.8	8.3	7.8	5.0	1.8	2.1	14.7
12/24/2002	13.3	n.d.	0.8	2.5	2.6	0.5	0.4	0.4	6.1
12/26/2002	0.8	n.d.	1.8	2.8	4.0	1.1	0.5	1.8	19.6
12/31/2002	3.0	n.d.	2.2	6.5	6.7	0.9	0.4	1.3	16.4
01/02/2003	6.8	n.d.	1.3	0.1	1.7	0.7	0.1	0.2	6.3
01/03/2003	11.0	n.d.	1.3	1.2	1.6	0.6	0.1	0.1	5.3
01/04/2003	11.8	n.d.	3.8	1.3	2.9	1.7	0.1	0.2	5.7
02/03/2003	58.9	n.d.	2.7	0.8	2.5	1.6	0.1	0.1	4.7
02/04/2003	36.6	n.d.	1.6	0.1	0.7	1.0	0.1	0.1	2.9
02/07/2003	2.7	n.d.	n.d.	n.d.	n.d.	21.1	7.4	2.7	25.2
02/08/2003	8.3	n.d.	n.d.	n.d.	n.d.	8.7	0.9	1.2	11.1
02/09/2003	14.8	n.d.	2.7	0.6	1.9	1.5	0.2	0.2	4.7
02/10/2003	3.2	n.d.	3.4	2.9	2.7	1.8	0.3	0.6	7.7
02/12/2003	2.6	n.d.	5.8	9.2	10.3	3.4	0.6	1.6	21.1
02/13/2003	13.9	n.d.	9.6	1.2	3.1	5.8	0.3	1.4	14.9
02/14/2003	21.3	n.d.	3.4	0.2	1.5	1.8	0.1	0.2	5.4
02/15/2003	6.7	n.d.	7.1	0.3	3.8	4.1	0.6	0.6	7.3
02/18/2003	17.5	n.d.	8.3	0.6	2.3	4.7	0.2	0.5	5.8
02/19/2003	23.2	n.d.	11.8	0.7	2.8	6.3	0.3	0.3	4.5
02/20/2003	36.1	n.d.	4.2	0.3	1.7	2.5	0.1	0.2	2.4
02/21/2003	43.7	n.d.	1.4	0.0	1.0	0.7	0.1	0.1	2.1
02/23/2003	4.1	n.d.	4.4	5.3	8.3	2.5	0.3	1.5	11.1
02/24/2003	18.2	n.d.	12.1	0.7	3.8	5.1	0.2	0.5	2.4
02/27/2003	15.6	n.d.	3.6	0.7	1.7	1.8	0.2	0.1	2.2
03/03/2003	11.1	n.d.	6.5	5.0	5.0	3.3	0.3	1.1	10.7
03/06/2003	12.3	n.d.	2.1	2.9	2.5	1.2	0.2	0.4	6.3

Table 52: Ion concentrations in daily rain samples at the Dan Nature Reserve. N.d.: not determined.

Date	Amount mm	HCO_3^- mg/L	Cl^- mg/L	NO_3^- mg/L	SO_4^{2-} mg/L	Na^+ mg/L	K^+ mg/L	Mg^{2+} mg/L	Ca^{2+} mg/L
12/16/2002	0.5	n.d.	4.1	4.6	4.8	2.1	0.6	0.6	4.4
12/20/2002	45.0	n.d.	3.0	0.7	1.8	1.6	0.1	0.1	1.6
12/21/2002	17.0	n.d.	n.d.	n.d.	n.d.	17.6	1.1	2.1	2.4
12/23/2002	1.0	n.d.	3.0	2.0	2.5	n.d.	n.d.	n.d.	n.d.
12/24/2002	5.0	n.d.	2.6	1.1	2.3	n.d.	n.d.	n.d.	n.d.
12/25/2002	5.0	n.d.	1.2	2.4	2.4	0.8	0.2	0.1	2.7
12/31/2002	3.5	n.d.	2.7	6.0	5.8	1.3	0.6	0.6	4.6
01/16/2003	6.0	n.d.	16.3	1.4	4.8	9.2	0.8	1.2	3.1
01/28/2003	22.5	n.d.	4.5	2.0	5.1	2.2	1.5	n.d.	8.3
02/08/2003	8.0	n.d.	n.d.	n.d.	n.d.	9.6	0.6	1.3	9.8
02/09/2003	13.0	n.d.	2.7	1.0	1.9	1.7	0.2	0.5	13.3
02/10/2003	7.5	n.d.	1.5	0.8	1.9	1.1	0.1	0.1	4.9
02/14/2003	21.0	n.d.	2.8	0.7	1.4	1.8	0.1	0.4	6.1
02/15/2003	23.0	n.d.	3.6	0.4	1.5	2.1	0.1	0.1	1.8
02/18/2003	20.0	n.d.	n.d.	n.d.	n.d.	2.0	0.1	0.1	0.7
02/19/2003	24.0	n.d.	n.d.	n.d.	n.d.	1.5	0.1	0.1	0.6
02/20/2003	35.0	n.d.	3.5	0.5	1.6	1.5	0.1	0.1	0.6
02/21/2003	50.0	n.d.	2.6	0.3	1.4	6.9	0.2	0.7	3.2
02/23/2003	4.0	n.d.	n.d.	n.d.	n.d.	6.4	0.2	0.6	1.8
02/24/2003	23.0	n.d.	9.3	0.5	3.4	7.8	0.5	1.1	3.7
02/25/2003	30.0	n.d.	7.1	0.5	2.3	4.1	0.2	0.4	0.9
02/27/2003	17.0	n.d.	2.7	1.2	2.4	1.3	0.2	0.7	4.4
03/04/2003	10.0	n.d.	8.8	2.9	6.4	4.5	0.4	0.7	8.9
03/05/2003	1.0	n.d.	9.4	3.2	7.6	6.0	0.8	1.4	17.6
03/06/2003	10.0	n.d.	2.0	1.6	2.1	1.3	0.1	0.1	3.9
03/07/2003	15.0	n.d.	1.8	1.7	2.1	1.1	0.1	n.d.	3.0
03/12/2003	9.0	n.d.	1.4	1.4	1.6	1.1	0.1	n.d.	2.1
12/18/2003	8.5	n.d.	1.1	0.9	1.5	0.7	0.1	n.d.	2.5

Table 53: Natural tracer concentrations from snow samples of different snow courses taken on Mount Hermon (Israel). N.d.: not determined.

Date	Altitude m	$\delta^{18}\text{O}$ ‰	$\delta^2\text{H}$ ‰	d	EC µS/cm	pH	HCO_3^- mmol/L	Cl mg/L	NO_3^- mg/L	SO_4^{2-} mg/L	Na^+ mg/L	K^+ mg/L	Mg^{2+} mg/L	Ca^{2+} mg/L	DOC mg/L	^3H TU	$\pm 2\text{s}$ TU	SiO_2 mg/L
02/23/2003	1389	-8.33	-43.3	23.3	9	7.00	n.d.	n.d.	n.d.	n.d.	n.d.	n.d.	n.d.	n.d.	0.68	n.d.	n.d.	n.d.
02/23/2003	1567	-7.47	-36.7	23.1	30	7.76	n.d.	n.d.	n.d.	n.d.	n.d.	n.d.	n.d.	n.d.	0.92	n.d.	n.d.	n.d.
02/23/2003	1700	-8.82	-47.1	23.5	9	6.45	n.d.	n.d.	n.d.	n.d.	n.d.	n.d.	n.d.	n.d.	0.89	n.d.	n.d.	n.d.
02/23/2003	1804	-9.91	-56.4	22.8	9	6.31	n.d.	n.d.	n.d.	n.d.	n.d.	n.d.	n.d.	n.d.	1.15	n.d.	n.d.	n.d.
02/23/2003	2050	-9.48	-52.3	23.5	5	6.50	n.d.	n.d.	n.d.	n.d.	n.d.	n.d.	n.d.	n.d.	1.17	n.d.	n.d.	n.d.
02/23/2003	2066	-10.16	-58.0	23.2	6	6.71	n.d.	n.d.	n.d.	n.d.	n.d.	n.d.	n.d.	n.d.	0.85	n.d.	n.d.	n.d.
12/21/2003	1393	-9.67	-47.4	30.0	33	5.76	0.60	n.d.	n.d.	n.d.	n.d.	n.d.	n.d.	n.d.	2.10	n.d.	n.d.	0.000
12/21/2003	1466	-8.96	-41.7	29.9	46	6.63	0.60	9.25	0.75	2.40	5.51	0.27	0.09	0.69	2.35	n.d.	n.d.	0.043
12/21/2003	1597	-8.60	-38.4	30.5	61	7.29	0.60	11.19	0.88	2.77	5.83	0.37	0.02	2.02	2.26	n.d.	n.d.	0.043
12/21/2003	1736	-9.64	-47.3	29.8	40	5.24	0.60	8.70	0.87	2.48	5.22	0.34	0.20	0.30	2.48	n.d.	n.d.	0.000
12/21/2003	1809	-8.65	-38.9	30.3	42	4.89	0.60	8.03	0.74	2.33	4.52	0.40	0.25	0.18	2.64	n.d.	n.d.	0.043
12/21/2003	1868	-9.26	-45.7	28.4	30	5.32	0.60	5.78	0.84	2.11	3.29	0.31	0.36	0.15	3.56	n.d.	n.d.	0.043
12/21/2003	1946	-8.45	-34.9	32.7	64	5.07	0.80	13.91	0.96	3.14	7.89	0.45	0.37	0.06	3.68	n.d.	n.d.	0.043
12/21/2003	2012	-9.36	-44.3	30.5	18	6.98	0.80	3.08	0.73	1.66	2.00	0.11	0.81	0.39	2.28	n.d.	n.d.	0.043
01/10/2004	1403	-8.29	-35.4	31.0	18	n.d.	n.d.	2.10	0.88	1.25	1.04	0.16	1.79	0.34	1.53	2.9	0.4	n.d.
01/10/2004	1500	-7.50	-33.9	26.1	7	n.d.	n.d.	0.68	0.87	0.30	0.02	0.07	1.96	0.04	1.15	2.9	0.4	n.d.
01/10/2004	1629	-8.15	-40.0	25.2	15	n.d.	n.d.	0.81	1.35	0.93	0.00	0.09	1.96	0.00	2.51	3.2	0.4	n.d.
01/10/2004	1725	-8.74	-40.3	29.6	15	n.d.	n.d.	1.29	0.77	0.95	0.46	0.16	1.87	0.11	1.34	2.6	0.4	n.d.
01/10/2004	1830	-8.95	-41.2	30.4	13	n.d.	n.d.	1.09	0.73	0.70	0.29	0.11	1.89	0.18	1.76	2.7	0.4	n.d.
01/10/2004	1927	-8.26	-34.1	31.9	21	n.d.	n.d.	1.79	0.67	1.17	0.82	0.10	1.79	0.10	1.24	2.7	0.4	n.d.
01/10/2004	2027	-8.41	-41.3	25.9	16	n.d.	n.d.	1.26	0.92	0.88	0.39	0.10	1.84	0.62	1.30	3.2	0.4	n.d.

continuation

Date	Altitude m	$\delta^{18}\text{O}$ ‰	$\delta^2\text{H}$ ‰	d	EC µS/cm	pH	HCO_3^- mmol/L	Cl ⁻ mg/L	NO_3^- mg/L	SO_4^{2-} mg/L	Na^+ mg/L	K^+ mg/L	Mg^{2+} mg/L	Ca^{2+} mg/L	DOC mg/L	³ H TU	$\pm 2\text{s}$ TU	SiO_2 mg/L
02/03/2004	1467	-6.78	-31.6	22.7	43	n.d.	0.50	0.85	1.84	0.11	0.26	0.07	0.03	8.93	n.d.	n.d.	n.d.	n.d.
02/03/2004	1737	-5.19	-17.6	24.0	16	n.d.	0.30	2.04	1.66	1.02	1.14	0.70	0.27	1.13	n.d.	n.d.	n.d.	n.d.
02/03/2004	1819	-3.97	-7.60	24.2	19	n.d.	0.10	2.18	1.85	1.19	1.24	0.64	0.43	0.32	n.d.	n.d.	n.d.	n.d.
02/03/2004	1923	-4.15	-8.90	24.3	19	n.d.	0.30	2.27	1.84	1.25	1.28	0.68	0.41	0.71	n.d.	n.d.	n.d.	n.d.
02/03/2004	2000	-5.36	-20.6	22.2	12	n.d.	0.20	1.83	2.16	0.96	1.02	0.13	0.01	0.92	n.d.	n.d.	n.d.	n.d.
02/18/2004	924	-6.38	-22.2	28.9	11	n.d.	0.30	1.12	1.70	0.02	0.41	0.08	0.09	1.81	n.d.	n.d.	n.d.	n.d.
02/18/2004	1010	-6.45	-23.7	27.9	4	n.d.	0.40	0.74	1.69	0.07	0.16	0.08	0.16	0.29	n.d.	n.d.	n.d.	n.d.
02/18/2004	1099	-6.44	-22.9	28.6	5	n.d.	0.30	n.d.	n.d.	n.d.	n.d.	n.d.	n.d.	n.d.	n.d.	n.d.	n.d.	n.d.
02/18/2004	1265	-5.14	-9.30	31.8	5	n.d.	0.40	0.84	1.18	0.12	0.22	0.03	0.47	0.92	n.d.	n.d.	n.d.	n.d.
02/18/2004	1319	-5.20	-13.8	27.8	7	n.d.	0.35	0.99	1.70	0.01	0.30	n.d.	0.14	0.78	n.d.	n.d.	n.d.	n.d.
02/18/2004	1444	-5.83	-23.4	23.3	6	n.d.	n.d.	n.d.	n.d.	n.d.	n.d.	n.d.	n.d.	n.d.	n.d.	n.d.	n.d.	n.d.
02/18/2004	1530	-5.96	-23.1	24.6	35	n.d.	0.40	1.15	1.84	0.41	0.47	0.09	0.12	5.59	n.d.	n.d.	n.d.	n.d.
02/18/2004	1646	n.d.	n.d.	n.d.	n.d.	n.d.	0.30	1.14	1.83	0.15	0.72	0.11	0.13	1.77	n.d.	n.d.	n.d.	n.d.
02/18/2004	1862	-6.18	-22.6	26.8	17	n.d.	0.40	2.24	1.89	0.72	1.41	0.13	0.14	1.42	n.d.	n.d.	n.d.	n.d.
02/18/2004	1958	-6.95	-40.0	15.7	6	n.d.	0.30	1.18	1.82	0.13	0.53	0.13	0.10	0.41	n.d.	n.d.	n.d.	n.d.
02/18/2004	2053	-5.09	-24.1	16.6	6	n.d.	0.40	1.01	1.33	0.03	0.33	0.04	0.47	0.85	n.d.	n.d.	n.d.	n.d.

Table 54: Natural tracer concentrations from snow samples of different snow profiles taken on Mount Hermon (Israel). N.d.: not determined.

Date	Altitude	Height	$\delta^{18}\text{O}$	$\delta^{2}\text{H}$	d	EC	pH	HCO_3^-	Cl^-	NO_3^-	SO_4^{2-}	Na^+	K^+	Mg^{2+}	Ca^{2+}	DOC
	m	cm	‰	‰		$\mu\text{S}/\text{cm}$		mmol/L	mg/L	mg/L	mg/L	mg/L	mg/L	mg/L	mg/L	mg/L
01/10/2004	2050	0	-8.10	-34.1	30.7	16	n.d.	n.d.	2.10	0.61	1.03	1.03	0.24	1.76	0.35	0.87
01/10/2004	2050	50	-7.42	-27.3	32.1	22	n.d.	n.d.	3.01	0.61	1.30	1.69	0.20	1.64	0.05	1.27
01/10/2004	2050	90	-8.74	-39.5	30.4	19	n.d.	n.d.	1.83	0.70	1.21	0.89	0.10	1.79	0.05	1.21
01/10/2004	2050	130	-9.26	-45.3	28.8	14	n.d.	n.d.	1.05	0.48	0.06	0.31	0.19	1.90	0.95	0.89
02/03/2004	2050	0	-4.54	-12.2	24.2	20	n.d.	0.50	1.66	1.81	0.99	0.94	0.07	0.45	0.59	n.d.
02/03/2004	2050	20	-7.18	-32.1	25.3	7	n.d.	0.30	0.86	1.71	0.29	0.30	0.07	0.49	1.99	n.d.
02/03/2004	2050	40	-6.13	-25.6	23.5	13	n.d.	0.25	1.61	1.96	0.97	0.81	0.09	0.39	1.51	n.d.
02/03/2004	2050	55	-7.55	-33.0	27.4	3	n.d.	0.30	0.59	1.39	0.00	0.09	0.07	0.51	0.62	n.d.
02/03/2004	2050	70	-7.78	-35.2	27.0	3	n.d.	0.30	0.51	1.40	0.14	0.03	0.04	0.57	0.56	n.d.
02/03/2004	2050	85	-8.55	-41.1	27.4	9	n.d.	0.30	0.87	1.43	0.05	0.32	0.06	0.43	1.44	n.d.
02/03/2004	2050	100	-8.87	-43.6	27.4	11	n.d.	0.35	0.64	1.43	0.10	0.16	0.06	0.34	2.22	n.d.
02/03/2004	2050	115	-8.72	-43.4	26.3	10	n.d.	0.25	1.32	1.76	0.24	0.66	0.10	0.03	1.04	n.d.
02/03/2004	2050	130	-8.52	-43.8	24.4	119	n.d.	0.90	2.74	1.92	2.22	1.80	0.29	0.61	13.6	n.d.
02/03/2004	2050	160	-8.33	-46.1	20.6	11	n.d.	0.30	0.65	1.66	0.08	0.10	0.06	0.47	2.97	n.d.

Table 55: Stable isotope composition ($\delta^{18}\text{O}$, $\delta^2\text{H}$) and amounts of daily rain in the Banias and Dan Nature Reserves.

Banias Nature Reserve					Dan Nature Reserve				
Date	Amount	$\delta^{18}\text{O}$	$\delta^2\text{H}$	d	Date	Amount	$\delta^{18}\text{O}$	$\delta^2\text{H}$	d
	mm	‰	‰	‰		mm	‰	‰	‰
12/20/02	47.0	-6.91	-38.30	16.98	12/16/02	0.5	-1.28	7.90	18.14
12/21/02	2.0	-12.39	-73.70	25.42	12/20/02	45.0	-6.68	-39.60	13.84
12/23/02	1.4	-2.80	6.30	28.70	12/21/02	17.0	-9.21	-50.00	23.68
12/24/02	13.3	-6.52	-23.80	28.36	12/23/02	1.0	-5.59	-17.00	27.72
12/24/02	13.3	-6.65	-22.30	30.90	12/24/02	5.0	-7.39	-37.90	21.22
12/26/02	0.8	-4.65	-18.30	18.90	12/25/02	5.0	-6.12	-20.30	28.66
12/31/02	3.0	-3.81	-17.20	13.28	12/31/02	3.5	-2.66	-9.90	11.38
01/02/03	6.8	-7.54	-43.70	16.62	01/04/03	13.0	-6.85	-39.30	15.50
01/03/03	11.0	-7.56	-44.30	16.18	01/16/03	6.0	-3.56	-8.50	19.98
01/04/03	11.8	-4.36	-19.20	15.68	01/18/03	6.0	-3.88	-11.30	19.74
02/03/03	58.9	-8.32	-45.70	20.86	01/20/03	12.5	-6.47	-40.20	11.56
02/04/03	36.6	-9.60	-53.70	23.10	01/21/03	14.0	-9.35	-57.40	17.40
02/07/03	2.7	-2.68	-4.20	17.24	01/28/03	22.5	-5.88	-29.70	17.34
02/08/03	8.3	-2.74	0.30	22.22	01/29/03	24.0	-9.38	-54.70	20.34
02/09/03	14.8	-4.85	-8.50	30.30	02/03/03	67.0	-8.67	-47.80	21.56
02/10/03	3.2	-5.14	-13.50	27.62	02/04/03	30.0	-9.85	-56.80	22.03
02/12/03	2.6	-0.86	1.80	8.68	02/08/03	8.0	-2.19	4.30	21.82
02/13/03	13.9	-8.17	-49.10	16.26	02/09/03	13.0	-4.31	-4.70	29.78
02/14/03	21.3	-6.76	-32.30	21.78	02/10/03	7.5	-6.57	-22.20	30.36
02/15/03	6.7	-7.82	-40.70	21.86	02/14/03	21.0	-7.44	-35.20	24.32
02/18/03	17.5	-4.70	-23.00	14.60	02/15/03	23.0	-6.26	-29.00	21.08
02/19/03	23.2	-5.23	-20.40	21.44	12/18/03	8.5	-9.55	-57.50	18.90
02/20/03	36.1	-7.41	-35.60	23.68	02/18/03	20.0	-4.96	-9.20	30.48
02/21/03	43.7	-7.84	-40.10	22.62	02/19/03	24.0	-7.16	-34.00	23.28
02/23/03	4.1	-4.93	-15.70	23.74	02/20/03	35.0	-8.33	-44.90	21.74
02/24/03	18.2	-11.47	-62.20	29.56	02/21/03	50.0	-4.43	-5.80	29.64
02/27/03	15.6	-8.45	-44.20	23.40	02/23/03	4.0	-6.36	-19.50	31.38
03/03/03	11.1	-3.68	-14.00	15.44	02/24/03	23.0	-9.58	-46.70	29.94
03/06/03	12.3	-8.14	-49.10	16.02	02/25/03	30.0	-6.14	-29.40	19.72
03/11/03	6.6	-5.70	-26.30	19.30	02/27/03	17.0	-8.91	-40.50	30.78
03/12/03	7.9	-5.42	-18.85	24.47	03/04/03	10.0	-3.00	-8.20	15.80
03/18/03	30.5	-7.98	-45.45	18.35	03/05/03	1.0	-2.22	-1.00	16.76
03/19/03	30.0	-5.09	-19.45	21.27	03/06/03	10.0	-7.98	-48.30	15.54
03/21/03	10.9	-5.81	-24.45	21.99	03/07/03	15.0	-8.81	-52.70	17.78
03/22/03	6.4	-4.49	-13.60	22.32	03/12/03	9.0	-4.58	-19.60	17.04
03/24/03	20.5	-5.65	-27.50	17.70	03/19/03	24.0	-7.41	-43.40	15.84
03/25/03	40.7	-8.12	-40.20	24.76	03/20/03	0.5	-3.58	-7.45	21.15
11/08/03	12.5	-4.05	-17.10	15.26	03/22/03	6.5	-5.33	-21.85	20.79
11/09/03	13.6	-4.63	-22.35	14.69	03/23/03	12.5	-5.74	-26.35	19.53

continuation

Banias Nature Reserve					Dan Nature Reserve				
Date	Amount	$\delta^{18}\text{O}$	$\delta^2\text{H}$	d	Date	Amount	$\delta^{18}\text{O}$	$\delta^2\text{H}$	d
	mm	‰	‰	‰		mm	‰	‰	‰
11/10/03	21.3	-4.84	-13.45	25.27	03/24/03	26.0	-4.23	-13.85	19.99
11/11/03	2.2	-2.75	0.95	22.91	03/25/03	47.0	-7.26	-34.75	23.29
11/24/03	0.4	2.18	20.35	2.95	03/26/03	4.5	-7.16	-35.15	22.09
11/28/03	2.0	1.05	20.50	12.14	11/08/03	18.5	-4.26	-16.25	17.83
12/04/03	8.4	-8.06	-54.35	10.13	11/09/03	13.0	-4.09	-19.10	13.62
12/07/03	22.0	-2.45	8.70	28.26	11/10/03	16.0	-4.42	-12.85	22.51
12/14/03	10.0	0.12	11.00	10.08	11/11/03	3.0	-2.44	1.00	20.48
12/17/03	23.6	-3.72	1.10	30.82	11/24/03	1.0	2.18	24.25	6.85
12/18/03	36.5	-8.30	-36.90	29.50	11/28/03	1.5	0.89	12.85	5.77
12/19/03	6.4	-8.28	-35.20	31.04	12/03/03	4.5	-4.51	-14.85	21.23
12/27/03	24.5	-11.88	-74.35	20.69	12/04/03	10.0	-8.35	-53.45	13.31
01/01/04	1.0	-2.66	-10.25	10.99	12/05/03	35.0	-9.27	-50.10	24.02
01/02/04	3.0	-3.48	-10.95	16.89	12/06/03	2.5	-5.32	-19.75	22.77
01/05/04	8.1	-3.09	-7.55	17.17	12/08/03	0.5	-8.59	-46.75	21.97
01/06/04	30.7	-6.27	-29.30	20.82	12/18/03	23.0	-2.89	4.30	27.38
01/07/04	30.5	-5.95	-17.70	29.90	12/19/03	5.5	-7.13	-25.45	31.59
01/08/04	7.5	-6.56	-22.95	29.49	12/20/03	0.5	-7.90	-34.10	29.10
01/12/04	8.0	-7.31	-42.40	16.08	12/26/03	11.6	-10.76	-65.15	20.89
01/13/04	43.8	-9.73	-63.60	14.24	12/28/03	28.0	-11.07	-68.95	19.61
01/14/04	12.6	-10.44	-70.45	13.07	01/01/04	4.0	-2.47	-6.50	13.22
01/15/04	2.0	-4.52	-25.40	10.76	01/05/04	7.5	-6.44	-31.20	20.28
01/22/04	12.6	-5.40	-28.55	14.61	01/06/04	28.0	-6.08	-26.35	22.29
01/23/04	67.5	-6.75	-26.40	27.60	01/07/04	28.0	-5.66	-15.65	29.59
01/24/04	14.5	-6.39	-20.65	30.47	01/08/04	10.0	-5.90	-19.20	27.96
01/25/04	11.1	-7.40	-38.95	20.25	01/09/04	14.0	-6.06	-19.75	28.73
01/26/04	28.9	-7.22	-36.05	21.67	01/12/04	5.5	-9.30	-43.35	31.01
01/27/04	2.0	-5.29	-22.45	19.83	01/13/04	38.0	-7.24	-60.05	-2.13
01/31/04	14.6	-5.25	-20.20	21.76	01/14/04	10.0	-8.41	-52.50	14.74
02/01/04	6.2	-7.36	-35.65	23.19	01/15/04	2.5	-4.23	-20.55	13.29
02/02/04	4.6	-3.44	-7.45	20.03	01/23/04	60.0	-4.24	-21.10	12.78
02/03/04	4.1	-2.36	2.60	21.48	01/24/04	17.5	-6.09	-21.65	27.07
02/10/04	3.2	-5.38	-18.10	24.90	01/25/04	12.0	-6.71	-34.95	18.69
02/11/04	5.8	-3.83	-18.30	12.34	01/26/04	34.0	-7.03	-34.00	22.24
02/13/04	18.7	-2.21	-4.40	13.28	01/27/04	2.0	-5.27	-26.40	15.76
02/15/04	10.2	-7.33	-37.05	21.59	01/31/04	13.0	-4.57	-19.90	16.66
02/16/04	20.0	-4.58	-4.55	32.09	02/01/04	7.0	-6.50	-33.90	18.10
02/18/04	6.0	-4.97	-19.75	19.97	02/02/04	4.0	-2.88	-5.05	17.99
02/19/04	8.2	-6.91	-33.40	21.84	02/03/04	5.5	-1.91	14.10	29.38
02/21/04	10.5	-3.28	-8.65	17.59	02/05/04	2.0	-4.28	-23.60	10.64
					02/10/04	0.3	-3.97	-19.85	11.91
					02/11/04	2.5	-1.58	-2.85	9.79
					02/13/04	15.0	-2.46	-2.90	16.74
					02/14/04	39.0	-8.53	-38.35	29.85
					02/15/04	13.0	-4.28	-3.60	30.64

continuation

Banias Nature Reserve					Dan Nature Reserve				
Date	Amount	$\delta^{18}\text{O}$	$\delta^2\text{H}$	d	Date	Amount	$\delta^{18}\text{O}$	$\delta^2\text{H}$	d
	mm	‰	‰	‰		mm	‰	‰	‰
					02/16/04	21.0	-5.11	-21.15	19.73
					02/18/04	7.0	-5.00	-22.15	17.81
					02/19/04	9.5	-6.06	-28.40	20.08
					02/21/04	11.0	-2.83	-8.70	13.94

Table 56: Stable isotope composition ($\delta^{18}\text{O}$, $\delta^2\text{H}$) and amounts of daily rain in Kibutz Mayan Barukh, the Nimrod Nature Reserve and Moshav Shear Yeshuv. N.d.: not determined.

Kibutz Mayan Barukh					Nimrod Nature Reserve					Moshav Shear Yeshuv				
Date	Amount	$\delta^{18}\text{O}$	$\delta^2\text{H}$	<i>d</i>	Date	Amount	$\delta^{18}\text{O}$	$\delta^2\text{H}$	<i>d</i>	Date	Amount	$\delta^{18}\text{O}$	$\delta^2\text{H}$	<i>d</i>
	mm	‰	‰	‰		mm	‰	‰	‰		mm	‰	‰	‰
10/29/03	2.2	-1.11	0.30	9.14	11/09/03	13.0	-4.89	-24.55	14.57	11/08/03	11.8	-4.27	-23.80	10.32
11/08/03	15.9	-4.87	-25.35	13.61	11/10/03	29.0	-5.35	-16.85	25.95	12/04/03	9.7	-8.11	-52.55	12.33
11/09/03	6.5	-4.20	-17.60	15.96	11/11/03	3.0	-3.48	-5.00	22.80	12/05/03	32.0	-9.12	-50.95	21.97
11/11/03	1.0	-1.60	5.45	18.21	11/24/03	6.0	-3.66	-7.75	21.49	12/06/03	6.7	-4.86	-15.55	23.29
11/24/03	0.7	0.41	9.05	5.77	12/04/03	12.0	-9.40	-63.95	11.25	12/17/03	16.5	-2.39	4.80	23.88
12/01/03	0.1	2.31	17.95	-0.53	12/04/03	6.0	-6.30	-27.60	22.76	12/18/03	44.8	-7.14	-31.45	25.63
12/03/03	2.2	-4.19	-15.75	17.77	12/07/03	4.0	-2.62	6.30	27.22	12/26/03	50.2	-10.59	-64.10	20.58
12/04/03	9.6	-8.81	-55.75	14.69	12/17/03	25.0	-4.61	-4.70	32.14	01/01/04	3.1	-3.52	-13.30	14.86
12/05/03	37.7	-5.70	-24.70	20.90	12/18/03	48.0	-8.58	-36.50	32.14	01/05/04	10.0	-2.49	-2.85	17.03
12/06/03	4.0	-5.36	-19.50	23.34	12/19/03	6.0	-8.82	-38.15	32.37	01/06/04	30.8	-5.76	-25.00	21.04
12/07/03	0.6	-2.71	1.90	23.58	12/27/03	31.0	-12.87	-81.60	21.36	01/07/04	24.3	-4.95	-12.55	27.05
12/14/03	0.5	-2.37	-5.10	13.82	12/28/03	n.d.	-13.02	-82.55	21.61	01/08/04	7.8	-6.10	-20.90	27.86
12/17/03	16.2	-2.96	-0.20	23.48	01/01/04	4.0	-4.23	-12.80	21.00	01/09/04	14.0	-6.02	-19.30	28.86
12/26/03	20.4	-10.09	-59.60	21.12	01/05/04	9.0	-3.82	-9.95	20.57	01/12/04	4.9	-6.38	-38.55	12.45
12/27/03	29.0	-10.76	-66.40	19.64	01/06/04	33.0	-6.84	-30.60	24.12	01/14/04	17.0	-9.91	-67.65	11.63
01/05/04	5.8	-3.33	-8.00	18.64	01/07/04	36.0	-6.84	-24.80	29.92	01/22/04	17.2	-4.12	-18.85	14.11
01/06/04	27.2	-6.20	-26.70	22.86	01/08/04	10.0	-7.62	-27.80	33.12	01/23/04	59.9	-5.81	-23.80	22.68
01/07/04	33.5	-5.27	-14.15	28.01	01/09/04	15.0	-6.79	-24.95	29.37	01/24/04	14.5	-5.69	-17.05	28.47
01/09/04	13.1	-6.19	-20.40	29.12	01/12/04	9.0	-8.99	-54.00	17.88	01/25/04	11.8	-6.61	-34.10	18.74
01/12/04	5.3	-6.10	-33.50	15.30	01/13/04	47.0	-10.62	-67.50	17.46	01/26/04	33.8	-6.93	-32.15	23.29
01/13/04	48.1	-9.25	-58.40	15.60	01/14/04	19.0	-11.70	-79.30	14.26	01/31/04	15.4	-4.70	-17.40	20.20
01/14/04	11.8	-6.86	-41.05	13.83	01/22/04	19.0	-7.60	-29.80	30.96	02/01/04	9.3	-6.47	-30.20	21.56

continuation

Kibutz Mayan Barukh					Nimrod Nature Reserve					Moshav Shear Yeshuv				
Date	Amount	$\delta^{18}\text{O}$	$\delta^2\text{H}$	d	Date	Amount	$\delta^{18}\text{O}$	$\delta^2\text{H}$	d	Date	Amount	$\delta^{18}\text{O}$	$\delta^2\text{H}$	d
	mm	‰	‰	‰		mm	‰	‰	‰		mm	‰	‰	‰
01/15/04	1.6	-3.82	-17.50	13.02	01/23/04	82.0	-7.27	-29.60	28.56	02/03/04	5.5	-1.63	5.35	18.39
01/22/04	18.8	-4.33	-23.10	11.50	01/24/04	23.0	-6.74	-24.45	29.47					
01/23/04	59.7	-6.08	-26.00	22.60	01/26/04	32.0	-7.80	-39.30	23.10					
01/24/04	17.1	-5.72	-16.90	28.82	01/31/04	18.0	-6.86	-30.30	24.60					
01/25/04	10.2	-6.87	-37.10	17.90	02/01/04	9.0	-8.04	-40.60	23.70					
01/25/04	10.2	-5.66	-20.10	25.14	02/02/04	5.0	-3.50	-4.50	23.46					
01/26/04	30.3	-7.14	-33.90	23.20	02/03/04	6.0	-3.22	-0.50	25.22					
01/27/04	1.6	-5.31	-24.80	17.70	02/11/04	15.0	-6.90	-33.35	21.85					
02/01/04	7.4	-6.77	-36.30	17.80	02/13/04	20.0	-4.03	-6.05	26.15					
02/02/04	2.7	-3.10	-6.30	18.60	02/14/04	22.0	-7.15	-25.30	31.86					
02/03/04	3.8	-1.93	7.00	22.40	02/15/04	15.0	-7.10	-25.40	31.40					
02/05/04	0.7	-3.66	-16.70	12.60	02/16/04	26.0	-5.63	-21.15	23.89					
02/10/04	0.2	-3.42	-15.25	12.07	02/18/04	8.0	-5.35	-22.55	20.25					
02/11/04	3.4	-2.23	-9.55	8.29	02/19/04	20.0	-7.45	-36.65	22.95					
02/13/04	15.5	-3.09	-9.50	15.18	02/21/04	15.0	-4.08	-10.30	22.30					
02/14/04	36.7	-7.13	-30.30	26.74										
02/15/04	14.0	-4.21	-5.05	28.63										
02/16/04	18.1	-4.82	-19.30	19.22										
02/18/04	3.2	-4.08	-18.70	13.90										
02/19/04	8.9	-6.00	-28.20	19.76										
02/21/04	15.1	-3.11	-11.30	13.58										

Table 57: Stable isotope composition ($\delta^{18}\text{O}$, $\delta^2\text{H}$) and amounts of weekly rain in the Banias and Dan Nature Reserves and Kibutz Mayan Barukh.

Banias Nature Reserve					Dan Nature Reserve					Kibutz Mayan Barukh				
Date	Amount	$\delta^{18}\text{O}$	$\delta^2\text{H}$	d	Date	Amount	$\delta^{18}\text{O}$	$\delta^2\text{H}$	d	Date	Amount	$\delta^{18}\text{O}$	$\delta^2\text{H}$	d
	mm	‰	‰	‰		mm	‰	‰	‰		mm	‰	‰	‰
01/19/03	26	-3.45	-7.30	20.30	01/19/03	22	-2.92	-5.40	17.96	11/12/03	38	-4.45	-16.90	18.70
01/26/03	23	-8.67	-54.00	15.36	01/26/03	24	-8.01	-48.30	15.78	12/08/03	54	-7.03	-36.45	19.75
02/16/03	46	-6.87	-34.90	20.02	01/30/03	62	-8.29	-46.10	20.22	12/20/03	83	-6.54	-25.85	26.47
02/20/03	41	-6.29	-31.90	18.42	02/06/03	90	-8.45	-44.20	23.40	12/29/03	47	-10.69	-63.85	21.63
02/24/03	92	-7.40	-36.10	23.10	02/12/03	22	-3.37	-2.90	24.06	01/19/04	67	-8.72	-53.85	15.91
02/28/03	63	-7.25	-28.00	30.00	02/16/03	43	-6.48	-32.90	18.90	01/31/04	51	-5.98	-27.55	20.25
11/03/03	5	-1.42	-2.50	8.86	02/20/03	41	-4.45	-20.20	15.40	02/08/04	13	-3.04	-9.40	14.88
11/12/03	53	-4.38	-15.95	19.09	02/24/03	86	-6.87	-31.30	23.66	02/23/04	28	-4.13	-16.80	16.20
12/01/03	2	1.12	18.80	9.84	02/28/03	49	-7.11	-27.50	29.34					
12/08/03	25	-5.20	-24.15	17.41	12/08/03	50	-2.44	5.65	25.17					
12/20/03	79	-6.46	-23.05	28.59	12/20/03	70	-6.49	-24.75	27.17					
12/29/03	49	-10.96	-66.75	20.89	12/29/03	43	-10.64	-65.25	19.83					
01/11/04	93	-5.72	-20.95	24.81	01/11/04	92	-5.43	-18.85	24.59					
01/19/04	74	-9.31	-60.30	14.18	01/19/04	62	-9.20	-58.75	14.85					
01/25/04	110	-6.40	-27.15	24.01	01/25/04	87	-5.59	-21.30	23.42					
01/31/04	67	-6.44	-31.30	20.18	01/31/04	54	-6.21	-29.00	20.68					
02/08/04	15	-4.19	-13.40	20.08	02/08/04	15	-3.96	-12.05	19.59					
02/18/04	75	-6.86	-32.15	22.73	02/18/04	121	-5.83	-22.35	24.25					
02/23/04	30	-4.91	-20.90	18.34	02/23/04	26	-4.48	-18.65	17.15					

Table 58: Stable isotope composition ($\delta^{18}\text{O}$, $\delta^2\text{H}$) and amounts of weekly rain in Moshav Neve Ativ, the Nimrod Nature Reserve and Moshav Shear Yeshuv. N.d.: not determined.

Moshav Neve Ativ					Nimrod Nature Reserve					Moshav Shear Yeshuv				
Date	Amount	$\delta^{18}\text{O}$	$\delta^2\text{H}$	d	Date	Amount	$\delta^{18}\text{O}$	$\delta^2\text{H}$	d	Date	Amount	$\delta^{18}\text{O}$	$\delta^2\text{H}$	d
	mm	‰	‰	‰		mm	‰	‰	‰		mm	‰	‰	‰
11/27/02	33	-5.78	-24.10	22.14	01/19/03	38	-4.77	-13.70	24.46	11/27/02	17	-3.52	-11.90	16.26
12/10/02	51	-8.06	-41.50	22.98	01/26/03	21	-9.43	-59.80	15.64	12/14/02	60	-6.22	-28.20	21.56
12/14/02	49	-7.42	-31.50	27.86	01/30/03	70	-8.76	-51.40	18.68	01/07/03	46	-5.36	-23.30	19.58
12/18/02	33	-8.97	-50.30	21.46	02/06/03	126	-9.73	-54.20	23.64	01/19/03	20	-2.57	-4.00	16.56
01/05/03	84	-6.95	-32.60	23.00	02/12/03	35	-4.93	-10.50	28.90	01/26/03	22	-7.81	-48.00	14.48
01/19/03	47	-5.14	-15.80	25.32	02/16/03	55	-7.73	-40.70	21.14	01/30/03	54	-7.88	-46.70	16.34
01/26/03	30	-10.26	-64.00	18.08	02/20/03	46	-5.77	-23.80	22.36	02/06/03	93	-8.50	-45.70	22.30
01/30/03	91	-9.56	-54.30	22.18	02/24/03	100	-8.25	-40.10	25.90	02/12/03	20	-3.26	-1.30	24.78
02/05/03	114	-9.96	-55.60	24.08	02/28/03	70	-7.94	-31.80	31.68	02/16/03	40	-4.87	-21.10	17.82
02/12/03	43	-5.50	-14.90	29.06	11/03/03	6	-1.38	-0.80	10.20	02/20/03	35	-3.90	-17.80	13.36
02/16/03	86	-8.73	-46.20	23.64	11/12/03	56	-5.01	-18.50	21.54	02/24/03	82	-6.82	-31.50	23.06
02/20/03	67	-6.35	-27.30	23.50	12/01/03	5	-1.68	2.10	15.50	02/28/03	54	-6.69	-25.90	27.62
02/24/03	127	-8.48	-41.80	26.04	12/08/03	28	-5.98	-29.55	18.25					
02/28/03	71	-7.32	-27.20	31.32	12/20/03	85	-7.18	-25.80	31.64					
11/03/03	11	-2.75	-8.85	13.11	12/29/03	54	-12.25	-74.90	23.06					
11/12/03	65	-5.44	-20.00	23.52	01/11/04	n.d.	-6.60	-24.60	28.16					
12/01/03	7	-2.23	-0.20	17.64	01/25/04	135	-7.26	-28.80	29.24					
12/08/03	39	-6.63	-31.25	21.75	01/31/04	75	-7.25	-35.85	22.11					
12/20/03	105	-8.52	-34.80	33.36	02/08/04	18	-4.96	-14.35	25.29					
12/29/03	60	-13.39	-82.50	24.58	02/18/04	129	-6.24	-23.05	26.87					
01/11/04		-7.32	-27.85	30.67	02/23/04	43	-6.20	-28.25	21.31					

Table 59: Stable isotope composition ($\delta^{18}\text{O}$, $\delta^2\text{H}$) and amounts of weekly rain in the Orevim catchment and Kibutz Shamir. N.d.: not determined.

Orevim					Kibutz Shamir				
Date	Amount	$\delta^{18}\text{O}$	$\delta^2\text{H}$	d	Date	Amount	$\delta^{18}\text{O}$	$\delta^2\text{H}$	d
	mm	‰	‰	‰		mm	‰	‰	‰
11/12/03	56	-5.16	-17.65	23.63	11/12/03	24	-4.12	-12.65	20.27
12/08/03	51	-5.38	-24.65	18.39	12/08/03	18	-5.11	-24.75	16.09
12/20/03	70	-6.46	-19.50	32.18	12/20/03	39	-5.44	-16.25	27.27
01/02/04	67	-10.72	-63.15	22.61	01/11/04	n.d.	-5.49	-19.85	24.07
01/11/04	n.d.	-6.11	-22.85	26.03	01/19/04	57	-8.56	-54.45	14.03
01/25/04	107	-6.33	-24.30	26.34	01/25/04	68	-5.34	-20.10	22.58
01/31/04	71	n.d.	n.d.	n.d.	01/31/04	59	-6.35	-30.25	20.55
02/10/04	21	-5.02	-14.90	25.22	02/10/04	16	-6.46	-19.50	32.18
02/18/04	76	-5.74	-21.30	24.58	02/18/04	61	-6.27	-22.95	27.21
02/23/04	19	-5.21	-21.10	20.58	02/23/04	16	-4.70	-19.85	17.71

<u>Code</u>	<u>Abbr.</u>	<u>Name in English</u>	<u>Typical Cases*</u> , all at 1200 UTC
1	RST _E	Red Sea Trough with the <u>Eastern</u> axis	2000 Nov 8
2	RST _W	Red Sea Trough with the <u>Western</u> axis	1996 Nov 14
3	RST _C	Red Sea Trough with the <u>Central</u> axis	2002 Nov 29
4	PT-W	Persian Trough (<u>Weak</u>)	2004 Jul 5
5	PT-M	Persian Trough (<u>Medium</u>)	2004 Jul 23
6	PT-D	Persian Trough (<u>Deep</u>)	1972 Jun 21
7	H _E	High to the <u>East</u>	2004 Feb 12
8	H _W	High to the <u>West</u>	2004 Jun 13
9	H _N	High to the <u>North</u>	2004 Feb 26
10	H _C	High over Israel (<u>Central</u>)	1985 Jan 5
11	L _E -D	Low to the <u>East</u> (<u>Deep</u>)	1994 Dec 2
12	CL _S -D	Cyprus Low to the <u>South</u> (<u>Deep</u>)	1992 Feb 3
13	CL _S -S	Cyprus Low to the <u>South</u> (<u>Shallow</u>)	1990 Feb 7
14	CL _N -D	Cyprus Low to the <u>North</u> (<u>Deep</u>)	1992 Jan 31
15	CL _N -S	Cyprus Low to the <u>North</u> (<u>Shallow</u>)	1998 Dec 25
16	L _W	cold Low to the <u>West</u>	2004 Jan 25
17	L _E -S	Low to the <u>East</u> (<u>Shallow</u>)	2002 Dec 18
18	SL _W	Sharav Low to the <u>West</u>	1984 Mar 9
19	SL _C	Sharav Low over Israel (<u>Central</u>)	1980 May 12

*To see typical cases on these dates, download the sea level pressure charts at 1200 UTC over the Eastern Mediterranean region, say 25E-45E, 25N-45N, from the NCEP/NCAR reanalysis, [/www.cdc.noaa.gov](http://www.cdc.noaa.gov).

Figure 66: Explanation of the synoptic systems classified for the Eastern Mediterranean region.

Table 60: Single altitude gradients determined on weekly bulk samples of up to five stations based on $\delta^{18}\text{O}$. NA = Neve Ativ, NNR = Nimrod Nature Reserve, BNR = Banias Nature Reserve, TDNR = Tel Dan Nature Reserve, MSY = Moshav Shear Yeshuv. N.d.: not determined.

Date	NA	NNR	BNR	TDNR	MSY	Slope	Intercept	r^2
	1000 m	750 m	360 m	227 m	100 m			
11/27/02	-5.78	n.d.	n.d.	n.d.	-3.52	-0.0025	-3.27	1.00
12/10/02	-8.06	n.d.	n.d.	n.d.	n.d.	n.d.	n.d.	n.d.
12/14/02	-7.42	n.d.	n.d.	n.d.	-6.22	n.d.	n.d.	n.d.
12/18/02	-8.97	n.d.	n.d.	n.d.	n.d.	n.d.	n.d.	n.d.
01/05/03	-6.95	n.d.	n.d.	n.d.	n.d.	n.d.	n.d.	n.d.
01/07/03	n.d.	n.d.	n.d.	n.d.	-5.36	n.d.	n.d.	n.d.
01/19/03	-5.14	-4.77	-3.45	-2.92	-2.57	-0.0030	-2.31	0.98 ** -0.0030
01/26/03	-10.26	-9.43	-8.67	-8.01	-7.81	-0.0027	-7.53	0.99 ** -0.0027
01/30/03	-9.56	-8.76	n.d.	-8.29	-7.88	-0.0016	-7.77	0.93 *
02/05/03	-9.96	n.d.	n.d.	n.d.	n.d.	n.d.	n.d.	n.d.
02/06/03	n.d.	-9.73	n.d.	-8.45	-8.50	-0.0021	-8.16	0.95 ** -0.0021
02/12/03	-5.50	-4.93	n.d.	-3.37	-3.26	-0.0026	-2.90	0.99 ** -0.0026
02/16/03	-8.73	-7.73	-6.87	-6.48	-4.87	-0.0036	-5.16	0.90 *
02/20/03	-6.35	-5.77	-6.29	-4.45	-3.90	-0.0023	-4.23	0.60
02/24/03	-8.48	-8.25	-7.40	-6.87	-6.82	-0.0020	-6.58	0.97 ** -0.0020
02/28/03	-7.32	-7.94	-7.25	-7.11	-6.69	-0.0008	-6.86	0.48
11/03/03	-2.75	-1.38	-1.42	n.d.	n.d.	-0.0019	-0.53	0.61
11/12/03	-5.44	-5.01	-4.38	n.d.	n.d.	-0.0017	-3.78	1.00 * -0.0017
12/01/03	-2.23	-1.68	1.12	n.d.	n.d.	-0.0054	2.87	0.94
12/08/03	-6.63	-5.98	-5.20	-2.44	n.d.	-0.0045	-2.42	0.76
12/20/03	-8.52	-7.18	-6.46	-6.49	n.d.	-0.0026	-5.67	0.88 *
12/29/03	-13.39	-12.25	-10.96	-10.64	n.d.	-0.0035	-9.74	0.99 ** -0.0035
01/02/04	n.d.	n.d.	n.d.	n.d.	n.d.	n.d.	n.d.	n.d.
01/11/04	-7.32	-6.60	-5.72	-5.43	n.d.	-0.0024	-4.86	1.00 ** -0.0024
01/19/04	n.d.	n.d.	-9.31	-9.20	n.d.	-0.0008	-9.01	1.00
01/25/04	n.d.	-7.26	-6.40	-5.59	n.d.	-0.0030	-5.09	0.94
01/31/04	n.d.	-7.25	-6.44	-6.21	n.d.	-0.0020	-5.74	1.00 ** -0.0020
02/08/04	n.d.	-4.96	-4.19	-3.96	n.d.	-0.0019	-3.51	1.00 -0.0019
02/10/04	n.d.	n.d.	n.d.	n.d.	n.d.	n.d.	n.d.	n.d.
02/18/04	n.d.	-6.24	-6.86	-5.83	n.d.	-0.0003	-6.19	0.02
02/23/04	n.d.	-6.20	-4.91	-4.48	n.d.	-0.0033	-3.72	1.00 ** -0.0033

Table 61: Single altitude gradients determined on weekly bulk samples of up to five stations based on $\delta^2\text{H}$. NA = Neve Ativ, NNR = Nimrod Nature Reserve, BNR = Banias Nature Reserve, TDNR = Tel Dan Nature Reserve, MSY = Moshav Shear Yeshuv. N.d.: not determined.

Date	NA	NNR	BNR	TDNR	MSY	Slope	Intercept	r^2
	1000 m	750 m	360 m	227 m	100 m			
11/27/02	-24.10	n.d.	n.d.	n.d.	-11.90	-0.0136	-10.54	1.000
12/10/02	-41.50	n.d.	n.d.	n.d.	n.d.	n.d.	n.d.	n.d.
12/14/02	-31.50	n.d.	n.d.	n.d.	-28.20	n.d.	n.d.	n.d.
12/18/02	-50.30	n.d.	n.d.	n.d.	n.d.	n.d.	n.d.	n.d.
01/05/03	-32.60	n.d.	n.d.	n.d.	n.d.	n.d.	n.d.	n.d.
01/07/03	n.d.	n.d.	n.d.	n.d.	-23.30	n.d.	n.d.	n.d.
01/19/03	-15.80	-13.70	-7.30	-5.40	-4.00	-0.0138	-2.51	0.990 ** -0.0138
01/26/03	-64.00	-59.80	-54.00	-48.30	-48.00	-0.0185	-45.81	0.972 ** -0.0185
01/30/03	-54.30	-51.40	n.d.	-46.10	-46.70	-0.0090	-44.95	0.962 * -0.0090
02/05/03	-55.60	n.d.	n.d.	n.d.	n.d.	n.d.	n.d.	n.d.
02/06/03	n.d.	-54.20	n.d.	-44.20	-45.70	-0.0148	-42.71	0.898
02/12/03	-14.90	-10.50	n.d.	-2.90	-1.30	-0.0150	0.40	0.998 ** -0.0150
02/16/03	-46.20	-40.70	-34.90	-32.90	-21.10	-0.0233	-23.80	0.864 *
02/20/03	-27.30	-23.80	-31.90	-20.20	-17.80	-0.0071	-20.73	0.227
02/24/03	-41.80	-40.10	-36.10	-31.30	-31.50	-0.0124	-30.13	0.936 **
02/28/03	-27.20	-31.80	-28.00	-27.50	-25.90	-0.0027	-26.76	0.210
11/03/03	-8.85	-0.80	-2.50	n.d.	n.d.	-0.0087	2.05	0.435
11/12/03	-20.00	-18.50	-15.95	n.d.	n.d.	-0.0063	-13.69	0.999 * -0.0063
12/01/03	-0.20	2.10	18.80	n.d.	n.d.	-0.0308	28.59	0.920
12/08/03	-31.25	-29.55	-24.15	5.65	n.d.	-0.0383	2.56	0.622
12/20/03	-34.80	-25.80	-23.05	-24.75	n.d.	-0.0125	-19.79	0.715 *
12/29/03	-82.50	-74.90	-66.75	-65.25	n.d.	-0.0223	-59.32	0.983 ** -0.0223
01/02/04	n.d.	n.d.	n.d.	n.d.	n.d.	n.d.	n.d.	n.d.
01/11/04	-27.85	-24.60	-20.95	-18.85	n.d.	-0.0112	-16.54	0.993 ** -0.0112
01/19/04	n.d.	n.d.	-60.30	-58.75	n.d.	-0.0117	-56.10	1.000
01/25/04	n.d.	-28.80	-27.15	-21.30	n.d.	-0.0121	-20.38	0.691
01/31/04	n.d.	-35.85	-31.30	-29.00	n.d.	-0.0128	-26.36	0.992 ** -0.0128
02/08/04	n.d.	-14.35	-13.40	-12.05	n.d.	-0.0040	-11.50	0.865
02/10/04	n.d.	n.d.	n.d.	n.d.	n.d.	n.d.	n.d.	n.d.
02/18/04	n.d.	-23.05	-32.15	-22.35	n.d.	0.0042	-27.74	0.044
02/23/04	n.d.	-28.25	-20.90	-18.65	n.d.	-0.0185	-14.37	1.000 ** -0.0185

Supplementary data – Chapter 6

Table 62: Physico-chemical parameters and natural tracer concentrations of the Bet HaMekhes spring from 2002 to 2004. N.d.: not determined.

Date	$\delta^{18}\text{O}$ ‰	$\delta^2\text{H}$ ‰	d	T °C	pH	EC µS/cm	DOC mg/L	SiO_2 mg/L	Ca^{2+} mg/L	Mg^{2+} mg/L	Na^+ mg/L	K^+ mg/L	HCO_3^- mg/L	SO_4^{2-} mg/L	Cl^- mg/L	NO_3^- mg/L
10/29/02	-6.38	-30.8	20.3	20.7	8.0	338	n.d.	n.d.	16.2	13.5	36.6	4.4	200	4.3	21.7	11.8
12/03/02	-6.38	-30.1	20.9	19.2	n.d.	355	1.1	26.6	16.8	12.9	33.3	4.7	177	4.1	21.0	11.7
01/10/03	-6.30	-29.7	20.7	18.9	8.2	358	0.9	24.3	16.8	12.7	36.5	4.7	183	4.4	21.6	12.7
06/19/03	-6.45	-30.4	21.2	21.1	8.5	351	n.d.	26.3	18.1	13.8	39.5	4.8	207	4.5	22.6	12.6
10/20/03	-6.46	-30.3	21.4	20.4	8.3	362	1.2	27.2	17.6	14.5	37.6	4.6	195	4.0	20.2	10.4
12/02/03	-6.44	-30.2	21.3	20.1	8.1	361	1.9	27.2	n.d.	n.d.	n.d.	n.d.	171	n.d.	n.d.	n.d.
01/04/04	-6.41	-30.5	20.7	17.8	8.4	356	n.d.	n.d.	15.5	13.3	31.4	3.9	189	4.3	20.8	10.4
02/08/04	-6.32	-29.4	21.2	19.8	8.3	367	1.3	n.d.	18.1	15.9	32.0	4.2	201	4.3	20.8	10.8
03/14/04	-6.39	-29.7	21.4	18.0	9.0	366	1.0	27.0	15.6	15.1	36.5	4.0	207	4.2	20.0	11.3
03/28/04	-6.34	-28.1	22.7	19.8	8.2	362	1.2	29.0	15.9	15.1	32.7	4.3	192	4.3	20.9	11.7
05/04/04	-6.32	-30.5	20.0	19.9	8.2	356	1.4	n.d.	16.0	14.5	30.5	4.1	195	1.2	20.0	10.0
05/31/04	-6.34	-31.6	19.1	20.8	8.2	359	0.9	n.d.	15.7	15.7	38.4	3.6	189	4.0	19.4	10.4
06/14/04	-6.30	-30.1	20.3	21.0	8.3	355	n.d.	25.5	n.d.	n.d.	n.d.	n.d.	n.d.	4.0	19.0	11.1
07/05/04	-6.38	-30.8	20.3	21.3	8.2	361	1.7	n.d.	17.2	14.7	35.3	4.2	198	2.9	19.7	10.3

Table 63: Physico-chemical parameters and natural tracer concentrations of the Divsha spring from 2002 to 2004. N.d.: not determined.

Date	$\delta^{18}\text{O}$ ‰	$\delta^{2}\text{H}$ ‰	d	T °C	pH	EC μS/cm	DOC mg/L	SiO_2 mg/L	Ca^{2+} mg/L	Mg^{2+} mg/L	Na^+ mg/L	K^+ mg/L	HCO_3^- mg/L	SO_4^{2-} mg/L	Cl^- mg/L	NO_3^- mg/L
10/29/02	-6.85	-32.8	22.0	21.3	8.2	302	n.d.	n.d.	27.9	11.7	19.3	3.4	187	8.3	15.0	9.9
12/03/02	-6.77	-33.1	21.1	20.0		321	0.8	31.6	25.4	11.5	20.1	3.2	183	8.2	14.6	9.7
01/10/03	-6.77	-32.8	21.4	20.6	8.4	329	n.d.	35.2	27.3	12.5	18.3	3.6	171	8.2	15.8	13.4
06/19/03	-6.82	-32.9	21.7	21.5	8.7	332	n.d.	34.5	27.9	12.4	21.7	4.3	177	7.3	17.6	14.5
10/20/03	-6.84	-32.7	22.0	21.2	8.4	327	1.0	36.1	24.1	12.6	20.4	3.1	177	6.3	14.6	10.2
12/02/03	-6.86	-32.7	22.1	19.9	8.5	325	1.5	33.8	23.3	14.4	17.8	3.1	177	6.6	14.4	10.4
01/04/04	-6.76	-33.0	21.1	19.0	8.4	318	1.8	n.d.	26.6	14.3	20.4	3.4	177	5.5	14.5	9.9
02/08/04	-6.91	-33.1	22.1	19.3	8.4	329	1.3	39.3	29.1	14.3	20.1	3.6	183	6.7	14.1	11.3
03/14/04	-6.82	-33.8	20.7	18.1	9.6	327	0.8	37.2	25.5	13.6	21.5	3.5	177	6.0	14.1	12.4
03/28/04	-6.77	-33.3	20.9	19.1	8.3	329	1.2	39.9	23.3	14.0	21.3	3.5	183	6.8	15.0	13.4
05/04/04	-6.65	-32.9	20.3	19.3	8.1	332	0.9	35.2	25.6	14.6	22.6	3.2	177	6.6	15.0	12.3
05/31/04	-6.69	-32.1	21.4	19.6	8.3	339	n.d.	33.8	26.6	15.1	23.5	3.2	177	6.6	16.5	11.7
06/14/04	-6.64	-32.5	20.7	19.7	8.3	333	n.d.	32.2	26.3	14.1	20.8	3.3	171	5.4	15.1	10.9
07/05/04	-6.85	-32.8	22.0	20.3	8.1	342	n.d.	n.d.	25.4	13.7	20.7	3.2	177	10.8	15.3	5.0

Table 64: Physico-chemical parameters and natural tracer concentrations of the Dupheila spring from 2002 to 2004. N.d.: not determined.

Date	$\delta^{18}\text{O}$ ‰	$\delta^{2}\text{H}$ ‰	d	T [°C]	pH	EC µS/cm	DOC mg/L	SiO_2 mg/L	Ca^{2+} mg/L	Mg^{2+} mg/L	Na^+ mg/L	K^+ mg/L	HCO_3^- mg/L	SO_4^{2-} mg/L	Cl^- mg/L	NO_3^- mg/L
10/09/02	-6.64	-30.8	22.3	19.7	8.0	394	n.d.	n.d.	39.0	15.5	23.3	6.0	207	8.9	20.7	10.6
10/29/02	-6.73	-32.4	21.4	21.4	7.8	341	n.d.	n.d.	31.2	12.6	22.8	4.8	207	7.9	16.6	13.3
12/03/02	-6.74	-33.2	20.7	20.8	n.d.	354	0.7	30.3	28.7	14.5	22.8	4.1	183	5.7	14.5	10.5
01/10/03	-6.66	-32.0	21.3	20.6	7.7	347	1.1	33.9	30.4	12.3	20.6	4.7	159	9.7	19.1	19.7
10/20/03	-6.75	-32.1	21.9	26.0	8.0	366	1.2	32.6	26.8	14.6	24.1	3.4	195	5.9	15.5	12.5
12/01/03	-6.83	-32.9	21.8	20.0	7.9	359	0.8	32.4	23.7	14.0	25.6	3.9	195	6.2	14.9	13.0
12/08/03	-6.73	-30.4	23.4	19.8	8.0	364	n.d.	n.d.	n.d.	n.d.	n.d.	n.d.	n.d.	6.7	16.9	13.3
01/06/04	-6.70	-32.1	21.5	19.8	8.0	357	0.9	30.2	27.5	13.7	22.0	3.0	195	6.6	16.5	14.4
01/19/04	-6.82	-33.5	21.1	17.3	8.4	319	1.8	30.7	25.8	10.7	18.0	2.9	134	9.3	17.0	20.7
02/10/04	-6.71	-31.3	22.4	18.5	8.1	318	1.1	n.d.	28.2	12.5	18.1	3.1	165	7.5	14.4	14.6
03/14/04	-6.68	-31.3	22.2	18.0	8.2	336	1.2	34.3	27.6	11.5	19.4	3.4	177	7.3	14.8	13.7
03/28/04	-6.67	-31.0	22.4	19.5	8.3	354	1.1	36.3	27.4	13.5	18.3	3.6	195	6.9	15.9	14.1
05/04/04	-6.62	-32.8	20.1	19.3	8.3	351	1.3	n.d.	29.9	14.4	21.0	3.6	201	6.1	15.4	12.1
05/31/04	-6.28	-31.4	18.8	19.1	8.1	334	0.8	32.6	20.2	14.3	27.5	3.1	177	3.9	16.4	8.1
05/31/04	-6.64	-32.3	20.8	19.8	8.4	362	0.7	32.0	30.1	14.5	25.6	3.7	195	5.2	14.8	11.6
06/15/04	-6.57	-34.0	18.6	19.5	8.3	360	1.2	31.9	30.5	16.8	23.8	3.7	195	6.0	15.5	12.4
07/07/04	-6.65	-34.0	19.2	19.8	7.9	364	n.d.	n.d.	29.9	15.0	22.3	3.9	195	4.9	15.7	12.8

Table 65: Physico-chemical parameters and natural tracer concentrations of the Elmin Jedida spring from 2002 to 2004. N.d.: not determined.

Date	$\delta^{18}\text{O}$ ‰	$\delta^2\text{H}$ ‰	d	T [°C]	pH	EC µS/cm	DOC mg/L	SiO_2 mg/L	Ca^{2+} mg/L	Mg^{2+} mg/L	Na^+ mg/L	K^+ mg/L	HCO_3^- mg/L	SO_4^{2-} mg/L	Cl^- mg/L	NO_3^- mg/L
10/29/02	-6.41	-30.0	21.3	20.4	7.5	379	n.d.	n.d.	29.5	15.1	26.0	3.9	229	5.4	20.4	17.1
12/03/02	-6.42	-30.5	20.9	20.2	n.d.	394	0.8	35.4	29.3	18.1	28.6	4.0	207	3.9	19.4	15.6
01/10/03	-6.39	-29.8	21.3	20.4	7.7	396	n.d.	36.0	28.9	14.8	25.1	4.3	207	5.3	20.2	17.0
06/19/03	-6.45	-31.1	20.5	21.1	7.8	398	n.d.	35.2	30.7	16.6	32.0	4.4	207	5.5	21.3	17.3
10/20/03	-6.45	-30.3	21.3	20.3	7.7	404	1.4	35.8	27.2	16.4	26.4	3.3	207	5.0	19.3	16.1
11/20/03	-6.31	-31.3	19.2	20.4	7.9	394	1.2	33.2	n.d.	n.d.	n.d.	n.d.	220	5.4	19.3	17.6
01/04/04	-6.41	-30.4	20.9	20.0	7.6	393	2.0	n.d.	26.8	17.9	25.5	3.5	214	5.0	19.5	15.8
02/08/04	-6.34	-30.1	20.6	20.9	7.7	393	1.2	32.4	27.5	17.3	24.3	3.8	214	5.2	19.6	16.1
03/14/04	-6.40	-29.6	21.6	20.0	7.8	406	1.1	34.9	24.0	18.5	29.0	3.7	214	5.6	19.0	16.7
03/28/04	-6.41	-30.7	20.6	20.4	7.9	405	0.7	37.5	25.1	17.1	26.9	3.8	223	5.2	19.5	16.6
05/04/04	-6.34	-29.7	21.0	20.3	7.6	401	1.3	n.d.	27.6	16.9	27.3	3.7	207	5.1	19.4	15.3
05/31/04	-6.34	-30.2	20.5	20.6	7.6	407	0.5	n.d.	26.9	18.6	29.2	3.4	201	5.1	19.2	15.5
06/14/04	-6.34	-29.6	21.1	20.6	7.7	403	n.d.	33.7	28.6	18.2	27.1	3.8	214	4.0	19.7	14.9
07/05/04	-6.31	-30.6	19.9	20.6	7.7	408	n.d.	n.d.	28.3	17.7	26.6	3.7	220	4.3	19.4	14.9

Table 66: Physico-chemical parameters and natural tracer concentrations of the Gonen spring from 2002 to 2004. N.d.: not determined.

Date	$\delta^{18}\text{O}$ ‰	$\delta^2\text{H}$ ‰	d	T °C	pH	EC µS/cm	DOC mg/L	SiO ₂ mg/L	Ca ²⁺ mg/L	Mg ²⁺ mg/L	Na ⁺ mg/L	K ⁺ mg/L	HCO ₃ ⁻ mg/L	SO ₄ ²⁻ mg/L	Cl mg/L	NO ₃ ⁻ mg/L
10/29/02	-6.79	-31.7	22.6	18.8	8.1	299	n.d.	n.d.	20.0	11.9	21.8	4.7	179	4.6	15.8	13.9
10/29/02	-6.74	-31.6	22.3	19.9	8.2	299	n.d.	n.d.	24.5	11.7	22.1	3.7	183	6.9	15.9	11.4
12/03/02	-7.00	-33.0	23.0	18.1	n.d.	311	1.0	32.2	25.9	11.6	19.6	3.9	159	7.0	15.6	11.1
01/10/03	-6.72	-32.4	21.4	18.1	8.2	323	1.1	30.7	26.5	12.1	20.3	4.1	165	7.1	16.1	14.2
06/19/03	-6.78	-32.8	21.5	19.7	8.7	307	n.d.	34.7	26.5	11.9	22.6	4.3	159	6.7	16.0	4.9
10/20/03	-6.80	-32.1	22.3	19.6	8.4	321	1.4	34.8	25.0	13.3	21.5	3.9	171	5.0	15.4	11.5
12/02/03	-6.76	-32.4	21.6	19.4	8.5	319	0.8	34.2	25.2	13.6	21.7	3.8	177	6.2	14.8	12.3
01/04/04	-6.75	-32.2	21.8	17.1	8.4	315	1.4	n.d.	22.5	14.6	20.5	3.5	162	5.8	14.4	10.9
03/14/04	-6.82	-32.4	22.2	17.0	8.6	315	0.9	36.1	22.9	12.6	21.8	3.7	183	6.4	14.0	13.6
03/28/04	-6.78	-34.6	19.7	18.3	8.3	312	1.0	37.0	21.9	11.8	19.4	3.7	165	6.0	14.0	13.4
05/04/04	-6.75	-33.6	20.4	18.8	8.2	309	1.1	n.d.	22.3	12.7	17.8	3.7	159	5.7	13.9	11.8
05/31/04	-6.68	-32.7	20.7	19.3	8.3	315	1.2	n.d.	23.3	13.6	21.2	3.2	165	5.8	13.9	12.2
06/14/04	-6.68	-31.3	22.2	19.6	8.3	311	0.9	28.9	23.8	14.3	21.0	3.5	165	5.6	13.7	11.9
07/05/04	-6.66	-33.0	20.2	20.4	8.3	332	n.d.	n.d.	25.1	13.3	19.9	3.4	177	4.7	15.3	11.5

Table 67: Physico-chemical parameters and natural tracer concentrations of the Hamroniya spring from 2002 to 2004. N.d.: not determined.

Date	$\delta^{18}\text{O}$ ‰	$\delta^2\text{H}$ ‰	d	T °C	pH	EC µS/cm	DOC mg/L	SiO_2 mg/L	Ca^{2+} mg/L	Mg^{2+} mg/L	Na^+ mg/L	K^+ mg/L	HCO_3^- mg/L	SO_4^{2-} mg/L	Cl^- mg/L	NO_3^- mg/L
10/29/02	-6.79	-32.3	22.0	n.d.	n.d.	n.d.	n.d.	n.d.	n.d.	n.d.	n.d.	n.d.	205	n.d.	n.d.	n.d.
12/03/02	-6.76	-33.3	20.8	19.7	n.d.	363	0.4	37.4	24.1	13.0	26.8	5.0	189	6.1	18.6	15.0
01/10/03	-6.82	-32.4	22.2	19.7	7.8	337	n.d.	38.0	21.8	12.4	24.5	5.5	165	6.2	17.2	16.4
06/19/03	-6.95	-33.8	21.8	18.7	8.9	335	n.d.	35.0	24.3	13.7	28.7	5.1	171	6.6	18.7	17.0
06/19/03	-6.98	-34.2	21.6	18.9	8.1	331	n.d.	34.1	23.2	12.4	23.0	5.2	166	6.5	17.9	17.2
10/20/03	-6.80	-32.2	22.2	19.4	7.8	365	n.d.	38.3	23.2	12.4	23.0	5.2	189	6.5	17.9	17.2
12/01/03	-6.79	-32.3	22.0	19.8	8.0	361	0.8	37.0	22.3	13.2	24.9	5.1	195	5.4	18.1	15.0
01/06/04	-6.74	-32.7	21.2	19.7	8.0	360	1.0	35.4	25.7	15.7	28.4	5.3	183	4.2	18.7	15.6
02/10/04	-6.88	-33.2	21.8	19.2	7.9	303	1.2	n.d.	19.6	13.1	22.1	4.5	159	5.9	14.7	14.3
03/14/04	-7.04	-34.7	21.6	17.8	7.9	325	0.9	38.3	19.3	13.4	23.3	4.0	177	6.6	15.2	13.8
03/28/04	-6.96	-34.2	21.5	18.2	8.1	333	1.0	41.4	20.3	14.6	21.4	4.6	183	6.4	15.9	14.6
04/20/04	-6.93	-31.9	23.5	18.4	8.0	341	1.6	35.7	21.7	13.7	23.1	4.0	183	6.0	15.7	14.5
05/04/04	-6.94	-34.3	21.2	18.5	8.1	331	1.1	n.d.	21.7	14.1	22.7	4.4	171	6.0	16.0	14.7
05/31/04	-6.77	-33.1	21.1	19.0	8.2	350	n.d.	36.5	23.4	14.7	23.9	4.6	171	4.8	17.1	14.2
06/15/04	-6.83	-34.9	19.8	19.0	8.2	351	0.8	n.d.	23.5	14.3	29.2	4.8	183	5.0	16.7	14.1
07/07/04	-6.74	-33.1	20.8	19.3	7.8	358	n.d.	n.d.	23.8	14.8	25.1	4.7	195	4.5	17.5	13.9

Table 68: Physico-chemical parameters and natural tracer concentrations of the Jalabina spring from 2002 to 2004. N.d.: not determined.

Date	$\delta^{18}\text{O}$ ‰	$\delta^2\text{H}$ ‰	d	T °C	pH	EC µS/cm	DOC mg/L	SiO_2 mg/L	Ca^{2+} mg/L	Mg^{2+} mg/L	Na^+ mg/L	K^+ mg/L	HCO_3^- mg/L	SO_4^{2-} mg/L	Cl^- mg/L	NO_3^- mg/L
10/29/02	-6.56	-31.2	21.3	20.2	7.8	308	n.d.	n.d.	16.1	11.1	35.6	3.8	190	4.4	17.6	11.9
12/03/02	-6.65	-31.6	21.6	20.1	n.d.	324	1.2	30.1	16.9	12.9	33.0	3.7	153	3.1	16.9	10.8
01/10/03	-6.54	-31.2	21.1	20.4	8.0	326	n.d.	27.0	15.9	11.7	30.7	3.7	165	4.3	17.9	12.5
06/19/03	-6.74	-32.3	21.6	20.3	8.3	324	n.d.	29.1	16.8	12.3	35.9	3.8	168	4.7	18.4	13.0
10/20/03	-6.63	-31.9	21.2	20.2	7.9	334	n.d.	31.1	n.d.	n.d.	n.d.	n.d.	183	4.2	19.0	12.7
11/20/03	-6.46	-32.2	19.5	20.5	7.8	335	1.4	26.5	14.9	13.0	31.6	3.3	189	4.1	17.3	8.2
01/04/04	-6.48	-30.6	21.2	15.4	8.3	334	4.1	n.d.	19.5	15.1	28.2	3.2	189	5.0	17.6	7.3
02/08/04	n.d.	n.d.	n.d.	20.4	8.0	326	1.0	27.3	16.0	14.2	28.6	3.1	180	4.4	17.1	10.8
03/14/04	-6.48	-30.6	21.2	15.8	8.5	343	1.1	29.7	19.4	14.8	27.7	2.9	189	5.5	16.7	9.5
03/28/04	-6.48	-30.6	21.2	16.9	8.0	340	1.4	33.9	18.9	14.2	27.4	3.2	201	5.4	16.4	8.7
05/04/04	-6.48	-30.6	21.2	18.4	8.0	328	1.4	n.d.	17.9	14.0	29.9	2.8	183	4.9	16.5	8.6
06/14/04	-6.48	-30.6	21.2	20.2	8.1	328	1.3	33.0	19.6	14.2	30.5	3.1	177	5.4	16.9	8.7
07/05/04	-6.48	-30.6	21.2	20.4	8.4	332	1.6	n.d.	16.1	13.5	32.3	3.6	189	3.1	16.9	10.5

Table 69: Physico-chemical parameters and natural tracer concentrations of the Notera spring from 2002 to 2004. N.d.: not determined.

Date	$\delta^{18}\text{O}$ ‰	$\delta^2\text{H}$ ‰	d	T °C	pH	EC µS/cm	DOC mg/L	SiO ₂ mg/L	Ca ²⁺ mg/L	Mg ²⁺ mg/L	Na ⁺ mg/L	K ⁺ mg/L	HCO ₃ ⁻ mg/L	SO ₄ ²⁻ mg/L	Cl ⁻ mg/L	NO ₃ ⁻ mg/L
10/29/02	-6.68	-31.7	21.7	19.8	8.0	313	n.d.	n.d.	22.4	12.8	23.3	5.0	184	6.6	17.8	14.8
12/03/02	-6.67	-31.4	22.0	19.2	n.d.	332	1.0	31.4	23.3	11.7	24.1	4.9	171	6.5	17.2	14.4
01/10/03	-7.36	-31.5	27.4	19.5	8.0	339	n.d.	28.4	21.5	12.7	25.1	5.3	165	6.6	17.6	14.5
06/19/03	-6.68	-31.7	21.7	19.6	8.4	319	n.d.	34.7	24.1	14.9	25.1	4.4	201	4.4	19.9	11.5
06/19/03	-6.67	-31.4	22.0	19.9	8.6	365	n.d.	33.0	19.7	12.2	23.2	5.8	159	7.7	18.2	17.5
10/20/03	-6.71	-31.5	22.2	19.5	8.3	340	2.4	34.2	19.6	14.9	22.0	4.5	171	6.2	17.0	14.3
12/02/03	n.d.	n.d.	n.d.	20.0	8.5	348	0.8	33.2	23.4	15.2	26.3	5.1	171	6.2	17.4	14.4
01/04/04	-6.63	-31.7	21.4	18.9	8.3	335	1.9	n.d.	21.1	15.0	24.7	4.5	171	6.1	16.7	13.7
02/08/04	n.d.	n.d.	n.d.	19.8	8.3	330	1.1	34.5	19.9	13.8	23.6	4.7	165	6.6	16.5	14.0
03/14/04	-6.59	-30.9	21.8	18.9	8.6	325	0.7	35.9	19.4	14.6	25.0	4.7	171	7.0	15.9	15.6
03/28/04	-6.42	-25.1	26.3	19.3	8.1	321	1.0	38.0	17.0	13.6	23.1	5.2	171	7.0	15.8	15.7
03/28/04	-6.57	-33.0	19.6	16.6	8.1	367	1.4	38.0	21.9	17.9	25.1	4.1	211	4.4	18.5	10.4
05/04/04	-6.59	-31.9	20.9	19.1	8.1	322	0.7	34.9	19.5	14.8	25.1	4.9	159	6.6	16.2	15.2
05/04/04	-6.49	-30.9	21.1	17.4	8.1	367	1.6	n.d.	23.7	18.6	25.0	3.4	192	4.2	18.7	9.3
05/31/04	-6.37	-32.6	18.4	19.4	8.2	333	1.0	33.8	20.5	16.4	25.6	5.0	171	6.3	16.4	14.6
05/31/04	-6.54	-33.0	19.4	18.5	8.2	378	1.2	34.9	24.3	19.3	27.5	3.6	201	4.5	20.0	9.6
06/14/04	-6.58	-31.3	21.3	19.7	8.2	332	0.9	n.d.	20.1	14.7	26.0	4.8	165	6.3	16.4	14.7
07/05/04	-6.53	-32.5	19.7	19.7	8.5	331	n.d.	n.d.	20.6	14.5	23.9	5.0	183	5.2	16.7	14.4

Table 70: Physico-chemical parameters and natural tracer concentrations of the Sion spring / stream from 2002 to 2004. N.d.: not determined.

Date	$\delta^{18}\text{O}$ ‰	$\delta^2\text{H}$ ‰	d	T °C	pH	EC µS/cm	DOC mg/L	SiO ₂ mg/L	Ca ²⁺ mg/L	Mg ²⁺ mg/L	Na ⁺ mg/L	K ⁺ mg/L	HCO ₃ ⁻ mg/L	SO ₄ ²⁻ mg/L	Cl ⁻ mg/L	NO ₃ ⁻ mg/L
02/28/03	n.d.	n.d.	n.d.	10.5	8.1	260	0.9	3.6	n.d.	n.d.	n.d.	n.d.	171	n.d.	n.d.	n.d.
03/02/03	n.d.	n.d.	n.d.	11.8	8.2	229	0.9	3.8	57.6	2.7	5.7	0.6	159	4.9	10.6	0.0
03/03/03	n.d.	n.d.	n.d.	10.7	8.1	241	n.d.	0.9	n.d.	n.d.	n.d.	n.d.	159	n.d.	n.d.	n.d.
03/10/03	n.d.	n.d.	n.d.	14.5	8.1	255	n.d.	4.1	47.3	2.7	5.5	0.4	153	5.2	8.9	1.4
03/10/04	n.d.	n.d.	n.d.	10.9	8.0	277	0.7	3.3	48.1	2.6	3.5	0.3	176	4.1	5.9	1.8
03/13/04	n.d.	n.d.	n.d.	11.5	8.1	282	n.d.	n.d.	n.d.	n.d.	n.d.	n.d.	153	n.d.	n.d.	n.d.
03/14/04	-7.75	-38.2	23.8	12.9	8.1	266	1.6	3.1	59.2	3.8	4.2	0.6	153	5.3	5.4	2.8
03/16/04	-7.63	-37.4	23.7	12.0	8.0	263	1.2	3.5	45.5	1.5	3.3	0.4	159	4.3	6.1	1.6
04/05/04	-7.82	-38.9	23.67	10.6	8.0	253	1.2	2.9	42.4	2.2	2.2	0.3	159	3.8	5.1	1.8

Table 71: Physico-chemical parameters and natural tracer concentrations of the Barid spring from 2002 to 2004. N.d.: not determined.

Date	$\delta^{18}\text{O}$ ‰	$\delta^2\text{H}$ ‰	d	T °C	pH	EC µS/cm	DOC mg/L	SiO ₂ mg/L	Ca ²⁺ mg/L	Mg ²⁺ mg/L	Na ⁺ mg/L	K ⁺ mg/L	HCO ₃ ⁻ mg/L	SO ₄ ²⁻ mg/L	Cl ⁻ mg/L	NO ₃ ⁻ mg/L
02/02/03	-7.36	-38.7	20.18	16.4	7.8	369	0.7	n.d.	54.8	1.9	3.6	0.6	186	6.0	6.9	5.4
10/19/03	-7.42	-39.4	19.96	16.0	7.9	321	n.d.	4.8	56.4	3.6	3.7	0.7	201	5.2	6.0	3.2
12/01/03	n.d.	n.d.	n.d.	15.3	8.0	323	0.4	4.8	68.8	3.5	3.7	0.7	220	5.5	6.2	3.8
03/15/04	-7.47	-33.9	25.82	15.5	8.0	312	1.4	n.d.	41.6	2.6	3.8	0.6	174	5.4	6.2	2.7
07/07/04	-7.54	-39.6	20.72	15.0	7.7	312	n.d.	n.d.	50.7	3.3	2.8	0.5	189	4.2	4.8	3.7

Table 72: Physico-chemical parameters and natural tracer concentrations of the Leshem spring from 2002 to 2004. N.d.: not determined.

Date	$\delta^{18}\text{O}$ ‰	$\delta^2\text{H}$ ‰	d	T °C	pH	EC µS/cm	DOC mg/L	SiO_2 mg/L	Ca^{2+} mg/L	Mg^{2+} mg/L	Na^+ mg/L	K^+ mg/L	HCO_3^- mg/L	SO_4^{2-} mg/L	Cl^- mg/L	NO_3^- mg/L
10/29/02	-7.47	-38.2	21.6	15.1	7.6	312	n.d.	n.d.	56.3	4.6	4.0	0.7	207	7.2	6.6	5.1
11/20/02	-7.49	-39.0	21.0	15.2	n.d.	325	0.9	n.d.	61.0	4.7	4.0	0.7	207	7.1	6.2	4.9
12/03/02	-7.46	-39.0	20.7	15.2	n.d.	349	1.5	5.1	59.7	4.5	3.9	0.7	207	7.3	6.4	5.0
12/09/02	-7.42	-39.0	20.4	15.2	n.d.	342	1.2	n.d.	65.5	5.1	3.7	0.7	201	7.3	6.3	5.1
12/10/02	-7.45	-39.3	20.3	15.2	n.d.	346	0.7	n.d.	60.9	4.9	4.0	0.7	195	7.4	6.3	5.0
12/11/02	n.d.	n.d.	n.d.	15.2	n.d.	349	0.7	n.d.	n.d.	n.d.	n.d.	n.d.	201	7.2	6.3	5.0
12/17/02	-7.56	-38.8	21.7	15.2	n.d.	331	0.9	n.d.	54.0	4.4	3.7	0.7	220	7.2	5.9	4.9
12/18/02	-7.48	-39.1	20.7	15.1	7.5	323	1.1	n.d.	58.6	4.3	3.5	0.7	195	7.0	5.8	5.1
12/20/02	-7.43	-39.6	19.8	15.0	n.d.	318	n.d.	n.d.	n.d.	n.d.	n.d.	n.d.	207	n.d.	n.d.	n.d.
12/23/02	-7.48	-39.0	20.8	15.2	7.7	325	n.d.	n.d.	n.d.	n.d.	n.d.	n.d.	238	n.d.	n.d.	n.d.
12/24/02	-7.36	-38.4	20.5	n.d.	7.7	n.d.	n.d.	n.d.	n.d.	n.d.	n.d.	n.d.	220	n.d.	n.d.	n.d.
12/26/02	-7.21	-38.0	19.7	15.3	7.6	314	0.9	n.d.	57.9	3.1	3.5	0.6	207	6.0	6.3	4.7
12/31/02	-7.54	-37.1	23.2	15.3	7.6	328	n.d.	n.d.	53.2	2.9	3.7	0.7	195	6.1	6.7	5.8
01/05/03	-7.28	-38.2	20.0	15.1	7.5	327	1.5	n.d.	44.6	2.9	3.3	0.7	192	6.2	6.5	5.4
01/13/03	-7.32	-38.3	20.3	15.0	7.6	326	0.9	n.d.	59.3	2.9	3.4	0.8	201	6.1	6.7	5.3
01/20/03	-7.35	-39.2	19.6	15.0	7.6	321	0.9	4.4	58.0	3.1	3.5	0.8	189	6.0	6.6	5.3
01/28/03	n.d.	n.d.	n.d.	15.0	7.5	321	0.7	n.d.	58.9	3.2	3.5	0.6	214	6.0	6.3	5.2
02/01/03	n.d.	n.d.	n.d.	15.0	n.d.	320	n.d.	n.d.	n.d.	n.d.	n.d.	n.d.	183	n.d.	n.d.	n.d.
02/02/03	-7.31	-37.9	20.6	15.1	7.5	331	0.9	n.d.	65.6	3.0	4.7	0.7	214	6.0	7.1	5.1
02/10/03	-7.26	-37.9	20.1	15.5	7.5	357	n.d.	4.4	68.6	3.1	3.6	0.6	207	5.9	7.4	5.3
02/16/03	-7.32	-38.5	20.1	15.5	7.7	343	n.d.	3.8	n.d.	n.d.	n.d.	n.d.	189	n.d.	n.d.	n.d.
02/24/03	-7.43	-39.6	19.9	n.d.	7.5	296	n.d.	3.5	n.d.	n.d.	n.d.	n.d.	223	n.d.	n.d.	n.d.
03/02/03	n.d.	n.d.	n.d.	15.6	7.4	293	n.d.	3.9	n.d.	n.d.	n.d.	n.d.	211	n.d.	n.d.	n.d.

continuation

Date	$\delta^{18}\text{O}$ ‰	$\delta^2\text{H}$ ‰	d	T °C	pH	EC µS/cm	DOC mg/L	SiO ₂ mg/L	Ca ²⁺ mg/L	Mg ²⁺ mg/L	Na ⁺ mg/L	K ⁺ mg/L	HCO ³⁻ mg/L	SO ₄ ²⁻ mg/L	Cl ⁻ mg/L	NO ₃ ⁻ mg/L
03/10/03	-7.35	-38.6	20.2	n.d.	n.d.	n.d.	n.d.	n.d.	49.8	1.2	3.7	0.5	207	4.3	7.3	n.d.
03/17/03	-7.39	-38.4	20.7	n.d.	n.d.	333	n.d.	n.d.	54.7	1.2	3.7	0.4	226	4.3	6.4	n.d.
03/24/03	-7.51	-39.9	20.2	n.d.	n.d.	n.d.	n.d.	n.d.	46.9	1.1	3.6	0.5	226	4.4	6.2	n.d.
03/31/03	-7.47	-39.5	20.3	n.d.	n.d.	n.d.	n.d.	n.d.	49.8	1.9	3.7	0.5	211	3.8	6.3	n.d.
04/07/03	-7.41	-37.3	22.0	n.d.	7.3	316	n.d.	4.4	62.3	2.3	3.4	0.4	207	4.6	5.9	0.6
04/14/03	-7.55	-38.9	21.5	n.d.	7.2	306	n.d.	4.3	52.8	2.0	3.5	0.6	214	4.6	5.7	1.0
04/21/03	-7.54	-38.5	21.8	n.d.	7.0	322	n.d.	4.2	63.0	2.6	3.9	0.6	201	4.6	6.2	n.d.
04/28/03	-7.52	-38.3	21.8	n.d.	7.4	308	n.d.	4.4	54.1	2.8	3.4	0.5	204	5.2	5.9	3.4
05/05/03	-7.69	-41.1	20.4	n.d.	7.6	300	1.1	4.1	55.4	3.1	3.4	0.5	207	4.8	5.6	3.7
05/12/03	-7.66	-41.0	20.2	n.d.	7.6	299	0.4	3.3	58.4	3.0	3.5	0.5	207	4.9	5.7	3.7
05/19/03	-7.61	-40.2	20.7	n.d.	7.6	298	0.4	3.2	55.5	3.3	3.2	0.6	217	4.9	5.7	3.8
05/26/03	-7.67	-40.7	20.7	n.d.	7.6	296	0.5	4.2	57.2	2.8	3.4	0.6	189	5.0	5.7	3.7
06/02/03	-7.68	-41.6	19.9	n.d.	7.5	298	1.3	3.2	53.2	2.9	3.1	0.5	204	4.8	5.5	3.7
06/09/03	-7.73	-41.3	20.6	n.d.	7.6	295	0.6	3.2	52.1	3.0	3.5	0.5	195	5.0	5.4	3.7
06/16/03	-7.64	-40.2	20.9	n.d.	7.5	335	n.d.	n.d.	n.d.	n.d.	n.d.	n.d.	207	n.d.	n.d.	n.d.
06/23/03	n.d.	n.d.	n.d.	n.d.	7.7	293	1.7	4.2	56.5	2.9	3.1	0.5	207	4.9	5.3	3.3
06/30/03	n.d.	n.d.	n.d.	n.d.	7.7	292	1.3	4.1	50.2	2.7	2.8	0.5	214	4.7	5.0	3.0
07/07/03	n.d.	n.d.	n.d.	n.d.	7.9	291	14.0	4.1	46.6	2.9	2.9	0.6	189	4.9	5.1	2.3
08/18/03	n.d.	n.d.	n.d.	n.d.	n.d.	n.d.	n.d.	n.d.	50.4	3.3	3.0	0.9	226	4.1	5.2	3.6
10/19/03	-7.45	-38.9	20.7	15.1	7.7	318	1.3	4.9	48.9	3.5	3.0	0.8	220	5.9	5.7	3.5
10/26/03	-7.42	-39.3	20.0	15.1	7.7	321	0.7	5.1	58.5	3.5	3.2	0.6	195	5.3	5.2	3.0
11/03/03	-7.32	-40.2	18.3	n.d.	7.7	321	1.0	4.8	48.5	3.8	3.5	0.5	250	5.0	5.5	3.9
11/09/03	-7.36	-39.5	19.3	15.3	7.9	322	1.0	4.9	51.9	3.8	3.2	0.6	220	6.2	5.6	3.9
11/30/03	-7.41	-38.1	21.2	n.d.	7.8	319	1.0	4.8	54.8	3.5	3.6	0.7	207	6.3	5.8	3.8
12/08/03	-7.19	-38.2	19.4	15.7	7.7	318	0.6	n.d.	52.1	4.1	3.7	0.6	244	5.5	6.0	4.1

continuation

Date	$\delta^{18}\text{O}$ ‰	$\delta^2\text{H}$ ‰	d	T °C	pH	EC µS/cm	DOC mg/L	SiO ₂ mg/L	Ca ²⁺ mg/L	Mg ²⁺ mg/L	Na ⁺ mg/L	K ⁺ mg/L	HCO ₃ ⁻ mg/L	SO ₄ ²⁻ mg/L	Cl ⁻ mg/L	NO ₃ ⁻ mg/L
12/14/03	-7.16	-38.3	19.0	16.1	n.d.	325	1.8	4.7	54.3	4.1	3.8	0.8	217	6.4	5.7	3.3
12/20/03	-7.03	-36.6	19.7	n.d.	7.6	336	6.2	n.d.	58.8	3.6	3.7	0.8	226	6.0	5.6	1.4
12/29/03	-7.03	-37.9	18.3	15.2	n.d.	341	0.8	5.0	54.1	3.9	3.9	0.8	214	6.5	5.8	4.1
01/04/04	-7.11	-37.0	19.9	16.3	7.7	352	2.0	n.d.	52.7	4.1	3.9	0.8	244	6.7	6.0	3.8
01/11/04	-7.13	-37.0	20.1	15.3	7.6	320	1.0	n.d.	58.7	3.9	3.9	0.6	226	6.8	6.1	4.3
01/19/04	-7.28	-36.7	21.5	15.2	7.6	325	0.5	4.2	59.3	2.9	4.2	0.5	220	6.0	6.6	4.2
02/01/04	-7.30	-38.8	19.6	15.8	7.5	342	1.1	5.2	62.6	2.5	4.3	0.6	226	5.3	6.1	3.3
02/08/04	-7.36	-37.8	21.1	16.0	7.5	335	1.0	4.4	61.4	2.2	3.6	0.7	214	5.5	6.0	4.1
02/17/04	-7.48	-39.4	20.4	n.d.	7.5	321	n.d.	n.d.	n.d.	n.d.	n.d.	n.d.	195	4.7	6.1	3.9
02/23/04	-7.55	-38.3	22.1	n.d.	7.5	331	n.d.	n.d.	60.1	2.6	3.9	0.6	171	4.3	6.2	4.0
03/04/04	-7.50	-37.8	22.2	15.6	7.8	324	n.d.	4.4	55.6	2.3	3.9	0.5	201	5.2	5.8	3.1
03/15/04	-7.58	-38.4	22.3	15.3	8.1	301	0.8	3.9	53.2	2.2	3.2	0.5	201	5.2	5.9	3.4
03/29/04	-7.55	-40.3	20.1	15.1	7.6	308	0.7	4.8	52.8	2.3	3.0	0.5	201	4.8	5.3	3.3
04/05/04	-7.62	-38.9	22.1	14.9	7.5	301	0.8	4.8	50.6	2.4	3.0	0.5	214	4.8	5.2	3.4
04/13/04	-7.66	-39.3	22.0	14.8	7.6	296	0.9	4.6	46.8	2.6	2.7	0.5	183	4.7	5.1	3.2
04/20/04	-7.72	-39.1	22.7	14.9	7.5	304	1.7	4.8	51.0	2.5	3.1	0.5	220	4.4	4.8	3.1
05/10/04	-7.73	-41.5	20.3	14.9	7.7	289	1.3	n.d.	53.6	1.7	3.7	0.6	192	3.8	5.2	3.1
06/01/04	-7.66	-41.3	20.0	14.7	n.d.	301	1.1	4.2	49.0	2.4	2.7	0.6	223	4.8	4.5	2.9
07/07/04	-7.50	-40.5	19.5	14.9	7.7	312	n.d.	n.d.	52.0	3.4	3.1	0.6	207	4.3	5.0	3.9

Table 73: Physico-chemical parameters and natural tracer concentrations of the Dan spring from 2002 to 2004. N.d.: not determined.

Date	$\delta^{18}\text{O}$ ‰	$\delta^2\text{H}$ ‰	d	T °C	pH	EC µS/cm	DOC mg/L	SiO_2 mg/L	Ca^{2+} mg/L	Mg^{2+} mg/L	Na^+ mg/L	K^+ mg/L	HCO_3^- mg/L	SO_4^{2-} mg/L	Cl^- mg/L	NO_3^- mg/L
10/29/02	-7.43	-37.6	21.8	15.8	7.4	330	n.d.	n.d.	57.2	4.9	4.3	0.8	250	8.9	7.6	n.d.
11/20/02	-7.40	-37.8	21.4	15.9	n.d.	343	n.d.	n.d.	45.7	5.4	3.9	0.7	244	8.3	6.9	4.9
12/03/02	-7.43	-38.3	21.1	15.8	n.d.	362	1.7	5.7	53.0	5.0	4.0	0.7	244	8.4	7.0	5.0
12/09/02	-7.47	-38.5	21.3	n.d.	n.d.	353	1.0	n.d.	64.2	5.4	4.2	0.8	226	8.4	6.9	4.9
12/10/02	-7.42	-38.5	20.9	15.9	n.d.	362	1.0	n.d.	60.1	4.9	3.8	0.7	220	n.d.	6.9	5.0
12/11/02	-7.46	-38.1	21.6	15.9	n.d.	361	0.9	n.d.	64.5	5.0	4.3	0.8	226	8.1	6.8	4.0
12/17/02	-7.49	-38.2	21.7	15.8	n.d.	350	1.2	n.d.	59.2	4.7	4.2	0.7	214	8.5	6.7	5.1
12/18/02	-7.40	-38.9	20.3	15.8	7.4	342	1.2	n.d.	67.3	5.0	3.7	0.7	268	8.0	6.4	5.1
12/20/02	-7.41	-38.3	21.0	15.7	n.d.	337	1.3	n.d.	60.9	4.6	3.9	0.7	171	8.0	6.7	5.3
12/23/02	-7.38	-38.4	20.6	15.6	7.6	338	n.d.	n.d.	n.d.	n.d.	n.d.	n.d.	201	n.d.	n.d.	n.d.
12/24/02	-7.27	-37.0	21.2	n.d.	7.6	n.d.	n.d.	n.d.	n.d.	n.d.	n.d.	n.d.	201	n.d.	n.d.	n.d.
12/26/02	-7.24	-37.3	20.6	15.7	7.7	329	0.9	n.d.	52.9	3.5	4.1	0.6	201	7.0	6.7	4.7
12/31/02	-7.43	-37.6	21.8	15.8	7.3	342	0.9	n.d.	78.6	3.4	4.7	0.7	214	7.3	7.2	5.8
01/05/03	n.d.	n.d.	n.d.	15.7	7.5	344	0.7	n.d.	46.3	3.6	4.1	0.7	207	7.5	7.0	5.3
01/13/03	-7.35	-37.9	20.9	15.8	7.6	346	1.1	n.d.	61.8	3.5	4.4	0.8	207	7.5	7.0	5.4
01/20/03	-7.38	-39.1	20.0	15.7	7.5	342	1.0	5.1	64.6	3.9	3.9	0.8	207	7.6	7.2	5.3
01/28/03	n.d.	n.d.	n.d.	n.d.	7.4	n.d.	1.1	n.d.	62.5	3.9	4.1	0.7	189	7.6	7.0	5.0
02/01/03	n.d.	n.d.	n.d.	15.6	n.d.	333	n.d.	n.d.	n.d.	n.d.	n.d.	n.d.	n.d.	n.d.	n.d.	n.d.
02/02/03	-7.35	-38.6	20.2	15.7	7.5	346	0.7	n.d.	64.1	3.9	4.1	0.8	207	7.2	7.2	5.4
02/10/03	-7.28	-38.2	20.0	16.0	7.4	370	0.8	n.d.	64.1	3.8	4.4	0.8	238	7.2	7.9	5.3
02/16/03	-7.30	-38.5	19.9	15.9	7.6	357	0.8	4.4	n.d.	n.d.	n.d.	n.d.	220	n.d.	n.d.	n.d.
02/24/03	-7.41	-39.9	19.3	16.9	7.4	328	0.6	4.2	n.d.	n.d.	n.d.	n.d.	207	n.d.	n.d.	n.d.

continuation

Date	$\delta^{18}\text{O}$ ‰	$\delta^2\text{H}$ ‰	d	T °C	pH	EC µS/cm	DOC mg/L	SiO ₂ mg/L	Ca ²⁺ mg/L	Mg ²⁺ mg/L	Na ⁺ mg/L	K ⁺ mg/L	HCO ₃ ⁻ mg/L	SO ₄ 2- mg/L	Cl ⁻ mg/L	NO ₃ ⁻ mg/L
03/02/03	-7.26	-39.2	18.9	16.2	7.4	311	0.6	4.7	n.d.	n.d.	n.d.	n.d.	214	n.d.	n.d.	n.d.
03/10/03	-7.38	-38.2	20.8	n.d.	n.d.	296	n.d.	n.d.	51.8	3.1	4.5	0.4	183	5.8	8.3	n.d.
03/17/03	-7.38	-37.9	21.2	n.d.	n.d.	343	n.d.	n.d.	50.6	3.8	4.4	0.5	214	6.3	8.0	2.9
03/24/03	-7.46	-37.8	21.9	n.d.	n.d.	356	n.d.	n.d.	52.9	3.7	4.4	0.5	207	6.3	7.9	3.9
03/31/03	-7.39	-37.9	21.2	n.d.	n.d.	303	n.d.	n.d.	50.0	3.6	4.4	0.5	189	5.9	7.6	n.d.
04/07/03	-7.42	-37.2	22.2	n.d.	7.4	341	n.d.	5.2	56.9	3.7	4.4	0.6	226	6.2	6.7	1.6
04/21/03	-7.47	-38.0	21.8	n.d.	7.3	334	n.d.	5.2	59.5	3.3	3.8	0.7	226	5.8	6.4	1.0
04/28/03	-7.41	-37.7	21.6	n.d.	7.4	338	n.d.	5.2	62.0	3.8	4.6	0.5	211	5.8	6.4	1.0
05/05/03	-7.54	-39.8	20.5	n.d.	7.5	331	1.1	n.d.	60.7	4.0	4.1	0.6	204	6.8	6.5	4.1
05/12/03	-7.57	-39.5	21.0	n.d.	7.5	337	0.8	n.d.	60.4	4.0	4.4	0.6	207	7.0	6.9	4.3
05/19/03	-7.57	-40.4	20.2	n.d.	7.5	334	0.8	n.d.	59.7	4.1	4.3	0.6	207	7.0	6.7	4.2
05/26/03	-7.62	-40.5	20.5	n.d.	7.5	335	1.2	n.d.	62.0	4.0	4.8	0.6	217	6.9	6.8	4.2
06/02/03	-7.58	-40.3	20.3	n.d.	7.5	333	1.4	n.d.	57.0	3.9	4.3	0.6	204	7.0	6.6	4.3
06/09/03	-7.68	-41.2	20.3	n.d.	7.8	294	1.3	n.d.	53.8	3.2	3.4	0.5	195	4.8	5.2	3.5
06/16/03	-7.58	-40.1	20.6	n.d.	7.5	335	n.d.	n.d.	61.8	4.1	4.1	0.6	207	7.2	6.5	4.2
06/23/03	n.d.	n.d.	n.d.	n.d.	7.7	328	1.1	5.1	57.6	3.8	3.7	0.6	207	5.5	5.6	2.8
06/30/03	n.d.	n.d.	n.d.	n.d.	7.7	323	1.2	5.1	57.4	4.0	4.1	0.7	214	5.4	5.4	2.8
08/18/03	n.d.	n.d.	n.d.	n.d.	n.d.	n.d.	n.d.	n.d.	52.0	4.4	4.0	0.5	195	5.5	5.8	4.0
10/19/03	-7.42	-38.3	21.1	16.0	7.6	355	1.6	6.1	51.9	5.0	4.8	0.8	220	7.5	6.8	3.5
10/26/03	-7.38	-38.7	20.3	16.0	7.6	352	0.6	5.7	55.5	4.5	4.2	0.6	207	7.8	6.3	4.1
11/03/03	n.d.	n.d.	n.d.	n.d.	7.6	353	n.d.	5.6	49.2	4.7	4.3	0.6	217	6.2	6.2	4.1
11/09/03	-7.35	-38.4	20.5	16.2	7.8	354	0.8	5.7	60.0	4.7	3.9	0.7	226	7.5	6.6	4.1
11/30/03	-7.35	-38.3	20.5	n.d.	7.7	355	0.8	5.7	55.6	5.1	4.3	0.7	214	7.6	6.8	3.9
12/08/03	-7.22	-37.8	19.9	16.1	7.7	346	0.8	n.d.	48.2	4.6	4.2	0.6	183	6.2	6.3	3.9
12/14/03	-7.19	-37.1	20.4	n.d.	7.8	354	n.d.	5.6	55.8	4.8	4.4	0.6	220	8.4	6.8	10.8

continuation

Date	$\delta^{18}\text{O}$ ‰	$\delta^2\text{H}$ ‰	d	T °C	pH	EC µS/cm	DOC mg/L	SiO_2 mg/L	Ca^{2+} mg/L	Mg^{2+} mg/L	Na^+ mg/L	K^+ mg/L	HCO_3^- mg/L	SO_4^{2-} mg/L	Cl^- mg/L	NO_3^- mg/L
12/20/03	-7.16	-36.0	21.3	n.d.	7.5	362	0.8	n.d.	54.4	3.9	4.3	0.7	192	7.6	6.7	3.9
12/29/03	-7.11	-38.3	18.6	16.0	n.d.	363	1.6	5.9	59.0	4.7	n.d.	0.7	223	7.6	6.5	4.1
01/04/04	-7.16	-37.2	20.1	16.3	7.6	383	1.7	n.d.	64.3	4.2	4.3	0.7	195	7.7	6.7	4.0
01/11/04	-7.16	-37.3	20.0	16.1	7.5	343	0.7	n.d.	56.3	4.5	4.5	0.6	201	7.6	6.5	4.3
01/19/04	-7.32	-36.9	21.7	15.9	7.6	345	0.9	4.9	52.8	4.0	4.2	0.6	220	7.2	7.0	5.2
02/01/04	-7.28	-37.2	21.1	16.3	7.5	357	1.3	5.6	52.4	3.9	4.5	0.6	195	6.6	6.6	4.1
02/08/04	-7.32	-37.9	20.7	16.4	7.5	353	1.9	5.0	62.1	3.5	4.6	0.7	192	6.6	6.5	4.2
02/17/04	-7.51	-38.6	21.4	n.d.	7.5	346	n.d.	n.d.	55.3	3.1	4.5	0.6	195	n.d.	n.d.	n.d.
02/23/04	-7.36	-36.7	22.2	n.d.	7.3	353	n.d.	n.d.	64.1	3.7	4.6	0.7	n.d.	5.8	7.0	4.6
03/04/04	-7.45	-37.7	21.9	16.4	7.6	351	n.d.	5.2	57.7	3.6	3.8	0.6	223	7.0	6.6	2.6
03/15/04	-7.61	-36.0	24.9	15.9	7.7	325	1.0	4.7	60.5	3.1	4.0	0.6	211	5.0	5.5	2.9
03/29/04	-7.46	-40.3	19.4	16.0	7.6	339	n.d.	5.7	57.0	4.2	4.5	0.6	207	7.0	6.5	4.3
04/05/04	-7.53	-38.4	21.8	15.9	7.5	337	n.d.	5.6	53.1	4.1	4.3	0.5	207	7.3	6.5	4.2
04/13/04	-7.53	-38.7	21.5	16.0	7.4	334	1.0	5.5	54.6	3.7	3.8	0.6	214	6.6	6.4	3.7
04/20/04	-7.56	-38.7	21.8	15.9	7.4	345	0.7	5.6	52.8	3.2	3.8	0.7	201	6.2	5.6	3.3
05/10/04	-7.47	-40.3	19.4	16.0	7.6	328	0.7	5.2	56.3	4.2	4.3	0.5	189	6.2	5.5	3.6
06/01/04	-7.57	-39.6	21.0	15.8	n.d.	341	1.0	5.1	57.9	3.4	3.9	0.6	189	6.4	5.5	3.2
06/16/04	-7.47	-39.9	19.9	15.8	7.6	336	0.8	n.d.	n.d.	n.d.	n.d.	n.d.	226	6.3	5.6	3.5
07/07/04	-7.49	-39.2	20.8	15.6	7.6	337	n.d.	n.d.	56.5	8.6	6.2	1.0	220	8.2	7.2	4.8

Table 74: Physico-chemical parameters and natural tracer concentrations of the Banias spring from 2002 to 2004. N.d.: not determined.

Date	$\delta^{18}\text{O}$ ‰	$\delta^2\text{H}$ ‰	d	T °C	pH	EC µS/cm	DOC mg/L	SiO_2 mg/L	Ca^{2+} mg/L	Mg^{2+} mg/L	Na^+ mg/L	K^+ mg/L	HCO_3^- mg/L	SO_4^{2-} mg/L	Cl^- mg/L	NO_3^- mg/L
10/09/02	-7.41	-37.0	22.3	15.5	7.4	431	n.d.	n.d.	71.5	10.6	9.2	1.4	232	59.4	10.6	5.2
11/20/02	-7.35	-37.3	21.6	15.6	n.d.	458	1.5	n.d.	73.6	11.5	9.7	1.7	256	62.2	10.9	5.6
12/03/02	-7.35	-37.3	21.5	15.7	n.d.	485	0.9	10.1	67.9	11.3	15.1	1.9	244	63.0	11.7	5.8
12/09/02	-7.39	-37.5	21.6	n.d.	n.d.	480	0.9	n.d.	74.2	10.5	11.0	1.7	226	63.7	12.1	5.8
12/10/02	-7.37	-38.2	20.8	15.6	n.d.	485	0.8	n.d.	74.1	11.5	11.2	1.7	232	62.3	11.7	6.0
12/11/02	-7.27	-37.0	21.2	15.6	n.d.	480	0.7	n.d.	72.2	11.6	11.7	1.8	232	56.7	12.1	6.8
12/12/02	-7.34	-34.5	24.2	15.7	n.d.	485	1.0	n.d.	n.d.	n.d.	n.d.	n.d.	244	n.d.	n.d.	n.d.
12/17/02	-7.41	-37.4	21.9	15.1	n.d.	450	1.1	n.d.	72.7	9.6	10.8	1.6	207	48.6	14.1	6.3
12/18/02	-7.36	-38.0	20.9	15.1	7.3	457	1.1	n.d.	72.9	9.5	12.1	1.5	214	51.0	16.5	6.3
12/19/02	-7.38	-38.0	21.0	15.1	7.4	465	0.8	n.d.	69.2	9.2	11.9	1.5	207	53.9	16.3	6.3
12/20/02	-7.43	-38.6	20.8	15.1	7.4	445	1.0	n.d.	71.8	9.0	11.0	1.5	214	52.7	13.7	5.8
12/23/02	n.d.	n.d.	n.d.	14.2	7.7	299	1.8	4.5	52.6	4.4	6.1	0.6	171	13.6	9.0	3.4
12/26/02	-7.55	-39.0	21.4	14.4	7.6	312	0.7	n.d.	n.d.	n.d.	n.d.	n.d.	183	10.5	10.6	10.5
12/31/02	-7.46	-38.0	21.7	14.8	7.5	328	0.9	n.d.	56.3	5.3	6.2	0.9	183	13.4	9.3	5.0
01/05/03	-7.42	-38.3	21.1	14.9	7.7	347	0.8	n.d.	60.3	5.9	6.6	0.9	183	18.5	10.0	5.4
01/13/03	-7.50	-37.9	22.1	14.6	7.4	333	0.8	n.d.	56.4	5.5	5.4	0.8	183	14.3	8.7	4.7
01/19/03	-7.51	-39.3	20.8	14.7	7.5	353	0.8	6.4	57.5	6.3	5.7	1.0	189	20.4	9.1	5.3
01/26/03	-7.50	-39.1	20.9	14.8	7.5	347	0.7	n.d.	55.2	6.1	6.0	0.9	177	17.9	9.8	5.3
02/02/03	-7.57	-38.7	21.8	14.8	7.5	337	0.7	n.d.	58.0	5.4	5.8	0.9	189	12.1	9.8	4.6
02/10/03	-7.49	-37.4	22.5	15.1	7.5	358	1.0	n.d.	57.8	5.3	6.2	0.8	201	11.2	10.0	5.4
02/16/03	-7.59	-39.2	21.5	14.8	7.5	335	0.8	4.1	57.2	4.0	6.5	0.7	195	8.7	11.4	3.7
02/24/03	-7.54	-39.0	21.3	n.d.	7.4	325	0.8	4.5	n.d.	n.d.	n.d.	n.d.	207	n.d.	n.d.	n.d.

continuation

Date	$\delta^{18}\text{O}$ ‰	$\delta^2\text{H}$ ‰	d	T °C	pH	EC µS/cm	DOC mg/L	SiO ₂ mg/L	Ca ²⁺ mg/L	Mg ²⁺ mg/L	Na ⁺ mg/L	K ⁺ mg/L	HCO ₃ ⁻ mg/L	SO ₄ ²⁻ mg/L	Cl ⁻ mg/L	NO ₃ ⁻ mg/L
03/02/03	n.d.	n.d.	n.d.	15.5	7.4	326	0.7	5.2	n.d.	n.d.	n.d.	n.d.	220	n.d.	n.d.	n.d.
03/10/03	-7.65	-39.4	21.8	15.1	7.9	343	1.3	n.d.	62.7	4.7	5.7	1.4	211	8.3	11.1	3.8
03/17/03	-7.47	-39.5	20.3	n.d.	n.d.	n.d.	n.d.	n.d.	42.1	4.9	5.7	0.7	153	7.0	8.8	3.7
03/24/03	-7.44	-39.2	20.3	n.d.	n.d.	n.d.	n.d.	n.d.	58.6	6.6	6.0	0.9	207	20.5	8.9	3.8
06/19/03	-7.48	-38.7	21.1	14.8	7.5	335	1.5	n.d.	57.4	7.5	6.1	0.9	195	21.3	8.3	4.5
08/18/03	n.d.	n.d.	n.d.	n.d.	n.d.	n.d.	n.d.	n.d.	n.d.	n.d.	n.d.	n.d.	207	n.d.	n.d.	n.d.
10/19/03	-7.49	-38.3	21.6	15.5	7.4	464	1.4	9.6	61.8	11.8	8.6	1.3	214	53.9	9.5	2.7
10/26/03	-7.51	-38.2	21.9	15.6	7.5	467	0.8	9.7	68.9	11.7	8.6	1.3	226	53.0	9.0	2.7
10/29/03	-7.36	-38.3	20.6	15.6	7.6	457	3.8	9.4	61.1	12.1	8.9	1.4	226	55.8	9.9	4.5
11/03/03	-7.35	-38.1	20.7	15.7	7.5	468	0.9	9.3	66.3	11.6	8.8	1.3	232	52.7	9.3	4.3
11/09/03	-7.46	-38.1	21.6	15.6	7.7	472	1.7	9.7	66.9	12.5	8.4	1.5	232	57.2	10.1	4.6
11/11/03	n.d.	n.d.	n.d.	15.7	7.5	472	1.3	10.0	68.8	13.5	9.1	1.4	220	56.3	10.0	5.1
11/30/03	-7.57	-38.6	21.9	n.d.	7.6	470	1.1	9.7	73.2	12.8	11.3	1.5	220	60.7	10.9	4.6
12/01/03	-7.35	-38.8	20.0	n.d.	7.8	475	0.7	9.3	69.6	11.9	9.6	1.4	232	57.2	10.0	4.4
12/08/03	-7.46	-37.8	21.9	15.9	7.6	470	0.7	n.d.	65.1	12.7	9.7	1.5	220	56.3	10.0	4.8
12/14/03	-7.47	-37.2	22.6	15.8	n.d.	475	1.5	9.1	66.0	13.6	9.6	1.4	223	59.3	9.7	3.9
12/21/03	-7.30	-36.8	21.6	n.d.	7.4	n.d.	2.2	n.d.	71.3	13.0	12.6	1.8	220	55.9	11.9	6.7
12/29/03	-7.41	-38.4	20.9	15.9	n.d.	499	0.7	10.0	64.5	12.8	9.1	1.5	232	57.3	10.4	5.1
01/04/04	-7.49	-38.0	21.9	15.6	7.5	435	0.7	n.d.	60.5	9.6	8.5	1.3	211	43.8	10.4	5.3
01/11/04	-7.54	-37.3	23.0	15.4	7.4	387	0.9	n.d.	59.7	8.0	8.2	1.0	201	27.7	9.8	5.2
01/14/04	-7.54	-37.9	22.5	n.d.	n.d.	n.d.	3.6	7.4	61.5	7.6	7.7	1.8	214	27.8	10.7	2.4
01/19/04	-7.62	-39.2	21.7	15.2	7.6	335	1.1	5.4	58.3	5.0	7.0	0.8	189	10.9	10.4	4.2
01/25/04	-7.58	-39.1	21.5	n.d.	7.6	349	0.8	5.2	56.4	4.6	6.3	0.8	201	10.2	9.4	3.8
02/01/04	-7.52	-38.5	21.6	15.4	7.5	351	0.9	6.5	55.4	4.3	5.9	0.8	207	9.5	7.7	3.7
02/08/04	-7.49	-38.0	21.9	15.9	7.5	355	1.4	5.6	56.5	6.0	5.7	0.7	195	10.4	9.0	3.8

continuation

Date	$\delta^{18}\text{O}$ ‰	$\delta^2\text{H}$ ‰	d	T °C	pH	EC µS/cm	DOC mg/L	SiO ₂ mg/L	Ca ²⁺ mg/L	Mg ²⁺ mg/L	Na ⁺ mg/L	K ⁺ mg/L	HCO ₃ ⁻ mg/L	SO ₄ ²⁻ mg/L	Cl ⁻ mg/L	NO ₃ ⁻ mg/L
02/17/04	-7.67	-39.5	21.8	n.d.	7.5	337	n.d.	n.d.	55.5	5.0	5.8	0.7	201	9.1	8.7	3.5
02/23/04	-7.58	-38.5	22.1	n.d.	7.4	344	n.d.	n.d.	59.3	4.8	5.4	0.7	207	6.6	8.1	3.5
03/04/04	-7.78	-39.1	23.2	14.9	7.7	303	2.2	4.7	54.1	3.7	5.4	0.4	189	6.6	7.7	2.4
03/14/04	-7.71	-39.1	22.5	14.5	7.9	317	1.1	5.0	52.9	4.4	4.7	0.6	201	7.1	6.8	2.3
03/29/04	-7.70	-39.7	22.0	14.7	7.5	325	1.0	6.6	47.7	5.2	4.9	0.6	201	11.2	7.0	3.2
04/05/04	-7.71	-38.4	23.3	14.2	7.5	311	0.9	6.3	46.2	5.3	4.5	0.6	192	10.5	6.6	3.1
04/13/04	-7.64	-37.8	23.3	14.4	7.5	328	0.9	6.6	51.9	5.9	5.4	0.9	192	14.4	7.1	3.3
04/20/04	-7.68	-37.5	23.9	14.6	7.5	343	0.6	6.6	49.5	6.0	5.2	0.8	207	14.0	6.6	3.1
05/11/04	-7.53	-38.2	22.1	14.9	7.8	342	0.8	11.2	55.7	7.4	6.1	0.7	189	19.5	6.8	3.5
06/01/04	-7.45	-37.3	22.3	15.0	n.d.	382	0.9	7.3	62.7	8.6	7.4	0.9	201	29.7	8.4	3.8
06/16/04	-7.44	-39.0	20.5	15.1	7.5	395	0.7	n.d.	59.0	9.7	7.5	0.9	204	32.7	7.8	3.9
07/12/04	-7.43	-41.6	17.9	15.3	7.4	427	n.d.	n.d.	60.9	10.1	7.1	1.1	214	38.2	8.4	4.3

Table 75: Physico-chemical parameters and natural tracer concentrations of the Kezinim spring from 2002 to 2004. N.d.: not determined.

Date	$\delta^{18}\text{O}$ ‰	$\delta^2\text{H}$ ‰	d	T °C	pH	EC µS/cm	DOC mg/L	SiO_2 mg/L	Ca^{2+} mg/L	Mg^{2+} mg/L	Na^+ mg/L	K^+ mg/L	HCO_3^- mg/L	SO_4^{2-} mg/L	Cl^- mg/L	NO_3^- mg/L
11/20/02	-7.27	-36.0	22.2	20.0	n.d.	572	1.3	n.d.	96.3	15.9	11.6	1.8	268	118.2	11.5	5.0
12/03/02	-7.29	-37.4	21.0	n.d.	n.d.	588	0.9	n.d.	92.8	16.7	11.5	1.9	238	119.3	12.1	5.1
12/10/02	-7.25	-36.5	21.5	19.8	n.d.	598	0.7	n.d.	93.0	17.6	11.4	2.0	244	114.8	11.6	4.8
12/11/02	-7.27	-35.8	22.4	19.8	n.d.	595	0.8	11.7	88.9	17.0	11.1	2.4	238	115.7	11.8	5.1
12/17/02	-7.33	-35.9	22.7	19.5	n.d.	576	0.9	n.d.	91.2	16.3	11.1	2.1	238	105.7	12.1	5.1
12/18/02	-7.28	-36.1	22.1	19.6	7.2	578	1.1	11.3	93.5	15.2	11.5	1.9	232	107.1	13.1	5.3
12/19/02	-7.25	-36.6	21.4	19.4	7.4	580	1.5	n.d.	90.4	15.7	11.1	2.2	238	106.9	13.6	5.5
12/20/02	-7.31	-37.6	20.9	19.3	7.5	586	1.3	n.d.	73.5	16.2	12.1	1.9	189	112.6	13.1	5.0
12/23/02	-7.34	-37.7	21.0	19.1	7.5	511	1.7	n.d.	76.0	12.6	9.0	1.7	226	86.3	11.2	4.1
12/26/02	-7.30	-38.6	19.8	18.8	7.2	501	1.0	n.d.	78.2	12.6	8.3	1.6	214	81.7	10.3	4.0
12/31/02	-7.26	-37.0	21.1	19.3	7.2	514	1.2	9.5	82.0	13.5	9.8	1.5	232	87.8	10.4	4.6
01/05/03	-7.26	-36.7	21.4	19.4	7.3	536	1.4	9.6	82.7	13.7	10.0	1.5	226	88.3	10.6	4.7
01/13/03	-7.27	-38.1	20.1	19.4	7.4	530	1.9	n.d.	76.9	13.2	9.8	1.6	214	87.2	10.4	4.3
01/19/03	-7.27	-37.9	20.3	19.2	7.4	547	1.8	10.6	81.5	13.6	9.4	1.6	214	93.2	10.4	4.8
01/26/03	-7.31	-38.6	19.9	19.6	7.3	541	0.8	n.d.	84.3	13.8	8.7	1.4	238	91.9	10.6	4.2
02/02/03	-7.29	-38.0	20.3	19.6	7.2	532	0.6	n.d.	79.7	13.9	8.7	1.4	226	86.1	10.2	4.2
02/10/03	-7.21	-36.6	21.0	19.5	7.2	551	0.7	10.1	88.9	13.1	9.0	1.4	232	82.9	11.4	5.0
02/16/03	-7.32	-36.7	21.9	19.5	7.3	518	0.8	8.4	85.2	13.1	8.9	1.5	232	83.7	11.1	4.5
02/24/03	-7.12	-37.3	19.7	19.5	7.2	485	0.7	8.0	n.d.	n.d.	n.d.	n.d.	244	n.d.	n.d.	n.d.
03/02/03	n.d.	n.d.	n.d.	19.4	7.3	489	1.6	7.9	n.d.	n.d.	n.d.	n.d.	250	n.d.	n.d.	n.d.
03/10/03	-7.22	-36.6	21.1	19.4	7.6	527	1.3	9.9	91.6	11.4	9.8	1.5	250	77.9	12.9	5.0
06/19/03	-7.23	-36.6	21.2	20.9	7.3	575	n.d.	11.6	89.3	15.4	9.6	1.7	244	118.9	10.9	4.7

continuation

Date	$\delta^{18}\text{O}$ ‰	$\delta^2\text{H}$ ‰	d	T °C	pH	EC µS/cm	DOC mg/L	SiO_2 mg/L	Ca^{2+} mg/L	Mg^{2+} mg/L	Na^+ mg/L	K^+ mg/L	HCO_3^- mg/L	SO_4^{2-} mg/L	Cl^- mg/L	NO_3^- mg/L
08/18/03	n.d.	n.d.	n.d.	n.d.	n.d.	n.d.	n.d.	n.d.	80.5	18.2	10.3	1.7	207	124.4	10.4	4.4
10/19/03	-7.22	-36.3	21.5	20.5	7.3	622	1.7	12.7	88.2	18.8	10.9	1.6	256	127.3	10.4	3.6
10/26/03	-7.23	-37.4	20.5	20.4	7.4	617	1.7	12.6	91.6	17.3	10.8	1.8	244	121.5	10.0	2.6
11/03/03	-7.16	-38.1	19.2	20.5	7.4	617	n.d.	n.d.	n.d.	n.d.	n.d.	n.d.	n.d.	n.d.	n.d.	n.d.
11/30/03	-7.36	-36.6	22.3	20.6	7.4	607	0.8	12.6	85.0	18.2	11.6	1.7	244	121.7	11.1	4.6
12/08/03	-7.29	-36.3	22.0	20.3	7.5	606	0.8	n.d.	84.1	18.3	11.1	1.9	238	121.6	10.7	4.7
12/14/03	-7.21	-35.5	22.2	20.5	7.6	612	1.0	12.2	83.8	18.1	12.3	1.8	238	129.5	11.1	3.5
12/21/03	-7.12	-35.1	21.9	n.d.	7.3	n.d.	1.4	n.d.	86.9	17.0	11.1	1.8	238	122.9	10.9	4.8
12/29/03	-7.23	-37.0	20.8	20.3	n.d.	635	1.0	12.5	91.0	16.7	10.6	1.7	220	122.8	10.7	4.5
01/04/04	-7.29	-36.4	21.9	20.1	7.4	631	0.8	n.d.	89.3	17.9	12.1	1.9	229	119.9	11.1	4.2
01/11/04	-7.33	-36.8	21.8	20.2	7.3	563	0.8	n.d.	82.8	16.1	10.9	1.6	226	107.1	10.9	4.7
01/19/04	-7.38	-37.1	22.0	19.8	7.4	534	0.9	9.6	74.6	13.9	9.3	1.2	229	93.4	10.4	4.2
01/25/04	-7.40	-37.6	21.7	n.d.	7.4	542	0.8	9.5	72.4	14.6	9.1	1.4	232	90.5	9.9	4.3
02/01/04	-7.18	-35.8	21.7	19.8	7.3	539	1.1	11.1	82.0	13.7	8.1	1.3	214	84.9	10.2	3.9
02/17/04	n.d.	n.d.	n.d.	n.d.	7.3	544	n.d.	n.d.	72.3	16.0	9.5	1.4	220	94.0	11.2	4.0
02/23/04	-7.19	-36.1	21.4	n.d.	7.3	547	n.d.	n.d.	85.8	13.5	9.3	1.4	n.d.	86.1	11.0	4.2
03/04/04	-7.33	-35.8	22.8	20.0	7.5	532	1.7	9.9	78.2	10.1	8.0	1.2	253	45.3	9.9	4.1
03/14/04	-7.30	-37.9	20.5	19.7	7.5	545	0.6	9.8	80.9	13.3	7.9	1.4	244	80.8	9.2	3.0
03/29/04	-7.30	-37.4	21.0	19.5	7.3	526	3.4	10.5	80.3	12.2	9.3	1.5	244	73.0	9.7	4.4
04/13/04	-7.30	-36.2	22.2	19.5	7.2	526	0.8	11.1	80.3	14.2	7.7	1.4	235	82.3	9.6	4.0
04/20/04	-7.30	-36.0	22.5	19.6	7.1	556	0.7	10.6	79.9	13.2	8.3	1.4	195	99.2	9.8	3.6
05/11/04	-7.28	-37.8	20.4	20.3	7.6	557	2.0	8.9	82.2	15.8	9.8	1.3	201	100.7	9.5	3.7
06/01/04	-7.16	-36.5	20.8	20.4	n.d.	590	1.7	11.4	80.3	16.7	9.4	1.6	207	108.7	9.7	3.7
07/12/04	-7.35	-39.2	19.6	20.5	n.d.	607	n.d.	n.d.	89.7	18.1	10.4	1.7	n.d.	122.1	10.6	4.7

Supplementary data – Chapter 7

Table 76: Characteristics of baseflow recessions in the Dan stream from 1969 to 2000. X_1 and X_2 both denote the interpolation points of the recession curve, X_0 is the time of the initial baseflow discharge (reconstructed from the recession curve), X_{end} is the end of the recession. Given are the recession constant α , the respective intercept β , the mean residence time of baseflow T_B , the initial baseflow discharge Q_0 , the estimated volume of water in the baseflow reservoir V_B , the recession length Δt_B and the baseflow reservoir change $V_{\Delta t B}$.

Hydr. Year		Date	LN(Q) m ³ /s	α -1/d	β	T_B d	Q_0 m ³ /s	V_B km ³	Δt_B d	$V_{\Delta t B}$ km ³
1970	X_0, X_1	06/01/70	2.15	-0.0018	45	563	8.59	0.42	238	0.144
	X_2	12/06/70	1.82							
	X_{end}	01/25/71								
1971	X_0, X_1	05/28/71	2.19	-0.0014	36	737	8.95	0.57	193	0.131
	X_2, X_{end}	12/07/71	1.93							
1976	X_0, X_1	05/18/76	2.27	-0.0015	42	671	9.66	0.56	190	0.138
	X_2, X_{end}	11/24/76	1.99							
1977	X_0, X_1	05/31/77	2.27	-0.0011	32	917	9.72	0.77	187	0.142
	X_2, X_{end}	12/04/77	2.07							
1978	X_0, X_1	07/05/78	2.30	-0.0017	48	599	9.93	0.51	236	0.167
	X_2	01/06/79	1.98							
	X_{end}	02/26/79								
1979	X_0, X_1	05/08/79	1.94	-0.0027	76	372	6.98	0.22	201	0.094
	X_2, X_{end}	11/25/79	1.40							
1980	X_0, X_1	08/08/80	2.27	-0.0032	91	317	9.74	0.27	140	0.095
	X_2	11/17/80	1.96							
	X_{end}	12/26/80								
1981	X_0, X_1	07/16/81	2.26	-0.0012	35	856	9.54	0.71	168	0.126
	X_2, X_{end}	12/31/81	2.06							
1982	X_0, X_1	07/05/82	2.06	-0.0017	51	588	7.82	0.40	172	0.101
	X_2, X_{end}	12/24/82	1.76							
1983	X_0, X_1	06/21/83	2.34	-0.0021	64	473	10.33	0.42	217	0.155
	X_2	12/31/83	1.93							
	X_{end}	01/24/84								
1984	X_0, X_1	06/30/84	2.21	-0.0013	42	744	9.08	0.58	215	0.146
	X_2	12/13/84	1.98							
	X_{end}	01/31/85								
1985	X_0, X_1	04/21/85	2.22	-0.0023	70	441	9.22	0.35	266	0.159
	X_2	12/06/85	1.70							
	X_{end}	01/12/86								
1986	X_0, X_1	04/22/86	1.96	-0.0029	89	344	7.08	0.21	200	0.093
	X_2	09/05/86	1.56							
	X_{end}	11/08/86								

continuation

Hydr. Year		Date	LN(Q) m ³ /s	α -1/d	β	T _B d	Q ₀ m ³ /s	V _B km ³	Δt_B d	V _{ΔtB} km ³
1987	X _{0, X₁}	06/30/87	2.24	-0.0014	45	722	9.38	0.58	175	0.126
	X ₂	12/05/87	2.02							
	X _{end}	12/22/87								
1988	X _{0, X₁}	04/21/88	2.31	-0.0011	36	906	10.06	0.79	328	0.239
	X ₂	02/24/89	1.97							
	X _{end}	03/15/89								
1989	X _{0, X₁}	04/15/89	2.04	-0.0035	111	285	7.66	0.19	302	0.123
	X ₂	10/12/89	1.40							
	X _{end}	02/11/90								
1990	X _{0, X₁}	05/31/90	1.72	-0.0035	113	284	5.61	0.14	244	0.079
	X ₂	09/06/90	1.38							
	X _{end}	01/30/91								
1991	X _{0, X₁}	05/29/91	1.99	-0.0028	92	355	7.34	0.23	190	0.093
	X ₂	10/01/91	1.64							
	X _{end}	12/05/91								
1992	X _{0, X₁}	04/18/92	2.33	-0.0007	23	1527	10.32	1.36	250	0.206
	X ₂	11/05/92	2.20							
	X _{end}	12/24/92								
1993	X _{0, X₁}	09/05/93	2.18	-0.0023	77	440	8.80	0.33	148	0.096
	X ₂	12/30/93	1.91							
	X _{end}	01/31/94								
1994	X _{0, X₁}	06/27/94	2.11	-0.0020	70	488	8.26	0.35	153	0.094
	X ₂	11/06/94	1.84							
	X _{end}	11/27/94								
1995	X _{0, X₁}	04/30/95	2.22	-0.0019	66	521	9.19	0.41	249	0.157
	X ₂	11/08/95	1.85							
	X _{end}	01/04/96								
1996	X _{0, X₁}	05/27/96	2.23	-0.0019	66	528	9.27	0.42	242	0.155
	X ₂	10/08/96	1.97							
	X _{end}	01/24/97								
1997	X _{0, X₁}	05/21/97	2.23	-0.0016	58	609	9.33	0.49	200	0.137
	X ₂	11/14/97	1.94							
	X _{end}	12/07/97								
1998	X _{0, X₁}	06/16/98	2.22	-0.0018	64	556	9.20	0.44	217	0.143
	X ₂	12/15/98	1.89							
	X _{end}	01/19/99								
1999	X _{0, X₁}	05/27/99	1.97	-0.0033	118	299	7.16	0.19	235	0.101
	X ₂	09/07/99	1.63							
	X _{end}	01/17/00								

Table 77: Characteristics of baseflow recessions in the Hermon stream from 1969 to 2000. X_1 and X_2 both denote the interpolation points of the recession curve, X_0 is the time of the initial baseflow discharge (reconstructed from the recession curve), X_{end} is the end of the recession. Given are the recession constant α , the respective intercept β , the mean residence time of baseflow T_B , the initial baseflow discharge Q_0 , the estimated volume of water in the baseflow reservoir V_B , the recession length Δt_B and the baseflow reservoir change $V_{\Delta t_B}$.

Hydr. Year		Date	LN(Q) m ³ /s	α -1/d	β	T_B d	Q_0 m ³ /s	V_B km ³	Δt_B d	$V_{\Delta t_B}$ km ³
1970	X_0	03/22/70	1.48							
	X_1	06/06/70	1.07	-0.0054	132.02	185	4.38	0.07	259	0.053
	X_2	11/04/70	0.25							
	X_{end}	12/06/70	0.34							
1971	X_0	04/17/71	1.69							
	X_1	07/07/71	1.16	-0.0065	162.66	153	5.43	0.07	228	0.056
	X_2	10/06/71	0.57							
	X_{end}	12/01/71	0.42							
1973	X_0	07/03/73	0.19							
	X_1	08/09/73	0.12	-0.0020	51.39	496	1.21	0.05	128	0.012
	X_2	10/07/73	0.00							
	X_{end}	11/08/73	-0.03							
1974	X_0	04/10/74	1.30							
	X_1	07/09/74	0.81	-0.0054	140.52	184	3.66	0.06	241	0.043
	X_2	09/13/74	0.45							
	X_{end}	12/07/74								
1975	X_0	03/27/75	1.43							
	X_1	07/22/75	0.69	-0.0063	165.34	159	4.18	0.06	227	0.044
	X_2	09/10/75	0.38							
	X_{end}	11/09/75								
1976	X_0	04/19/76	1.36							
	X_1	07/17/76	0.85	-0.0058	153.50	174	3.91	0.06	215	0.042
	X_2	09/22/76	0.46							
	X_{end}	11/20/76								
1977	X_0	04/24/77	1.38							
	X_1	08/13/77	0.65	-0.0066	177.74	152	3.99	0.05	222	0.040
	X_2	10/10/77	0.27							
	X_{end}	12/02/77	0.16							
1979	X_0	03/09/79	0.50							
	X_1	07/12/79	0.13	-0.0029	80.99	341	1.64	0.05	263	0.026
	X_2	09/08/79	-0.04							
	X_{end}	11/27/79								

continuation

Hydr. Year		Date	LN(Q) m ³ /s	α -1/d	β	T _B d	Q ₀ m ³ /s	V _B km ³	Δt_B d	V _{$\Delta t B$} km ³
1980	X ₀	04/04/80	1.02							
	X ₁	08/12/80	0.64	-0.0029	82.69	341	2.78	0.08	248	0.042
	X ₂	12/08/80	0.30							
	X _{end}	12/08/80	0.30							
1981	X ₀	03/27/81	0.90							
	X ₁	09/10/81	0.49	-0.0025	70.89	403	2.47	0.09	256	0.040
	X ₂	11/01/81	0.36							
	X _{end}	12/08/81								
1983	X ₀	03/22/83	1.69							
	X ₁	07/23/83	0.86	-0.0068	197.52	148	5.41	0.07	234	0.055
	X ₂	09/30/83	0.39							
	X _{end}	11/11/83								
1986	X ₀	05/12/86	0.37							
	X ₁	08/18/86	0.08	-0.0030	91.27	331	1.45	0.04	172	0.017
	X ₂	10/03/86	-0.06							
	X _{end}	10/31/86	-0.07							
1987	X ₀	03/27/87	1.26							
	X ₁	09/11/87	0.65	-0.0036	111.46	276	3.53	0.08	258	0.051
	X ₂	10/21/87	0.51							
	X _{end}	12/10/87								
1988	X ₀	03/07/88	1.58							
	X ₁	07/20/88	0.84	-0.0055	170.69	182	4.85	0.08	283	0.060
	X ₂	10/04/88	0.42							
	X _{end}	12/15/88	0.39							
1992	X ₀	03/06/92	1.78							
	X ₁	09/17/92	1.00	-0.0040	129.78	252	5.91	0.13	262	0.083
	X ₂	10/26/92	0.85							
	X _{end}	11/23/92								
1997	X ₀	04/10/97	0.80							
	X ₁	08/30/97	0.32	-0.0034	117.82	291	2.23	0.06	204	0.028
	X ₂	10/15/97	0.16							
	X _{end}	10/31/97								

Table 78: Characteristics of baseflow recessions in the Senir stream from 1969 to 2000. X_1 and X_2 both denote the interpolation points of the recession curve, X_0 is the time of the initial baseflow discharge (reconstructed from the recession curve), X_{end} is the end of the recession. Given are the recession constant α , the respective intercept β , the mean residence time of baseflow T_B , the initial baseflow discharge Q_0 , the estimated volume of water in the baseflow reservoir V_B , the recession length Δt_B and the baseflow reservoir change $V_{\Delta t_B}$.

Hydr. Year		Date	LN(Q) m ³ /s	α -1/d	β	T_B d	Q_0 m ³ /s	V_B km ³	Δt_B d	$V_{\Delta t_B}$ km ³
1971	X_0	04/17/71	0.79							
	X_1	10/05/71	0.47	-0.0019	48	525	2.21	0.10	233	0.036
	X_2	11/26/71	0.37							
	X_{end}	12/06/71								
1972	X_0	04/11/72	0.66							
	X_1	07/10/72	0.45	-0.0023	59	431	1.94	0.07	271	0.034
	X_2	11/24/72	0.14							
	X_{end}	01/07/73	0.21							
1979	X_0	03/09/79	0.27							
	X_1	04/25/79	0.16	-0.0023	65	426	1.31	0.05	263	0.022
	X_2	10/23/79	-0.27							
	X_{end}	11/27/79								
1983	X_0	03/22/83	1.38							
	X_1	08/14/83	0.54	-0.0058	170	172	3.98	0.06	301	0.049
	X_2	09/30/83	0.26							
	X_{end}	01/17/84								
1986	X_0	02/15/86	0.50							
	X_1	05/02/86	0.27	-0.0031	92	328	1.65	0.05	227	0.023
	X_2	09/13/86	-0.14							
	X_{end}	09/30/86								
1987	X_0	03/26/87	1.95							
	X_1	05/13/87	1.44	-0.0107	327	94	7.02	0.06	215	0.051
	X_2	08/16/87	0.42							
	X_{end}	10/27/87								
1992	X_0	02/05/92	2.41							
	X_1	09/19/92	0.71	-0.0075	244	133	11.14	0.13	290	0.114
	X_2	10/25/92	0.44							
	X_{end}	11/21/92								
1997	X_0	04/10/97	0.45							
	X_1	08/31/97	0.13	-0.0022	76	450	1.57	0.06	207	0.022
	X_2	10/29/97	0.00							
	X_{end}	11/03/97								
1998	X_0	03/30/98	0.59							
	X_1	07/18/98	0.33	-0.0024	82	425	1.80	0.07	266	0.031
	X_2	11/02/98	0.08							

	Xend	12/21/98								
1999	X0	04/03/99	0.24							
	X1	05/26/99	0.07	-0.0033	114	307	1.27	0.03	278	0.020
	X2	09/08/99	-0.27							
	Xend	01/06/00								

Table 79: Characteristics of baseflow recessions in the Jordan River from 1991 to 2000. X_1 and X_2 both denote the interpolation points of the recession curve, X_0 is the time of the initial baseflow discharge (reconstructed from the recession curve), X_{end} is the end of the recession. Given are the recession constant α , the respective intercept β , the mean residence time of baseflow T_B , the initial baseflow discharge Q_0 , the estimated volume of water in the baseflow reservoir V_B , the recession length Δt_B and the baseflow reservoir change $V_{\Delta t_B}$.

Hydr. Year		Date	LN(Q) m ³ /s	α -1/d	β	T_B d	Q_0 m ³ /s	V_B km ³	Δt_B d	$V_{\Delta t_B}$ km ³
1992	X_0	02/06/92	3.87							
	X_1	03/21/92	3.59	-0.0065	212	155	48.13	0.64	289	0.545
	X_2	08/11/92	2.67							
	X_{end}	11/21/92								
1993	X_0	03/09/93	3.45							
	X_1	04/26/93	2.91	-0.0114	374	88	31.65	0.24	296	0.232
	X_2	07/15/93	2.00							
	X_{end}	12/30/93								
1994	X_0	03/14/94	3.18							
	X_1	04/01/94	2.91	-0.0151	501	66	23.97	0.14	254	0.134
	X_2	06/21/94	1.68							
	X_{end}	11/23/94								
1995	X_0	02/08/95	3.50							
	X_1	03/24/95	3.01	-0.0111	373	90	32.97	0.26	329	0.250
	X_2	06/17/95	2.06							
	X_{end}	01/03/96								
1997	X_0	04/10/97	3.12							
	X_1	05/16/97	2.55	-0.0158	542	63	22.55	0.12	242	0.121
	X_2	07/16/97	1.58							
	X_{end}	12/08/97								
1998	X_0	03/31/98	3.11							
	X_1	05/09/98	2.58	-0.0135	468	74	22.32	0.14	245	0.138
	X_2	07/14/98	1.69							
	X_{end}	12/01/98								
1999	X_0	04/03/99	2.23							
	X_1	05/06/99	1.66	-0.0171	599	58	9.29	0.05	250	0.046
	X_2	06/10/99	1.06							
	X_{end}	12/09/99	1.51							

Table 80: Hydrological characteristics of runoff events in the Hermon stream in 2002/03 and 2003/04. Q denotes discharges where Q_{initial} , Q_{final} and Q_{peak} are the discharges at the beginning, and at the end of the event and during peak flow, respectively. Temporal features are given as T: times, where T_{start} , T_{end} , T_{peak} are the start, end or peak time of the runoff event. T_{duration} , T_{BF} , T_{interval} and T_{response} denote the duration of the runoff event, the duration of baseflow preceding the event, the interval between events and the time between the start and the peak of the runoff event, respectively. The antecedent precipitation index (API) is calculated as the 2-day or 5-day sum of precipitation preceding the storm event.

Hydr. Year	I	T_{start}	Q_{initial} m ³ /s	T_{end}	Q_{final} m ³ /s	T_{peak}	Q_{peak} m ³ /s	T_{duration} d	T_{BF} d	T_{interval} d	T_{response} h	$Q_{\text{peak}}/Q_{\text{initial}}$	$Q_{\text{final}}/Q_{\text{initial}}$	2-day API mm	5-day API mm	
2002/03	1	12/20/02 00:41	3.2	12/24/02 13:19	4.2	12/20/02 06:03	41.0	4.5				5.4	12.9	1.3	60	82
						12/21/02 00:54	12.8				0.8					
	2	01/28/03 11:35	3.7	02/03/03 02:52	4.8	01/29/03 18:24	26.0	5.6	34.9	39.7	30.8	7.0	1.3	40	61	
						01/30/03 10:20	13.6				0.7					
	3	02/03/03 14:56	4.8	02/08/03 09:05	6.8	02/04/03 15:13	55.0	4.8	0.5	5.2	24.3	11.5	1.4	96	96	
						02/04/03 22:32	21.6				0.3					
	4	02/13/03 13:08	6.8	02/14/03 08:12	14.0	02/14/03 01:05	37.1	0.8	5.2	9.1	12.0	5.5	2.1	35	41	
	5	02/14/03 08:12	14.0	02/16/03 19:45	12.0	02/15/03 08:51	42.6	2.5	0.0	1.3	24.7	3.0	0.9	28	45	
	6	02/18/03 19:14	8.6	02/20/03 19:44	20.0	02/19/03 12:13	46.7	2.0	4.5	4.1	17.0	5.4	2.3	41	47	
2003/04	7	02/20/03 19:44	20.0	02/24/03 06:41	18.8	02/21/03 14:28	135.0	3.5	0.0	2.1	18.7	6.8	0.9	80	121	
	8	03/18/03 12:40	8.9	03/24/03 07:08	15.6	03/19/03 23:03	68.7	5.8	22.2	26.4	34.4	7.7	1.7	61	61	
	9	03/24/03 07:08	15.6	03/31/03 11:40	15.6	03/26/03 15:33	98.0	7.2	0.0	6.7	56.4	6.3	1.0	45	82	
	1	01/13/04 22:02	4.4	01/22/04 10:22	4.7	01/14/04 11:28	46.7	8.5			13.4	10.6	1.1	56	64	
						01/23/04 21:06	41.0				9.4					
	2	01/23/04 07:17	4.7	01/26/04 01:52	9.6	01/24/04 05:03	57.5	2.8	0.9	0.3	21.8	12.4	2.1	82	95	
						01/24/04 11:47	47.3				0.3					
	3	01/26/04 01:52	9.6	01/31/04 10:57	7.6	01/27/04 10:15	29.3	5.4	0.0	2.9	32.4	3.0	0.8	31	124	
	4	02/16/04 09:20	7.3	02/19/04 02:28	11.3	02/17/04 00:48	21.2	2.7	15.9	20.6	15.5	2.9	1.6	0	42	
	5	02/19/04 02:28	11.3	02/21/04 14:15	10.3	02/19/04 20:42	25.6	2.5	0.0	2.8	18.2	2.3	0.9	41	47	
	6	02/21/04 4:15	10.3	02/23/04 03:02	11.0	02/22/04 01:59	20.8	1.5	21.1	2.2	11.7	2.0	1.1	50	126	

Table 81: Hydrological characteristics of runoff events in the Senir stream in 2002/03 and 2003/04. Q denotes discharges where Q_{initial} , Q_{final} and Q_{peak} are the discharges at the beginning, and at the end of the event and during peak flow, respectively. Temporal features are given as T: times, where T_{start} , T_{end} , T_{peak} are the start, end or peak time of the runoff event. T_{duration} , T_{BF} , T_{interval} and T_{response} denote the duration of the runoff event, the duration of baseflow preceding the event, the interval between events and the time between the start and the peak of the runoff event, respectively. The antecedent precipitation index (API) is calculated as the 2-day or 5-day sum of precipitation preceding the storm event.

Hydr. Year	I	T_{start}	Q_{initial} m ³ /s	T_{end}	Q_{final} m ³ /s	T_{peak}	Q_{peak} m ³ /s	T_{duration} d	T_{BF} d	T_{interval} d	T_{response} h	$Q_{\text{peak}}/Q_{\text{initial}}$	$Q_{\text{final}}/Q_{\text{initial}}$	2-day API mm	5-day API mm	
2002/03	1	12/09/02 23:36	0.8	12/18/02 00:46	1.2	12/11/02 11:35	5.3	8.0				36.0	6.7	1.6	32	68
						12/12/02 08:12	4.5			0.9		56.6				
	2	12/18/02 00:46	1.2	01/03/03 12:47	2.7	12/18/02 09:56	2.3				6.1	9.2				
						12/20/02 08:13	179.4	16.5	0.0	1.9		55.5	144.0	2.2	65	93
						12/21/02 02:20	28.0			6.1		73.6				
						12/25/02 04:27	9.2			0.8		171.7				
	3	01/03/03 12:47	2.7	01/15/03 09:27	3.0	01/04/03 22:01	16.4	11.9	0.0	10.7		33.2	6.1	1.1	22	32
	4	01/20/03 23:27	2.7	01/27/03 00:00	2.7	01/21/03 16:28	4.5	6.0	5.6	16.8		17.0	1.7	1.0	27	33
	5	01/27/03 00:00	2.7	02/03/03 19:03	7.3	01/28/03 20:56	20.6	7.8	0.0	7.2		44.9	7.7	2.7	41	41
						01/30/03 01:49	20.2			1.2		73.8				
	6	02/03/03 19:03	7.3	02/08/03 03:11	12.5	02/04/03 09:50	59.4			5.3		201.8				
						02/04/03 16:17	60.1	4.3	0.0	0.3		21.2	8.2	1.7	93	93
	7	02/08/03 03:11	12.5	02/13/03 19:14	12.9	02/09/03 07:32	17.4			5.3		14.8				
						02/10/03 18:24	18.1	5.7	0.0	1.5		63.2	1.4	1.0	14	26
	8	02/13/03 19:14	12.9	02/18/03 21:39	15.3	02/14/03 03:26	52.6	5.1	0.0	3.4		8.2	4.1	1.2	35	39
						02/15/03 11:03	39.0			1.3		39.8				
	9	02/18/03 21:39	15.3	02/24/03 10:49	26.2	02/20/03 04:40	42.0			4.7		31.0				
						02/21/03 18:12	92.5	5.5	0.0	1.6		68.5	6.0	1.7	92	139
						02/24/03 08:25	25.5			2.6		130.8				

continuation

Hydr. Year	I	T _{start}	Q _{initial} m ³ /s	T _{end}	Q _{final} m ³ /s	T _{peak}	Q _{peak} m ³ /s	T _{duration} d	T _{BF} d	T _{interval} d	T _{response} h	Q _{peak/Q_{initial}}	Q _{final/Q_{initial}}	2-day API mm	5-day API mm
10	02/24/03 10:49	26.2	03/18/03 20:26	15.7	02/24/03 17:29 02/25/03 19:27 02/27/03 18:10 03/04/03 03:41 03/07/03 05:52	38.2 36.9 31.4 27.3 24.8	22.4 0.0 1.1 4.4 3.1	0.0	0.4 1.9 1.9 4.4 3.1	6.7 32.6 79.4 184.9 259.0	1.5	0.6	24	117	
11	03/18/03 20:26	15.7	03/24/03 07:08	23.7	03/19/03 21:47	46.1	5.4	0.0	12.7	25.3	2.9	1.5	50	50	
12	03/24/03 07:08	23.7	04/18/03 12:48	16.0	03/24/03 22:20 03/25/03 17:50	38.6 36.9	0.0 5.4	0.0	5.0 0.8	15.2 34.7	0.0	0.0	50	90	
2003/04	1	01/06/04 16:34	1.3	01/13/04 19:31	3.8	01/07/04 15:26 01/08/04 09:00 01/10/04 06:51	18.8 12.9 11.0	7.1	0.0	0.8 0.7 1.9	54.6 40.4 86.3	3.6 0.7 0.0	0.7 2.8 2.1	61	67
2	01/13/04 19:31	3.8	01/22/04 14:09	4.3	01/14/04 10:11	39.0	8.8	0.0	4.1	14.7	10.4	1.1	60	65	
3	01/22/04 14:09	4.3	02/13/04 10:30	9.0	01/24/04 08:54 01/26/04 14:19 01/27/04 09:40 02/01/04 01:27	84.8 24.4 44.9 13.2	21.8 0.0 0.0 0.0	0.0	9.9 2.2 0.8 4.7	42.8 96.2 115.5 227.3	19.7	2.1	77	96	
4	02/13/04 10:30	9.0	03/21/04 14:02	9.5	02/14/04 13:54 02/15/04 23:52 02/16/04 21:43 02/17/04 19:53 02/19/04 15:48 02/22/04 03:12	28.0 22.7 34.0 34.4 32.5 34.8	0.0 37.1	0.0	2.5	27.4 61.4 83.2 105.4 149.3 208.7	3.9	1.1	15	27	

Table 82: Hydrological characteristics of runoff events in the Orevim stream in 2002/03 and 2003/04. Q denotes discharges where Q_{initial} , Q_{final} and Q_{peak} are the discharges at the beginning, and at the end of the event and during peak flow, respectively. Temporal features are given as T: times, where T_{start} , T_{end} , T_{peak} are the start, end or peak time of the runoff event. T_{duration} , T_{BF} , T_{interval} and T_{response} denote the duration of the runoff event, the duration of baseflow preceding the event, the interval between events and the time between the start and the peak of the runoff event, respectively. The antecedent precipitation index (API) is calculated as the 2-day or 5-day sum of precipitation preceding the storm event.

Hydr. Year	I	T_{start}	Q_{initial}	T_{end}	Q_{final}	T_{peak}	Q_{peak}	T_{duration}	T_{BF}	T_{interval}	T_{response}	$Q_{\text{peak}}/Q_{\text{initial}}$	$Q_{\text{final}}/Q_{\text{initial}}$	2-day API	5-day API	
			m^3/s		m^3/s		m^3/s	d	d	d	h			mm	mm	
2002/03	1	12/20/02 01:39	0.1	12/22/02 13:00	0.1	12/20/02 04:53	0.3	2.5				3.2	3.0	1.5	102	136
	2	01/03/03 06:46	0.1	01/05/03 01:21	0.2	01/04/03 14:17	0.2	1.8	11.7	15.4	31.5	1.5	1.2	27	35	
	3	01/27/03 09:29	0.1	01/31/03 11:50	0.5	01/29/03 16:41	8.6	4.1	22.3	25.1	55.2	75.7	4.2	58	95	
	4	02/03/03 21:25	0.4	02/08/03 05:15	0.7	02/04/03 14:02	16.0	4.3	3.4	5.9	16.6	38.3	1.7	117	117	
	5	02/13/03 22:40	0.8	02/15/03 07:22	1.1	02/14/03 04:52	3.4	1.4	5.7	9.6	6.2	4.2	1.4	66	87	
	6	02/15/03 07:22	1.1	02/16/03 14:45	0.9	02/15/03 11:51	6.0	1.3	0.0	1.3	4.5	5.4	0.8	40	100	
	7	02/19/03 10:11	0.8	02/24/03 08:29	1.7	02/21/03 15:08	18.0	4.9	2.8	6.1	53.0	21.6	2.1	110	165	
	8	02/24/03 08:29	1.7	02/27/03 08:26	2.5	02/26/03 08:26	5.8	3.0	0.0	4.7	48.0	3.4	1.5	51	94	
	9	02/27/03 08:26	2.5	02/28/03 17:20	2.3	02/27/03 23:45	5.4	1.4	0.0	1.6	15.3	2.1	0.9	27	111	
	10	03/06/03 14:00	1.1	03/08/03 04:49	1.2	03/06/03 17:27	2.5	1.6	5.9	6.7	3.4	2.3	1.0	31	37	
	11	03/12/03 06:04	0.8	03/15/03 12:11	0.7	03/12/03 11:16	1.6	3.3	4.1	5.7	5.2	2.0	0.9	24	26	
	12	03/19/03 03:08	0.7	03/21/03 16:59	1.3	03/19/03 21:59	15.4	2.6	3.6	7.4	18.8	23.3	1.9	113	113	
	13	03/22/03 13:50	1.5	03/23/03 20:43	1.4	03/22/03 17:10	3.3	1.3	0.9	2.8	3.3	2.2	0.9	22	137	
	14	03/24/03 09:43	1.5	03/30/03 21:03	1.2	03/26/03 07:57	14.3	6.5	0.5	3.6	46.2	9.5	0.8	60	114	
						03/24/03 13:59	6.4				1.9			44	68	
						03/25/03 17:41	9.4				1.2			82	118	

continuation

Hydr. Year	I	T _{start}	Q _{initial} m ³ /s	T _{end}	Q _{final} m ³ /s	T _{peak}	Q _{peak} m ³ /s	T _{duration} d	T _{BF} d	T _{interval} d	T _{response} h	Q _{peak} /Q _{initial}	Q _{final} /Q _{initial}	2-day API mm	5-day API mm	
2003/04	1	01/14/04 02:56	0.4	01/18/04 20:17	0.5	01/14/04 09:33	12.5	4.7				6.6	28.4	1.2	68	81
	2	01/22/04 14:57	0.5	01/26/04 00:52	1.1	01/24/04 05:41	15.4	3.4	3.8	9.8		38.7	30.5	2.1	146	180
	3	01/26/04 00:52	1.1	01/31/04 10:08	1.1	01/27/04 11:22	8.0	5.4	0.0	3.2		34.5	7.5	1.0	43	207
					01/26/04 07:52	3.8					2.1			54	234	
	4	02/01/04 01:28	1.1	02/03/04 15:15	1.1	02/02/04 02:31	1.8	2.6	0.6	5.6		25.0	1.7	1.0	19	19
	5	02/03/04 15:15	1.1	02/05/04 16:48	0.9	02/03/04 21:11	2.5	2.1	0.0	1.8		5.9	2.4	0.9	15	30
	6	02/14/04 11:05	0.7	02/23/04 20:17	1.0	02/17/04 00:09	7.7	9.4	8.8	13.1		61.1	10.2	1.3	70	87

Table 83: Hydrological characteristics of runoff events in the Sion stream in 2002/03 and 2003/04. Q denotes discharges where Q_{initial} , Q_{final} and Q_{peak} are the discharges at the beginning, and at the end of the event and during peak flow, respectively. Temporal features are given as T: times, where T_{start} , T_{end} , T_{peak} are the start, end or peak time of the runoff event. T_{duration} , T_{BF} , T_{interval} and T_{response} denote the duration of the runoff event, the duration of baseflow preceding the event, the interval between events and the time between the start and the peak of the runoff event, respectively. The antecedent precipitation index (API) is calculated as the 2-day or 5-day sum of precipitation preceding the storm event.

Hydr. Year	I	T_{start}	Q_{initial} m ³ /s	T_{end}	Q_{final} m ³ /s	T_{peak}	Q_{peak} m ³ /s	T_{duration} d	T_{BF} d	T_{interval} d	T_{response} h	$Q_{\text{peak}}/Q_{\text{initial}}$	$Q_{\text{final}}/Q_{\text{initial}}$	2-day API mm	5-day API mm	
2002/03	1	12/10/02 04:13	0.0	12/10/02 23:15	0.1	12/10/02 08:14	0.2	0.8				4.0	2080.0	1160.0	90	90
	2	12/19/02 20:04	0.1	12/23/02 23:33	0.0	12/20/02 05:51	3.4	4.1	8.9	9.9	9.8	29.0	0.0	102	136	
	3	01/29/03 16:28	0.0	01/29/03 18:57	0.3	01/29/03 18:57	0.3	0.1	36.7	40.5	2.5	10.0	10.0	58	95	
	4	02/04/03 04:18	0.0	02/13/03 23:04	0.1	02/04/03 19:52	0.2	9.8	5.4	6.0	15.6	160.0	94.0	117	117	
	5	02/13/03 23:04	0.1	02/14/03 17:27	0.4	02/14/03 01:21	1.3	0.8	0.0	9.2	2.3	14.3	4.5	66	87	
	6	02/15/03 07:14	0.5	02/18/03 18:11	0.2	02/15/03 10:36	0.7	3.5	1.3	1.4	3.4	1.6	0.5	40	100	
	7	02/18/03 18:11	0.2	02/19/03 03:38	0.5	02/18/03 22:17	0.7	0.4	0.0	3.5	4.1	3.0	1.9	24	65	
	8	02/19/03 03:38	0.5	02/20/03 12:46	0.6	02/19/03 09:37	1.7	1.4	0.0	0.5	6.0	3.7	1.3	54	70	
	9	02/20/03 12:46	0.6	02/21/03 01:05	0.7	02/20/03 20:56	1.1	0.5	0.0	1.5	8.2	1.9	1.2	73	97	
	10	02/21/03 01:05	0.7	02/22/03 07:19	0.7	02/21/03 11:05	2.1	1.3	0.0	0.6	10.0	2.8	1.0	110	165	
	11	03/18/03 00:00	0.3	03/20/03 11:44	0.3	03/19/03 23:03	1.0	2.5	23.7	26.5	47.1	3.0	0.8	113	113	
	12	03/26/03 08:23	0.3	03/26/03 20:24	0.4	03/26/03 14:22	0.9	0.5	5.9	6.6	6.0	3.3	1.4	60	114	
	13	04/02/03 20:07	0.3	06/13/03 00:00	0.0	04/07/03 12:30	0.8	71.2	7.0	11.9	112.4	2.3	0.0			
2003/04	1	01/14/04 08:05	0.0	01/15/04 19:16	0.0	01/14/04 10:39	1.3	1.5				2.6	64.6	0.0	68	81
	2	01/23/04 19:15	0.0	01/26/04 00:25	0.0	01/24/04 07:46	0.5	2.2	8.0	9.9	12.5	25.5	0.0	146	180	
	3	02/29/04 15:53	0.0	04/11/04 00:00	0.0	03/08/04 16:13	1.2	41.3				192.3	41.3	0.0		

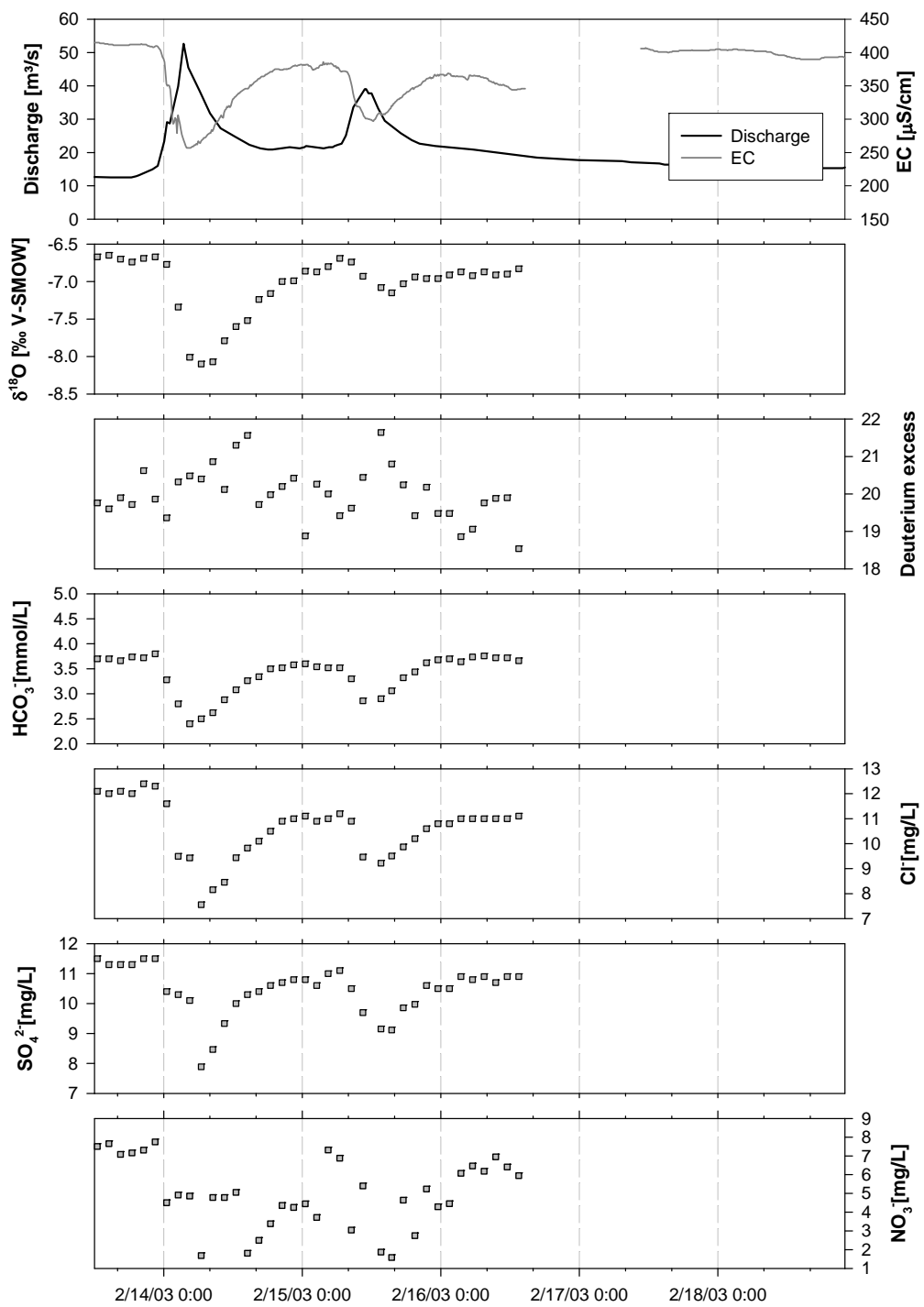


Figure 67: Time-series of discharge, electrical conductivity, temperature, $\delta^{18}\text{O}$, deuterium excess and major anions during 2/14/2003-2/18/2003 in the Senir stream.

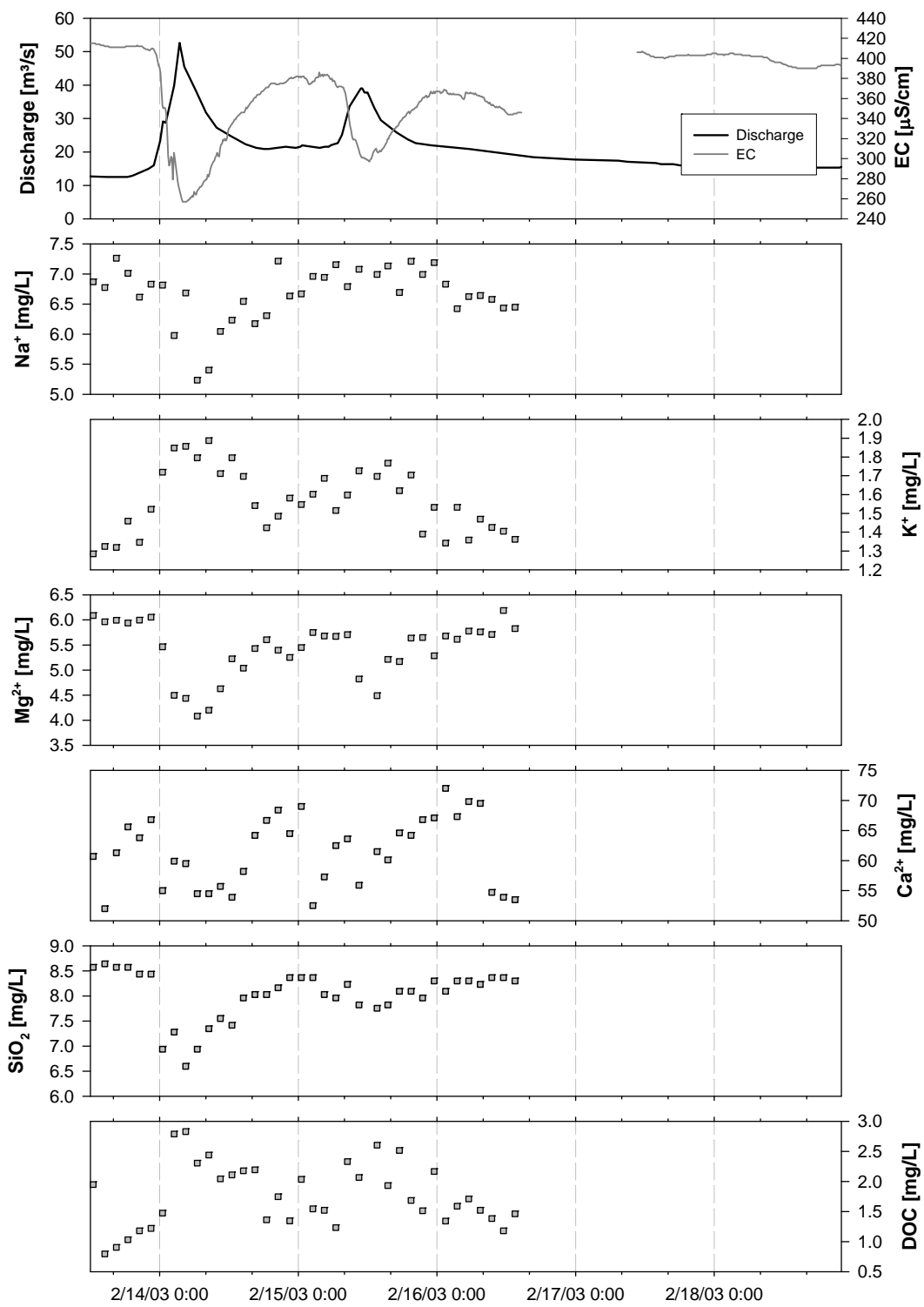


Figure 68: Time-series of discharge, electrical conductivity, temperature, major cations, SiO_2 and DOC during 2/14/2003-2/18/2003 in the Senir stream.

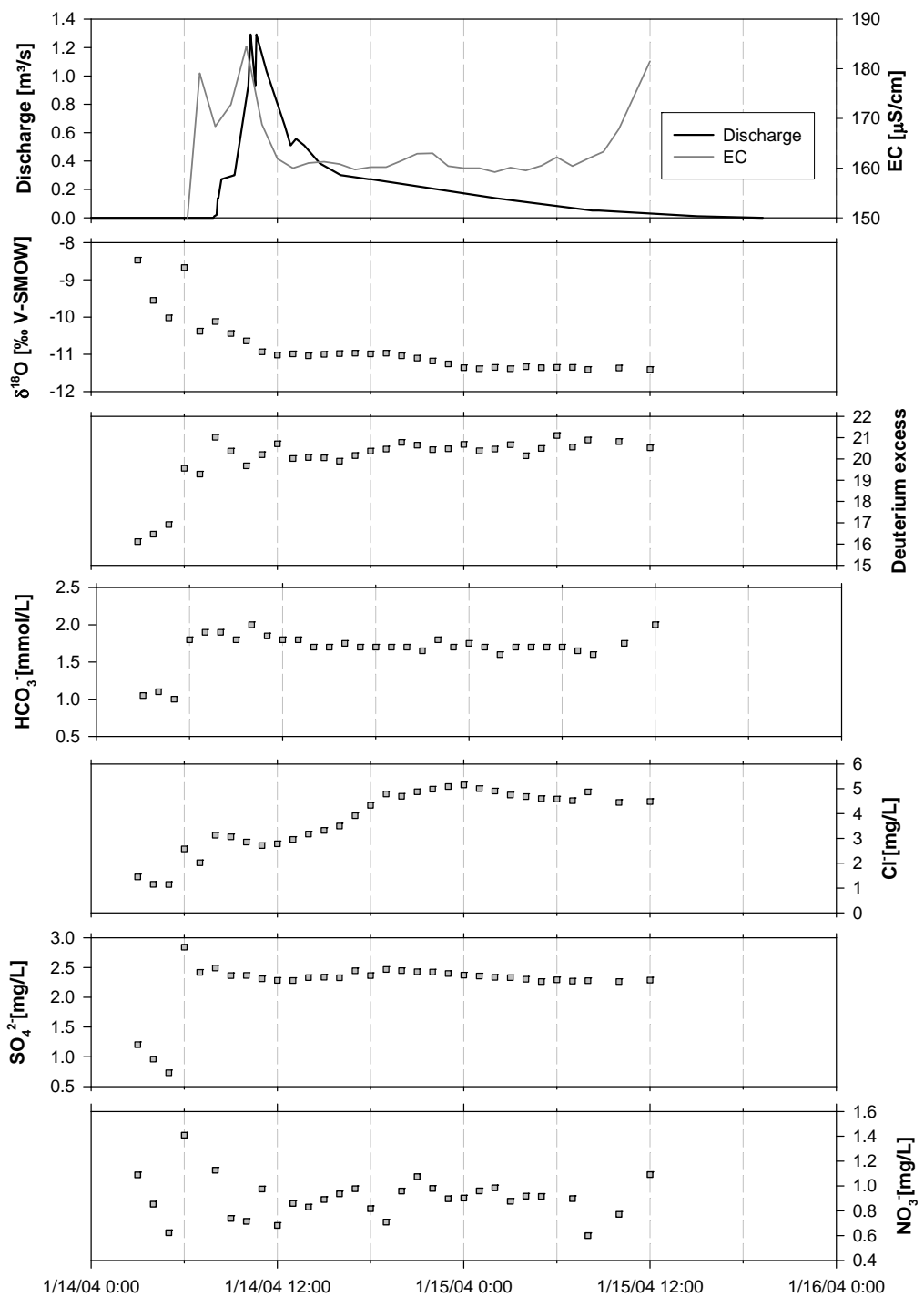


Figure 69: Time-series of discharge, electrical conductivity, temperature, $\delta^{18}O$, deuterium excess and major anions during 1/14/2004-1/18/2004 in the Sion stream.

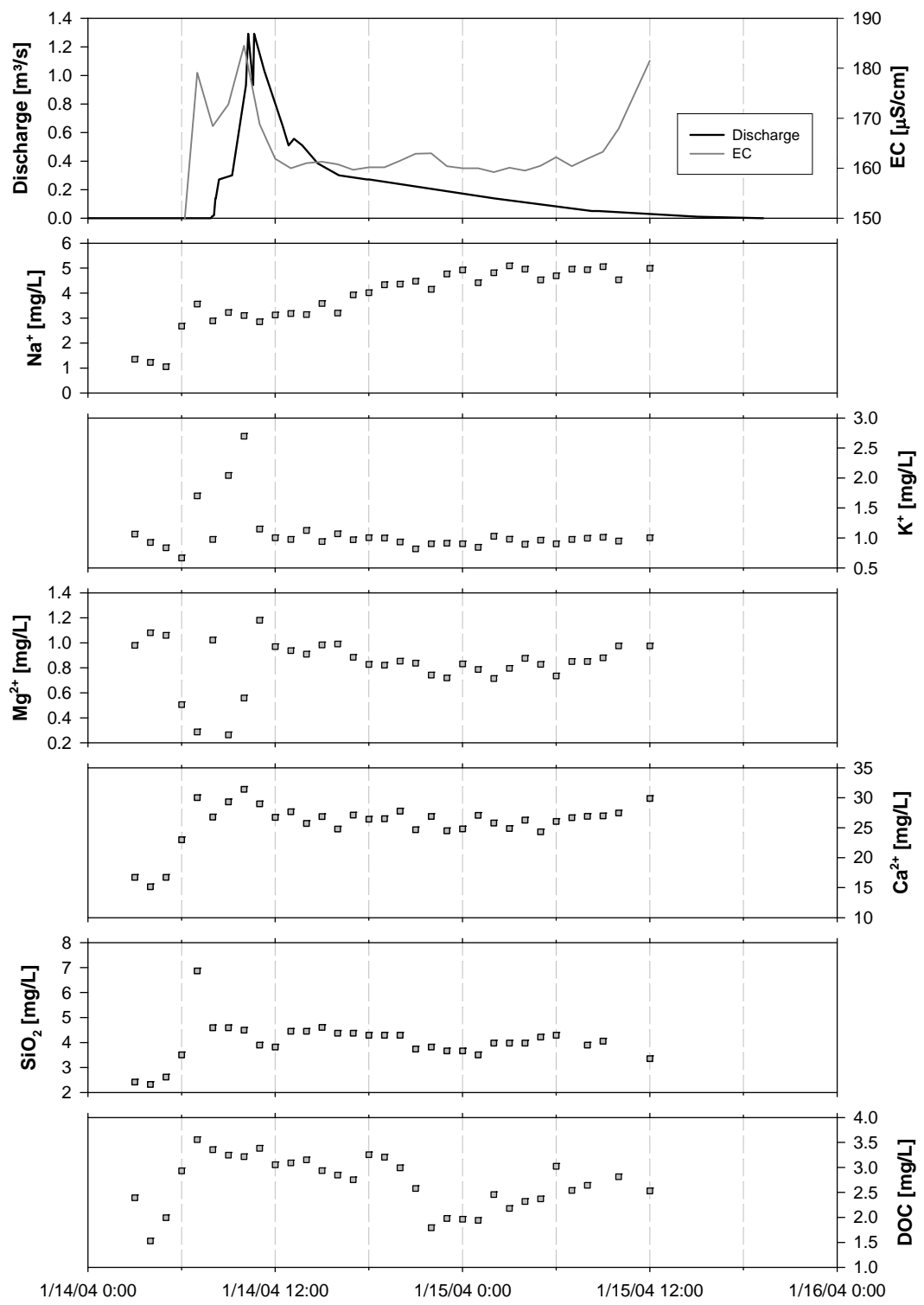


Figure 70: Time-series of discharge, electrical conductivity, temperature, major cations, SiO_2 and DOC during 1/14/2004-1/18/2004 in the Sion stream.

Table 84: Discharge and natural tracer concentrations of the investigated Hermon runoff event (1/13-1/22/2004). N.d.: not determined.

Date/Time	Q m ³ /s	δ ² H ‰	δ ¹⁸ O ‰	d ‰	Cl ⁻ mg/L	NO ₃ ⁻ mg/L	SO ₄ ²⁻ mg/L	HCO ₃ ⁻ mmol/L	Na ⁺ mg/L	K ⁺ mg/L	Mg ²⁺ mg/L	Ca ²⁺ mg/L	SiO ₂ mg/L	DOC mg/L	TSS mg/L	EC µS/cm	T °C
1/12/2004 12:00	4.39	-36.2	-7.1	20.6	12.5	7.6	36.44	3.70	10.48	1.44	11.05	69.2	10.2	1.17	12	440	15.6
1/12/2004 14:00	4.39	-37.1	-7.14	20.1	12.3	7.3	36.08	3.70	10.38	1.38	10.87	70.4	10.1	1.40	27	439	15.4
1/12/2004 16:00	4.39	-36.9	-7.09	19.9	12.2	5.7	36.02	3.70	10.41	1.51	10.80	69.0	9.9	1.35	8	437	15.1
1/13/2004 0:00	4.39	-36.6	-7.13	20.5	12.5	8.2	36.82	3.60	10.61	1.57	11.13	69.1	10.4	1.41	41	435	14.7
1/13/2004 12:00	4.39	-35.4	-7.18	22.0	12.0	7.3	35.74	3.75	10.17	1.43	10.92	69.2	10.0	n.d.	25	436	15.7
1/13/2004 16:00	4.39	-35.8	-7.2	21.8	12.0	5.0	35.88	3.90	10.23	1.43	10.08	69.8	9.9	3.73	11	435	15.8
1/13/2004 18:00	4.39	-36.2	-7.29	22.1	11.2	6.8	33.14	3.80	8.60	1.38	10.46	62.6	10.6	1.10	n.d.	432	15.7
1/13/2004 19:00	4.39	-36.0	-7.3	22.4	11.1	6.5	33.04	3.70	8.52	1.41	10.74	63.3	10.4	1.49	n.d.	433	15.6
1/13/2004 20:00	4.39	-36.3	-7.29	22.0	11.1	6.6	33.01	3.70	9.17	1.36	9.84	63.8	10.4	1.35	n.d.	419	15.5
1/13/2004 21:00	4.39	-35.6	-7.25	22.4	11.0	7.0	32.83	3.60	9.76	1.31	10.03	67.0	10.3	1.55	n.d.	432	15.5
1/13/2004 22:00	4.39	-36.1	-7.28	22.1	10.8	6.6	32.30	3.50	8.99	1.56	9.66	66.6	10.3	1.66	n.d.	433	15.4
1/13/2004 23:00	4.65	-36.3	-7.24	21.6	10.7	6.2	32.03	3.55	9.05	1.48	9.54	64.4	10.3	1.35	n.d.	436	15.3
1/14/2004 0:00	5.25	-35.8	-7.22	21.9	12.1	7.4	38.56	3.70	9.43	1.70	10.09	67.2	10.5	1.43	n.d.	448	15.0
1/14/2004 1:00	5.25	-35.9	-7.26	22.2	12.3	7.8	37.54	3.60	9.29	1.77	10.55	67.4	10.6	1.83	n.d.	427	14.8
1/14/2004 2:00	5.70	-36.4	-7.3	22.0	11.0	6.3	32.53	3.40	8.19	1.88	10.07	65.1	11.0	2.09	n.d.	410	14.6
1/14/2004 3:00	5.70	-37.0	-7.36	21.9	11.4	8.3	28.24	3.40	8.97	2.14	9.11	58.7	10.9	1.90	n.d.	414	14.5
1/14/2004 4:00	5.55	-44.9	-8.33	21.8	8.8	5.1	20.17	2.90	7.10	2.58	7.36	47.0	10.4	3.30	n.d.	402	14.4
1/14/2004 5:00	13.20	-46.8	-8.53	21.5	8.5	6.0	18.31	2.70	8.13	2.94	6.83	41.8	10.3	3.65	n.d.	394	14.3
1/14/2004 6:00	13.20	-47.0	-8.54	21.3	8.1	5.9	17.67	2.60	7.18	2.96	6.63	42.3	10.5	3.53	n.d.	367	13.2
1/14/2004 7:00	20.40	-50.4	-8.8	20.0	7.3	5.8	14.84	2.40	7.09	3.30	6.48	36.2	10.6	5.14	n.d.	327	12.5

Date/Time	Q m ³ /s	δ ² H ‰	δ ¹⁸ O ‰	d ‰	Cl mg/L	NO ₃ ⁻ mg/L	SO ₄ ²⁻ mg/L	HCO ₃ ⁻ mmol/L	Na ⁺ mg/L	K ⁺ mg/L	Mg ²⁺ mg/L	Ca ²⁺ mg/L	SiO ₂ mg/L	DOC mg/L	TSS mg/L	EC µS/cm	T °C
1/14/2004 8:00	22.80	-46.3	-8.4	20.9	8.5	6.3	19.16	2.60	6.76	2.67	7.24	46.7	10.0	4.07	n.d.	306	12.0
1/14/2004 10:00	39.84	-48.8	-8.59	19.9	8.0	6.1	17.53	2.45	8.26	3.30	6.63	42.2	10.6	4.34	1681	276	11.2
1/14/2004 11:00	46.10	-50.1	-8.83	20.6	7.1	5.6	15.18	2.50	7.15	3.31	5.74	37.2	10.4	4.20	2177	267	11.0
1/14/2004 12:00	33.36	-52.3	-9.03	20.0	7.0	5.0	14.73	2.50	7.09	3.19	5.71	36.6	10.6	3.63	1907	274	11.1
1/14/2004 13:00	24.00	-50.2	-8.97	21.5	7.5	5.3	15.72	2.45	7.09	2.74	6.02	42.6	10.9	4.05	n.d.	294	11.6
1/14/2004 14:00	20.00	-48.8	-8.63	20.3	8.1	6.2	16.95	2.70	8.02	2.87	6.72	40.7	11.4	3.84	929	311	12.2
1/14/2004 15:00	16.40	-46.3	-8.42	21.0	8.6	6.3	17.55	2.50	8.11	2.67	7.89	41.6	11.5	3.88	n.d.	328	12.6
1/14/2004 16:00	14.80	-44.8	-8.21	20.8	8.9	7.4	18.59	2.90	8.59	2.56	7.32	45.0	11.2	3.17	272	340	13.0
1/14/2004 17:00	14.80	-43.0	-8.02	21.2	9.3	7.7	19.04	2.95	9.06	2.38	8.32	46.8	11.3	2.67	287	348	13.2
1/14/2004 18:00	13.20	-42.1	-7.92	21.3	9.5	8.0	19.95	3.10	8.84	2.38	8.33	49.5	11.4	2.73	240	354	13.4
1/14/2004 19:00	13.20	-41.4	-7.84	21.3	9.7	8.2	20.06	3.10	8.77	2.47	8.63	47.6	11.3	2.81	233	357	13.5
1/14/2004 20:00	13.20	-41.5	-7.8	20.9	9.8	8.4	20.10	3.00	8.07	2.32	8.04	50.4	11.2	2.61	199	358	13.6
1/14/2004 21:00	13.20	-40.5	-7.75	21.6	9.7	8.3	19.34	3.10	8.23	2.13	8.01	51.1	11.1	2.17	181	361	13.7
1/14/2004 22:00	12.40	-40.8	-7.68	20.6	9.8	8.2	19.40	3.20	8.48	1.99	8.16	52.1	10.9	2.53	135	361	13.8
1/14/2004 23:00	12.00	-40.4	-7.71	21.2	10.2	8.9	20.50	3.20	8.91	1.90	9.73	51.8	10.7	2.28	155	361	13.9
1/15/2004 0:00	12.00	-40.7	-7.72	21.0	9.6	8.2	19.12	3.15	7.91	2.03	8.03	51.6	10.6	2.11	183	361	13.9
1/15/2004 1:00	12.00	-40.9	-7.8	21.5	9.6	8.0	18.85	3.15	8.41	2.01	7.77	51.4	10.6	1.82	188	362	14.0
1/15/2004 2:00	12.00	-41.8	-7.77	20.3	9.5	8.2	18.69	3.10	8.08	1.95	8.08	52.0	10.4	2.06	189	360	14.0
1/15/2004 3:00	12.00	-41.5	-7.81	21.0	9.4	8.1	18.48	3.10	6.69	1.76	8.37	49.8	10.5	2.25	153	358	14.0
1/15/2004 4:00	11.66	-42.1	-7.8	20.3	9.4	7.9	18.33	3.10	8.39	1.78	7.59	49.0	10.6	1.64	135	358	14.0
1/15/2004 5:00	11.66	-40.7	-7.84	22.0	10.2	8.6	19.71	3.12	8.74	1.77	8.77	56.6	10.6	1.52	130	358	14.0
1/15/2004 6:00	11.66	-41.3	-7.8	21.2	10.0	8.7	19.50	3.20	8.77	1.75	8.85	57.2	10.7	2.05	131	358	14.0
1/15/2004 7:00	9.62	-41.3	-7.78	21.0	9.2	7.8	18.16	3.10	7.68	1.77	8.22	51.4	10.6	1.74	128	359	14.1
1/15/2004 8:00	9.62	-41.2	-7.77	20.9	9.4	7.8	18.46	3.25	9.05	1.81	8.55	52.9	10.6	1.72	118	362	14.2
1/15/2004 9:00	9.62	-40.4	-7.77	21.8	9.4	7.6	18.97	3.30	8.03	1.84	8.67	50.3	10.5	1.46	119	364	14.3
1/15/2004 11:00	9.62	-38.3	-7.65	23.0	10.2	8.1	19.72	3.10	8.22	1.82	8.66	54.6	10.6	2.51	63	365	14.6

Date/Time	Q m ³ /s	δ ² H ‰	δ ¹⁸ O ‰	d ‰	Cl mg/L	NO ₃ ⁻ mg/L	SO ₄ ²⁻ mg/L	HCO ₃ ⁻ mmol/L	Na ⁺ mg/L	K ⁺ mg/L	Mg ²⁺ mg/L	Ca ²⁺ mg/L	SiO ₂ mg/L	DOC mg/L	TSS mg/L	EC µS/cm	T °C
1/15/2004 14:00	8.60	-38.4	-7.61	22.5	10.0	7.8	20.49	3.10	9.00	1.68	9.12	59.0	10.6	2.27	66	372	14.9
1/15/2004 17:00	8.94	-38.1	-7.56	22.3	10.2	7.3	20.45	3.20	7.79	1.68	9.08	53.9	10.8	2.01	57	373	15.1
1/15/2004 20:00	7.82	-37.3	-7.51	22.8	10.4	7.6	20.82	3.25	8.70	1.72	8.97	56.7	10.9	1.24	49	378	14.9
1/15/2004 23:00	7.82	-37.3	-7.5	22.7	11.2	8.5	20.95	3.30	8.95	1.58	9.10	59.6	11.0	1.55	52	377	14.7
1/16/2004 2:00	6.78	-36.8	-7.38	22.2	10.5	7.8	18.95	3.30	8.39	1.61	8.73	52.8	11.1	1.34	45	377	14.8
1/16/2004 5:00	6.78	-36.9	-7.33	21.8	11.1	7.5	19.06	3.20	8.22	1.80	8.94	58.0	11.0	1.75	46	380	14.9
1/16/2004 8:00	6.78	-36.5	-7.4	22.8	10.6	7.8	18.53	3.35	8.43	1.73	8.71	59.5	10.9	1.74	17	383	15.0
1/16/2004 11:00	6.26	-36.7	-7.41	22.6	10.5	7.4	18.19	3.40	7.80	1.51	8.34	58.4	10.6	1.26	19	384	15.6
1/16/2004 14:00	6.26	-36.2	-7.34	22.5	10.6	6.9	18.34	3.40	8.11	1.66	8.52	56.8	10.7	1.40	15	386	16.1
1/16/2004 17:00	6.26	-36.4	-7.32	22.2	10.6	7.6	18.68	3.40	8.61	1.64	8.28	58.6	11.1	2.07	17	389	16.0
1/16/2004 20:00	6.26	-36.3	-7.39	22.8	10.7	7.4	18.88	3.45	8.90	1.59	8.46	59.2	11.0	1.50	20	391	15.5
1/16/2004 23:00	6.26	-36.6	-7.33	22.0	10.7	7.3	19.18	3.50	8.67	1.57	8.94	61.4	10.6	1.69	18	392	15.1
1/17/2004 2:00	5.55	-36.2	-7.34	22.5	10.6	7.2	19.04	3.50	8.06	1.40	8.34	61.8	10.5	1.74	12	393	14.9
1/17/2004 5:00	5.55	-37.3	-7.41	22.0	10.6	6.3	19.03	3.50	7.94	1.51	8.31	63.9	10.3	2.31	6	394	14.7
1/17/2004 8:00	5.55	-36.8	-7.33	21.8	10.8	7.1	19.44	3.60	8.08	1.41	8.32	59.9	10.1	1.27	n.d.	393	14.7
1/17/2004 14:00	5.55	-36.6	-7.38	22.5	11.1	7.0	20.01	3.50	8.67	1.44	8.36	64.7	10.0	1.34	n.d.	392	15.8
1/17/2004 20:00	5.10	-35.7	-7.31	22.8	10.7	6.6	19.52	3.40	8.78	1.47	9.25	62.0	9.9	1.66	n.d.	394	15.3
1/18/2004 2:00	5.10	-35.9	-7.35	23.0	10.4	6.5	19.27	3.40	7.81	1.45	8.05	60.9	9.7	0.95	n.d.	395	14.7
1/18/2004 8:00	5.10	-35.3	-7.36	23.6	10.6	6.6	19.87	3.50	8.36	1.37	7.85	59.2	9.7	1.44	n.d.	395	14.6
1/20/2004 0:00	4.95	-38.8	-7.245	19.2	12.0	6.2	21.50	3.55	8.30	1.07	7.71	66.6	9.1	0.68	n.d.	398	n.d.
1/21/2004 0:00	4.80	-37.8	-7.255	20.2	11.7	5.9	21.49	3.60	8.57	1.66	7.98	64.5	8.4	1.59	n.d.	389	n.d.
1/22/2004 0:00	4.65	-38.2	-7.275	20.0	11.7	6.0	22.80	3.65	8.77	1.02	7.79	66.2	8.4	0.94	n.d.	400	n.d.
1/22/2004 12:00	4.80	-36.7	-7.33	21.9	11.2	5.4	22.30	3.70	8.08	1.25	8.12	65.2	8.3	1.17	n.d.	399	n.d.

Table 85: Discharge and natural tracer concentrations of the investigated Orevim runoff event (1/13-1/18/2004). N.d.: not determined.

Date/Time	Q m ³ /s	δ ² H ‰	δ ¹⁸ O ‰	d ‰	Cl ⁻ mg/L	NO ₃ ⁻ mg/L	SO ₄ ²⁻ mg/L	HCO ₃ ⁻ mmol/L	Na ⁺ mg/L	K ⁺ mg/L	Mg ²⁺ mg/L	Ca ²⁺ mg/L	SiO ₂ mg/L	DOC mg/L	TSS mg/L	EC µS/cm	T °C
1/12/2004 12:00	0.27	-29.9	-6.42	21.5	19.6	16.7	9.33	2.85	19.29	3.35	15.56	29.8	29.0	2.22	33	370	15.4
1/12/2004 14:00	0.31	-29.3	-6.39	21.8	19.5	17.7	9.36	2.80	19.58	3.31	17.20	29.8	28.5	2.51	34	362	14.8
1/12/2004 16:00	0.29	-29.7	-6.43	21.8	19.3	17.1	9.31	2.80	19.61	3.38	13.66	30.0	28.4	2.82	42	361	14.6
1/13/2004 0:00	0.36	-29.0	-6.41	22.3	18.9	15.2	10.36	2.80	17.08	3.99	13.72	28.3	26.9	3.72	67	341	13.5
1/13/2004 12:00	0.31	-29.8	-6.41	21.5	20.5	17.2	10.68	2.60	20.25	3.60	13.61	29.9	27.3	3.23	48	348	15.9
1/13/2004 17:00	0.31	-32.1	-6.56	20.4	19.2	15.9	9.79	2.50	21.46	3.34	13.54	27.7	28.5	2.53	31	350	15.3
1/13/2004 18:00	0.31	-31.3	-6.56	21.2	19.3	16.1	9.82	2.40	18.78	3.52	13.98	28.2	28.7	2.60	34	350	15.2
1/13/2004 19:00	0.31	-32.3	-6.5	19.8	19.1	16.0	9.77	2.40	20.53	3.47	13.65	28.2	28.4	2.53	29	350	15.0
1/13/2004 20:00	0.31	-29.9	-6.56	22.5	19.7	16.4	9.77	2.50	22.16	3.65	13.21	26.6	28.6	2.52	38	350	14.9
1/13/2004 21:00	0.31	-31.1	-6.59	21.6	19.5	15.9	9.77	2.40	19.31	3.75	12.06	27.5	28.6	2.62	36	346	14.8
1/13/2004 22:00	0.31	-31.4	-6.58	21.2	19.3	16.5	9.70	2.60	21.26	3.30	12.95	28.4	28.0	2.84	25	346	14.8
1/13/2004 23:00	0.31	-31.5	-6.61	21.4	19.4	16.6	9.78	2.45	19.46	3.49	13.13	24.3	27.8	2.73	31	346	14.7
1/14/2004 0:00	0.31	-31.6	-6.62	21.4	19.1	16.3	9.60	2.40	20.43	3.67	13.31	29.1	27.6	2.90	n.d.	345	14.7
1/14/2004 1:00	0.34	-32.0	-6.6	20.9	18.8	15.8	9.54	2.45	19.59	3.36	14.11	28.1	28.3	3.21	32	344	14.6
1/14/2004 2:00	0.44	-33.1	-6.6	19.8	18.6	15.3	9.45	2.80	19.49	3.68	12.78	26.0	27.2	3.07	n.d.	340	14.6
1/14/2004 3:00	0.59	-34.7	-6.69	18.8	18.2	15.1	9.30	2.35	19.95	3.74	13.25	26.1	26.8	3.30	80	337	14.5
1/14/2004 4:00	0.59	-33.7	-6.74	20.3	18.4	14.5	9.56	2.50	19.36	3.99	12.52	27.1	26.6	3.80	55	338	14.3
1/14/2004 5:00	0.64	-34.1	-6.72	19.7	18.7	14.7	10.29	2.50	19.34	4.73	13.30	28.1	25.7	4.80	150	336	14.1
1/14/2004 6:00	1.39	-35.7	-6.87	19.3	18.0	14.8	11.15	2.70	18.14	5.48	13.60	26.7	24.2	5.94	223	336	13.9
1/14/2004 7:00	3.45	-34.9	-6.92	20.4	18.6	15.4	14.02	2.35	15.81	7.23	11.07	27.5	22.6	8.61	708	296	12.2

Date/Time	Q m ³ /s	δ ² H ‰	δ ¹⁸ O ‰	d ‰	Cl mg/L	NO ₃ ⁻ mg/L	SO ₄ ²⁻ mg/L	HCO ₃ ⁻ mmol/L	Na ⁺ mg/L	K ⁺ mg/L	Mg ²⁺ mg/L	Ca ²⁺ mg/L	SiO ₂ mg/L	DOC mg/L	TSS mg/L	EC µS/cm	T °C
1/14/2004 8:00	5.03	-41.1	-7.63	19.9	13.3	10.8	11.13	1.90	12.25	5.01	9.34	20.5	18.9	6.42	410	247	11.2
1/14/2004 9:00	12.50	-43.3	-7.86	19.6	11.5	9.0	9.82	1.80	10.44	4.22	8.24	21.3	18.0	6.93	733	234	10.7
1/14/2004 10:00	12.06	-44.9	-8.08	19.7	9.4	7.8	8.76	1.50	10.11	4.66	7.38	20.2	17.1	7.50	978	204	10.3
1/14/2004 11:00	12.06	-48.1	-8.43	19.3	7.3	5.9	6.96	1.65	7.89	3.63	5.88	16.5	15.6	6.12	897	177	10.4
1/14/2004 12:00	7.33	-49.1	-8.62	19.9	7.2	6.0	6.89	1.25	8.48	3.05	4.93	17.3	15.7	5.77	300	185	10.5
1/14/2004 13:00	4.65	-48.1	-8.47	19.7	8.4	6.4	7.39	1.50	8.36	3.10	7.02	17.7	16.2	5.56	228	191	10.8
1/14/2004 14:00	4.65	-47.5	-8.36	19.3	9.2	7.1	7.80	1.50	9.38	3.30	7.10	19.0	17.1	6.06	154	203	11.1
1/14/2004 15:00	3.75	-46.3	-8.18	19.1	8.4	7.0	7.11	1.60	n.d.	3.06	7.88	19.7	18.1	4.99	106	212	11.3
1/14/2004 16:00	3.55	-45.1	-8.05	19.4	10.7	8.7	8.65	1.50	10.74	2.82	8.66	20.4	18.3	5.28	92	224	11.5
1/14/2004 17:00	3.65	-43.1	-7.86	19.7	10.4	7.8	8.54	1.90	10.13	2.76	8.29	19.8	19.1	5.51	60	225	11.5
1/14/2004 18:00	3.35	-43.6	-7.84	19.1	11.0	8.3	8.60	1.60	11.36	3.23	9.36	20.3	18.9	5.50	61	226	11.5
1/14/2004 19:00	3.35	-43.6	-7.84	19.1	10.6	8.7	8.76	1.85	10.50	3.12	9.41	19.5	19.5	5.22	46	229	11.6
1/14/2004 20:00	2.43	-43.1	-7.78	19.2	10.8	8.2	8.66	1.55	10.40	3.26	8.77	21.5	19.7	6.18	47	231	11.6
1/14/2004 21:00	2.43	-42.2	-7.74	19.7	10.9	9.0	8.96	1.90	10.51	2.68	8.85	20.2	19.9	5.12	39	235	11.6
1/14/2004 22:00	2.43	-41.7	-7.67	19.7	11.8	9.3	9.37	1.70	11.46	3.03	8.93	22.2	20.3	5.20	37	241	11.7
1/14/2004 23:00	1.65	-40.8	-7.55	19.6	12.3	9.0	9.42	1.90	11.29	2.95	9.24	22.9	20.6	6.13	41	248	11.9
1/15/2004 0:00	1.65	-40.4	-7.53	19.9	12.4	9.8	9.38	1.85	11.93	3.37	10.37	23.4	21.1	4.64	36	255	12.1
1/15/2004 1:00	1.65	-39.5	-7.46	20.2	13.0	10.5	9.71	1.95	11.39	3.10	10.06	23.1	21.7	4.81	38	262	12.3
1/15/2004 2:00	1.17	-38.9	-7.43	20.6	12.9	10.6	9.53	1.95	12.69	2.92	11.31	24.0	22.1	4.55	39	270	12.4
1/15/2004 3:00	1.17	-39.1	-7.38	19.9	13.2	11.2	9.64	1.95	13.16	3.44	10.30	25.0	22.3	4.65	42	276	12.7
1/15/2004 4:00	1.17	-38.2	-7.38	20.8	13.6	11.3	9.74	1.95	13.28	3.15	11.39	26.6	22.4	5.06	43	282	12.9
1/15/2004 5:00	1.17	-38.5	-7.33	20.2	14.1	12.3	10.17	2.05	12.90	3.24	12.59	25.8	22.9	4.73	40	288	13.0
1/15/2004 6:00	0.89	-37.5	-7.3	20.9	14.3	12.5	9.99	2.20	13.36	3.20	10.75	27.0	23.6	4.94	40	292	13.2
1/15/2004 7:00	0.89	-36.5	-7.23	21.4	14.6	13.4	10.15	2.10	12.98	3.31	12.31	27.3	23.6	4.64	49	297	13.4
1/15/2004 8:00	0.89	-36.7	-7.27	21.5	14.5	13.3	10.02	2.30	15.03	3.32	12.28	27.6	24.3	4.32	41	301	13.5
1/15/2004 9:00	0.89	-36.7	-7.22	21.1	15.2	13.8	10.28	2.30	13.36	3.33	12.37	27.0	24.5	4.37	33	305	13.8

Date/Time	Q m ³ /s	δ ² H ‰	δ ¹⁸ O ‰	d ‰	Cl mg/L	NO ₃ mg/L	SO ₄ ²⁻ mg/L	HCO ₃ mmol/L	Na ⁺ mg/L	K ⁺ mg/L	Mg ²⁺ mg/L	Ca ²⁺ mg/L	SiO ₂ mg/L	DOC mg/L	TSS mg/L	EC µS/cm	T °C
1/15/2004 10:00	0.78	-36.3	-7.22	21.5	15.6	14.7	10.55	2.20	15.90	3.41	13.18	26.7	25.0	4.30	29	309	14.0
1/15/2004 11:00	0.78	-36.5	-7.17	20.9	16.1	15.4	10.68	2.20	15.93	3.74	12.73	29.0	25.0	3.69	29	312	14.2
1/15/2004 12:00	0.78	-35.9	-7.13	21.2	16.0	15.5	10.65	2.70	14.91	3.75	13.26	29.2	25.7	4.08	28	313	14.4
1/15/2004 13:00	0.78	-35.9	-7.04	20.4	15.2	15.3	10.29	2.30	13.74	3.35	14.21	27.0	26.2	4.56	n.d.	315	14.6
1/15/2004 16:00	0.75	-35.9	-7.01	20.2	15.6	15.9	10.38	2.30	15.88	3.27	14.37	27.5	26.6	4.15	n.d.	320	15.0
1/15/2004 19:00	0.75	-35.5	-6.98	20.3	15.6	15.6	10.33	2.50	14.70	3.57	13.66	28.1	27.0	4.10	n.d.	324	14.9
1/15/2004 22:00	0.72	-35.1	-6.96	20.5	15.6	16.0	10.38	2.40	15.59	3.09	15.75	29.1	27.3	4.35	n.d.	328	14.5
1/16/2004 1:00	0.66	-33.6	-6.79	20.7	16.1	16.9	10.64	2.50	16.52	3.02	17.46	28.1	27.9	3.62	n.d.	331	14.5
1/16/2004 4:00	0.66	-29.9	-6.9	21.4	16.7	17.5	10.73	2.55	16.12	3.24	15.13	30.1	28.7	3.94	n.d.	335	14.6
1/16/2004 7:00	0.62	-32.9	-6.86	21.9	16.8	18.0	10.70	2.60	16.56	3.08	15.20	27.3	29.2	3.37	n.d.	337	14.8
1/16/2004 10:00	0.62	-32.3	-6.84	22.5	16.9	18.6	10.66	2.50	16.63	3.16	14.72	28.4	29.4	3.56	n.d.	340	15.8
1/16/2004 16:00	0.62	-31.7	-6.82	22.9	17.2	18.9	10.54	2.50	16.70	3.24	14.24	29.6	30.1	3.66	n.d.	344	17.1
1/16/2004 22:00	0.57	-32.3	-6.75	21.8	18.8	19.1	11.25	2.60	17.86	4.15	16.33	29.7	30.8	3.43	n.d.	347	15.6
1/17/2004 4:00	0.57	-31.5	-6.76	22.5	18.0	19.6	10.57	2.55	18.98	3.39	15.41	30.0	31.5	3.54	n.d.	348	14.9
1/17/2004 10:00	0.57	-31.7	-6.71	22.0	18.0	19.9	10.43	2.50	17.30	3.33	13.80	30.7	31.5	2.97	n.d.	346	15.9
1/17/2004 16:00	0.57	-31.6	-6.72	22.1	18.1	19.1	10.31	2.35	16.15	3.29	14.23	27.7	30.5	3.69	n.d.	343	16.6
1/17/2004 22:00	0.53	-31.5	-6.64	21.6	17.9	19.6	10.20	2.60	17.89	3.22	14.74	30.0	31.1	2.69	n.d.	346	15.5
1/18/2004 4:00	0.53	-31.7	-6.72	22.0	18.0	19.8	10.21	2.55	17.53	3.31	16.04	30.0	31.1	2.91	n.d.	347	15.3
1/18/2004 10:00	0.53	-31.8	-6.69	21.7	17.7	19.3	10.00	2.60	18.98	3.04	14.05	26.7	31.2	2.90	15	347	15.3

Table 86: Discharge and natural tracer concentrations of the investigated Senir runoff event (2/14-2/18/2003). N.d.: not determined.

Date/Time	Q m ³ /s	δ ² H ‰	δ ¹⁸ O ‰	d ‰	Cl ⁻ mg/L	NO ₃ ⁻ mg/L	SO ₄ ²⁻ mg/L	HCO ₃ ⁻ mmol/L	Na ⁺ mg/L	K ⁺ mg/L	Mg ²⁺ mg/L	Ca ²⁺ mg/L	SiO ₂ mg/L	DOC mg/L	TSS mg/L	EC µS/cm	T °C
2/13/2003 12:30	12.50	-33.6	-6.67	19.8	12.1	7.5	11.50	3.70	6.87	1.29	6.09	60.7	8.6	1.95	n.d.	414	n.d.
2/13/2003 14:30	12.50	-33.6	-6.65	19.6	12.0	7.7	11.30	3.70	6.78	1.32	5.96	52.0	8.6	0.79	n.d.	412	n.d.
2/13/2003 16:30	12.50	-33.7	-6.7	19.9	12.1	7.1	11.30	3.66	7.26	1.32	5.99	61.3	8.6	0.91	n.d.	411	n.d.
2/13/2003 18:30	12.85	-34.2	-6.74	19.7	12.0	7.2	11.30	3.74	7.01	1.46	5.94	65.6	8.6	1.03	n.d.	412	n.d.
2/13/2003 20:30	13.20	-32.9	-6.69	20.6	12.4	7.3	11.50	3.72	6.61	1.35	6.00	63.8	8.4	1.18	n.d.	412	n.d.
2/13/2003 22:30	16.00	-33.5	-6.67	19.9	12.3	7.7	11.50	3.80	6.83	1.52	6.06	66.8	8.4	1.22	n.d.	409	n.d.
2/14/2003 0:30	29.13	-34.8	-6.77	19.4	11.6	4.5	10.40	3.28	6.82	1.72	5.47	55.0	6.9	1.47	n.d.	360	n.d.
2/14/2003 2:30	52.62	-38.4	-7.34	20.3	9.5	4.9	10.30	2.80	5.98	1.85	4.50	59.9	7.3	2.79	n.d.	294	n.d.
2/14/2003 4:30	38.62	-43.6	-8.01	20.5	9.4	4.9	10.10	2.40	6.68	1.86	4.44	59.5	6.6	2.83	n.d.	258	n.d.
2/14/2003 6:30	31.75	-44.4	-8.1	20.4	7.6	1.7	7.89	2.50	5.24	1.80	4.08	54.5	6.9	2.31	n.d.	268	n.d.
2/14/2003 8:30	27.25	-43.7	-8.07	20.9	8.2	4.8	8.47	2.62	5.40	1.89	4.20	54.5	7.3	2.44	n.d.	286	n.d.
2/14/2003 10:30	24.75	-42.2	-7.79	20.1	8.5	4.8	9.34	2.88	6.05	1.71	4.63	55.7	7.6	2.04	n.d.	311	n.d.
2/14/2003 12:30	22.30	-39.5	-7.6	21.3	9.4	5.1	10.00	3.08	6.23	1.80	5.22	53.9	7.4	2.11	n.d.	335	n.d.
2/14/2003 14:30	22.30	-38.6	-7.52	21.6	9.8	1.8	10.30	3.26	6.54	1.70	5.04	58.2	8.0	2.18	n.d.	347	n.d.
2/14/2003 16:30	21.25	-38.2	-7.24	19.7	10.1	2.5	10.40	3.34	6.17	1.54	5.43	64.2	8.0	2.19	n.d.	361	n.d.
2/14/2003 18:30	20.90	-37.3	-7.16	20.0	10.5	3.4	10.60	3.50	6.31	1.42	5.61	66.7	8.0	1.36	n.d.	371	n.d.
2/14/2003 20:30	21.60	-35.8	-7	20.2	10.9	4.4	10.70	3.52	7.22	1.49	5.40	68.4	8.2	1.75	n.d.	374	n.d.
2/14/2003 22:30	21.25	-35.5	-6.99	20.4	11.0	4.3	10.80	3.58	6.63	1.58	5.25	64.5	8.4	1.35	n.d.	380	n.d.
2/15/2003 0:30	21.95	-36.0	-6.86	18.9	11.1	4.4	10.80	3.60	6.67	1.55	5.45	69.0	8.4	2.04	n.d.	382	n.d.
2/15/2003 2:30	21.25	-34.7	-6.87	20.3	10.9	3.7	10.60	3.54	6.96	1.60	5.75	52.5	8.4	1.55	n.d.	377	n.d.
2/15/2003 4:30	21.60	-34.4	-6.8	20.0	11.0	7.3	11.00	3.52	6.94	1.69	5.68	57.3	8.0	1.52	n.d.	383	n.d.
2/15/2003 6:30	22.65	-34.1	-6.69	19.4	11.2	6.9	11.10	3.52	7.15	1.52	5.67	62.5	8.0	1.23	n.d.	374	n.d.
2/15/2003 8:30	33.63	-34.3	-6.74	19.6	10.9	3.0	10.50	3.30	6.79	1.60	5.71	63.6	8.2	2.33	n.d.	350	n.d.

Date/Time	Q m ³ /s	δ ² H ‰	δ ¹⁸ O ‰	d ‰	Cl ⁻ mg/L	NO ₃ ⁻ mg/L	SO ₄ ²⁻ mg/L	HCO ₃ ⁻ mmol/L	Na ⁺ mg/L	K ⁺ mg/L	Mg ²⁺ mg/L	Ca ²⁺ mg/L	SiO ₂ mg/L	DOC mg/L	TSS mg/L	EC µS/cm	T °C
2/15/2003 10:30	38.20	-35.0	-6.93	20.4	9.5	5.4	9.70	2.86	7.08	1.73	4.82	55.9	7.8	2.07	n.d.	308	n.d.
2/15/2003 13:37	29.50	-35.0	-7.08	21.6	9.2	1.9	9.15	2.90	6.99	1.70	4.49	61.5	7.8	2.60	n.d.	308	n.d.
2/15/2003 15:30	25.80	-36.4	-7.15	20.8	9.5	1.6	9.12	3.06	7.13	1.77	5.21	60.1	7.8	1.93	n.d.	320	n.d.
2/15/2003 17:30	22.30	-36.0	-7.03	20.2	9.9	4.6	9.86	3.32	6.69	1.62	5.17	64.6	8.1	2.52	n.d.	336	n.d.
2/15/2003 19:30	22.65	-36.1	-6.94	19.4	10.2	2.7	9.97	3.44	7.21	1.70	5.64	64.2	8.1	1.68	n.d.	348	n.d.
2/15/2003 21:30	21.95	-35.5	-6.96	20.2	10.6	5.2	10.60	3.62	6.99	1.39	5.65	66.8	8.0	1.51	n.d.	360	n.d.
2/15/2003 23:30	20.90	-36.2	-6.96	19.5	10.8	4.3	10.50	3.68	7.19	1.53	5.29	67.1	8.3	2.17	n.d.	366	n.d.
2/16/2003 1:30	20.90	-35.8	-6.91	19.5	10.8	4.5	10.50	3.70	6.83	1.34	5.68	72.0	8.1	1.34	n.d.	367	n.d.
2/16/2003 3:30	20.90	-36.1	-6.87	18.9	11.0	6.1	10.90	3.64	6.42	1.53	5.61	67.3	8.3	1.59	n.d.	364	n.d.
2/16/2003 5:30	20.90	-36.3	-6.92	19.1	11.0	6.5	10.80	3.74	6.63	1.36	5.78	69.8	8.3	1.71	n.d.	365	n.d.
2/16/2003 7:30	18.45	-35.2	-6.87	19.8	11.0	6.2	10.90	3.76	6.64	1.47	5.76	69.5	8.2	1.52	n.d.	362	n.d.
2/16/2003 9:30	18.45	-35.4	-6.91	19.9	11.0	6.9	10.70	3.72	6.58	1.43	5.71	54.7	8.4	1.38	n.d.	354	n.d.
2/16/2003 11:30	18.45	-35.3	-6.9	19.9	11.0	6.4	10.90	3.72	6.44	1.41	6.19	53.9	8.4	1.18	n.d.	349	n.d.
2/16/2003 13:30	18.45	-36.1	-6.83	18.5	11.1	5.9	10.90	3.66	6.45	1.36	5.83	53.5	8.3	1.46	n.d.	345	n.d.

Table 87: Discharge and natural tracer concentrations of the investigated Sion runoff event (1/14-1/16/2004). (At times, Sion discharge was just a trickle and was recorded as “zero” by the gauges of the Hydrological Service.) N.d.: not determined.

Date/Time	Q m ³ /s	δ ² H ‰	δ ¹⁸ O ‰	d ‰	Cl ⁻ mg/L	NO ₃ ⁻ mg/L	SO ₄ ²⁻ mg/L	HCO ₃ ⁻ mmol/L	Na ⁺ mg/L	K ⁺ mg/L	Mg ²⁺ mg/L	Ca ²⁺ mg/L	SiO ₂ mg/L	DOC mg/L	TSS mg/L	EC µS/cm	T °C
1/14/2004 3:00	0.000	-51.6	-8.47	16.1	1.45	1.09	1.20	1.05	1.35	1.06	0.98	16.71	2.42	2.39	94	92	n.d.
1/14/2004 4:00	0.000	-59.9	-9.55	16.5	1.15	0.85	0.96	1.10	1.23	0.93	1.08	15.16	2.32	1.53	120	85	n.d.
1/14/2004 5:00	0.000	-63.2	-10.02	16.9	1.15	0.62	0.73	1.00	1.06	0.83	1.06	16.73	2.62	1.99	316	92	n.d.
1/14/2004 6:00	0.010	-49.8	-8.67	19.6	2.58	1.41	2.84	1.80	2.67	0.67	0.50	22.98	3.51	2.93	1090	142	n.d.
1/14/2004 7:00	0.000	-63.8	-10.38	19.3	2.02	n.d.	2.42	1.90	3.57	1.70	0.29	30.02	6.87	3.56	24110	179	n.d.
1/14/2004 8:00	0.020	-59.9	-10.12	21.0	3.13	1.13	2.49	1.90	2.89	0.98	1.02	26.77	4.60	3.36	4545	168	n.d.
1/14/2004 9:00	0.300	-63.2	-10.44	20.4	3.07	0.74	2.36	1.80	3.23	2.04	0.26	29.32	4.60	3.25	11315	173	n.d.
1/14/2004 10:00	0.932	-65.4	-10.64	19.7	2.85	0.72	2.37	2.00	3.10	2.70	0.56	31.42	4.50	3.22	12530	185	n.d.
1/14/2004 11:00	1.032	-67.2	-10.93	20.2	2.71	0.98	2.31	1.85	2.85	1.15	1.18	28.97	3.90	3.39	4650	169	n.d.
1/14/2004 12:00	0.648	-67.5	-11.02	20.7	2.78	0.68	2.28	1.80	3.13	1.00	0.97	26.74	3.82	3.06	3403	162	n.d.
1/14/2004 13:00	0.556	-67.9	-10.99	20.0	2.96	0.86	2.28	1.80	3.18	0.97	0.94	27.67	4.45	3.09	2323	160	n.d.
1/14/2004 14:00	0.384	-68.3	-11.04	20.1	3.18	0.83	2.33	1.70	3.14	1.13	0.91	25.72	4.45	3.15	1486	161	n.d.
1/14/2004 15:00	0.300	-68.0	-11.00	20.1	3.33	0.89	2.34	1.70	3.58	0.94	0.98	26.86	4.61	2.94	852	161	n.d.
1/14/2004 16:00	0.300	-68.0	-10.98	19.9	3.50	0.94	2.33	1.75	3.20	1.07	0.99	24.79	4.37	2.85	757	161	n.d.
1/14/2004 17:00	0.272	-67.6	-10.97	20.2	3.92	0.98	2.45	1.70	3.93	0.97	0.88	27.12	4.37	2.75	630	160	n.d.
1/14/2004 18:00	0.272	-67.6	-10.99	20.4	4.33	0.82	2.36	1.70	4.02	1.01	0.83	26.41	4.29	3.25	436	160	n.d.
1/14/2004 19:00	0.138	-67.3	-10.97	20.5	4.79	0.71	2.47	1.70	4.34	1.00	0.82	26.49	4.29	3.21	280	160	n.d.
1/14/2004 20:00	0.138	-67.5	-11.04	20.8	4.70	0.96	2.45	1.70	4.36	0.93	0.85	27.77	4.29	2.99	263	162	n.d.
1/14/2004 21:00	0.138	-68.2	-11.10	20.7	4.88	1.08	2.43	1.65	4.48	0.82	0.84	24.66	3.74	2.58	191	163	n.d.
1/14/2004 22:00	0.138	-69.0	-11.18	20.4	4.98	0.98	2.42	1.80	4.15	0.90	0.74	26.89	3.82	1.79	306	163	n.d.

Date/Time	Q m ³ /s	δ ² H ‰	δ ¹⁸ O ‰	d ‰	Cl ⁻ mg/L	NO ₃ ⁻ mg/L	SO ₄ ²⁻ mg/L	HCO ₃ ⁻ mmol/L	Na ⁺ mg/L	K ⁺ mg/L	Mg ²⁺ mg/L	Ca ²⁺ mg/L	SiO ₂ mg/L	DOC mg/L	TSS mg/L	EC µS/cm	T °C
1/14/2004 23:00	0.138	-69.6	-11.26	20.5	5.09	0.90	2.40	1.70	4.77	0.91	0.72	24.49	3.66	1.98	180	160	n.d.
1/15/2004 0:00	0.138	-70.2	-11.36	20.7	5.16	0.90	2.37	1.75	4.93	0.90	0.83	24.82	3.66	1.96	265	160	n.d.
1/15/2004 1:00	0.000	-70.7	-11.39	20.4	5.01	0.96	2.36	1.70	4.42	0.84	0.79	27.06	3.51	1.94	341	160	n.d.
1/15/2004 2:00	0.138	-70.3	-11.35	20.5	4.91	0.98	2.34	1.60	4.81	1.03	0.71	25.78	3.98	2.46	113	159	n.d.
1/15/2004 3:00	0.050	-70.5	-11.39	20.7	4.76	0.88	2.33	1.70	5.09	0.98	0.80	24.87	3.98	2.18	99	160	n.d.
1/15/2004 4:00	0.050	-70.5	-11.33	20.2	4.69	0.92	2.30	1.70	4.96	0.90	0.88	26.26	3.98	2.32	73	160	n.d.
1/15/2004 5:00	0.050	-70.4	-11.36	20.5	4.60	0.92	2.26	1.70	4.53	0.96	0.83	24.33	4.22	2.37	62	161	n.d.
1/15/2004 6:00	0.050	-69.7	-11.35	21.1	4.59	n.d.	2.29	1.70	4.69	0.90	0.74	26.07	4.29	3.02	53	162	n.d.
1/15/2004 7:00	0.050	-70.2	-11.35	20.6	4.52	0.90	2.27	1.65	4.96	0.98	0.85	26.66	n.d.	2.54	37	160	n.d.
1/15/2004 8:00	0.050	-70.4	-11.41	20.9	4.87	0.60	2.28	1.60	4.94	1.00	0.85	26.91	3.90	2.64	n.d.	162	n.d.
1/15/2004 9:00	0.010	n.d.	n.d.	n.d.	n.d.	n.d.	n.d.	n.d.	5.06	1.01	0.88	26.96	4.06	n.d.	n.d.	163	n.d.
1/15/2004 10:00	0.010	-70.1	-11.37	20.8	4.45	0.77	2.26	1.75	4.54	0.95	0.98	27.46	n.d.	2.81	n.d.	168	n.d.
1/15/2004 12:00	0.000	-70.8	-11.41	20.5	4.49	1.09	2.29	2.00	4.99	1.00	0.98	29.89	3.35	2.53	n.d.	182	n.d.

CURRICULUM VITAE

Dipl.-Ing. Heike Brielmann

Huernbeckstrasse 22 • 80939 München

h.brielmann@gmx.de

Date of birth: 16. November 1976

Place of birth: Rostock

Education & University	
10/2005 – 03/2008	PostDoc at the Helmholtz Zentrum München, Institute of Groundwater Ecology
	Subject: The impact of anthropogenically induced temperature changes on shallow groundwater ecosystems
	Workgroup Molecular Microbiology, Dr. Tillmann Lueders
	AQUITHERM – Life Science Foundation
04/2002 - 09/2005	Ph.D. student at the GSF - Research Center, Institute of Hydrology
	Subject: Recharge and discharge dynamics in the Upper Jordan River catchment and their alteration with global change
	Supervisor: Prof. Dr. Klaus-Peter Seiler, Prof. Dr. M. I. Litaor
	BMBF-Project GLOWA
10/1995 - 10/2001	Student at the University of Rostock. Land management and Environmental Protection
	Thesis: Sequentially extracted P-fractions of P-enriched peat soils in Israel and Germany
	Supervisor: Prof. Dr. Peter Leinweber
	EU-Project PROWATER
Additional professional experience	
08/2001 – 12/2001	Technical assistant, MIGAL Galilee Technology Center, Kiryat Shmona, Israel – Workgroup Geohydrology
11/1998 – 08/2000	Technical assistant, University of Rostock, Institute of Geodesy and Geoinformatics
04/2000 - 05/2000	Intern, PROWA Black & Veatch GmbH, Rostock
11/1999 – 01/2000	Intern, Engineering Consultant „Ingenieurbüro für Planung und Konstruktion“, Wismar
07/1998 – 08/1998	Intern, Office for Ecological Studies, Dr. Norbert Brielmann, Rostock